OMEGA-3 FATTY ACID SUPPRESSION OF SILICA-INDUCED INFLAMMATION AND AUTOIMMUNE DISEASE

By

Kathryn Alexandria Wierenga

A DISSERTATION

Submitted to
Michigan State University
in partial fulfillment of the requirements
for the degree of

Biochemistry and Molecular Biology–Environmental Toxicology – Doctor of Philosophy

2021

ABSTRACT

OMEGA-3 FATTY ACID SUPPRESSION OF SILICA-INDUCED INFLAMMATION AND AUTOIMMUNE DISEASE

By

Kathryn Alexandria Wierenga

Exposure to the respirable toxicant crystalline silica ($cSiO_2$) is etiologically linked to systemic lupus erythematosus and other human autoimmune diseases. An estimated 2 million Americans are exposed to $cSiO_2$ occupationally, including approximately 100,000 exposed to levels above the National Institute for Occupational Safety and Health's recommended exposure limit. Clearance of inhaled $cSiO_2$ is very slow, thus repeated inhalation of $cSiO_2$ activates a chronic immune response in the lungs. Animal models suggest that continued over-activation of immune cells results in production of antibodies against the host, ultimately culminating in the development of systemic autoimmunity. Intriguingly, previous studies performed in Dr. Pestka's lab discovered that dietary supplementation with ω-3 polyunsaturated fatty acids (ω-3 PUFAs), an intervention known to improve disease status in patients with lupus and other autoimmune diseases, blocks $cSiO_2$-triggered autoimmunity in lupus-prone NZBWF1 mice. In these studies, the dietary ω-3 PUFA docosahexaenoic acid (DHA) attenuated many of the inflammatory and autoimmune disease endpoints induced by $cSiO_2$, including inflammatory gene expression; pulmonary immune cell infiltration; local and systemic chemokine, cytokine, and autoantibody production; and development of glomerulonephritis. This thesis builds upon previous work employing this model for environment-triggered autoimmunity to determine 1) the effect of DHA supplementation in a Western-style diet, 2) the associate between tissue ω-3 content and disease severity, and 3) the mechanisms of DHA protection and $cSiO_2$ toxicity in *in vitro* macrophage models.

Here, supplementation with DHA dose-dependently decreased several features of $cSiO_2$-triggered autoimmunity in a lupus-prone mouse model fed a diet mimicking the micro-and macro-nutrient composition of Western dietary patterns. DHA was as effective in this sub-optimal diet as in previous studies where DHA is provided on the background of a diet optimized for rodent health.

A meta-analysis of three publications employing DHA supplementation to protect against $cSiO_2$-triggered lupus identified strong correlations between red blood cell ω-3 fatty PUFA levels and autoimmune and inflammatory endpoints, which highlights the benefits of monitoring patients' fatty acid profiles when implementing a dietary intervention to augment ω-3 PUFA levels.

A key event in the development of systemic inflammation in this model is $cSiO_2$-induced toxicity of the alveolar macrophage (AM). *In vitro* studies in this thesis demonstrated that enriching the macrophage membrane with DHA influences macrophage phenotype and suppresses inflammatory and cytotoxic pathways induced by $cSiO_2$ and other inflammatory stimuli. Specifically, it was identified that DHA inhibits $cSiO_2$-induced inflammasome activation in part by interfering with gene expression of inflammasome components. Further investigations employing next generation RNA sequencing revealed that DHA suppressed many LPS-induced transcripts, and induced genes associated with inflammation resolution, identifying putative mechanisms for the protective effects of DHA supplementation *in vitro*. Lastly, a novel self-replicating AM model was used to investigate $cSiO_2$ engulfment, cell death, and cytokine release *in vitro*. Here, DHA inhibited $cSiO_2$-induced cell death and inflammatory cytokine release without influencing particle phagocytosis, highlighting the potential for this dietary intervention to protect against $cSiO_2$-triggered autoimmunity by preventing $cSiO_2$-induced toxicity in AMs.

Taken together, these studies provide greater insight into ω-3 PUFA-mediated protection against inflammation and autoimmune disease triggered by the inhaled toxicant $cSiO_2$.

Copyright by
KATHRYN ALEXANDRIA WIERENGA
2021

ACKNOWLEDGMENTS

It is humbling to reflect on how many people supported and encouraged me as I pursued this PhD. There is simply not enough room to thank all of them here, nevertheless, I am still grateful and humbled by their love and support.

To Dr. Pestka, words cannot adequately describe my gratitude. You are truly the best mentor I could have asked for. You have taught me so much about science, leadership, and teamwork. Your confidence in me has given me confidence in myself.

To my committee members, Dr. Dan Jones, Dr. John LaPres, Dr. Sophia Lunt, and Dr. Julia Busik, I am so appreciative of your guidance and grateful for every tough question you threw at me. Thank you so much for your support.

I enjoyed meeting and collaborating with so many excellent scientists and people throughout the course of of this project. I want to especially thank Dr. Andrew Olive and Sean Thomas, who advanced the MPI cell project to a level I could never have achieved on my own.

This research would not have been possible without funding from the NIEHS, the Lupus Foundation of America, and the Robert and Carol Deibel family endowment. It also would have been impossible without the financial administrative support I received from the the BMB and FSHN departments and the EITS program.

I have had the greatest joy of working alongside so many amazing people in the Pestka and Harkema labs. First, to Dr. Harkema, thank you for all your advice, on both lab- and life-related matters, and for always keeping me on my toes in lab meetings. To Jim and Ryan, thank you for being a constant source of positivity and fun. Working and chatting with both of you always brightened my day.

To Melissa, even though we only worked together briefly, you taught me how to think critically and work efficiently as a graduate student. Thank you for setting such a high bar.

To Kristen and Jo, thank you for making Dr. Pestka's lab feel like home, and for being such dear friends to me. I learned so much from both of you.

To Dan and Preeti, your hard work and determination always pushed me to work harder. Your bravery to travel around the world to pursue your careers is inspirational.

To all the bright and motivated undergrads I worked with - Liz, Augie, Alexa, Shamya, Adrianna, Riley - thank you for working hard, for making me laugh, and for keeping me up to date on ”what the kids are saying these days”.

To my fellow grad students, Lauren and Olivia, I am so excited to watch you succeed and thankful to have shared part of my graduate school experience with you.

To all my friends and colleagues at MSU, thank you for the commiserating, the advice, and the encouragement.

The ups and downs of graduate school continually reminded me how very blessed I am to have a rock-solid support system in my family, the Wierengas and the Royers. Thank you for cheering for me every step of the way and for reminding me what really matters. I love you all so much.

And last, but not least, to John - Thank you for always spurring me on to be my best, but still loving me exactly as I am. You are the greatest husband, teammate, and friend.

TABLE OF CONTENTS

LIST OF TABLES xii

LIST OF FIGURES xiii

KEY TO ABBREVIATIONS xviii

CHAPTER 1 INTRODUCTION AND LITERATURE REVIEW 1
1.1 INTRODUCTION 2
1.1.1 CHAPTER SUMMARIES 3
1.2 LITERATURE REVIEW 5
1.2.1 Lupus, silica, and dietary Omega-3 fatty acids 5
1.2.2 The role of alveolar macrophages in initiating $cSiO_2$-induced autoimmunity 15
1.2.3 Can DHA protect AMs from $cSiO_2$-induced toxicity? 30
1.2.4 Conclusion 40

CHAPTER 2 INFLUENCE OF TOTAL WESTERN DIET ON DOCOSAHEXAENOIC ACID SUPPRESSION OF SILICA-TRIGGERED LUPUS FLARING IN NZBWF1 MICE 41
2.1 ABSTRACT 42
2.2 INTRODUCTION 42
2.3 MATERIALS AND METHODS 45
2.3.1 Animals. 45
2.3.2 Fatty acid analyses. 46
2.3.3 Diet formulation. 46
2.3.4 $cSiO_2$. 47
2.3.5 Experimental design. 48
2.3.6 IRG expression. 50
2.3.7 Cytokine analyses. 51
2.3.8 Autoantibody ELISAs. 51
2.3.9 BALF cell quantitation and identification. 51
2.3.10 Lung histopathology. 52
2.3.11 Immunohistochemistry and morphometry of lungs 52
2.3.12 Kidney histopathology. 53
2.3.13 Statistical analysis. 53
2.4 RESULTS 54
2.4.1 DHA intake increases ω-3 PUFA content in red blood cells and tissues. . . 54
2.4.2 DHA supplementation suppresses $cSiO_2$-induced IRG response in the lungs. 58
2.4.3 DHA intake suppresses $cSiO_2$-induced cytokine elevations in the BALF. . 59
2.4.4 DHA consumption suppresses $cSiO_2$-induced pulmonary immune cell infiltration, including B and T lymphocytes and ELS neogenesis. 61

2.4.5 $cSiO_2$-induced autoantibody production is attenuated by DHA supplementation. . . . 62
2.4.6 DHA intake protects against $cSiO_2$-induced lesions in the kidney. . . . 64
2.5 DISCUSSION . . . 65
2.6 ACKNOWLEDGEMENTS . . . 69

CHAPTER 3 REQUISITE ω-3 HUFA BIOMARKER THRESHOLDS FOR PREVENTING MURINE LUPUS FLARING . . . 70
3.1 ABSTRACT . . . 71
3.2 INTRODUCTION . . . 71
3.3 MATERIALS AND METHODS . . . 74
3.3.1 Experimental design. . . . 74
3.3.2 Fatty acid analyses. . . . 77
3.3.3 Determination of the RBC ω-3 HUFA Score and the O3I. . . . 79
3.3.4 Data analysis and statistics. . . . 79
3.4 RESULTS . . . 80
3.4.1 DHA supplementation dose-dependently increases ω-3 HUFA Score uniformly across RBC and tissues. . . . 80
3.4.2 Elevated RBC ω-3 HUFA Scores negatively correlate with IRG expression in the lung. . . . 80
3.4.3 Higher RBC ω-3 HUFA Scores correspond to reduced pro-inflammatory cytokines and leukocyte infiltration in BALF. . . . 81
3.4.4 Increased RBC ω-3 HUFA Scores are associated with reduced ectopic lymphoid structure (ELS) neogenesis and autoantibody production. . . . 83
3.4.5 Higher RBC ω-3 HUFA Scores were associated with delayed disease progression. . . . 88
3.4.6 Higher O3I were associated with reduced autoimmune pathogenesis. . . . 88
3.5 DISCUSSION . . . 92
3.6 ACKNOWLEDGMENTS . . . 100

CHAPTER 4 DOCOSAHEXAENOIC ACID SUPPRESSES SILICA-INDUCED INFLAMMASOME ACTIVATION AND IL-1 CYTOKINE RELEASE BY INTERFERING WITH PRIMING SIGNAL . . . 101
4.1 ABSTRACT . . . 102
4.2 INTRODUCTION . . . 103
4.3 MATERIALS AND METHODS . . . 104
4.3.1 RAW-WT and RAW-ASC macrophage models. . . . 104
4.3.2 Preparation of bone marrow-derived macrophages (BMDMs). . . . 105
4.3.3 $cSiO_2$ and other crystals. . . . 106
4.3.4 DHA preparation. . . . 106
4.3.5 Experimental design. . . . 107
4.3.6 IL-1 cytokine analyses. . . . 108
4.3.7 Caspase-1 activity. . . . 109
4.3.8 Cell death. . . . 109
4.3.9 PPARγ transcription factor assay. . . . 110

4.3.10 qRT-PCR. . . . 110
4.3.11 SDS-PAGE and western blot. . . . 110
4.3.12 Fatty acid analysis. . . . 112
4.3.13 Statistical analyses. . . . 113
4.4 RESULTS . . . 113
4.4.1 Nigericin- and $cSiO_2$-induced IL-1β release is LPS- and ASC-dependent. . . 113
4.4.2 $cSiO_2$-Induced caspase-1 activation is LPS- and ASC-dependent. . . . 114
4.4.3 Nigericin- and $cSiO_2$-induced IL-1α release differ with regard to LPS- and ASC-dependence. . . . 115
4.4.4 Nigericin- but not $cSiO_2$-induced cell death is inflammasome-dependent. . 118
4.4.5 DHA is efficiently incorporated into RAW-ASC cell phospholipids. . . . 119
4.4.6 DHA inhibits nigericin-induced IL-1 cytokine release and cell death. . . . 120
4.4.7 DHA suppresses $cSiO_2$-induced IL-1 cytokine release and caspase-1 activation but not cell death. . . . 121
4.4.8 DHA suppresses IL-1 cytokine release triggered by alum and MSU crystals. 123
4.4.9 DHA interferes with LPS priming by activating PPARγ. . . . 124
4.5 DISCUSSION . . . 126
4.6 ACKNOWLEDGMENTS . . . 131

CHAPTER 5 SINGLE CELL TRANSCRIPTOMICS TO INVESTIGATE DOCOSAHEXAENOIC ACID SUPPRESSION OF LPS-INDUCED INFLAMMATORY GENE EXPRESSION . . . 132
5.1 ABSTRACT . . . 133
5.2 INTRODUCTION . . . 133
5.3 MATERIALS AND METHODS . . . 135
5.3.1 Animals and euthanasia. . . . 135
5.3.2 MPI cell isolation and culture. . . . 135
5.3.3 DHA supplementation and membrane incorporation. . . . 136
5.3.4 LPS exposure. . . . 137
5.3.5 Western blotting. . . . 137
5.3.6 qPCR. . . . 138
5.3.7 Single cell isolation, library preparation, and sequencing. . . . 138
5.3.8 Filtering and generation of Seurat object. . . . 139
5.3.9 SCENIC analysis. . . . 140
5.3.10 Heatmaps. . . . 140
5.3.11 Data visualization and statistics. . . . 140
5.4 RESULTS . . . 141
5.4.1 Clustering is driven by LPS treatment and cell cycle phase. . . . 141
5.4.2 DHA influences expression of genes involved in proliferation, the antioxidant response, lipid metabolism, and immune suppression at 0 h. . . . 141
5.4.3 LPS-induced inflammatory gene expression is preceded by cellular pathways promoting transcription. . . . 144
5.4.4 DHA suppresses genes involved in cholesterol synthesis at 1 h post-LPS exposure and inflammatory signaling pathways at 4 h post-LPS exposure. . 148

5.4.5 Distinct subsets of LPS-treated cells are driven by NF-κB signaling and IFN signaling. . . . 151
5.5 DISCUSSION . . . 153
5.6 ACKNOWLEDGMENTS . . . 157

CHAPTER 6 OPTIMIZATION OF A SELF-REPLICATION IN VITRO MODEL FOR ALVEOLAR MACROPHAGES TO STUDY CRYSTALLINE SILICA TOXICITY . . . 158
6.1 ABSTRACT . . . 159
6.2 INTRODUCTION . . . 160
6.3 MATERIALS AND METHODS . . . 162
6.3.1 Animals. . . . 162
6.3.2 MPI cell isolation and culture. . . . 162
6.3.3 AM isolation and culture. . . . 163
6.3.4 BMDM isolation and culture. . . . 163
6.3.5 Flow cytometry. . . . 164
6.3.6 qPCR. . . . 164
6.3.7 Scanning electron microscropy. . . . 165
6.3.8 $cSiO_2$ phagocytosis assay. . . . 165
6.3.9 ELISAs. . . . 166
6.3.10 Statistical analysis and data visualization. . . . 166
6.4 RESULTS . . . 167
6.4.1 MPI and AMs similarly express lineage-specific markers that decline over time. . . . 167
6.4.2 Addition of TGFβ prolongs AM-like state of MPI cells. . . . 169
6.4.3 TMPI cells and AMs phagocytose $cSiO_2$ particles and undergo cell death at similar rates. . . . 170
6.4.4 Engulfment of $cSiO_2$ particles leads to loss of outer membrane ruffling, apoptotic blebbing, and membrane rupture. . . . 171
6.4.5 Loss of lysosome integrity precedes $cSiO_2$-induced cell death in TMPI cells. 171
6.4.6 AM and TMPI cells exhibit high expression and release of the alarmin IL-1α. . . . 174
6.4.7 DHA decreases $cSiO_2$-induced cell death and cytokine release in TMPI cells. . . . 175
6.5 DISCUSSION . . . 177
6.6 ACKNOWLEDGMENTS . . . 182

CHAPTER 7 CONCLUSIONS AND FUTURE DIRECTIONS . . . 183
7.1 CONCLUSION . . . 184
7.2 FUTURE RESEARCH . . . 185
7.2.1 Profile the presence and phenotype of macrophages in the lung following acute $cSiO_2$ exposure *in vivo*. . . . 185
7.2.2 Relate metabolite profile in the BALF to inflammatory endpoints triggered by $cSiO_2$. . . . 186

7.2.3 Use genetically modified TMPI cells to elucidate pathways of $cSiO_2$ uptake and toxicity and/or protection by DHA. . . . 187
7.2.4 Instill edited TMPI cells into the murine lung to mechanisms of interest in vivo. . . . 188
7.2.5 Investigate the influence of other HUFAs, including ω-6 HUFA arachidonic acid and ω-3 HUFA eicosapentaenoic acid on the phenotype and function of MPI cells. . . . 189

APPENDICES . . . 191
APPENDIX A CHAPTER 2 SUPPORTING FIGURES AND TABLES . . . 192
APPENDIX B CHAPTER 3 SUPPORTING FIGURES AND TABLES . . . 199
APPENDIX C CHAPTER 4 SUPPORTING FIGURES . . . 202
APPENDIX D CHAPTER 5 SUPPORTING FIGURES AND TABLES . . . 205
APPENDIX E CHAPTER 6 SUPPORTING FIGURES . . . 209
APPENDIX F REAGENTS AND MATERIALS . . . 214
APPENDIX G FULL LIST OF PUBLISHED MANUSCRIPTS . . . 220

BIBLIOGRAPHY . . . 222

LIST OF TABLES

Table 1.1: $cSiO_2$ enhances and DHA suppresses many inflammatory end points targeted by drugs either approved or in clinical trials for treatment of autoimmune disease 13

Table 1.2: Cellular events induced by $cSiO_2$ and suppressed by DHA 40

Table 2.1: Experimental diet formulations 46

Table 2.2: Fatty acid content of experimental diets as determined by GLC. 48

Table 2.3: Red blood cell fatty acid content as determined by GLC. 55

Table 3.1: Composition of experimental diets. 76

Table 3.2: Fatty acid profiles of experimental diets as determined by gas-liquid chromatography. 78

Table 3.3: Summary of ω-3 HUFA intervention trials in lupus patients. 97

Table 4.1: DHA supplementation modulates phospholipid profile of RAW-ASC cells. . . . 119

Table A.1: Lung fatty acid content as determined by GLC. 194

Table A.2: Liver fatty acid content as determined by GLC. 195

Table A.3: Kidney fatty acid content as determined by GLC. 196

Table A.4: Spleen fatty acid content as determined by GLC. 197

Table A.5: Histopathology severity scores, lungs 198

Table A.6: Urinary protein at 18, 20, and 22 wk of age. 198

Table B.1: Fatty acid content of RBCs for Studies 1,2,and 3. 201

Table D.1: Fatty acid profile of Veh- and DHA-supplemented MPI cells 208

LIST OF FIGURES

Figure 1.1: Putative role for type 1 IFN in $cSiO_2$-induced systemic lupus erythematosus . . 11

Figure 1.2: $cSiO_2$-induced autoimmune pathogenesis is suppressed by ω-3 HUFAs 15

Figure 1.3: Origin and contribution of alveolar macrophages during homeostasis, injury, and resolution in the mouse 18

Figure 1.4: Particle deposition mechanisms in the respiratory tract 21

Figure 1.5: $cSiO_2$ triggers multiple interconnected events involved in NLRP3 inflammasome activation. 27

Figure 1.6: Putative anti-inflammatory mechanisms of ω-3 HUFAs 33

Figure 2.1: Experimental diets have unique fatty acid compositions 47

Figure 2.2: Experimental design 49

Figure 2.3: $cSiO_2$ instillation and experimental diets did not affect body weight changes over time. 49

Figure 2.4: RBC fatty acid composition is influenced by modulation of dietary lipids. . . . 56

Figure 2.5: Individual tissues show distinct patterns of fatty acid incorporation. 57

Figure 2.6: DHA supplementation attenuates $cSiO_2$-induced interferon-regulated gene expression in the lungs. 59

Figure 2.7: DHA consumption suppresses $cSiO_2$-triggered cytokine release. 60

Figure 2.8: DHA supplementation with SFA and ω-6 PUFA reduction suppress $cSiO_2$-induced immune cell accumulation in BALF. 61

Figure 2.9: DHA supplementation impedes perivascular and peribronchiolar lymphocyte infiltration, and the neogenesis of ELS. 63

Figure 2.10: DHA intake suppresses $cSiO_2$-induced lupus-associated autoantibodies in the BALF and the plasma. 64

Figure 2.11: DHA intake inhibits $cSiO_2$-induced glomerulonephritis. 65

Figure 2.12: DHA supplementation against the complex background of the Western diet suppresses $cSiO_2$-triggered flaring and progression of lupus in NZBWF1 mice. 67

Figure 3.1: RBC ω-3 HUFA score increases with DHA intake in NZBWF1 mice and can be predicted based on diet composition in $cSiO_2$-treated NZBWF1 mice. 81

Figure 3.2: ω-3 HUFA scores are consistent across multiple tissues in $cSiO_2$-treated NZBWF1 mice. 82

Figure 3.3: RBC ω-3 HUFA score negatively correlates with IFN-regulated gene expression in $cSiO_2$-triggered NZBWF1 mice. 83

Figure 3.4: Increasing RBC ω-3 HUFA score corresponds to reduced inflammatory cytokines in the lung alveolar fluid of $cSiO_2$-triggered NZBWF1 mice. 84

Figure 3.5: Elevated RBC ω-3 HUFA scores are associated with reduced mononuclear cell infiltration into lung alveolar fluid of $cSiO_2$-triggered NZBWF1 mice. . . . 85

Figure 3.6: High RBC ω-3 HUFA scores correspond with suppression of ELS neogenesis, anti-dsDNA response, and disease progression in $cSiO_2$-triggered NZBWF1 mice. 86

Figure 3.7: Increased RBC ω-3 HUFA scores correlate with reductions in a broad array of autoantibodies relative to specificity and isotype in the plasma and BALF of $cSiO_2$-treated NZBWF1 mice. 87

Figure 3.8: The Omega-3 Index (O3I) negatively correlates with IRG expression in $cSiO_2$-triggered NZBWF1 mice. 89

Figure 3.9: Heightened O3Is correspond with suppression of leukocyte infiltration, ELS development, and disease progression in $cSiO_2$-triggered NZBWF1 mice. . . . 90

Figure 3.10: RBC ω-3 HUFA score and O3I both negatively correlate with inflammatory/autoimmune indicators and pulmonary immune cell infiltration. 91

Figure 4.1: Experimental design. 108

Figure 4.2: Nigericin- and $cSiO_2$-induced IL-1β release are LPS- and ASC-dependent in RAW macrophages. 114

Figure 4.3: $cSiO_2$-induced caspase-1 activation in RAW macrophages is LPS- and ASC-dependent. 116

Figure 4.4: Nigericin- and $cSiO_2$-induced IL-1α release is LPS- and ASC-dependent in RAW macrophages. 117

Figure 4.5: Nigericin-induced cell death is LPS- and ASC-dependent while $cSiO_2$-induced cell death is LPS- and ASC-independent in RAW macrophages. 118

Figure 4.6: DHA is incorporated into RAW-ASC macrophage phospholipids at the expense of oleic acid (OA). 120

Figure 4.7: DHA supplementation suppresses nigericin-induced IL-1β and IL-1α release and cell death in RAW-ASC macrophages. 121

Figure 4.8: DHA inhibits $cSiO_2$-induced IL-1β and IL-1α release but not cell death in RAW-ASC macrophages. 122

Figure 4.9: DHA supplementation suppresses $cSiO_2$-induced caspase-1 activation in RAW-ASC macrophages. 123

Figure 4.10: Alum- and MSU crystal-induced IL-1 cytokine release is suppressed by DHA. . 124

Figure 4.11: DHA supplementation downregulates LPS-induced inflammasome gene expression and intracellular IL-1 cytokines in RAW-ASC cells. 125

Figure 4.12: PPARγ is involved in DHA-mediated suppression of LPS-induced *Il1a* and *Il1b* 126

Figure 4.13: Putative model for the protective effects of DHA against nigericin- and $cSiO_2$-induced inflammasome activation, IL-1 cytokine release, and death in macrophages 131

Figure 5.1: Timeline for treatment and collection of samples for single cell RNA sequencing 139

Figure 5.2: Uniform manifold approximation and projection (UMAP) reveals factors that drive clustering 142

Figure 5.3: DHA influences expression of genes involved in lipid metabolism, antioxidant response, and immune regulation 143

Figure 5.4: Gene expression changes induced by LPS at 1 and 4 h 146

Figure 5.5: Heatmap of differentially expressed genes at 1 and 4h post-LPS treatment . . . 147

Figure 5.6: DHA suppresses genes associated with cholesterol synthesis and inflammatory signaling pathways 149

Figure 5.7: DHA suppresses inflammatory signaling pathways at 4h post-LPS treatment . . 150

Figure 5.8: DHA suppresses IFN-regulated genes 151

Figure 5.9: Cells with high expression of IFN-driven genes are distinct from cells with high expression of NF-κB-driven genes. 153

Figure 6.1: MPI cells lose their AM-like phenotype over time 167

Figure 6.2: MPI cells lose expression of AM-specific surface markers and gene expression over time 168

Figure 6.3: Addition of TGFβ to the cell culture media extends the AM-like phenotype of MPI cells 170

Figure 6.4: Kinetics of $cSiO_2$ uptake and $cSiO_2$-induced cell death is similar among AMs, early MPI cells, and early TMPI cells 172

Figure 6.5: Scanning electron microscopy or cells treated with $cSiO_2$ for 1 and 16 h. 173

Figure 6.6: Lysosomal membrane integrity decreases over time in $cSiO_2$ exposed TMPIs . 174

Figure 6.7: $cSiO_2$ elicits IL-1 cytokine release from AMs, early MPI, and TMPI cells but not from BMDM or late MPI cells 175

Figure 6.8: DHA suppresses cell death, lysosomal membrane permeability, and IL-1 cytokine release following $cSiO_2$ exposure 176

Figure 7.1: Short term exposure to DHA and ARA suppresses cell death, IL-1β, and IL-1 gene expression 190

Figure A.1: Correlation between RBC and tissues for SFA, MUFA, ω-6 PUFA, and ω-3 PUFA 193

Figure B.1: O3I increases with DHA intake in NZBWF1 mice. 199

Figure B.2: RBC O3Is do not closely reflect tissue EPA+DHA levels. 200

Figure C.1: Visualization of ASC-CFP specks in RAW-ASC cells stimulated with LPS, nigericin and/or $cSiO_2$. 203

Figure C.2: Assessment of NF-κB activation. 204

Figure D.1: DHA supplementation results in increased DHA levels in the phospholipid membrane at the expense of oleic acid and arachidonic acid 205

Figure D.2: Quality control metrics before and after filtering 206

Figure D.3: DHA inhibits NF-κB signaling pathway 207

Figure D.4: Heatmap of regulon scores reveals cluster of cells with high expression of *Stat1, Stat2*, and *Irf7* regulons 207

Figure E.1: AMs cultured over time lose AM-specific gene and surface marker expression . 209

Figure E.2: FBS supplemented media slows cell death in response to $cSiO_2$ 210

Figure E.3: Short term incubation with TGFβ increases expression of AM-specific genes. . 211

Figure E.4: Cells with high rates of $cSiO_2$ engulfment show loss of lysosomal membrane integrity following $cSiO_2$ exposure 212

Figure E.5: MPI cells and BMDM have different patterns of cytokine release following LPS stimulation 213

Figure E.6: DHA supplementation enhances DHA in the TMPI cell membrane at the expense of oleic acid and arachidonic acid 213

KEY TO ABBREVIATIONS

AAb	Autoantibody
AAg	Autoantigen
AD	Autoimmune disease
AEC	Alveolar epithelial cell
AGES	Age, Gene/Environment Susceptibility Study
AM	Alveolar macrophages
ANA	Anti-nuclear antibodies
ANCA	Anti-neutrophil cytoplasmic antibodies
ANOVA	Analysis of variance
ARA	Arachidonic acid
ASC	Apoptosis-associated speck-like protein containing a CARD
AUC	Area under the recovery curve
BAFF	B-cell activating factor
BALF	Bronchoalveolar lavage fluid
BALT	Bronchus-associated lymphoid tissue
BMDM	Bone marrow-derived macrophage
BSA	Bovine serum albumin
CFP	Cyan fluorescent protein
CON	Control
$cSiO_2$	Crystalline silica
CVD	Cardiovascular disease
d	day
DAMP	Danger-associated molecular pattern
DC	Dendritic cell
DEG	Differentially expressed gene

DHA	Docosahexaenoic acid
DPA	Docosapentaenoic acid
DPPC	Dipalmitoylphosphatidylcholine
dsDNA	Double-stranded DNA
ELS	Ectopic lymphoid structure
EPA	Eicosapentaenoic acid
FAME	Fatty acid methyl ester
FBS	Fetal bovine serum
FMLP	N-Formylmethionine-leucyl-phenylalanine
g	gram
GLC	Gas-liquid chromatography
GO	Gene ontology
GPCR	G-protein-coupled receptor
GSDMD	Gasdermin D
H&E	Hematoxylin and Eosin
h	hour
HUFAs	Highly unsaturated fatty acid
IFN	Interferon
iNOS	Inducible nitric oxide synthase
IPE	Isopent ethyl
IRG	Interferon-regulated gene
I/R	Ischemia/reperfusion
LA	Linoleic acid
LAP	Latency-associated peptide
LBP	LPS binding protein
LDH	Lactate dehydrogenase
LDL	Low-density lipoprotein

LMP	Lysosomal membrane permeabilization
LPS	Lipopolysaccharide
LTBPs	Latent TGFβ binding proteins
LXR	Liver X receptor
mAb	Monoclonal antibody
MESA	Multi-ethnic Study of Atherosclerosis
Miles	Michigan Lupus Epidemiology and Surveillance
min	minute
MK	Maximum kill
MSU	Monosodium urate
MTWD	Modified total western diet
NEFA	Non-esterified fatty acid
NET	Neutrophil extracellular trap
NHANES	National Health and Nutrition Examination Survey
NSAID	Non-steroidal anti-inflammatory drug
O3I	Omega-3 Index
OA	Oleic acid
P/S	Penicillin-streptomycin
PASH	Periodic acid-Schiff hematoxylin
PBMC	Peripheral blood mononuclear cell
PBS	Phosphate-buffered saline
pDC	Plasmacytoid dendritic cell
PLA2	Phospholipase A2
PMN	Polymorphonuclear leukocyte
PS	Phosphatidylserine
PUFAs	Polyunsaturated fatty acid
RBC	Red blood cell

RCN	Relative copy number
RCT	Randomized controlled trial
Rv	Resolvin
ROS	Reactive oxygen species
ROUT	Robust regression and outlier removal
RPMI	Roswell Park Memorial Institute
RXR	Retinoid X Receptor
s	second
scRNAseq	Single cell RNA sequencing
SD	Standard deviation
SEM	Standard error of the mean, Scanning electron microscopy
SFA	Saturated fatty acid
SLICC	Systemic Lupus International Collaborating Clinics
SPM	Specialized pro-resolving mediators
TAG	Tri-acyl glycerol
TiO_2	Titanium dioxide
TLC	Thin layer chromatography
TLO	Tertiary lymphoid organ
TLR	Toll-like receptor
TULIP	Treatment of Uncontrolled Lupus via the Interferon Pathway
VEH	Vehicle
UMAP	Uniform manifold approximation and projection
wk	week
WT	Wild type

CHAPTER 1

INTRODUCTION AND LITERATURE REVIEW

1.1 INTRODUCTION

The development of autoimmune disease in genetically susceptible individuals can be influenced by the exposome, which is defined as the total measure of environmental exposures over one's lifetime [1]. This includes elements of our diet, such as the dietary omega-3 (ω-3) highly unsaturated fatty acid (HUFA) docosahexaenoic acid (DHA) and inhaled toxicants, such as the respirable particle crystalline silica ($cSiO_2$). This thesis explores how DHA and $cSiO_2$ influence autoimmune disease development in lupus prone mice and toxicity in alveolar macrophages (AMs).

Human epidemiological studies link $cSiO_2$ exposure to the development of lupus and other autoimmune diseases [2]. Pre-clinical studies employing lupus-prone mouse models found that the rampant pulmonary inflammation triggered by $cSiO_2$ culminates in loss of immune tolerance and the development of systemic autoimmunity [3]. Intriguingly, dietary supplementation with ω-3 HUFAs, an intervention known to improve disease status in patients with lupus and other autoimmune diseases, blocks $cSiO_2$-triggered autoimmunity these animals [4].

The current literature suggest that modulation of dietary lipids could be used to attenuate the inflammatory response. There is currently no cure for lupus, and treatment options focus on reducing the symptoms and preventing immune-mediated tissue damage. Many of the drugs employed to treat systemic inflammation in patients with lupus, such as methotrexate, corticosteroids, and cyclophosphamide, have undesirable side effects, including nausea, headache, and fatigue [5, 6]. While dietary modulation may not completely prevent disease progression, it could allow patients to see improvements at lower doses of drugs, thus minimizing the collateral damage of these treatments. This approach is consistent with the National Institutes of Health's 10-year strategic plan to focuses on precision nutrition, which was announced in 2020, and includes the goal of reducing the burden of disease in clinical settings (https://www.nih.gov/news-events/news-releases/nih-releases-strategic-plan-accelerate-nutrition-research-over-next-10-years).

The work presented in this dissertation builds upon previous studies in Dr. Pestka's lab by investigating the efficacy of DHA on the background of a Western-style diet and linking the protective effects of DHA supplementation to augmented ω-3 levels in the red blood cells and tissues.

This thesis also employs a novel, self-replicating AM model to investigate the effects of DHA and $cSiO_2$ *in vitro*. The AM is the first line of defense against inhaled particles, thus understanding how DHA influences the AM response to $cSiO_2$ is essential in elucidating how DHA protects against $cSiO_2$-triggered autoimmunity *in vivo*.

1.1.1 CHAPTER SUMMARIES

Chapter 1, the current chapter, provides an extensive literature review highlighting 1) clinical and preclinical studies that investigate how the exposome contributes to autoimmune disease, 2) the role of AMs in potentiating $cSiO_2$-triggered pathologies, and 3) the immunomodulatory effects of ω-3 HUFAs, and how they may attenuate $cSiO_2$-induced damage in the lung. The first section of the literature review (Lupus, silica, and dietary omega-3 fatty acids) was published in Toxicologic Pathology in 2019, and can be accessed online (doi: 10.1177/0192623319878398).

Previous *in vivo* studies in our lab provided the dietary ω-3 HUFA DHA on the background of the AIN-93G diet, which is optimized for rodent health. In **Chapter 2**, we investigated the effect of DHA supplementation on the background of a modified total Western diet, which is formulated to mimic micro- and macro-nutrient levels observed in a typical American diet. Furthermore, levels of saturated and ω-6 fatty acids were reduced to explore the potential for these fatty acids to exacerbate the inflammatory response. Animals were instilled with 1 mg of $cSiO_2$ once per week for four weeks, to mimic chronic particle exposure. Here, we found that DHA supplementation reduced many $cSiO_2$-induced inflammatory and autoimmune endpoints. Reduction of ω-6 and saturated fats modestly suppressed some of these endpoints, but was far less protective than DHA alone. This chapter was published as a co-first authored manuscript with my colleague Kristen Gilley in PLoS One in 2020, and can be accessed online (doi: 10.1371/journal.pone.0233183).

Chapter 3 is a meta-analysis of data from three previously published *in vivo* studies from our lab, including the study described in the second chapter [4, 7, 8]. Here, red blood cell ω-3 levels were negatively correlated with expression of interferon-regulated genes, proinflammatory cytokine production, leukocyte infiltration, ectopic lymphoid structure development, pulmonary and

systemic autoantibody production, and severity of kidney lesions. This chapter was published in Frontiers in Immunology in 2020, and can be accessed online (doi: 10.3389/fimmu.2020.01796).

Chapter 4 investigates the cellular mechanisms of $cSiO_2$-induced toxicity and protection by DHA in ASC-transfected RAW 264.7 cells. Wild-type (WT) RAW 264.7 cells do not express the ASC protein, which is an adapter protein required for inflammasome activation. ASC-transfected cells capable of inflammasome activation released significantly more IL-1β and IL-1α than WT cells, highlighting the role of the inflammasome in mediating $cSiO_2$-triggered damage. Furthermore, supplementing ASC-transfected RAW 264.7 cells with DHA significantly reduced inflammasome activation as observed by IL-1 cytokine gene expression and release and caspase-1 activation. Activation of PPARγ was identified as a putative mechanism for DHA's protective effects. The PPARγ agonist Rosiglitazone suppressed lipopolysaccharide (LPS)-induced *Il1a* and *Il1b* in a manner similar to DHA. A PPARγ antagonist reversed this effect. This chapter was published in Frontiers in Immunology in 2019, and can be accessed online (doi: 10.3389/fimmu.2019.02130).

In **Chapter 5,** MPI cells, a non-transformed, self-replicating macrophage model were employed to further elucidate how DHA supplementation influences macrophage gene expression, with and without treatment with LPS for 1 and 4 h. Single cell RNA sequencing was used to provide insight into the heterogeneity of the MPI cell population and the differences between cells within the same treatment group in their transcriptional response to LPS or DHA. Supplementation for 24 h induced genes associated with a pro-resolving phenotype. DHA significantly decreased genes associated with cholesterol synthesis, many of which were among the first genes upregulated by LPS (1 h post-LPS). The ability for DHA to reverse this metabolic pathway may represent an unexplored mechanism for opposing the inflammatory response to LPS. A 4 h treatment with LPS resulted in a small population of cells primarily expressing interferon-driven genes, and these cells were separate from a larger population with high expression of NF-κB driven genes. DHA suppressed both sets of LPS-induced genes. This chapter is in preparation to be submitted for publication.

Chapter 6 explores the cellular response to $cSiO_2$ in an optimized MPI cell model that allows them to retain their AM-like morphology for an extended period of time in culture. First, it

was identified that though MPI cells are very similar to AMs during a short period following their isolation, they begin to lose this phenotype and become more like a recruited, monocyte-derived macrophage. Addition of the cytokine TGFβ in the culture media upregulated AM-specific genes and surface markers, including Siglec F, MARCO, and CD11c. It was also determined that these cells responded similarly to AMs in terms of the rate of $cSiO_2$ engulfment, loss of lysosomal membrane integrity, cell death, and IL-1 cytokine release. Lastly, DHA suppressed $cSiO_2$-induced cell death, lysosomal membrane permeability, and IL-1 cytokine release without influencing the rate or extent of phagocytosis. This chapter is in preparation to be submitted for publication.

Finally, **Chapter 7** discusses conclusions that can be drawn from this body of work, and includes proposals for future experiments to build upon these findings. These include 1) employing flow cytometry and RNA sequencing to thoroughly profile monocyte and macropahge subpopulations present following an acute exposure to $cSiO_2$, 2) investigating the protective effects of DHA-derived metabolites following exposure to $cSiO_2$, 3) exploring the role of other classes of fatty acids *in vitro*, and 4) using MPI cells derived from knock-out mice or genetically engineered *in vitro* to perform mechanistic studies to better elucidate the impact of $cSiO_2$ and DHA on this cell line.

Supplementary information from Chapters 2-6 are presented as **Appendices A-E**, respectively. **Appendix F** contains a list of key reagents along with their manufacturer and product number and **Appendix G** contains a list of publications during the duration of this degree.

1.2 LITERATURE REVIEW

1.2.1 Lupus, silica, and dietary Omega-3 fatty acids

1.2.1.1 Lupus results from gene-environment interactions.

Systemic lupus erythematosus (lupus) is a prototypical autoimmune disease characterized by inflammation and a loss of self-tolerance. There are an estimated 250,000 patients in the US with lupus [9], and this is likely an underestimate, as lupus is frequently misdiagnosed [10]. This dev-

astating disease disproportionately impacts women of child-bearing age and of non-Caucasian descent. Lupus begins with benign but detectable elevations in plasma autoantibodies and inflammatory biomarkers, but eventually develops into full-scale systemic autoimmune disease. Rampant autoantibodies form immune complexes with their cognate autoantigens and can deposit in the kidney, triggering glomerulonephritis and ultimately renal failure if left untreated. While the genome is the primary predisposing factor for autoimmunity, environmental factors such as toxicants [11] and diet [12] modulate underlying hereditary susceptibilities, playing major roles in the development and/or exacerbation of symptoms. To illustrate the interactive actions of such factors, we review here investigations in a widely used preclinical mouse model of lupus demonstrating that 1) early autoimmune disease onset can be triggered by the respiratory toxicant $cSiO_2$ and 2) this triggering can be ameliorated by consumption of the dietary ω-3 fatty acid DHA.

1.2.1.2 $cSiO_2$ is an autoimmune trigger.

$cSiO_2$ is the most abundant mineral on earth and an estimated 2.3 million Americans are exposed to $cSiO_2$ occupationally [13]. Exposure to $cSiO_2$ is critical to the development of the human disease silicosis, which presents as chronic inflammation with severe fibrosis in the lungs and culminates in the loss of lung function [14]. High levels of $cSiO_2$ and other silicates are present in the lungs of miners exposed to high levels of coal dust containing $cSiO_2$, indicating that the dust cannot be cleared from the lungs following chronic exposure [15]. Clearance of inhaled $cSiO_2$ from the lung has also been shown to be extremely slow in rodents [16], thus repeated inhalation of $cSiO_2$ activates a persistent inflammatory response in the lungs [17]. Continued over-activation of immune cells coupled with the release of cellular material following $cSiO_2$-induced cell death results in production of antibodies against host antigens, contributing to the development of systemic autoimmunity [18, 3].

The etiological linkage between $cSiO_2$ exposure and the development of autoimmunity is supported by human epidemiological studies, as reviewed by Parks and Cooper [19]. The review's authors concluded that existing data met the Sir Bradford Hill criteria for establishing causality

[20]; specifically, there was strength and consistency in the association between $cSiO_2$ exposure and lupus. This was observed across different study designs and populations, there was an obvious exposure-response gradient, and epidemiological findings are consistent with mechanistic studies in animals. More recently, a National Institute for Environmental Health Sciences expert panel evaluated the role of environmental factors in autoimmune disease and concluded that $cSiO_2$ contributes to multiple autoimmune diseases, including lupus, rheumatoid arthritis, systemic sclerosis, and anti-neutrophil cytoplasmic autoantibody (ANCA) vasculitis [11].

1.2.1.3 ω-3 HUFAs counter inflammation and autoimmunity.

Consumption of ω-3 HUFAs has been shown to ameliorate chronic inflammatory and autoimmune diseases [21, 22, 23]. A recent meta-analysis showed that higher blood ω-3 HUFA levels are associated with a decrease in all-cause mortality [24]. Here, we use the term HUFA to fatty acids chain lengths greater than or equal to 20 carbons and containing 2 or more double bonds, while the term polyunsaturated fatty acid (PUFA) encompasses both HUFAs and their 18-carbon precursors. While HUFAs may be elongated and desaturated from their precursor PUFAs, this process in mammals is highly inefficient [25], making the HUFA levels in the body highly dependent on what is obtained in the diet. The major ω-3 HUFAs eicosapentaenoic acid (EPA), docosapentaenoic acid (DPA), and DHA are abundant in oily fish. Since the Western diet is lacking in fish and, in general, marine fatty acids [26, 27], the most effective way to increase ω-3 HUFAs is through dietary supplementation [28, 29]. Indeed, after multivitamins, fish oil is the second most widely used supplement in the US [30]. Crude fish oil or semi-purified mixtures of ω-3 HUFAs EPA, DPA, and DHA have been utilized in clinical trials for cardiovascular disease, inflammatory diseases, and autoimmune diseases [31], including lupus (reviewed elsewhere [32]). While there have been many supportive findings, there are also inconclusive results, leaving many open questions about the dose required to achieve beneficial effects as well as the mechanisms behind ω-3 HUFAs' protective actions.

1.2.1.4 Preclinical evidence that dietary DHA consumption prevents $cSiO_2$-triggered lupus.

To investigate contributions of the exposome to onset and progression of lupus, we have employed the NZBWF1 mouse, a widely used animal model that mimics human lupus [33, 34]. As in humans, lupus development in NZBWF1 mice primarily occurs in females. These mice develop robust autoantibody responses and lupus nephritis around 32 wk of age and typically will die within a year. Intriguingly, when these mice are intranasally instilled with $cSiO_2$, they develop lupus about 3 months earlier than vehicle-treated animals [3]. Our lab has focused on understanding the early inflammatory events that lead to $cSiO_2$-triggered onset of lupus in this model, as well as the potential to block $cSiO_2$-triggered inflammation using dietary intervention with ω-3 HUFAs [3, 35, 7]. In a recent study [4], 6-wk old female NZBWF1 mice were introduced to diets enriched with 0, 0.4 or 1% DHA, which are calorically equivalent to human doses of 0, 2 or 5 g/d, respectively. These mice were intranasally instilled with 1 mg $cSiO_2$ at 8, 9, 10, and 11 wk of age. Cohorts were then sacrificed at 1, 5, 9, and 13 wk after the final instillation and bronchoalveolar lavage fluid (BALF), lungs, kidneys, and blood were collected for analysis. Mice exposed to $cSiO_2$ developed glomerulonephritis at 13 wk post-instillation, but this response was blocked by DHA feeding.

DHA's protective effects against $cSiO_2$-induced kidney inflammation were specifically linked to reduced myeloid and lymphoid cell recruitment and proliferation in the lung [4]. Cell counts from the BALF of $cSiO_2$–treated NZBWF1 mice revealed a robust increase in immune cells at 9 and 13 wk post-instillation, with the main cell types being macrophages and neutrophils; at 13 wk, lymphocytes were also present in the BALF. $cSiO_2$–triggered elevations of these cells were significantly suppressed by feeding DHA, both at the low and high doses. Relatedly, following hematoxylin and eosin (H&E) staining, we observed perivascular and peribronchiolar lymphoid cell infiltration in $cSiO_2$-instilled mice, suggesting the development of ectopic lymphoid structures (ELS) [3, 4, 36]. This was confirmed by immunohistochemical staining for T cells, B cells, and follicular dendritic cells (DCs). The infiltrating lymphoid cells clearly adopted a germinal center-like formation, with lymphoid cells surrounding aggregated follicular DCs and yielding IgG-producing plasma cells [37]. Intriguingly, DHA supplementation impeded formation of ELS in the lung at all

time points.

In lupus and other autoimmune diseases, ELS can serve as a platform for the development of autoantibodies [36, 38]. Using an autoantigen microarray, we identified numerous autoantibodies in the BALF and plasma that were upregulated in response to $cSiO_2$, beginning at 5 wk post-instillation and becoming highly robust at 9 and 13 wk [39]. These included IgG, IgM, and IgA isotypes. In mice that consumed diets supplemented with DHA, $cSiO_2$-induced autoantibody production was suppressed. Importantly, known human lupus markers, namely anti-DNA, anti-RNP, anti-SM, anti-histone, anti-double-stranded DNA (dsDNA), anti-Ro/SSA, anti-La/SSB, and anti-complement autoantibodies [40], were suppressed by feeding DHA.

1.2.1.5 Type 1 interferon response is induced by $cSiO_2$ but suppressed by DHA supplementation.

Recently, we analyzed gene expression in the lungs and the kidneys using a multiplex platform targeting 770 immune-related genes to assess the effects $cSiO_2$ exposure and DHA consumption on mRNA signatures over time in female NZBWF1 mice [41]. These analyses were performed on samples from the experiment detailed above [4], as well as in animals sacrificed either one day following a single $cSiO_2$ exposure or one day after the fourth exposure. Just one day after the last of four weekly $cSiO_2$ doses, genes related to inflammation as well as innate and adaptive immunity were dramatically increased in lungs of animals fed the control diet but were significantly reduced in mice fed DHA diets. Importantly, mRNA signatures in lungs of $cSiO_2$-treated mice fed the control diet over 13 wk reflected progressive amplification of type 1 interferon (IFN)- and chemokine-related gene pathways, in addition to other immune-related pathways [41]. At all timepoints, these lung signatures were suppressed in mice fed DHA.

IFN signaling is strongly implicated in the development of autoimmune diseases, with type 1 IFN – and more specifically IFN-α – being associated with the development of lupus [42]. Early studies using the lupus-prone NZBWF1 mouse model showed that induction of type I IFN using polyinosinic:polycytidylic acid accelerated the disease onset [43]. In 1979, it was reported that

patients with autoimmune disease had increased levels of circulating IFN, and in lupus patients both type I and type II IFN were observed [44]. In the late 1990s and early 2000s, there were multiple reports that patients administered IFN-α to treat certain malignancies and hepatitis C developed lupus-like symptoms, further strengthening the connection between type I IFN and the development of lupus [45, 46, 47]. In 2003, Baechler et al. showed that expression of IFN target genes was closely correlated with disease activity and severity [48]. Of high relevance to our model, it was recently reported that $cSiO_2$-induced cell death and self-dsDNA release could induce a type I IFN response in mice via the cytosolic receptor STING (stimulator of interferon genes) [49, 50]. These findings were extended to humans, showing that patients with silicosis had an increase in circulating dDNA as well as activation of the pathway sensing DNA and inducing a type I IFN response in the lung tissue [49].

1.2.1.6 Proposed role for type 1 IFN in $cSiO_2$-induced autoimmunity.

When $cSiO_2$ is inhaled it can induce cell death (e.g. apoptosis, pyroptosis, and necroptosis) in multiple cell types in the lung, including AMs and neutrophils (**Figure 1.1**). If dead cells are not properly cleared, cellular debris accrues. Of note, impaired efferocytosis (i.e. phagocytosis of dead/dying cells) is implicated in lupus and other autoimmune diseases, resulting in insufficient clearance of cellular debris, including host nucleic acids [51]. In addition, $cSiO_2$ has been shown to induce formation of neutrophil extracellular traps (NETs) via a mechanism known as NETosis, leading to the extrusion of nuclear contents that further contribute to extracellular DNA accumulation [52]. While it is well established that viral nucleic acids can trigger an IFN response, endogenous nucleic acids released by dying and NETosing cells can as well [42, 53]. Many cell types can recognize double stranded and single stranded nucleic acids through various receptors, including toll like receptors and cytosolic nucleic acid sensors such as STING [50], ultimately leading to the release of type I IFNs. In lupus, one of the key cell types implicated in this response is the plasmacytoid dendritic cell (pDC), which primarily releases IFN-α [42].

Based on published studies and our findings, we propose that the type I IFN response plays

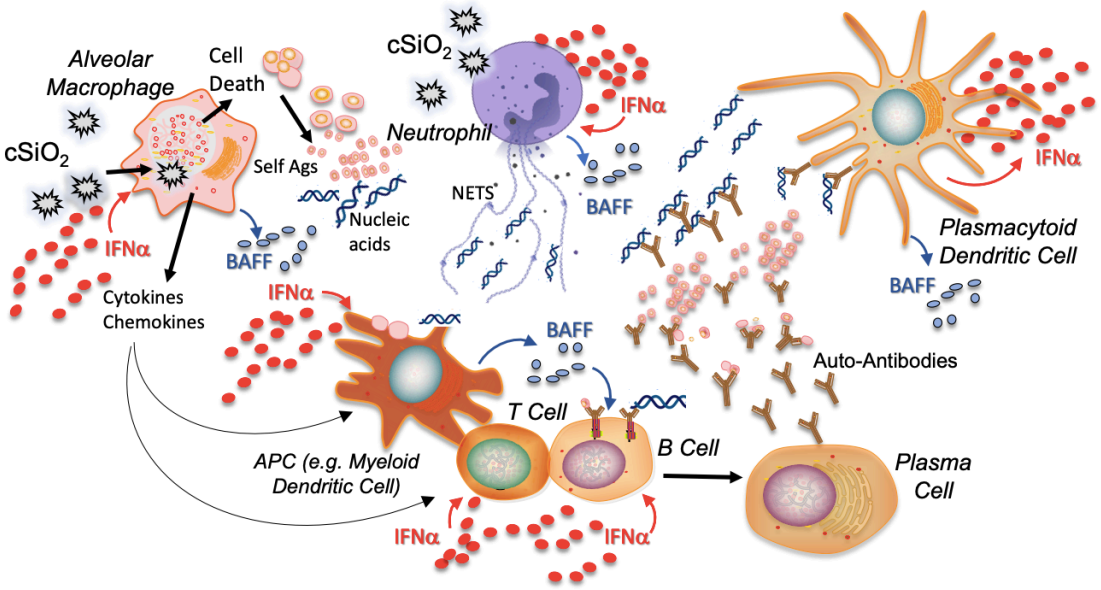


Figure 1.1: Putative role for type 1 IFN in $cSiO_2$-induced systemic lupus erythematosus. When inhaled, $cSiO_2$ induces cell death in multiple cell types present in the lung (e.g., neutrophils and macrophages), leading to the extracellular release of host nucleic acids. $cSiO_2$ also stimulates release of neutrophil extracellular traps (NETs) that contribute to the accumulation of extracellular DNA. Extracellular nucleic acids, either viral or innate, induce the release of type I interferon (IFN) from many immune cell types. In lupus, plasmacytoid DCs (pDCs) are recognized as a primary producer of IFNα, the major type I IFN. Extracellular DNA along with other uncleared cellular debris can be presented by antigen-presenting cells, promoting the development of autoreactive B and T cells. This process is enhanced directly by IFNα and by other cytokines and chemokines, such as B-cell activating factor (BAFF), released from immune cells in response to IFNα. Autoreactive plasma cells will produce autoantibodies against host antigens, forming DNA-containing immune complexes that can be recognized by pDCs to further drive this cycle. *Adapted from Chasset and Arnaud (2018).*[54]

a central role in $cSiO_2$-triggered autoimmunity. IFN-α can act on multiple cell types and many of its actions promote a feed-forward loop to drive the type I IFN response. For example, IFN-α can induce additional NETosis [55] and can also act on macrophages, leading to the release of proinflammatory chemokines and cytokines that stimulate antigen presentation and T and B cell activation. Additionally, IFN-α can act directly on myeloid DCs to promote antigen presentation. In the case of $cSiO_2$-triggered autoimmunity, host antigens are likely be presented due to the impaired clearance of cellular debris. IFN-α can further promote B cell maturation into plasma cells. In lupus, these may be autoreactive plasma cells producing autoantibodies against host antigens, in-

cluding host DNA. These DNA-containing immune complexes can be recognized by pDCs, leading to additional release of IFN-α [54].

Of high relevance to human autoimmunity, IFN-α elicits the release of B-cell activating factor (BAFF) from multiple cell types [56, 57]. The main role of BAFF is to promote B-cell maturation, increasing the release of autoantibodies and driving this feed-forward cycle. BAFF is the target of the drug Belimumab (Benlysta^{TM}), which was approved by the FDA in 2011, making it the first drug in 52 years approved to treat lupus in adults [58]. In April 2019, Benlysta became the first approved treatment for pediatric lupus [59]. Of high relevance to our model, we have found that $cSiO_2$ induces elevated BAFF in the BALF and plasma of NZBWF1 mice and that elevation of this critical B-cell maturation factor is dose-dependently suppressed by DHA supplementation [7].

1.2.1.7 Can ω-3 HUFA supplementation be used as a precision medicine tool against lupus?

$cSiO_2$ treatment markedly increases expression of several cytokines and receptors that are pathogenic in the progression of lupus. Importantly, dietary DHA reversed this effect (**Table 1.1**) [4, 7]. Relevant to the treatment of lupus, several of the cytokines identified in our preliminary and published studies are pharmacological targets for drugs already approved or currently in clinical trials for the treatment of lupus and other autoimmune diseases [60, 54, 61, 62, 63, 64, 58]. Notably, two the recently completed TULIP-1 and TULIP-2 trials found that Anifrolumab, a monoclonal antibody against the IFN-α receptor IFNAR1, reduced flares in lupus patients and allowed them to decrease their maintenance dose of glucocorticoids [65]. Like Anifrolumab, many of the therapies in development are monoclonal antibodies, which are extremely expensive [66]. For example, a Belimumab dosing regimen costs approximately $35,000 per year, placing a substantial financial burden on uninsured patients and their families [58, 67]. While ω-3 HUFA supplementation might not eliminate the need for these drugs, it has the potential to interfere with many of these targets simultaneously for less than few dollars a day, reducing the need for high doses of expensive drugs over prolonged periods of time.

Recently, a population study conducted under the aegis of the Michigan Lupus Epidemiology

Table 1.1: $cSiO_2$ enhances and DHA suppresses many inflammatory end points targeted by drugs either approved or in clinical trials for treatment of autoimmune disease.

Target	$cSiO_2$	DHA	Treatment	Drug
IFNα	↑	↓	IFNα mAb	Rontalizumab, Sifalimumab
			IFNAR1 mAb	Anifrolumab
			IFNα vaccine	Interferon-α-kinoid (IFN-K)
BAFF	↑	↓	BAFF mAb	Belimumab (Benlysta™)
IL-6	↑	↓	IL-6R mAb	Tocilizumab
			IL-6 mAb	Sirukumab
TNF-α	↑	↓	TNF-α mAb	Infliximab
MCP-1	↑	↓	Neutralize MCP-1	Emapticap
CD3	↑	↓	CD3 mAb	Muromonab-CD3

BAFF, B-cell activating factor; IFN, interferon; IL-6, interleukin-6; MCP-1, monocyte chemotactic protein 1; TNF-α, tumor necrosis factor alpha; mAB, monoclonal antibody.

& Surveillance (MILES) Program reported that higher dietary intake of ω-3 fatty acids, and lower dietary ω-6:ω-3 ratios, were favorably associated with patient-reported outcomes, particularly self-reported lupus activity and sleep quality [12]. To harness the protective effects of DHA and other ω-3 HUFAs, it is important to understand how they act. When consumed, fatty acids are incorporated into the cell membrane [28], and the resulting levels of ω-3 and ω-6 HUFAs in the membrane can have direct, often opposing, effects on inflammatory pathways in the cell [68]. For example, ω-3 HUFAs can 1) impede lipid raft formation to prevent aggregation and activation of transmembrane receptors involved in inflammatory signaling [69], 2) be cleaved from the membrane to generate free HUFAs [70, 71] that bind to intra- and extra-cellular receptors to promote anti-inflammatory signaling pathways [72, 73, 74, 75], and 3) be metabolized to downstream metabolites with anti-inflammatory and pro-resolving qualities [**RN653**, 76, 77]. EPA and DHA can directly compete with ω-6 HUFAs for incorporation into the cell membrane, resulting in decrease availability of ω-6 HUFA arachidonic acid to act as a substrate for proinflammatory prostaglandins, thromboxanes, and leukotrienes [**RN654**]. These mechanisms will be discussed in greater detail in Section 1.3.

Because altering the HUFA balance of the membrane to favor ω-3 HUFAs can have a direct im-

pact on promoting resolution over inflammation, it is critical to gauge their content in the phospholipid membrane. Assessing the phospholipid content of one's red blood cells (RBCs) as a biomarker of HUFA status in tissues is now quite simple with several companies providing relatively inexpensive, at-home finger prick tests [78]. From just one drop of blood collected and stabilized on filter paper, dozens of major fatty acids, including ω-3 and -6 HUFAs, can be quantified. We favor using the ω-3 HUFA score over other alternative approaches to reflect the ω-3 content in the RBCs of our mice. The HUFA score is calculated as the major ω-3 HUFAs as a percent of total HUFAs [79], while other widely used indices present EPA and DHA as a percent of total fatty acids. There are a few advantages to presenting the ω-3 content using the HUFA score. First, HUFAs have similar chemical properties and will be modified – or degraded – at similar rates. Therefore, the HUFA score should remain relatively constant despite methodological differences [68]. Second, the major ω-6 and ω-3 HUFAs are the primary substrates for known proinflammatory and anti-inflammatory lipid mediators [28, 68]. Limiting analysis to the HUFA pool allows the clinician to better estimate potential competition between ω-6- and ω-3-derived metabolites. Finally, the HUFA score is predictable from dietary fat intake, which would be important for developing a personalized nutritional intervention [80].

Taken together, intranasal exposure of lupus-prone mice to $cSiO_2$ induces a type I IFN gene signature that precedes ELS induction in the lung, with lymphoid cell infiltration occurring as early as 1 wk post-instillation and worsening over the course of the disease. ELS neogenesis evokes vigorous elevations of diverse autoantibodies in the BALF and plasma that form immune complexes with their cognate antigens and deposit in the kidneys, ultimately resulting in glomerulonephritis. When animals are fed DHA, the IFN-related genes are suppressed, ELS development is blocked, autoantibodies are reduced, and animals present much less severe glomerulonephritis (**Figure 1.2**). Because DHA consumption results in an enrichment of ω-3 HUFAs in the phospholipids, measuring the HUFA score of patients could be ideal for developing strategies to effectively combat inflammatory and autoimmune diseases. Ultimately, a precision medicine strategy for an individual would require at least two tactics to potentiate the ω-3 HUFA score: 1) increasing ω-3 HUFA intake

by dietary supplementation and 2) reducing consumption of foods that contain high amounts of ω-6 HUFAs. This strategy may protect and benefit patients with lupus or other autoimmune diseases, individuals genetically predisposed to these diseases, or individuals environmentally exposed to $cSiO_2$ and other autoimmune disease triggers.

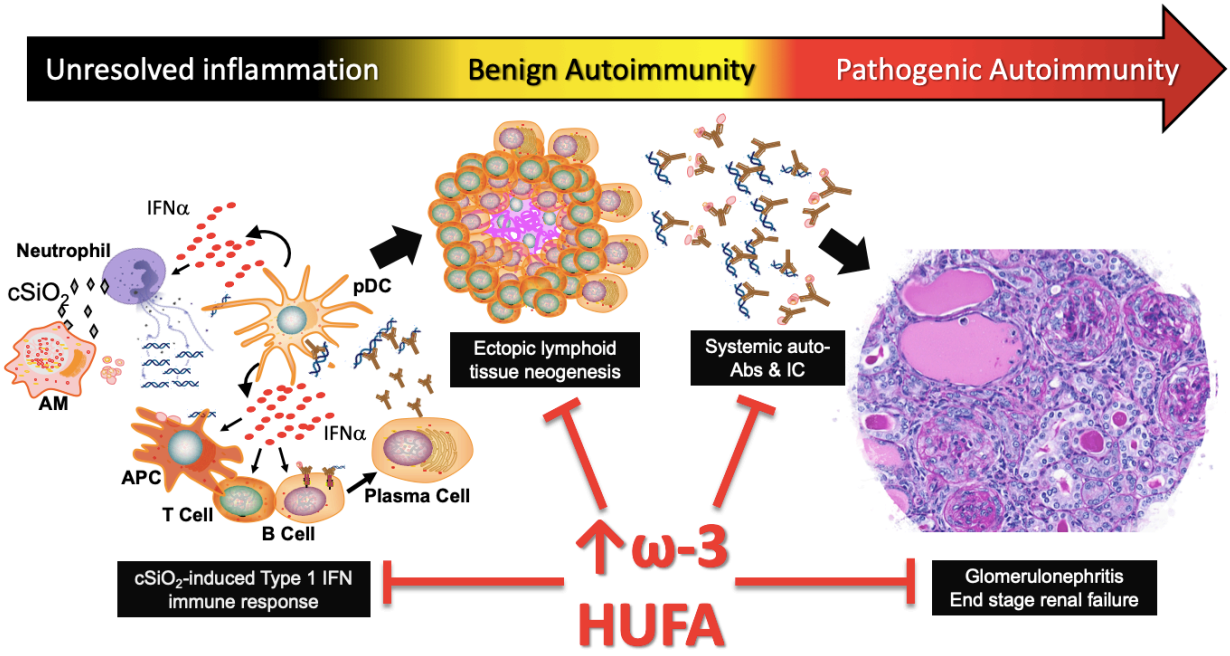


Figure 1.2: $cSiO_2$-induced autoimmune pathogenesis is suppressed by ω-3 HUFAs. The $cSiO_2$-induced type I interferon (IFN) gene signature promotes ectopic lymphoid structure neogenesis in the lungs and production of pathogenic autoantibodies that form immune complexes (ICs) with host antigens. This culminates in systemic autoimmunity and glomerulonephritis. When mice are fed diets rich in DHA, autoimmune pathogenesis is suppressed. Improved disease status and decreased inflammatory end points are associated with an increase in ω-3 highly unsaturated fatty acids (HUFAs) in the cell phospholipid membrane. Biomarkers that evaluate membrane fatty acids, such as the HUFA score, are crucial to developing ω-3 supplementation strategies to prevent or ameliorate inflammatory and autoimmune disease.

1.2.2 The role of alveolar macrophages in initiating $cSiO_2$-induced autoimmunity

1.2.2.1 Distinct phenotype, function, and origin of tissue macrophages.

Macrophages (based on the Greek words "makro", meaning big, and "phagein", meaning eat) were discovered by Russian biologist Elie Metchnikoff, "the father of natural immunity". Though

Metchnikoff was not the first to observe phagocytosis, his work solidified the importance of phagocytosis in immune defense and homeostasis, through the clearing of dead cells [81]. While the phagocytic functions of macrophages provide the namesake for these cells, they also play key roles in antigen presentation, recruiting and activating incoming immune cells through release of chemokines and cytokines, propagating signals that initiate resolution of inflammation, and repairing damaged tissue [82].

Under homeostatic conditions, most tissues are populated by self-renewing, tissue resident macrophages. During tissue damage or disease, circulating monocytes are attracted to the site by chemical mediators released by injured or infected cells [82]. In the tissue, these monocytes differentiate into mature macrophages, which contribute to immune defense by phagocytosing pathogens, releasing additional chemokines and cytokines to attract additional immune cells, presenting antigens to cells of the adaptive immune system, and clearing dead and dying cells. Macrophages also metabolize fatty acids to downstream bioactive lipid mediators, such as prostaglandins, thromboxanes, and leukotrienes, which contribute to the inflammatory response, and specialized pro-resolving mediators (SPMs), that act to suppress inflammatory signaling and initiate tissue repair and resolution [83, 84].

Macrophages can adopt distinct phenotypes based on external signals in their microenvironment. A common paradigm applied to understand the phenotypes of macrophages is to classify them as M1 or M2, or as classically or alternatively activated macrophages [84, 85]. While these distinctions do not perfectly capture the diverse repertoire of macrophage phenotypes observed *in vivo*, they provide a paradigm to understand the differences between macrophages involved in promoting inflammation or resolution. M1-like macrophages are considered to be inflammatory while M2-like macrophages have characteristics that promote resolution (i.e. release of anti-inflammatory cytokines and SPMs, increased phagocytosis). Most resident macrophages, including AMs, adopt a more pro-resolving phenotype to promote tissue healing following an inflammatory response [82]. Infiltrating monocyte-derived macrophages generally adopt an M1-like phenotype, with a more robust inflammatory response, but shift to an M2-like phenotype during the resolution

phase of inflammation. Furthermore, monocyte-derived macrophages recruited to the tissue during inflammation can remain in the tissue following resolution and adopt a phenotype similar to tissue-resident macrophages [82].

1.2.2.2 AMs are the immune sentinels of the alveoli.

Origin of AMs and role in maintaining alveolar homeostasis. AMs are the resident immune cells of the alveoli [86]. Unlike interstitial macrophages, the resident immune cell of the lung interstitium that is continually repopulated by circulating monocytes, AMs are long-lived and self-replicating. Like other resident macrophages (e.g., Kupffer cells in the liver, Langerhans cells in the skin), AMs are derived from fetal liver monocytes during development (**Figure 1.3A**) [87]. The local microenvironment induces differentiation into mature AMs [88, 89]. Specifically, the growth factor GM-CSF and cytokine TGFβ have been shown to be essential for AM development and maintenance in the alveoli [90, 91]. Both of these signals promote expression and activation of PPARγ. Genes and pathways induced by this receptor are involved in lipid metabolism and induction of scavenger receptors that promote phagocytosis. This is critical for the AM roles of 1) maintaining surfactant homeostasis and 2) constantly clearing the alveolar space of inhaled microbes and particles.

The AM phenotype is uniquely tailored to meet the requirements of protecting the alveolar space. Its inflammatory response is relatively subdued, as it would be deleterious for the AM to trigger an immune response to every foreign object it encounters, yet the AM can induce a robust inflammatory response in situations that pose a major threat to the lung. Interactions between AMs and alveolar epithelial cells (AECs) maintain a state of immune quiescence in the alveoli in the absence of pathogenic stimuli (**Figure 1.3B**) [92]. This is mediated by various mechanisms, by i) binding of surface proteins between AECs and AMs, such as AEC PD1 to AM PDL1, AEC CD200r to AM CD200, AEC CD47 to AM SIRP1α, ii) cytokines like IL-10 and TGFβ secreted from AECs, and iii) extracellular vesicles secreted by AMs that contain SOCS proteins to suppress inflammatory STAT signaling in AECs. Repeated injury to the alveoli permanently perturb these

interactions, resulting in chronic disease and pathogenesis in the lung.

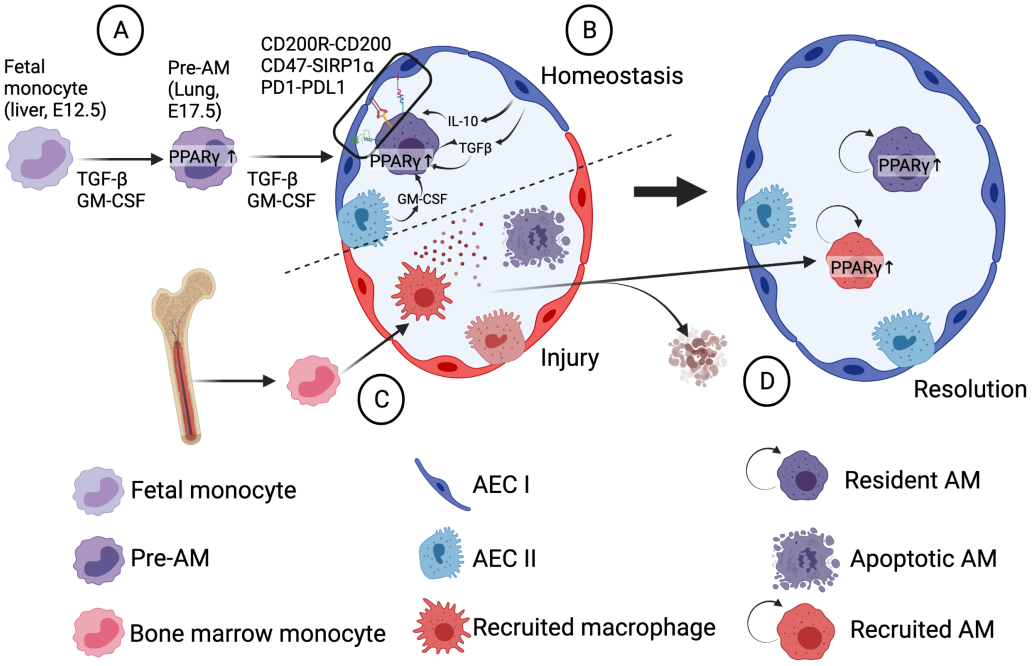


Figure 1.3: Origin and contribution of alveolar macrophages during homeostasis, injury, and resolution in the mouse. A. Resident macrophages are derived from fetal monocytes, which are present in the mouse fetal liver at 12.5 gestational days. These migrate to the developing lung, and differentiate to pre-alveolar macrophages (pre-AMs) in the presence TGFβ and GM-CSF. The sustained presence of TGFβ and GM-CSF promotes the development of mature alveolar macrophages (AMs) during the first few weeks of life. **B.** Signals within the alveolar environment keep AMs in a quiescent state and promote their continued self-renewal. **C.** Tissue injury and loss of AMs due to cell death results in recruitment of bone marrow-derived circulating monocytes, which differentiate into inflammatory macrophages. **D.** During resolution, recruited monocyte-derived macrophages either undergo apoptosis or remain in the lungs, where they adopt a similar phenotype to tissue resident AMs. Both recruited and resident AMs can self-renew to repopulate the alveoli. *Created with Biorender.com*

Repopulation of the alveoli by monocyte-derived macrophages in lung injury and infection: Beneficial or detrimental? When injury or infection eliminates resident AMs from the alveoli, the alveolar niche is repopulated by macrophages derived from circulating monocytes (**Figure 1.3C**) [93]. While this process is necessary to control infection, it also may contribute to chronic inflammation and irreversible lung damage due to the inflammatory phenotype of recruited monocytes. For example, the presence of monocyte-derived macrophages bolster the immune response to influenza infection [94], and their more pro-inflammatory phenotype protect against future respiratory infections [95]. On the other hand, preventing recruitment of monocytes to the lung can alleviate disease severity and tissue damage in chronic lung diseases [94]. These recruited monocyte-derived macrophages can remain in the lung for extended periods of time, where they adopt a phenotype similar, but not identical, to the tissue resident AMs (**Figure 1.3D**).

The role of monocyte-derived macrophages in chronic lung diseases is complex. In a mouse model of bleomycin-induced fibrosis, the repopulation of resident AMs by recruited monocytes contributes to disease progression due to their pro-fibrotic nature [96, 97, 98, 99]. Depleting monocyte-derived macrophages ameliorated development of bleomycin-induced fibrosis, while depleting resident AMs has no effect. The pro-fibrotic, monocyte-derived macrophages have an immature phenotype with low expression of AM surface marker Siglec F [98]. Contrary to this, a mouse model of silica-induced fibrosis showed a protective effect of monocyte-derived macrophages [100]. Here, inhibiting recruitment of monocyte-derived macrophages resulted in a transition from nodular lesions to diffuse fibrosis, that, in humans, is a hallmark of disease progression and a poor prognosis. This finding suggests that, in the $cSiO_2$-triggered silicosis mouse model, monocyte-derived macrophages prevent diffusion of nodular lesions, attenuating the development of fibrosis.

To summarize, while it is evident that depleted AMs are replenished by monocyte-derived macrophages, it is yet unclear whether this process helps or harms the lungs in the context of particle-induced toxicity.

1.2.2.3 Deposition and clearance of inhaled particles.

There are five primary modes for particle deposition that determine where it deposits in the lung (**Figure 1.4 A-B**) [101, 102]. First, impaction is the inability for large objects (typically >10 μm in diameter) to change direction due to inertia. This usually occurs in the large airways and nasal passages, where changes in flow direction are abrupt. Second, interception, which is deposition due to particles contacting the airway surface due to their shape or size, is most common for inhaled fibers, such as asbestos. Third, sedimentation, also known as settling, is when small particles (1-5 μm) deposit due to gravity. This is most common in the alveoli and small airways, where airflow velocities are low. Fourth, diffusion, also known as Brownian motion, is the primary mode of sedimentation for nanoparticles (<1 μm), which can reach the distal airways and move randomly by diffusion until they come in contact with the airway epithelium. Finally, electrostatic precipitation is deposition of charged particles due to electrostatic interactions with the airway walls.

Inhaled particles can be cleared by both chemical and physical means (**Figure 1.4C**). Chemical clearance refers to the dissolution of particles or parts of particles that are soluble within the lung environment [103]. During this process, particle components may bind to proteins to be cleared via the circulatory system. Particles are considered insoluble if the rate at which they could be solubilized is negligible relative to their rate of physical clearance. Physical clearance mechanisms differ depending on the area in the lung where the particle deposits as well as its size [105, 103]. Particles depositing in the trachea, bronchi, and bronchioles can be cleared via the mucociliary escalator and by coughing. These regions of the airway are populated by secretory cells (primarily goblet cells) that secrete the necessary components of mucus, as well as ciliated cells. The cilia lining the airway epithelium beat constantly to direct the mucus layer upward to the larynx, where it enters the gastrointestinal tract [106]. Particles that reach the respiratory bronchioles and alveoli are primarily cleared through phagocytosis by AMs. Particle-laden AMs are believed to migrate out of the alveoli, either within the lumen or through the interstitium, to be removed via the mucociliary escalator [105]. Nanoparticles can be cleared by additional mechanisms, including epithelial cell endocytosis and interstitial translocation, which can lead to particle transfer to the lymphatic and

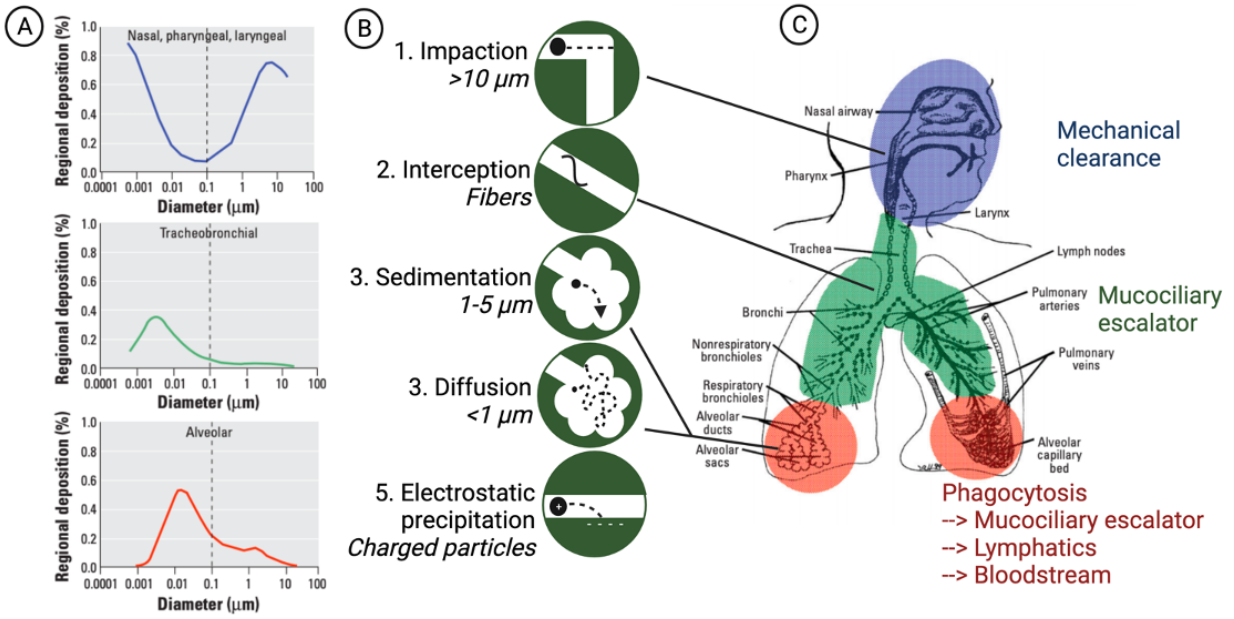


Figure 1.4: Particle deposition mechanisms in the respiratory tract. A. Particles deposit by different mechanisms and in different locations of the respiratory tract based on their physical characteristics. The largest and smallest particles deposit in the upper airways, while mid-sized particles can penetrate deeper to reach the tracheobronchial and alveolar regions. **B.** Large particles (>10 μm) deposit by impaction in the upper airways, fibers deposit by interception due to their shape, 1-5μm particles and <1μm particles deposit in the distal airways by sedimentation and diffusion, respectively, and charged particles deposit based on electrostatic interaction with the airway wall. **C.** Large particles are cleared from the upper airway by mechanical clearance (i.e. coughing), particles in the trachea and bronchi are cleared by movement via the mucociliary escalator, and small particles in the distal airways are phagocytosed by alveolar macrophages or diffuse into the interstitium. Particle-containing macrophages may translocate to ciliated airways to be transported via the mucociliary escalator, or they may migrate to the lymphatics and bloodstream. *Adapted from Oberdorster 2005 and Prata 2017.* [103, 104] *Created with Biorender.com*

blood circulation resulting in their presence in extrapulmonary sites. Nanoparticles can even be taken up by sensory neurons in the nasal passage and trachea, allowing them to infiltrate the central nervous system [103].

Though critical to understanding mechanisms of particle-induced toxicity, there are several limitations to rodent models of particle exposure. First, differences in lung architecture between rodents and primates influence the deposition and clearance of inhaled particles. Rodents, which lack respiratory bronchioles and have smaller alveolar ducts, clear particles more rapidly than hu-

mans and monkeys [107]. A direct comparison between rats and monkeys found that diesel exhaust and coal dust accumulates in the rat alveolar lumen and ducts, while in monkeys the particles evenly distribute between the lumen and the interstitial and pleural spaces [108]. Second, within rodent models of particle exposure, substantial variation arises from strain [109, 110] and species differences [111]. For example, mice more effectively clear carbon black particles and have reduced immune cell infiltration following particle exposure compared to rats [111].

1.2.2.4 Fate of respirable $cSiO_2$: Effective clearance vs particle overload.

Respirable crystalline silica is defined as $cSiO_2$ particles <10 μm in diameter [112]. Based on the discussion above, respirable $cSiO_2$ is expected to deposit primarily in the alveoli, where the primary mechanism of clearance is phagocytosis by AMs. AMs rapidly engulf particles *in situ*, with a study in rats showing up to 80% of 3 and 10 μm plastic microspheres engulfed within 24 h [113]. Similarly, a 1982 study showed that 2/3 of AMs recovered from BALF from rats 12 h post exposure to a sub-pathogenic dose of $cSiO_2$ had engulfed particles [114]. This high number of $cSiO_2$-containing AMs was observed through 42 d post-exposure, at which time it decreased to 25%, and no increase in cell death was observed at either timepoint. During this time, the amount of $cSiO_2$ per macrophage continually decreased, possibly as $cSiO_2$-containing macrophages were cleared from the alveoli.

Onset of $cSiO_2$-induced lung diseases in experimental models does not occur immediately [17, 115, 116], suggesting that the continued presence of the particle drives pulmonary pathology. This may be due to an excess or repeated exposure that overwhelms the clearance ability of the macrophage, resulting in sustained presence of the particle in the lung, a process termed "particle overload". Free $cSiO_2$ that is not taken up by AMs can translocate to the interstitium and be engulfed by interstitial macrophages, which may be the case when particle burden overwhelms the clearance ability of AMs [117, 16]. Accumulation of $cSiO_2$-engorged macrophages, often referred to as "dust cells", are frequently observed in structured lymphocyte-macrophage aggregates that sequester $cSiO_2$, known as silicotic nodules or granulomas. In a detailed review of the fate of inhaled

$cSiO_2$, it was suggested that the location of granulomas can be used to infer the intended location of $cSiO_2$-filled dust cells. In rats, granulomas were observed in the bronchus-associated lymphoid tissue (BALT), lung-associated lymph nodes, and the pleura. These sites are consistent with the proposed pathway of dust cell translocation from the lung interstitium to the bronchial lumen via the BALT and through pleural lymphatics to lung associated lymph nodes [16]. The detriment of overwhelming the AM clearance ability in the lungs is highlighted in a recent study where rats were treated with a single intratracheal instillation of a high dose of $cSiO_2$ [118]. Particles were detected in the lung up to 96 wk following the exposure, and $cSiO_2$ treated rats had an increase in immune cell infiltration, fibrosis, granuloma formation, and development of neoplastic lesions compared to saline-instilled controls.

A series of studies found that augmenting the number of phagocytes present in the alveoli and their chemotactic abilities could protect against the pathologic effects of $cSiO_2$ particle overload [119, 120]. Mice that were intratracheally instilled with chemotactic factor N-formyl-L-methionine-leucyl-phenylalanine (FMLP) 2-3 wk following a single dose of $cSiO_2$ had reduced development of pulmonary fibrosis than mice instilled with vehicle. Immediately following FMLP administration, mice had an increased number of $cSiO_2$-filled phagocytes and cell-free $cSiO_2$ in the BALF, suggesting that the augmented chemotaxis promotes $cSiO_2$ clearance via the mucociliary escalator. At 16 wk following the $cSiO_2$ exposure, FMLP-exposed mice had significantly less $cSiO_2$, particularly in the interstitium and lymph nodes, likely due to the enhanced clearance observed at the earlier timepoint.

1.2.2.5 AM death and release of DAMPs.

$cSiO_2$-induced cell death. In a comprehensive review of mechanisms of $cSiO_2$-induced toxicity in the lung [17], it was noted that particles with greater toxicity to AMs are less effectively cleared and are more likely to promote lung pathologies. A 1987 study [121] measured the particle lung burden in rats 3 and 38 d following the exposure period to $cSiO_2$ and the less cytotoxic titanium dioxide (TiO_2) [122]. Using these data, the review author determined that animals could be exposed

to approximately three times more TiO_2 than $cSiO_2$ before reaching particle overload. Others showed that *ex vivo* macrophages from bronchoalveolar lavage of rats exposed $cSiO_2$ had reduced chemotactic ability compared to those from rats exposed to TiO_2 [123]. Thus, the impairment of particle clearance in the lung is due in part to AM dysfunction and cell death.

In an elegant live-cell imaging study [124], Joshi and Knecht investigated the kinetics of $cSiO_2$-induced cell death *in vitro* using the MH-S alveolar macrophage model. Here, they observed that $cSiO_2$ triggered apoptosis in 80% of cultured macrophages, while the other 20% underwent necrotic cell death. They observed that one of the first events triggering apoptosis following $cSiO_2$ was lysosomal membrane permeabilization (LMP), though this was not observed in the cells undergoing necrosis. Previous studies have also shown that loss of lysosomal membrane integrity is a key event following $cSiO_2$ phagocytosis [125, 126, 127]. The molecular mechanisms linking LMP to cell death have been reviewed previously [128]. If apoptotic cells are not cleared by other macrophages (a process known as efferocytosis), apoptosis is followed by secondary necrosis, which likely also occurs *in vivo* as a result of impaired efferocytosis due to $cSiO_2$ exposure [129]. Interestingly, impairment in efferocytotic capacity is implicated in multiple autoimmune disease [130], implying that individuals with autoimmune disease might be particularly susceptible to flares induced by inhaled particles.

DAMP release. Cell death following exposure to $cSiO_2$ leads to release of alarmins and damage-associated molecular patterns (DAMPs) that promote additional inflammatory signaling pathways, including NLRP3 inflammasome activation [131, 132, 133]. The terms DAMPs and alarmins are often used interchangeably to define endogenous proteins that trigger inflammation in the absence of pathogenic stimuli. However, they have also been defined separately, with DAMPs referring to immune-activating molecules released from dead cells and alarmins referring to immune-activating molecules released from living cells [134]. Many molecules fall into both categories, including toll-like receptor 4 (TLR4) agonist HMGB1 and IL-1α, which are both implicated in potentiating $cSiO_2$-induced inflammation in the lung [135, 136, 132].

A recent study showed that intratracheal instillation of $cSiO_2$ with an HMGB1 neutralizing antibody induced less inflammation in the lung induced than did $cSiO_2$ alone [136]. Studies investigating the role of IL-1α show that IL-1α knockout mice or mice treated with IL-1α neutralizing antibodies have decreased inflammation following $cSiO_2$ or intranasal lipopolysaccharide (LPS) exposure [137, 132]. Interestingly, particle-triggered IL-1α release has been shown to be a unique feature of alveolar macrophages compared to other macrophages, and the increase in IL-1α in the lung following $cSiO_2$ exposure is the result of AM cell death [138]. In an *in vitro* tri-culture system composed of THP-1 macrophages, A549 alveolar epithelial cells, and Ea.Hy926 basolateral cells, addition of the IL-1 receptor agonist IL-1RA to the media reduced inflammatory cytokine gene expression and release following exposure to $cSiO_2$ and silica nanoparticles [139]. IL-33 is also released following $cSiO_2$ exposure *in vivo* and follows a similar time-course to IL-1α release, though its role in promoting particle-induced inflammation has not been specifically investigated [132].

1.2.2.6 $cSiO_2$ activates the NLRP3 inflammasome.

Overview of inflammasome activation. A third form of cell death triggered by $cSiO_2$ particles is pyroptosis, which is associated with inflammasome activation, specifically the NLRP3 inflammasome. Unlike necrotic and apoptotic cell death, which can be induced directly by $cSiO_2$ alone *in vitro*, NLRP3 inflammasome activation requires two signals [140]. First, the inflammasome must be primed (Signal 1), which can occur by activating NF-κb family transcription factors that evoke gene expression of inflammasome components and IL-1 cytokines. Microbial components (e.g. LPS), cytokines (e.g. IL-1β, IL-6), and alarmins (e.g. IL-1α, HMGB1) can all act as priming signals. Subsequently, Signal 2 promotes NLRP3 oligomerization, caspase-1 activation, and processing of pro-IL-1β and pro-IL-18 to mature IL-1β and IL-18 [140]. The alarmin IL-1α, is also released upon inflammasome activation [141]. These potent pro-inflammatory cytokines bind the IL-1 receptor IL-1R on immune cells to drive inflammation, including further inflammasome activation [132]. Over-activation of the NLRP3 inflammasome is implicated in multiple chronic

inflammatory and autoimmune diseases, including lupus [142]. Importantly, mice lacking components of the NLRP3 inflammasome have markedly reduced development of $cSiO_2$-triggered inflammation and fibrosis [140].

Mechanisms of NLRP3 inflammasome activation. Though it is clear that particles, including volcanic ash, cholesterol crystals, silica nanoparticles and $cSiO_2$ [143, 144, 145], act as Signal 2 for inflammasome activation, there is no consensus on exactly how this activation occurs or whether the diverse NLRP3 inflammasome triggers share a specific molecular event or pathway to activate the multi-protein complex [146]. A recent review highlights the various molecular mechanisms involved in activation of the NLRP3 inflammasome [147]. These include i) ion flux (including potassium efflux, calcium mobilization, and possibly chloride influx), ii) reactive oxygen species (ROS) production, iii) lysosomal destabilization resulting in release of cathepsin enzymes, and iv) synthesis and release of oxidized mitochondrial DNA, likely following mitochondrial damage. The NLRP3 inflammasome can also be non-canonically activated, in which activation of caspase-11 (caspase 4/5 in humans) triggers NLRP3 inflammasome activation, likely via potassium efflux. Certainly, the events listed above likely occur concurrently in response to many inflammasome activators, but it remains to be seen if one will be defined as the common trigger for NLRP3 inflammasome activation.

Inflammasome activating events triggered by $cSiO_2$. $cSiO_2$ induces interconnected cellular events that ultimately converge on NLRP3 inflammasome activation, including LMP, potassium efflux, and ROS generation, and mitochondrial damage, making it difficult to identify a single unifying mechanism (**Figure 1.5**). Many have shown that phagocytosis and LMP are critical steps in particle-induced inflammasome activation [140, 148, 145, 125, 126, 149, 150]. LMP may lead to inflammasome activation through the release of cathepsin enzymes [125, 126, 150], ROS leakage [151], or calcium influx and mobilization from the endoplasmic reticulum [152]. Alternatively, others have shown that macrophages treated with cytochalasin D, which inhibits actin polymerization and particle phagocytosis, still undergo NLRP3 inflammasome activation in response to $cSiO_2$

[153]. Here, they found that potassium efflux, which can be induced by membrane curvature without complete phagocytosis, is sufficient to trigger inflammasome activation in response to particles. Notably, release of cathepsin B from permeabilized lysosomes may also trigger potassium efflux [133].

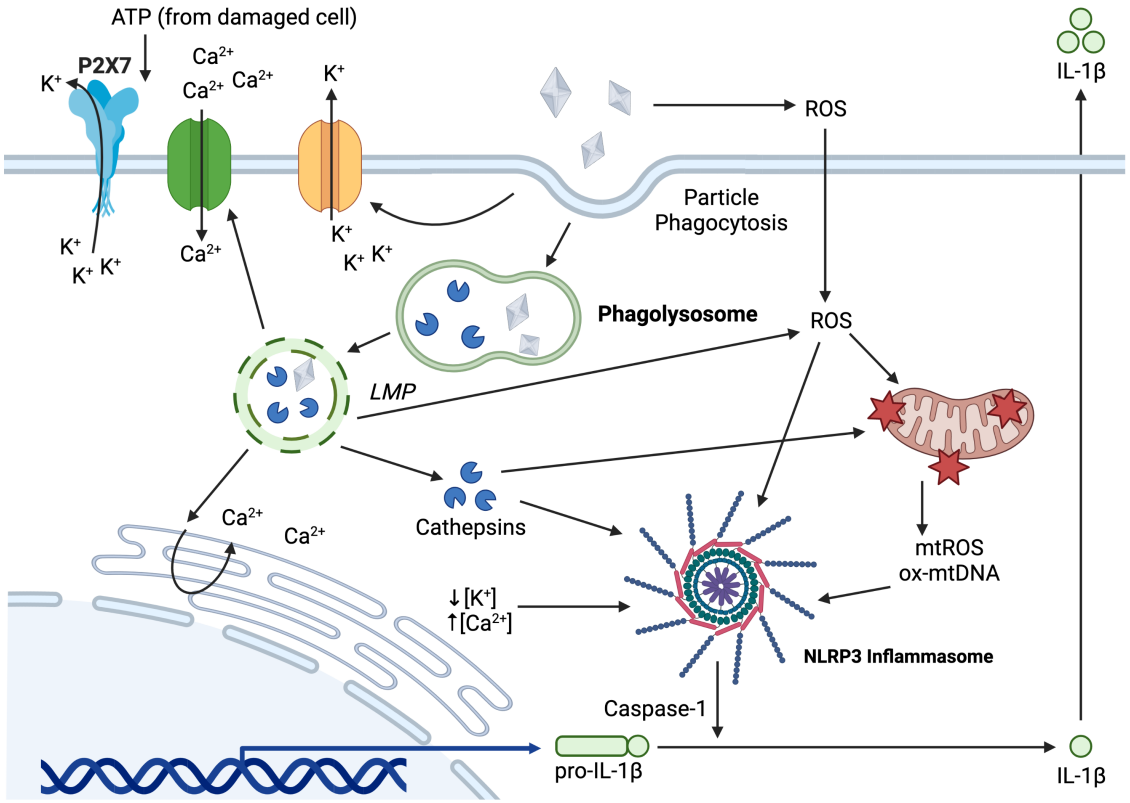


Figure 1.5: $cSiO_2$ triggers multiple interconnected events involved in NLRP3 inflammasome activation. Though the exact mechanism of NLRP3 inflammasome activation particles is unknown, many of the putative activators are triggered by exposure to $cSiO_2$. Phagocytosis of $cSiO_2$ particles triggers potassium efflux as a result of membrane curvature, while ATP from neighboring, damaged cells activates P2X7 channels to further promote potassium efflux. $cSiO_2$ within the phagolysosome can induce lysosomal membrane permeabilization (LMP), which can trigger calcium influx through TRPM2 channels as well as calcium mobilization from the endoplasmic reticulum. These changes to intracellular ion concentrations are one proposed mechanism of inflammasome activation. LMP also leads to release of cathepsin enzymes and ROS, both of which are postulated to activate the inflammasome directly. Extracellular $cSiO_2$ particles can also generate reactive oxygen species (ROS), which can lead to mitochondrial damage and release of mitochondrial ROS and oxidized mitochondrial DNA, both of which have been shown to activate the inflammasome. Regardless of the mechanism of activation, the end result of inflammasome activation is processing of pro-IL-1β to mature IL-1β by mature caspase-1, which is activated autoproteolytically when the inflammasome assembles. *Created with Biorender.com*

ROS production has also been put forth as a critical event for inflammasome activation. $cSiO_2$ particles themselves are capable of generating ROS [154], exposure to $cSiO_2$ induces ROS generation *in vitro* [151, 155], and inhalation of $cSiO_2$ induces prolonged ROS presence in the lung [115]. In the absence of an inflammasome priming signal, ROS production precedes apoptosis [151]. While inhibition of ROS can prevent $cSiO_2$-induced inflammasome activation [140], the source of the ROS is unclear, with some results suggesting that $cSiO_2$-triggered ROS is dependent on the phagocyte NADPH oxidase [148] and others suggesting dependence on mitochondrial ROS only [125, 156]. Excess ROS production can lead to generation of oxidized mitochondrial DNA, which is postulated to directly activate the NLRP3 inflammasome [157]. Alternatively, ROS production can activate TRPM2 channels to allow calcium influx, which contributes to the hypothesis that ion flux is indispensable for inflammasome activation [152, 156].

To summarize, while the occurrence of some events in response to $cSiO_2$ and other particles are generally agreed upon (i.e. lysosomal and mitochondrial damage, ROS production, ion flux), the order, timing, and requirement of such events for inflammasome activation remains unresolved.

1.2.2.7 $cSiO_2$-triggered AM dysfunction may contribute to ELS neogenesis.

Studies performed in our lab and others identify a link between $cSiO_2$ exposure and the development of ELS [4, 158, 159, 160], sometimes termed tertiary lymphoid organs (TLO), or inducible bronchus associated lymphoid tissue (iBALT) when localized to the lung [36]. In the first section of this Chapter (Silica, Lupus, and Dietary Omega-3 Fatty Acids), we reviewed the impact of type I IFN signaling on ectopic lymphoid development. In this section, we will focus on potential mechanisms hinging on the role of AMs.

A recent review suggests that ELS develops resulted from inflammatory cytokine-driven activation and proliferation of local fibroblasts leading to chemokine production and recruitment of immune cells, including DCs, B cells, and T cells [161]. These recruited lymphoid cells adopt an organized structure, that can include the formation of high endothelial venules (specialized blood vessels present that allow efficient lymphocyte recruitment to lymphoid organs [162]) and lym-

phatic vessels [163]. The progression of these events requires sustained inflammatory signaling, which, as described, is consistent with *in vivo* models of $cSiO_2$ exposure [4]. The activation of and damage to AMs by $cSiO_2$, as described above, may serve as a key event contributing to ELS development.

Fibroblast activation. The first step of ELS development, fibroblast activation, is also critical to development of fibrosis. Fibrosis is a defining trait of silicosis, the most recognizable lung pathology caused by $cSiO_2$ inhalation [14]. The cytokine TGFβ, which promotes pulmonary fibrosis [164], is expressed in high levels in the lung following exposure to $cSiO_2$ [165]. Transient overexpression of IL-1β, released from AMs following $cSiO_2$-triggered inflammasome activation, has been shown to trigger TGFβ expression in the lung [166]. Furthermore, IL-1β can increase ITGB8 on lung fibroblasts, which is an integrin the converts latent TGFβ to its active form [167]. Human studies of patients with idiopathic pulmonary fibrosis have documented T- and B-cell aggregates, pointing to a potential interaction between ELS and development of fibrosis [168].

Immune cell recruitment. Since AMs regulate migration and activation of other immune cells under homeostatic conditions [92], damage to or dysfunction of these cells could influence immune cell recruitment and function. For example, AM depletion results in increased migration and antigen presentation capacity of DCs [169, 170, 171]. Also, in an *in vivo* model of allergic asthma, introducing AMs from non-asthmatic mice reduced dendritic cell uptake of antigens and the number of antigen-containing DCs in the draining lymph node [172]. Furthermore, AMs induce the development of $FoxP3^+$ T-regulatory cells in the absence of inflammatory stimuli, which is an important mechanism in promoting airway tolerance to inhaled allergens [173].

Putative model of $cSiO_2$-induced ELS development. Work from our lab and others suggest that IL-1α released following AM injury may contribute to the development of ELS [159, 138]. IL-1α released by dying AMs following exposure to inhaled particles contributes to DC migration, which was shown to be crucial to particle-triggered development of iBALT [138]. Similar results

were observed by Neyt et al. in the context of influenza infection: intratracheal administration of IL-1α exacerbated iBALT formation while infected Il1r-/-, which lack the IL-1 receptor, did not develop iBALT in response following infection [174]. IL-1α release may also promote expression of chemokines that recruit immune cells to ELS. Neyt et al. [174] found that gene expression of *Cxcl13*, a chemokine also known as B-cell chemoattractant and implicated in the development of ELS, was reduced in Il1r-/-, further suggesting a role for IL-1α in ELS development.

Recently published findings from our lab in which lupus-prone animals were subjected an acute exposure to $cSiO_2$ are consistent with the proposed pathway of AM cell death $\rightarrow$ IL1α release $\rightarrow$ CXCL13 expression $\rightarrow$ ELS formation. Specifically, we observed a decrease in macrophage cell counts 1 d following $cSiO_2$ instillation, high levels of IL-1α in the BALF sustained throughout the 28 d experiment, an increase in *Cxcl13* gene expression peaking at 14 d post-instillation, and infiltration of T-cells at 14 d post-instillation and B-cells 21 d post-instillation [159]. We observed that the number of macrophages rapidly returned to and then exceeded the number observed in vehicle-instilled animals, likely due to recruitment of monocyte-derived macrophages. Chronic exposure studies from our lab find that *Cxcl13* gene expression is markedly increased in the lungs of mice beginning at 9 wk following the final intranasal instillation with $cSiO_2$ and continuing to rise at 13 wk post-instillation, mirroring the increase in recruited macrophages [175]. This is consistent with the timing of the appearance of B-cells, T-cells, and follicular DCs in the lung, and with the induction of autoantibodies in the bronchoalveolar lavage fluid [4]. Taken together, our findings are consistent with the hypothesis that $cSiO_2$-induced damage to AMs triggers ELS neogenesis.

1.2.3 Can DHA protect AMs from $cSiO_2$-induced toxicity?

1.2.3.1 Clinical and preclinical evidence that ω-3 HUFAs benefit lung health.

There is extensive preclinical and clinical evidence that supplementation with dietary ω-3 HUFAs EPA and DHA can protect against inhaled particles [176, 177, 178, 179, 180]. Importantly, work

from our lab and others has further shown that ω-3 supplementation can be effective when initiated after particle exposure, indicating that this intervention has the potential to be used both prophylactically and therapeutically [178, 181]. ω-3 supplementation has been demonstrated to be efficacious for other lung pathologies as well, such as asthma [182] and chronic obstructive pulmonary disease [183]. A meta-analysis published earlier this year analyzing data from three population-based cohort studies (the Multi-Ethnic Study of Atherosclerosis (MESA), the Framingham Heart Study, and the Age, Gene/Environment Susceptibility-Reykjavik Study (AGES-Reykjavik)) identified that higher blood DHA levels were associated with a lower risk of hospitalization or death due to interstitial lung disease and fewer lung imaging abnormalities [184], further contributing to a protective role for DHA in the lung.

As discussed in Section 1.2.1 (Silica, Lupus, and Dietary ω-3 Fatty Acids) dietary supplementation with DHA ameliorates immune cell infiltration in the lung, ELS neogenesis, cytokine and autoantibody levels in the BALF and plasma, inflammatory and autoimmune gene expression in multiple organs, and the development of glomerulonephritis [4, 7, 39]. While ω-3 HUFAs influences multiple immune cells [185], many of which are implicated in the development of autoimmune diseases, this section specifically will focus on how EPA and DHA modulate the inflammatory response in the macrophage, and how this may protect against cSiO_2-induced toxicity.

1.2.3.2 DHA and EPA alter phospholipid profiles of AMs.

ω-3 and ω-6 PUFAs are termed "essential" as they must be obtained in the diet due to the inability of humans to synthesize these fats endogenously [186]. Ingested fats are primarily in the form of triglycerides, which are broken down to free fatty acids in the intestine and taken up by intestinal epithelial cells, where they are packaged into chylomicrons to be circulated throughout the body. From here, they can be used in individual tissues as fuel or deposited in the adipose tissue for storage. Dietary fatty acids are incorporated into the phospholipid membrane via the Land's Cycle, in which a fatty acid is cleaved from a phospholipid by phospholipase A2 (PLA2) to generate a free fatty acid and a lysophospholipid. The lysophospholipid is then able to accept a new acylated fatty

acid, which is catalyzed by a lysophospholipid acyltranserase [187]. William Lands (for whom the Land's Cycle is named) also found that acyltransferases preferentially incorporate PUFAs into the sn-2 position of the phospholipid (that is, the second carbon in the triglyceride backbone) [188]. ω-3 and ω-6 PUFAs are incorporated at a similar rate, which makes their presence in most tissue membranes highly dependent on their availability in the diet [189].

Dietary consumption of ω-3 HUFA-containing food or supplements results increases ω-3 HUFA levels in human samples, including serum and plasma phospholipids, red blood cells, and platelets [190, 191, 192, 193]. ω-3 HUFAs can also be enriched in immune cells, including immune cells and their precursors, including mononuclear cells, neutrophils, monocytes, T-cells, and B-cells [194, 195, 196, 191, 193]. Modulating the membrane lipid composition can change its physical properties, potentially altering the immune response (**Figure 1.6**). ω-3 HUFAs have been shown to increase membrane fluidity and elasticity [197, 198, 199, 200], which may influence processes such as phagocytosis and LMP. Furthermore, ω-3 and ω-6 HUFAs in the membrane can act as substrates for the production of downstream metabolites, including pro-inflammatory lipid mediators (leukotrienes, prostaglandins, thromboxanes) and SPMs (resolvins, maresins, protectins, lipoxins) [31, 84]. SPMs very likely play a role in ω-3 HUFA-dependent protection against cSiO_2-induced toxicity. Detailed information about SPMs' mechanisms of actions can be found in several excellent reviews [201, 202, 84, 203].

1.2.3.3 DHA and EPA improve phagocytosis and efferocytosis.

Early studies into the effects of unsaturated fatty acids on phagocytosis found that increasing the degree of unsaturation in the membrane enhanced phagocytosis, regardless of whether the membrane was enriched with ω-3 or ω-6 PUFAs [204, 205]. However, more recent work suggests that much of the DHA- or EPA-mediated effects on phagocytosis are through the actions of downstream metabolites. For example, a recent study demonstrated that incubating human PBMCs in commercially available fish oil supplements enhanced phagocytosis, but that this could be reversed by inhibiting enzymes involved in production of ω-3 derived metabolites [206]. Among these metabolites are

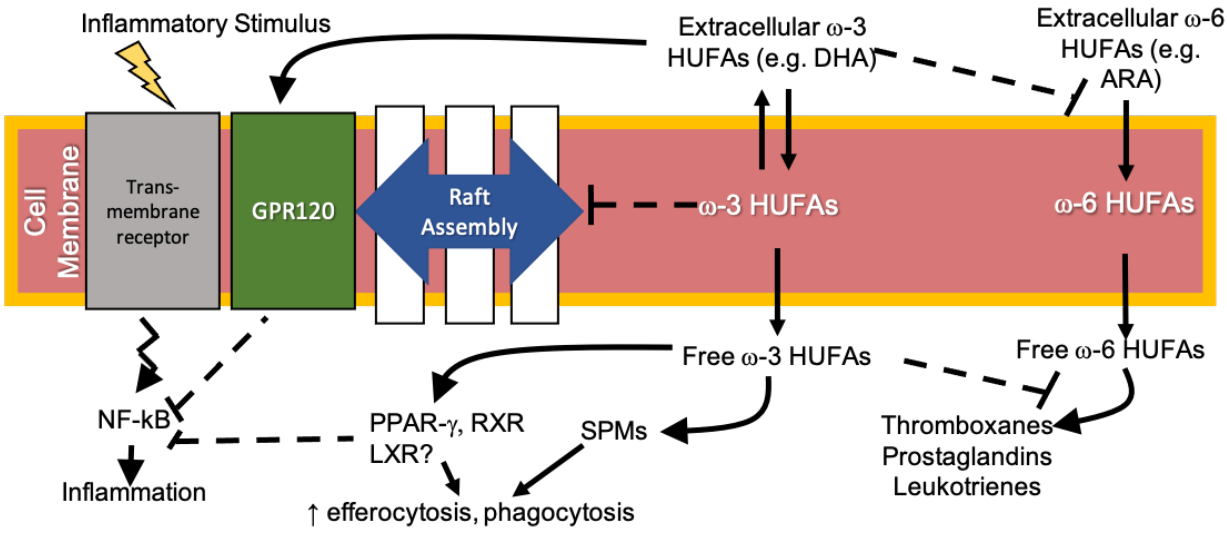


Figure 1.6: Putative anti-inflammatory mechanisms of ω-3 HUFAs. Within the membrane, the ω-3 highly unsaturated fatty acids (HUFAs) EPA and DHA influence lipid raft formation, inhibiting the aggregation of receptors involved in pro-inflammatory signaling. HUFAs can also be cleaved from the membrane, both extracellularly and intracellularly by phospholipases. Free EPA and DHA activate transmembrane receptors involved in blocking pro-inflammatory signaling pathways, such as GPR40 and GPR120, as well as the nuclear receptor PPARγ, which can inhibit NF-κb dependent transcription. Both EPA and DHA can be metabolized to downstream specialized pro-resolving mediators (SPMs) which also inhibit inflammatory signaling pathways. EPA and DHA can directly compete with arachidonic acid for incorporation into the cell membrane, as well as for metabolism to downstream inflammatory eicosanoids. *Adapted from Calder 2017.* [31]

the SPMs resolvin D1 (RvD1) and resolvin E1 (RvE1), which improve phagocytosis *in vitro* and bacterial clearance *in vivo* in mice [207, 208]. Similar results have been observed *in vitro* with human monocyte derived macrophages [209].

ω-3-derived lipid metabolites also promote efferocytosis, which is crucial in the resolution of inflammation. A series of studies has identified that 1) RvD1 is reduced while thromboxanes are increased in necrotic areas of atherosclerotic plaques [77], 2) thromboxanes released from necrotic cells impair efferocytosis [210], and 3) RvD1 stimulates efferocytosis of necrotic cells by promoting fatty acid oxidation and oxidative phosphorylation [211, 210]. RvD1 has also been shown to promote efferocytosis by macrophages in the lung following ischemia/reperfusion (I/R)-induced lung injury, resulting in decreased neutrophil infiltration. In the same study, the researchers found that mediators released from senescent cells impaired efferocytosis, but that this could be reversed

with RvD1 treatment *in vitro* [212]. A similar I/R lung injury model demonstrated that another D-series resolvin, RvD5, also promoted efferocytosis by increasing expression of phospholipase D2 (PLD2) [213]. Previous work has shown that PLD1 and PLD2 are involved in actin polymerization and cell protrusion [214], and they coordinate to facilitate phagocytosis [215].

A recently published study from Dr. Pestka's laboratory has shown that supplementing RAW 264.7 macrophages with DHA prior to triggering apoptotic cell death results in enhanced uptake of apoptotic cells by AM-like MPI cells *in vitro* [216] and by AMs *in vivo* (unpublished). Interestingly, supplementing MPI cells did not improve their ability to engulf apoptotic cells. DHA supplementation prior to inducing apoptosis may result in RvD1 release by the apoptotic cells, as observed by necrotic cells in atherosclerotic plaques discussed above [210]. Another hypothesized mechanism for DHA-enhanced clearance is through increased oxidation of PUFA groups within phosphatidylserine (PS) exposed on the apoptotic cell surface, which is a recognized "eat me" signal on apoptotic cells [217, 218, 219]. A 2014 study [220] found that increasing the PUFA content (namely, linoleic acid, C18:2n6) at the sn2 position of phosphatidylserine resulted in oxidized PS products at the expense of PS-bound linoleic acid. This corresponded with enhanced efferocytosis of apoptotic cells induced by H_2O_2 exposure. Furthermore, selective cleavage of oxidized PS by lipoprotein-associated PLA2 resulted in impaired efferocytosis. DHA has six double bonds and is also incorporated at the sn2 position of the phospholipid, thus DHA supplementation likely augments levels of oxidized PS in a manner similar to linoleic acid supplementation. In support of this hypothesis, preliminary investigations performed in our laboratory suggest that lipoprotein-associated PLA2 can similarly reverse the increase in efferocytosis of apoptotic cells supplemented with DHA (unpublished).

1.2.3.4 DHA and EPA can modulate lipid raft formation.

Increasing ω-3 fatty acids in the phospholipid membrane influences the presence and composition of lipid rafts, which are cholesterol-enriched domains of the membrane with increased order and rigidity (tighter packing and decreased fluidity) [221, 198]. Lipid rafts can act to organize or ag-

gregate membrane bound proteins, thus influencing signaling pathways initiated by transmembrane receptors. Multiple immunological events depend on lipid raft formation, including IgE receptor signaling and T- and B-cell receptor activation [222, 223]. Studies in cancer cells have found that ω-3-mediated changes to lipid rafts can suppress oncogenic signaling pathways and tumor growth [224, 225].

In macrophages, lipid rafts facilitate aggregation of receptors involved in inflammatory signaling pathways, such as TLR4 and the IFNγ receptor IFNAR1. In macrophages, *in vitro* treatment with EPA and DHA inhibited recruitment of CD14 and TLR4 into lipid rafts without changing their total surface expression [226, 227, 69]. These studies also showed a reduction in TLR4 dimerization [69] and interactions between TLR4 and CD14 [227, 228], ultimately resulting in reduced NF-κB activation and inflammatory gene transcription. DHA also reduced the presence of IFNγR1 in lipid rafts without changing its surface expression [229]. This study, performed in the context of *M. tuberculosis* infection, found that these changes led to impaired phagolysosomal maturation and inability to control bacterial replication. Other studies *in vivo* have found that ω-3 HUFAs impair IFNγ signaling [230]. While this response is undesirable in the context of bacterial infection, it may be beneficial in the context of lupus and other autoimmune diseases characterized by excessive IFN signaling [42].

1.2.3.5 Impact of DHA and EPA on cell death.

Cytoprotective effects of ω-3 HUFAs *in vivo*. Just as $cSiO_2$ triggers cell death through various pathways, ω-3 HUFAs have been shown to prevent multiple forms of cell death. In a 2021 study, rats fed ω-3 HUFAs prior to administration of the chemotherapeutic methotrexate had decreased apoptosis in enterocytes, which was coupled with reduced intestinal injury and a reduction in inflammatory biomarkers in the intestinal mucosa [231]. In another study, decreased levels of pyroptosis in the liver following I/R injury in rats fed a DHA-enriched diet was attributed to activation of the PI3K/AKT pathway, which promotes cell survival and proliferation [232]. In FAT-1 mice, which have augmented levels of endogenous ω-3 HUFAs due to expression the *C. elegans*

FAT-1 ω-3 fatty acid desaturase [233], apoptotic cell death was reduced compared to WT mice following traumatic brain injury or cerebral microinfarction [234, 235]. This was associated with a reduction in ROS. Similar findings have been observed for mice on fish-oil supplemented diets [234]. To summarize, the cytoprotective effects of DHA and EPA in these studies are primarily mediated by a decrease in inflammatory gene expression and attenuation of ROS levels, both of which are discussed in greater detail below.

Cytotoxic effects of ω-3 HUFAs on cancer cells *in vitro*. There are many studies that report cytotoxic effects of ω-3 HUFAs on cancer cells. *In vitro* cancer cells appear to be particularly sensitive to DHA- and EPA-induced cell death (typically administered at 50-200 μM) [236, 237, 238]. Similar concentrations applied to primary immune cell populations *in vitro* can inhibit inflammatory cytokine production and cell death (25-100 μM), but high concentrations (exceeding 200 μM) can still have cytotoxic effects [239, 231, 232, 238, 240]. The finding that moderate concentrations of ω-3 PUFAs may preferentially target cell death in tumor cells, but not primary cells, has exciting implications for cancer research.

1.2.3.6 Reduction in oxidative stress by EPA and DHA.

While low to moderate levels of ROS play critical roles in regulating cell function and homeostasis, excess production results in damage to the cell through modifications to DNA, proteins, and lipids. High levels of ROS are associated with chronic inflammatory disorders, including cardiovascular disease, cancer, and neurodegenerative disorders [241]. As discussed previously, environmental toxicants such as $cSiO_2$ can trigger ROS development beyond what the cell is equipped to handle, and likely plays a major role in connecting $cSiO_2$ to the development of multiple pathologies.

ω-3 PUFA supplementation *in vitro* and *in vivo* reduces intracellular ROS levels [235, 242] and specifically nitric oxide levels [243, 244]. The antioxidant activity of ω-3 PUFAs may be mediated in part by their ability to reduce inducible nitric oxide synthase (iNOS) expression [245, 243, 244, 246] and promote expression and activity of antioxidant proteins such as glutathione peroxidase,

heme oxygenase, catalase, and NADPH:quinone oxidoreductase [247, 248, 242]. These effects might attributed to activation of NRF2, a transcription factor that promotes expression of multiple proteins with anti-oxidant capabilities [249, 250, 244]. As noted in the previous section, ROS levels increase in the lung following particle exposure [115], and are also involved in activating the NLRP3 inflammasome [140]. Notably, both rodent and human studies show that ω-3 PUFAs can protect against ROS induced by cigarette smoke [251, 180], PM2.5 [176, 177, 179], and synthetic particles [178].

An argument that has been put forth against the use of ω-3 PUFA supplementation is their potential to increase levels of lipid peroxidation [252]. The variety of methods for assessing the presence of ROS has resulted in opposing claims regarding the impact of ω-3 PUFAs on oxidative stress. Some studies show that supplementation with ω-3 PUFAs may increase markers of lipid peroxidation [253, 252], yet numerous other studies link the beneficial effects of ω-3 PUFAs to their antioxidant capabilities [254, 247, 234, 248, 235, 242, 244]. Here, it is important to consider what individual markers of oxidative stress may reveal about the redox state of the cell. An increase in markers of lipid peroxidation indicate that lipids have been oxidized at the expense of another molecule that may have more detrimental effects when oxidized, such as DNA. Consistent with this hypothesis, DHA and EPA have been shown to have modest free radical scavenging activity [248] and studies reporting lipid peroxidation with ω-3 HUFAs report concomitant decreases in inflammatory markers [255, 253].

1.2.3.7 EPA and DHA promote inhibition of NF-κB through transmembrane and nuclear receptors.

GPR120. The G-protein coupled receptor GPR120 (gene symbol *Ffar4*) has been termed "the ω-3 fatty acid receptor", as it is activated by ω-3 HUFAs DHA and EPA. This receptor has insulin sensitizing effects mediated by its expression in the gut and adipose tissue, and anti-inflammatory effects mediated by its expression on macrophages and other immune cells [256]. GPR120 is expressed by immune cells, including AMs, in both the murine and human lung [257, 258].

Oh et al. [259] reported that DHA and EPA block TLR and TNF-alpha signaling pathways in RAW 264.7 and peritoneal macrophages through activation of GPR120. Here, the authors found that ligand binding caused receptor-associated β-arrestin 2 to prevent interaction of the proteins TAK1 and TAB1, which is required for downstream NF-κB activation. The inhibitory effect of GPR120 activation on LPS-induced gene expression was confirmed by Yan et al. [73], who also showed that adding DHA could also inhibit both the priming and activating steps of inflammasome activation in a β-arrestin 2-dependent manner.

Studies have reported that GPR120 is necessary for both the neuro- and hepatoprotective effects of ω-3 PUFAs [260, 261, 262]. These effects were reported to be mediated through inhibition of inflammasome activation [260] and inflammatory gene expression [262] in microglia, apoptosis in neurons [262], and NF-κB activation in Kupffer cells [261]. ω-3 HUFAs also suppress inflammatory signaling pathways through GPR120 in other cell types, including DCs, adipocytes, intestinal epithelial cells, and hypothalamic neurons [263, 186].

A recent study found that intranasal administration of a GPR120 agonist improved airway resistance in mice exposed to ozone, cigarette smoke, and house dust mite [257]. This protective response was not observed in mice that did not express the receptor. The GPR120 agonist also decreased immune cell infiltration and inflammatory gene expression in animals exposed to cigarette smoke and ozone. The authors observed expression of GPR120 on CD11c-, Siglec F-, and GR-1-expressing cells in the BALF, which includes AM, DCs, and monocytes. Staining of lung sections found high GPR120 expression in the epithelium of the mid and lower airways and in the airway smooth muscle cells. Taken together, these results suggest that GPR120 activation is likely involved in the anti-inflammatory effects of ω-3 HUFAs in the lung.

GPR40. The other recognized receptor EPA and DHA is GPR40 (gene symbol *Ffar1*). This receptor is not as ubiquitously expressed as GPR120 [258], yet it appears to play similar roles [186]. Like GPR120, GPR40 promotes insulin sensitivity. The anti-inflammatory actions of GPR40 are less well-described. Though Oh et al. reported minimal GPR40 expression in adipose tissue, peri-

toneal macrophages, bone marrow-derived macrophages, and RAW 264.7 macrophages [259], Yan et al. found that GPR40 is expressed in THP-1 cells, and that silencing its expression reduced the ability of DHA to inhibit inflammasome activation [73]. GPR40 has also been reported to mediate EPA-dependent neuroprotection, as EPA's inhibitory effects on inflammasome activation in microglial cells are absent in GPR40$^{-/-}$ mice [260]. Others have reported that activation of GPR40 in neutrophils can promote their chemotaxis, phagocytosis, and release of pro-resolving lipid mediators during *E. coli* infection [264].

PPARγ. Another anti-inflammatory mechanism of ω-3 HUFAs that is likely at play in AMs is via binding the nuclear receptor PPARγ [31]. PPARγ is expressed at high levels in AMs relative to other macrophage populations [88]. Genes induced by PPARγ are associated with an anti-inflammatory, pro-resolving macrophage phenotype, thus allowing the AM to suppress immune activation in the alveoli [265]. Related to this, loss of PPARγ expression in the lung is associated with an exacerbated inflammatory response in animal models of influenza infection [266, 267, 268], sarcoidosis [269], and sepsis [270], while administration of PPARγ agonists piaglitazone reduced NF-κB and inflammatory gene expression in a mouse model of sepsis [271].

Both ω-3 HUFA and their metabolites are believed to be endogenous ligands for PPARγ [31]. *In vitro* studies in macrophages show that ω-3 HUFA-driven polarization to an M2-like phenotype [272] as well as suppression of NF-κB signaling [273, 274] depends in part on PPARγ. There are multiple putative mechanisms proposed for how PPARγ mediates its immunomodulatory effects, including direct induction of pro-resolving genes and interacting with NF-κB to promote its degradation, preventing NF-κB from binding to DNA, or acting as a transcriptional repressor to DNA-bound NF-κB [74, 275].

Activation of PPARγ target genes requires heterodimerization of PPARγ with the retinoid x receptor (RXR) [276, 277], which itself is a proposed target of DHA [278]. RXR can also heterodimerize with the liver X receptor (LXR). Many of the actions of LXRs and LXR:RXR heterodimers overlap with PPARγ, including induction of lipid metabolism and anti-inflammatory

genes and trans-repression of inflammatory transcription factors [276, 279]. Though a role for LXRs and RXRs in mediating the effects of ω-3 HUFAs has been proposed, it is unclear if this is possible in the absence of PPARγ.

1.2.4 Conclusion

In conclusion, many mechanisms of toxicity triggered by $cSiO_2$ in AMs, including ROS production, inflammatory gene expression, increased cell death, and impaired clearance of dead cells, may be reversed by dietary ω-3 HUFAs (**Table 1.2**). Investigation into these mechanisms will provide additional insight into how dietary DHA can protect against $cSiO_2$-triggered autoimmune disease development in lupus-prone NZBWF1 mice. The literature reviewed here as well as the data presented in subsequent chapters of this thesis improve our understanding of the role of two elements of the exposome, which can be modified by dietary and lifestyle changes to ameliorate disease.

Table 1.2: Cellular events induced by $cSiO_2$ and suppressed by DHA.

	$cSiO_2$	DHA
Apoptosis	↑	↓
Pyroptosis	↑	↓
Oxidative stress	↑	↓
Inflammasome activation	↑	↓
Inflammatory gene expression	↑	↓
Efferocytosis	↓	↑

CHAPTER 2

INFLUENCE OF TOTAL WESTERN DIET ON DOCOSAHEXAENOIC ACID SUPPRESSION OF SILICA-TRIGGERED LUPUS FLARING IN NZBWF1 MICE

Gilley KN[1,2], Wierenga KA[1,3,4], Chauhan PS[2], Wagner JG[4,5], Lewandowski RP[5], Lock AL[6], Harkema JR[4,5], Benninghoff AD[7], Pestka JJ[2,4]

[1]These authors contributed equally to this work

[2]Department of Food Science and Human Nutrition, Michigan State University, East Lansing, MI

[3]Department of Biochemistry and Molecular Biology, Michigan State University, East Lansing, MI

[4]Institute for Integrative Toxicology, Michigan State University, East Lansing, MI

[5]Department of Pathobiology and Diagnostic Investigation, Michigan State University, East Lansing, MI

[6]Department of Animal Science, Michigan State University, East Lansing, MI

[7]Department of Animal, Dairy and Veterinary Sciences and USTAR Applied Nutrition Research, Utah State University, Logan, UT

Author Contributions: KW and KN: study design, data analyses/interpretation, manuscript preparation. PS, JW, RL: data analysis/interpretation. AL: fatty acid analysis. JH, AB: data analysis/interpretation, manuscript preparation. JP: planning, coordination, oversight, manuscript preparation/submission, and project funding.

Originally published in PLoS ONE :

https://doi.org/10.1371/journal.pone.0233183

2.1 ABSTRACT

Lupus is a debilitating multi-organ autoimmune disease clinically typified by periods of flare and remission. Exposing lupus-prone female NZBWF1 mice to crystalline silica ($cSiO_2$), a known human autoimmune trigger, mimics flaring by inducing interferon-regulated gene (IRG) expression, inflammation, ectopic lymphoid structure (ELS) development, and autoantibody production in the lung that collectively accelerate glomerulonephritis. $cSiO_2$-triggered flaring in this model can be prevented by supplementing mouse diet with the ω-3 polyunsaturated fatty acid (PUFA) docosahexaenoic acid (DHA). A limitation of previous studies was the use of purified diet that, although optimized for rodent health, does not reflect the high American intake of saturated fatty acid (SFA), ω-6 PUFAs, and total fat. To address this, we employed here a modified Total Western Diet (mTWD) emulating the 50th percentile U.S. macronutrient distribution to discern how DHA supplementation and/or SFA and ω-6 reduction influences $cSiO_2$-triggered lupus flaring in female NZBWF1 mice. Six-week-old mice were fed isocaloric experimental diets for 2 wk, intranasally instilled with $cSiO_2$ or saline vehicle weekly for 4 wk, and tissues assessed for lupus endpoints 11 wk following $cSiO_2$ instillation. In mice fed basal mTWD, $cSiO_2$ induced robust IRG expression, proinflammatory cytokine and chemokine elevation, leukocyte infiltration, ELS neogenesis, and autoantibody production in the lung, as well as early kidney nephritis onset compared to vehicle-treated mice fed mTWD. Consumption of mTWD containing DHA at the caloric equivalent to a human dose of 5 g/d dramatically suppressed induction of all lupus-associated endpoints. While decreasing SFA and ω-6 in mTWD modestly inhibited some disease markers, DHA addition to this diet was required for maximal protection against lupus development. Taken together, DHA supplementation at a translationally relevant dose was highly effective in preventing $cSiO_2$-triggered lupus flaring in NZBWF1 mice, even against the background of a typical Western diet.

2.2 INTRODUCTION

Systemic lupus erythematosus (lupus) is a devastating multi-organ autoimmune disease (AD) that adversely affects 1.5 million Americans, primarily women of child-bearing age [9]. While

the genome is a primary predisposing factor for lupus, it is now recognized that environmental exposures over a lifetime can exacerbate or ameliorate disease activity [280, 19]. The initiating step in lupus is loss of tolerance to nuclear self-antigens, resulting in production of autoreactive antibodies and formation of circulating immune complexes [9]. These complexes deposit in the tissues, where they promote activation and infiltration of circulating mononuclear cells leading to organ damage. In the kidney, this manifests as glomerulonephritis that, if left untreated, culminates in end-stage renal failure. Lupus patients typically experience quiescent periods with low disease activity intermittently interrupted by episodes of disease flaring marked by increased symptom severity and active organ damage [281].

Genome-driven mouse models of lupus have been used to elucidate mechanisms of disease pathogenesis and to evaluate efficacy of interventions [282]. Similar to human lupus, female NZBWF1 mice are more likely to develop lupus than their male counterparts [283]. These mice display steady, gradual expansion of autoreactive B and T cells, proinflammatory cytokine and chemokine expression, elevations of autoantibodies, and development of organ damage, thus mimicking the periods of remission in human lupus that precede flaring. Also similar to human lupus, flare-associated disease activity can be initiated and organ damage accelerated in these models by several triggers, including UV exposure [284, 285], epidermal injury [286], and interferon (IFN)-α-expressing adenovirus injection [158, 56, 287].

Exposure to the respirable toxicant crystalline silica ($cSiO_2$) dust is also a known trigger of lupus and other ADs in humans and animals (reviewed in [288, 289, 290]). In lupus-prone female NZBWF1 mice, intranasal instillation with $cSiO_2$ mimics flaring by triggering autoimmunity onset three months earlier than controls [175, 3]. When introduced into the lungs, $cSiO_2$ initiates chronic sterile inflammation that progresses from local to systemic autoimmunity [291]. Due to their small size (approximately 2 μm), $cSiO_2$ particles deposit in the alveoli where alveolar macrophage phagocytose them, ultimately triggering phagolysosome permeabilization. This in turn activates the inflammasome resulting in IL-1β and IL-18 release, as well as cell death by pyroptosis, apoptosis, and necrosis [292, 124]. Because of the slow clearance of $cSiO_2$ from the

lung, particles released after cell death are again phagocytosed, evoking a vicious cycle of inflammation and cell death. In $cSiO_2$-instilled female NZBWF1 mice, we observed the development of ectopic lymphoid structures (ELS) and autoantibodies in bronchoalveolar lavage fluid (BALF) and plasma [4, 3]. Circulating autoantibodies bind their cognate autoantigens resulting in immune complexes that deposit in the kidney, promoting inflammation. Collectively, findings in NZBWF1 mice confirm that, following airway exposure to $cSiO_2$, the lung serves as a nexus triggering flares of systemic autoimmunity and glomerulonephritis.

Conventional treatments for managing lupus, such as glucocorticoids, have considerable adverse effects, while newer immunotherapies are expensive and benefit only a sub-population of lupus patients [293]. Therefore, new interventions to prevent or delay lupus flaring are needed. Results of human and animal studies suggest that consumption of ω-3 PUFAs from marine sources can both prevent and resolve inflammation and autoimmune disease, as reviewed previously [32, 31, 23]. At the mechanistic level, ω-3 PUFAs modulate immune function by altering; 1) ω-6 incorporation into phospholipids, 2) production of bioactive lipid mediators; 3) intracellular signaling, transcription factor activity, and gene expression; and, 4) membrane structure and ultimately function [31]. These mechanisms may be at play in the protective effects seen in human lupus trials employing ω-3 supplementation [294, 295, 296]. Relative to animal studies, we previously assessed the impact of supplementing purified rodent diet with ω-3 PUFA docosahexaenoic acid (DHA) on genome-driven autoimmunity in female NZBWF1 mice [35]. Dietary DHA dose-dependently increased ω-3 PUFA content in the erythrocytes, lungs, kidneys, and spleen while also suppressing the $cSiO_2$-triggered the triggered inflammatory response. Remarkably, the decrease in inflammatory response correlated with reduced $cSiO_2$-triggered leukocyte infiltration in the kidneys and resultant glomerulonephritis [4, 175, 7].

To better parallel human food consumption in rodent feeding studies, the total Western diet (TWD) was formulated to emulate typical American intakes of macro- and micro-nutrients on an energy density basis for rodents [297, 298]. The TWD is based on 50th percentile intakes reported in the Centers for Disease Control National Health and Nutrition Examination Survey (NHANES)

for 2007–2008, which were adjusted for differences in caloric intake. Overall, the TWD is not necessarily extreme in the level of any given nutrient, but rather reflects the overall U.S. dietary pattern. The TWD has fewer calories from protein and carbohydrate sources and twice that from fat as compared to the AIN-93G diet, the standard diet fed to rodents in nutritional studies to date. The new TWD diet contains more SFA and monounsaturated fatty acids (MUFAs), less PUFAs, more complex carbohydrates, and twice the level of simple sugars. As such, the TWD better represents typical U.S. nutrition intakes, making it very useful for studies employing animal models of human health and disease [299]. Here, we employed a modified TWD (mTWD) based on U.S. macronutrient intake to assess the impact of DHA supplementation with or without SFA and ω-6 PUFA reduction on $cSiO_2$-induced lupus endpoints in NZBWF1 mice. The findings reported herein provide important new insights into the translatability of DHA's effects on lupus flaring in this novel mouse model.

2.3 MATERIALS AND METHODS

2.3.1 Animals.

Experimental animal procedures were reviewed and approved by Michigan State University's Institutional Animal Care and Use Committee (AUF # PROTO201800113) in accordance with the guidelines of the National Institute of Health. Female lupus-prone NZBWF1 mice were obtained at 6 wk of age from Jackson Laboratories (Bar Harbor, ME), housed 4 per cage, and allowed free access to feed and water. Only females were included in this study, as the incidence and severity of lupus symptoms is less pronounced in male NZBWF1 mice [34]. Animals were maintained under a 12 h light/dark cycle with regulated temperature (21–24°C) and humidity (40–55%). Mice were monitored daily by animal facility staff, observed for signs of distress such as rapid heart rate and lethargy, and weighed weekly in case of unexplained weight loss. Veterinary staff was alerted to any potential issues or advised for further monitoring. Following silica installation, animals were under observation for approximately 1 h immediately following the procedure to identify any adverse events and observed again approximately 4 h post-instillation.

2.3.2 Fatty acid analyses.

Total fatty acid concentrations in diets and tissues were determined by gas liquid chromatography (GLC) as previously described [7]. Total erythrocyte fatty acids were measured by OmegaQuant Analytics LLC. (Sioux Falls, SD).

2.3.3 Diet formulation.

Table 2.1 summarizes formulations of the four isocaloric experimental diets used in this study. Since the focus of this study was on macronutrients, a modified version of the TWD (mTWD) was used as a basal diet for all experimental groups, with the modification being that micronutrients were provided by the standard AIN-93G vitamin and mineral mixes.

Table 2.1: Experimental diet formulations.

	Experimental Diet			
	CON	**↑DHA**	**↓SF.ω6**	**↓SF.ω6 ↑DHA**
Ingredient	*(g/Kg)*			
Casein	190.00	190.00	190.00	190.00
L-Cystine	2.85	2.85	2.85	2.85
Corn Starch	230.00	230.00	230.00	230.00
Maltodextrin	70.00	70.00	70.00	70.00
Sucrose	256.62	256.62	256.62	256.62
Corn oil	16.50	16.50	3.30	3.30
Soybean oil	29.40	29.40	5.90	5.90
Anhydrous milkfat	36.30	36.30	7.20	7.20
Lard	28.00	28.00	5.60	5.60
Beef tallow	24.80	24.80	5.00	5.00
Cholesterol	0.40	0.40	0.52	0.52
Cellulose	30.00	30.00	30.00	30.00
AIN-93 Mineral Mix	40.59	40.59	40.59	40.59
AIN-93 Vitamin Mix	11.60	11.60	11.60	11.60
Choline Bitartrate	2.90	2.90	2.90	2.90
TBHQ Antioxidant	0.03	0.03	0.03	0.03
Extra virgin olive oil[a]	30.00	0.00	138.00	108.00
DHA-enriched algal oil[b]	0.00	30.00	0.00	30.00

[a]Olive oil contained 678 g/kg oleic acid and 84 g/kg linoleic acid, as reported by the USDA, FDC ID 748648. [b]Algal oil contained 395 g/kg DHA and 215 g/kg oleic acid, as reported by manufacturer.

Experimental diets were prepared as follows: 1) control diet (CON) was the basal mTWD with

no other alterations; 2) DHA-supplemented diet (↑DHA) was prepared by replacing 30 g/kg of olive oil in the mTWD (composed primarily of the ω-9 monosaturated fatty acid oleic acid) with 30 g/kg DHASCO microalgal oil containing 40% DHA (provided by Dr. Kevin Hadley, Martek Biosciences Corporation Columbia, MD); 3) reduced SFA and ω-6 diet (↓SF.ω6) was prepared by replacing a portion of SFA and ω-6 in the mTWD with olive oil; and 4) ↓SF.ω6 diet supplemented with DHA (↓SF.ω6↑DHA) was prepared by supplementing with DHASCO microalgal oil as indicated above. GLC analysis confirmed the expected changes in amounts of ω-3 PUFAs, ω-6 PUFAs, and SFAs in the four experimental diets (**Table 2.2, Figure 2.1**). Experimental diets were prepared fresh biweekly, flushed with nitrogen, vacuum sealed, and stored at -20°C until use. Mice were provided fresh diet every day to prevent oxidation of the fatty acids. Palatability was assessed for the first 2 wk of the experiment to ensure proper consumption.

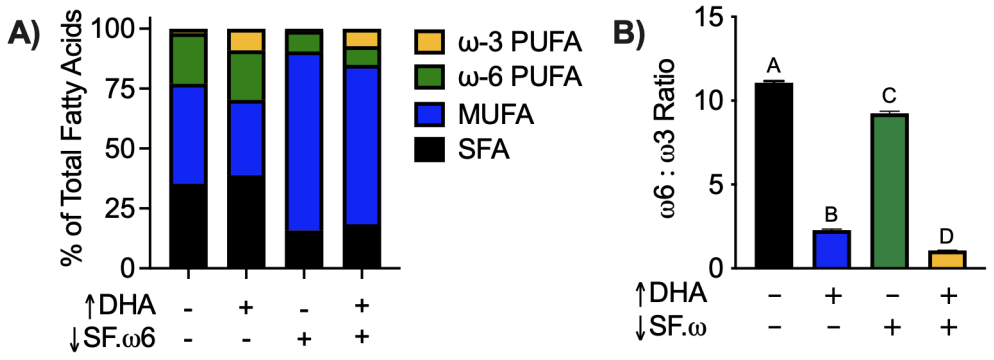


Figure 2.1: Experimental diets have unique fatty acid compositions. A. DHA supplementation (↑DHA) increased the percentage of total ω-3 PUFAs at the expense of monounsaturated fatty acids (MUFAs). Saturated fatty acids (SFAs) and ω-6 polyunsaturated fatty acids (PUFAs) were reduced in the ↓SF.ω6 diet while MUFAs were increased. **B.** Both ↑ DHA and ↓SF.ω6 diets had lower ω-6:ω-3 ratio than the control (CON) diet. Bars without the same letters differ ($p<0.001$).

2.3.4 $cSiO_2$.

$cSiO_2$ (Min-U-Sil® 5, 1.5–2.0 μm average particle size, U.S. Silica [Mapleton, PA]) was acid washed and oven-dried before addition of sterile phosphate buffered saline (PBS) [3]. Stock suspensions were prepared fresh in PBS prior to use, and suspensions were sonicated and vortexed for

Table 2.2: Fatty acid content of experimental diets as determined by GLC.

		Experimental Diet			
		CON	**↑DHA**	**↓SF.ω6**	**↓SF.ω6↑DHA**
Common Name	**Chemical Formula**	*(% of total fatty acids, mean ± SD)*			
Lauric	**C12:0**	0.65 ± 0.01^{A}	1.49 ± 0.03^{B}	0.14 ± 0.01^{C}	0.83 ± 0.01^{D}
Myristic	**C14:0**	2.87 ± 0.06^{A}	5.54 ± 0.05^{B}	0.53 ± 0.01^{C}	2.51 ± 0.02^{D}
Pentadecanoic	**C15:0**	0.29 ± 0.00^{A}	0.30 ± 0.00^{A}	0.07 ± 0.00^{B}	0.06 ± 0.00^{B}
Palmitic	**C16:0**	22.24 ± 0.16^{A}	22.63 ± 0.05^{B}	10.87 ± 0.06^{C}	11.00 ± 0.01^{C}
Palmitoleic	**C16:1ω7**	1.15 ± 0.03^{A}	1.46 ± 0.02^{B}	0.57 ± 0.02^{C}	0.84 ± 0.00^{D}
Stearic	**C18:0**	8.49± 0.04^{A}	8.26 ± 0.03^{B}	3.61 ± 0.03^{C}	3.37 ± 0.01^{D}
Oleic	**C18:1ω9**	39.19 ± 0.38^{A}	29.00 ± 0.08^{B}	72.63 ± 0.08^{C}	64.41 ± 0.03^{D}
Linoleic	**C18:2ω6**	21.07 ± 0.21^{A}	20.62 ± 0.18^{B}	8.57 ± 0.04^{C}	7.82 ± 0.04^{D}
Arachidic	**C20:0**	0.21 ± 0.03^{A}	0.17 ± 0.01^{A}	0.29 ± 0.00^{B}	0.28 ± 0.01^{B}
alpha-Linolenic	**C18:3ω3**	1.90 ± 0.03^{A}	1.81 ± 0.04^{B}	0.93 ± 0.01^{C}	0.87 ± 0.02^{C}
Behenic	**C22:0**	0.10 ± 0.01^{A}	0.11 ± 0.01^{A}	0.10 ± 0.01^{A}	0.11 ± 0.00^{A}
Lignoceric	**C24:0**	0.04 ± 0.01^{A}	0.05 ± 0.01^{A}	0.03 ± 0.00^{A}	0.05 ± 0.00^{A}
Eicosapentaenoic	**C20:5ω3**	0.00 ± 0.00^{A}	0.13 ± 0.00^{B}	0.00 ± 0.00^{A}	0.10 ± 0.01^{C}
Docosahexaenoic	**C22:6ω3**	0.00 ± 0.00^{A}	7.09 ± 0.20^{B}	0.00 ± 0.00^{A}	6.34 ± 0.08^{C}
Total SFA		35.28 ± 0.21^{A}	38.84 ± 0.05^{B}	15.80 ± 0.08^{C}	18.39 ± 0.02^{D}
Total MUFA		41.74 ± 0.36^{A}	31.49 ± 0.10^{B}	74.70 ± 0.10^{C}	66.49 ± 0.01^{D}
Total ω-3 PUFA		1.90 ± 0.03^{A}	9.04 ± 0.19^{B}	0.93 ± 0.01^{C}	7.31 ± 0.05^{D}
Total ω-6 PUFA		21.07 ± 0.21^{A}	20.62 ± 0.18^{B}	8.57 ± 0.04^{C}	7.82 ± 0.04^{D}
ω-6 : ω-3 ratio		11.07 ± 0.10^{A}	2.28 ± 0.07^{B}	9.24 ± 0.13^{C}	1.12 ± 0.01^{D}

Data presented as mean ± SD. Difference between diets compared by ordinary one-way ANOVA followed by Tukey's multiple comparison test. Unique letters indicate significant differences between groups (p<0.05). GLC, gas-liquid chromatography; SFA, saturated fatty acid; MUFA, monounsaturated fatty acid; PUFA, polyunsaturated fatty acid.

1 min before intranasal instillation of each animal.

2.3.5 Experimental design.

Figure 2.2 depicts the experimental design for this study. Briefly, groups (n = 8) of mice were fed one of the four isocaloric experimental diets beginning at 6 wk of age. 7 mice from the ↓SF.ω6↑DHA diet group were analyzed, as one animal succumbed to an unrelated illness prior to termination of the experiment. After 2 wk, groups of mice were anesthetized with 4% isoflurane and intranasally instilled with 1.0 mg $cSiO_2$ in 25 μL PBS or 25 μL PBS vehicle (VEH) as described previously [3]. Body weights were monitored weekly and urine assessed biweekly for proteinuria using clinical dipsticks (Cortez Diagnostics, Calabasas, CA). $cSiO_2$ instillation and experimental

diets did not affect body weight changes over the course of the study (**Figure 2.3**) and proteinuria was not detectable (**Supplementary Table A.6)**.

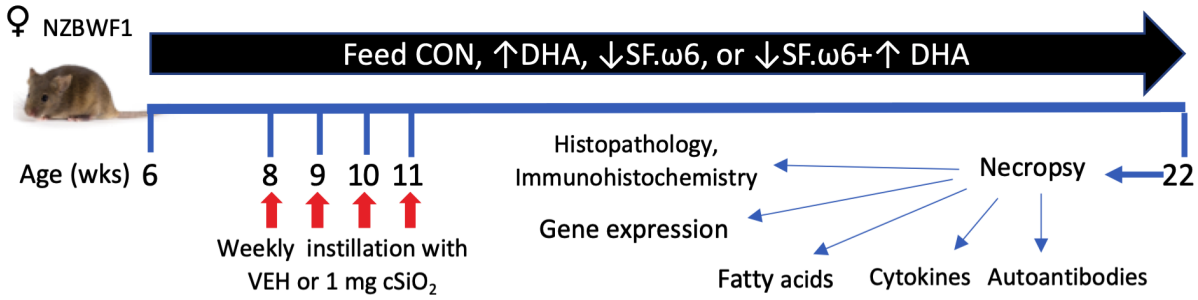


Figure 2.2: Experimental design. Feeding of experimental diets was begun in 6 wk old female NZBWF1 mice. At 8 wk of age, mice were intranasally instilled with $cSiO_2$ once per wk for 4 wk. Body weights were measured weekly, and urine was collected weekly from 18 wk of age onward to monitor the development of proteinuria. Animals were necropsied at 22 wk of age, 11 wk following the final $cSiO_2$ instillation. Plasma, bronchoalveolar lavage fluid (BALF), and tissues were collected for analysis.

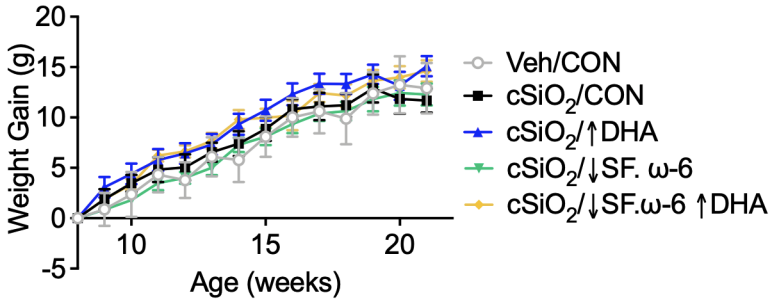


Figure 2.3: $cSiO_2$ instillation and experimental diets did not affect body weight changes over time. Mice were weighed weekly to identify differences in weight gain between diet groups. No significant differences were observed between treatment groups ($p<0.05$).

At 22 wk of age (11 wk following the final $cSiO_2$ exposure), mice were euthanized by intraperitoneal injection with 56 mg/kg body weight sodium pentobarbital and exsanguination via the abdominal aorta. This time point was selected to capture ectopic lymphoid tissue neogenesis in the lungs following $cSiO_2$ exposure prior to and during onset of glomerulonephritis based on previous studies [4, 7]. Blood was collected with heparin-coated syringes and centrifuged at 3500 *x*g for 10 min at 4°C for separation of red blood cells (RBCs) and plasma, which were then stored at

-80°C. BALF was collected from whole lungs as described previously [300] and stored at -80°C for cytokine and autoantibody analysis. The left lung lobe was fixed with 10% (v/v) neutral buffered formalin (Fisher Scientific, Pittsburgh, PA) at constant pressure (30 cm H_2O) for minimum of 1 h, stored in formalin for 24 h, and then formalin was exchanged to 30% ethanol for long term storage and further processing for histology and immunohistochemistry. The caudal lung lobe was removed, held in RNAlater (Thermo Fisher Scientific, Wilmington, DE) overnight at 4°C, then stored at -80°C for RNA analysis. The right lung, kidney, liver, and spleen were snap-frozen in liquid nitrogen and stored at -80°C for fatty acid analyses.

2.3.6 IRG expression.

Total RNA was extracted from the lung using TriReagent (Sigma Aldrich, St. Louis, MO) per manufacturer's protocol. Extracted RNA was purified with a Zymo RNA Clean and Concentrator Kit, including DNase digestion to remove any possible DNA contamination (Zymo Research, Irvine, CA, catalog number R1017). Total RNA was quantified using a NanoDrop-100 (Thermo Fisher Scientific) and reverse transcribed to cDNA at 50 ng/μL with a High Capacity cDNA Reverse Transcription Kit (Thermo Fisher Scientific, Waltham, MA). TaqMan Assays were then performed on a SmartChip Real-Time PCR System in technical triplicates for 15 IRGs and 3 housekeeping genes (*Actb, Gapdh, Hprt*). The IFN score was calculated using 15 IRGs that were significant upregulated in $cSiO_2$ treated mice relative to VEH-treated mice (*Ccl7, Zbp1, Ifi44, Ifit1, Irf7, Isg15, Mx1, Oas1, Oas2, Oasl1, Psmb8, Rsad2, Siglec1, Ccl8, Cxcl10*), as determined by Student's t-test for parametric data or Mann-Whitney U test for non-parametric data.

For each gene, the copy number relative to the average expression of *Gapdh, Hprt*, and *Actb* was calculated. First, the ΔCt was calculated for each gene by subtracting the mean Δ Ct of the two housekeeping genes from the gene of interest. The relative copy number (RCN) was calculated as previously described [301, 302] using the following equation: $RCN= 2^{(-\Delta Ct)}*100$

Missing values were replaced with ½ the minimum RCN for each gene. For example, the minimum RCN of *Zbp1* was 0.75, thus samples with missing values for *Zbp1* were assigned an

RCN of 0.37. Then, outliers within each treatment group were identified using robust outlier test (ROUT) with a *Q* value of 0.05%. After removing outliers, each gene was autoscaled by subtracting the mean expression of each sample and dividing by the standard deviation. The IFN score was calculated by summing the autoscaled expression for each gene within a given sample. All genes were given equal weight.

2.3.7 Cytokine analyses.

Cytokine levels in BALF and plasma were analyzed with Immune Monitoring 48-plex ProcartaPlex Mouse Luminex Bead-based Immunoassay (Thermo Fisher Scientific, catalog number EPX480-20834-901) according to the manufacturer's protocols at the Michigan State University Flow Cytometry Core using a Luminex 200.

2.3.8 Autoantibody ELISAs.

Autoantibody ELISA kits from Alpha Diagnostic International were utilized as per kit protocols for IgG-specific anti-double-stranded DNA (Alpha Diagnostic, San Antonio, TX, dsDNA, Catalog number 5120), and total anti-nuclear antigens (IgG + IgM + IgA) (ANA/EN, Catalog number 5210) in the BALF and plasma. Samples were read on a FilterMax F3 Multimode plate reader (Molecular Devices, San Jose, CA) at 450 nm.

2.3.9 BALF cell quantitation and identification.

Total viable cell numbers in BALF were determined by Trypan Blue exclusion. Cytological slides from BALF were prepared, allowed to air dry, and stained with Diff-Quick (Fisher Scientific). Differential cell counts for macrophages/monocytes, lymphocytes, neutrophils, and eosinophils in BALF were determined using morphological criteria from 200 total cells on cytological slides. Remaining BALF was centrifuged at 2400 *x*g for 15 min, and supernatant collected and stored at -80°C.

2.3.10 Lung histopathology.

Randomly oriented, serial sections of formalin-fixed left lung lobes were routinely processed and embedded in paraffin. Tissue sections (5 μm) were deparaffinized and stained with hematoxylin and eosin (H&E) for histopathology. Tissues were scored semi-quantitatively by a board-certified veterinary pathologist in a blinded fashion for: (a) presence of lymphoid aggregates within perivascular and peribronchiolar regions; (b) histologically evident ectopic lymphoid tissues; (c) presence of alveolar proteinosis; (d) alveolitis (defined as the increased accumulation in the alveolar parenchyma of neutrophils, lymphocytes, and mononuclear/macrophages); (e) alveolar type II epithelial cell hyperplasia; and (f) mucous cell metaplasia in bronchiolar epithelium. Lungs were individually graded for these lesions as percent of total pulmonary tissue examined based on the following criteria: (0) no changes compared to control mice; (1) minimal (<10%); (2) slight (10–25%); (3) moderate (26–50%); (4) severe (51–75%); or (5) very severe (>75%) of total area affected.

2.3.11 Immunohistochemistry and morphometry of lungs

Immunohistochemistry was performed on formalin-fixed, paraffin embedded, left lung lobe for identification of B and T cell infiltration using a anti-CD45R (1:600 rat anti-CD45R monoclonal antibody from Becton Dickinson, Franklin Lakes, NJ, catalog # 550286) and a anti-CD3 antibody (1:250 rabbit anti-CD3 polyconal antibody from Abcam, Cambridge, MA catalog # ab5690), respectively, as described previously [16, 30]. Slides were digitally scanned using a VS110 (Olympus, Hicksville, NY) virtual slide system. At least 100 images were then captured at 20X magnification using systematic random sampling with NewCast software (Visiopharm, Hoersholm, Denmark). Volume densities of $CD45R^+$ or $CD3^+$ cells in the bronchial and perivascular areas of the lungs were estimated using a point grid over the randomly sampled images with the STEPanizer 1.8 Stereology Tool. The number of points landing directly on the $CD45R^+$ or $CD3^+$ cells were counted and the volume density or percentage of $CD45R^+$ and $CD3^+$ per reference area was calculated.

2.3.12 Kidney histopathology.

Fixed kidneys were sectioned, paraffin-embedded, cut and stained with either H&E or Periodic acid-Schiff and hematoxylin (PASH), and evaluated for lupus nephritis by a board-certified veterinary pathologist using a modified International Society of Nephrology/Renal Pathology Lupus Nephritis Classification system [303]. Slide sections were graded as follows: (0) no tubular proteinosis and normal glomeruli; (1) mild tubular proteinosis with multifocal segmental proliferative glomerulonephritis and occasional early glomerular sclerosis and crescent formation; (2) moderate tubular proteinosis with diffuse segmental proliferative glomerulonephritis, early glomerular sclerosis and crescent formation; and (3) marked tubular proteinosis with diffuse global proliferative and sclerosing glomerulonephritis.

2.3.13 Statistical analysis.

Statistical analysis was performed using GraphPad Prism Version 8 (GraphPad Software, La Jolla California USA, www.graphpad.com). First, suspected outliers were verified using the ROUT with a conservative Q value of 1%, meaning that there was <1% chance of excluding a data point as an outlier in error. Data that did not meet the normality assumption as determined by the Shapiro-Wilk test ($p<0.01$) were analyzed using a the Kruskal-Wallis non-parametric test with Dunn's post-hoc test for selected multiple comparisons. Data that did not meet the equal variance assumption as determined by the Brown-Forsythe test ($p<0.01$) were analyzed by the Brown-Forsythe/Welch ANOVA with Dunnett's T3 post-hoc test for multiple comparisons. Otherwise, data meeting both normality and variance assumptions were analyzed using a standard one-way ANOVA with Sidak's post-hoc test for multiple comparisons. The groups were compared as follows:

1) VEH/CON vs. $cSiO_2$/CON; 2) $cSiO_2$/CON vs $cSiO_2$/↑DHA; 3) $cSiO_2$/CON vs. $cSiO_2$/↓SF.ω6; 4) $cSiO_2$/↑DHA vs. $cSiO_2$/↓SF.ω6↑DHA; 5) $cSiO_2$/↓SF.ω6 vs. $cSiO_2$/↓SF.ω6↑DHA; 6) $cSiO_2$/CON vs. $cSiO_2$/↓SF.ω6↑DHA.

For samples where every individual in the VEH/CON group was undetectable, a one-sample t-test was performed on the $cSiO_2$/CON group to confirm that $cSiO_2$-induced changes were signif-

icantly different from the limit of quantification. Then, the appropriate statistical test was applied to compare the remaining groups, as described above. In all instances, a significant effect of the diet group was inferred when the adjusted $p<0.05$.

2.4 RESULTS

2.4.1 DHA intake increases ω-3 PUFA content in red blood cells and tissues.

Previous studies have shown that the Omega-3 Index, obtained by measuring DHA and EPA as a percent of total RBC fatty acids, is correlated with the ω-3 PUFA content in other tissues [304, 305, 306]. We assessed this, as well as correlations between RBCs and tissues for SFAs, MUFAs, and ω-6 PUFAs. Individual tissues showed unique total fatty acid (FA) profiles, with varying degrees of similarity to each other and to RBCs. In general, correlations between RBCs and tissues were higher for ω-3 and ω-6 PUFAs than for SFAs and MUFAs (**Supplemental Figure A.1**). This is consistent previous studies demonstrating high correlations between dietary and tissue levels of fatty acids that cannot be produced endogenously, such as essential ω-3 and ω-6 PUFAs [307, 308, 309, 310]. The most consistent trend across all tissues was a concurrent decrease of the major ω-6 PUFA arachidonic acid (ARA) as DHA levels increased (**Figures 2.4 and 2.5**).

RBCs had higher levels total PUFA than tissues (40% of RBC fatty acids). The PUFA pool in RBCs was composed primarily of linoleic acid (LA), ARA, and DHA. Total ω-3 incorporation into RBCs was ∼3-fold greater in mice that consumed ↑DHA or ↓SF.ω6↑DHA diets compared to those fed CON or ↓SF.ω6 diets (**Table 2.3, Figure 2.4 A-B**). Both DHA (22:6ω3) and EPA (20:5ω3) contributed to the increase in total ω-3 PUFA. The increase in EPA observed with DHA supplementation is consistent with published studies performed *in vitro* and *in vivo* [311, 312].

In the RBCs, reducing dietary SFA and ω-6 PUFAs had only a minor impact on SFA content (approximately 4%) and reduced RBC total ω-6 levels by approximately 10%, with the greatest change observed in LA (18:2ω6). Alternatively, combining DHA supplementation with ω-6 reduction resulted in decreased RBC ω-6 content by over 50%. The decrease in ω-6 PUFAs with DHA supplementation was largely due to changes in ARA.

Table 2.3: Red blood cell fatty acid content as determined by GLC.

		VEH / CON	$cSiO_2$ / CON	$cSiO_2$ /↑DHA	$cSiO_2$ / ↓SF.ω6	$cSiO_2$ / ↓SF.ω6↑DHA
Common Name	**Chemical Formula**	*(% of total fatty acids, mean ± SD)*				
Myristic	**C14:0**	0.22 ± 0.01^{A}	0.23 ± 0.03^{A}	0.33 ± 0.06^{B}	0.13 ± 0.02^{C}	0.22 ± 0.02^{A}
Palmitic	**C16:0**	24.87 ± 0.48^{A}	25.47 ± 0.67^{A}	27.20 ± 0.49^{B}	24.71 ± 0.72^{A}	27.05 ± 0.38^{B}
Palmitelaidic	**C16:1ω7t**	0.14 ± 0.01^{A}	0.15 ± 0.01^{A}	0.14 ± 0.01^{A}	0.07 ± 0.01^{B}	0.06 ± 0.01^{B}
Palmitoleic	**C16:1ω7**	0.45 ± 0.05^{A}	0.45 ± 0.06^{A}	0.60 ± 0.08^{B}	0.32 ± 0.04^{C}	0.41 ± 0.03^{A}
Stearic	**C18:0**	16.00 ± 0.40^{A}	16.29 ± 0.84^{A}	15.83 ± 0.18^{A}	14.84 ± 0.75^{B}	13.45 ± 0.41^{C}
Elaidic	**C18:1ω9t**	0.67 ± 0.02^{A}	0.69 ± 0.04^{A}	0.62 ± 0.04^{B}	0.27 ± 0.02^{C}	0.24 ± 0.02^{C}
Oleic	**C18:1ω9**	14.77 ± 0.23^{A}	15.03 ± 0.43^{A}	12.99 ± 0.55^{B}	21.70 ± 0.19^{C}	20.00 ± 0.29^{D}
Linoelaidic	**C18:2ω6t**	0.10 ± 0.01^{A}	0.11 ± 0.01^{AB}	0.12 ± 0.03^{AB}	0.08 ± 0.01^{BC}	0.07 ± 0.01^{C}
Linoleic	**C18:2ω6**	10.83 ± 0.34^{A}	10.97 ± 0.39^{A}	14.30 ± 0.78^{B}	7.96 ± 0.35^{C}	9.70 ± 0.47^{D}
Arachidic	**C20:0**	0.14 ± 0.01^{A}	0.13 ± 0.03^{A}	0.13 ± 0.03^{A}	0.12 ± 0.03^{A}	0.11 ± 0.02^{A}
gamma-Linolenic	**C18:3ω6**	0.05 ± 0.01^{A}	0.06 ± 0.01^{A}	0.05 ± 0.01^{AB}	0.05 ± 0.00^{AB}	0.03 ± 0.01^{B}
Eicosenoic	**C20:1ω9**	0.27 ± 0.01^{AC}	0.28 ± 0.02^{ABC}	0.18 ± 0.04^{C}	0.49 ± 0.06^{B}	0.29 ± 0.03^{AB}
alpha-Linolenic	**C18:3ω3**	0.08 ± 0.01^{AB}	0.08 ± 0.01^{B}	0.09 ± 0.01^{B}	0.04 ± 0.01^{AC}	0.04 ± 0.01^{C}
Eicosadienoic	**C20:2ω6**	0.29 ± 0.03^{A}	0.30 ± 0.03^{A}	0.30 ± 0.03^{A}	0.21 ± 0.01^{B}	0.18 ± 0.01^{B}
Behenic	**C22:0**	0.13 ± 0.04^{A}	0.10 ± 0.02^{B}	0.10 ± 0.02^{AB}	0.07 ± 0.01^{B}	0.09 ± 0.02^{B}
Dihomo-g-linolenic	**C20:3ω6**	1.37 ± 0.14^{A}	1.26 ± 0.09^{A}	1.43 ± 0.20^{A}	1.42 ± 0.08^{A}	1.24 ± 0.14^{A}
Arachidonic	**C20:4ω6**	19.92 ± 0.49^{A}	18.91 ± 0.87^{B}	6.84 ± 0.56^{C}	19.14 ± 0.45^{B}	5.11 ± 0.49^{D}
Lignoceric	**C24:0**	0.24 ± 0.05^{A}	0.18 ± 0.07^{AB}	0.20 ± 0.06^{AB}	0.14 ± 0.03^{B}	0.19 ± 0.01^{AB}
Eicosapentaenoic	**C20:5ω3**	0.30 ± 0.03^{A}	0.25 ± 0.02^{B}	2.98 ± 0.16^{C}	0.20 ± 0.02^{D}	4.73 ± 0.18^{E}
Nervonic	**C24:1ω9**	0.20 ± 0.04^{AC}	0.14 ± 0.06^{AB}	0.13 ± 0.04^{B}	0.21 ± 0.04^{C}	0.26 ± 0.02^{C}
Docosatetraenoic	**C22:4ω6**	2.23 ± 0.09^{A}	2.22 ± 0.13^{A}	0.22 ± 0.03^{B}	1.98 ± 0.15^{C}	0.14 ± 0.01^{B}
Docosapentaenoic ω6	**C22:5ω6**	0.47 ± 0.03^{A}	0.47 ± 0.03^{A}	0.05 ± 0.01^{B}	0.51 ± 0.04^{A}	0.03 ± 0.01^{C}
Docosapentaenoic ω3	**C22:5ω3**	0.79 ± 0.06^{AB}	0.75 ± 0.08^{A}	0.87 ± 0.04^{BD}	0.46 ± 0.05^{C}	0.90 ± 0.04^{D}
Docosahexaenoic	**C22:6ω3**	5.50 ± 0.16^{A}	5.50 ± 0.19^{A}	14.35 ± 0.49^{B}	5.06 ± 0.17^{C}	15.00 ± 0.28^{B}
Total SFA		41.58 ± 0.62^{AC}	42.39 ± 0.72^{AB}	43.79 ± 0.45^{B}	40.01 ± 1.13^{C}	41.32 ± 0.35^{AC}
Total MUFA		16.50 ± 0.21^{A}	16.73 ± 0.46^{A}	14.65 ± 0.57^{B}	23.06 ± 0.19^{C}	21.26 ± 0.30^{D}
Total ω-3 PUFA		6.67 ± 0.16^{A}	6.58 ± 0.17^{A}	18.27 ± 0.56^{B}	5.76 ± 0.21^{C}	20.67 ± 0.27^{D}
Total ω-6 PUFA		35.25 ± 0.68^{A}	34.30 ± 0.89^{A}	23.40 ± 0.14^{B}	31.18 ± 0.90^{C}	16.49 ± 0.37^{D}
ω-3 Index		5.80 ± 0.15^{A}	5.75 ± 0.18^{A}	17.32 ± 0.56^{B}	5.27 ± 0.17^{C}	19.74 ± 0.28^{D}

Data presented as mean ± SD. Difference between diets compared by ordinary one-way ANOVA followed by Tukey's multiple comparison test. Unique letters indicate significant differences between groups (p<0.05). GLC, gas-liquid chromatograph; FA, saturated fatty acid; MUFA, monounsaturated fatty acid; PUFA, polyunsaturated fatty acid.

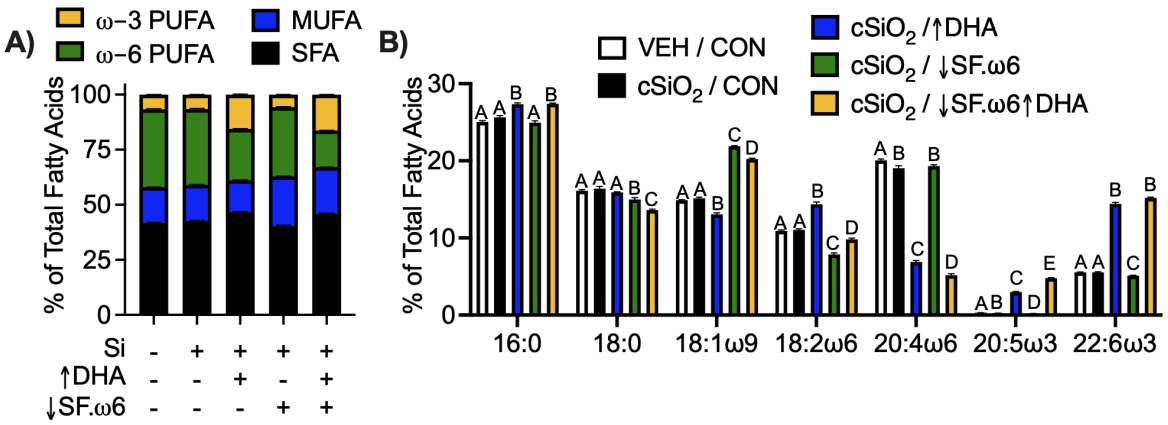


Figure 2.4: RBC fatty acid composition is influenced by modulation of dietary lipids. A. Major fatty acid sub-types and the **B.** 7 most abundant fatty acids in red blood cells (RBCs) were compared across treatment groups. Fatty acid concentrations were determined by gas-liquid chromatography and expressed as percent of total. Statistically significant differences in polyunsaturated fatty acids (PUFAs), monounsaturated fatty acids (MUFAs), and saturated fatty acids (SFAs) are indicated in **Table 2.3**. Different letters indicate statistically significant differences between treatment groups for individual fatty acids (p<0.05).

The lung was the only organ where a significant change in total FA composition was observed in response to $cSiO_2$ (**Supplementary Table A.1, Figure 2.5 A-B**). Here, $cSiO_2$ exposure induced an increase in SFA in the form of palmitic acid (C16:0) from ∼30% (similar to RBC levels) to ∼50%. Palmitic acid is the fatty acid moiety of dipalmitoylphosphatidylcholine (DPPC), a major component of pulmonary surfactant. This increase in palmitic acid appears to be at the expense of stearic acid and oleic acid (OA, C18:1ω9). OA was decreased further by DHA supplementation, but increased slightly in the ↓SF.ω-6 diets. Trends within the PUFA fraction are similar to those observed in the RBCs, with ω-3 PUFAs significantly increased by DHA supplementation.

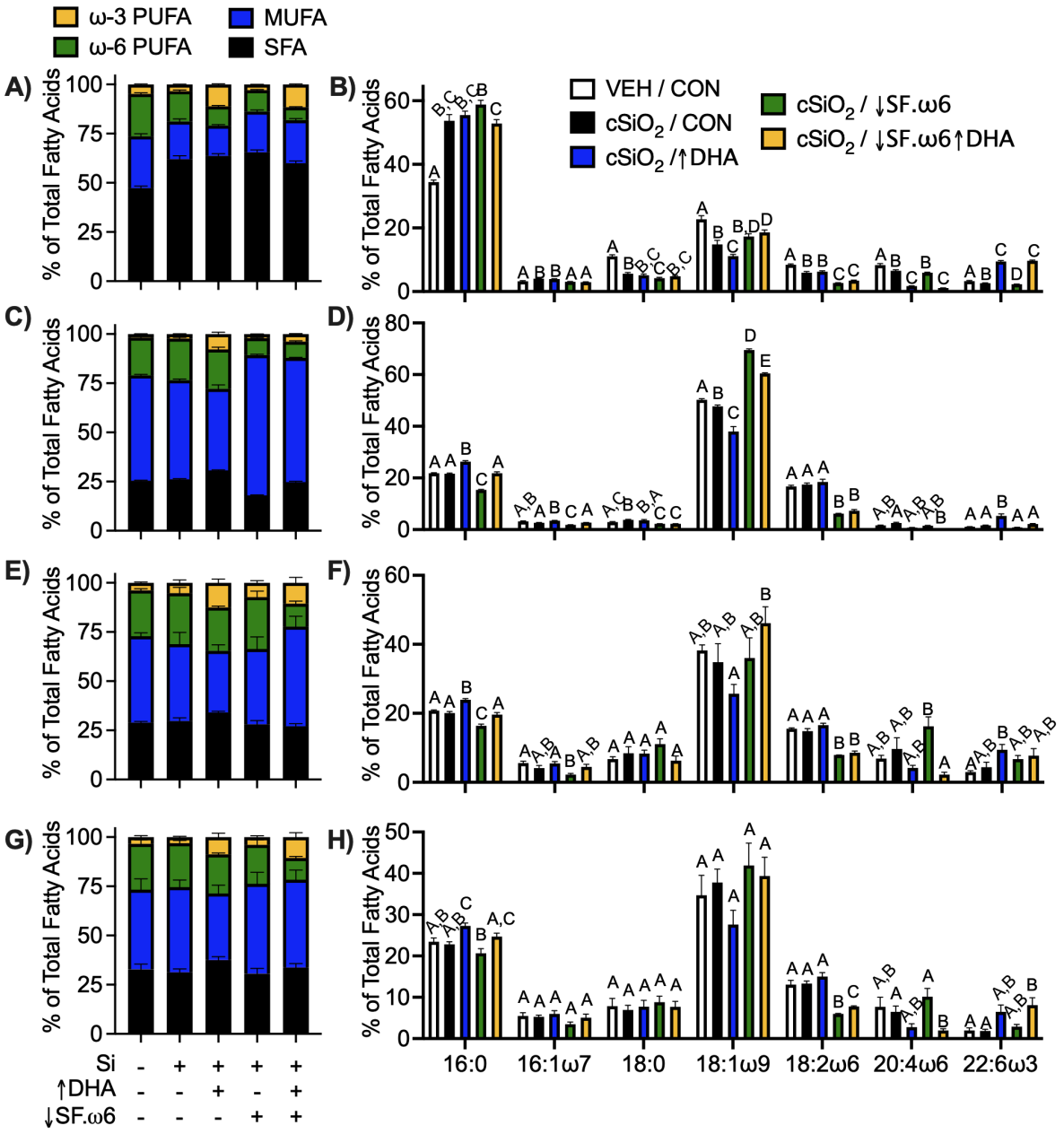


Figure 2.5: Individual tissues show distinct patterns of fatty acid incorporation. A,C,E,G. Total fatty acid content was determined by gas-liquid chromatography and expressed as percent of total. The distribution of saturated fatty acids (SFAs), monounsaturated fatty acids (MUFAs), and polyunsaturated fatty acids (PUFAs) was compared between tissues. Statistically significant differences are indicated in Supplementary Tables A.1-A.4. **B,D,F,H**. The 7 most abundant fatty acids in each tissue were expressed as percent of total. Different letters indicate statistically significant differences between treatment groups for individual fatty acids ($p<0.05$).

The liver appeared to be the organ most reflective of dietary fat intake. In the liver, plasma non-esterified fatty acids (NEFAs) obtained from adipose tissue lipolysis or from dietary fatty acids are packaged into lipoproteins to be distributed throughout the body or stored in lipid droplets as triacylglycerides (TAGs) [313, 314, 315]. Furthermore, TAGs present in the liver are highly similar to the dietary FA composition, especially when dietary fat remains consistent over time. MUFA levels were greatest in the liver (**Supplementary Table A.2, Figure 2.5 C-D**), with OA composing ∼40% of total liver fatty acids in the CON and ↑DHA diets and ∼60% in the ↓SF.ω6 diet and ↓SF.ω6↑DHA diets. This is notable because OA is the major FA in olive oil, which replaced corn oil (composed primarily of LA) in the ↓SF.ω-6 diet. A reduction in SFA and ω-6 PUFAs (mainly in palmitic acid and LA, respectively) was observed in animals fed the ↓SF.ω6 diet. SFA in the liver was comparable to levels in the spleen and kidney (∼15%) (**Figure 2.5 E,G**).

The total FA composition of the kidney (**Supplementary Table A.3, Figure 2.5 E-F**) and spleen (**Supplementary Table A.4, Figure 2.5 G-H**) were nearly identical. Unlike RBCs and the liver, there was no clear change in OA in these tissues. Changes in SFA levels across all diets were also minimal. In both tissues, there was a clear decrease in LA with the ↓SF.ω6 diets. The increase in DHA in these tissues was evident, though not as dramatic as observed in the RBC, lung, and liver.

2.4.2 DHA supplementation suppresses $cSiO_2$-induced IRG response in the lungs.

The effects of dietary treatments on $cSiO_2$-induced IRG expression in the lung were compared using an IFN score, encompassing 15 genes with known functions in response to IFN signaling. Expression of each of these genes was significantly induced (p<0.05) following $cSiO_2$ exposure. The IFN score was calculated for each sample by taking the sum of the autoscaled expression of each gene (see Methods section 2.3.6). The IFN score was elevated significantly (p<0.05) in $cSiO_2$-instilled mice fed CON but suppressed nearly to baseline in those fed the ↑DHA diet (**Figure 2.6A**). The IFN score in $cSiO_2$-treated mice fed the ↓SF.ω6↑DHA diet was reduced compared to those fed CON or ↓SF.ω6. The mRNA expression profiles for four representative genes, *Irf7, Cxcl9, Isg15*, and *Oas1* are illustrative of the expression pattern for individual IRGs (**Figure 2.6B**).

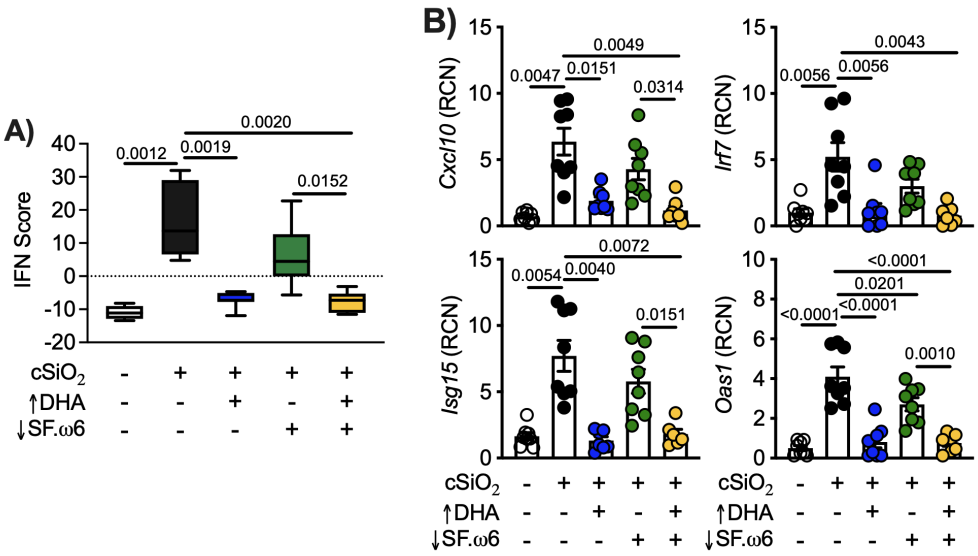


Figure 2.6: DHA supplementation attenuates $cSiO_2$-induced interferon-regulated gene expression in the lungs. A. The interferon (IFN) score was calculated by combining the auto-scaled expression of 15 differentially expressed IFN-regulated genes (*Ccl7, Zbp1, Ifi44, Ifit1, Irf7, Isg15, Mx1, Oas1, Oas2, Oasl1, Psmb8, Rsad2, Siglec1, Ccl8, Cxcl10*) for each animal. **B.** Expression of four representative interferon-regulated genes (IRGs). RCN is relative copy number. Values of $p<0.1$ are shown, with $p<0.05$ considered statistically significant.

2.4.3 DHA intake suppresses $cSiO_2$-induced cytokine elevations in the BALF.

As we have observed in prior studies employing AIN-93G diet [175, 7, 3], $cSiO_2$ instillation of mice fed CON diet induced a range of cytokines in BALF that are associated with leukocyte infiltration and the inflammatory response (**Figure 2.7**). Levels of the monocyte chemoattractant proteins MCP-1 (**Figure 2.7A**) and MCP-3 (**Figure 2.7B**) tended to be lower in the BALF of $cSiO_2$-treated animals fed ↑DHA, with significant suppression occurring in mice fed ↓SF.ω6↑DHA. Though not all changes were statistically significant, similar observations were made for TNF-α (**Figure 2.7C**), IL-1α (**Figure 2.7D**), IL-6 (**Figure 2.7E**), and IL-18 (**Figure 2.7F**), which are known for their roles in inflammation and lupus development. Furthermore, T-helper cytokines IL-17A (**Figure 2.7G**) and IL-22 (**Figure 2.7H**), which recruit Th17 cells and polarize macrophages toward a proinflammatory M1 phenotype, were upregulated by $cSiO_2$ in CON-fed mice and downregulated in mice fed ↓SF.ω6↑DHA and ↑DHA, respectively.

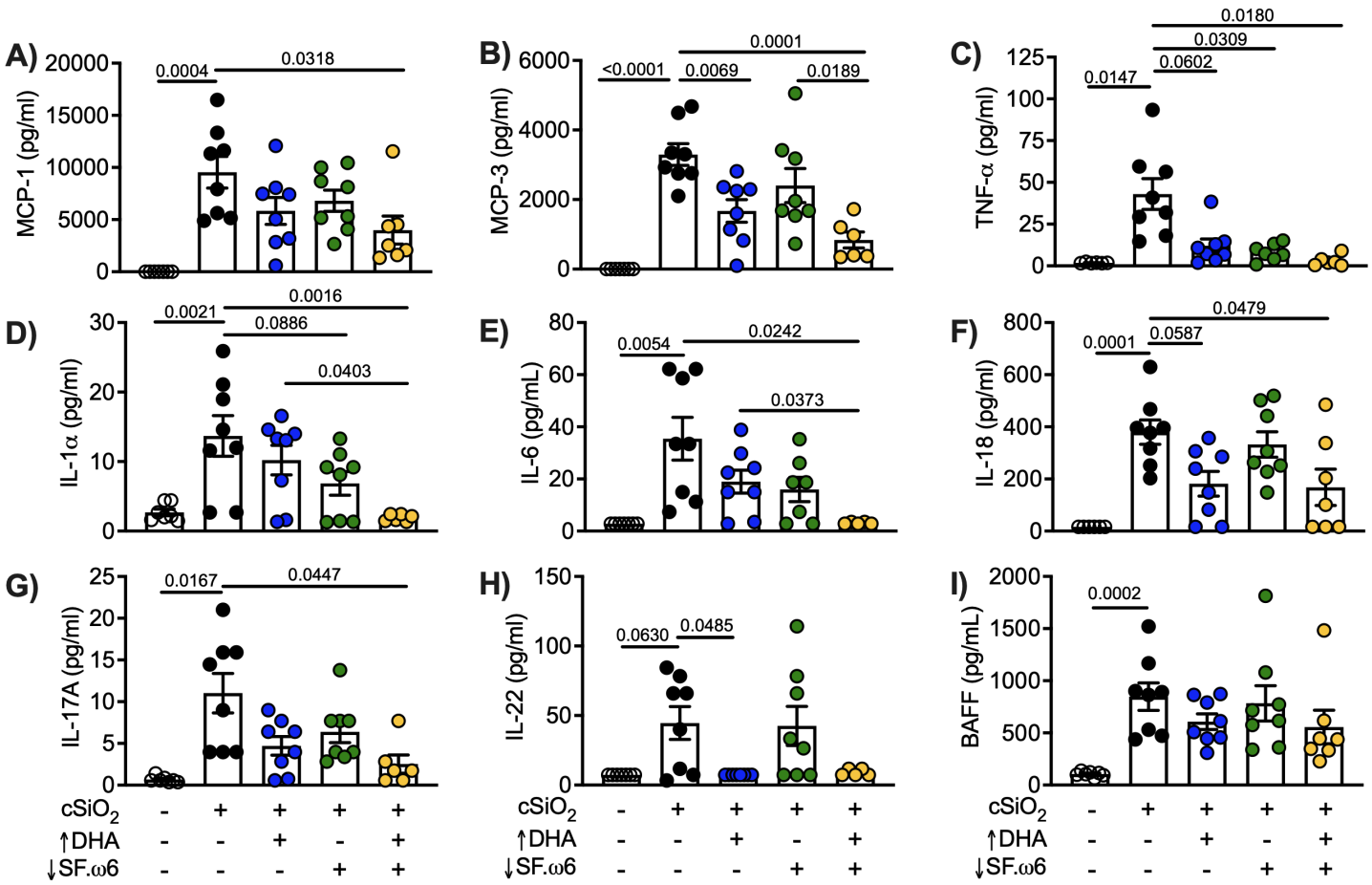


Figure 2.7: DHA consumption suppresses $cSiO_2$-triggered cytokine release. Cytokine levels in the bronchoalveolar lavage fluid (BALF) were assessed using antibody bead array. Values of $p<0.1$ are shown, with $p<0.05$ considered statistically significant.

Finally, while $cSiO_2$ instillation induced elevation of B cell activating factor (BAFF) (**Figure 2.7I**) in the BALF of CON-fed mice, this response was not affected by feeding ↑DHA, ↓SF.ω6, or ↓SF.ω6↑DHA. Overall, DHA supplementation with or without SFA and ω-6 PUFA suppression alleviated induction of many cytokines involved in lupus pathogenesis.

2.4.4 DHA consumption suppresses $cSiO_2$-induced pulmonary immune cell infiltration, including B and T lymphocytes and ELS neogenesis.

Further consistent with prior investigations utilizing AIN-93G diet [16, 30], intranasal instillation with $cSiO_2$ increased total cells (**Figure 2.8A**), monocytes (**Figure 2.8B**), neutrophils (**Figure 2.8C**), and lymphocytes (**Figure 2.8D**) in the BALF of mice at experiment termination. Notably, total cell and monocyte accumulation were inhibited in mice fed ↑DHA, ↓SF.ω6, and ↓SF.ω6↑DHA diets. Similar trends were observed with the increase for neutrophils and lymphocytes, though not all were statistically significant.

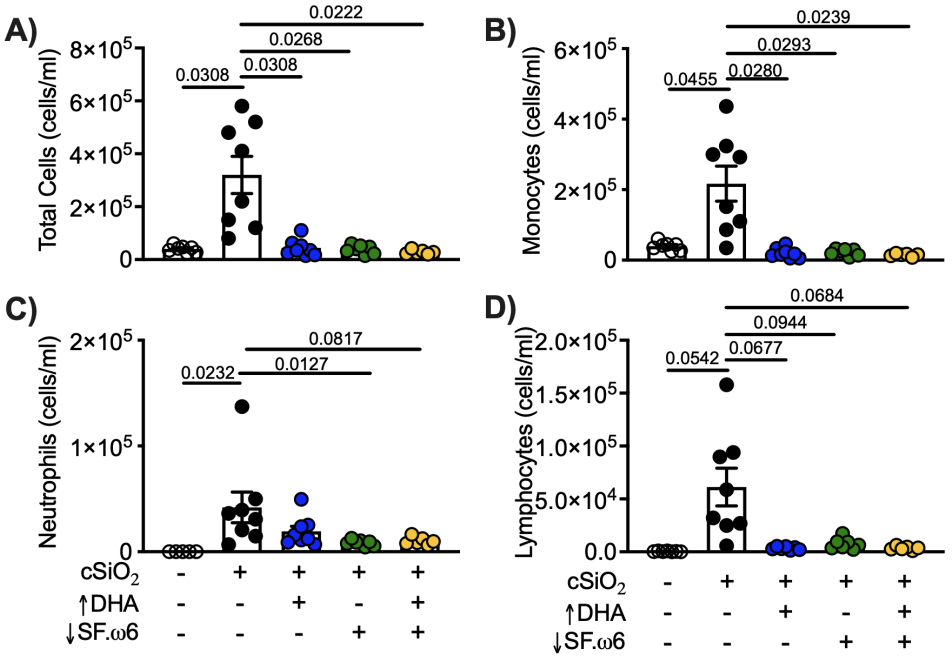


Figure 2.8: DHA supplementation with SFA and ω-6 PUFA reduction suppress $cSiO_2$-induced immune cell accumulation in BALF. Bronchoalveolar lavage fluid (BALF) was collected at experiment termination and **A.** total cells, **B.** monocytes, **C.** neutrophils, and **D.** lymphocytes enumerated. Values of $p<0.1$ are shown, with $p<0.05$ considered statistically significant.

Histological assessment of H&E-stained lung tissue from $cSiO_2$-instilled mice fed CON showed robust peribronchiolar and perivascular leukocytic infiltration (**Figure 2.9, Supplementary Table A.5**). Immunohistochemical staining further indicated $cSiO_2$-induced development of ELS in the lung, as evidenced by the organized accumulation of B cells ($CD45R^+$) and T cells ($CD3^+$) (**Figure 2.9A**). $cSiO_2$-induced cell infiltration and ELS neogenesis were suppressed in mice fed ↑DHA and ↓SF.ω6↑DHA diets, but unlike the observations in BALF, not affected in mice fed the ↓SF.ω6 diet. Morphometric analysis confirmed that $cSiO_2$ treatment of mice fed CON diets elicited accumulation of B cells (**Figure 2.9B**) and T cells (**Figure 2.9C**) in the lung, further suggestive of ELS neogenesis, and that this response was markedly suppressed in mice fed ↑DHA and ↓SF.ω6↑DHA diets.

2.4.5 $cSiO_2$-induced autoantibody production is attenuated by DHA supplementation.

Elevations in anti-dsDNA and anti-nuclear autoantibodies are hallmarks of lupus flaring and progression. Mice in the $cSiO_2$/CON group exhibited significant increases for both of these autoantibodies in both BALF and plasma compared to VEH/CON (**Figure 2.10**). Consumption of ↑DHA, ↓SF.ω6, or ↓SF.ω6↑DHA diets significantly reduced $cSiO_2$-anti-dsDNA responses in BALF (**Figure 2.10A**), whereas plasma responses were reduced only in mice fed the ↑DHA diet (**Figure 2.10B**). Anti-nuclear antibody (ANA) responses followed similar trends (**Figure 2.10 C-D**).

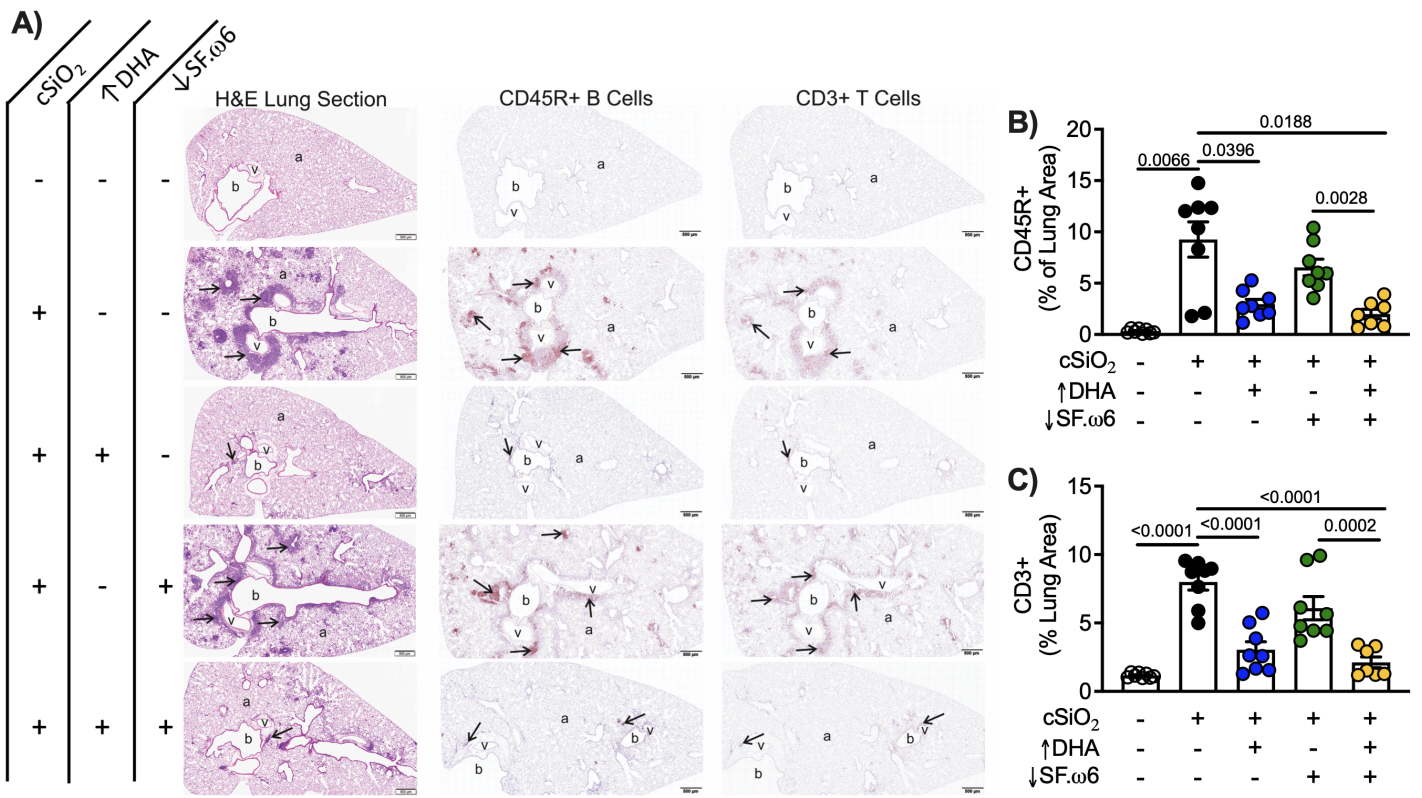


Figure 2.9: DHA supplementation impedes perivascular and peribronchiolar lymphocyte infiltration, and the neogenesis of ELS. A. Light photomicrographs of lung tissue sections from mice intranasally instilled with $cSiO_2$ (+) or saline (-), fed a diet with (+) or without (-) DHA supplementation, and with (+) or without (-) SF.ω6 reduction. Lung sections were stained with H&E (first column), immunohistochemically stained for $CD45R^+$ B lymphoid cells (arrows; brown chromagen; second column), or $CD3^+$ T lymphoid cells (arrows; brown chromagen; third column). Peribronchiolar and perivascular accumulations of B and T lymphoid cells (ectopic lymphoid structures [ELS]; arrows) were present in $cSiO_2$-exposed mice fed diets without DHA supplementation but not in the lung of control mice intranasally instilled with saline and fed CON (row one). Minimal perivascular and peribronchiolar accumulations of B and T lymphoid cells were seen in the lungs of mice on experimental diets. **Abbreviations**:a–alveolar parenchyma, b–bronchiolar airway, v–blood vessel. Morphometric analysis was used to quantitatively determine the volume density of **B.** $CD45R^+$ and **C.** $CD3^+$ area in the measured lung area. Values of $p<0.1$ are shown, with $p<0.05$ considered statistically significant.

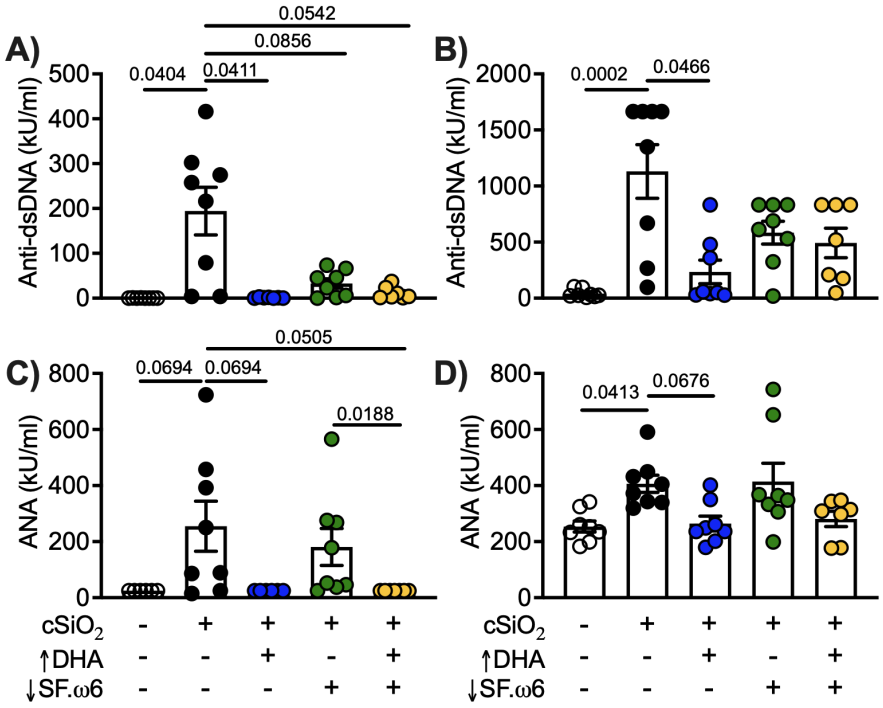


Figure 2.10: DHA intake suppresses $cSiO_2$-induced lupus-associated autoantibodies in the BALF and the plasma. Effects of $cSiO_2$ and experimental diets on anti-dsDNA antibodies (**A,B**) and anti-nuclear antibodies (ANA) (**C,D**) in bronchoalveolar lavage fluid (BALF) (**A,C**) and plasma (**B,D**). Values of $p<0.1$ are shown, with $p<0.05$ considered statistically significant.

2.4.6 DHA intake protects against $cSiO_2$-induced lesions in the kidney.

Naïve female NZBWF1 mice typically display glomerulonephritis around 35 wk of age [316] and die of kidney failure within 1 year. Previous studies in our lab and others have shown that exposure to $cSiO_2$ accelerates this phenotype, with nephritis being first observed within 3 months after the final $cSiO_2$ instillation (i.e. age 22 wk) in mice fed the AIN-93G diet [3]. While proteinuria was not evident up to experiment termination (**Supplementary Table A.6**), histopathological analysis indicated that multifocal segmental proliferative glomerulonephritis was more severe in kidneys of mice after $cSiO_2$ instillation fed CON and ↓SF.ω6 compared to mice fed DHA-supplemented diets (**Figure 2.11**).

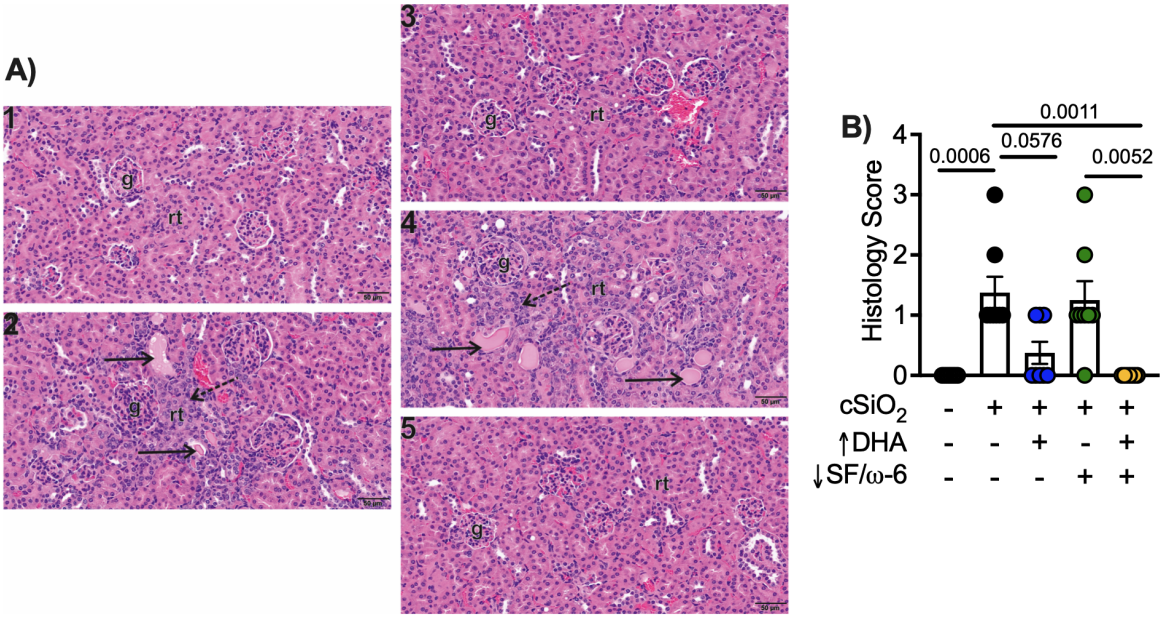


Figure 2.11: DHA intake inhibits $cSiO_2$-induced glomerulonephritis. A. Light photomicrographs of kidney tissue sections from mice intranasally instilled with saline alone (1) or with $cSiO_2$ (2–5). Animals were fed the control (CON) diet (1, 2) or ↑DHA diet (3). Others were fed the ↓SF.ω6 without DHA (4) or with DHA supplementation (↓SF.ω6↑DHA, 5). No renal histopathology was evident in saline-instilled control mice (1) or $cSiO_2$-instilled mice fed DHA (3, 5). In contrast, $cSiO_2$-instilled mice fed diets without DHA supplementation (2, 4) had renal histopathology characteristic of a membranoproliferative glomerulonephritis characterized by hypercellular glomeruli with thickened mesangial tissue, tubular proteinosis (solid arrows), and tubular epithelial hyperplasia (stippled arrows). **Abbreviations**: g–glomerulus, rt–renal tubules. **B.** Quantification of renal histology score, based on the following scoring criteria: No proteinosis, normal glomeruli (0); multifocal segmental proliferative glomerulonephritis (1); multifocal segmental proliferative glomerulonephritis and occasional glomerular sclerosis and crescent formation (2); diffuse global segmental proliferative glomerulonephritis (3). Values of $p<0.1$ are shown, with $p<0.05$ considered statistically significant.

2.5 DISCUSSION

The TWD represents typical eating patterns in the U.S, making it highly appropriate for investigating how modulation of dietary lipids affects flaring and progression in preclinical models of lupus. The results presented herein indicate for the first time that translationally relevant DHA supplementation against the complex background of the Western diet is highly effective in protecting against $cSiO_2$-triggered IRG expression, cytokine/chemokine release, leukocyte infiltration, ELS neogenesis, autoantibody production in the lungs as well as glomerulonephritis (summarized

in **Figure 2.12**). While some disease endpoints were modestly attenuated by reducing SFAs and ω-6 PUFAs through increasing the ω-9 PUFA content with olive oil, further DHA supplementation to this diet was required for maximal protection against lupus development. Finally, consistent with the observed effects in the lung, consumption of DHA-amended diets prevented early onset of glomerulonephritis in $cSiO_2$-exposed mice. Together, these findings suggest that ω-3 supplementation to a Western diet without substantial diet changes may be protective against lupus flaring.

The observation that DHA can suppress IRG responses is highly significant because IFN signaling has been centrally linked to lupus disease activity in preclinical and clinical studies. In NZBWF1 mice, adenovector-mediated delivery of IFN-α, a major type I IFN, induces the development of lupus [317]. Gonzalez-Quintial, et al. [318] demonstrated in C57Bl6 mice, which are not genetically predisposed to lupus, that early-life virus exposure combined with adult exposure to $cSiO_2$ results in the production of lupus-like symptoms, including autoantibody production and glomerulonephritis. Likewise, the IRG signature is closely related to the flaring and pathogenesis of lupus symptoms in human patients [319, 42, 320]. Randomized, double-blind, placebo-controlled Phase IIb clinical trials indicated that sifalimumab, an anti-IFN-α monoclonal antibody [321], and anifrolumab, a type I IFN receptor antagonist [322], reduced lupus symptoms. Recently, a large, double-blind, placebo-controlled Phase 3 clinical trial (TULIP-2) was finalized and documented that intravenous anifrolumab lowered overall disease activity, reduced skin disease, and enabled oral corticosteroid tapering [65]. Accordingly, the finding here that DHA supplementation of CON and ↓SF.ω6 diets lowered the IRG response is potentially relevant from a translational perspective.

Our analysis of tissue fatty acid content confirmed that the ω-3 PUFA content of the RBC, presented both as the Omega-3 Index and as total ω-3 PUFA, is reflective of ω-3 PUFA levels in the diet [323]. We found here that Omega-3 Indexes for mice fed ↑DHA and ↓SF.ω6↑DHA diets were three times higher than those fed CON or ↓SF.ω6 diets. These trends were consistent with %EPA+DHA levels in the tissues. Alternatively, the effects of feeding ↓SF.ω6 diet on the Omega-3 Index and the %EPA+DHA in tissues were minimal compared to CON-fed animals. This may explain why the ↓SF.ω6 diet provided minimal protection against the $cSiO_2$-induced inflammatory

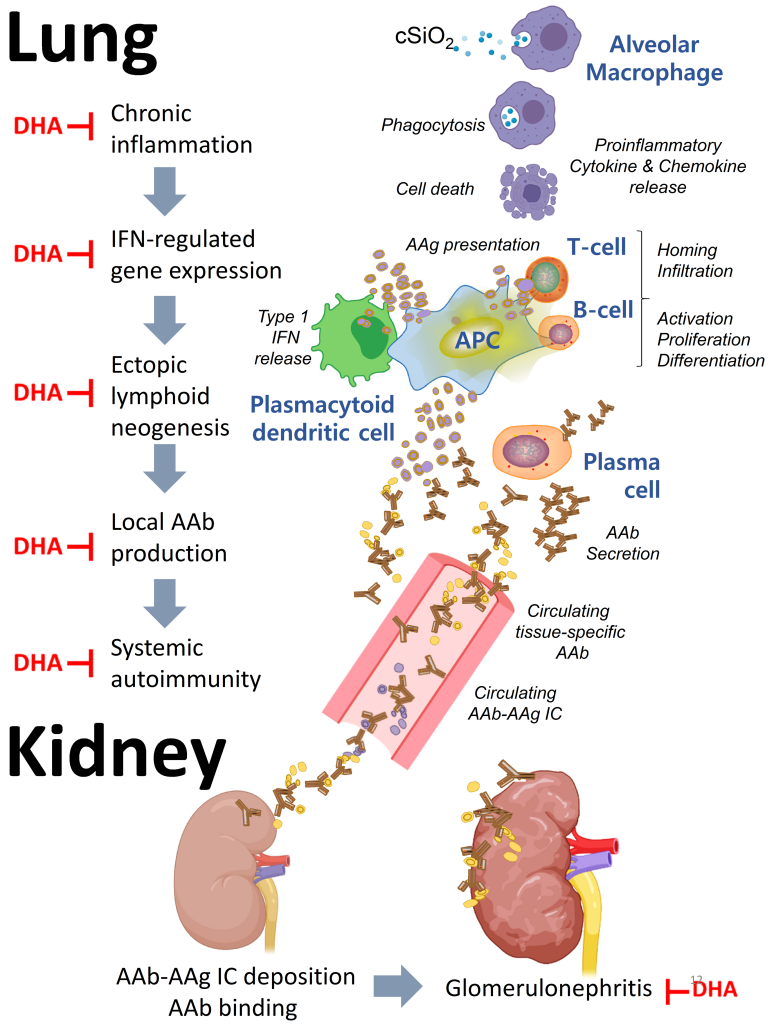


Figure 2.12: DHA supplementation against the complex background of the Western diet suppresses $cSiO_2$-triggered flaring and progression of lupus in NZBWF1 mice. The results presented here and in other investigations suggest that $cSiO_2$ promotes cell death in alveolar macrophages, resulting in the release of proinflammatory cytokines and chemokines that recruit and activate additional immune cells, including T-cells and B-cells. Accumulation of cellular debris results in uptake and presentation of autoantigens (AAg) to T- and B-cells. Among the cellular debris are host nucleic acids, which stimulate the production of Type I IFN from plasmacytoid dendritic cells. Type I IFN promotes cytokine release, antigen uptake, and maturation of B cells to plasma cells, which produce autoantibodies (AAb) against host antigens both locally and systemically. Upon binding their cognate AAgs, Aabs can form immune complexes that ultimately deposit in the kidney inflicting damage. The red $\perp$ indicates steps where DHA supplementation has been demonstrated to interfere with this pathway.

response. Additionally, the ↓SF.ω-6 diet had a minor impact on tissue and RBC SFA levels and did not alter levels of long chain ω-6 PUFAs. Though there was a reduction in total ω-6 PUFA levels, this was accomplished primarily by reduction of LA (18:2ω6) rather than ARA (20:4ω6).

Our results suggest that the balance of long chain ω-3 and ω-6 PUFAs in the cell membrane might be critical to promoting inflammation or resolution. One explanation for this observation is that ω-3 and ω-6 PUFAs are substrates for downstream bioactive lipid metabolites. It is well established that lipid metabolites derived from the "arachidonic acid cascade" have primarily inflammatory actions, especially in the case of acute inflammation [324]. Over the last two decades, many metabolites of ω-3 PUFAs have been identified as having anti-inflammatory and pro-resolving properties [203]. A recent study demonstrated that the plasma and RBC levels of ω-3 PUFA were highly correlated with the production of ω-3 PUFA-derived lipid mediators, many of which are involved in the resolution of inflammation. Similarly, supplementation with EPA and DHA led to a decrease in ω-6 PUFAs, namely ARA, as well as decreased ω-6-PUFA derived metabolites [28, 325]. Shifting the membrane composition to favor long chain ω-3 PUFAs rather than ω-6 PUFAs, such as arachidonic acid, may enhance the pro-resolving phenotype promoted by ω-3 PUFA-derived lipid mediators.

Despite a limited number of studies, there is evidence that increasing levels of long chain ω-3 PUFAs in lupus patients leads is protective against inflammation, a process that likely involves the action of bioactive lipid metabolites. A recent study showed strong associations between dietary PUFA intake from fish and the ω-3 status in lupus patients. Further, the RBC ω-3 levels were negatively associated with levels of C-reactive protein [326]. Others have reported that lupus patients had lower levels of plasma ω-3 PUFAs [327] and plasma resolvin D1, an anti-inflammatory metabolite of DHA than healthy controls [328]. Multiple human studies in lupus and other rheumatic diseases have shown decreased disease activity in patients receiving ω-3 supplementation [24], but few studies have investigated the impact of modulating other dietary lipids, such as ω-6 PUFAs and SFAs. To date, there has been no extensive study of the membrane fatty acid content or plasma lipidome of lupus patients. Investigation in this area–both in preclinical and clinical settings–is necessary to elucidate potential benefit of ω-3 PUFA supplementation in individuals with lupus.

To summarize, DHA supplementation at a translationally relevant dose was highly effective in preventing cSiO_2-triggered lupus flaring in NZBWF1 mice fed a Western diet. Future perspectives

should include understanding how the TWD may impact the ameliorative effects of lower DHA doses in this model over time and how these responses are influenced by ω-6, SFA, and total fat content. Ultimately, well-designed clinical trials will be needed to confirm the value of ω-3 PUFA supplementation for the prevention and treatment of lupus in humans.

2.6 ACKNOWLEDGEMENTS

The authors would like to thank the MSU histology core for their assistance and expertise in the processing and staining of the tissues presented herein.

CHAPTER 3

REQUISITE ω-3 HUFA BIOMARKER THRESHOLDS FOR PREVENTING MURINE LUPUS FLARING

Wierenga KA[1,2], Strakovsky RS[2,3], Benninghoff AD[4], Rajasinghe LD[3], Lock AL[5], Harkema JR[2,6], Pestka JJ[2,7].

[1]Department of Biochemistry and Molecular Biology, Michigan State University, East Lansing, MI

[2]Institute for Integrative Toxicology, Michigan State University, East Lansing, MI

[3]Department of Food Science and Human Nutrition, Michigan State University, East Lansing, MI

[4]Department of Animal, Dairy and Veterinary Sciences and USTAR Applied Nutrition Research, Utah State University, Logan, UT

[5]Department of Animal Science, Michigan State University, East Lansing, MI [6]Department of Pathobiology and Diagnostic Investigation, Michigan State University, East Lansing, MI

[7]Department of Microbiology and Molecular Genetics, Michigan State University, East Lansing, MI

Author Contributions: KW: investigation, data curation, data analysis/interpretation, figure preparation, manuscript preparation, and project funding. RS, AB, LR, JH: data analysis/interpretation and manuscript preparation. AL: tissue, red blood cells, and diet fatty acid analysis. JP: initial study design, manuscript preparation, supervision, and project funding.

Originally published in Frontiers in Immunology

https://doi.org/10.3389/fimmu.2020.01796

3.1 ABSTRACT

Lupus is a systemic autoimmune disease typified by uncontrolled inflammation, disruption of immune tolerance, and intermittent flaring – events triggerable by environmental factors. Preclinical and clinical studies reveal that consumption of the marine ω-3 highly unsaturated fatty acids (HUFAs) eicosapentaenoic acid (EPA) and docosahexaenoic acid (DHA) might be used as a precision nutrition intervention to lessen lupus symptoms. The anti-inflammatory and pro-resolving effects of ω-3 HUFAs are inextricably linked to their presence in membrane phospholipids. The ω-3 HUFA score, calculated as [100 × (ω-3 HUFAs/(ω-3 HUFAs + ω-6 HUFAs))] in red blood cells (RBCs), and the Omega-3 Index (O3I), calculated as [100 × ((DHA+EPA)/total fatty acids)] in RBCs, are two biomarkers potentially amenable to relating tissue HUFA balance to clinical outcomes in individuals with lupus. Using data from three prior preclinical DHA supplementation studies, we tested the hypothesis that the ω-3 HUFA score and the O3I inversely correlate with indicators of autoimmune pathogenesis in the $cSiO_2$-triggered lupus flaring model. The three studies employed both low and high fat rodent diets, as well as more complex diets emulating the U.S. dietary pattern. The ω-3 HUFA scores in RBCs were comparatively more robust than the O3I at predicting HUFA balances in the kidney, liver, spleen, and lung. Importantly, increases in both the ω-3 HUFA score (>40%) and the O3I (>10%) were strongly associated with suppression of $cSiO_2$-triggered (1) expression of interferon-regulated genes, proinflammatory cytokine production, leukocyte infiltration, and ectopic lymphoid structure development in the lung, (2) pulmonary and systemic autoantibody production, and (3) glomerulonephritis. Collectively, these findings identify achievable ω-3 HUFA scores and O3I thresholds that could be targeted in future human intervention studies querying how ω-3 HUFA consumption influences lupus and other autoimmune diseases.

3.2 INTRODUCTION

Systemic lupus erythematosus (lupus) is a prototypic, multifaceted autoimmune disease characterized by uncontrolled inflammation, disruption of self-tolerance, and intermittent episodes of

disease flaring often triggered by environmental factors [10]. Lupus-associated autoimmune pathogenesis elicits irreversible damage in the kidney and other organs, sometimes culminating in death. The overactive immune response in lupus is typically managed with glucocorticoids, which have deleterious effects associated with long-term use, including organ damage, osteoporosis, diabetes, and increased risk of cardiovascular disease (CVD) [329, 5]. Both animal and human studies indicate that consumption of marine ω-3 highly unsaturated fatty acids (HUFAs) docosahexaenoic acid (DHA) and eicosapentaenoic acid (EPA) may potentially alleviate the severity of chronic inflammatory and autoimmune diseases [reviewed in [31, 330, 23]], suggesting this precision nutrition approach might be a steroid-sparing intervention for lupus.

Human studies support the contention that ω-3 HUFA consumption may benefit lupus patients. In observational studies, low ω-3 HUFA intake is associated with exacerbated disease activity, adverse serum lipids, and atherosclerotic plaques in lupus patients [331], and a recent study by the Michigan Lupus Epidemiology and Surveillance (MiLES) program reported that positive patient-reported outcomes were associated with high consumption of ω-3 fatty acids and low dietary ω-6:ω-3 ratios [12]. Most intervention trials implementing ω-3 HUFA supplementation in lupus patients report lessening of symptoms [332, 333, 334, 335, 336, 294, 295, 337, 338, 296]. However, there is variability across studies with some trials failing to show positive results. Key limiting factors contributing to disparities among investigations in humans include inadequate patient numbers; lack of consideration of effects of concurrent pharmacotherapies; variability in ω-3 HUFA dosages, sources, and supplementation durations; and failure to monitor ω-3 HUFA tissue levels in patients. This final point is immensely critical because the pro-resolving and anti-inflammatory properties of dietary ω-3 HUFAs are inextricably linked to the extent of their presence in the cell membrane [68]. Importantly, pro-inflammatory ω-6 HUFAs, generated by elongation of shorter chain ω-6 polyunsaturated fatty acids (PUFAs), that dominate the typical Western diet compete with ω-3 HUFAs for occupancy at the sn2 position of phospholipids, thereby diminishing their anti-inflammatory and pro-resolving effects [68]. In clinical studies, many factors influence the efficiency ω-3 HUFA incorporation, including patient compliance, individual differences in absorption, genetic variation

in lipid metabolizing genes, and consumption of competing ω-6 PUFAs [339]. Accordingly, for any clinical trial of marine ω-3 HUFA supplementation, it is essential to measure the balance of ω-3 HUFA levels both at baseline and throughout the study.

Animal models of lupus are an essential tool for understanding how gene-environment interactions influence development of the disease in humans. The NZBWF1 mouse is genetically predisposed to the development of autoimmune disease and has been widely used for over five decades as a preclinical lupus model for investigating mechanisms of disease pathogenesis, effects of environmental exposures, and efficacy of pharmacological and immunotherapeutic interventions [33]. Female NZBWF1 mice spontaneously develop lupus at around 7 months of age, much earlier than males, and rarely live past 12 months [340, 341], mimicking the sex bias observed in human lupus. Inclusion of marine ω-3 HUFAs in the diet delays lupus onset and extends survival in this strain [342, 343, 344, 345, 346, 35]. Our laboratory has recently developed a novel model for lupus flaring involving intranasal instillation of female NZBWF1 mice with crystalline silica ($cSiO_2$). Frequent, high exposure to $cSiO_2$ particles in occupations such as construction, mining, and farming is etiologically linked to multiple human autoimmune diseases, including lupus [347, 348, 2, 19]. In this model, autoimmune disease is triggered 3 months earlier than vehicle-treated controls, as reflected in the lung by pro-inflammatory and interferon-regulated gene (IRG) upregulation, mononuclear cell infiltration, ectopic lymphoid structure (ELS) neogenesis, and autoantibody production. In the kidney, we see concurrent induction of glomerulonephritis [175, 3]. Importantly, dietary supplementation with the ω-3 HUFA DHA ameliorates $cSiO_2$-triggered lupus flaring in female NZBWF1 mice [4, 175, 7, 3], and this intervention is effective against the background of three unique diets [4, 7, 8].

The ω-3 HUFA score [79] and the Omega-3 Index (O3I) [349] are two interrelated red blood cell (RBC) biomarkers potentially applicable for associating tissue HUFA balance with disease outcomes in both preclinical and clinical studies. The ω-3 HUFA score reflects the total ω-3 HUFAs as a percent of total HUFAs (ω-3, ω-6, and ω-9 HUFAs), while the O3I is the sum of DHA and EPA as a percent of total fatty acids. The goal of the present study was to test the hypothesis that

the ω-3 HUFA score and the O3I inversely correlate with indicators of inflammation and autoimmune pathogenesis during $cSiO_2$-triggered lupus flaring in NZBWF1 mice. Data used to test this hypothesis were drawn from three unique DHA supplementation studies recently published by our laboratory [4, 7, 8] that employed both purified mouse diets, as well as more complex diets reflecting Western eating patterns. Our findings indicate that increases in both the O3I and the ω-3 HUFA score were strongly associated with suppression of autoimmune pathogenesis in this preclinical mouse model of toxicant-triggered lupus flaring. Importantly, these preclinical results identify the ω-3 HUFA score and O3I thresholds potentially required for successful intervention against lupus and other autoimmune diseases.

3.3 MATERIALS AND METHODS

3.3.1 Experimental design.

Data used for this study were collected from our previously published investigations based on three DHA feeding studies [4, 175, 7, 8] (all raw data provided in Supplemental Information for the online article). Each study used female NZBWF1 mice obtained from Jackson Laboratories (Bar Harbor, ME). Female mice were used in these studies due to the sexual dimorphism observed in both human lupus and the NZBWF1 mouse model [33]. Experimental protocols were designed and performed in accordance with National Institutes of Health guidelines and approved by the Institutional Animal Care and Use Committee at Michigan State University (AUF # 01/15-021-00; AUF # PROTO201800113). Upon arrival, mice were randomly assigned to experimental groups and housed four per cage with access to food and water provided *ad libitum*. Animal facilities were maintained at constant temperature (21–24°C) and humidity (40–55%) with a 12 h light/dark cycle. One animal in Study 3 was euthanized for health concerns unrelated to $cSiO_2$ exposure or lupus development [8].

Experimental diets contained specified amounts of DHA against unique dietary backgrounds as summarized in **Table 3.1**. Study 1 used a modified high fat American Institute of Nutrition-93G diet (HF-AIN-93G) containing 134 g fat/kg diet (30% kcal fat), formulated with corn oil (10 g/kg),

soybean oil (64 g/kg), and high-oleic safflower oil (60 g/kg) [175, 7]. High-oleic safflower oil was substituted with 10, 30, or 60 g/kg microalgal oil containing 40% (w/w) DHA (DHASCO, provided by Dr. Kevin Hadley, Martek Biosciences Corporation, Columbia, MD). The resulting experimental diets yielded 0.4, 1.2, or 2.4% (w/w) DHA, respectively. Analyses were only performed on animals fed diets containing 0, 0.4, and 1.2% (w/w) DHA because no additional protection was seen when comparing the 1.2% (w/w) DHA diet to the 2.4% (w/w) DHA diet. Furthermore, animals fed the 2.4% (w/w) DHA diet achieved an ω-3 HUFA score of $\sim$90%, which is much higher than those achieved in the other studies and beyond levels observed in humans [80]. Study 2 employed the AIN-93G diet containing 70 g fat/kg diet (17% kcal fat), composed of corn oil (10 g/kg) and high-oleic safflower oil (60 g/kg) [4]. High-oleic safflower oil was replaced with 10 or 25 g/kg DHASCO to yield experimental diets containing 0.4 and 1% (w/w) DHA, respectively. Study 3 utilized a modified total Western diet (MTWD) and a MTWD with 40% less saturated fats and ω-6 HUFAs (MTWD $\downarrow$SF.ω-6) [8]. Both MTWDs contained 164 g fat/kg diet (34.5% kcal fat), composed of soybean oil, anhydrous milk fats, olive oil, lard, beef tallow, corn oil, cholesterol, and high-oleic safflower oil. Olive oil was replaced by 30 g/kg DHASCO to achieve 1.2% (w/w) DHA.

In each study, groups of female mice (n = 7–8/group) were initiated on experimental diets at age 6 wk and maintained on those same diets until experiment termination. To limit oxidation of dietary lipids, diets were prepared every 2 wk, vacuum-sealed and stored at −20°C, and provided fresh every 1–2 d. Two weeks later (age 8 wk), mice were anesthetized with 4% isoflurane and intranasally instilled with 1 mg $cSiO_2$ (Min-U-Sil-5, 1.5–2.0 μm average particle size, U.S. Silica, Berkeley Springs, WV) in 25 μL PBS or PBS vehicle (VEH) every wk for 4 wk. The total amount of $cSiO_2$ provided over the course of the experiment (4 mg per mouse) was chosen to approximate half of a recommended human lifetime exposure as established by the Occupational Safety and Health Administration [3]. Mice were euthanized by intraperitoneally injecting 56 mg/kg BW sodium pentobarbital 11–13 wk after the final $cSiO_2$ exposure. Selected tissue analyses were conducted as described for Study 1 [7], Study 2 [4, 175], and Study 3 [8]. These included fatty acid profiling (RBC, lung, kidney, spleen, liver), IRG expression (lung), pro-inflammatory cytokines

(bronchoalveolar lavage fluid [BALF]), lymphocyte infiltration (lung), ELS development (lung), pulmonary and systemic autoantibody expression (BALF, plasma), and glomerulonephritis (kidney).

Table 3.1: Composition of experimental diets.

	Experimental Diets									
	Study 1*			Study 2*			Study 3*			
Basal Diet	HF AIN-93G			AIN-93G			MTWD		Low SF/w6 MTWD	
DHA (en%)	0%	0.96%	2.40%	0%	0.87%	2.62%	0%	2.63%	0%	2.63%
DHA (%w/w)	0%	0.40%	1.20%	0%	0.40%	1%	0%	1%	0%	1%
Macronutrient	*(g/Kg)*									
Carbohydrates										
Corn Starch	366	366	366	398	398	398	230	230	230	230
Maltodextrin (Dyetrose)	121	121	121	132	132	132	70	70	70	70
Sucrose	92	92	92	100	100	100	257	257	257	257
Cellulose	46	46	46	50	50	50	30	30	30	30
kcal (% of total)	53.3	53.3	53.3	63.2	63.2	63.2	49.4	49.4	49.4	49.4
Proteins										
Casein	184	185	184	200	200	200	190	190	190	190
L-Cysteine	3	3	3	3	3	3	3	3	3	3
kcal (% of total)	16.7	16.7	16.7	19.7	19.7	19.7	16.1	16.1	16.1	16.1
Fats										
Soybean Oil	64	64	64	-	-	-	29	29	6	6
Anhydrous Milkfat	-	-	-	-	-	-	36	36	7	7
Olive Oil[a,b]	-	-	-	-	-	-	30	0	138	108
Lard	-	-	-	-	-	-	28	28	6	6
Beef Tallow	-	-	-	-	-	-	25	25	5	5
Corn Oil[a,c]	10	10	10	10	10	10	16	16	3	3
Cholesterol	-	-	-	-	-	-	0.4	0.4	0.5	0.5
High-Oleic Safflower Oil[a,d]	60	50	30	60	50	35	-	-	-	-
DHA-enriched Algal Oil[a,e]	0	10	30	0	10	25	0	30	0	30
kcal (% of total)	30.0	30.0	30.0	17.1	17.1	17.1	34.5	34.5	34.5	34.5
Other										
AIN93G Mineral Mix	32	32	32	35	35	35	41	41	41	41
AIN93G Vitamin Mix	19	19	19	10	10	10	12	12	12	12
Choline Bitartrate	2	2	2	3	3	3	3	3	3	3
TBHQ Antioxidant	0.01	0.01	0.01	0.01	0.01	0.01	0.03	0.03	0.03	0.03

*Diet compositions from Studies 1, 2, and 3 can be found in Bates et al. 2016, Bates et al. 2015, and Gilley et al. 2020. [a]Based on oil composition reported by manufacturer. [b]Olive oil contained 678 g/kg oleic acid and 84 g/kg linoleic acid, as reported by the USDA, FDC ID 748648. [c]Corn oil contained 612 g/kg linoleic acid and 26 g/kg oleic acid. [d]High-oleic safflower oil contained 750 g/kg oleic acid and 140 g/kg linoleic acid. [e]Algal oil contained 395 g/kg DHA and 215 g/kg oleic acid, as reported by manufacturers.

3.3.2 Fatty acid analyses.

Experimental diets from Studies 1, 2, and 3, tissues from Studies 1 and 3, and RBCs from Study 1 were analyzed by GLC at Michigan State University as described previously using a GC2010 Gas Chromatograph (Shimadzu, Columbia, MD) equipped with a CP-Sil 88 WCOT (wall-coated open tubular) fused-silica column (100 m × 0.25 mm i.d. × 0.2-μm film thickness; Varian Inc., Lake Forest, CA) with hydrogen as carrier gas [7]. A standard cocktail of fatty acids characteristic of erythrocytes was used to identify phospholipid fatty acids, which were quantified as a percentage of total identified fatty acids after response factor correction. Analysis of RBCs from Studies 2 and 3 was performed by OmegaQuant Analytics, LLC (Sioux Falls, SD), an independent CLIA-certified laboratory.

To verify fatty acid compositions, final diets were analyzed by gas liquid chromatography (GLC) as described above and presented in **Table 3.2**. The dietary fatty acid composition was used to calculate predicted RBC $\omega-3$ HUFA scores. We used a modification of Lands' equation [80] as follows, where HC3 = 3.0, HC6 = 0.70, PC3 = 0.0555, PC6 = 0.0441, HI3 = 0.005, CO = 5.0, and Ks = 0.175.

$$\text{Predicted } \omega-3 \text{ HUFA Score} =$$

$$100 - \frac{100}{1+(HC6/en\%H6)(1+en\%H3/HC3)} + \frac{100}{(1+(PC6/en\%H6)(1+en\%P3/PC3+en\%H3/HI3+en\%O/CO+en\%P6/KS))}$$

En%P6 was the en% of linoleic acid (C18:2ω6), en%P3 was the en% of alpha-linolenic acid, en%H6 was the en% of arachidonic acid (C20:4ω6), and en%H3 was the en% of EPA (C20:5ω3), docosapentaenoic acid (DPA) (C22:5ω6), and DHA (C22:6ω3). En%O (other fatty acids) was calculated for each diet by subtracting en%P6, P3, H6, and H3 from the total en% of fat in the diet. In diet formulations with no measurable arachidonic acid, EPA, DPA, or DHA, the values for en%H6 or H3 were replaced with 0.001, a value much smaller than the estimated en%H6 or H3 in the Western diet.

Table 3.2: Fatty acid profiles of experimental diets as determined by GLC.

		Experimental Diets									
		Study 1			Study 2			Study 3			
	Basal Diet	HF AIN-93G			AIN-93G			MTWD		Low SF/N6 MTWD	
	DHA (en%)	0%	0.96%	2.40%	0%	0.87%	2.62%	0%	2.63%	0%	2.63%
	DHA (%w/w)	0%	0.40%	1.20%	0%	0.40%	1%	0%	1%	0%	1%
Common Name	Chemical Formula	*(% of total fatty acids)*									
Lauric	C12:0	0.07 ± 0.00	0.30 ± 0.06	0.75 ± 0.03	0.04 ± 0.00	0.62 ± 0.00	1.42 ± 0.07	0.65 ± 0.01	1.49 ± 0.03	0.14 ± 0.01	0.83 ± 0.01
Myristic	C14:0	0.18 ± 0.01	0.97 ± 0.21	2.57 ± 0.11	0.16 ± 0.01	1.79 ± 0.02	4.15 ± 0.21	2.87 ± 0.06	5.54 ± 0.05	0.53 ± 0.01	2.51 ± 0.02
Pentadecanoic	C15:0	0.03 ± 0.00	0.03 ± 0.00	0.03 ± 0.00	0.03 ± 0.00	0.02 ± 0.00	0.03 ± 0.00	0.29 ± 0.00	0.30 ± 0.00	0.07 ± 0.00	0.06 ± 0.00
Palmitic	C16:0	8.31 ± 0.12	8.94 ± 0.33	10.05 ± 0.11	5.64 ± 0.04	6.82 ± 0.02	7.79 ± 0.02	22.24 ± 0.16	22.24 ± 0.05	10.87 ± 0.06	11.00 ± 0.01
Palmitoleic	C16:1ω7	0.09 ± 0.00	0.18 ± 0.02	0.34 ± 0.01	0.08 ± 0.00	0.41 ± 0.00	0.86 ± 0.03	0.13 ± 0.01	0.10 ± 0.00	0.13 ± 0.01	0.12 ± 0.01
Stearic	C18:0	2.61 ± 0.04	2.58 ± 0.07	2.47 ± 0.03	0.03 ± 0.00	0.04 ± 0.00	0.04 ± 0.00	8.49± 0.04	8.26 ± 0.03	3.61 ± 0.03	3.37 ± 0.01
Oleic	C18:1ω9	46.36 ± 0.87	42.55 ± 2.21	35.56 ± 1.05	71.08 ± 0.13	62.40 ± 0.08	53.26 ± 0.50	39.19 ± 0.38	29.00 ± 0.08	72.63 ± 0.08	64.41 ± 0.03
Linoleic	C18:2ω6	36.55 ± 0.70	36.09 ± 1.14	34.51 ± 0.70	19.17 ± 0.10	18.94 ± 0.01	15.08 ± 0.79	21.07 ± 0.21	20.62 ± 0.18	8.57 ± 0.04	7.82 ± 0.04
Arachidic	C20:0	0.32 ± 0.01	0.31 ± 0.01	0.28 ± 0.00	0.31 ± 0.00	0.28 ± 0.00	0.24 ± 0.00	0.21 ± 0.03	0.17 ± 0.01	0.29 ± 0.00	0.28 ± 0.01
Alpha-linolenic	C18:3ω3	3.15 ± 0.08	3.25 ± 0.08	3.26 ± 0.09	0.36 ± 0.01	0.37 ± 0.00	0.32 ± 0.01	1.90 ± 0.03	1.81 ± 0.04	0.93 ± 0.01	0.87 ± 0.02
Behenic	C22:0	0.28 ± 0.01	0.28 ± 0.01	0.28 ± 0.01	0.22 ± 0.00	0.21 ± 0.00	0.20 ± 0.00	0.10 ± 0.01	0.11 ± 0.01	0.10 ± 0.01	0.11 ± 0.00
Lignoceric	C24:0	0.13 ± 0.01	0.12 ± 0.01	0.12 ± 0.00	0.14 ± 0.00	0.13 ± 0.00	0.12 ± 0.00	0.04 ± 0.01	0.05 ± 0.01	0.03 ± 0.00	0.05 ± 0.00
Eicosapentaenoic	C20:5ω3	0.00 ± 0.00	0.00 ± 0.00	0.01 ± 0.00	0.00 ± 0.00	0.09 ± 0.00	0.20 ± 0.01	0.00 ± 0.00	0.13 ± 0.00	0.00 ± 0.00	0.10 ± 0.01
Docosahexaenoic	C22:6ω3	0.00 ± 0.00	2.47 ± 0.74	7.74 ± 0.43	0.00 ± 0.00	5.40 ± 0.05	14.20 ± 0.65	0.00 ± 0.00	7.09 ± 0.20	0.00 ± 0.00	6.34 ± 0.08
Total Saturated Fat		12.1 ± 0.2	13.7 ± 0.7	16.8 ± 0.2	8.3 ± 0.1	11.5 ± 0.1	15.4 ± 0.1	35.28 ± 0.21	38.84 ± 0.05	15.80 ± 0.08	18.39 ± 0.02
Total MUFA		47.8 ± 0.9	44.0 ± 2.2	37.1 ± 1.1	71.9 ± 0.1	63.5 ± 0.1	54.7 ± 0.5	41.74 ± 0.36	31.49 ± 0.10	74.70 ± 0.10	66.49 ± 0.01
Total ω-6 PUFA		36.7 ± 0.7	36.1 ± 1.14	34.6 ± 0.7	19.2 ± 0.1	18.9 ± 0.1	15.1 ± 0.8	21.07 ± 0.21	20.62 ± 0.18	8.57 ± 0.04	7.82 ± 0.04
Total ω-3 PUFA		3.2 ± 0.1	5.8 ± 0.9	11.1 ± 0.4	0.4 ± 0.00	5.9 ± 0.1	14.7 ± 0.1	1.90 ± 0.03	9.04 ± 0.19	0.93 ± 0.01	7.31 ± 0.05
ω-6:ω-3 Ratio		11.6 ± 0.3	6.4 ± 0.9	3.12 ± 0.13	52.8 ± 1.3	3.2 ± 0.0	1.0 ± 0.1	11.07 ± 0.10	2.28 ± 0.07	9.24 ± 0.13	1.12 ± 0.01

Abbreviations: GLC, gas-liquid chromatography; MUFA, monounsaturated fatty acid; PUFA, polyunsaturated fatty acid.

3.3.3 Determination of the RBC ω-3 HUFA Score and the O3I.

The ω-3 HUFA score and O3I were determined for RBCs and all available tissues of each animal. The ω-3 HUFA score is the sum of EPA (C20:5ω3), DPA (C22:5ω3), and DHA (C22:6ω3) as a percentage of the most abundant HUFAs (C20:5ω3, C22:5ω3, C22:6ω3, C20:3ω6, C20:4ω6, C22:4ω6, C22:5ω6, C20:3ω9) [79].

$$\omega{-}3 \text{ HUFA Score} = 100\% * \frac{EPA+DPA+DHA}{TotalHUFA}$$

The O3I was calculated by taking the sum of EPA and DHA as a percent of total fatty acids [349]. In tissues, this value is referred to as EPA + DHA.

$$\text{Omega}{-}3 \text{ Index (O3I)} = 100\% * \frac{EPA+DHA}{TotalFA}$$

3.3.4 Data analysis and statistics.

All correlations to inflammatory endpoints used ω-3 HUFA scores and O3Is measured in RBCs. Data were analyzed using Graph Pad Prism 8.0.0 (GraphPad Software, San Diego, CA, www.graphpad.com). Inflammatory endpoints that were undetectable were replaced with half of the minimum value for the individual endpoint. The robust regression and outlier removal (ROUT) method was used to identified outliers, which were excluded from further analysis ($Q = 0.5\%$). For all endpoints, <10% of data points were identified as outliers. Where appropriate, non-normal data were $\log_{10}$ transformed and analyzed using linear regression. To account for experimental and methodological differences, all log transformed inflammatory and autoimmune endpoints were standardized prior to performing correlations across multiple experiments. When the best-fit values of the slope and y-intercept were not significantly different between experiments, raw data from each experiment were combined and re-analyzed to obtain a single linear regression model. Correlation analyses were performed on raw data using Spearman's Correlation due to non-normality of the data (per Shapiro-Wilk Test, $p < 0.05$). For correlations to autoantibody classes and sub-types, autoantibody groups were determined based on location and function of cognate autoantigens. Within a given

group, signal intensities for individual autoantibodies were normalized and summed to obtain a group score for each animal, as described previously [39]. The score was used to perform correlation analyses against the RBC ω-3 HUFA score. In analyses comparing diet groups, data are presented as mean ± SEM with n = 7–8 mice per group. To compare the O3I and ω-3 HUFA scores of animals positive or negative for nephritis, the non-parametric Mann-Whitney Rank Sum test was used. A p-value < 0.05 was considered statistically different for all study outcomes.

3.4 RESULTS

3.4.1 DHA supplementation dose-dependently increases ω-3 HUFA Score uniformly across RBC and tissues.

The effects of substituting various amounts of DHA-rich microalgal oil for high oleic acid safflower oil (HF AIN-93G, Study 1; AIN-93G, Study 2) or olive oil in (MTWD and MTWD ↓SF.ω6, Study 3) on resultant tissue and RBC ω-3 HUFA scores were compared. Regardless of diet, increasing the DHA content up to 2.6 en% (human equivalent dose of ∼5 g/d) dose-dependently increased RBC ω-3 HUFA scores (**Figure 3.1A**). These increases closely correlated (R^2 = 0.93–0.99, p < 0.05) with predicted ω-3 HUFA scores calculated from diet composition using Lands' equation (**Figure 3.1B**). ω-3 HUFA scores were relatively consistent across all tissues, both for basal and DHA-supplemented diets (**Figure 3.2 A,C**). DHA-dependent increases in RBC ω-3 HUFA score closely correlated (p < 0.001) with those in lung (r_s = 0.87), spleen (r_s = 0.84), and kidney (r_s = 0.72) for Study 1 (**Figures 3.2 A-B**), and in lung (r_s = 0.90), spleen (r_s = 0.89), liver (r_s = 0.86), and kidney (r_s = 0.95) for Study 3 (**Figures 3.2 C,D**). Using the O3I as a measure of fatty acid content resulted in lower and more varied correlations (r_s = 0.27–0.88, **Supplementary Figure B.2 B,D**).

3.4.2 Elevated RBC ω-3 HUFA Scores negatively correlate with IRG expression in the lung.

Elevated IRG expression is highly associated with flaring and increased disease severity in lupus [54]. It was demonstrated in Studies 2 and 3 that IRG expression is upregulated in cSiO_2-exposed NZBWF1 mice and that this is suppressed by DHA supplementation [175, 8]. Here, an interferon

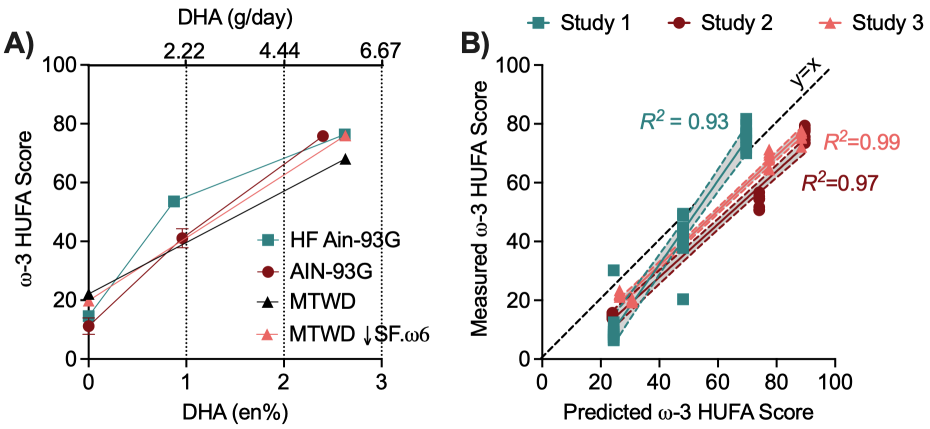


Figure 3.1: RBC ω-3 HUFA score increases with DHA intake in NZBWF1 mice and can be predicted based on diet composition in $cSiO_2$-treated NZBWF1 mice. Animals were fed different diets for Studies 1 (HF AIN-93G), 2 (AIN-93G), and 3 (MTWD and MTWD ↓SF.ω6) with or without DHA (see Table 3.1) as indicated by individually colored lines and symbols. At experiment termination, red blood cells (RBCs) were analyzed for fatty acids by GLC. **A.** Increasing en% of DHA in the diet elevated ω-3 HUFA score similarly across all experimental diets. Data presented as mean ± SEM. **B.** The ω-3 HUFA score is predictable based on the en% of major ω-3 and ω-6 fatty acids using Lands' equation. Individual animals represented by individual data points. For all regression analyses, R^2 is reported next to the corresponding line and p<0.001 Shaded bands around regression lines represent 95% confidence intervals.

(IFN) score was generated by combining the autoscaled expression of 12 IRGs measured in animals fed AIN-93G, MTWD, and MTWD ↓SF.ω6 [8]. Resultant IFN scores negatively correlated with ω-3 HUFA scores (R^2 = 0.29, p < 0.0001, **Figure 3.3A**). This negative correlation is illustrated for representative IRGs including *Isg15* (R^2 = 0.32, p < 0.0001, **Figure 3.3B**), *Psmb8* (R^2 = 0.32, p < 0.0001, **Figure 3.3C**), *Irf7* (R^2 = 0.26, p < 0.0001, **Figure 3.3D**), and *Oasl1* (R^2 = 0.30, p < 0.0001, **Figure 3.3E**). Overall, the autoscaled plots indicate that ω-3 HUFA scores above 40% were associated with reduced IRG scores and individual gene expression (**Figure 3.3**).

3.4.3 Higher RBC ω-3 HUFA Scores correspond to reduced pro-inflammatory cytokines and leukocyte infiltration in BALF.

Intranasal instillation of $cSiO_2$ elicits local sterile inflammation in the lungs of NZBWF1 mice that is associated with elevated proinflammatory cytokines, chemokines, and mononuclear cell influx, all of which can be suppressed by DHA supplementation [4, 7, 8]. Here it was found that IL-6 (R^2

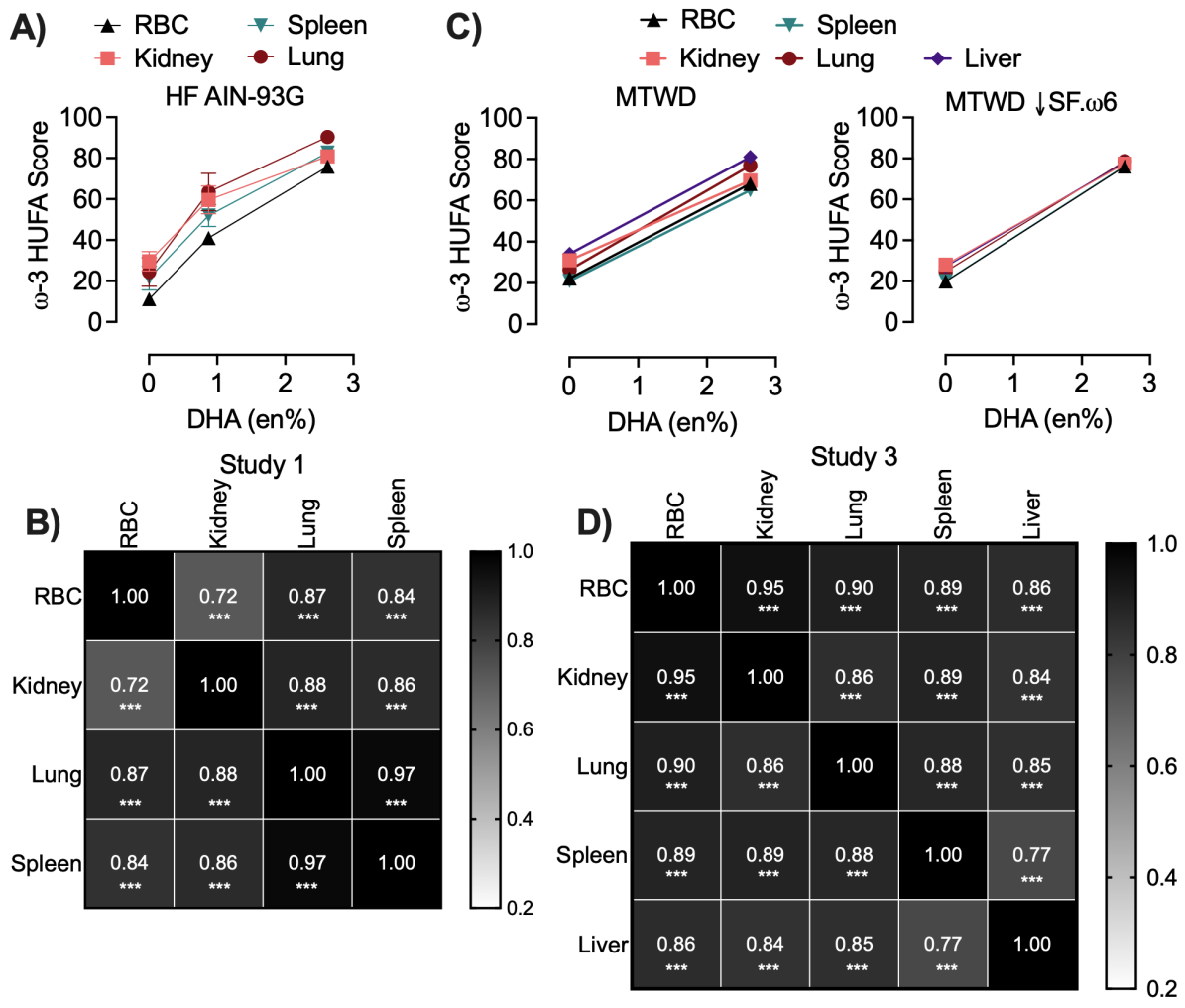


Figure 3.2: ω-3 HUFA scores are consistent across multiple tissues in $cSiO_2$-treated NZBWF1 mice. Mouse tissues from **A,B.** Study 1 (HF AIN-93G diet) and **C,D.** Study 3 (MTWD and MTWD ↓SF.ω6 diets) were analyzed separately to assess the impact of DHA in tissue fatty acid incorporation. Study 2 is not included because only RBCs were analyzed in this study. **A,C.** ω-3 HUFA scores increased similarly across tissues with DHA supplementation. Data presented as mean ± SEM. **B,D.** Pearson's correlation was used to assess correlations between the ω-3 HUFA score across different tissues (***p<0.001).

= 0.26, p = 0.0001, **Figure 3.4A**), MCP-1 (R^2 = 0.29, p < 0.0001, **Figure 3.4B**), and TNF-α (R^2 = 0.39, p < 0.0001, **Figure 3.4C**) concentrations in the BALF were negatively correlated with the ω-3 HUFA score. Consistent with these findings, numbers of macrophages (R^2 = 0.40, p < 0.0001, **Figure 3.5A**), lymphocytes (R^2 = 0.35, p < 0.0001, **Figure 3.5B**), and neutrophils (R^2 = 0.12, p = 0.0029, **Figure 3.5C**) in BALF also negatively correlated with the ω-3 HUFA score in all three

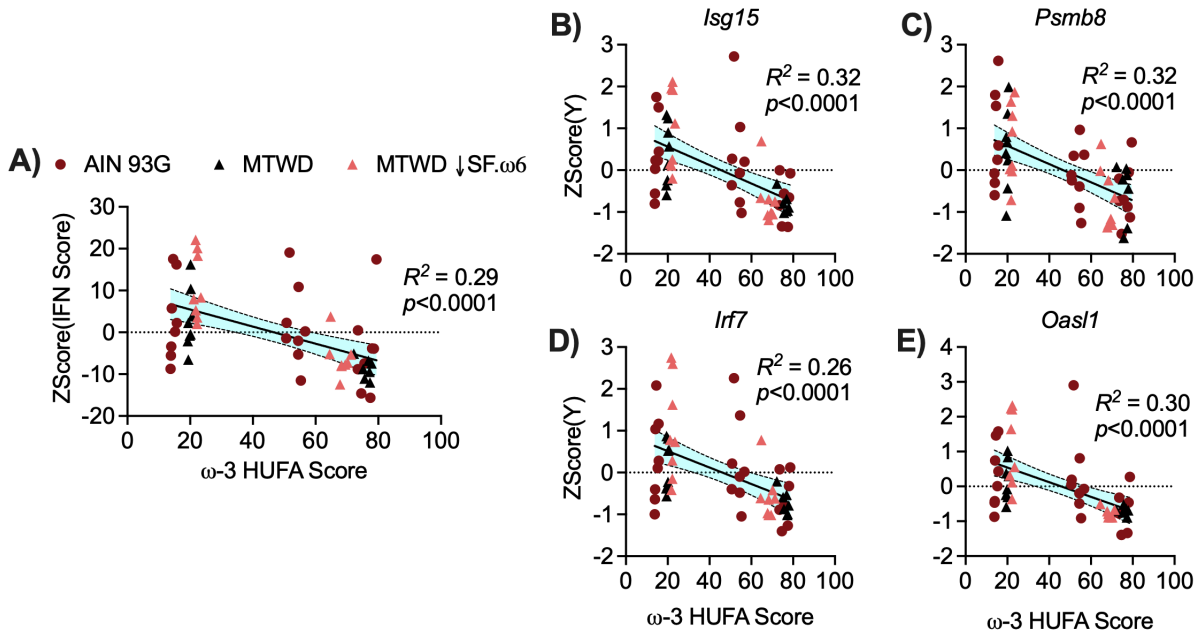


Figure 3.3: RBC ω-3 HUFA score negatively correlates with IFN-regulated gene expression in $cSiO_2$-triggered NZBWF1 mice. A. An interferon (IFN) score was calculated to include 12 IFN-related genes significantly induced by $cSiO_2$ exposure (*Ccl7, Zbp1, Ifi44, Ifit1, Irf7, Isg15, Mx1, Oas2, Oasl1, Psmb8, Rsad2, Siglec1*). These genes were presented as fold-change relative to vehicle-instilled animals. Missing values and outliers were handled as described in the Methods section. Expression was standardized by autoscaling (subtracting the mean expression of the gene and dividing by the standard deviation of the expression of the gene). Standardized scores of all genes for each sample were summed to achieve the IFN score. **B-E.** Representative genes used in the calculation of the IFN score including **B.** *Isg15*, **C.** *Psmb8*, **D.** *Irf7*, and **E.** *Oasl1* reflect the trend observed in the combined IFN score. All values were plotted against the ω-3 HUFA score and the resulting data analyzed by simple linear regression. Regression coefficients were considered statistically significant at $p<0.05$. Shaded bands around regression lines represent 95% confidence intervals.

studies. Though some R^2 values are relatively low, there is a consistent negative linear relationship with all endpoints assessed. Consonant with IRG expression, reductions in these inflammatory responses was most apparent when ω-3 HUFA scores exceeded 40%.

3.4.4 Increased RBC ω-3 HUFA Scores are associated with reduced ectopic lymphoid structure (ELS) neogenesis and autoantibody production.

Central to $cSiO_2$-triggered autoimmunity in NZBWF1 mice is the appearance of ELS in the lung composed of germinal center-like organization of B- and T-cells [7]. These structures promote the

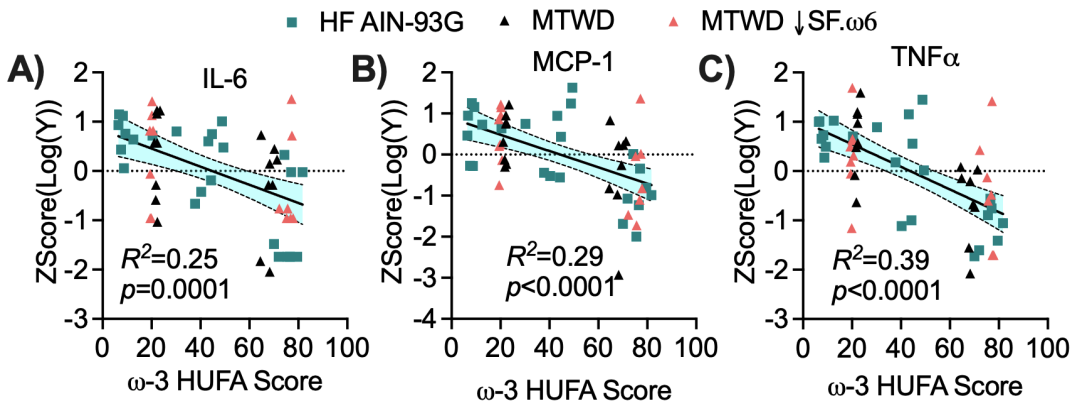


Figure 3.4: Increasing RBC ω-3 HUFA score corresponds to reduced inflammatory cytokines in the lung alveolar fluid of $cSiO_2$-triggered NZBWF1 mice. Bronchoalveolar fluid (BALF) was analyzed for the proinflammatory cytokines **A.** IL-6, **B.** MCP-1, and **C.** TNFα by ELISA in Study 1 and by a multiplexed bead based assay in Study 3. To compare across experiments, data was linearized by $\log_{10}$ transformation and standardized by autoscaling. The normalized and standardized data were plotted against the ω-3 HUFA score for each animal. When each diet was assessed individually, the resultant linear models were not found to be significantly different from one another, indicating that the data sets could be combined and analyzed simultaneously. The combined data were analyzed by a simple linear regression and goodness of fit presented as R^2. Regression coefficients were considered statistically significant at $p<0.05$. Shaded bands around regression lines represent 95% confidence intervals.

development of autoreactive plasma cells and the production of autoantibodies. Notably, their formation is suppressed by DHA supplementation [4, 7, 8]. Consistent with those observations, very strong, negative linear correlations were observed between the ω-3 HUFA score and $CD3^+$ (R^2 = 0.45, $p < 0.0001$) and $CD45R^+$ ($R^2 = 0.62$, $p < 0.0001$) lung tissue in Studies 1, 2, and 3 (**Figure 3.6 A-B**). Similar correlations were observed for anti-dsDNA in BALF ($R^2 = 0.35$, $p < 0.0001$) and plasma ($R^2 = 0.24$, $p < 0.0001$) as measured by ELISA (**Figure 3.6 C-D**). Again, ω-3 HUFA scores over 40% were associated with reduced ELS development and anti-dsDNA production. A further feature of Study 2 was the use of high throughput autoantigen microarray for in-depth analysis of autoantibodies relative to specificity and isotype [39]. Robust negative correlations were found between ω-3 HUFA score and IgG and IgM autoantibodies in both BALF and plasma with specificity for a broad range of host antigens (most r_s values between −0.4 and −0.6, significance indicated by asterisks) (**Figure 3.7**).

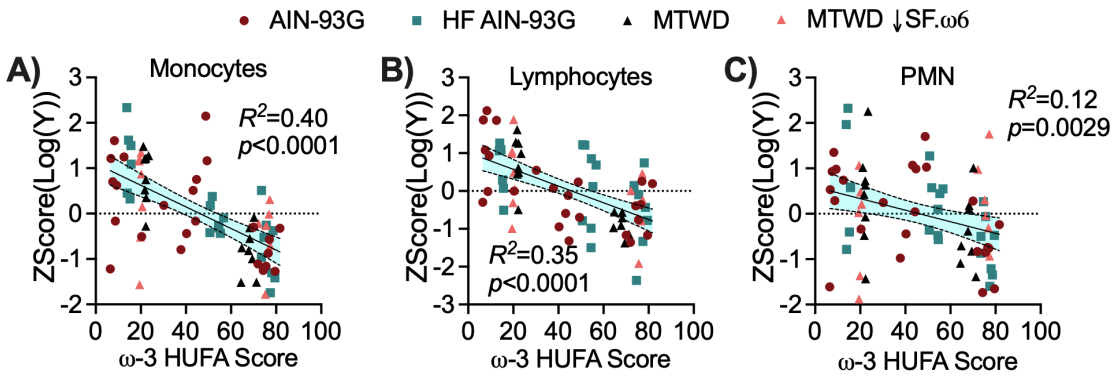


Figure 3.5: Elevated RBC ω-3 HUFA scores are associated with reduced mononuclear cell infiltration into lung alveolar fluid of $cSiO_2$-triggered NZBWF1 mice. Bronchoalveolar lavage fluid (BALF) was assessed for **A.** macrophages, **B.** lymphocytes, and **C.** neutrophils by differential cell counts, as determined by morphological assessment of 200 total cells on cytological slides. Counts between diet groups were normalized by log transformation and standardized by autoscaling. The normalized and standardized data was plotted against the ω-3 HUFA score for each animal. The data was analyzed by a simple linear regression and goodness of fit presented as R^2. Regression coefficients were considered statistically significant at $p<0.05$. Shaded bands around regression lines represent 95% confidence intervals.

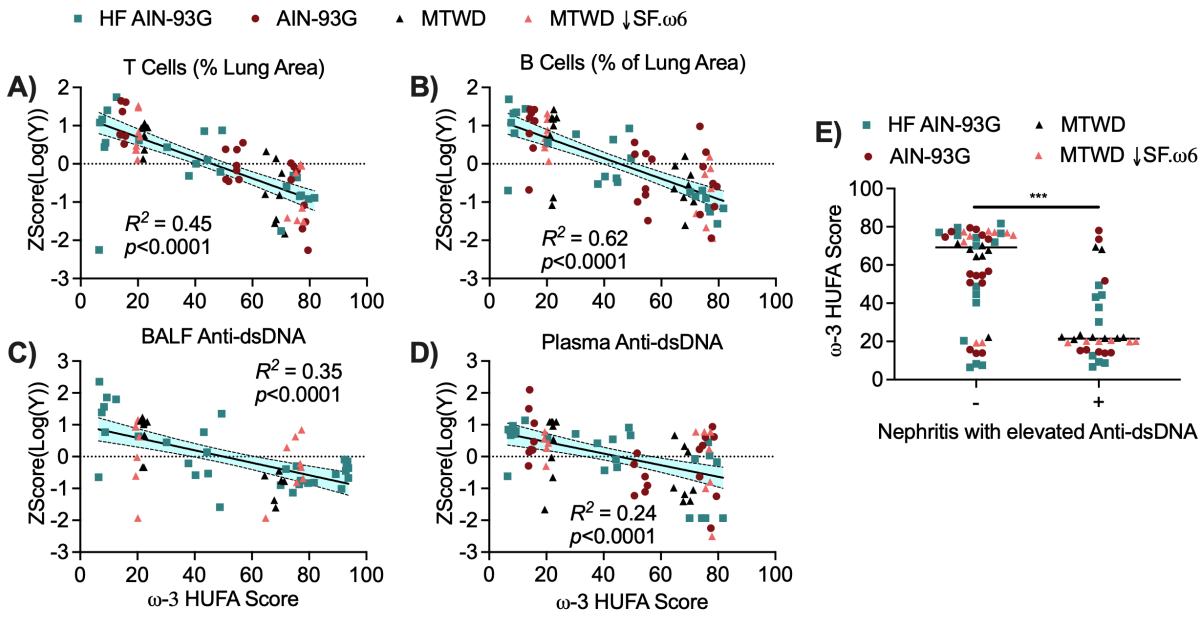


Figure 3.6: High RBC ω-3 HUFA scores correspond with suppression of ectopic lymphoid structure (ELS) neogenesis, anti-dsDNA response, and disease progression in cSiO$_2$-triggered NZBWF1 mice. A-D. Ectopic lymphoid structure (ELS) neogenesis was assessed by measuring the volume density of **A.** T cells (CD3$^+$) and **B.** B cells (CD45R$^+$), respectively, in the bronchial and perivascular regions of the lung. Anti-dsDNA was measured in **C.** bronchoalveolar lavage fluid (BALF) and **D.** plasma by ELISA. Percent area covered by T or B cells and anti-dsDNA levels were $\log_{10}$ transformed to normalize followed by autoscaling to standardize across experiments. These values were plotted against the ω-3 HUFA score and the resulting data analyzed by simple linear regression. Goodness of fit of the linear regression was presented as R^2. Regression coefficients were considered statistically significant at $p<0.05$. Shaded bands around regression lines represent 95% confidence intervals. **E.** Mice positive for renal lesions and elevated plasma anti-dsDNA IgG (significantly different from mean of the Veh-treated group, $p<0.05$) had significantly lower median ω-3 HUFA scores than mice in the the group negative for these endpoints, as assessed by the non-parametric Mann-Whitney U-test (***$p<0.001$). Quantification of renal histopathology score was based on the following scoring criteria: No proteinosis, normal glomeruli (0); multifocal segmental proliferative glomerulonephritis (1); multifocal segmental proliferative glomerulonephritis and occasional glomerular sclerosis and crescent formation (2); diffuse global segmental proliferative glomerulonephritis (3). Animals receiving any score $\geq$1 were categorized as positive for renal lesions.

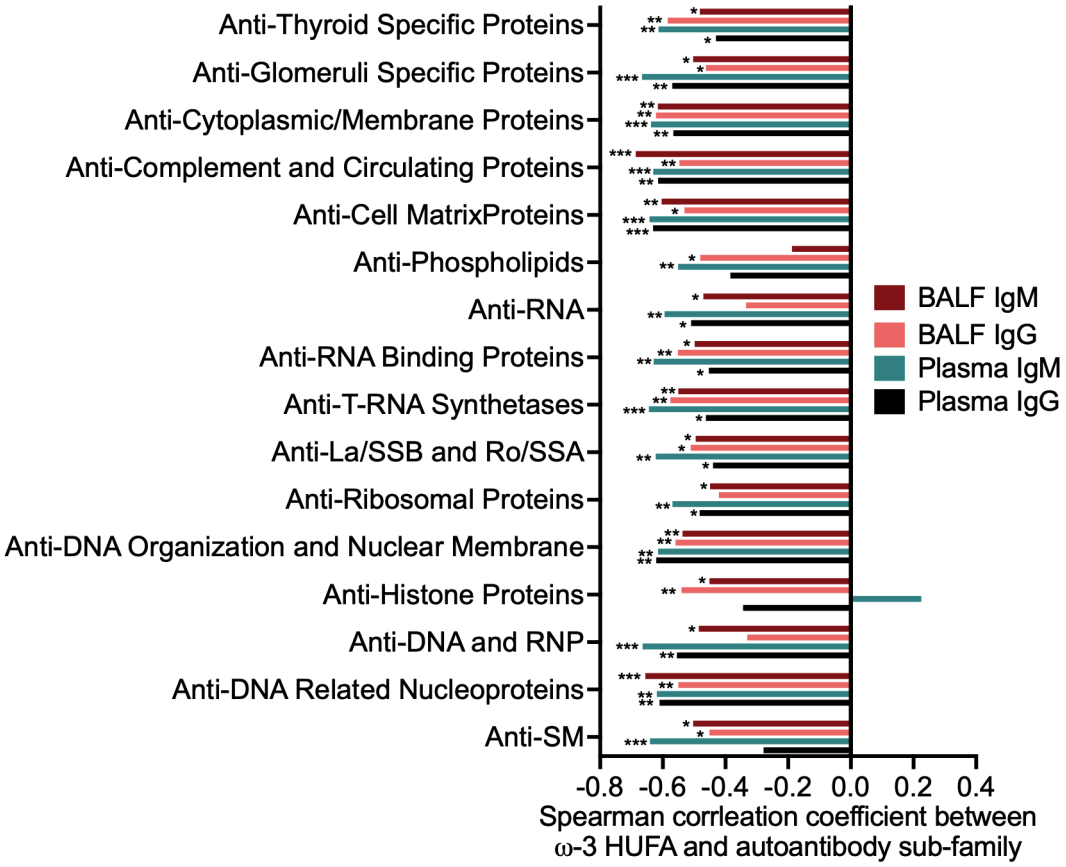


Figure 3.7: Increased RBC ω-3 HUFA scores correlate with reductions in a broad array of autoantibodies relative to specificity and isotype in the plasma and BALF of $cSiO_2$-treated NZBWF1 mice. Autoantigen coated protein arrays were used for profiling four isotypes of autoantibody (IgG, IgM, IgA, and IgE) in plasma and bronchoalveolar lavage fluid (BALF) in Study 2. The final intensity value of each autoantibody was expressed as an autoantibody score. Individual autoantibodies were grouped according to the function of their cognate antigens (group names shown on y-axis) as described in the Methods section. The scores of each autoantibody in this group were combined to obtain an overall score for each group. This score was related to the ω-3 HUFA score using Spearman's correlation coefficient. *p<0.05, **p<0.01, ***p<0.001.

3.4.5 Higher RBC ω-3 HUFA Scores were associated with delayed disease progression.

Early glomerulonephritis onset and production of autoantibodies is a critical outcome of $cSiO_2$-triggered systemic autoimmunity that was prevented by dietary DHA supplementation in Studies 1, 2, and 3 [4, 7, 8]. We defined lupus disease progression in animals as the presence of renal lesions combined with elevated plasma anti-dsDNA IgG in $cSiO_2$-treated animals compared to the mean of the vehicle-treated group ($p < 0.05$). This is reflective of the SLICC criteria published in 2013, which stated that combination of biopsy confirmed nephritis in the presence of either ANA or anti-dsDNA antibodies is sufficient for classification of lupus in humans [350]. Mice negative for both renal lesions and plasma anti-dsDNA IgG had significantly higher ω-3 HUFA scores (median of 69.18, 95% CI 54.46–74.59) compared to animals positive for both endpoints (median of 21.43, 95% CI 19.44–30.21) (**Figure 3.6E**). Consistent with the above findings for inflammation and autoimmunity indicators, ω-3 HUFA scores below $\sim$40% were associated with disease progression.

3.4.6 Higher O3I were associated with reduced autoimmune pathogenesis.

O3Is for Study 1 increased with en% DHA in the diet to a much lesser extent than those for Studies 2 and 3 (**Supplementary Figure B.1**). When assessing DHA's effects on the O3I in tissues, responses followed the rank order of kidney > lung > spleen > RBC for Study 1, whereas for Study 3 the rank order was RBC > kidney > lung > spleen > liver (**Supplementary Figure B.2 A,C**). Previous reports of the RBC O3I for animals fed similar diets were much more similar to those observed in Studies 2 and 3 (in the range of 6–14%) [304]. Together these observations suggest that there were methodological issues with the fatty acid analysis in Study 1, possibly due to fatty acid decomposition. Therefore, correlation analyses between O3Is and inflammation and autoimmunity indicators were performed only for Studies 2 and 3.

O3Is significantly correlated with decreased IFN scores (**Figure 3.8A**) and with downregulated expression of the representative IRGs *Isg15* ($R^2 = 0.28$, $p < 0.0001$, **Figure 3.8B**), *Psmb8* ($R^2 = 0.32$, $p < 0.0001$, **Figure 3.8C**), *Irf7* ($R^2 = 0.25$, $p = 0.0001$, **Figure 3.8D**), and *Oasl1* ($R^2 = 0.30$,

$p < 0.0001$, **Figure 3.8E**). Furthermore, high O3Is were strongly associated with suppression of $cSiO_2$-triggered increases in numbers of macrophages ($R^2 = 0.33$, $p < 0.0001$, **Figure 3.9A**) and lymphocytes ($R^2 = 0.40$, $p < 0.0001$, **Figure 3.9B**) in BALF, as well as decreased ELS neogenesis in the lung as reflected by B-cell ($R^2 = 0.52$, $p < 0.0001$, **Figure 3.9C**) and T-cell ($R^2 = 0.45$, $p < 0.0001$, **Figure 3.9D**) accumulation. Importantly, autoscaled plots consistently suggested that O3Is above 10% were associated with reduced IRG expression, leukocyte infiltration, and ELS development (**Figures 3.8** and **3.9**). Lastly, O3Is were significantly lower in mice (median of 5.44, 95% CI 5.30–5.85) that showed development of lupus as indicated by renal lesions and elevated anti-dsDNA compared to mice negative for both of these endpoints (median of 17.48, 95% CI 14.83–19.67) (**Figure 3.9E**).

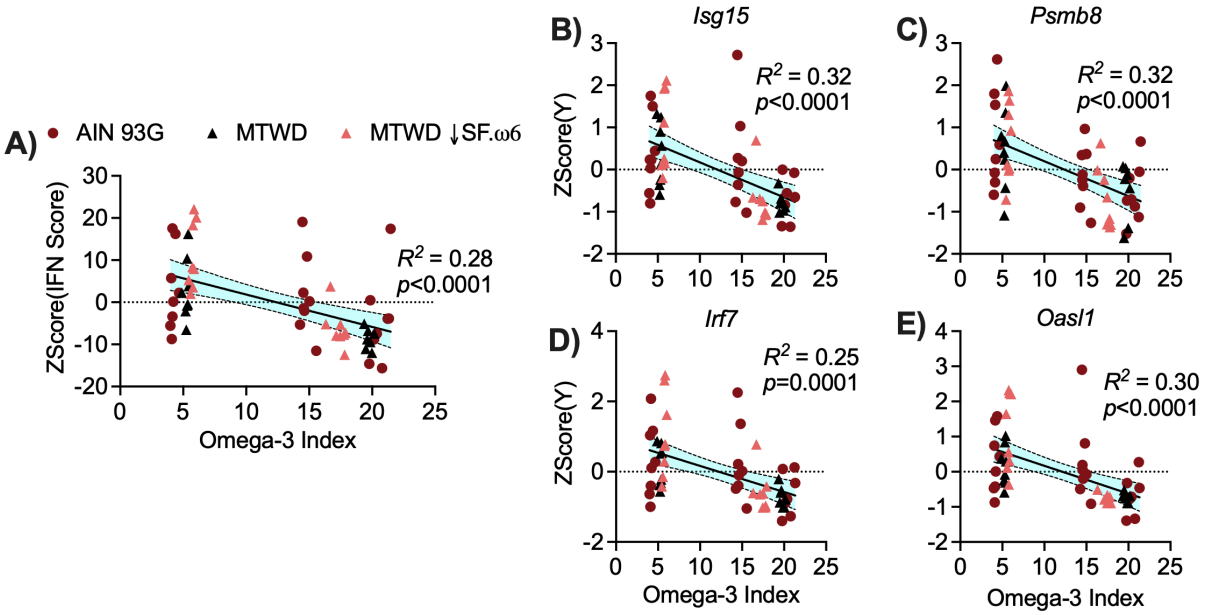


Figure 3.8: The Omega-3 Index (O3I) negatively correlates with IRG expression in $cSiO_2$-triggered NZBWF1 mice. A. Interferon (IFN) scores and expression of the IFN-regulated genes (IRGs) **B.** *Isg15*, **C.** *Psmb*, **D.** *Irf7*, and **E.** *Oasl1* expression were calculated as described in Figure 3.3. The autoscaled IFN scores and the expression of each gene was plotted against the O3I and the resulting data analyzed by simple linear regression. Regression coefficients were considered statistically significant at $p<0.05$. Shaded bands around regression lines represent 95% confidence intervals.

Correlations between inflammation/leukocyte infiltration indicators and RBC ω-3 HUFA scores and O3I for individual animals in Studies 1, 2, and 3 were assessed by Spearman's correlation

analysis. Both ω-3 HUFA scores and the O3I were found to similarly negatively correlate with most endpoints in each study, suggesting that both biomarkers were comparable in predicting DHA's disease-preventive effects (**Figure 3.10**). The only endpoint that showed an opposing trend was the number of polymorphonuclear (PMN) leukocytes measured in the BALF. These differences may be due to the fact that the animals in each experiment were sacrificed at slightly different times post $cSiO_2$ instillation. It appears that animals sacrificed at later dates show an increasing strength in the correlation between ω-3 content and PMN (study 3 sacrificed at 11 wk, study 2 sacrificed at 13 wk, study 1 sacrificed at 12 wk). This may be due to increased disease severity leading to more pronounced neutrophil infiltration between treatment groups.

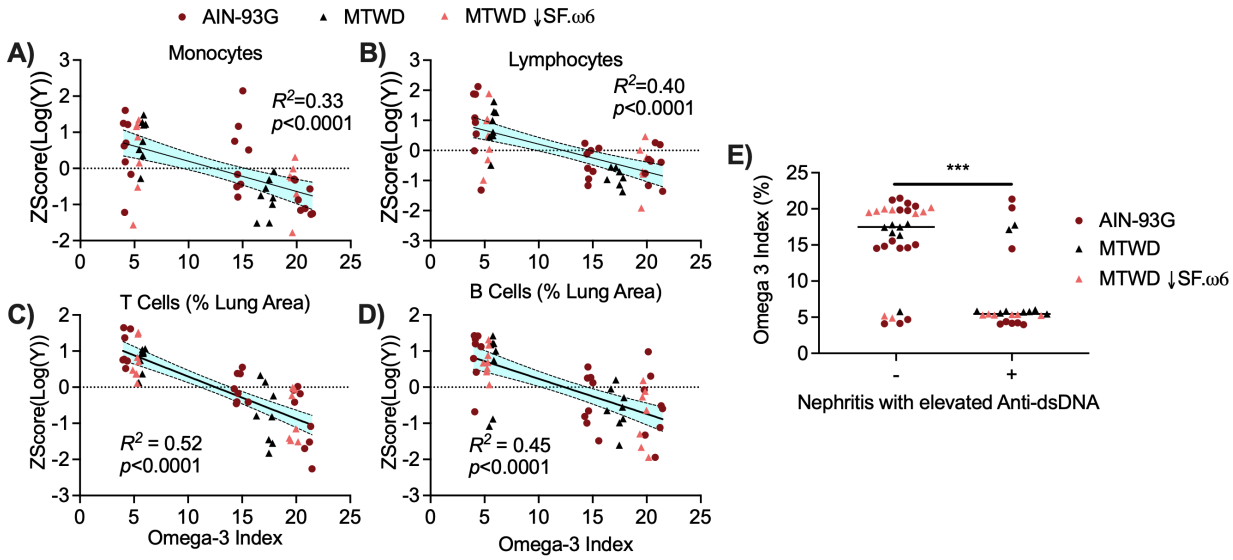


Figure 3.9: Heightened O3Is correspond with suppression of leukocyte infiltration, ELS development, and disease progression in $cSiO_2$-triggered NZBWF1 mice. A. Macrophage and **B.** lymphocyte infiltration, as well as **C.** B-cell$^+$ and **D.** T-cell$^+$ lung tissue were negatively correlated with the Omega-3 Index (O3I). **E.** Mice positive for renal lesions and elevated plasma anti-dsDNA IgG (significantly different from mean of the Veh-treated group, $p<0.05$) had significantly lower median O3Is than mice in the the group negative for these endpoints, as assessed by the non-parametric Mann-Whitney U-test (***$p<0.001$). For **A-D**, data were analyzed by a simple linear regression and goodness of fit presented as R^2. Regression coefficients were considered statistically significant at $p<0.05$. Shaded bands around regression lines represent 95% confidence intervals.

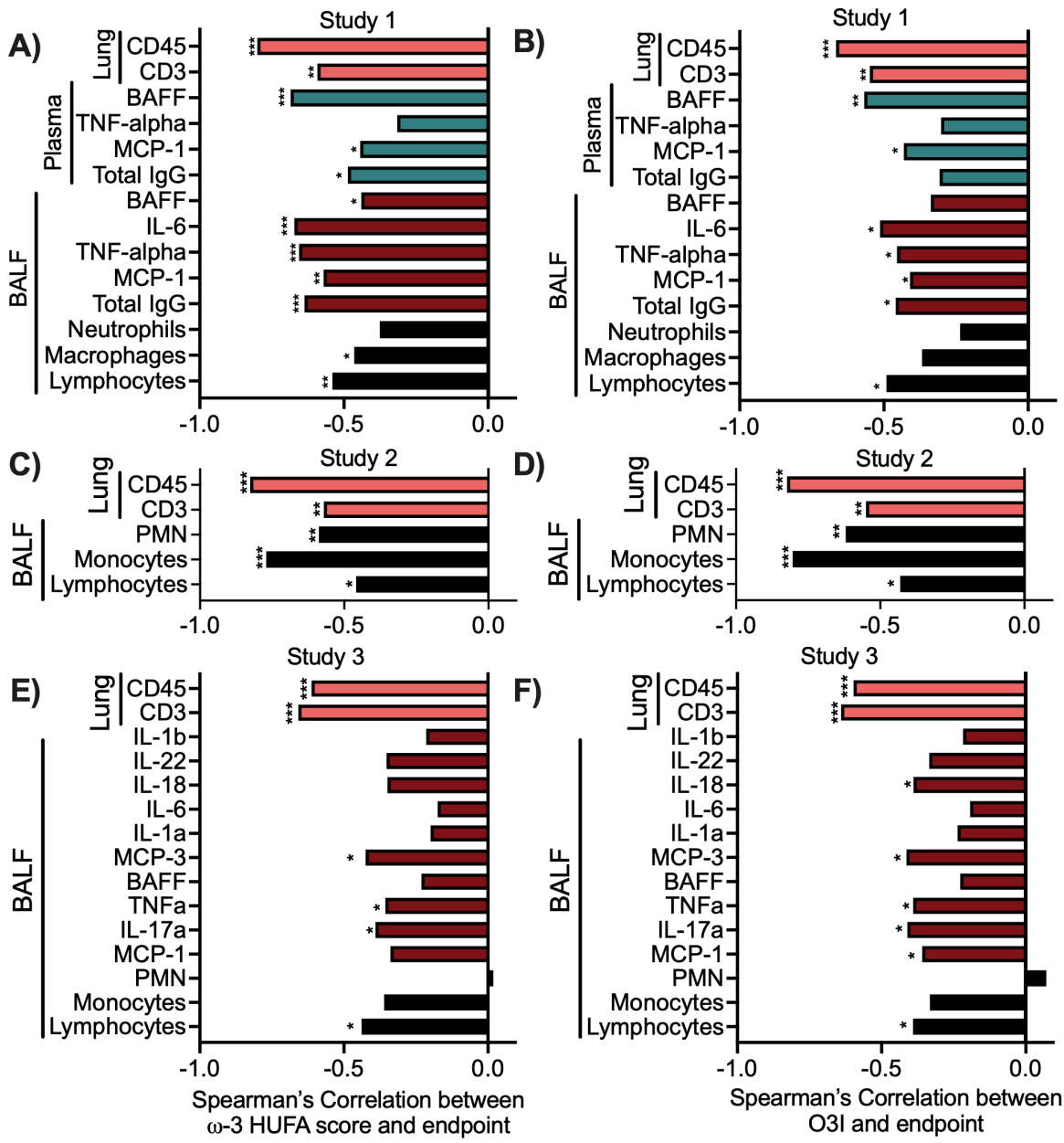


Figure 3.10: RBC ω-3 HUFA score and O3I both negatively correlate with inflammatory/autoimmune indicators and pulmonary immune cell infiltration. Correlation between inflammatory endpoints and red blood cell (RBC) ω-3 HUFA scores and Omega-3 Indexes (O3Is) for individual animals was assessed by Spearman's correlation coefficient, due to non-normal distribution of samples. Many endpoints in **A-B.** Study 1 (HF AIN-93G diet), **C-D.** Study 2 (AIN-93G diet), and **E-F.** Study 3 (MTWD and MTWD ↓SF.ω6 diets) were significantly negatively correlated with both the ω-3 HUFA score and the O3I. *p<0.05, **p<0.01, ***p<0.001.

3.5 DISCUSSION

Murine lupus models typically display gradual increases in autoantibodies prior to glomerulonephritis and thus mimic quiescent disease prior to flaring-associated organ damage [282]. Here, airway exposure to $cSiO_2$ was used to mimic flaring in NZBWF1 mice by promoting persistent sterile inflammation, cell death, robust expression of IRGs, and development of autoantibody-producing ELS in the lung [175, 7, 3]. These autoantibodies and resultant immune complexes can accumulate in the kidney, accelerating glomerulonephritis [351, 352]. We report here for the first time that increasing two biomarkers of ω-3 HUFA tissue content, the ω-3 HUFA score and the O3I, by dietary DHA supplementation is highly associated with suppression of $cSiO_2$-triggered lupus flaring. Benchmark thresholds for these biomarkers were further identified that may be highly relevant to future clinical use of ω-3 HUFA supplementation as an intervention against lupus and other autoimmune diseases.

As has been reviewed previously [291], autoimmune disease onset and progression following $cSiO_2$ inhalation likely begins with unresolvable inflammation and rampant cell death in the lung, overwhelming the ability of alveolar macrophages to clear autoantigen-containing debris by efferocytosis [353]. The presence of host nucleic acids released from dying cells may stimulate a type I IFN response [42, 53]. Type I IFNs, including IFN-α, promote autoantigen presentation to infiltrating B- and T-cells and induce the release of additional cytokines such as B-cell activating factor (BAFF) [56, 57], the target of the monoclonal antibody drug Benlysta, approved for treatment of adult lupus in 2011 and pediatric lupus in 2019. BAFF stimulates the maturation of B-cells into autoantibody-producing plasma cells. The resultant DNA-containing immune complexes induce further release of IFN-α, sustaining this cycle [54]. Marine ω-3s and their metabolites attenuate multiple steps of this putative pathway, resulting in protection against $cSiO_2$-triggered autoimmunity. Several studies indicate that DHA is capable of blocking key inflammatory pathways and promoting a more pro-resolving phenotype in macrophages, which enhances their ability to efferocytose dying cells, thereby preventing aberrant production of type 1 IFNs, pro-inflammatory cytokines, and chemokines [272, 185, 354]. Together, these inhibitory actions could dampen the

subsequent inflammatory and downstream autoimmune responses. As shown here, increasing both the ω-3 HUFA score or the O3I correlated with reductions in IRG, cytokine, chemokine expression, B- and T-cell infiltration, autoantibody production, and glomerulonephritis induced by $cSiO_2$ exposure.

In 2020, the National Institutes of Health announced at 10 years strategic plan focusing on precision nutrition—a "holistic approach to developing comprehensive and dynamic nutritional recommendations relevant to both individual and population health" (https://www.niddk.nih.gov/about-niddk/strategic-plans-reports/strategic-plan-nih-nutrition-research). Selection of dietary lipids would be central to the development on an individual's precision nutrition plan. The strong correlations between the ω-3 biomarkers and inflammatory endpoints suggest that the balance between ω-3 and ω-6 fatty HUFAs in the cell membrane is critical to promoting inflammation or resolution [355]. At the translational level, there are a variety of factors that will influence the incorporation of dietary HUFAs into the cell membrane of individuals. ω-3 and ω-6 HUFAs compete for incorporation into the membrane phospholipids at the sn2 position, thus increasing the levels of ω-6 fatty acids in the diet will reduce the ω-3 HUFA incorporation in the tissue and vice versa [68]. It has also been shown that the bioavailability of ω-3 supplements is enhanced when provided with a meal rich in other fats [312]. Finally, single nucleotide polymorphisms (SNPs) in lipid metabolizing genes are associated with altered levels of various fatty acids observed in the RBCs and tissues [356, 357], and variations in lipid metabolizing genes are associated with the efficacy of ω-3 supplementation in CVD [358]. Therefore, in preclinical and clinical ω-3 HUFA intervention studies, it is vital to measure of the balance of ω-3 and ω-6 HUFAs.

Measuring an individual's tissue HUFA status can be readily accomplished with low-cost commercial tests that are performed using dried blood spots [78]. The alteration of RBC ω-3 and ω-6 fatty acids observed following dietary interventions is reflected in multiple tissues. Similarly, other studies have shown membrane fatty acid profiles of various immune cells, including monocytes, macrophages, T-cells, and B-cells, are also influenced by ω-3 supplementation [359]. Of the two biomarkers studied, the O3I (i.e., DHA + EPA as a percent of total erythrocyte fatty acids) has been

extensively validated in human clinical studies and is more widely implemented. A critical advantage of the O3I is the wealth of literature utilizing this biomarker, which was proposed for use as a risk factor for CVD in 2004. The widespread use of this biomarker has allowed for meta-analyses to identify O3I levels that show protection against a variety of disease endpoints, particularly in the field of CVD and coronary heart disease (CHD). In instances where storage conditions, extraction protocols, and analytical techniques remain consistent across studies and samples, the O3I is preferable because it can be understood in the context of previous studies. If inconsistencies among these factors are a concern, defining fatty acid levels using the ω-3 HUFA score might be more advantageous.

A major advantage of the ω-3 HUFA score is its consistency across tissues and blood fractions and recalcitrance to differences in storage conditions and analytical techniques. Since HUFAs have similar chemical properties, they are degraded at similar rates [68]. This appeared to be critical factor in our studies, where we found that ω-3 HUFA scores in RBCs were similarly impacted by en% DHA across all three studies, whereas the O3I was less robust (**Figure B.1**). This observation is supported by a previous study that investigated the stability of dried blood spot fatty acids over the course of 4 wk when stored at 4 and −20°C. Bell et al. observed a 15–30% decrease in individual HUFAs stored at 4°C for 28 d, while the ω-3 HUFA score decreased by only 8% [360]. Because our samples were stored and processed under different conditions among experiments, we favored the use of the ω-3 HUFA score for this study. With the ω-3 HUFA score, we saw slightly higher correlations in many of the endpoints assessed, which may be in part due to the reduced variability observed in the HUFA score compared to the O3I. Another advantage shown here (**Figure 3.1B**) and previously [80] is that the ω-3 HUFA score can be predicted from dietary fat intake, making it an important tool when developing personalized nutritional interventions. Finally, focusing on the HUFA pool gives the clinician insight into the potential for the generation of anti-inflammatory ω-3 and proinflammatory ω-6 HUFA metabolites [28, 68].

There are multiple mechanisms by which ω-3 and ω-6 HUFAs directly influence inflammatory pathways in the cell [361]. First, by increasing membrane fluidity and impeding lipid raft forma-

tion, DHA and EPA can interfere with activation of transmembrane receptors associated with inflammatory signaling [228]. Second, both extracellular and intracellular phospholipases can cleave HUFAs from the membrane [70, 362]. Resultant free DHA and EPA may activate transmembrane receptors or intracellular receptors associated with suppressing proinflammatory signaling [72, 73]. Specifically, ω-3 HUFAs have been shown to antagonize TLR activation [363, 364] and interfere with NF-κB-dependent transcription by activating PPARγ [272, 74]. Third, both DHA and EPA are metabolized to form specialized pro-resolving mediators (SPMs) such as maresins, resolvins, protectins, and anti-inflammatory epoxide metabolites [325, 365]. SPMs inhibit inflammatory signaling [366, 367] and promote efferocytosis of dead cells [368], both of which are critical to halting autoimmune disease pathogenesis.

Besides competing for cell membrane incorporation, ω-3 HUFAs can inhibit ω-6 HUFA metabolism to downstream proinflammatory eicosanoids (e.g., thromboxanes, prostaglandins, and leukotrienes) [68]. Lipid metabolites derived from the arachidonic acid cascade have primarily inflammatory actions, especially during acute inflammation. Shifting the HUFA balance to favor ω-3 HUFAs rather than ω-6 HUFAs, such as arachidonic acid, may enhance the pro-resolving phenotype promoted by ω-3 derived lipid mediators. A recent study demonstrated that the plasma and red blood cell levels of ω-3 HUFAs were highly correlated with the production of downstream lipid mediators [325]. Similarly, supplementation with EPA and DHA led to a decrease in ω-6 HUFAs, namely arachidonic acid, as well as decreased ω-6 HUFA-derived metabolites.

It is likely that the anti-inflammatory actions of ω-3 HUFAs and their downstream metabolites are at play in the inflammatory processes driving lupus symptoms. Among lupus patients, higher ω-3 HUFA levels or more frequent consumption of fish correlate with reduced disease activity [12, 326]. In 2011, it was reported that lupus patients had lower amounts of ω-3 HUFAs in RBC and plasma than observed in healthy controls [327], and a subsequent study showed a negative correlation between adipose ω-3 levels and disease activity [331]. More recently, it was shown that individuals with lupus had decreased levels of plasma resolvin D1, an anti-inflammatory metabolite of DHA, as compared to healthy controls [328]. To date, there has been no extensive study of the

membrane fatty acid content or plasma lipidome of lupus patients. Investigation in this area is necessary to elucidate potential benefit of ω-3 supplementation in human patients.

The majority of clinical trials utilizing ω-3 fatty acid supplementation to combat disease have been specific to CVD. Over the past three decades, randomized control trials (RCTs) have produced inconclusive results, with some showing benefit and others not. There are a variety of potential reasons for this inconsistency, as thoroughly reviewed by Rice et al. [369]. Reasons include, among other things, insufficient dose of ω-3 HUFAs and inadequate duration of supplementation. Analysis of the results of some CVD studies reveal that that there can be significant overlap in the O3I in treatment vs. control group at trial completion, which would explain why researchers did not observe any effect with supplementation [370, 371]. Additionally, there is a lack of consistency in measuring the fatty acid content in trial participants. The authors concluded that assessment of the ω-3 status of study participants, both at baseline and throughout the study, is critical to implementing an effective nutritional intervention. A recently published large scale RCT showing positive results with EPA supplementation met many of the suggestions put forth by Rice et al. [369]: (i) the EPA dose given (4 g/d) was $\sim$4-fold greater than other contemporaneous trials, (ii) the study had an average duration of 4.9 years, (iii) the baseline EPA levels were identical between the placebo and treatment group, and (iv) the plasma EPA content at 1 year was 5-fold higher than at baseline [372]. This study, as well as other recent RCTs showing beneficial effects of ω-3 supplementation have been reviewed in detail by O'Keefe et al. [373].

Compared to CVD, there have been very few trials investigating the impact of ω-3 supplementation on lupus outcomes, all of which have very few subjects (n < 100) (**Table 3.3**). Recent reviews on this subject [32, 330] reveal that approximately half of the clinical trials performed employing ω-3 supplementation in lupus patients report a reduction in disease activity [332, 374, 294, 295, 338, 296]. Many studies that did not observe a reduction in disease activity reported improvements in other areas, such as a reduction in serum triglycerides [335, 336] or biomarkers of inflammation and oxidative stress [334, 335]. A critical impediment to evaluating the efficacy of ω-3 supplementation in these trials is the inconsistency in measuring and reporting the ω-3 levels

in subjects. Among lupus studies reporting fatty acid levels, there is variability in units used for reporting [mol% [335, 336], wt% [327, 337, 296], mg/mL [294]], the source [platelets [335, 336, 294, 296], RBCs [327, 338], plasma phospholipids [327, 337]], and the fatty acids reported. To more definitively identify ω-3 levels that are protective against lupus symptoms and flaring requires frequent measurement and consistent reporting of ω-3 status in human patients, in addition to more robust clinical trials.

Table 3.3: Summary of ω-3 HUFA intervention trials in lupus patients.

Year	Author	FA dose (EPA+DHA)	Supplementation type	N	Trial duration	Measured fatty acids	Fatty acids reported	Result
1989	Clark et al.	1.8g, 5.4g	MaxEPA fish oil capsules	12	5 wk	Yes - platelets	ARA, EPA, DHA	Decreased Triglycerides and cholesterol
1991	Walton et al.	5.6 g	MaxEPA fish oil capsules	27	12 wk	Yes - RBCs	not reported	Improved disease status
1993	Clark et al.	4.4 g	MaxEPA fish oil capsules	21	1 yr	Yes - Platelets	ARA, EPA, DHA	Improvement, but not in renal function or disease activity
2004	Duffy et al.	0.9 g	MaxEPA fish oil capsules	52	24 wk	Yes - Platelets	EPA, DHA	Improved disease status
2005	Nakamura et al.	1.8 g	EPA, ethyl esters	6	3 mo	Yes – Plasma PL	LA, DGLA, ARA, ALA, EPA, DPA, DHA	Decreased oxidative stress (8-isoprostane)
2008	Wright et al.	3 g	Omacor, EPA/DHA methyl esters	60	24 wk	Yes - Platelets	ARA, EPA, DHA	Decreased SLAM-R, BILAG, FMD, isoprostanes
2013	Bello et al.	3 g	Lovaza, EPA/DHA ethyl esters	85	12 wk	No	-	No change
2015	Arriens et al.	4.5g	Metagenics fish oil capsules	32	6 mo	No	-	Improved disease status
2015	Lozovoy et al.	300 mg	Fish oil capsules (no brand)	62	4 mo	No	-	Decreased SLEDAI, increased adiponectin, decreased leptin
2017	Borges et al.	1.28 g	Naturalis HiOmega3 fish oil capsules	49	12 wk	No	-	Decreased CRP

Abbreviations: ARA, arachidonic acid; EPA, eicosapentaenoic acid; DHA, docosahexaenoic acid; LA, linoleic acid; DGLA, dihomo-gamma linoleic acid; ALA, alpha linolenic acid; DPA, docosapentaenoic acid; SLAM-R, systemic lupus activity measure – revised; BILAG, British Isles lupus assessment group; FMD, flow mediated dilation; SLEDAI, systemic lupus erythematosus disease activity index; CRP, C-reactive protein. Citations: Clark 1989 [335], Walton 1991 [338], Clark 1993 [336], Duffy 2004 [294], Nakamura 2005 [337], Wright 2008 [296], Bello 2013 [333], Arriens 2015 [332], Lozovoy 2015 [295], Borges 2017 [334]

The recent studies identifying the protective effects of ω-3 supplementation in CVD support the potential benefit for a similar dietary intervention in lupus. Notably, patients with lupus have an increased risk of myocardial infarction and CVD mortality relative to the general population

[375]. A key mechanism proposed to link these chronic diseases is increased oxidative stress [376, 241]. A 2012 clinical trial with >700 participants reported that 4 g/d IPE (iscosapent ethyl, an ethyl ester of EPA) for 12 wk significantly decreased plasma oxidized low density lipoprotein (oxLDL) [377], an oxidized biomarker implicated in CVD. Similarly, urinary F2 isoprostanes, produced by the non-enzymatic oxidation of arachidonic acid and a widely accepted marker for oxidative stress, were decreased by supplementation with 4 g/d of either DHA or EPA in a study of 59 hypertensive patients with type 2 diabetes [378] A specific member of the F2-isoprostane family, 8-isoprostane, was found to be decreased in with ω-3 supplementation in lupus patients, as measured in both the platelets and urine (**Table 3.3**) [337, 296].

In the present study, O3Is above 10% and ω-3 HUFA scores >40% appeared to be associated with absence of disease progression. This is consistent with studies showing decreased mortality from CVD in populations where the ω-3 HUFA score is >40% [379] and associating increased ω-3 HUFA scores to a reduction in chronic pain [380]. In 2004, Harris and von Schacky proposed that an O3I > 8% was associated with decreased risk of death from CHD, while O3I < 4% was associated with increased risk [381], based on a small clinical trial of 57 subjects. In 2017, a meta-analysis of 10 cohort studies, with a combined n > 27,505, confirmed these cutoffs [382]. Because there are far fewer clinical studies investigating the role of ω-3 HUFAs in rheumatic disease, and even fewer that present enough fatty acid information to calculate the ω-3 HUFA score, it is difficult to identify a protective ω-3 HUFA score or O3I for lupus. However, a study performed in patients with rheumatoid arthritis showed that increasing the ω-3 HUFA score from $\sim$30 to $\sim$40% resulted in decreased joint swelling, pain, various inflammatory markers, and non-steroidal anti-inflammatory drug (NSAID) and glucocorticoid use [382].

Providing sufficient levels of ω-3 supplementation is paramount to achieving ω-3 HUFA levels capable of reducing symptoms involved in lupus flares. A recent study presented an equation to predict the change in the O3I using the baseline O3I and the supplemented dose of EPA and DHA [323]. These findings suggested that individuals with a baseline O3I around 4%, a level typical for many individuals consuming a Western diet, would require 1,500 mg/d EPA + DHA for 13 wk to

achieve an O3I of 8%. Though many ω-3 supplementation trials in lupus patients use doses >1,500 mg/d, the results presented herein suggest that a human equivalent dose of $\sim$5 g/d may be necessary to provide protection against a variety of lupus associated endpoints. Consumption of 5 g/d ω-3 HUFAs has been determined as safe by the European Food Safety Authority after analyzing the impact of ω-3 HUFAs on endpoints such as bleeding time, immune function, and changes in blood LDL-cholesterol [383].

A potential limitation of this study is the limited range of doses of DHA provided (0, 2, and 5 g/d human equivalent dose), which may contribute to the relatively low R^2 value observed between the ω-3 biomarkers and some inflammatory endpoints. Additional intermediate doses of DHA, and corresponding intermediate ω-3 levels, may allow for a more accurate regression model. Other informative modifications to the diet would include using EPA as the primary source of dietary ω-3 HUFAs, providing ω-3 HUFAs as phospholipids rather than triglycerides, or varying levels of ω-6 fatty acids to determine the extent to which ω-6 HUFAs impact levels of ω-3 biomarkers and lupus-associated inflammatory endpoints. Finally, it should be recognized that DHA was administered here prophylactically. Since the most severe lupus symptoms are episodic and associated with flaring, the study design of our experiments is most relevant to periods of disease remission achievable by treatment with glucocorticoids, antimalarials, and immunosuppressants — drugs that have many adverse side effects [6]. ω-3 supplementation might be amenable as a substitute or adjunct therapy for these strong drugs to prevent flaring and prolong the quiescent state. However, the prophylaxis model does not mimic the human situation where ω-3 supplementation is provided after the onset of overt symptoms. Thus, further research is needed on the effects of ω-3 supplementation to treat ongoing lupus flares.

To summarize, we demonstrated with this study that both ω-3 HUFA scores and O3Is of mice fed a wide range of diets supplemented with DHA could be related to numerous lupus-associated inflammatory endpoints. This determination is highly relevant to current and future trials investigating the effect of ω-3 supplementation in inflammatory and autoimmune diseases. Our results suggest that measurement of RBC ω-3 levels allows clinicians and administrators of randomized

clinical trials to assess the efficacy of the supplementation strategy employed, as well as confirming compliance. Precision nutritional interventions can be designed to reduce consumption of ω-6 fatty acids while simultaneously supplementing with ω-3 HUFAs, with the objective of achieving an ω-3 HUFA score or O3I that may protect against lupus flaring and autoimmune disease progression.

3.6 ACKNOWLEDGMENTS

We would like to thank Jason Polreis and Bill Harris of OmegaQuant Analytics for their assistance in the red blood cell analysis, Elizabeth Ross for assistance in manuscript preparation, and Melissa Bates and Kristen Gilley for coordination of the animal studies.

CHAPTER 4

DOCOSAHEXAENOIC ACID SUPPRESSES SILICA-INDUCED INFLAMMASOME ACTIVATION AND IL-1 CYTOKINE RELEASE BY INTERFERING WITH PRIMING SIGNAL

Wierenga KA[1,2†], Wee J[3†‡], Gilley KN[3], Rajasinghe LD[3], Bates MA[2,3], Gavrilin MA[4], Holian A[5], Pestka JJ[2,3,6*]

[1]Department of Biochemistry and Molecular Biology, Michigan State University, East Lansing, MI

[2]Institute for Integrative Toxicology, Michigan State University, East Lansing, MI

[3]Department of Food Science and Human Nutrition, Michigan State University, East Lansing, MI

[4]Division of Pulmonary, Critical Care and Sleep Medicine, Ohio State University, Columbus, OH

[5]Department of Biomedical and Pharmaceutical Sciences, Center for Environmental Health Sciences, University of Montana, Missoula, MT

[6]Department of Microbiology and Molecular Genetics, Michigan State University, East Lansing, MI

[†]These authors contributed equally to this work

Author Contributions: KW and JW: study design, data analyses/interpretation, and manuscript preparation. KG: data analysis/interpretation. LR: data analysis/interpretation and manuscript preparation. MB: optimization of RAW-ASC model and data analysis/interpretation. MG: data analysis/interpretation and generation of RAW-ASC model. AH: experimental design, data interpretation, manuscript writing, and project funding. JP: planning, coordination, oversight, manuscript preparation/submission, and project funding.

Originally published in Frontiers in Immunology :

https://doi.org/10.3389/fimmu.2019.02130

4.1 ABSTRACT

Occupational exposure to respirable crystalline silica ($cSiO_2$) has been etiologically linked to human autoimmunity. Intranasal instillation with $cSiO_2$ triggers profuse inflammation in the lung and onset of autoimmunity in lupus-prone mice; however, dietary supplementation with the ω-3 polyunsaturated fatty acid docosahexaenoic acid (DHA) abrogates these responses. Inflammasome activation, IL-1 cytokine release, and death in alveolar macrophages following $cSiO_2$ exposure are early and critical events that likely contribute to triggering premature autoimmune pathogenesis by this particle. Here we tested the hypothesis that DHA suppresses $cSiO_2$-induced NLRP3 inflammasome activation, IL-1 cytokine release, and cell death in the macrophage. The model used was the murine macrophage RAW 264.7 cell line stably transfected with the inflammasome adapter protein ASC (RAW-ASC). Following priming with LPS, both the canonical activator nigericin and $cSiO_2$ elicited robust inflammasome activation in RAW-ASC cells, as reflected by IL-1β release and caspase-1 activation. These responses were greatly diminished or absent in wild-type RAW cells. In contrast to IL-1β, $cSiO_2$ induced IL-1α release in both RAW-ASC and to a lesser extent in RAW-WT cells after LPS priming. $cSiO_2$-driven effects in RAW-ASC cells were confirmed in bone-marrow derived macrophages. Pre-incubating RAW-ASC cells with 10 and 25 μM DHA for 24 h enriched this fatty acid in the phospholipids by 15- and 25-fold, respectively, at the expense of oleic acid. DHA pre-incubation suppressed inflammasome activation and release of IL-1β and IL-1α by nigericin, $cSiO_2$, and two other crystals – monosodium urate and alum. DHA's suppressive effects were linked to inhibition of LPS-induced *Nlrp3*, *Il1b*, and *Il1a* transcription, potentially through the activation of PPARγ. Finally, nigericin-induced death was inflammasome-dependent, indicative of pyroptosis, and could be inhibited by DHA pretreatment. In contrast, $cSiO_2$-induced death was inflammasome-independent and not inhibited by DHA. Taken together, these findings indicate that DHA suppresses $cSiO_2$-induced inflammasome activation and IL-1 cytokine release in macrophages by acting at the level of priming, but was not protective against $cSiO_2$-induced cell death.

4.2 INTRODUCTION

Occupational exposure to airborne crystalline silica ($cSiO_2$) has been linked to the prevalence of autoimmune disease [289]. We have previously demonstrated that $cSiO_2$ triggers the early onset and progression of systemic autoimmunity and glomerulonephritis in lupus-prone female NZBWF1 mice [3]. In this model, intranasal instillation with $cSiO_2$ induces profuse inflammation in the lung characterized by cytokine and chemokine secretion, lymphocyte infiltration, and autoantigen release. Collectively, these processes promote the development of pulmonary ectopic lymphoid structures (ELS) that drive autoimmune pathogenesis. Remarkably, supplementing the NZBWF1 mouse diets with the ω-3 polyunsaturated fatty acid (ω-3 PUFA) docosahexaenoic acid (C22:6 ω-3; DHA), a widely used dietary supplement extracted from cold-water fish, blocks $cSiO_2$-triggered inflammation, ectopic lymphoid neogenesis, systemic autoimmunity, and nephritis [4, 7]. Accordingly, supplementation with DHA and other ω-3 PUFAs may be an effective intervention against triggering of lupus onset, flaring, and/or progression by environmental agents such as $cSiO_2$. However, the mechanisms behind DHA's suppression of $cSiO_2$-accelerated pulmonary and systemic autoimmunity are unclear.

Phagocytosis by alveolar macrophages (AMs) is a primary line of defense against respirable particles. After $cSiO_2$ is phagocytosed, it induces lysosomal membrane permeabilization that in turn elicits NLRP3 inflammasome oligomerization and caspase-1 activation [384, 385, 125, 126]. Caspase-1 selectively cleaves pro-IL-1β to mature IL-1β, and induces cell death via pyroptosis [140, 386, 387]. The latter results in release of inflammatory mediators, alarmins, autoantigens, and reemergence of the $cSiO_2$ particles into the alveolar space. Continuous repetition of this sequence promotes recruitment and activation of additional leukocytes in the lung, culminating in chronic inflammation and autoimmunity [384]. Other crystals, including monosodium urate (MSU) [388], alum [125], and cholesterol [145], have also been shown to activate the NLRP3 inflammasome.

NLRP3 inflammasome activation requires a priming signal such as the pathogen-associated lipopolysaccharide (LPS), which upregulates expression of inflammasome components and IL-1 cytokines [389]. Importantly, cytokines (e.g., IL-1β, TNF-α, and IL-6) and endogenous dan-

ger signals such as alarmins can similarly elicit this priming effect. The canonical alarmin IL-1α is constitutively expressed in myriad cell populations, including macrophages under steady state conditions, but its expression can be upregulated by proinflammatory or stress-associated stimuli [142]. Rabolli et al. [132] reported that macrophages are a main source of IL-1α in the lung and that $cSiO_2$ can induce release of this cytokine. Like IL-1β, IL-1α binds the IL-1R1 receptor on AM, consequently activating NF-κB-driven expression of inflammasome proteins [142]. Release of IL-1β and IL-1α in concert with the sustained presence of $cSiO_2$ [390] then allows a feed-forward loop of inflammasome activation and pyroptotic cell death within macrophages that is capable of perpetually activating inflammation and autoimmune pathogenesis.

Previous studies suggest that DHA and other ω-3 PUFAs potentially interfere with $cSiO_2$-induced NLRP3 inflammasome activation, release of IL-1 cytokines, and death of AMs [391, 392, 393, 394, 73]. However, elucidation of how ω-3 PUFAs influence these responses is inherently difficult due to low numbers of AMs isolatable from animals or humans. The murine RAW 264.7 (RAW) cell line is a widely used macrophage model that has been cited in mechanism studies nearly 10,000 times since its discovery in 1977 by Raschke et al. [395]. Importantly, the wild-type RAW (RAW-WT) cells lack the inflammasome adapter ASC (apoptosis-associated speck-like protein containing a CARD domain) that is crucial for NLRP3 inflammasome assembly [396]. This can be rectified by transfection with the ASC gene thereby rendering this cell line capable of mounting an inflammasome response similar to primary AMs [397]. Herein, we employed RAW-ASC and RAW-WT cells with and without inflammasome priming to test the hypothesis that DHA suppresses $cSiO_2$-induced NLRP3 inflammasome activation, IL-1 cytokine release, and cell death in the macrophage.

4.3 MATERIALS AND METHODS

4.3.1 RAW-WT and RAW-ASC macrophage models.

Murine-derived wild-type RAW 264.7 (RAW-WT) cells were purchased from the American Type Culture Collection (ATCC® TIB-71™). RAW-ASC cells were obtained by transfection with a

fusion CFP-ASC protein. The open-reading frame of ASC was amplified from cDNA by PCR and inserted at the C-terminus of cyan fluorescent protein (CFP) of pLenti-CFP plasmid generated on the basis of pLenti6/V5 (Invitrogen Life Technologies, Carlsbad, CA) resulting in a fusion CFP-ASC protein, as described previously [398]. Plasmid containing the fusion CFP-ASC protein (designated pLenti-CFP-ASC) was verified by Sanger sequencing. The lentiviral system was generated in the packaging cell line HEK293-FT (Invitrogen Life Technologies) and transfected with pLenti-CFP-ASC and helper plasmids pCMVΔR8.2 and pMD.G using Lipofectamine 2000 (Invitrogen Life Technologies). Cell culture medium containing virus was harvested at 48 and 72 h post-transfection, filtered, and concentrated at 3,200 *x*g for 30 min in Centricon C-20 columns, 100,000 MWCO (Millipore Sigma, Burlington, MA) resulting in a titer of 1–2E7 TU/ml. To restore inflammasome function, RAW 264.7 lacking expression of endogenous ASC were transduced with CFP-ASC lentivirus at 2–5 multiplicity of infection (MOI) in the presence of 6 μg/ml polybrene. After lentiviral transduction, 10–15% cells expressed fluorescent protein. Stably transduced cells were then selected with 5 μg/ml of blasticidin (InvivoGen) for 10 d, resulting in 90% fluorescent cells as observed by fluorescent microscopy. Both cell types were cultured in phenol red-free RPMI 1640 medium (Thermo Fisher Scientific, Waltham, MA) supplemented with 10% FBS (Thermo Fisher Scientific) and 1% Penicillin-streptomycin (Invitrogen Life Technologies) and sub-cultured every 2–4 d [302, 396].

4.3.2 Preparation of bone marrow-derived macrophages (BMDMs).

All experimental protocols involving animals were reviewed and approved by the Institutional Animal Care and Use Committee at Michigan State University in accordance with the National Institutes of Health guidelines (AUF # PROTO201800113). Femurs were removed from 8 to 14 wk old C57BL/6J mice and marrow was flushed from the bone with ice cold PBS. Cells were dissociated by pipetting and filtered through a 40 μm cell strainer. Cells were pelleted and resuspended in 1 mL red blood cell lysis buffer (Thermo Fisher Scientific) and incubated at room temperature for 10 min. An additional 10 mL PBS were added and cells were pelleted, counted, and plated at 5 $\times 10^6$

cells per 100 mm petri dish in DMEM (Thermo Fisher Scientific) supplemented with 10% FBS, 1% Penicillin-streptomycin, and 20% L929 supernatant as previously described [399]. Medium was refreshed every 2–3 d. Adherent macrophages were used in experiments at 7 d after isolation.

4.3.3 $cSiO_2$ and other crystals.

$cSiO_2$ (Min-U-Sil-5, Pennsylvania Glass Sand Corp, Pittsburgh, PA) was prepared as previously described [400]. Briefly, $cSiO_2$ was suspended in 1 M HCl and washed for 1 h at 100°C. Following cooling, $cSiO_2$ was washed 3 times with sterile water and dried at 200°C overnight. For treatments, acid washed $cSiO_2$ was suspended in fresh, sterile Dulbecco's phosphate-buffered saline (DPBS, pH 7.4). Similarly, MSU crystals (InvivoGen) were suspended in DPBS at 5 mg/mL per the manufacturer's instructions. A 20 mg/mL stock suspension of alum crystals (InvivoGen) was prepared in sterile water and diluted 1:4 with PBS before use. All crystal suspensions were stored at 4°C for no longer than 2 wk. Prior to use, crystal suspensions were vortexed thoroughly, sonicated for 1 min and added dropwise to wells to achieve the desired concentrations.

4.3.4 DHA preparation.

DHA-bovine serum albumin (BSA) complexes were used to supplement cell culture media at physiologically relevant doses. The complexes were prepared as previously described [229, 401]. Briefly, a 15% solution of fatty acid-free, endotoxin-, and fatty acid-free BSA (Millipore Sigma) was prepared in serum-free RPMI. Stocks of DHA (Cayman Chemical, Ann Arbor, MI) were diluted in EtOH to 11.76 mg/mL. A volume of the DHA corresponding to 20 mg DHA was transferred to glass tube and EtOH evaporated under a steady stream of N_2. DHA was then dissolved in 4 mL of 0.05 M Na_2CO_3 for a final concentration of 5 mg/mL. The tube was flushed with N_2 gas, vortexed, and incubated at room temperature for 1 h. DHA in Na_2CO_3 and 15% w/v BSA in RPMI were added to serum-free RPMI to obtain a final concentration of 2.5 mM DHA and 0.833 mM BSA (3:1 molar ratio). The tube was flushed with N_2 and gently mixed for 30 min. The DHA-BSA

complex solution was filter sterilized and aliquoted. Complexes were capped with N_2 and stored at −20°C for no longer than 3 months.

4.3.5 Experimental design.

Approaches used for this study are summarized in **Figure 4.1**. For comparison of RAW-WT or RAW-ASC macrophages, cells were plated at 3×10^5 cells/well in 12-well plates, 1.5×10^5 cells/well in 24-well plates, or 1.7×10^5 cells/well in 96-well plates in order to achieve 70–90% confluency at the time of treatment. Unless otherwise noted, cells were cultured for 24 h in complete RPMI (phenol red-free RPMI 1640, 10% FBS, 1% penicillin-streptomycin), washed once with sterile DPBS and primed for 2 h with 20 ng/mL LPS in serum deprived RPMI (phenol red-free RPMI 1640, 0.25% FBS, 1% penicillin-streptomycin). Following priming with LPS (from *Salmonella enterica* serotype typhimurium containing <1% protein impurities, Millipore Sigma), $cSiO_2$, nigericin (Millipore Sigma), MSU, alum, or vehicle (DPBS for $cSiO_2$ and <0.3% EtOH for nigericin) was added to cultures dropwise. Cells were incubated with nigericin for 30 to 120 min, with $cSiO_2$ for 1 to 4 h, and with MSU or alum for 8 h. Culture supernatants were collected for cytokine ELISAs and lactate dehydrogenase (LDH) assays, and cells were collected for RNA and protein extraction. For DHA supplementation studies, cells were seeded at 2.5×10^5 cells/well in 12-well plates or 1.25×10^5 cells/well in 24-well plates, as established in prior experiments to achieve 70–90% confluency at the time of treatment. Cells were grown 24 h in complete RPMI. Wells were then washed once with DPBS and media was replaced with RPMI containing 0.25% FBS and 10 or 25 μM DHA as a 3:1 complex with BSA [229, 402]. Non-supplemented media (0 μM DHA) containing BSA was used as a vehicle control. After 24 h, wells were washed with DPBS and subjected to treatments as described above.

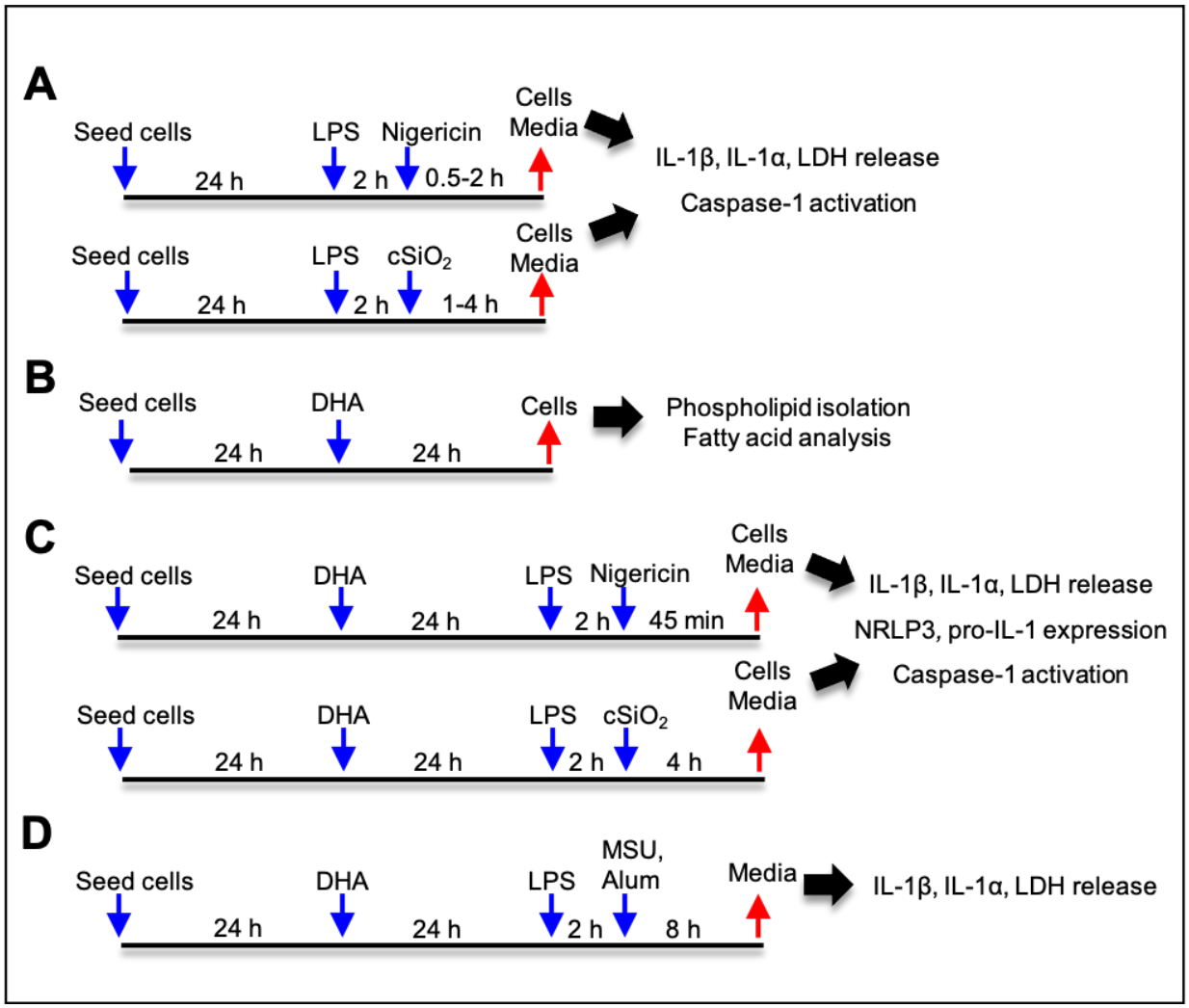


Figure 4.1: Experimental design. Studies focused on **A.** characterization of $cSiO_2$- and nigericin-induced inflammasome activation, IL-1 cytokine release and cell death in RAW-WT and RAW-ASC macrophages, **B.** assessing effects of DHA supplementation on the fatty acid profile of membrane phospholipids, **C.** determining how DHA impacts inflammasome activation, IL-1 cytokine release and cell death, and **D.** assessing how DHA impacts inflammasome activation by monosodium urate (MSU) and alum crystals.

4.3.6 IL-1 cytokine analyses.

IL-1β and IL-1α release was measured using the mouse IL-1β/IL-1F2 DuoSet® ELISA and mouse IL-1α/IL-1F1 DuoSet® ELISA (R&D Systems, Minneapolis, MN) per the manufacturer's instructions.

4.3.7 Caspase-1 activity.

Caspase-1 activation was determined in LPS-primed and unprimed RAW-ASC cells using the FAM-FLICA *in vitro* caspase-1 kit (ImmunoChemistry Technologies, LLC, Bloomington, MN). This kit employs the fluorescent inhibitor probe FAM-YVAD-FMK to label active caspase-1 enzyme in living cells. To investigate the effect of $cSiO_2$ on caspase-1 activation in RAW-ASC cells, 1.5 x 10^5 cells per well were seeded in complete RPMI medium in a clear bottomed, black walled 24-well plate. After 24 h, cells were subjected to the treatments described above, with the exception that 15 μL of FAM-FLICA reagent (20x) was added 2 h before the end of incubation. Following treatment, plates were spun at 100 *x*g for 2 min to recover detached cells. Cells were gently washed with the provided wash buffer and centrifuged at 100 *x*g for 2 min three times. Cells were imaged with the EVOS FL Auto Cell Imaging System (Invitrogen Life Technologies) with 40x objective using the GFP light cube. For multi-well analysis, total green fluorescence intensity was measured at 492 ex and 520 em using surface scan mode of EnSpire™ Multilabel Plate Reader (PerkinElmer Inc., Waltham, MA). Total fluorescence intensity was normalized to total amount of protein as measured by Pierce™ BCA Protein Assay Kit (Thermo Fisher Scientific). Results from two separate experiments were combined and expressed as fold change relative to treatment control.

4.3.8 Cell death.

At the conclusion of the nigericin or $cSiO_2$ treatment periods, cell death was assessed by release of LDH as previously described [403]. Briefly, 10% Triton X-100 (Millipore Sigma) was added to control wells designated for quantification of maximum kill (MK) at 2% (v/v) to induce maximum cell lysis. Media was collected from MK and sample wells and 50 μL media from each well added to an untreated, flat-bottomed 96-well plate. Serum-deprived RPMI was used as the sample blank and serum-deprived RPMI with 10% Triton-X was used as the MK blank. LDH reagent solution was prepared fresh as described [403] and 100 μL added to each well. Plates were incubated in the dark at room temperature for 15 min and read on a FilterMax F3 Multimode plate reader (Molecular Devices, San Jose, CA) at an absorbance wavelength of 492 nm. Cytotoxicity of samples was

calculated as follows: 100% x [($sample_{abs}$ - sample $blank_{abs}$)/(MK_{abs} - MK $blank_{abs}$)]. Remaining cell culture medium was stored at −20°C until cytokine analysis.

4.3.9 PPARγ transcription factor assay.

Samples were prepared using a Nuclear Extraction Kit (Active Motif Inc., Carlsbad, CA) per the manufacturer's instructions. Protein content of the nuclear extracts was quantified by Pierce™ BCA Protein Assay Kit (Thermo Fisher Scientific). PPARγ activity in nuclear extracts was assessed using the TransAM® PPARγ Transcription Factor ELISA kit (Active Motif Inc). Activity was expressed as fold-change relative to control.

4.3.10 qRT-PCR.

Following 6 h incubation with 20 ng/mL LPS, RNA was extracted using RNeasy Mini spin columns provided with the RNeasy Mini Kit (Qiagen, Germantown, MD). Following extraction, reverse transcription was performed using a High Capacity RNA to cDNA Reverse Transcription Kit (Invitrogen Life Technologies). Quantitative real-time qPCR was performed using specific Taqman probes for selected genes involved in NLRP3 inflammasome formation (*Nlrp3* Assay ID Mm00840904_m1, *Il1b* Assay ID Mm01336189_m1, *Il1a* Assay ID Mm00439620_m1, *Casp1* Assay ID Mm004438023_m1; Thermo Fisher Scientific) on the Applied Biosystems™ QuantStudio™ 7 real-time PCR system. Data were analyzed with Applied Biosystems™ Thermo Fisher Cloud using the RQ software and the relative quantification method. *Gapdh* (Assay ID Mm99999915 _g1; Thermo Fisher Scientific) was used as the housekeeping gene. Relative copy number (RCN) for each gene was normalized to expression of *Gapdh* and calculated as described previously [301].

4.3.11 SDS-PAGE and western blot.

RAW-ASC macrophages were lysed in RIPA buffer containing Halt Protease Inhibitor (RIPA-HPI; Thermo Fisher Scientific). To assess IL-1α in supernatant, protein was concentrated by precipitation with methanol and chloroform [404]. Briefly, 600 μL of methanol:chloroform (4:1) was

added to 600 μL media supernatant. Samples were centrifuged at 12,000 *x*g for 5 min and the upper methanol layer removed. Methanol (600 μL) was added, samples were vortexed and centrifuged again. Supernatant was removed, and the pellet was dried under a gentle stream of N_2. The pellet was then resuspended in 60 μL RIPA-HPI. For assessment of NF-κB activation, nuclear and cytoplasmic extracts were prepared using a NE-PER Nuclear and Cytoplasmic Extraction Kit (Thermo Fisher Scientific) supplemented with Halt Protease Inhibitor according to the manufacturer's instructions and as previously described [405].

Protein lysates and supernatant concentrates were diluted in Laemmli sample buffer containing 5% β-mercaptoethanol and separated on a 4–20% gradient gel (Bio-Rad Laboratories, Hercules, CA) with 1x TGS buffer (Bio-Rad Laboratories). Protein was transferred to a Trans-Blot® Turbo™ RTA Mini low fluorescent PVDF membrane (Bio-Rad Laboratories) using Trans-Blot® Turbo™ gel transfer stacks (Bio-Rad Laboratories) and the Trans-Blot® Turbo™ Transfer Device (Bio-Rad Laboratories) as directed by the manufacturer. Efficient protein transfer was confirmed by staining membranes with a solution containing Coomassie Brilliant Blue R-250 Dye. The membranes were placed in an iBind Western Device (Thermo Fisher Scientific) and the primary and secondary antibody solutions and washes were added to the corresponding chambers. Dilutions of antibodies were made with the iBind Fluorescent Detection Solution Kit (Thermo Fisher Scientific) according to the manufacturer's protocol. The primary antibodies, namely goat anti-IL-1β (R&D Systems), rabbit anti-IL-1α (Cell Signaling Technology, Danvers, MA), rabbit anti-caspase-1 (p20) (Adipogen, San Diego, CA), mouse anti-IκBα (Cell Signaling Technology), rabbit anti-p-IKKα/β (Cell Signaling Technology), and rabbit anti-NF-κB p65 (Cell Signaling Technology), were diluted at 1:1000 for cell lysates or 1:500 for supernatant and placed into the primary antibody chamber. Rabbit anti-GAPDH (Cell Signaling Technology) and rabbit anti-beta-actin (Cell Signaling Technology) were diluted 1:1000 and 1:2000, respectively, and used for normalization of proteins detected in the lysate or cytoplasmic fraction. Mouse anti-PCNA (Cell Signaling Technology) was diluted 1:1000 and used for normalization of proteins detected in the nuclear fraction. Similarly, the secondary antibodies (donkey anti-goat IRDye 800CW, goat anti-mouse 800CW, goat anti-rabbit 680RD) from

LI-COR Biosciences System (LI-COR Biosciences, Lincoln, NE, USA) were diluted at 1:3000 and placed into their corresponding chamber. The membranes were left in the iBind system for >2.5 h at room temperature before scanning with the LI-COR Odyssey Infrared Imaging System (LI-COR Biosciences).

Data shown are mean percent of total FA ± SEM (n = 8 per group) as determined by GLC. FA levels significantly different from control (0 μM DHA) represented by asterisks (*$p < 0.05$, **$p < 0.01$).

4.3.12 Fatty acid analysis.

Cells were seeded at a density of 1.5×10^6 cells per 100 mm dish. After 24 h in complete RPMI, wells were washed once with DPBS and media switched to serum-deprived RPMI supplemented with 25 μM DHA as described above. After 24 h, cells were washed once with DPBS, collected in ice-cold DPBS, and pelleted at 1,000 *x*g for 3 min. Cell pellets were resuspended in 1.4 mL ice-cold DPBS as previously described [83]. Each sample was divided in half and stored in 1.6 mL screw-cap tubes in order to perform the phospholipid isolation in technical duplicates. Samples were then snap frozen and stored at −80°C until further analysis. Total lipids were extracted according to the method by Bligh and Dyer [406] and phospholipids were isolated by solid phase extraction as described previously [305]. Isolated phospholipids were stored at −80°C in a 3:1 solution of hexane/isopropanol until methylation. The exogenous heptadecanoic acid, C17:0 (NuChek Prep, Elysian, MN), was added to isolated phospholipids as an internal standard. Samples were methylated using methanolic BF_3 (Millipore Sigma) as previously described [76]. Fatty acid methyl esters (FAMEs) were analyzed by gas chromatography using a Shimadzu GC equipped with a flame ionization detector. Samples were separated on a JW DB-23 30 m capillary column (Agilent, Santa Clara, CA) with an inner diameter of 0.25 μm and a flow rate of 0.82 mL/min, with helium as the carrier gas. The injection temperature and detector temperature were 250°C and the column temperature ranged from 120 to 240°C. A 16-standard FAME mix (NuChek Prep) was used to identify peaks of interest.

4.3.13 Statistical analyses.

Student's t-tests were used to compare two groups when applicable. If groups were determined non-parametric or determined to have unequal variance by the Shapiro-Wilk test for normality or the F-test for equal variance, respectively, they were analyzed using the Mann-Whitney U test. Comparison of multiple groups was accomplished by one-way ANOVA, and comparison of individual groups was accomplished using Tukey's test. If groups were determined non-parametric or determined to have unequal variance by the Shapiro-Wilk test for normality or the F-test equal variance, respectively, they were analyzed by the Kruskal-Wallis test. In this case, post-hoc comparison of individual groups was accomplished using Dunn's test.

4.4 RESULTS

4.4.1 Nigericin- and $cSiO_2$-induced IL-1β release is LPS- and ASC-dependent.

To confirm that ASC transfection conferred a functional inflammasome, the effects of the K^+ ionophore nigericin, a prototypical activator of the NLRP3 inflammasome, were compared in RAW-ASC and RAW-WT cells. Nigericin elicited marked IL-1β secretion in LPS-primed RAW-ASC cells, but not RAW-ASC cells (**Figure 4.2A**). Robust IL-1β release was evident in LPS-primed RAW-ASC cells as early as 30 min after nigericin treatment (**Figure 4.2B**). IL-1β release from LPS-primed RAW-WT cells was negligible at all time points, verifying lack of inflammasome activity. As found with nigericin, $cSiO_2$ induced abundant IL-1β release in LPS-primed RAW-ASC cells within 1 h but not in RAW-WT or unprimed RAW-ASC cells (**Figures 4.2 C-D**). In response to both nigericin and $cSiO_2$, release of IL-1β by RAW-ASC cells included both the inactive precursor and the bioactive mature form (**Figure 4.2E**). Collectively, IL-1β release in response to either activating stimulus was dependent on the presence of a priming signal and a functional inflammasome. Under identical experimental conditions, primary BMDM released IL-1β in an LPS-dependent manner in response to nigericin and $cSiO_2$ (**Figure 4.2F**) suggesting the RAW-ASC model was a relevant surrogate to investigate inflammasome activation in the macrophage.

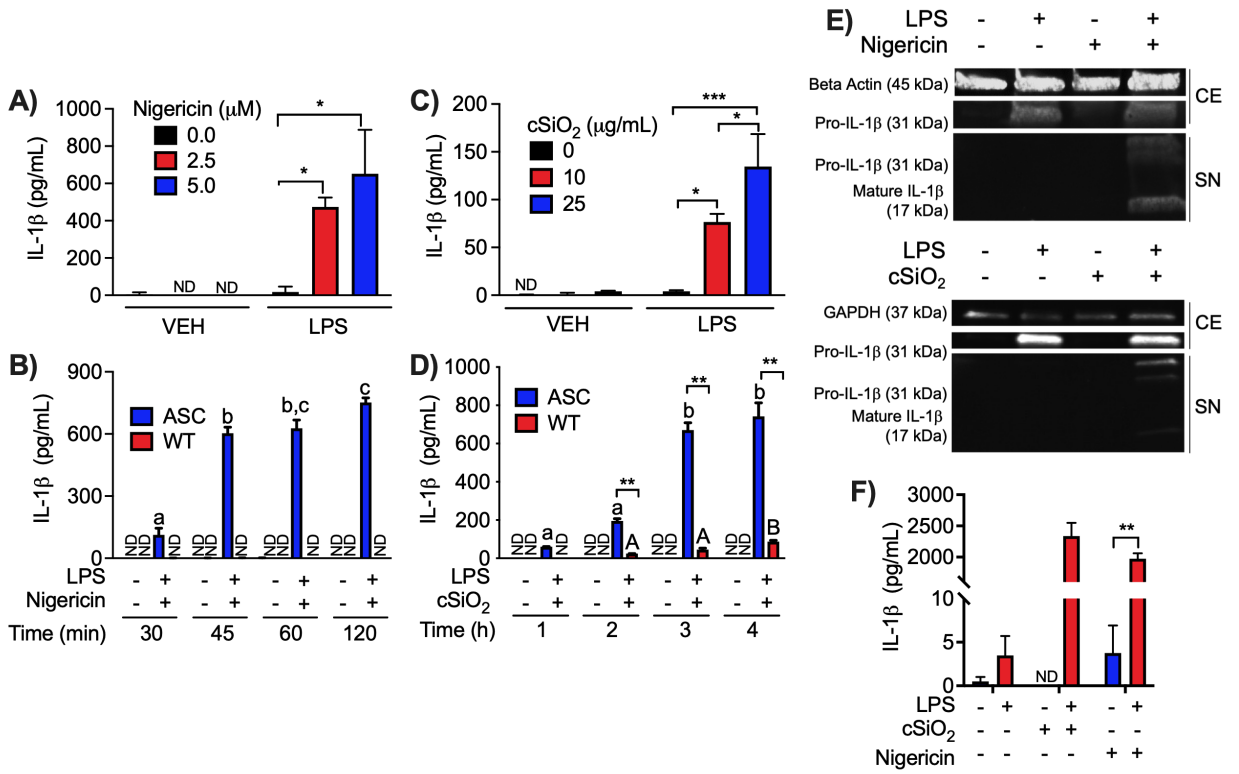


Figure 4.2: Nigericin- and $cSiO_2$-induced IL-1β release are LPS- and ASC-dependent in RAW macrophages. A,C. RAW-ASC cells were pretreated with 20 ng/ml LPS for 2 h, incubated with 0, 2.5, or 5.0 μM nigericin for 45 min, or 0, 10, or 25 μg/ml $cSiO_2$ for 4 h, and then release of IL-1β measured. **B,D**. RAW-ASC and RAW-WT were pretreated with vehicle (VEH) or LPS for 2 h, incubated with VEH or 10 μM nigericin or 25 μg/ml $cSiO_2$. IL-1β release was assessed at the indicated times. **E.** Pro-IL-1β was present in the cell extracts (CE) of RAW-ASC macrophages treated with LPS, but only secreted into the supernatant (SN) with nigericin or $cSiO_2$ treatment. IL-1β in the supernatant contained both the precursor and cleaved forms. **F.** Bone marrow-derived macrophages (BMDMs) were pretreated with VEH or LPS (20 ng/ml) for 2 h, incubated with VEH or 5 μM nigericin or 25 μg/ml $cSiO_2$ and IL-1β release then assessed at 45 min or 4 h, respectively. Data presented as mean $\pm$ SEM, n = 3. ND = not detectable. Asterisks indicate significant differences between cell type (**B,D**) or treatment group (**A,C,E**) (*p<0.05, **p<0.01). Different letters indicate significant differences between treatment groups within each cell type (**B,D**) (p<0.05). ELISA data are representative of three independent experiments. Western blots are representative of two independent experiments.

4.4.2 $cSiO_2$-Induced caspase-1 activation is LPS- and ASC-dependent.

During NLRP3 inflammasome activation, caspase-1 is post-translationally modified by cleavage to its mature, active form. FAM-YVAD-FMK, a fluorescent dye that binds intracellularly to cleaved, active caspase-1, was used to compare $cSiO_2$-induced caspase-1 activation in RAW-ASC and RAW-

WT cells. Caspase-1 was activated by $cSiO_2$ only in LPS-primed RAW-ASC cells, confirming inflammasome-dependent activation (**Figure 4.3A**). These results were confirmed by Western blot analysis of cleaved caspase-1 in the media supernatant in RAW-ASC cells treated with both LPS and $cSiO_2$ (**Figure 4.3B**). Consistent with these results, we observed the formation of ASC specks following LPS priming and $cSiO_2$ or nigericin treatment (**Supplementary Figure C.1A**).

4.4.3 Nigericin- and $cSiO_2$-induced IL-1α release differ with regard to LPS- and ASC-dependence.

Nigericin evoked a robust IL-1α response in LPS-primed RAW-ASC cells, but not unprimed cells (**Figure 4.4A**). The IL-1α response was detectable in supernatants of LPS-primed RAW-ASC cells within 30 min of nigericin addition but was not evident in LPS-primed RAW-WT supernatants up to 120 min following nigericin treatment (**Figure 4.4B**).

$cSiO_2$-induced IL-1α release in RAW-ASC cells also required LPS pretreatment (**Figure 4.4C**). In contrast to nigericin findings, IL-1α concentrations in culture supernatants of $cSiO_2$-treated RAW-WT cells were 30–50 % of that observed in $cSiO_2$-treated RAW-ASC cells (**Figure 4.4D**). These results suggest that $cSiO_2$-induced release of some IL-1α occurs via mechanisms that do not involve NLRP3 inflammasome activation. IL-1α detected in the media of RAW-ASC cells was primarily the 17 kDa mature form (**Figure 4.4E**). Finally, as found in RAW-ASC cells, primary BMDM released IL-1α in response to nigericin and $cSiO_2$ in an LPS-dependent manner (**Figure 4.4F**).

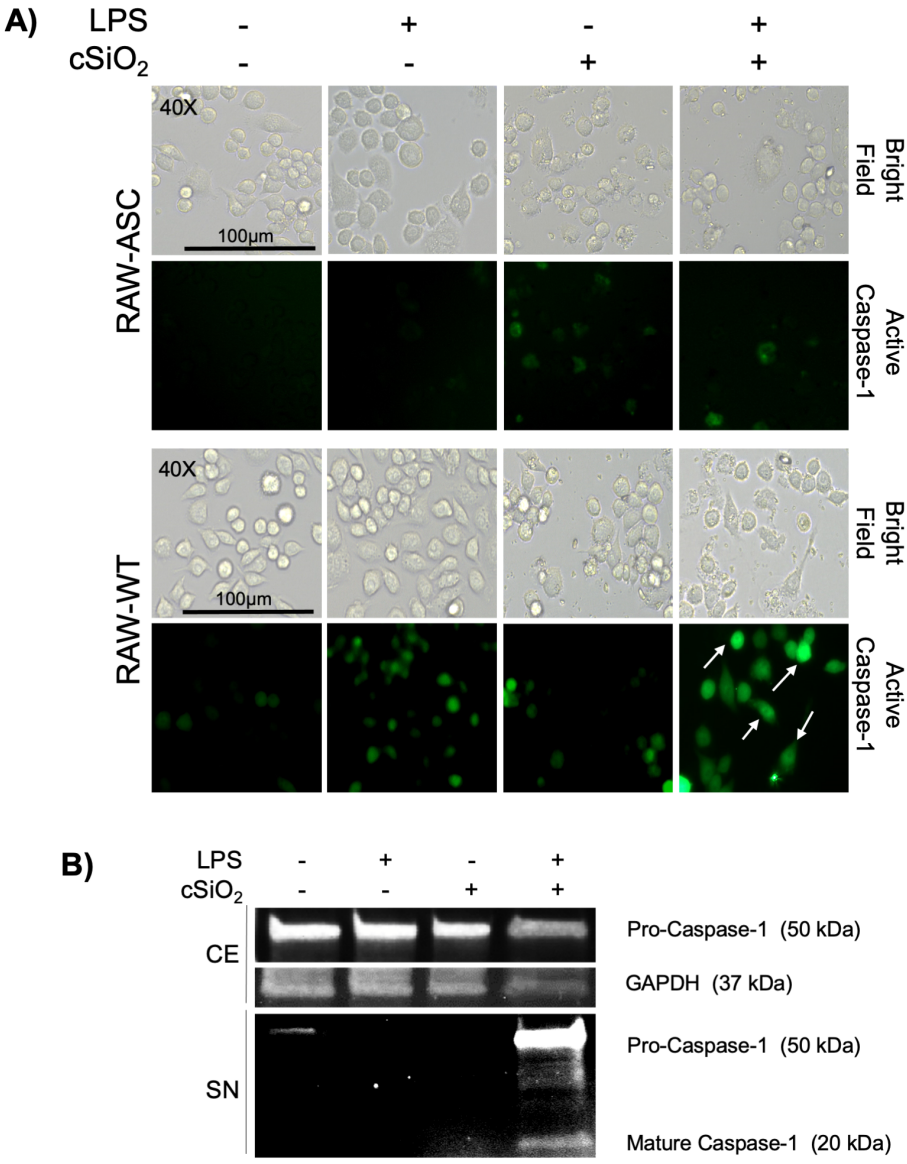


Figure 4.3: $cSiO_2$-induced caspase-1 activation in RAW macrophages is LPS- and ASC-dependent. A. RAW-WT and RAW-ASC cells were pretreated with vehicle (VEH) or 20 ng/ml LPS for 2 h and then incubated with VEH or 25 μg/ml $cSiO_2$ for 4 h. Caspase-1 activation was assessed using fluorescent inhibitor probe FAM-YVAD-FMK. Treatment with LPS and $cSiO_2$ induced minimal activation of caspase-1 in RAW-WT cells while RAW-ASC cells show robust activation of caspase-1 as indicated by green fluorescence (white arrows). Cells imaged using an EVOS FL Auto Cell Imaging System; images representative of three independent experiments. **B.** Pro-caspase-1 was constitutively expressed in RAW-ASC macrophages and detectable in cell extracts (CE). Pro-caspase-1 and cleaved, active caspase-1 (p20) were only present in supernatant (SN) of cells treated with both LPS and $cSiO_2$; Western blots representative of two independent experiments.

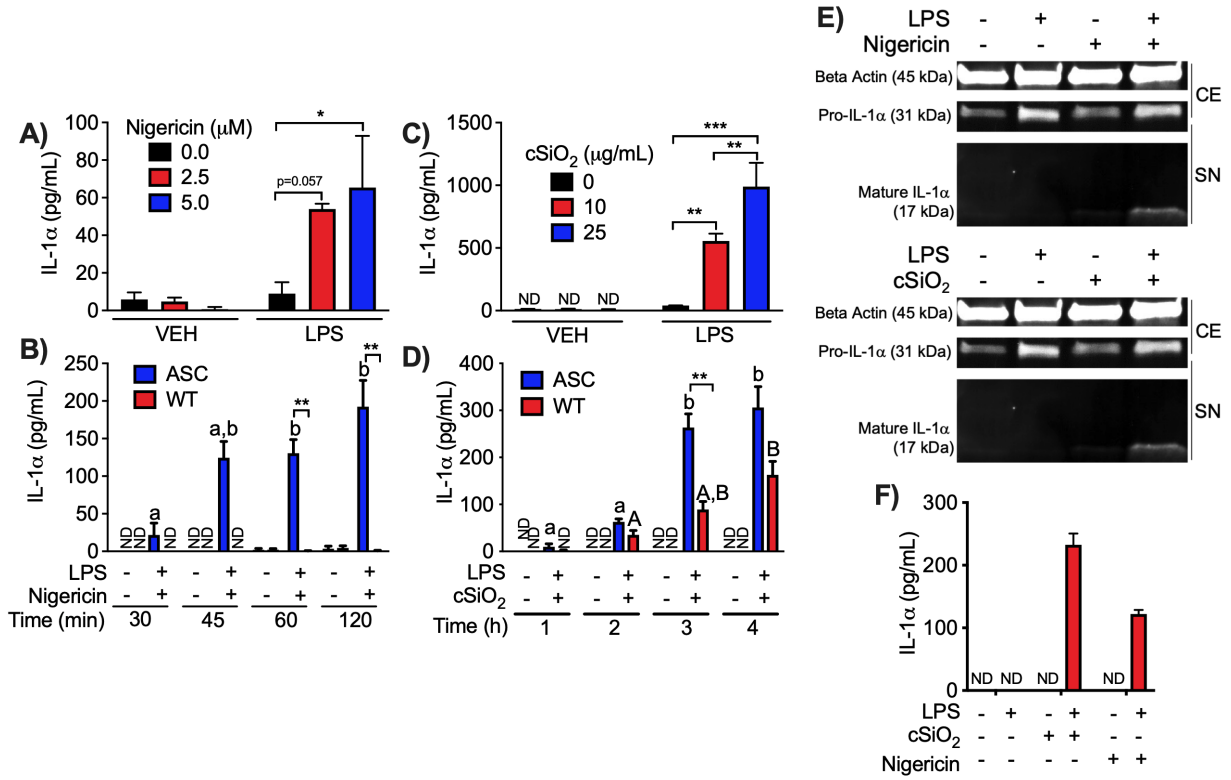


Figure 4.4: Nigericin- and $cSiO_2$-induced IL-1α release is LPS- and ASC-dependent in RAW macrophages. A,C. RAW-ASC cultures were pretreated with vehicle (VEH) or 20 ng/ml LPS for 2 h, incubated with 0, 2.5, or 5.0 μM nigericin for 45 min, or 0, 10, or 25 μg/ml $cSiO_2$ for 4 h, and then release of IL-1α measured. **B,D.** RAW-ASC and RAW-WT were pretreated with VEH or LPS for 2 h, incubated with VEH, 10 μM nigericin, or 25 μg/ml $cSiO_2$ and release of IL-1α measured at the times indicated. **E.** Pro-IL-1α was constitutively expressed and slightly upregulated in cell extracts (CE) of RAW-ASC macrophages treated with LPS, but only secreted into the supernatant (SN) with 5 μM nigericin or 25 μg/ml $cSiO_2$ treatment. Both pro-IL-1α and mature IL-1α were detected in the supernatant. To detect IL-1α in the supernatant, LPS priming was extended to 5 h and protein concentrated 10x by methanol-chloroform precipitation. **F.** Bone marrow-derived macrophages (BMDMs) were pretreated with VEH or LPS (20 ng/ml) for 2 h, incubated with VEH or 5 μM nigericin or 25 μg/ml $cSiO_2$ and IL-1α release then assessed at 45 min or 4 h, respectively. Data presented as mean $\pm$ SEM, n = 3. ND = not detectable. Asterisks indicate significant differences between cell type **(B,D)** or treatment group **(A,C,E)** (*p<0.05, **p<0.01). Different letters indicate significant differences between treatment groups within each cell type (**B,D**) (p<0.05). ELISA data are representative of three independent experiments. Western blots are representative of two independent experiments.

4.4.4 Nigericin- but not $cSiO_2$-induced cell death is inflammasome-dependent.

Nigericin treatment induced LDH release in LPS-primed RAW-ASC cells but not in unprimed ones (**Figure 4.5A**). Concordant with these findings, nigericin elicited LDH release in RAW-ASC but not RAW-WT cells following LPS priming (**Figure 4.5B**) suggesting that death was inflammasome-dependent and thus consistent with pyroptosis.

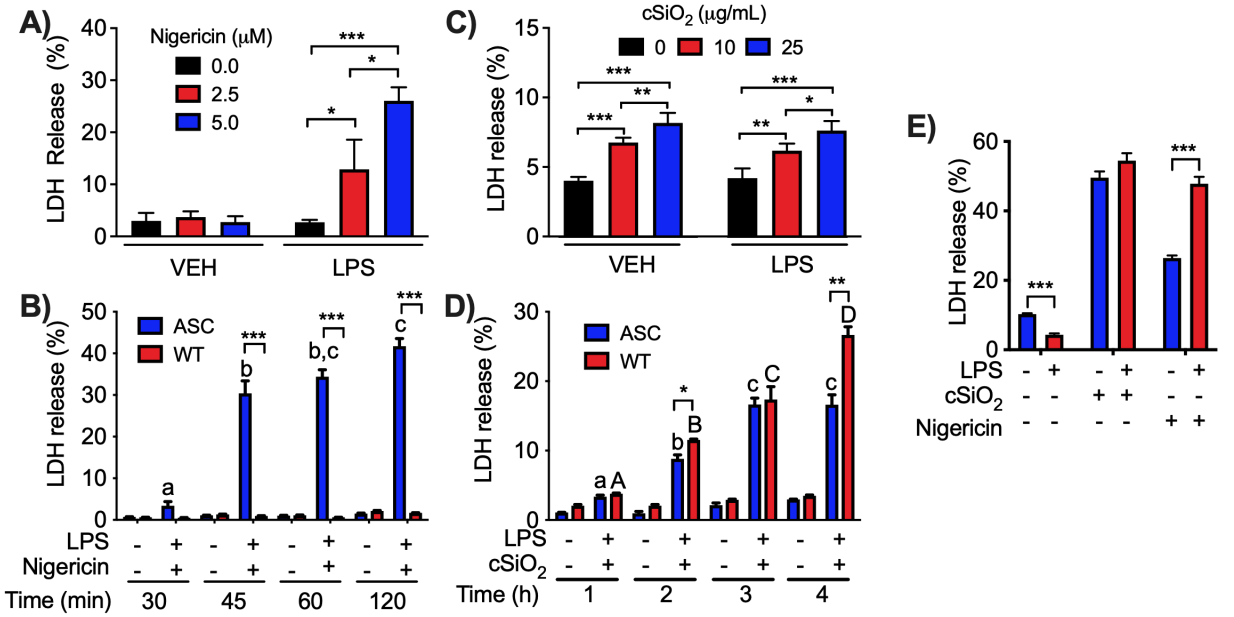


Figure 4.5: Nigericin-induced cell death is LPS- and ASC-dependent while $cSiO_2$-induced cell death is LPS- and ASC-independent in RAW macrophages. A,C. RAW-ASC cultures were pretreated with vehicle (VEH) or 20 ng/ml LPS for 2 h, incubated with 0, 2.5, or 5.0 μM nigericin for 45 min or 0, 10, or 25 μg/ml $cSiO_2$ for 4 h, and then lactate dehydrogenase (LDH) release measured. **B,D.** RAW-ASC and RAW-WT macrophages were pretreated with VEH or 20 ng/ml LPS for 2 h, incubated with VEH, 10 μM nigericin, or 25 μM $cSiO_2$ and then LDH release assessed at the indicated times. **E.** Bone marrow-derived macrophages (BMDMs) were pretreated with VEH or LPS (20 ng/ml) for 2 h, incubated with VEH or 5 μM nigericin or 25 μg/ml $cSiO_2$ and then LDH release assessed at 45 min or 4 h, respectively. Data presented as mean ± SEM, n = 3. ND = not detectable. Asterisks indicate significant differences between cell type (**B,D**) or treatment group (**A,C,E**) (*p<0.05, **p<0.01). Different letters indicate significant differences between treatment groups within each cell type (**B,D**) (p<0.05). Representative of three independent experiments.

Unlike nigericin, $cSiO_2$ induced LDH release in both LPS-primed and unprimed RAW-ASC cells (**Figure 4.5C**) and was largely equivalent in RAW-ASC and RAW-WT cells (**Figure 4.5D**), strongly indicating that $cSiO_2$-induced cell death is not strictly inflammasome dependent and py-

roptotic. Consistent with our findings in RAW-ASC cells, nigericin-induced cell death in BMDM was LPS-dependent whereas $cSiO_2$-induced cell death was LPS-independent (**Figure 4.5E**).

4.4.5 DHA is efficiently incorporated into RAW-ASC cell phospholipids.

Following 24 h incubation with DHA, delivered as a complex with BSA, the fatty acid was dose-dependently incorporated into the phospholipid fraction of RAW-ASC cells (**Figure 4.6A**). This occurred largely at the expense of oleic acid (OA) (**Figure 4.6B**), the major unsaturated fatty acid in the FBS present in the culture medium [407]. Along with DHA incorporation, there were significant decreases in ω-9 palmitoleic acid and ω-6 eicosadienoic acid and a significant increase in ω-3 eicosapentaenoic acid, which can be formed by enzymatic retroconversion of DHA (**Table 4.1**).

Table 4.1: DHA supplementation modulates phospholipid profile of RAW-ASC cells.

		DHA in Serum Deprived Media		
		0 μM DHA	10 μM DHA	25 μM DHA
Fatty Acid	**Common Name**	*Mean ± SEM (% of total)*		
C14:0	Myristic Acid	2.94 ± 0.29	3.27 ± 0.28	4.90 ± 0.84**
C16:0	Palmitic Acid	31.15 ± 3.10	31.34 ± 0.79	38.59 ± 1.25**
C16:1ω9	Palmitoleic Acid	4.67 ± 1.04	3.13 ± 0.25	2.29 ± 0.50**
C18:0	Stearic Acid	15.60 ± 9.05	22.03 ± 0.47	18.01 ± 1.21
C18:1ω9	Oleic Acid	36.68 ± 4.32	22.23 ± 1.25**	9.77 ± 0.34**
C18:2ω6	Linoleic Acid	0.63 ± 0.88	1.26 ± 0.11	0.78 ± 0.71
C20:2ω6	Eicosadienoic Acid	4.16 ± 0.92	1.13 ± 0.68**	0.00 ± 0.00**
C20:4ω6	Arachidonic Acid	3.27 ± 0.67	2.30 ± 0.47	1.80 ± 1.15
C20:5ω3	Eicosapentaenoic Acid	0.00 ± 0.00	0.00 ± 0.00	1.13 ± 0.71
C22:4ω6	Adrenic Acid	0.00 ± 0.00	0.15 ± 0.33	0.35 ± 0.79
C22:5ω3	Docosapentaenoic Acid	0.00 ± 0.00	0.17 ± 0.38	0.18 ± 0.40
C22:5ω6	Docosapentaenoic Acid	0.00 ± 0.00	0.14 ± 0.31	0.00 ± 0.00
C22:6ω3	Docosahexaenoic Acid	0.91 ± 0.53	12.85 ± 0.49**	22.20 ± 1.42**

Data shown are mean percent of total FA ± SEM (n = 6 per group) as determined by gas-liquid chromatography. Fatty acid levels are significantly different from control (0 μM DHA) represented by asterisks **p<0.01.

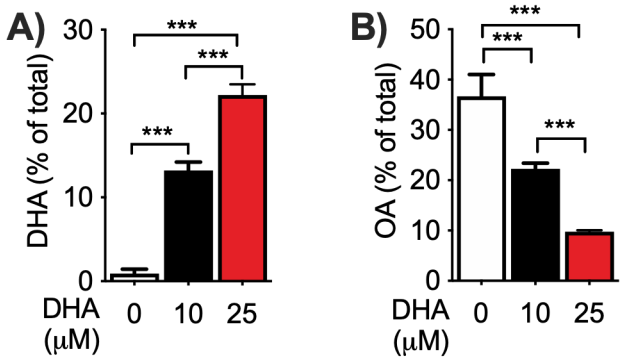


Figure 4.6: DHA is incorporated into RAW-ASC macrophage phospholipids at the expense of oleic acid (OA). RAW-ASC cells were incubated in serum-deprived media containing DHA-BSA complexes or BSA vehicle for 24 h. Cell phospholipids were extracted and analyzed for fatty acid content by gas-liquid chromatography. The major unsaturated fatty acid in the cell membrane of Veh-treated cells is oleic acid (OA), which is the primary fatty acid component of fetal bovine serum (FBS). Incubation with DHA **A.** increased membrane content of DHA while **B.** decreasing the membrane content of OA. See Table 4.1 for complete fatty acid profile. Data presented as mean $\pm$ SEM, n = 3. Asterisks indicate significant difference (**p<0.01). Representative of two independent experiments.

4.4.6 DHA inhibits nigericin-induced IL-1 cytokine release and cell death.

When RAW-ASC cells were pretreated with DHA and then primed with LPS, nigericin-induced release of IL-1β (**Figure 4.7A**) and IL-1α (**Figure 4.7B**) were suppressed by the ω-3 fatty acid in a concentration-dependent manner. DHA's effects corresponded to decreased intracellular pro-IL-1β and pro-IL-1α, as well as diminished extracellular mature IL-1β and IL-1α (**Figures 4.7 D,E**). Finally, DHA pretreatment blocked nigericin-induced LDH release (**Figure 4.7C**), suggesting that DHA inhibits pyroptotic cell death.

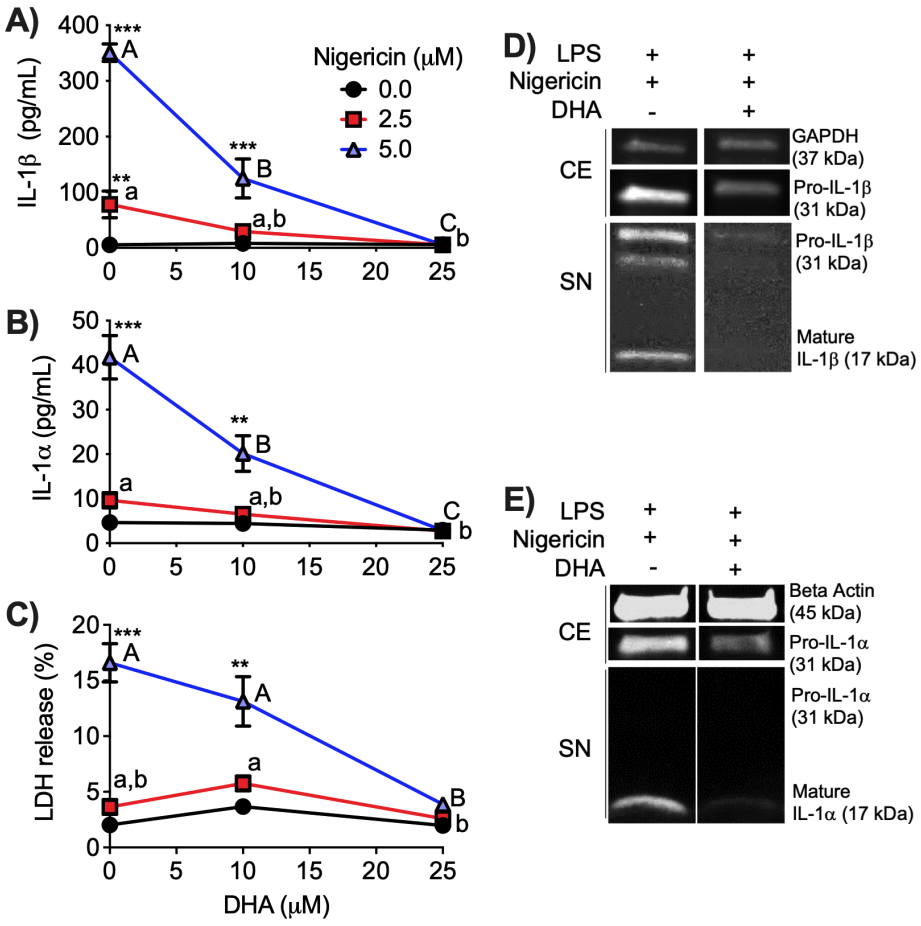


Figure 4.7: DHA supplementation suppresses nigericin-induced IL-1β and IL-1α release and cell death in RAW-ASC macrophages. A-C. RAW-ASC cells were incubated in serum-deprived RPMI containing DHA (0, 10, or 25 μM) or vehicle (BSA) for 24 h. Cells were pretreated with 20 ng/ml LPS for 2 h, incubated with 0, 2.5, or 5.0 μM nigericin for 45 min, and then release of IL-1β, IL-1α, and lactate dehydrogenase (LDH) release measured. **D-E.** The presence of mature IL-1β and IL-1α in the supernatant were determined by Western blotting. For Western blots of IL-1α, LPS priming was extended to 5 h and supernatant concentrated 10x by methanol-chloroform precipitation. Data presented as mean $\pm$ SEM, n = 3. Significant differences between DHA-supplemented groups represented as different letters (uppercase for 5 μM group, lowercase for 2.5 μM group). Significant differences from vehicle control at each DHA concentration represented by asterisks (*p<0.05, **p<0.01). ELISAs and LDH assay are representative of three independent experiments. Western blots are representative of two independent experiments.

4.4.7 DHA suppresses cSiO$_2$-induced IL-1 cytokine release and caspase-1 activation but not cell death.

DHA concentration-dependently suppressed cSiO$_2$-induced release of IL-1β (**Figure 4.8A**) and IL-1α (**Figure 4.8B**) and inhibited cSiO$_2$-induced caspase-1 activation (**Figure 4.9**) and ASC speck

formation (**Supplementary Figure C.1B)**. DHA's inhibitory effects corresponded to reduced levels of intracellular pro-IL-1β and pro-IL-1α and extracellular IL-1β and IL-1α (**igures 4.8 D,E**). However, DHA did not affect cell death induced by $cSiO_2$ (**Figure 4.8C**), further suggesting that $cSiO_2$-induced cell death did not involve inflammasome activation and pyroptosis.

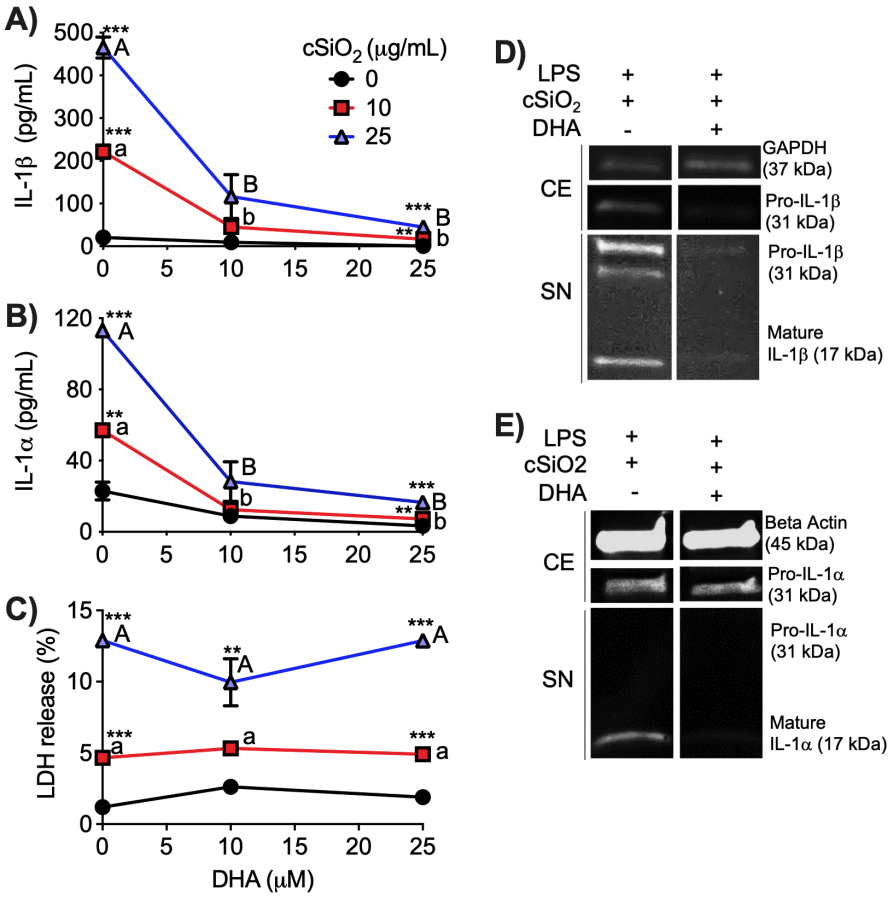


Figure 4.8: DHA inhibits $cSiO_2$-induced IL-1β and IL-1α release but not cell death in RAW-ASC macrophages. A-C. RAW-ASC cells were incubated in serum-deprived RPMI containing DHA (0, 10, or 25 μM) or vehicle (BSA) for 24 h. Cells were pretreated with 20 ng/ml LPS for 2 h, incubated with 0, 10, or 25 μg/ml $cSiO_2$ for 4 h, and then release of IL-1α, IL-1β, and lactate dehydrogenase (LDH) release measured. **D-E** The presence of mature IL-1β and IL-1α in the supernatant were determined by Western blotting. For Western blots of IL-1α, LPS priming was extended to 5 h and supernatant concentrated 10x by methanol-chloroform precipitation. Data presented as mean $\pm$ SEM, n = 3. Significant differences between DHA-supplemented groups represented as different letters (uppercase for 5 μM group, lowercase for 2.5 μM group). Significant differences from vehicle control at each DHA concentration represented by asterisks (**p<0.01). ELISAs and LDH assay are representative of three independent experiments. Western blots are representative of two independent experiments.

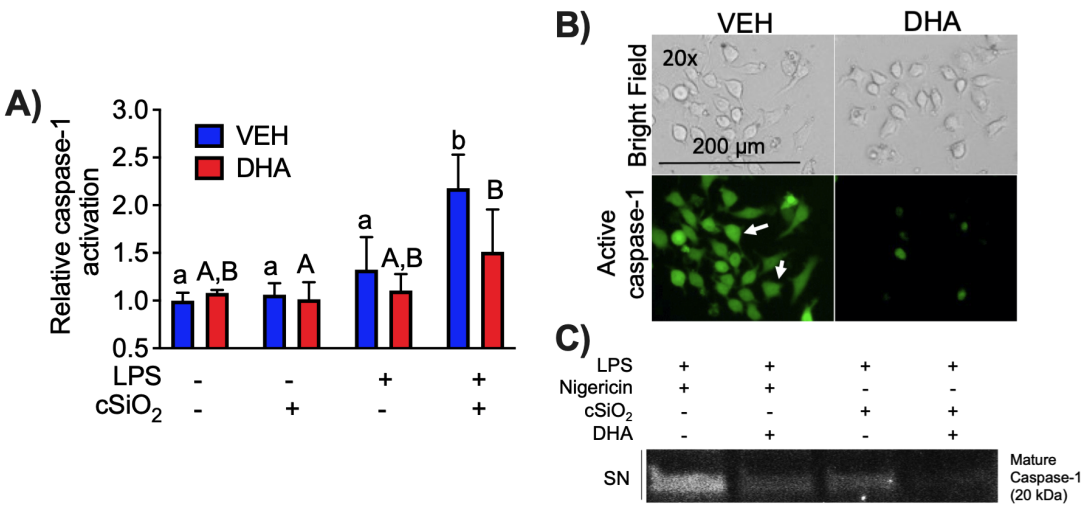


Figure 4.9: DHA supplementation suppresses $cSiO_2$-induced caspase-1 activation in RAW-ASC macrophages. A. RAW-ASC cells were incubated in serum-deprived RPMI containing DHA (25 μM) or vehicle (BSA) for 24 h. Cultures were then primed with 20 ng/ml LPS for 2 h and incubated with or without 25 μg/ml $cSiO_2$ for 4 h. Caspase-1 activation was assessed using fluorescent probe FAM-YVAD-FMK. A fluorescent microplate assay indicated that DHA suppressed $cSiO_2$-induced caspase-1 activation. Fluorescence data pooled from two independent experiments and presented as mean $\pm$ SEM, n = 6. Significant differences between groups represented as different letters (p<0.05). **B.** Representative photomicrographs indicating that cells treated with LPS and $cSiO_2$ showed robust activation of caspase 1 as indicated by green fluorescence (white arrows) and this was attenuated by supplementation with DHA. Cells were imaged using an EVOS FL Auto Cell Imaging System. Images are representative of three independent experiments. **C.** Western blot analysis confirmed that DHA suppressed both the cleavage and release of active caspase-1 (p20) into the supernatant. Western blot data are representative of two independent experiments.

4.4.8 DHA suppresses IL-1 cytokine release triggered by alum and MSU crystals.

Following priming with LPS, both alum (**Figures 4.10 A-B**) and MSU (**Figures 4.10 D-E**) induced robust release of both IL-1α and IL-1β. In both instances, release of IL-1 cytokines was ablated by supplementation with DHA. Unlike $cSiO_2$-induced LDH release, responses to alum and MSU were extremely modest, slightly potentiated by LPS priming, and negligibly affected by DHA (**Figures 4.10 C,F**).

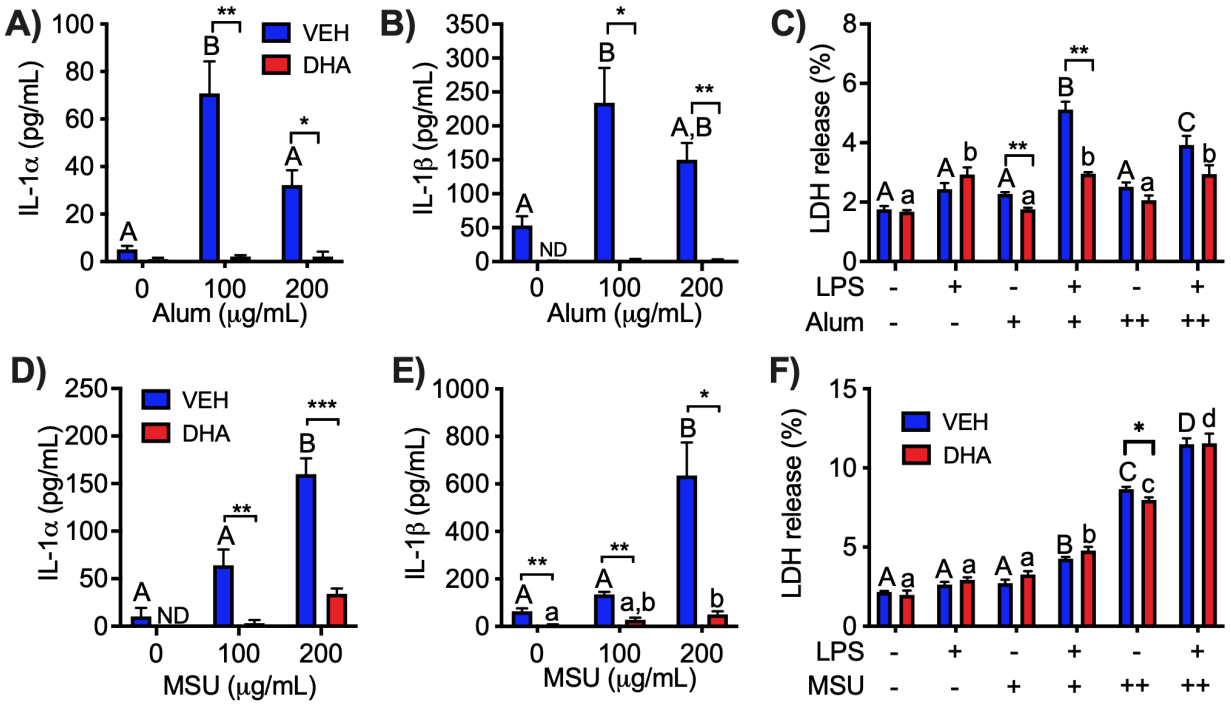


Figure 4.10: Alum- and MSU crystal-induced IL-1 cytokine release is suppressed by DHA. RAW-ASC cells were incubated in serum-deprived RPMI containing DHA (25 μM) complexed with BSA or vehicle (BSA only) for 24 h. Cells were pretreated with 20 ng/ml LPS for 2 h, incubated with 0 (-), 100 (+), or 200 (++) μg/ml **A-C.** alum or **D–F.** monosodium urate MSU for 8 h, and then release of IL-1α, IL-1β, and lactate dehydrogenase (LDH) measured. Data presented as mean ± SEM, n = 3. Asterisks indicate significant differences between DHA and BSA treated cells (*p<0.05, **p<0.01). Different letters indicate significant differences between treatment groups within each VEH treated cells (uppercase letters) or DHA treated cells (lowercase letters) (p<0.05). Data representative of three independent experiments.

4.4.9 DHA interferes with LPS priming by activating PPARγ.

DHA pretreatment significantly suppressed LPS-induced expression of *Nlrp3* and *Il1b* (**Figure 4.11**). A similar trend (p = 0.100) of DHA inhibition was observed for LPS-induced *Il1a* mRNA expression. DHA potentially inhibits IL-1 cytokine and NLRP3 transcription by activating PPARγ, a well-known transrepressor of NF-κB [74]. To test this possibility, PPARγ binding activity was measured in nuclear extracts of RAW-ASC cells treated with DHA or with the PPARγ agonist rosiglitazone as a positive control. Significantly more active PPARγ was detectable in nuclear extracts from the rosiglitazone- and DHA-treated cells than those from vehicle-treated cells (**Figure**

4.12A). Consistent with these findings, both rosiglitazone- and DHA-mediated suppression of IL-1 cytokine gene expression was suppressed in cells treated with the PPARγ antagonist SR16832 (**Figure 4.12B**). Although LPS treatment induced phosphorylation of IKKα/β, degradation of IκBα, NF-κB phosphorylation, and nuclear translocation of NF-κB (**Supplementary Figure C.2**), none of these effects were influenced by DHA.

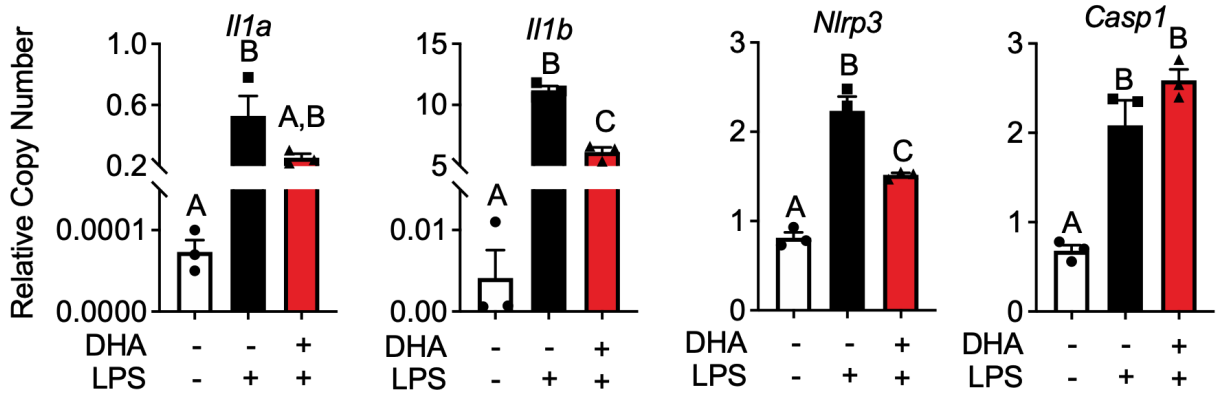


Figure 4.11: DHA supplementation downregulates LPS-induced inflammasome gene expression and intracellular IL-1 cytokines in RAW-ASC cells. RAW-ASC cells were incubated in serum-deprived RPMI containing DHA (25 μM) or vehicle (BSA) for 24 h. Cultures were then incubated with 20 ng/ml LPS for 6 h. Assessment of mRNA levels by qRT-PCR showed that LPS priming induced *Nlrp3*, *Casp1*, *Il1b*, and *Il1a* mRNA expression and upregulation of *Nlrp3*, *Il1b*, and *Il1a* was suppressed by DHA. Gene expression represented as copy number relative to *Gapdh*. Data presented as mean $\pm$ SEM, n = 3. Letters indicate significant differences between groups (p<0.05). Data are representative of two independent experiments.

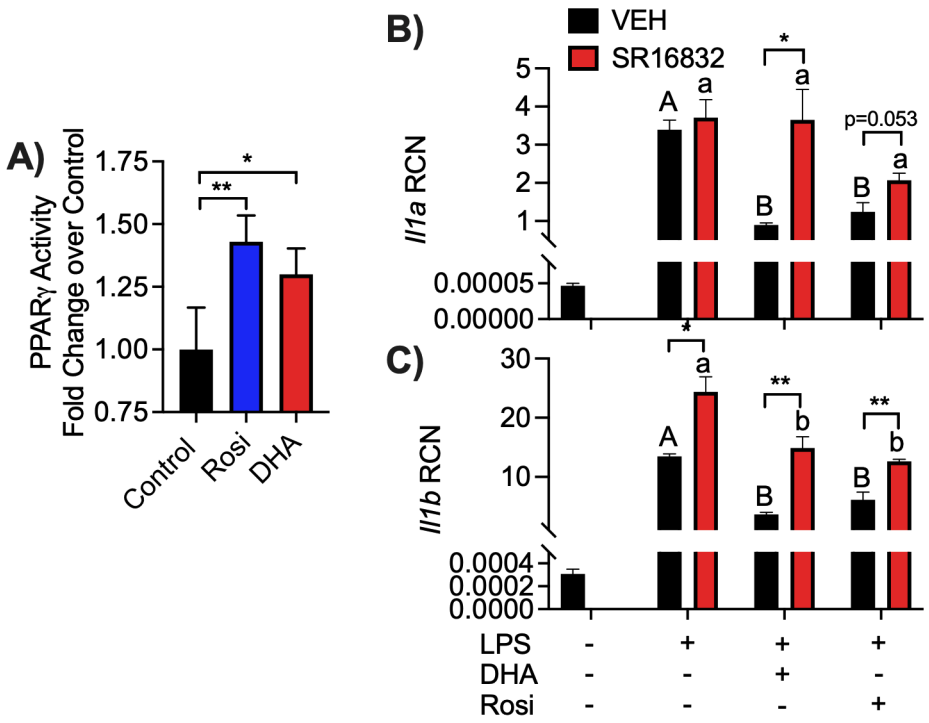


Figure 4.12: PPARγ is involved in DHA-mediated suppression of LPS-induced *Il1a* and *Il1b* **A.** A TransAM™ PPARγ transcription factor assay was used to assess PPARγ activity in nuclear extracts of DHA (10 μM) and PPARγ agonist rosiglitazone (10 μM) treated RAW-ASC cells. Data presented as mean ± SEM, n = 2. Asterisks indicate significant relative to the control (*p<0.05, **p<0.01). **B-C.** RAW-ASC cells were incubated in serum-deprived RPMI containing DHA (10 μM), rosiglitazone (10 μM), PPARγ antagonist SR16832 (100 nM), or vehicle (BSA) for 24 h. Cultures were then incubated with 20 ng/ml LPS for 3.5 h. Assessment of mRNA levels by qRT-PCR showed that the PPARγ antagonist SR16832 blocked DHA and rosiglitazone-dependent suppression of LPS-induced gene expression. Gene expression represented as copy number relative to Gapdh. Asterisks indicate significant differences between DHA and BSA treated cells (*p<0.05, **p<0.01). Data presented as mean ± SEM, n = 3. Different letters indicate significant differences between treatment groups within VEH treated cells (uppercase letters) or SR16832 treated cells (lowercase letters) (p<0.05). Representative of two independent experiments.

4.5 DISCUSSION

Dysregulation of inflammasomes has been implicated as a contributing factor in lupus and other autoimmune diseases [408]. Airway exposure to $cSiO_2$ triggers prolific inflammation in the lung and onset of localized and systemic autoimmunity in lupus-prone mice, but inclusion of DHA in the diet abrogates these effects [4, 7, 35]. The early mechanisms for DHA's ameliorative actions are as yet unclear. To address this knowledge gap, we tested the hypothesis that DHA suppresses $cSiO_2$-

induced NLRP3 inflammasome activation, IL-1 cytokine release, and cell death in the macrophage. Like BMDM, RAW-ASC cells were found to be capable of robust NLRP3 inflammasome activation, and therefore suitable surrogates to investigate DHA's effects on macrophage responses to $cSiO_2$. We report for the first time that DHA at physiologically relevant concentrations interferes with $cSiO_2$-induced inflammasome activation and release of mature IL-1α and IL-1β but not with cell death. As depicted in **Figure 4.13**, DHA likely acts at the level of priming (i.e., Signal 1), as evidenced by its suppression of LPS-induced *Nlrp3*, *Il1b*, and *Il1a* gene expression that influenced later responses to $cSiO_2$ or nigericin (Signal 2). Importantly, suppression by DHA was linked to increased PPARγ activity.

An early and critical response to airborne $cSiO_2$ exposure is robust release of IL-1 cytokines by AMs [132]. Thus, it is noteworthy that DHA suppressed release of both mature IL-1α and IL-1β following treatment with $cSiO_2$ and other inflammasome activators (MSU, alum, and the canonical inflammasome inducer nigericin). Although IL-1α and IL-1β share many characteristics, there are distinctions in the mechanisms by which they are expressed, processed, and released. Pro-IL-1α is constitutively expressed in many cell types, including immune cells where it can be further upregulated by physiological stimuli, including oxidative stress, hormonal stimulation, and exposure to cytokines (including IL-1β and IL-1α itself) [142]. Pro-IL-1β is primarily expressed by immune cells and is rapidly induced by inflammatory stimuli. Both exist as 31 kDa precursors that can be cleaved to 17–18 kDa mature forms [409]. IL-1α is bioactive in both the precursor and mature forms, however, it has been reported that IL-1α activity is enhanced upon cleavage by calpains, which may be activated by $cSiO_2$-induced Ca^{2+} influx [410]. IL-1β is only active in its mature form and can be cleaved by caspase-1 during inflammasome activation. IL-1β may also be cleaved in a caspase-independent manner by proteases produced by other immune cell types [411]. Additionally, both pro-IL-1α and pro-IL-1β released from dying cells can be processed by extracellular proteases [409].

Unlike most cytokines, IL-1 cytokines lack secretory sequences targeting them to the endoplasmic reticulum and Golgi apparatus for processing and release from the cell. Rather, mature IL-1β

has been shown to be released through pores formed by gasdermin D (GSDMD) [412, 413, 414]. Though it has not been confirmed experimentally, it is conceivable that mature IL-1α may also be released in this manner. During inflammasome activation, GSDMD is cleaved by caspase-1, whereupon the N-terminal fragment localizes to the cell membrane and oligomerizes to form pores [386]. A further feature of GSDMD pores is their capacity to collapse the plasma membrane, causing lytic pyroptotic cell death and releasing additional alarmins and cytokines that act as priming signals for the NLRP3 inflammasome [411, 386, 132].

Since $cSiO_2$ clearance from the lung is very slow [16], the persistent presence of this particle elicits repeated cycles in AMs involving phagocytosis of free $cSiO_2$ $\rightarrow$ phagolysosome permeabilization $\rightarrow$ death $\rightarrow$ release of cell autoantigens and reemergence of free $cSiO_2$. Like $cSiO_2$, other exogenous and endogenous crystals (e.g., alum and MSU, respectively) also evoke phagolysosome permeabilization [125, 415, 416]. These crystals elicit pyroptosis [417] as well as inflammasome-independent cell death via apoptotic and necrotic pathways [418, 124]. Our data here suggest that crystal-induced death in RAW-ASC cells was, to a large extent, inflammasome-independent. The release of IL-1α during other types of death associated with inhalation of crystalline substances [419, 420, 386, 418] is consistent with our observation of this cytokine in cell supernatant following $cSiO_2$ treatment of LPS-treated RAW-WT cells.

Numerous preclinical and clinical studies show consuming long chain ω-3 PUFAs such as DHA and eicosapentaenoic acid (C20:5 ω-3; EPA) can reduce chronic inflammatory and autoimmune conditions [31, 35]. Western diets tend to exclude these pro-resolving ω-3s and more typically contain high concentrations of proinflammatory ω-6 PUFAs like linoleic acid (C18:2 ω-6; LA) and arachidonic acid (C20:4 ω-6; ARA) found in plant- and animal-derived lipids. Americans consume many times more ω-6s than ω-3s, so tissue phospholipid fatty acids skew heavily toward ω-3 deficiency [421]. Several marine algae proficiently catalyze formation of DHA and EPA. Oily fish (e.g., salmon, mackerel) and small crustaceans (e.g., krill) bioconcentrate ω-3s into their membrane phospholipids by consuming the marine microalgae [422]. Individuals can increase DHA and EPA tissue incorporation and correct ω-3 deficiency by consuming fish or dietary supplements with fish

oil, krill oil, or microalgal oil.

Following dietary supplementation, DHA concentrations in the lung and other tissues in the lupus-prone NZBWF1 mouse correlate with decreased $cSiO_2$-triggered autoimmune pathogenesis [4, 7]. Significantly, levels of *in vitro* DHA incorporation observed in the present study are similar to those found *in vivo* for mice fed diets supplemented with DHA, suggesting that *in vitro* concentrations of DHA (10 and 25 μM) used here are physiologically relevant. Our findings are consistent with prior reports that DHA suppresses NLRP3 inflammasome activation in other primary and transformed macrophage cell lines stimulated by nigericin [423, 73]. The demonstration here that DHA suppresses expression of three NF-κB dependent genes is concordant with reports that activity of this transcription factor might be inhibited by ω-3 PUFAs, both *in vitro* and *in vivo* [31]. Notably, our laboratory has previously shown that intranasally instilling mice with $cSiO_2$ upregulates many NF-κB targets, including but not limited to MCP-1, TNFα, BAFF, and IL-6. The expression of these genes is significantly reduced in animals supplemented with dietary DHA, suggesting involvement of this pathway *in vivo* [4, 175, 7].

Our finding here that DHA activates PPARγ is consistent with other studies in RAW 264.7 cells [424, 425] and in other macrophage cell lines [74]. PPARγ's capacity to interfere with NF-κB-dependent gene expression [426] might partially explain DHA interference with IL-1 and NLRP3 gene expression. The exact mechanism of PPARγ-dependent inhibition of NF-κB appears to depend on the gene being upregulated. We found here that DHA did not impede nuclear translocation of NF-κB. A similar scenario has been observed for *iNos* expression in RAW 264.7 cells. In that case, PPARγ-dependent suppression of *iNos* does not impact NF-κB binding but rather represses LPS-induced *iNos* expression by preventing the recruitment of the proteasome machinery required to clear co-repressors from the *iNos* promoter [427]. In a separate study in RAW 264.7 cells, activated PPARγ interacts directly with NF-κB to prevent it from binding to the *Il12* promoter [428]. Other studies in human colonic cells and mouse embryonic fibroblast studies reveal that PPARγ has E3 ligase activity, and can induce degradation of NF-κB [273]. Still others show that PPARγ promotes nuclear export of NF-κB in Caco-2 cells [429].

We cannot exclude the possibility of other mechanisms besides PPARγ that might contribute to our findings [430, 431]. For example, ω-3 PUFAs have been shown to affect the physical properties of the cell membrane. Both TLR4 and IL-1R1 activation require the oligomerization of multiple receptors, a process that requires structural alteration of the plasma membrane [432, 69]. Increased phospholipid ω-3 PUFA content reduces the formation of lipid rafts, thus suppressing inflammatory signaling pathways that depend on clustering of transmembrane receptors [224, 432, 69]. Alternatively, free DHA can be cleaved from the membrane and act as a ligand for anti-inflammatory receptors. *In vitro* studies reveal that DHA activates G-protein coupled receptors (GPCRs) FFAR1/GPR40 and FFAR4/GPR120 [272, 73]. Previous studies indicate that activation of FFAR1/GPR40 and FFAR4/GPR120 by extracellular free DHA prevents TAB1 from binding TAK1, which is a necessary step in LPS-induced NF-κB activation [259]. Finally, DHA-derived metabolites, many of which are termed specialized pro-resolving mediators (SPMs), are associated with the resolution of inflammation. Many reports of the bioactivity of SPMs support their potential to attenuate inflammasome activation [433, 434, 435, 436, 392, 437], potentially by binding to GPCRs involved in inhibiting NF-κB signaling [433, 202, 392, 438, 439]. In general, these mechanisms culminate in inhibition of NF-κB, which we did not observe in our model. Accordingly, while outside the scope of this study, further clarification is needed to delineate the relative contributions of PPARγ-dependent and –independent mechanisms that might contribute to DHA-mediated suppression of IL-1 cytokine and NLRP3 gene expression.

Taken together, we have demonstrated that increasing the DHA content of membrane phospholipids suppresses cSiO_2-induced inflammasome activation and release of IL-1 cytokines and that these effects are potentially linked to PPARγ activation and interference with NF-κB-driven gene expression (**Figure 4.13**). Understanding how DHA and other ω-3 PUFAs influence crystal-mediated pathogenesis could potentially lead to harnessing dietary modulation of the lipidome as an intervention against chronic inflammatory and autoimmune diseases involving the inflammasome.

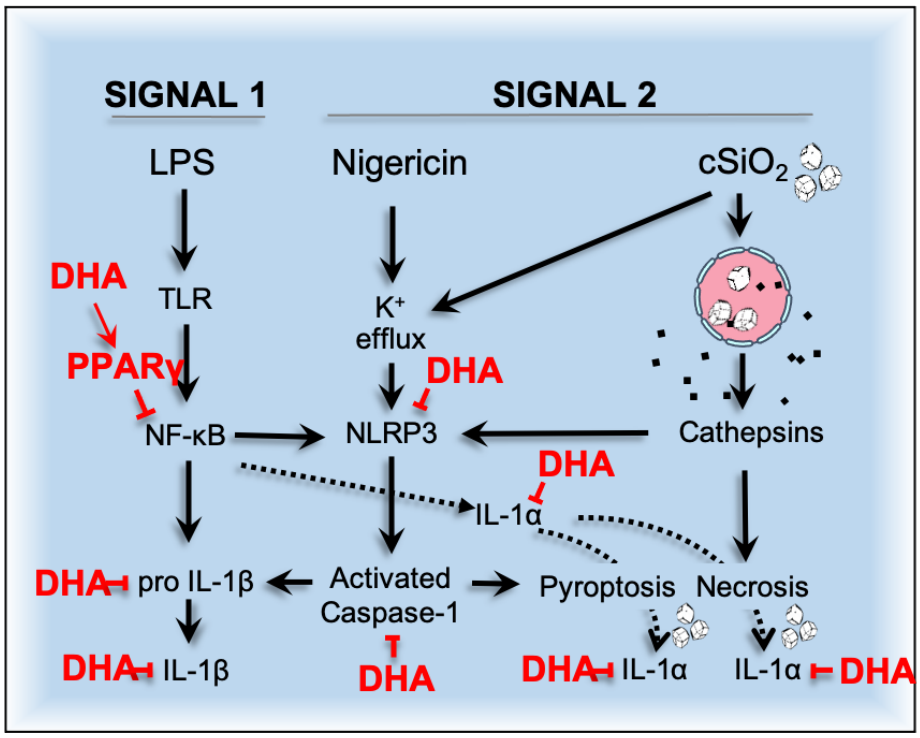


Figure 4.13: Putative model for the protective effects of DHA against nigericin- and $cSiO_2$-induced inflammasome activation, IL-1 cytokine release, and death in macrophages. DHA inhibits nigericin- and $cSiO_2$-induced inflammasome activation as measured by IL-1β maturation and release and caspase-1 activation. DHA also suppresses nigericin- and $cSiO_2$-induced IL-1α cleavage and release and cell death. Cell death is wholly suppressed by DHA in nigericin-treated macrophages but only partially suppressed in $cSiO_2$-treated macrophages. Collectively, these inhibitory effects are linked to suppression of genes (*Nlrp3*, *Il1b*, and *Il1a*) regulated by the transcription factor NF-κB.

4.6 ACKNOWLEDGMENTS

We would like to thank Dr. Hui-Ren Zhou, Augie Evered, and Elizabeth Ross for their excellent technical support and advice.

CHAPTER 5

SINGLE CELL TRANSCRIPTOMICS TO INVESTIGATE DOCOSAHEXAENOIC ACID SUPPRESSION OF LPS-INDUCED INFLAMMATORY GENE EXPRESSION

Wierenga KA[1,2], Westendorp B[3], Harkema JR[2,4] Pestka JJ[2,5,6]

[1]Department of Biochemistry and Molecular Biology, Michigan State University, East Lansing, MI

[2]Institute for Integrative Toxicology, Michigan State University, East Lansing, MI

[3]Department of Biomolecular Health Sciences, Utrecht University, Utrecht, NL

[4]Department of Pathobiology and Diagnostic Investigation, Michigan State University, East Lansing, MI

[5]Department of Food Science and Human Nutrition, Michigan State University, East Lansing, MI

[6]Department of Microbiology and Molecular Genetics, Michigan State University, East Lansing, MI

Author Contributions: KW: study design, data analyses/interpretation, chapter preparation. BW: data analysis/interpretation. JH: study design, project funding. JP: study design, oversight, chapter preparation, project funding.

5.1 ABSTRACT

Preclinical and clinical studies suggest that consumption of ω-3 fatty acids reduces inflammation associated with chronic diseases, in part by inhibiting proinflammatory cytokine and interferon-regulated gene expression in macrophages. Here we tested the hypothesis that the ω-3 docosahexaenoic acid (DHA) interferes with LPS-induced polarization of primary macrophages to inflammatory phenotypes. The impact of LPS and DHA on macrophage polarization was assessed by single cell RNA sequencing (scRNAseq). Self-renewing primary murine macrophages derived from fetal livers were cultured with 25 μM DHA or vehicle for 24 h and then treated with 20 ng/ml LPS for 1 and 4 h. Single cells were isolated and libraries prepared per the 10x Genomics workflow, followed by RNA sequencing on the Illumina NovaSeq platform. Downstream analysis of >30,000 genes expressed by over 10,000 high-quality cells revealed distinct clusters associated with time and treatment. These clusters were explored by investigating genes differentially expressed among experimental groups. Changes induced by DHA alone were consistent with a pro-resolving phenotype and a dampened inflammatory response to LPS. Among the first genes induced by LPS were cholesterol synthesis genes, many of which were reduced by DHA both before and after LPS treatment. Finally, a subsets of LPS-treated cells was identified that expressed high levels of NF-κB-driven genes and interferon-related genes, both of which were effectively suppressed with DHA supplementation.

5.2 INTRODUCTION

Macrophages, a highly plastic immune cell population, can be polarized to a range of phenotypes that promote or resolve inflammation. Pro-resolving macrophages repair damaged tissue, phagocytose and clear dead cells, and suppress the inflammatory response. A skewing of macrophages towards a more proinflammatory phenotype is observed in chronic inflammatory and autoimmune conditions, such as atherosclerosis [440], obesity [441], rheumatoid arthritis [85], and lupus [442]. Hence, interventions that suppress macrophage activation and promote resolution may be able to alleviate chronic inflammation and autoimmune diseases.

Pathogen-derived stimuli are often used to activate immune cells to study their inflammatory response. Bacterial lipopolysaccharide (LPS) is a prototypical stimulus for inducing a robust inflammatory response *in vitro* and *in vivo* [443]. LPS is a component of the gram-negative bacterial cell wall and a potent agonist for the pattern recognition receptor toll-like receptor 4 (TLR4). TLR4 activates multiple signaling pathways that involve MAP kinases, NF-κB, and interferon (IFN) response factors, resulting in time-dependent upregulation of genes associated with inflammation [444, 445]. Genes associated with transcriptional machinery are among the first induced, followed by a large repertoire of inflammatory cytokines and IFN genes. In the absence of additional stimulation, modest TLR4-stimulated inflammation is self-resolving. Thus, pro-inflammatory genes and their protein products peak at specific timepoints and followed by rapid degradation. However, in situations of unresolved inflammation, many of these genes may remain elevated, contributing to pathophysiological effects [446, 447].

Chronic and autoimmune diseases often result from aberrant inflammatory signaling, making it critical to identify ways to subdue the inflammatory response or hasten its resolution. Preclinical and clinical studies reveal that ω-3 polyunsaturated fatty acids (PUFAs) ameliorate symptoms and reduce biomarkers in inflammatory diseases, including rheumatoid arthritis [448], cardiovascular disease [381, 373], and lupus [32, 449]. Studies employing supplementation of macrophages *in vitro* with long chain ω-3 PUFAs docosahexaenoic acid (DHA) and eicosapentaenoic acid (EPA) have provided insight into how these dietary lipids influence inflammatory pathways [31, 185, 354]. Multiple potential mechanisms have been put forth that differ depending on the experimental context, including cell type and inflammatory stimuli.

A shortcoming of most mechanistic studies on ω-3 PUFAs *in vitro* is the utilization of cloned macrophage cell lines. To address this limitation, here we tested the hypothesis that DHA-mediated transcriptomic changes prior to an inflammatory trigger would polarize primary macrophages towards a phenotype resistant to transcriptional changes induced by LPS. Single cell RNA sequencing (scRNAseq) was employed to gain insight into how DHA influences LPS-triggered inflammatory gene expression in a novel, self-renewing primary macrophage model, derived from the fetal liver,

known as MPI cells [450].

5.3 MATERIALS AND METHODS

5.3.1 Animals and euthanasia.

C57BL/6J mice (strain # 000664) were obtained from The Jackson Laboratory (Bar Harbor, ME). Experimental protocols were approved by the Institutional Animal Care and Use Committee at MSU (AUF # PROTO201800113). Mice were given free access to food and drinking under controlled conditions (humidity: 40–55%; lighting: 12-h light/dark cycles; and temperature: 24 $\pm$ 2°C) as described previously [4, 3]. MPI cells were isolated from fetuses carried by pregnant dams at 14-18 gestational d. Dams were euthanized by CO_2 inhalation for 10 min to ensure death to neonates, which are resistant to anoxia. Cervical dislocation was used as a secondary form of death for the dam. Fetuses were immediately removed, and loss of maternal blood supply served as a secondary form of death for the fetuses.

5.3.2 MPI cell isolation and culture.

MPI cells were generated from livers excised from murine fetuses at 14-18 gestational days, as previously described [450]. Briefly, livers were dissociated into a single cell suspension in sterile phosphate buffered saline (PBS), filtered through a 70 μm nylon filter (Corning), and centrifuged at 220 *x*g for 5 min. Cells were washed twice with sterile PBS, resuspended in MPI media (RPMI media (Thermo Fisher) containing 10% fetal bovine serum (FBS, R&D Systems), 1% penicillin-streptomycin (P/S, Thermo Fisher) and 30 ng/mL murine GM-CSF (Peprotech), and plated in 10-cm treated culture dishes (1 liver/dish). The following day, half of the media was replaced with fresh media. Media was refreshed in this manner every 2-3 d, until an adherent monolayer was achieved (about 1-2 wk). At this time, cells were frozen for cryostorage or used for experiments. Initially, cells cultured under aseptic conditions have a round morphology and proliferate slowly, but after approximately 5-10 passages, cells become spindleoid and proliferate rapidly. All cells used for experiments in this study were between passage 10 and 20, which are spindle-shaped and

highly proliferative.

5.3.3 DHA supplementation and membrane incorporation.

DHA was prepared as a 3:1 complex with fatty-acid free bovine serum albumin (BSA) as previously described [354, 402]. DHA-supplemented media was prepared in serum deprived MPI media (0.25% FBS, 1% P/S, 30 ng/mL mGM-CSF). The serum concentration was reduced to maximize DHA's incorporation into the phospholipid membrane by removing competing fatty acids present in serum. We have previously showed using RAW264.7 cells that this protocol results in significant incorporation of DHA into the phospholipid membrane at the expense of oleic acid, the major unsaturated fatty acid found in fetal bovine serum [354]. The same was true of MPI cells used in this study (**Supplementary Figure D.1, Supplementary Table D.1**).

To measure phospholipid fatty acid content, cell pellets were stored in 100% methanol at -80 until analysis by gas-liquid chromatography (GLC) with flame ionization detection at OmegaQuant Analytics, LLC. Cell pellet samples were transferred to a screw-cap glass vial which contained 1,2-ditricosanoyl-sn-glycero-3-phosphocholine as an internal standard (di-C23:0 PL) (Avanti Polar Lipids, USA) where they were extracted with a modified Folch extraction. A portion of the organic layer was taken and spotted on thin-layer chromatography (TLC) plate that was developed with 8:2:0.15 (hexane:ethyl ether:acidic acid) to separate the lipid fractions. After the TLC plate was dry the phospholipid band was scrapped into a screw-cap glass vial with methanol containing 14% boron trifluoride (Sigma-Aldrich, St. Louis, MO). The vial was briefly vortexed and heated in a hot bath at 100˚C for 10 min. After cooling, HPLC grade water and hexane (EMD Chemicals, USA) were added sequentially the tubes were recapped, vortexed and centrifuged help to separate layers. An aliquot of the hexane layer was transferred to a GC vial. GC was carried out using a GC2010 Gas Chromatograph (Shimadzu Corporation, Columbia, MD) equipped with a SP2560, 100-m fused silica capillary column (0.25 mm internal diameter, 0.2 μm film thickness; Supelco, Bellefonte, PA).

Fatty acids were identified by comparison with a standard mixture of fatty acids (GLC 782,

NuCheck Prep, Elysian, MN) and an internal standard (C23:0 FAME, NuCheck Prep, Elysian, MN) which was also used to determine individual fatty acid calibration curves. The di-C23:0 PL was used to calculate recovery efficiency of the assay and applied to all fatty acids. The following 24 fatty acids (by class) were identified: saturated (14:0, 16:0, 18:0, 20:0, 22:0 24:0); cis monounsaturated (16:1, 18:1, 20:1, 24:1); trans (16:1, 18:1, 18:2), cis ω-6 polyunsaturated (18:2, 18:3, 20:2, 20:3, 20:4, 22:4, 22:5); cis ω-3 polyunsaturated (18:3, 20:5, 22:5, 22:6). Fatty acid composition was expressed as a percent of total identified fatty acids and concentrations as μg/vial of cell pellets.

5.3.4 LPS exposure.

Cells were treated with 20 ng/mL LPS (Salmonella enterica serotype typhimurium containing <1% protein impurities, Millipore Sigma) unless otherwise noted. LPS stock solution was prepared in sterile PBS. The solution was thoroughly vortexed and sonicated before use, and dilutions were prepared in serum-deprived MPI media.

5.3.5 Western blotting.

Whole cell lysate was isolated as previously described [354], with Halt™ Protease and Phosphatase inhibitors (Thermo Fisher) included in RIPA buffer (Thermo Fisher Scientific) during lysis. Protein was quantified using a Pierce™ BCA protein assay (Thermo Fisher), after which all samples were adjusted to the same concentration. Samples were loaded in lanes of pre-cast 4-20% Mini-Protean TGX Protein Gels (Bio-Rad) and electrophoresis performed at 100V for 90 min in a Bio-Rad mini-PROTEAN tetra vertical electrophoresis chamber. Proteins were transferred to a 0.45 μm low fluorescence PVDF membrane (Bio-Rad) using the Bio-Rad TransBlot Turbo System, per the manufacturer's instructions. Antibody binding was performed using an iBind Flex apparatus per the manufacturer's instructions using the iBind Flex fluorescence detection solution kit. The following primary antibodies (Cell Signaling Technologies) used at the indicated dilution: Rabbit anti-Actin (1:4000), Rabbit anti-NFκB (1:1000), Rabbit anti-phospho-NFκB (1:1000), Mouse anti-

IκB (1:1000), Rabbit anti-phospho-IκB kinase (1:1000). The following Licor (Lincoln, Nebraska) near infrared fluorescent secondary antibodies used at the indicated dilution: IRDye 680 RD Goat anti-Rabbit IgG (1:4000), IRDye 800 CW Donkey anti-Rabbit (1:3000), IRDye 800 CW Donkey anti-Mouse (1:3000). Blots were read using a Licor Odyssey Imaging System.

5.3.6 qPCR.

Cells were treated in 12-well plates with 25 μM DHA/8.3 μM BSA or Veh (8.3 μM BSA) for 24 h and 20 ng/mL LPS for 1 and 4 h. Approximately 5 x 10^5 cells were collected for RNA extraction using RNeasy Mini Kit spin columns (Qiagen). RNA was quantified using a NanoDrop-1000 (Thermo Scientific) and reverse transcribed to cDNA with reagents from a High Capacity RNA to cDNA reverse transcriptase kit (Thermo Fisher). Resultant cDNA was diluted to a concentration between 10-50 ng/μL. qPCR was performed on a QuantStudio 7 instrument using a Gene Expression Taqman Master mix (Thermo Fisher) and Taqman probes (Thermo Fisher). Gene expression was calculated as the relative copy number, as previously described [301, 354].

5.3.7 Single cell isolation, library preparation, and sequencing.

The overall experimental design is depicted in **Figure 5.1**. MPI cells were seeded in 6 well plates at -48 h in complete media. At -24 h, media was changed to contain 25 μM DHA or Veh (8.3 μM BSA) and 0.25% FBS. At time 0 h (24 h after DHA supplementation), cells were treated with 20 ng/mL LPS. Treatment conditions are identified as follows:

1. Con (collected at -24 h)
2. Veh (treated with 8.3 μM BSA, collected at 0 h)
3. DHA (treated with 25 μM DHA + 8.3 μM BSA, collected at 0 h)
4. Veh.LPS1 (treated with 8.3 μM BSA, collected 1 h post-LPS)
5. DHA.LPS1 (treated with 25 μM DHA + 8.3 μM BSA, collected at 1 h post-LPS)
6. Veh.LPS4 (treated with 8.3 μM BSA, collected 4 h post-LPS)
7. DHA.LPS4 (treated with 25 μM DHA + 8.3 μM BSA, collected at 4 h post-LPS).

Sample start times were staggered to allow collection of all samples simultaneously, after the indicated treatment times. Cells were lifted from 6-well plates using Accutase® (Millipore Sigma), and washed twice with ice cold sterile PBS to remove residual enzyme. Cell viability immediately after lifting and prior to single cell isolation was assessed by Trypan Blue exclusion. All treatment groups had a viability of >90%. Single cells were isolated and RNA libraries prepared using the 10x Chromium SingleCell 3' RNAseq kit (v3 Chemistry, 10X Genomics), per the manufacturer's instructions. Sample quality control was performed at the Michigan State University Genomics Core followed by sequencing at Novogene. Libraries were sequenced on an Illumina Novaseq using S4 chemistry, obtaining >100K reads/cell. Reads were demultiplexed with the mkfastq option of CellRanger 2.1.1 [451].

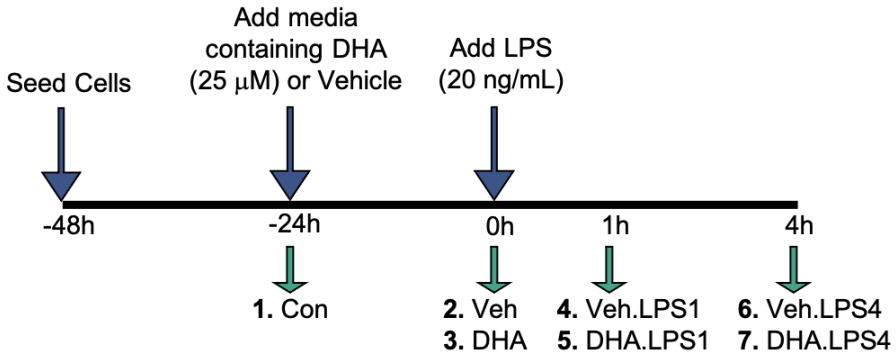


Figure 5.1: Timeline for treatment and collection of samples for single cell RNA sequencing. MPI cells were seeded in 6 well plates at -48 h in complete media. At -24 h, media was changed to contain 25 μM DHA or Veh (8.3 μM BSA) and 0.25% FBS. At time 0 h (after 24 h DHA supplementation) cells were treated with 20 ng/mL LPS. Sample start times were staggered to allow collection of all samples simultaneously, after the indicated treatment times.

5.3.8 Filtering and generation of Seurat object.

Data were filtered to remove low quality cells. Only cells with over 2 x 10^4 unique UMI reads mapping to at least 2000 unique genes or more were included. Furthermore the percentage of counts mapping to mitochondrial genes should not exceed 20% (**Supplementary Figure D.2**). The remaining cells were then subjected to normalization with the sctransform function in Seurat, an R toolkit for single-cell genomics [452]. The Uniform Manifold Approximation and Projection

(UMAP) technique for data dimensionality reduction. Clusters were identified using the FindClusters function in Seurat.

5.3.9 SCENIC analysis.

SCENIC was used to detect which transcription factor programs were most strongly affected by DHA in 4 h LPS-treated cells [453]. Briefly, the SCENIC workflow consists of three steps: 1) the GENIE3 package is used to identify genes co-expressed with transcription factors, 2) the RcisTarget package is used to perform *cis*-regulatory motif analyses of co-expressed genes to identify potential binding targets for the transcription factor in question, and 3) the AUCell package is used to calculate the area under the recovery curve (AUC) by integrating the expression ranks for a defined set of genes (in this case, genes comprising defined regulons) for individual cells.

5.3.10 Heatmaps.

Heatmaps were generated using the pheatmap tool in R Studio, based on scaled gene expression data or regulon AUC values for individual cells. Ward's criteria was used as the clustering method. The "cutree_columns" function was used to break the heatmap into clusters. No scaling was applied as the input values were already scaled for individual cells and regulons.

5.3.11 Data visualization and statistics.

Plots were prepared in R Studio version 1.1.442 (using ggplot2 [454]) and in GraphPad Prism version 9.1.0 (San Diego, California, USA, www.graphpad.com). Non-parametric versions of statistical tests were used where appropriate, as noted in figure legends.

5.4 RESULTS

5.4.1 Clustering is driven by LPS treatment and cell cycle phase.

Seurat identified ten distinct clusters of cells, which visually separated into four time-associated groups (**Figure 5.2A**). When individual cells were colored according to treatment group, it was evident that 24 h serum deprivation resulted in a separation from the control group (**Figure 5.2B**). Cells treated with and without LPS for 1 or 4 h separated from one another in the UMAP projection. Veh- and DHA-treated cells clustered closely together. Hence, serum deprivation and LPS treatment had a greater effect on the gene expression profile than DHA supplementation.

The Seurat CellCycleScoring tool was used to gain insight into how treatments influenced proliferation of macrophages *in vitro*. Cell cycle phase scores, based on genes expressed in the G2M and S phases, were calculated for individual cells. We chose not to regress out the influence of cell cycle, as serum deprivation and LPS treatment appeared to have a greater influence on cell clustering. Treatment groups that received serum-deprived media had a reduced number of cycling cells (**Figure 5.2 C-D**). This was reduced further with DHA treatment at 0 and 1 h and treatment with LPS at 4 h.

5.4.2 DHA influences expression of genes involved in proliferation, the antioxidant response, lipid metabolism, and immune suppression at 0 h.

We identified 36 differentially expressed genes in the DHA treatment group compared to the Veh treatment group at 0 h (no LPS treatment) (**Figure 5.3A**). Of these, 13 were downregulated and 23 were upregulated. Gene ontology analysis only returned pathways that overlapped with 2 or 3 of the differently expressed genes, which made it difficult to determine the relevance of these results. Owing to the small number of genes, we chose to forego the GO analysis and instead performed literature searches to identify the cellular pathways involved with the differentiated expressed genes.

DHA increased genes involved in lipid uptake and synthesis, including *Cd36* (a scavenger receptor involved in lipid uptake), *Plin2* (associated with lipid droplet formation), and *Lipa* (lipase

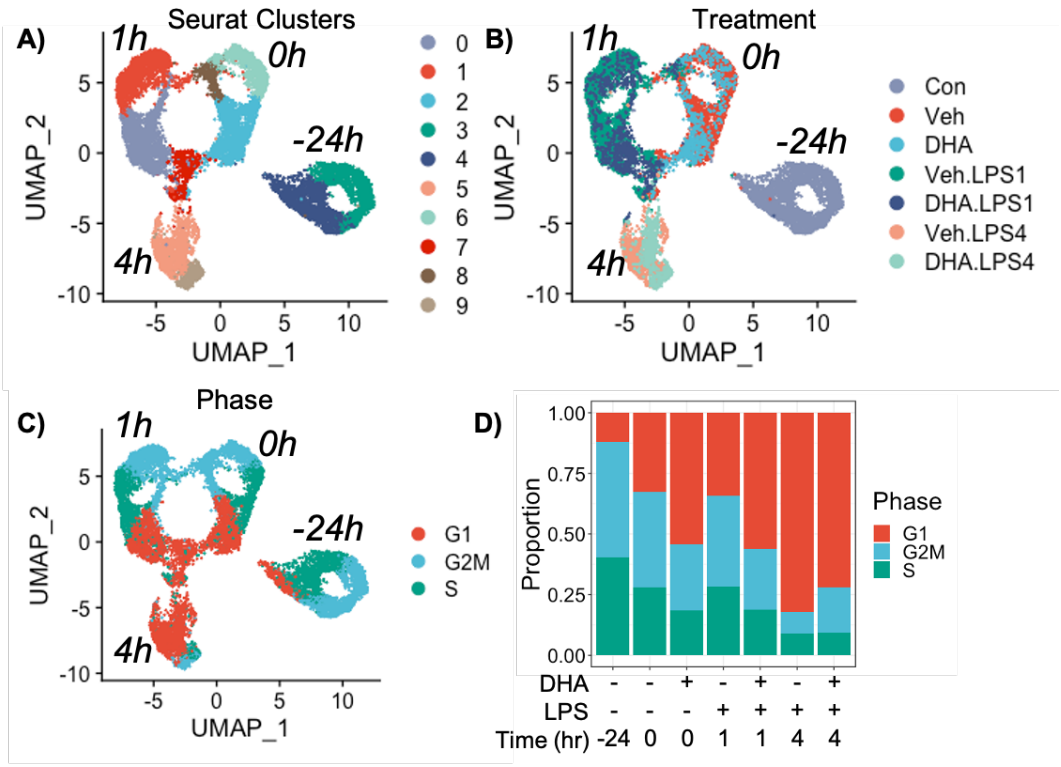


Figure 5.2: Uniform manifold approximation and projection (UMAP) reveals factors that drive clustering. **A.** Unbiased Seurat Clustering identified ten distinct clusters which separated into four larger groups. **B.** Labeling individual cells according to treatment showed that cells clustered into groups based on serum deprivation (-24 h vs 0, 1, and 4 h) and by duration of LPS treatment (0 h vs 1 h vs 4 h). **C.** Cell cycle phase scores were applied to each cell using the Seurat CellCycleScoring tool. Cells within the same phase clustered together within the groupings were separated based on serum deprivation and time of LPS treatment. **D.** Serum deprivation, addition of DHA, and 4 h treatment with LPS all reduced the number of cycling cells. All UMAP plots were generated using the Seurat FeaturePlot tool.

involved in lysosomal degradation of lipids). DHA-treated cells had lower expression levels of genes involved in cholesterol synthesis (*Scd1, Scd2, Pmvk, Cyp51, Hmgcs1, Fdps*). Changes to cholesterol synthesis may be in response to changes to membrane fluidity that occur with PUFA incorporation into phospholipids [455].

DHA decreased synthesis of histone genes (*Hist2h2ac, Hist1h2ae, Hist1h2ap*), which is associated with a decline in DNA synthesis [456], and increased the apoptotic transcription factor *Ddit3*, which is consistent with the observed decrease in cycling cells. Previous studies have shown that treatment with high concentrations of DHA are capable of inducing apoptosis *in vitro* in breast

cancer cells [457]. We conclude that though our DHA treatment did reduce cell proliferation, the concentration was not high enough to trigger excess cell death by apoptosis.

Other genes differentially regulated by DHA play roles in the antioxidant response (*Hmox1, Sqstm1, Chchd10, Gclm*), metal homeostasis (*Mt1, Mt2, Slc39a10, Ftl1, Fth1*), and inflammatory pathways (*Ifi202b, Cd300a, Cx3cr1*). We observed that DHA augmented expression of multiple genes shown to be induced by NRF2, including *Cd36, Sqstm1, Hmox1, Ftl1, Fth1*, and *Gclm* [458, 459]. Bulk qPCR was used to confirm expression of *Hmox1* and *Sqstm1*, which encode the proteins heme oxygenase-1 and sequestosome-1 and play roles in reducing reactive oxygen species and promoting autophagosome formation, respectively [460, 461] (**Figure 5.3B**).

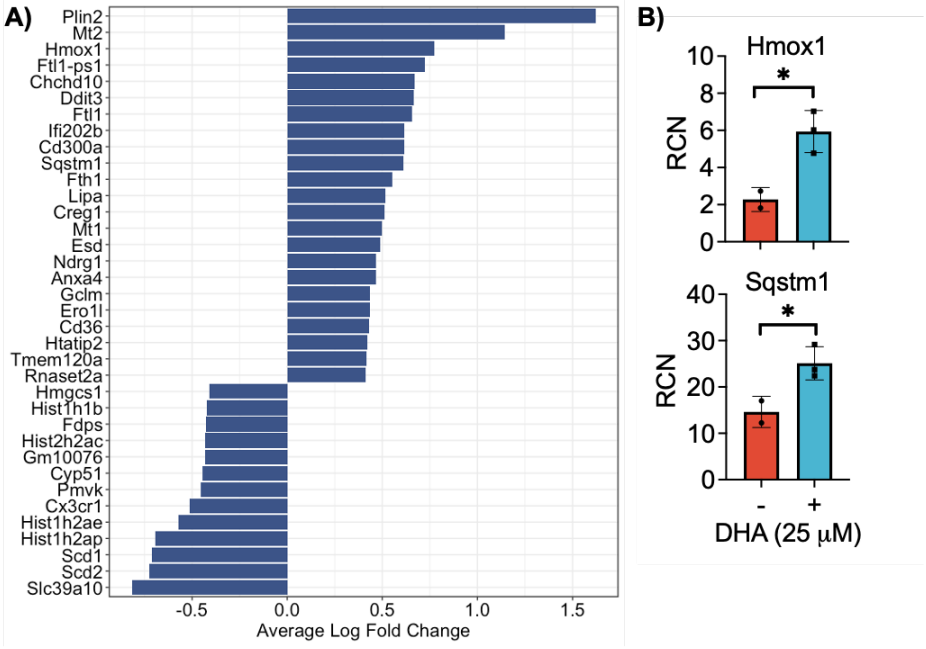


Figure 5.3: DHA influences expression of genes involved in lipid metabolism, antioxidant response, and immune regulation. A. Differentially expressed genes (DEGs) were identified using the Seurat FindMarkers tool, with thresholds set to select genes with >1.5-fold change (Adjusted p-value < 0.001) in gene expression and genes expressed in at least half in the Veh or DHA groups. **B.** Expression of *Hmox1* and *Sqstm1*, two genes induced by DHA treatment, was confirmed using bulk qPCR of samples treated in parallel with treatments for single cell isolation. Asterisks indicated significant differences (*p<0.05) between Veh (-) and DHA (+) groups, as assessed by Student's t-tests.

Some differentially expressed genes have functions that are unknown or not well described, though many are implicated in pathways involved in oxidative stress, cell proliferation, and the

immune response. For example, it has been shown that mutations in *Chchd10* are associated with impaired mitochondrial genome maintenance following oxidative stress [462]. *Ifi202b* (also known as p202) suppresses IFN gene signaling by binding to dsDNA and preventing its access to nucleic acid sensors in the cell [463]. *CD300a* is an inhibitory receptor expressed on many immune cell populations [464]. *Cx3cr1* has been reported to have both protective and pro-inflammatory effects in different disease contexts [465], and *Ndrg1* acts as a tumor suppressor in some cancers and a tumor promoter in others [466]. We also observed increased expression of *Anxa4*, which was shown to be upregulated in human and mouse M2-polarized macrophages *in vitro* [467]. Altogether, these changes are possibly indicative of a shift in macrophage phenotype at time 0 h to be more resilient against subsequent inflammatory triggers.

5.4.3 LPS-induced inflammatory gene expression is preceded by cellular pathways promoting transcription.

Analysis with Seurat FindMarkers revealed 88 differentially expressed genes after 1 h LPS treatment and 417 differentially expressed genes with 4 h LPS treatment, with 52 genes shared between the two groups (**Figure 5.4A**). Among the genes differentially expressed at 1 h, 81 were upregulated and 7 were downregulated; and among the genes differentially expressed at 4 h, 205 were upregulated and 212 were downregulated.

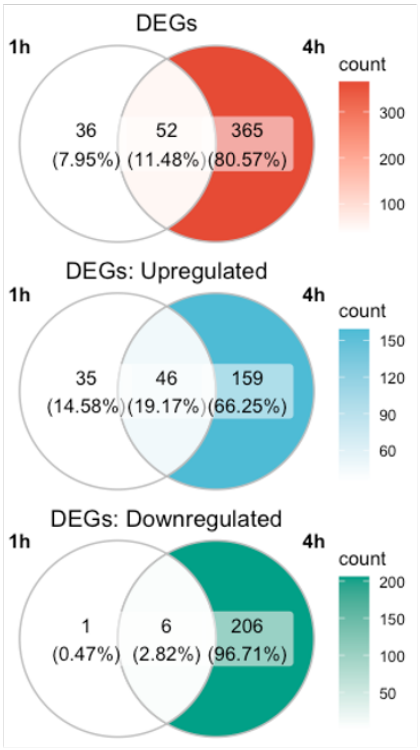
The Enrichr database [468] was used to identify GO Biological Process terms associated with differentially expressed genes. Genes upregulated at 1 h were enriched in pathways involved in regulating transcription as well as inflammatory pathways, like cellular response to cytokine stimulus and response to lipopolysaccharide (**Figure 5.4B**). This suggests that at 1 h, many genes were setting the stage for the much greater transcriptional response subsequently observed. Indeed, at 4 h, most upregulated genes are involved in inflammatory signaling pathways, while downregulated genes are involved in cell proliferation.

Heatmaps were generated to visualize the gene expression pattern among individual cells (**Figure 5.5**, additional details in figure legend). Cells were annotated by cell cycle and treatment (horizon-

tal colored lines above heatmap). As in the UMAP plots, unbiased clustering of cells resulted in near-perfect separation by LPS treatment group. Within treatment groups, cells clustered according to cell cycle phase.

Cluster 1 contained genes that were most strongly induced at 4 h post-LPS exposure, some of which were also upregulated at 1 h. A large number of altered genes code for cytokines or were proteins involved in inflammatory signaling pathways. Interestingly, some chemokines at 1 h post-LPS (*Ccl2, Ccl3, Ccl4*) appeared to be more robustly expressed in cells in G1 phase compared to cells in G2M or S phase. Though the number of cells in G2M and S phase at 4 h post-LPS was much lower than 1 h, a similar pattern was observed where genes such as *Il1a, Il1b*, and *Oasl1* had higher expression in G1 phase cells compared to cycling cells. Cluster 2 contained genes that were induced by 1 h treatment with LPS, and either remained constant or decreased at 4 h LPS treatment. These included transcription factors (*Junb, Ier2, Egr1*), genes involved in negative feedback of inflammatory signaling (*Zfp36, Dusp2, Nfkbiz*), and genes involved in promoting inflammatory signaling (*Nlrp3, Tnf, Traf*). Genes in clusters 3 and 4 were associated with proliferation, though their roles of the genes in cluster 3 are less well defined than those of cluster 4. Cluster 3 and 4 genes were all downregulated with 4 h LPS treatment.

A)



B)

Upregulated by LPS at 1 h Term	Adj. P-Value
Regulation of transcription from RNA polymerase II promoter	$5.33*10^{-8}$
Positive regulation of transcription from RNA pol II promoter	$3.66*10^{-8}$
Cellular response to cytokine stimulus	$6.03*10^{-8}$
Cytokine-mediated signaling pathway	$6.45*10^{-7}$
Regulation of I-kappaB kinase/NF-kappaB signaling	$6.29*10^{-7}$
Response to lipopolysaccharide	$5.81*10^{-7}$
Upregulated by LPS at 4 h Term	**Adj. P-Value**
Cellular response to lipopolysaccharide	$2.34*10^{-13}$
Cytokine-mediated signaling pathway	$7.76*10^{-13}$
Cellular response to cytokine stimulus	$6.54*10^{-12}$
Response to lipopolysaccharide	$4.09*10^{-11}$
Cellular response to molecule of bacterial origin	$5.88*10^{-8}$
Lipopolysaccharide-mediated signaling pathway	$9.65*10^{-8}$
Downregulated by LPS at 4 h Term	**Adj. P-Value**
Mitotic sister chromatid segregation	$1.65*10^{-12}$
DNA metabolic process	$5.71*10^{-8}$
Mitotic spindle organization	$5.80*10^{-8}$
Microtubule cytoskeleton organization involved in mitosis	$9.34*10^{-7}$
Sister chromatid segregation	$1.20*10^{-6}$
Chromosome condensation	$2.46*10^{-6}$

Figure 5.4: Gene expression changes induced by LPS at 1 and 4 h. A. Differentially expressed genes (DEGs) were identified using the Seurat FindMarkers tool, with thresholds set to select genes with >2-fold change in gene expression and genes expressed in at least half of either group being compared. Venn diagrams of DEGs at 1 h only (right circle), 4 h only (left circle), and at both timepoints (intersection) were generated to visualize the quantity of DEGs in each group. **B.** The Enrichr database was used to identify GO Biological Process terms for the indicated groups of genes. The six most enriched pathways are shown, as determined by the size of the adjusted *p*-value.

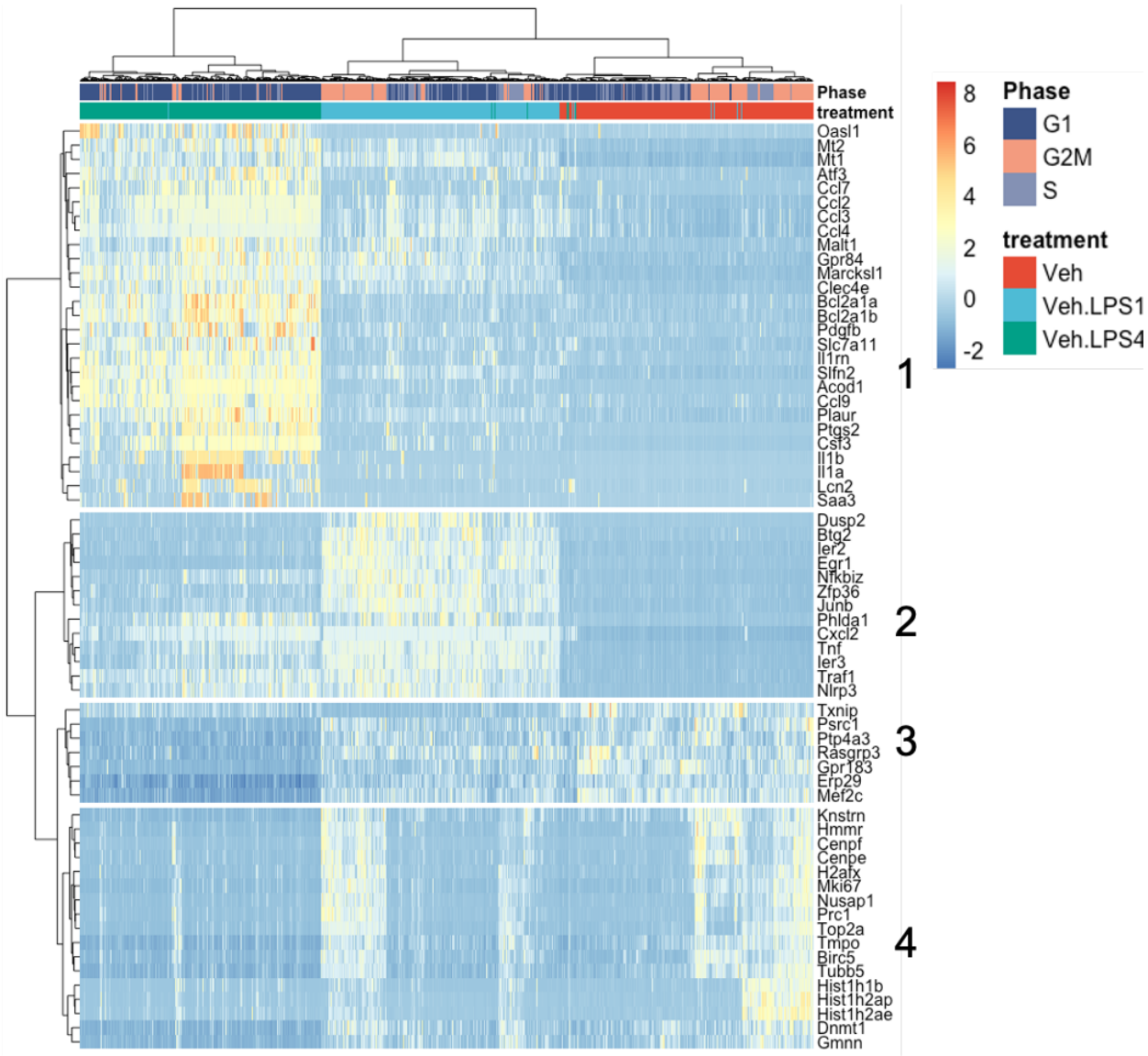


Figure 5.5: Heatmap of differentially expressed genes at 1 and 4h post-LPS treatment. 500 cells were randomly selected from the Veh, Veh.LPS1, and Veh.LPS4 groups and genes upregulated >6-fold or downregulated >3-fold were used to generate a heatmap. Cells were annotated according to their cell cycle phase and treatment group. Genes were split into 4 clusters, identifying genes that increased expression from 1 h LPS to 4 h LPS (Cluster 1), genes that peaked at 1 h LPS (Cluster 2), genes suppressed by LPS at 4 h (Cluster 3, many associated with cell survival), and genes associated with cycling cells (Cluster 4), which were also suppressed at 4 h.

5.4.4 DHA suppresses genes involved in cholesterol synthesis at 1 h post-LPS exposure and inflammatory signaling pathways at 4 h post-LPS exposure.

Of the 156 genes induced by LPS at 1 h, 11 genes were significantly suppressed by DHA (**Figure 5.6A**). Among these 11 genes, more than half were involved in cholesterol synthesis, including *Cyp51, Hmgcs, Hmgcr, Insig, Ldlr, Sc5d*, and *Idi1* (**Figure 5.6B**). This is consistent with recent studies investigating the role of lipid metabolism in macrophages, where it has been shown that LPS-induced cholesterol synthesis promotes macrophage activation [469, 83]. Of the remaining genes, *Rasgef1b* and *Rgs1* are involved in G-protein signaling, *Gpr84* is a GPCR known to be involved in activating inflammatory pathways in macrophages [470], and *Phlda1* expression is observed to be increased in inflammatory macrophages in atherosclerotic plaques [471] (**Figure 5.6C**).

It was further determined that 77 of the 494 genes induced by LPS at 4 h were suppressed by DHA (**Figure 5.7A**). GO Biological Processes were identified for the differentially expressed genes that were 1) decreased by DHA, 2) increased in LPS and suppressed by DHA, 3) increased by LPS (**Figure 5.7B**). LPS-induced genes that were suppressed by DHA were enriched for pathways such "cytokine mediated signaling pathway" and "cellular response to type I interferon". Assessment of selected genes annotated as "cellular response to LPS" and "cytokine-mediated signaling pathway" show that DHA completely suppressed certain genes while only mildly suppressing, or having no effect, on others (**Figure 5.7 C-D**). The group of genes annotated as "cellular response to LPS" contained chemokines (*Ccl5, Ccl2, Ccl3*), cytokines (*Tnf, Tgfb1*), and other genes promoting pro-inflammatory signaling pathways (*Pde4b, Nfkb1, Cd14, Tnfrsf1b*). LPS also upregulates many genes that regulate inflammation by degrading mRNA coding inflammatory cytokines (*Zc3h12a*) or inhibiting inflammatory signaling pathways (*Tnip3, Tnip1, Tnfaip3, Nfkil3*). Many of the genes annotated as "cytokine-mediated signaling pathway" are involved in or induced by type I IFN signaling (*Ifit1, Isg15, Xaf1, Oas2, Cxcl10, Irf9, Irf7*). Suppression of type I IFN genes observed in scRNAseq was further confirmed using bulk qPCR (**Figure 5.8**).

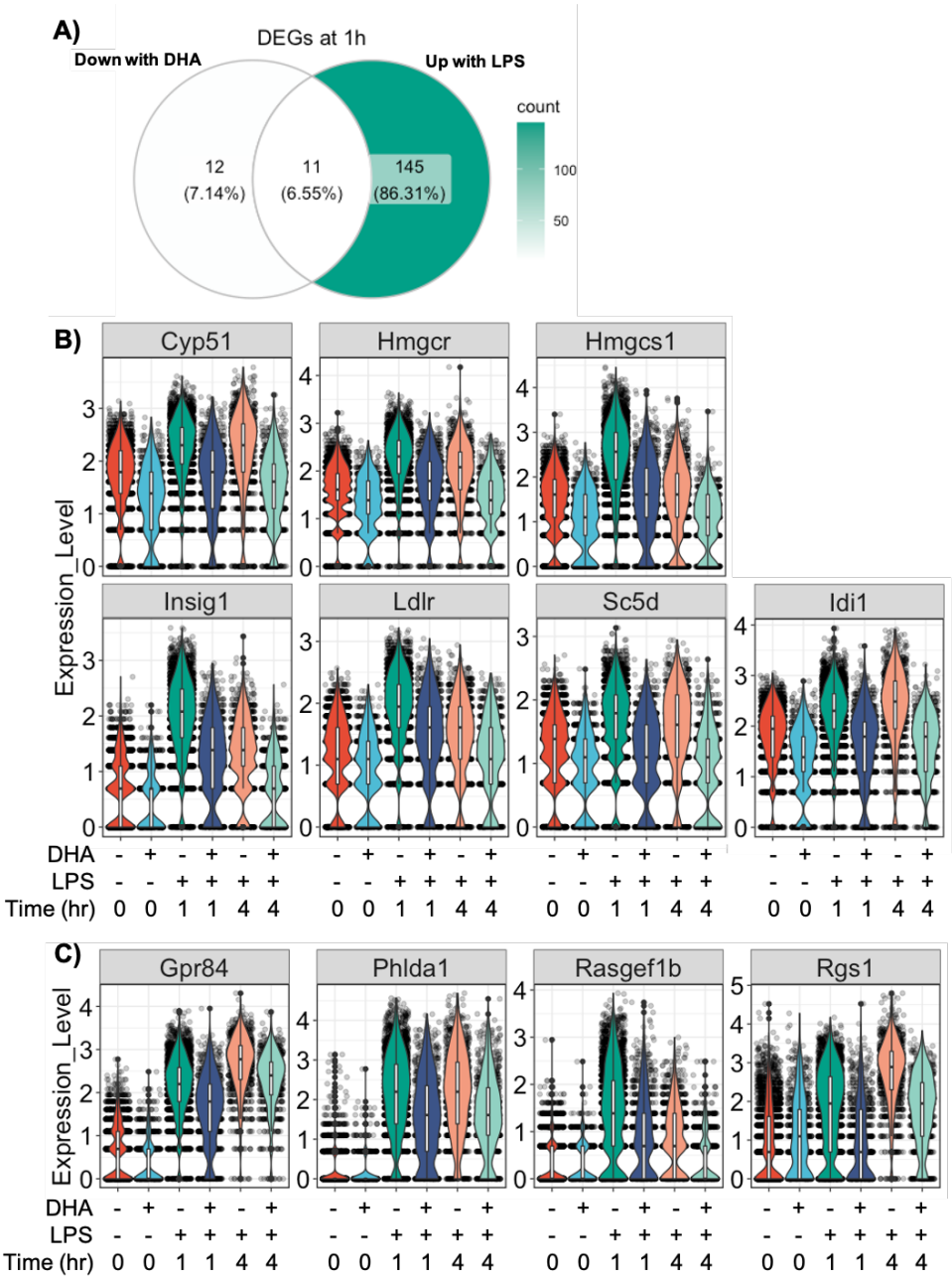
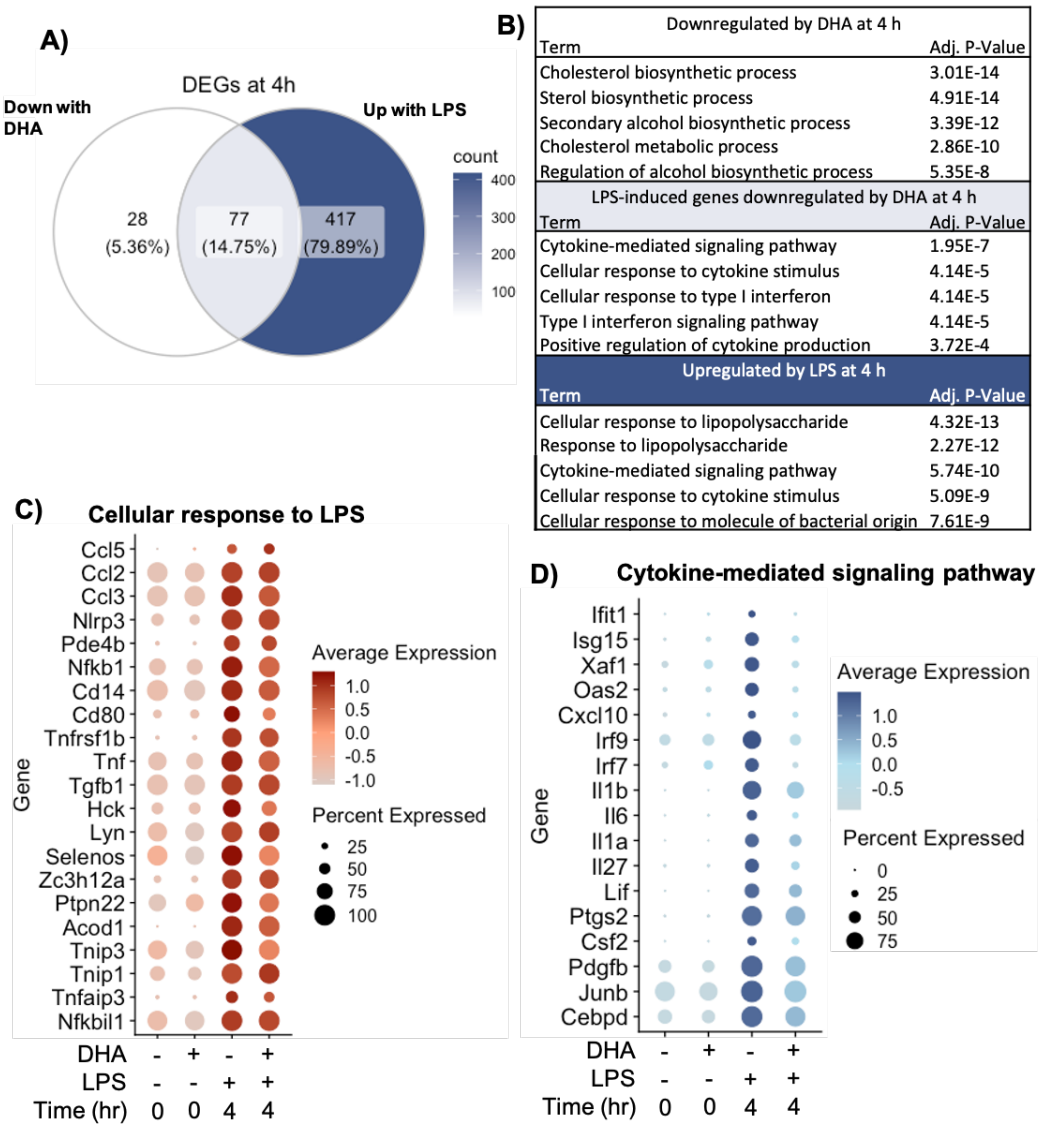


Figure 5.6: DHA suppresses genes associated with cholesterol synthesis and inflammatory signaling pathways. A. Differentially expressed genes (DEGs) were identified by using the Seurat FindMarkers tool, with thresholds set to select genes with >1.5-fold change in expression and genes expressed in at least 25% of groups being compared. DEGs in the "Down with DHA" circle of the Venn diagram are downregulated in DHA.LPS1 relative to Veh.LPS1 and DEGs in the "Up with LPS" circle are upregulated in Veh.LPS1 relative to Veh. The intersection represents LPS-induced genes suppressed by DHA at 1h. **B.** 7 of the 11 LPS-induced genes suppressed by DHA were involved in the cholesterol synthesis pathway, and nearly all were also suppressed by DHA under control (no LPS) conditions and at 4 h post-LPS treatment. **C.** Other LPS-induced genes suppressed by DHA at 1 h are also suppressed by DHA at 4 h LPS treatment, but not without LPS.



Downregulated by DHA at 4 h	
Term	Adj. P-Value
Cholesterol biosynthetic process	3.01E-14
Sterol biosynthetic process	4.91E-14
Secondary alcohol biosynthetic process	3.39E-12
Cholesterol metabolic process	2.86E-10
Regulation of alcohol biosynthetic process	5.35E-8
LPS-induced genes downregulated by DHA at 4 h	
Term	Adj. P-Value
Cytokine-mediated signaling pathway	1.95E-7
Cellular response to cytokine stimulus	4.14E-5
Cellular response to type I interferon	4.14E-5
Type I interferon signaling pathway	4.14E-5
Positive regulation of cytokine production	3.72E-4
Upregulated by LPS at 4 h	
Term	Adj. P-Value
Cellular response to lipopolysaccharide	4.32E-13
Response to lipopolysaccharide	2.27E-12
Cytokine-mediated signaling pathway	5.74E-10
Cellular response to cytokine stimulus	5.09E-9
Cellular response to molecule of bacterial origin	7.61E-9

Figure 5.7: DHA suppresses inflammatory signaling pathways at 4h post-LPS treatment. **A.** Differentially expressed genes (DEGs) were identified by using the Seurat FindMarkers tool, with thresholds set to select genes with >1.5-fold change in gene expression and genes expressed in at least 25% of groups being compared. DEGs in the "Down with DHA" circle of the Venn diagram are downregulated in DHA.LPS4 relative to Veh.LPS4 and DEGs in the "Up with LPS" circle of the Venn diagram are upregulated in Veh.LPS4 relative to Veh. The intersection represents LPS-induced genes suppressed by DHA at 1h. **B.** The Enrichr database was used to identify GO Biological Process terms for the indicated groups of genes. The five most enriched pathways are shown, as determined by the size of the adjusted P-value. **C.** Input genes enriched in the "Cellular response to LPS" and **D.** "Cytokine-mediated signaling pathway" GO terms were presented using the Seurat DotPlot feature, where the size of the dot indicates the percent of cells expressing the gene and the depth of the dot color indicates the average expression of the gene across the cells in which it is expressed.

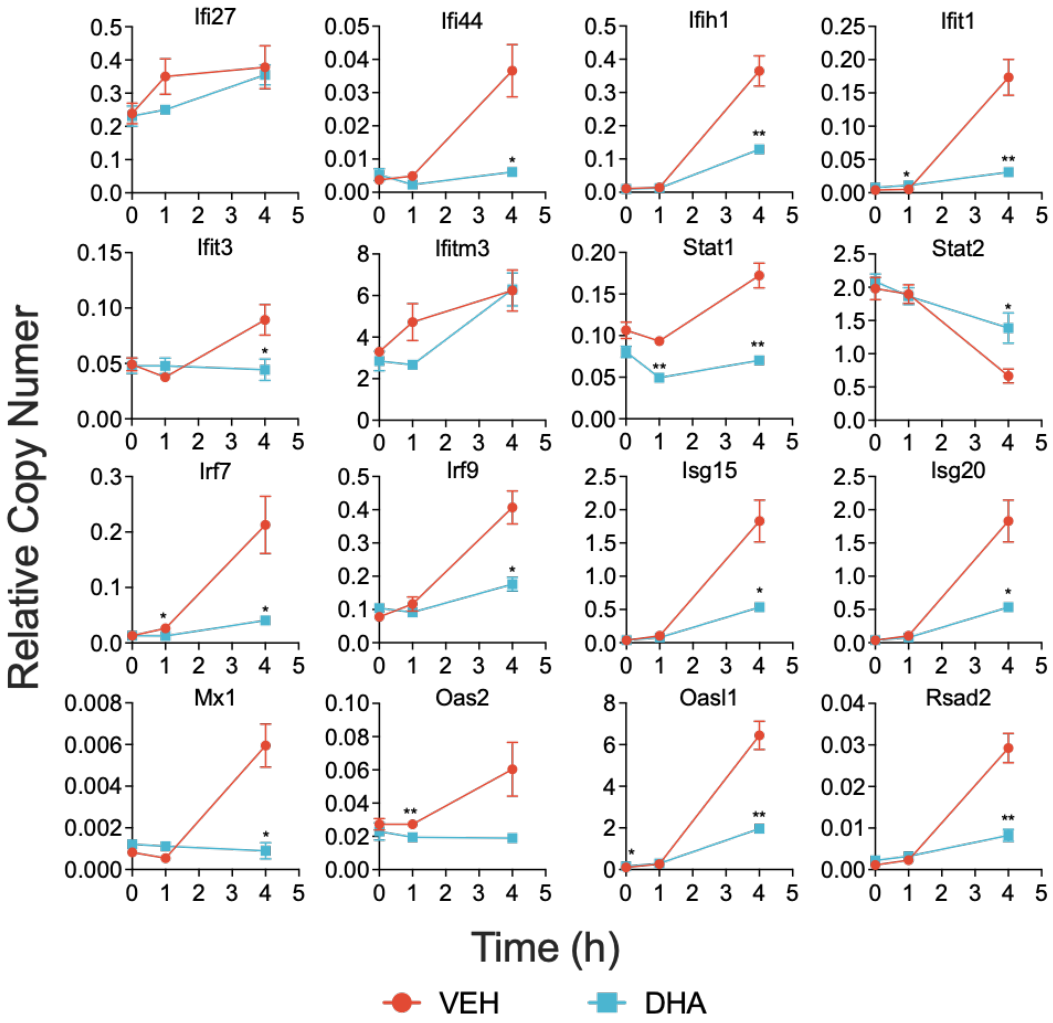


Figure 5.8: DHA suppresses IFN-regulated genes. A panel of interferon (IFN)-regulated genes was investigated by bulk qPCR in samples treated with LPS for 1 and 4 h. Cells were pre-treated with DHA (25 μM) or Veh (8.3 μM BSA) for 24 h prior to LPS treatment. Asterisks indicate significant differences (*p<0.05, **p<0.01) between the DHA and Veh groups, n=3.

5.4.5 Distinct subsets of LPS-treated cells are driven by NF-κB signaling and IFN signaling.

To identify which transcription factor programs (regulons) were most strongly expressed after 4h LPS in an unbiased manner, we determined regulon scores for individual cells using SCENIC workflow in R [453]. Regulons consist of a group of co-expressed genes known to be induced by the same transcription factor, whose expression is also increased with expression of the target genes, and SCENIC assigns a regulon score to each individual cell. Among the most significantly expressed regulons, we identified transcription factors involved in NF-κB signaling (*Nfkb1, Rel*)

and IFN signaling (*Irf7, Stat1*) (**Figure 5.9A**). The *Nfkb1* and *Rel* genes encode NF-κB family members p50 and c-Rel, respectively. The p50 subunit dimerizes with the p65 subunit, forming the most abundant of the Rel/NF-κB heterodimers [472, 473]. Upregulation of the *Nfkb1* and *Rel* regulons was already observed at 1 h, which increased at 4 h post-LPS treatment. DHA suppressed the *Rel* regulon at 1 h and both the *Rel* and *Nfkb1* regulons at 4 h. The *Irf7* and *Stat1* regulons were significantly increased at 4 hours post LPS, and almost completely suppressed by DHA.

LPS-induced degradation of IκB allows p65 translocation to the nucleus, where it binds to NF-κB response elements to promote inflammatory gene expression. The effects of LPS and DHA on the NF-κB pathway were further verified by Western blotting (**Supplementary Figure D.3**). LPS induced phosphorylation of IκB-kinase (IKK) α/β, which phosphorylates IκB to initiate its degradation, and p65 after both 30 and 60 min of treatment. At 30 min following LPS treatment, LPS induced degradation of the inhibitor protein IκB, which retains the NF-κB p65 subunit in the cytoplasm. Importantly, DHA effectively inhibited phosphorylation of both IκB kinase alpha/beta and NF-κB p65 at 30 and 60 min and furthermore, blocked IκB degradation at 30 min. DHA-mediated retention of the p65 subunit in the cytoplasm likely resulted in decreased expression of NF-κb-driven genes as observed here.

When investigating the regulon scores for individual cells, it was identified that a cluster of cells with high expression of genes in the *Irf7* and *Stat1* regulons among cells treated with LPS for 4h. This cluster appeared to be separate from cells with high expression of genes in the *Nfkb1* regulon (**Supplementary Figure D.4**). Plots were generated to map *Nfkb1* and *Irf7* regulon expression on the cells with the highest expression of these regulons. When cells in the top quartile (Q4) of expression for each regulon were identified (**Figure 5.9B**), it was revealed that the majority of the cells with the highest expression of these regulons originated from the Veh.LPS4 treatment group (**Figure 5.9 C-D**). There was a separate and smaller population of DHA-treated cells with high *Irf7* regulon expression that was distinct from the larger population with high *Nfkb1* expression. Thus DHA acted on two distinct populations that expressed *Nfkb1*- and *Irf7*-driven genes.

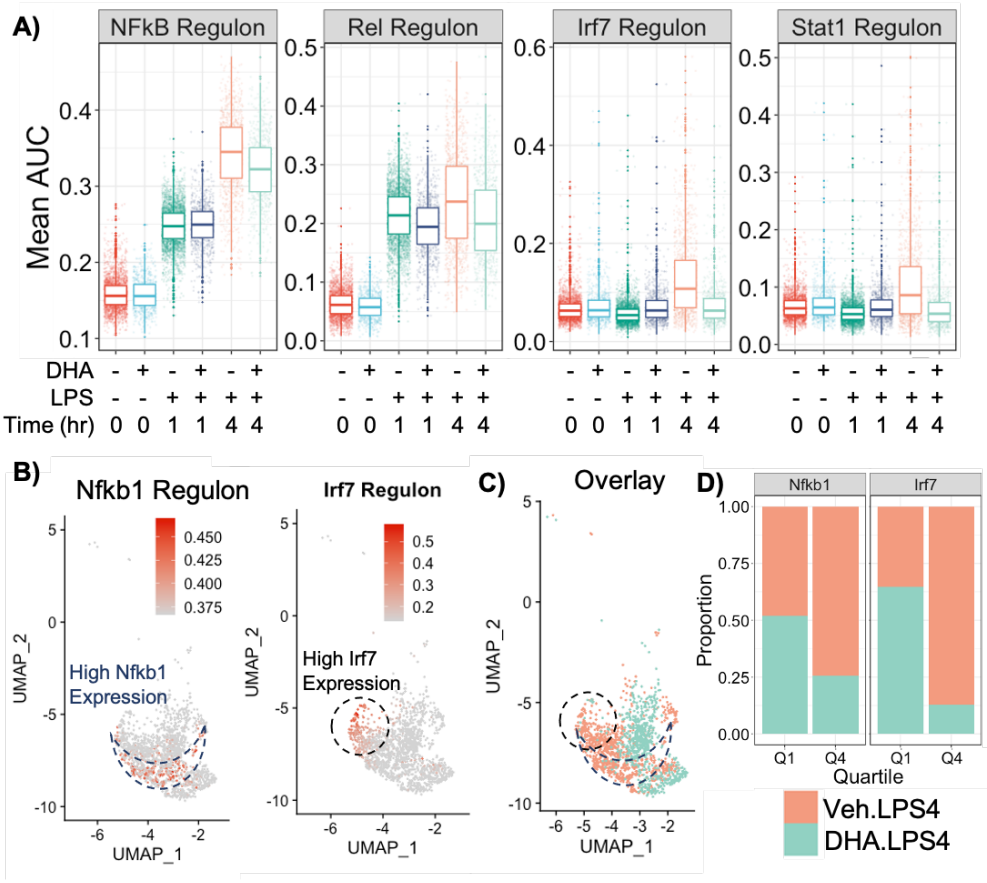


Figure 5.9: Cells with high expression of IFN-driven genes are distinct from cells with high expression of NF-κB-driven genes. **A.** Regulon scores for cells in each group were generated using the SCENIC workflow. Boxplots for regulon scores across all cells were generated to identify differences between treatment groups. *Irf7* and *Stat1* regulons scores only increased for cells treated with LPS for 4 h, but *Nfkb1* and *Rel* regulon scores were already increased at 1 h and remained high at 4 h. **B.** The Seurat FeaturePlot tool was used to color cells in the top quartile of *Irf7* or *Nfkb1* regulon expression. Only cells treated with LPS for 4 h were assessed (Veh.LPS4 and DHA.LPS4 treatment groups). Cells with the highest *Irf7* and *Nfkb1* regulon scores were separate from each other in the UMAP projection. **C.** The Seurat DimPlot tool was used to color cells according to treatment. Most regions with high *Irf7* or *Nfkb1* regulon scores were in the Veh.LPS4 group rather than the DHA.LPS4 group. **D.** Cells were separated into quartiles based on their *Irf7* and *Nfkb1* regulon scores. The proportion of cells in each quartile that belonged to the Veh.LPS4 and DHA.LPS4 treatment groups were presented to show that fewer DHA-treated cells are found among cells with high expression of *Irf7*- and *Nfkb1*-driven genes.

5.5 DISCUSSION

As an innate immune population, macrophages act as sentinels to signal the presence of foreign molecules while simultaneously functioning to destroy or sequester invading microbes or injurious

particles. Cytokines released by macrophages modulate the phenotype and function of incoming immune cells, influencing the inflammatory response. Sets of genes are upregulated in conjunction with each other at specified times, triggering a sequence of responses in the cell and extracellular milieu. Here we used single cell RNA sequencing to scrutinize patterns of LPS-induced gene expression in a primary, heterogeneous self-renewing macrophage model and query how the DHA intervention influences the LPS-induced inflammatory response. The use of this novel technique allowed us to capture heterogeneity within a single population of treated cells, with groups of cells within the same LPS treatment group expressing different sets of inflammatory genes. This approach allowed us to ascertain that cells with high expression of NF-κB- and IFN-driven genes minimally overlapped with each other. We also observed that genes involved in cholesterol synthesis are among the first genes induced by LPS, and that many of these genes are suppressed by DHA. While others have reported induction of cholesterol synthesis as a mechanism for propagating LPS-triggered inflammation, the potential for DHA to target this pathway has not been explored.

The signaling pathways induced by TLR4 activation have been thoroughly described [474, 443]. Briefly, *in vivo* serum and serum used to supplement cell culture media *in vitro* contain LPS-binding protein (LBP), which transports LPS to the transmembrane receptor CD14. CD14 facilitates binding of LPS to TLR4, which functions as a dimer. TLR4 activation induces divergent signaling pathways initiated by the adapter protein MyD88 or by TRIF/TRAM. MyD88-dependent signaling results in activation of the kinase TAK1, which phosphorylates IKKα/β. IKKα/β phosphorylates IκB, which frees the transcription factor NF-κB to translocate to the nucleus. TAK-1 can also phosphorylate MAP kinases, including JNK and p38. Following endocytosis of the TLR4 receptor complex, TRIF/TRAM activate IKKi and TBK1, which phosphorylate Irf3. Phosphorylated Irf3 then translocates to the nucleus where it initiates type I IFN signaling. A recent study showed IRF7 is activated in a similar manner to IRF3 in BMDMs [475].

In vitro and *in vivo* treatment with ω-3 PUFAs influence the activation and phenotype of immune cells in situations of chronic and acute inflammation, with many studies pointing to their

potential to inhibit inflammatory gene express driven by NF-κB [31]. *In vivo*, dietary supplementation with ω-3 PUFAs elevates their presence in the phospholipid membranes in individual tissues, red blood cells, and blood lipid pools [28, 8], and this has been shown to decrease plasma levels of inflammatory cytokines [449, 354]. There are various mechanisms by which ω-3 PUFAs may suppress inflammation. Free extracellular DHA or EPA may bind to GPCRs (i.e. GPR40 and GPR120) to induce in signaling pathways that interfere with NF-κB signaling. Similarly, free intracellular ω-3 PUFAs are ligands for PPARγ, which may interfere with transcription of inflammatory genes. The increase in ω-3 PUFAs in the phospholipid membrane is often at the expense of ω-6 PUFAs, decreasing the amount of substrate available for production of ω-6-derived pro-inflammatory lipid mediators while simultaneously increasing levels of anti-inflammatory ω-3-derived metabolites [476]. An increase in membrane ω-3 PUFAs may also influence lipid raft formation, altering aggregation and activation of transmembrane receptors that initiate inflammatory signaling pathways (reviewed in [31]).

RNA sequencing revealed that DHA and LPS have opposing roles in regulating expression of genes involved in cholesterol synthesis, which may be another mechanism by which DHA suppresses inflammatory signaling. All the genes suppressed by DHA at 1 h post-LPS treatment are targets of the transcription factors SREBP1a and SRBP1c [477, 478, 479], which have been shown to be inhibited by DHA supplementation *in vitro* and *in vivo* [480, 481]. Furthermore, many of these genes were significantly reduced by DHA in the absence of inflammatory stimulus. An increase in intracellular cholesterol promotes TLR4 signaling by providing structure for lipid rafts, which promote aggregation of TLR4 receptors with CD14 [469, 482]. cholesterol synthesis genes were among the earliest genes induced by LPS, many of which were significantly reduced by DHA in this study, potentially reducing availability of cholesterol for lipid rafts formation and reducing TLR4 signaling. DHA-mediated reduction of intracellular cholesterol could also prevent type I IFN induction by release of mitochondrial DNA [483], which is shown to be released when excess intracellular levels of cholesterol compromise the mitochondrial membrane [484].

Many of the genes induced by LPS at 1 h are involved in promoting transcription of inflam-

matory genes observed at the 4 h timepoints, while others initiate pro-resolving pathways that lead to shutting down the inflammatory response. This is consistent with previously published bulk mRNA studies investigating early, middle, and late gene expression patterns in macrophages from several species treated with LPS [444, 485, 445, 486]. These studies assessed timepoints that extended beyond 4 h, and found that while many inflammatory cytokines and chemokines peak at 4 h, induction of most IFN-regulated genes occurs slightly later. Here, within the population of cells treated with LPS for 4 h, a specific subset of cells had high expression of IFN-regulated genes. These may be cells that are temporally "ahead" of their other cells within this treatment group. In contrast, very few DHA-treated cells exhibited high IFN-regulated gene expression, suggesting that DHA slows or inhibits cells from undergoing this transcriptional change.

Recent studies in our lab have focused on how DHA mediates inflammatory and autoimmune pathways triggered by the environmental toxicant $cSiO_2$ in lupus-prone mice [41]. In previous *in vivo* studies, we have observed that DHA supplementation significantly reduces expression of type I IFN-regulated genes in lupus-prone mice intranasally exposed to $cSiO_2$ [41]. Of high translational relevance, increased IFN-regulated gene expression is observed in patients with lupus experiencing flares [42]. Using the same panel of genes employed *in vivo*, we found that many IRGs were significantly enhanced by LPS at 4 hours and suppressed by DHA. In both our *in vivo* and *in vitro* experiments, DHA suppresses the type I IFN pathway more strongly than other inflammatory pathways (i.e. NF-κB signaling). This may suggest that anti-inflammatory pathways induced by DHA more specifically target IFN signaling.

This study had several limitations. First, extending the time window could provide greater detail regarding the pathways most effectively targeted by DHA. Also, even though we identified that upstream inflammatory pathways (i.e. NF-κB signaling) that were influenced by DHA supplementation, there is further need to confirm the effects on other key proteins associated with the pathways identified, or on resultant metabolites produced (i.e. cholesterol synthesis). Furthermore, the influence on cholesterol synthesis genes may have been due to the presence of a fatty acid in general and not specific to DHA. Finally, although the *in vitro* macrophage model used here is sim-

ilar to an inflammatory monocyte-derived macrophage, it might not precisely mimic tissue-specific macrophage populations observed *in vivo*. Thus, many of the pathways identified here need to be confirmed in other translationally relevant models.

In conclusion, our findings contribute to identifying mechanisms by which the ω-3 PUFA DHA may impede inflammatory signaling pathways induced by LPS. Our analyses uncovered cholesterol synthesis as a potential metabolic pathway differentially modulated by DHA and LPS that may be central to DHA-mediated suppression of TLR4-dependent signaling. We also observed that DHA suppresses IFN-driven genes to a greater extent than NF-κB-driven genes, which provides a new perspective on how the multifaceted TLR4-induced signaling pathway is influenced by DHA. Many of the findings reported herein herald lines of future research to investigate dietary interventions to combat inflammation and the development of autoimmune disease.

5.6 ACKNOWLEDGMENTS

We would like to thank Anthony Bach for his assistance with the execution of single cell isolation and Illumina library preparation.

CHAPTER 6

OPTIMIZATION OF A SELF-REPLICATION IN VITRO MODEL FOR ALVEOLAR MACROPHAGES TO STUDY CRYSTALLINE SILICA TOXICITY

Wierenga KA[1,2], Thomas S[3], Olive A[3], Jack Harkema [2,4] and James J. Pestka[2,3,5]

[1]Department of Biochemistry and Molecular Biology, Michigan State University, East Lansing, MI

[2]Institute for Integrative Toxicology, Michigan State University, East Lansing, MI

[3]Department of Microbiology and Molecular Genetics, Michigan State University, East Lansing, MI

[4]Department of Pathobiology and Diagnostic Investigation, Michigan State University, East Lansing, MI

[5]Department of Food Science and Human Nutrition, Michigan State University, East Lansing, MI

Author Contributions: KW: study design, data analyses/interpretation, chapter preparation. ST: study design, data analyses/interpretation. AO, JH: study design, project funding. JP: study design, oversight, chapter preparation, project funding.

6.1 ABSTRACT

Occupational exposure to crystalline silica ($cSiO_2$) is associated with multiple airway diseases and etiologically linked to development of autoimmune disease. While much has been learned about $cSiO_2$ toxicity in inbred and transgenic mice, there is need to meld these findings with mechanistic studies in primary alveolar macrophages (AM), the primary line of defense against inhaled particles. This is, however, precluded by the paucity of AMs recoverable from a single mouse ($\sim$1 x 10^5 cells). A potential solution to this problem comes from Max Planck Institute (MPI) cells, a self-replicating AM surrogate obtained by culturing fetal liver monocytes with the recombinant cytokine GM-CSF. While MPI cells are initially similar to AMs in morphology and gene expression, we have found that they lose this phenotype after 1 month in culture. Here, we hypothesized that supplementing cell culture media with TGFβ, recently identified as critical to the development and maintenance of AMs in the lungs, would prolong an AM-like phenotype in MPI cells. We compared conventional MPI cells cultured with 30 ng/mL GM-CSF alone to MPI cells cultured with 30 ng/mL GM-CSF and 20 ng/mL TGFβ, referred hereafter as TMPI cells. After approximately 1 month, light and scanning electron microscopy revealed that TMPI cells retained an ovoid morphology with numerous outer plasma membrane ruffles found in primary AM, while conventional MPI cells adopted a more fusiform morphology with loss of membrane ruffling, respectively. When phenotype was assessed on the basis of gene expression (*Cd14, Siglecf, Marco, PPARγ, Car4, Fabp4, Itgax*) by qPCR and cell markers (Siglec F, CD11c, and CD14) by flow cytometry, TMPI cells were found to retain the AM and early MPI phenotypes, whereas late MPI cells (i.e. cultured for $\geq$ 1 month) lost the phenotype coincident with the aforementioned morphological changes. At the functional level, $cSiO_2$ was rapidly phagocytosed and could induce IL-1α release and cell death in AM, early MPI, and both early and late TMPI cells, however, these properties were lost in late MPI cells. Finally, when the effects of incubation with the ω-3 fatty acid docosahexaenoic acid (DHA) were assessed in the TMPI cell model, the fatty acid prevented $cSiO_2$-induced cell death and IL-1 cytokine release without affecting phagocytosis of the particle. Taken together, TMPI cells recapitulate *ex vivo* AMs even after extended culturing. Their high isolation yield and

self-replicating capabilities make them an attractive and accessible AM model for investigating toxicological mechanisms and interventions, as demonstrated here for $cSiO_2$-induced toxicity and protection by DHA, respectively.

6.2 INTRODUCTION

The unique environments and repertoire of self and foreign antigens present in divergent tissues of the body demand a specialized immune populations to regulate which stimuli should be tolerated and which should initiate an inflammatory response. Major components of the innate immune system are tissue resident macrophages that are functionally distinct from each other and circulating bone-marrow derived macrophages (BMDMs) [86]. These include Kupffer cells of the liver, Langerhans cells of the skin, microglia of the brain, red pulp macrophages of the spleen, and interstitial and alveolar macrophages (AMs) of the lung [86]. AMs are particularly critical as a first line of innate immune defense against particles and microbes entering the airway [93].

A particle of considerable public health significance and high risk for occupational exposures is crystalline silica ($cSiO_2$) [14]. $cSiO_2$ is recognized to cause chronic debilitating lung disease and is a known risk factor for several autoimmune diseases including rheumatoid arthritis [487], scleroderma [129, 348], and systemic lupus erythematosus [19, 288, 488]. Following entry into the lung, $cSiO_2$ is rapidly phagocytosed by AMs [16]. When presented at sub-toxic concentrations, $cSiO_2$ particles are effectively cleared, but exposures that overwhelm the clearance ability of the AMs trigger various forms of cell death including apoptosis, necrosis, and pyroptosis and concomitant pro-inflammatory cytokine and chemokine release [17, 16]. Collectively, these events promote immune cell infiltration and tissue injury with rampant local inflammation. $cSiO_2$ can also impede the ability of the AM to clear dead cell debris, a process known as efferocytosis [129]. Inadequate efferocytosis is associated with many autoimmune conditions, as accumulation of host antigens can result in an immune response against the host [51]. Interestingly, recent *in vivo* studies have identified a protective role of the ω-3 fatty acid docosahexaenoic acid (DHA) against $cSiO_2$-triggered inflammation and autoimmunity in the lung [4, 7, 181]. At the mechanistic level, *in vitro* studies

with primary AM and cloned macrophages suggest that DHA i) suppresses $cSiO_2$-induced cytokine release [354] and ii) enhances the efferocytotic capacity of *in vitro* macrophages [216].

Because AMs play such a critical role in the $cSiO_2$-induced toxicity and autoimmune disease triggering, it is essential to better understand how this specific macrophage phenotype interacts with and responds to this particle, and how manipulation of membrane fatty acids with ω-3 fatty acids influence this response. While mechanistic studies of the inflammatory response to lung-specific stimuli such as $cSiO_2$should ideally employ primary AMs, these experiments require both a large number of cells and the ability to maintain these cells *ex vivo* for long periods of time. Unfortunately, AM replicate slowly and only small numbers can be recovered from a single mouse (1×10^5) [489]. This requires that large numbers of mice to be sacrificed to allow sufficient AM for high throughput *in vitro* mechanistic experiments with multiple treatment groups. Furthermore, AM can not be cultured for extended time periods. As a result, many *in vitro* studies investigating responses to airborne particles and microbes have relied on BMDMs or transformed macrophage cell lines [490, 148, 125, 97]. While these macrophage models are applicable in certain contexts, they do not adequately mimic the AM response to inflammatory stimuli [491, 450, 354].

AMs are a long-lived and self-replicating and like most tissue resident macrophages, are derived from embryonic precursors [492]. AMs arise from fetal liver monocytes, which migrate to the lung and develop into mature AMs in the presence of cytokines such as GM-CSF and TGFβ shortly after birth. The continued presence of these factors is necessary for the maintenance and self-renewal of AMs in the lung [91]. Previous studies have shown that culturing cells from the fetal liver in GM-CSF generates cells functionally and phenotypically similar to alveolar macrophages, which have been termed Max Planck Institute (MPI) cells [450]. Furthermore, including GM-CSF in the culture medium also prolongs the viability and self-replicative capacity of *ex vivo* AMs [489]. However, in our hands, both MPI cells and *ex vivo* AMs lose AM-like morphology, phenotype, and surface markers upon prolonged culturing even when cultured with recombinant GM-CSF. Recently, it has been documented that inclusion of TGFβ in the cell culture media can prevent this phenotypic shift in *ex vivo* AMs, allowing them to be cultured for prolonged periods of time while still providing

AM-like responses to various inflammatory stimuli [493].

Here, we hypothesized that supplementing cell culture media with TGFβ will prolong an AM-like phenotype in MPI cells making them suitable for mechanistic studies of $cSiO_2$ toxicity. We refer to the TGFβ-supplemented cultures as TMPI cells. AMs, BMDMs, MPI, and TMPI cells were compared to confirm that the TMPI cells were functionally and phenotypically similar to AMs despite prolonged *ex vivo* culture. Live-cell imaging was then used to confirm that TMPI cells and AMs had similar kinetics of $cSiO_2$ phagocytosis and cell death and to investigate $cSiO_2$ -induced lysosomal membrane permeabilization. In addition to phagocytosing and undergoing cell death at a similar rate, TMPI cells and AMs both release IL-1α following exposure to $cSiO_2$, which was not observed for BMDMs. Finally, the potential for DHA to mitigate $cSiO_2$ -induced toxicity in MPI cells as assessed.

6.3 MATERIALS AND METHODS

6.3.1 Animals.

Experimental protocols were approved by the Institutional Animal Care and Use Committee at MSU (AUF # PROTO201800113). C57Bl6 mice (cat # 000664) were obtained from Jackson Laboratories (Bar Harbor, ME). Mice were given free access to food and drinking under controlled conditions (humidity: 40–55%; lighting: 12 h light/dark cycles; and temperature: 24 $\pm$ 2°C) as described previously [4, 3]. Pregnant dams at 6-10 wk of age and 14-18 gestational days were euthanized to obtain murine fetuses. AMs were isolated from male and female mice older than 10 wk of age. BMDMs were obtained from male and female mice 6 wk of age and older.

6.3.2 MPI cell isolation and culture.

MPI cells were obtained as previously described [450]. Briefly, pregnant dams were euthanized by CO_2 inhalation for 10 min to ensure death to neonates, which are resistant to anoxia. Cervical dislocation was used as a secondary form of death for the dam. Fetuses were immediately removed, and loss of maternal blood supply served as a secondary form of death for the fetuses. Cells were

initially cultured in MPI media (Roswell Park Memorial Institute medium [RPMI, Thermo Fisher] containing 10% fetal bovine serum [FBS, R&D Systems], 1% penicillin-streptomycin [P/S, Thermo Fisher], and 30 ng/mL recombinant mGM-CSF [Peprotech]). Media was refreshed every 2-3 d. When cells reached 70-90% confluency, they were lifted by incubating for 10 min with 37°C PBS containing 10 mM EDTA, followed by gentle scraping. After approximately 1 wk, adherent cells adopted a round, AM-like morphology. At this time, stocks were frozen for future use. Thawed stocks were plated in untreated petri dishes with either MPI media or TMPI media (MPI media supplemented with 20 ng/mL recombinant hTGFβ1 [Peprotech]) and sub-cultured as described above.

6.3.3 AM isolation and culture.

Mice were euthanized by CO_2 exposure followed by exsanguination via the inferior vena cava. Lungs were lavaged as previously described [489]. Cells were then resuspended in MPI or TMPI media and plated in untreated 48- or 24- well plates. AMs were lifted from plates using Accutase™ (BioLegend). AMs retained their morphology and phenotype for approximately 2 wk in culture, and were discarded if this morphology was lost. qPCR and flow cytometry confirmed that AMs cultured in MPI media without TGFβ lost AM-specific genes and surface markers over time (**Supplementary Figure E.1**).

6.3.4 BMDM isolation and culture.

C57Bl6 mice were euthanized by CO_2 exposure followed by cervical dislocation. Both femurs were cut on one end to expose the bone marrow, placed cut side down in 0.6 mL tubes, and centrifuged at 16,000 *x*g for 25 s. Marrow from multiple mice was pooled, dissociated to a single cells suspension in sterile PBS and pelleted by centrifuging at 220 *x*g for 5 min. The pellet was resuspended in mouse RBC lysis buffer (Alfa Aeser) and incubated at room temperature for 5 min. The RBC lysis buffer was diluted with 2 volumes of PBS and the cell suspension passed through a nylon 70 μm filter (Corning). Cells were pelleted a second time and resuspended in RPMI media containing 10%

FBS, 1% P/S, and 20% L929 media [399]. Approximately 5 x 10^6 cells were plated per dish in 10 cm untreated petri dishes. Media was refreshed every 2-3 d. Cells were used for assays when fully differentiated after 7 d.

6.3.5 Flow cytometry.

All plated cells were lifted in warm PBS with 10 mM EDTA for 5-10 min and washed twice in PBS before being stained. AMs that were stained immediately following isolation were resuspended in PBS and filtered prior to staining. An antibody cocktail of PE CD170, APC CD11c, APC/Cyanine7 CD14, and FC Block (Biolegend) was prepared in PBS at 1:400 dilution. Cells were incubated in the antibody cocktail for 20 min at room temperature protected from light. Stained cells were washed three times with PBS, resuspended in PBS, and passed through a 70 μm nylon filter immediately prior to analysis. Flow cytometry was performed on a LSR II Flow Cytometer (BD Biosciences) at the Michigan State University Flow Cytometry Core.

6.3.6 qPCR.

RNA was isolated from $\sim$5 x 10^5 cells using RNeasy mini kits (Qiagen), typically yielding 100-400 ng RNA. RNA was then reverse transcribed to cDNA using a High Capacity cDNA reverse transcription kit (Thermo Fisher) on a Stratagene Robocycler 40. Quantitative real-time qPCR was performed using specific Taqman probes (Thermo Fisher) for TGFβ (*Tgfb1*), TGFβ receptors (*Tgfbr1, Tgfbr2*), selected genes used to distinguish AMs from other macrophage populations (*Cd14, Siglecf, Marco, PPARγ, Car4, Fabp4, Itgax*), and cytokines (*Il1a, Il1b, Il10*) on an Applied Biosystems™ QuantStudio™ 7 real-time PCR system. Data were analyzed with Applied Biosystems™ Thermo Fisher Cloud using the RQ software and the relative quantification method. *Gapdh* was used as the housekeeping gene. Relative copy number (RCN) for each gene was normalized to expression of *Gapdh* and calculated as described previously [301].

6.3.7 Scanning electron microscropy.

Suspensions of AMs or MPI cells were diluted to 2.5 x 10^5 cells/mL, and 100 μL pipetted directly upon glass 12 mm diameter, 0.13-0.16 mm thick circular coverslips (Electron Microscopy Sciences), which were placed in the bottom of 6-well plates. Cells were allowed to settle for 2-3 min, then 1 mL of media was added to fill the well. For $cSiO_2$-treated cells, 25 $\mu g/cm^2$ $cSiO_2$ (Min-U-Sil 5 ®, U.S. Silica) was added dropwise and the plate was centrifuged for 1 min at 16 *x*g to ensure even settling of particles. Cells were fixed at designated intervals (1 and 16 h following $cSiO_2$ exposure). To fix cells, the coverslips were removed from the wells, submerged in 4% glutaraldehyde in 0.1 M sodium phosphate buffer at pH 7.4 and placed in a graded ethanol series (25%, 50%, 75%, 95%) for 10 min at each step followed by 3 min changes in 100% ethanol.

Samples were critical point dried in a Leica Microseystems model EM CPD300 critical point drier (Leica Microsystems, Vienna, Austria) using CO_2 as the transitional fluid. Coverslips were then mounted on aluminum stubs using epoxy glue (System's Three Quick Cure 5, Systems Three Resins, Auburn WA). Samples were coated with osmium at $\sim$ 10 nm thickness in an NEOC-AT osmium chemical vapor deposition coater (Meiwafosis Co, Osaka, Japan) and examined in a JEOL 7500F (field emission emitter) scanning electron microscope (JEOL, Tokyo, Japan).

6.3.8 $cSiO_2$ phagocytosis assay.

To assess phagocytosis of $cSiO_2$ particles, MPI cells, AMs, and BMDMs were seeded at 0.25 cells/cm^2 in 48- or 96-well plates to observe engulfment of surrounding silica particles. The following day, the media was removed, wells were rinsed 1x with sterile PBS, and FluoroBrite DMEM (Thermo Fisher) with 50 nM LysoTracker Red (Thermo Fisher) was added to cells to label lysosomes. Cells were incubated 30 min at 37°C, washed 1x with sterile PBS, and media replaced with FluoroBrite DMEM containing 10% FBS and 200 nM SYTOX Green nucleic acid stain (Thermo Fisher). After 30 min to allow LysoTracker dye to equilibrate, $cSiO_2$ was added dropwise to a final density of 25-100 $\mu g/cm^2$. Cells were imaged over time on an EVOS FL2 fluorescent microscope (Thermo Fisher) with an on-stage, temperature control CO_2 incubator and 2-4 images were

acquired per well. LysoTracker dye was detected with the Texas Red light cube and SYTOX Green detected on the GFP light cube.

Images were analyzed using analysis pipelines built in the CellProfiler software [494]. $cSiO_2$ engulfment was assessed by quantifying the number of $cSiO_2$-filled cells, which have a higher pixel intensity than non-$cSiO_2$-filled cells due to the accumulation of the particles. To avoid counting aggregated $cSiO_2$ particles, a threshold was applied to capture only shapes with high solidity and low compactness. Lysosomal integrity and cell death were quantified by counting LysoTracker Red^+ and SYTOX $Green^+$ cells, respectively.

For *in vitro* experiments, FBS is often removed or substantially decreased in the cell culture media to prevent interference from proteins and lipids present in the serum. We observed that removing FBS from the media resulted in an increased rate of cell death and a decrease in the phagocytic capacity of the cells (**Supplementary Figure E.2**). Thus, we chose to use media supplemented with 10% FBS for all *in vitro* experiments assessing $cSiO_2$ phagocytosis, cell death, and cytokine release.

6.3.9 ELISAs.

Cells were treated with $cSiO_2$ or with LPS plus nigericin as described in the figure legends. Cell-free supernatant was collected and the cytokines IL-1α, IL-1β, IL-10, GM-CSF, and TGFβ analyzed using DuoSet ELISA kits (R&D Systems) per the manufacturer's instructions.

6.3.10 Statistical analysis and data visualization.

Statistical analysis and data visualization were performed using Prism Version 8 (GraphPad) or R studio as indicated in the figure legends. $SYTOX^+$, $LysoTracker^+$, and $cSiO_2$-filled cells were quantified using CellProfiler. Data are presented, unless otherwise indicated, as the mean $\pm$ the standard deviation. For parametric data, one-way ANOVA followed by Tukey's post-hoc test was used to identify significant differences between multiple groups, and Student's t-tests were used to

compare two groups. Non-parametric one-way ANOVAs and Mann-Whitney U tests were used to compare multiple groups and two groups, respectively, for non-parametric data.

6.4 RESULTS

6.4.1 MPI and AMs similarly express lineage-specific markers that decline over time.

Consistent with previous reports that MPI cells are phenotypically and morphologically similar to AMs [450, 495, 496], MPI cells grown for 2 wk *ex vivo* in the presence of GM-CSF adopt a distinct fried-egg-like morphology akin to AMs (**Figure 6.1A**). Scanning electron microscopy revealed that the AM and early MPI cell surface have numerous outer membrane ruffles (**Figure 6.1B**). However, when MPI cells were cultured >1 month (MPI P14 in **Figure 6.1A**, MPI P17 in **Figure 6.1B**), they underwent a morphological shift from an AM-like, ovoid morphology with numerous outer plasma membrane ruffles, to a smaller, fusiform morphology with loss of membrane ruffles. MPI cells cultured <1 month are hereafter referred to as "early MPI" and cells cultured >1 month referred to as "late MPI".

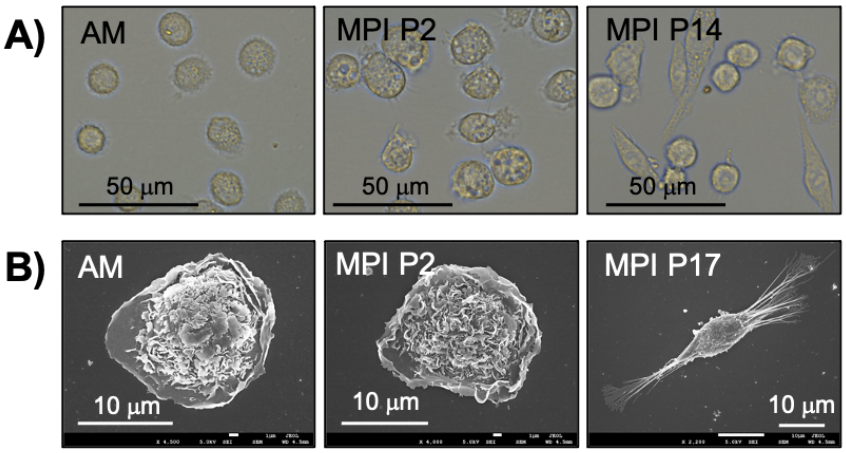


Figure 6.1: MPI cells lose their AM-like phenotype over time. Alveolar macrophages (AMs) and early (P2) MPI cells have similar morphology, with **A.** a round "fried-egg-like" morphology observed by light microscopy, and **B.** a ruffled membrane observed by scanning electron microscopy. After prolonged time in culture (∼1 month, P14 and P17 in **A** and **B**, respectively), MPI cells adopt a smaller, more spindleoid appearance with a decrease in membrane ruffling. Images were taken at 60x magnification for light microscopy and at 4500x, 4000x, and 2200x for AM, P2 MPI, and P17 MPI, respectively.

When AM-specific surface markers and gene expression were compared, we found high similarity between AMs and early passage MPI cells for Siglec F, CD11c, and CD14 protein levels and gene expression (**Figure 6.2**). Late MPI cells had low expression of AM-like surface markers and genes, but high gene and protein expression of CD14 (**Figure 6.2A**). Additionally, early passage MPI and AMs express similar levels of *PPARγ, Car4, Il1a,* and *Fabp4*, a transcriptional target of PPARγ (**Figure 6.2B**).

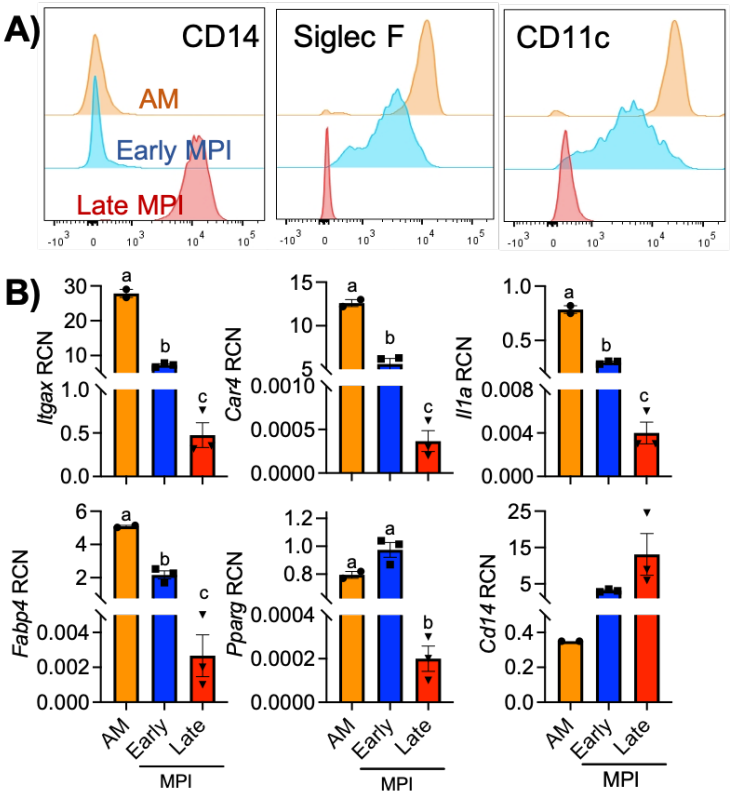


Figure 6.2: MPI cells lose expression of AM-specific surface markers and gene expression over time. A. Alveolar macrophages (AMs) and MPI cells were assessed for surface expression of the proteins CD14, Siglec F, and CD11c. MPI were lifted using warm 10 mM EDTA in PBS and washed twice in PBS before staining. AMs were stained immediately upon isolation from the bronchoalveolar lavage fluid. Cells were incubated for 20 min in an antibody cocktail containing PE-CD170, APC-CD11c, APC/Cyanine7-CD14, and FC Block (Biolegend) diluted 1:4000 in PBS at room temperature protected from light. Stained cells were washed three times with PBS, resuspended in PBS, and filtered immediately prior to analysis. **B.** qPCR analysis confirmed expression of CD11c and CD14 expression (genes *Itgax* and *Cd14*, respectively), while also revealing that early MPI cells express AM-identifying genes *Car4, PPARγ,* and *Fabp4* and have high basal expression *Il1a*. Data compared using one-way ANOVA followed by Tukey's multiple comparisons test. Bars labeled with unique letters are significantly different ($p<0.05$).

6.4.2 Addition of TGFβ prolongs AM-like state of MPI cells.

Based on a prior report that cytokine TGFβ is critical to AM development and homeostasis [91], we hypothesized that TGFβ may also promote maintenance of AM-like phenotype in MPI cells. In preliminary experiments, treating early MPI cells for 24 h with 10 ng/mL TGFβ induced the genes *PPARγ, Car4*, and *Itgax* (**Supplementary Figure E.3A**), all of which are highly expressed by AMs (**Figure 6.2B**). To assess the influence of continued supplementation with TGFβ, we cultured conventional MPI cells in control media or media containing 20 ng/mL TGFβ hereafter referred to as TMPI cells. After 15 passages (approximately 2 months of culturing), TMPI cells retained a round, AM-like morphology (**Figure 6.3A**) and continued expressing AM-identifying genes (**Figure 6.3B**). Conversely, conventional MPI cells cultured in control media lost expression of AM-identifying genes *Siglecf, Marco,* and *PPARγ* and began expressing *Cd14*, which is a common marker for monocyte-derived macrophages recruited to the lung [497] (**Figure 6.3B**).

Interestingly, although both TMPI and MPI cells expressed *Tgfb1* throughout the time course, expression of the TGFβ receptors *Tgfbr1* and *Tgfbr2* decreased in the MPI cells while remaining elevated in TMPI cells (**Figure 6.3B, Supplementary Figure E.3B**). Consistent with this observation, addition of TGFβ to MPI cells that had already lost the AM-like morphology did not regain this morphology, as observed by light microscopy over multiple passages (data not shown), likely due to the loss of expression of the receptor. Expression of Siglec F and CD14 was confirmed by flow cytometry (**Figure 6.3C**). At the time when MPI cells begin to lose the AM like phenotype, two populations are present: SiglecF^{hi}CD14^{low} and SiglecF^{low}CD14^{hi}. At passage 8, 89.2% and 96.5% of MPI and TMPI, respectively, were SiglecF^{hi}CD14^{low}. By passage 15, 85.8% of the MPI cells adopted the SiglecF^{low}CD14^{hi} phenotype. At the same passage, 62.8% of TMPI cells retained the SiglecF^{hi}CD14^{low} phenotype, while 15.2% have present the SiglecF^{low}CD14^{hi} phenotype.

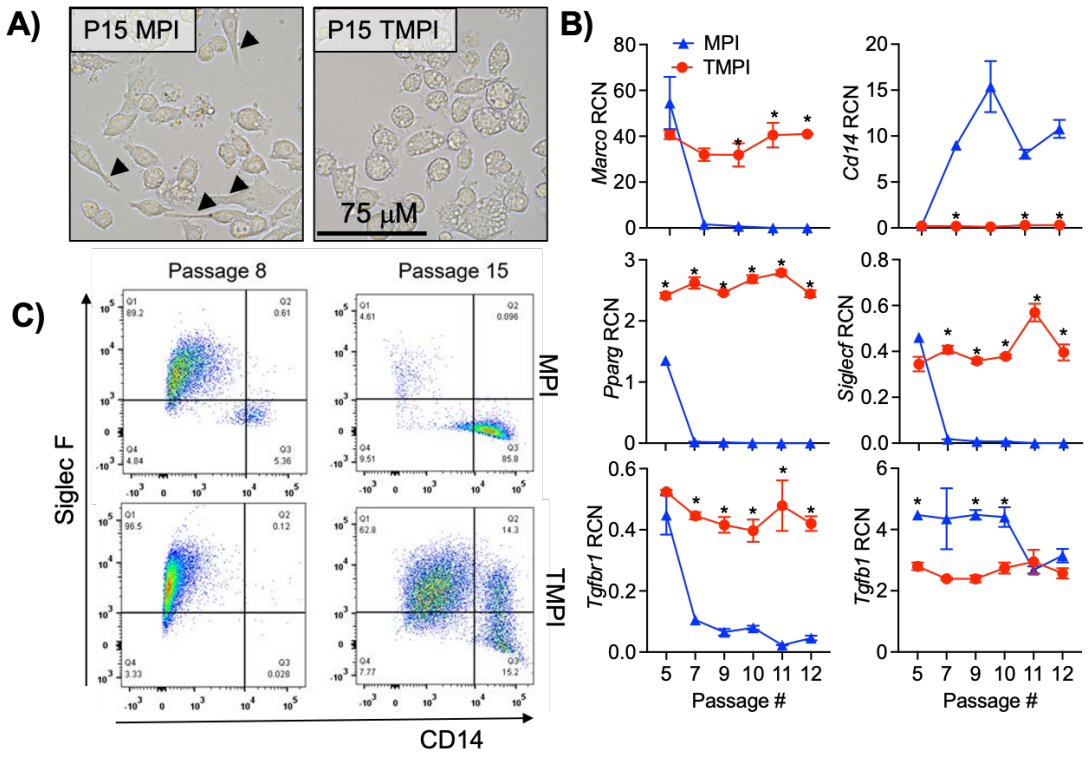


Figure 6.3: Addition of TGFβ to the cell culture media extends the AM-like phenotype of MPI cells. A. MPI cells cultured in TGFβ (TMPI) maintain an ovoid, alveolar macrophage (AM)-like morphology in culture while MPI cells in control media (MPI) change to a spindleoid morphology (arrows). **B.** Changes in gene expression levels with continued passage of MPI and TMPI was assessed by qPCR. AM-specific genes *Marco, PPAR*γ, and *Siglecf* decreased in MPI, but remained high in TMPI over time, while *Cd14* expression increased in MPI, but not TMPI. Both cell types maintained expression of *Tgfb1*, but MPI cells lost expression of the TGFβ receptor, *Tgfbr1*. Asterisks indicate significant (p<0.05) differences between MPI and TMPI cells at the same passage number, as determined by Student's t-test. **C.** MPI and TMPI cells were lifted using warm 10 mM EDTA in PBS and washed twice in PBS before staining. Cells were incubated for 20 min in an antibody cocktail containing PE-CD170, APC/Cyanine7-CD14, and FC Block diluted 1:4000 in PBS at room temperature protected from light. Stained cells were washed three times with PBS, resuspended in PBS, and filtered immediately prior to analysis on a BD LSR II flow cytometer. The top left quandrant of each plot contains SiglecF^{hi}CD14^{low} cells while the bottom right quadrant contains SiglecF^{low}CD14^{hi} cells.

6.4.3 TMPI cells and AMs phagocytose cSiO$_2$ particles and undergo cell death at similar rates.

The functional implications associated with the observed phenotypic changes, specifically with respect to the macrophage response to cSiO$_2$, were further investigated. Early MPI, early TMPI, and AMs showed similar rates of cSiO$_2$engulfment and cell death (**Figure 6.4A**). Late MPI cells

exhibited poor phagocytosis while late TMPI cells effectively phagocytosed $cSiO_2$, though to a lesser extent than early MPI or TMPI cells. The lack of phagocytosis by late MPI cells coincided with decreased rates of cell death (**Figure 6.4A**). Rates of phagocytosis by BMDMs were similar to AMs, but were accompanied by higher levels of cell death (nearly 80% at 8 h, compared to <40% for AMs and 10-50% for TMPI cells). Representative images shown in **Figure 6.4B**.

6.4.4 Engulfment of $cSiO_2$ particles leads to loss of outer membrane ruffling, apoptotic blebbing, and membrane rupture.

Scanning electron microscopy revealed that most TMPI cells exposed to $cSiO_2$ for 1 h appeared to be engulfing the particles (**Figure 6.5A**). While many cells retained outer membrane ruffling, some had begun to lose this feature (**Figure 6.5A**, panel 1, solid arrow). Some cells appeared to be migrating (**Figure 6.5A**, panel 1, dashed arrow) and others extended pseudopodia to grab nearby particles (**Figure 6.5A**, panel 2). At 16 h following $cSiO_2$ exposure, nearly all cells had lost membrane ruffling (**Figure 6.5B**). The remaining viable TMPI cells exhibited extended long, fine pseudopodia (**Figure 6.5B**, panel 1, arrows). Many cells appeared to be undergoing various stages and types of cell death including apoptotic blebbing (**Figure 6.5B**, panel 3), and complete membrane rupture, indicative of primary or secondary necrosis, which also involved release of free $cSiO_2$ particles (**Figure 6.5B**, panel 2).

6.4.5 Loss of lysosome integrity precedes $cSiO_2$-induced cell death in TMPI cells.

The relationship of $cSiO_2$ engulfment to loss of lysosomal integrity and cell death was assessed in TMPI cells over time using LysoTracker Red, a dye that accumulates in acidic organelles, and SYTOX Green, respectively. Loss of lysosomal membrane integrity followed phagocytosis of $cSiO_2$, but preceded cell death (**Figure 6.6A**). Representative images at 0 and 7 h shown in **Figure 6.6B**. This is consistent with prior studies establishing that phagocytosis of $cSiO_2$ by AMs induces lysosomal permeabilization, triggering cell death [498, 126]. Comparable results were found in AM, early MPI cells, and BMDMs but not late MPI cells (**Supplementary Figure E.4**).

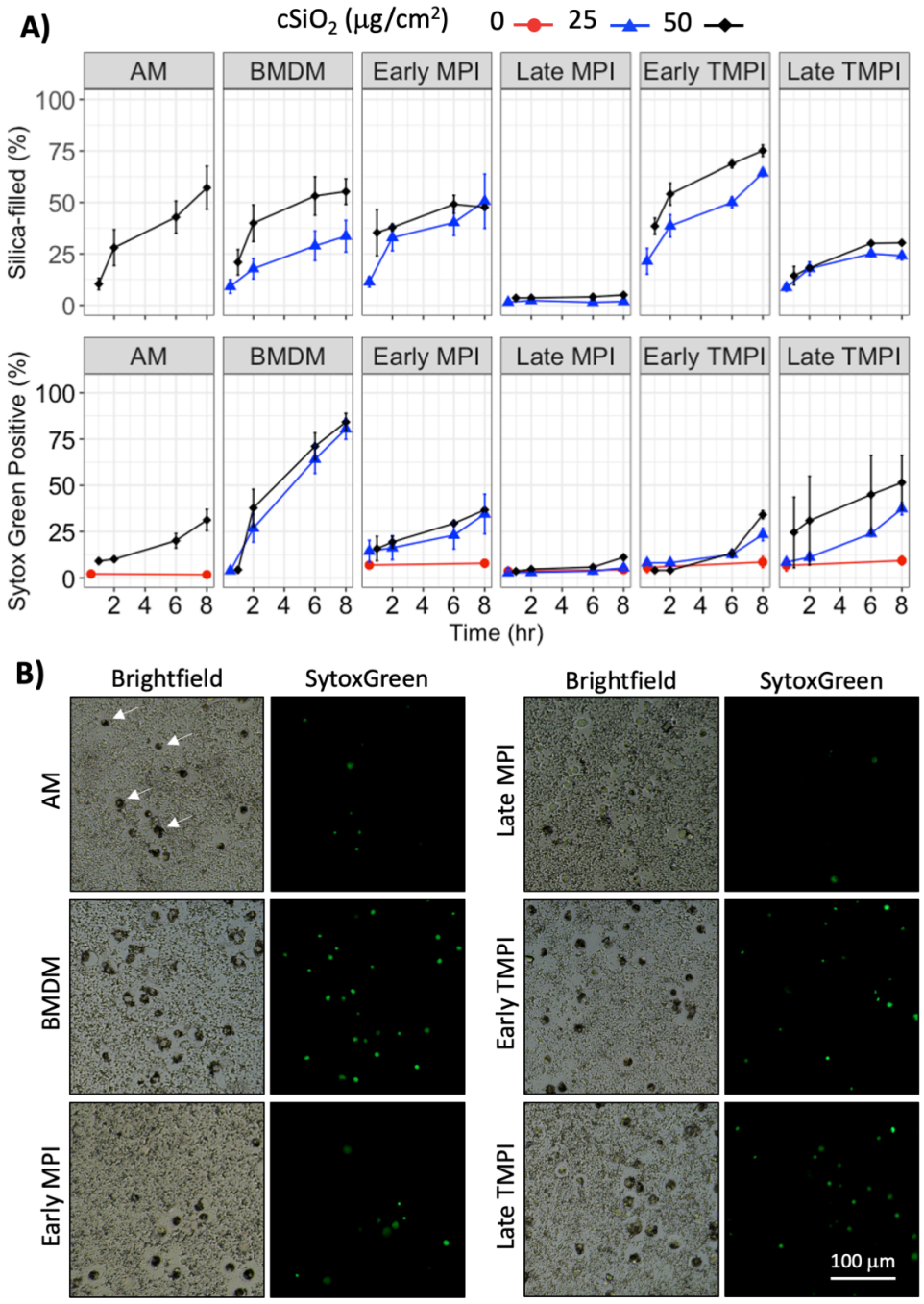


Figure 6.4: Kinetics of $cSiO_2$-induced cell death and $cSiO_2$ uptake is similar among AMs, early MPI cells, and early TMPI cells. A. Alveolar macrophages (AM), bone marrow-derived macrophages (BMDMs), MPI cells, and TMPI cells were seeded in 96-well plates. After 24 h, media was replaced with FluoroBrite DMEM containing 200 nM SYTOX green and 10% FBS. $cSiO_2$ was added dropwise to cells at the indicated densities. Images were taken at 0, 2, 6, and 8 h using an EVOS FL2 fluorescent microscope using an onstage temperature- and CO_2-controlled incubator, protected from light. $cSiO_2$-filled and $SYTOX^+$ cells were quantified using the CellProfiler software. **B.** Representative images of $SYTOX^+$ and $cSiO_2$-filled cells (white arrows in AM panel, top right) treated with 50 $\mu g/cm^2$ silica for 8 h, 20x magnification.

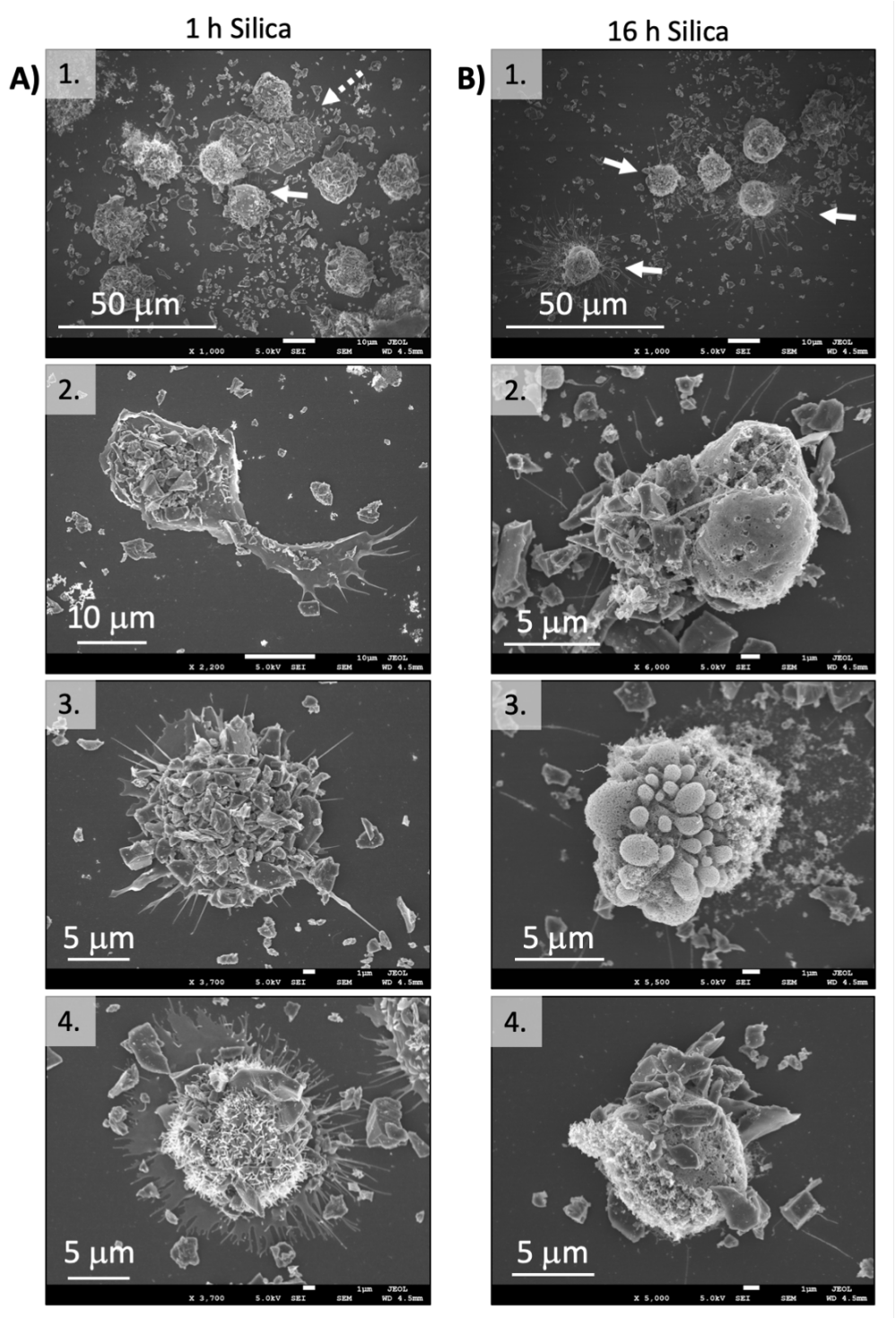


Figure 6.5: Scanning electron microscopy or cells treated with $cSiO_2$ for 1 and 16 h. 2.5 *10^4 cells grown on 12 mm diameter glass coverslips. Cells were treated with 25 μg/cm^2 and fixed in 4% glutaraldehyde in 0.1 M sodium phosphate buffer at pH 7 at **A.** 1 h and **B.** 16 h following $cSiO_2$ exposure. Samples were critical-point dried and samples coated with osmium prior to analysis on a JEOL 700F scanning electron microscope.

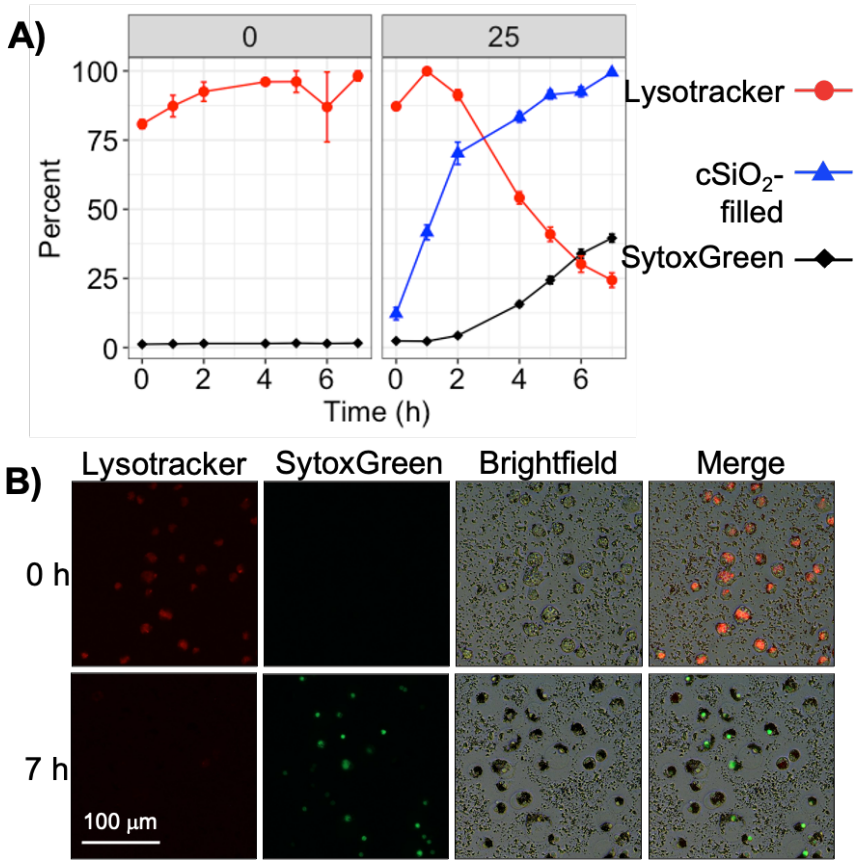


Figure 6.6: Lysosomal membrane integrity decreases over time in $cSiO_2$ exposed TMPIs. A. TMPI cells were stained with LysoTracker Red (50 nM) in FluoroBrite DMEM for 30 min. Media was then replaced with FluoroBrite DMEM containing 200 nM SYTOX Green and 10% FBS. After 30 min to allow LysoTracker staining to equilibrate, $cSiO_2$ was added dropwise at 25 μg/cm^2. Images were taken at the indicated timepoints using an EVOS FL2 fluorescent microscope with an onstage temperature- and CO_2-controlled incubator protected from light. SYTOX$^+$, LysoTracker$^+$, and $cSiO_2$-filled cells were quantified using the CellProfiler software. **B.** Representative images of cells treated with 25 μg/mL $cSiO_2$ at 0 and 7 h, 20x magnification.

6.4.6 AM and TMPI cells exhibit high expression and release of the alarmin IL-1α.

IL-1α has been shown to be central to particle-induced inflammation. *In vivo* and *ex vivo* studies suggest AMs are the primary source of IL-1α in the lung following inhalation of $cSiO_2$, likely as a result of cell death [138, 132]. Initial characterizations of MPI cells by Fejer and coworkers showed that AMs and MPI cells release high level of IL-1α and low levels of IL-10 in response to a 24 h exposure to LPS, while the opposite is true in BMDMs [450]. This response was replicated

in our preliminary studies (**Supplementary Figure E.5**). We also found that AMs and early MPI cells have higher basal *Il1a* expression than BMDMs and late MPI cells (**Figure 6.2B**). IL-1α was released from AMs, early MPI and TMPI cells, as well as late TMPI cells when exposed to $cSiO_2$ for 8 h (**Figure 6.7A**). A modest amount of IL1β was released from early MPI and early and late TMPI, and a slight, though not significant, increase in IL-1β release was observed in AMs in response to $cSiO_2$ (**Figure 6.7B**). IL-1 release was not evident from BMDMs or late MPI cells.

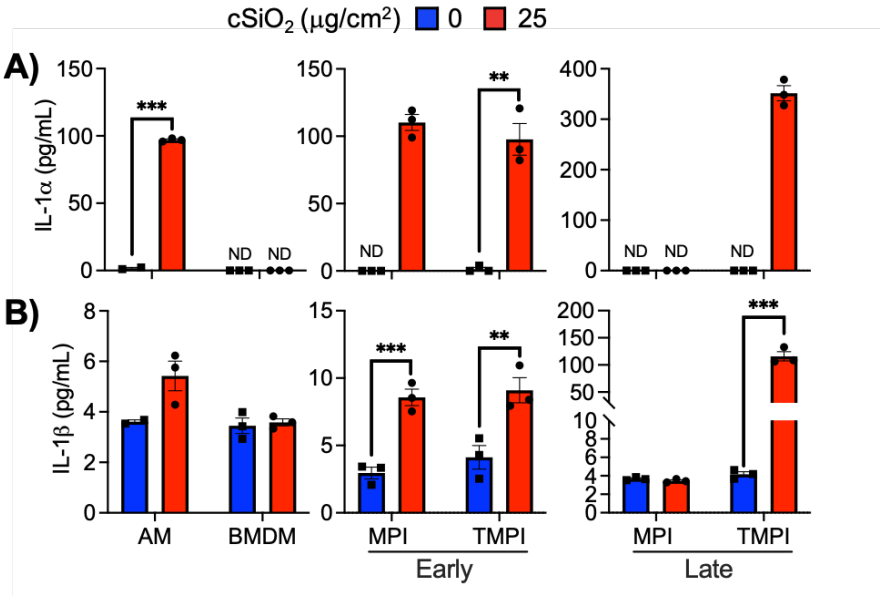


Figure 6.7: $cSiO_2$ elicits IL-1 cytokine release from AMs, early MPI, and TMPI cells but not from BMDM or late MPI cells. **A.** Alveolar macrophages (AMs), bone marrow-derived macrophages (BMDMs), early and late TMPI and MPI cells were treated with 25 $\mu g/cm^2$ $cSiO_2$ for 8 h, and supernatant was collected to assess release of the cytokines IL-1α **A.** and IL-1β **B.** by ELISA. Asterisks indicative of significant differences between groups (**p<0.01, ***p<0.001), as assessed by Student's t-tests between relevant groups. ND = not detected.

6.4.7 DHA decreases $cSiO_2$-induced cell death and cytokine release in TMPI cells.

To test the protective effects of DHA, we incubated TMPI cells with media containing DHA (25 μM) and BSA (8.3 μM BSA) or BSA alone (8.3 μM BSA) for 24 h. Media was changed to DHA-free media to limit observations to the protective effects of DHA incorporated in the cell membrane. DHA delayed $cSiO_2$-induced lysosomal membrane permeabilization and cell death without

impacting phagocytosis (**Figure 6.8A**). In a similar manner, DHA reduced in IL-1α and IL-1β release (**Figure 6.8B,C**) in response to both $cSiO_2$ exposure and nigericin treatment following LPS priming, which acts as a positive control for inflammasome activation.

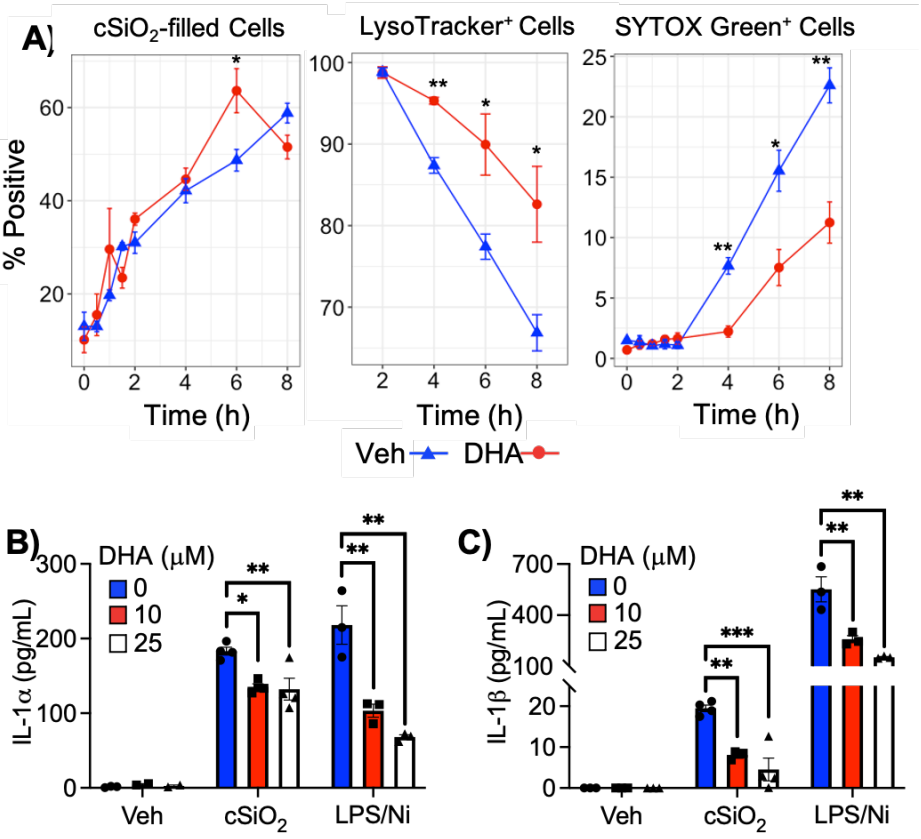


Figure 6.8: DHA suppresses cell death, lysosomal membrane permeability, and IL-1 cytokine release following $cSiO_2$ exposure. A. TMPI cells were treated with 25 μM DHA or Veh (8.3 μM BSA) for 24 h in complete TMPI media. Media was removed, wells washed once with PBS to remove excess DHA or Veh, followed by staining with 50 nM LysoTracker Red for 30 min. Media was replaced by 200 nM SYTOX Green in FluoroBrite DMEM with 10% FBS. $cSiO_2$ was added dropwise at 25 $\mu g/cm^2$. Images were taken at the indicated timepoints using an EVOS FL2 fluorescent microscope with an onstage temperature- and CO_2-controlled incubator protected from light. $SYTOX^+$, $LysoTracker^+$, and $cSiO_2$-filled cells were quantified using the CellProfiler software. RStudio and ggplot2 were used to prepare plots. **B-C.** Cells were incubated with DHA at indicated concentrations. The 0 uM DHA group was treated with 8.3μM BSA. Cells were then treated with 25 $\mu g/cm^2$ $cSiO_2$ for 8 h or LPS for 3 h followed by nigericin for 45 min as a positive control for inflammasome activation. Supernatant was assessed for IL-1α **(B)** and IL-1β **(C)** by ELISA. Asterisks indicate significant differences between groups (*p<0.05, **p<0.01, ***p<0.001), as assessed by Student's t-tests between 0 and 25 μM DHA at individual timepoints **(A)** and by one-way ANOVA comparing DHA concentrations **(B,C)**.

6.5 DISCUSSION

As a long-lived, resident macrophage population, AMs have unique phenotypes and functions that are shaped by the alveolar environment including efficient phagocytosis to clear inhaled particles and microbes, efferocytosis of cellular corpses and debris resulting from cell death, and maintenance of surfactant homeostasis. AMs play a critical role in fine tuning the inflammatory response and preventing excessive responses to non-threatening exposures, while maintaining the capacity to "sound the alarm" when necessary [92]. Prior studies have demonstrated that MPI cells generated by culturing fetal liver cells with GM-CSF are self-replicating and have AM-like phenotype [450]. However, we have found that this phenotype is lost upon prolonged culturing. We observed that this phenotypic shift resulted in the presence of two distinct populations of cells in culture: SiglecF^{hi}CD14^{low} cells and SiglecF^{low}CD14^{hi} cells, and the shift towards a population of SiglecF^{low}CD14^{hi} cells corresponds with the loss other AM marker genes. Consistent with recent studies showing that TGFβ is critical for AM development and maintenance [91], we demonstrate for the first time that including TGFβ in the cell culture media prolongs the AM-like phenotype and function of MPI cells. As was observed for AM, TMPI cells efficiently phagocytosed $cSiO_2$ and responded by releasing of IL-1 cytokines, undergoing lysosomal membrane permeabilization, and dying. Importantly, DHA suppressed $cSiO_2$-induced IL-1 cytokine release and cell death without affecting phagocytosis of the particle. Thus, TMPI cells recapitulate *ex vivo* AMs even after extended culturing and should be suitable for uncovering mechanisms of and interventions against particle toxicity.

The observations that TGFβR1 and TGFβR2 were expressed in early but not late MPI cells was highly relevant because they suggested that late MPI were resistant to supplementation with TGFβ. Notably, the late MPI cells still expressed *Tgfb1*, but expression of both *Tgfbr1* and *Tgfbr2* was decreased with loss of the AM-like phenotype. TGFβ signaling is complex, as both TGFβ and its receptors are regulated through a variety of post-translational modifications [499, 500]. TGFβ itself is secreted in a complex consisting of proteins and glycoproteins that neutralize the active protein. The release of these inhibitory factors is highly dependent on the extracellular en-

vironment. Specifically, elastase and metalloproteases degrade bound glycoproteins and cleave the latent TGFβ binding protein (LTBP), while integrin mediated structural changes release active TGFβ from the latency-associated peptide (LAP). In addition to regulation by covalent modifications, the activation of the TGFβ receptor is dependent in part upon the localization of the receptor on the plasma membrane, as both TGFβR1 and TGFβR2 are consistently endocytosed and either degraded or recycled back to the plasma membrane. Notably, TGFβ itself can enhance the presence of this receptor on the membrane [501]. Latent TGFβ released by AMs *in vivo* is activated by α-V-β-6 integrins expressed on the type II alveolar epithelial cells, resulting in increased levels of the active protein which can signal in an autocrine manner to maintain the unique phenotype of AMs. This feed-forward loop is absent for *in vitro*, which may explain why addition of exogenous active TGFβ prevents the loss of the AM-like phenotype in MPI cells.

Consistent with previous reports [91], short- and long-term supplementation with TGFβ enhanced expression of the nuclear PPARγ, which drives many AM characteristics, including lipid metabolism, phagocytic capacity, and regulation of inflammation [88, 265]. PPARγ signaling enhances efferocytosis and phagocytosis by upregulating scavenger receptors (e.g. CD36 and Fcγ) and attenuates pro-inflammatory cytokine release by inhibiting inflammatory signaling pathways and inducing genes with anti-inflammatory properties [265, 431, 74]. A recent study showed that in AMs, loss of PPARγ impaired mitochondrial function and led to increased apoptotic cell death [502]. PPARγ induces a repertoire of genes involved in lipid metabolism, allowing AMs to metabolize the lipid-rich surfactant present in the alveoli [503, 269]. Notably, many lipids are endogenous receptors of PPARγ, and constant exposure to surfactant ensures robust activation of this transcription factor [504]. The environment clearly plays a role in the induction of PPARγ, as short-term exposure to TGFβ *in vitro* or GM-CSF treatment *in vivo* is sufficient to promote expression of this transcription factor [505, 91]. Similarly, donor macrophages from the bone marrow or even from distinct organs will adopt a PPARγ-driven transcriptional profile similar to resident AMs due to extracellular signals present in the alveolar niche [506, 88].

Though recruited macrophages can become nearly identical to AMs, the scavenger receptor

MARCO appears to be specific to fetal monocyte-derived AMs [95, 88]. Our findings confirmed previous reports showing that MPI cells, but not BMDMs, express MARCO [495]. Supplementation with TGFβ prolonged the expression of this AM-specific receptor. The functional implications of this have been explored in the context of adenovirus infection, where it was found that the MARCO-expressing MPI cells were more rapidly infected than BMDMs [495]. Of high relevance to this work, MARCO is also implicated in AM uptake of $cSiO_2$ and other particles in C57Bl6 mice [507, 508].

Other phenotypic differences previously observed for AMs, BMDMs, and MPI cells were replicated in this study, including the differential expression of CD14 and Siglec F [137, 450]. Two key functional differences observed in this study between BMDMs and AMs were induction of cell death and IL-1α release by $cSiO_2$. Though BMDMs were able to engulf $cSiO_2$ particles at a rate similar to AMs and AM-like MPI cells (i.e. early MPI, early TMPI, late TMPI), they quickly succumbed to cell death, while AMs and AM-like MPI cells remained viable many hours following $cSiO_2$ phagocytosis. A delay in cell death may be important for appropriate clearance of particles, potentially allowing the AMs to be transported out of the alveoli before they die [17]. AMs and AM-like MPI cells also released significantly more IL-1α than BMDMs or late MPI cells in response to $cSiO_2$. This is consistent with other studies showing that AMs express high levels of IL-1α relative to other cells in the lung and other macrophage sub-types, and that they release this cytokine in response to particle exposure [138, 132]. Studies employing MPI cells have also observed that these cells release more IL-1α than BMDM in response to other inflammatory stimuli such as LPS and adenovirus [137, 450, 495].

In vivo studies have shown that IL-1α plays a major role in the inflammatory response following exposure to various stimuli, including particles, pathogens, and LPS [450, 138, 174, 132]. Notably, these studies observed the formation of ectopic lymphoid structures (ELS, also known as inducible bronchoalveolar lymphoid tissue, iBALT) induced by environmental particles and by viruses in an IL-1α-dependent manner [138, 174]. Previous work in our laboratory has shown that acute and chronic $cSiO_2$ exposure promotes ELS neogenesis in lupus prone animals, and that this can

be inhibited by dietary supplementation with DHA [4, 3, 159]. Here, inclusion of DHA in the cell culture medium prior to $cSiO_2$ treatment led to reduced cell death of AMs and a concurrent reduction in the release of IL-1α, providing clues as to how DHA may suppress $cSiO_2$-induced ELS development *in vivo*.

The anti-inflammatory effects of DHA on TMPI cells have important implications for developing dietary supplementation strategies to protect against $cSiO_2$-triggered inflammation and lung pathology *in vivo*. Work by our lab and others has investigated the potential mechanisms by which DHA suppresses inflammatory gene expression and cell death following particle exposure. In a RAW264.7 cell model and in the MPI cells, we have observed that DHA and treatment with the PPARγ agonist rosiglitazone similarly reduce gene expression of *Il1a* and *Il1b*, and that this can be reversed by PPARγ antagonists. The high expression of PPARγ in AMs and MPI cells make them an excellent model to investigate potential PPARγ-mediated effects of DHA supplementation, such as increased phagocytosis and inhibition of inflammatory signaling pathways. Other mechanisms by which ω-3 fatty acids may suppress the inflammatory response include 1) direct binding to GPCRs (i.e. GPR120 and GPR40), 2) influencing lipid rafts via following incorporation in the lipid membrane, 3) metabolism to specialized pro-resolving mediators, and 4) reduction in inflammatory ω-6 metabolites by competing for space in the lipid membrane. Advancements in this area of research have been thoroughly reviewed [31, 509, 510]. Further research is warranted to understand which of these mechanisms are at play in protecting against $cSiO_2$ -induced toxicity in AMs specifically and the lung as a whole.

Increased dietary or blood levels of ω-3 fatty acids is associated with improved outcome in a variety of lung diseases, including chronic obstructive pulmonary disease (COPD, reviewed in [511]), acute lung injury and acute respiratory distress syndrome [512]. A recent meta-analysis investigating data from the Framingham Heart Study, Age, Gene/Environment Susceptibility-Reykjavik Study (AGES-Reykjavik), and the Multi-Ethnic Study of Atherosclerosis (MESA) found that higher plasma phospholipid or red blood cell membrane DHA levels were associated with a decreased risk of hospitalization, a decreased risk of death from interstitial lung disease, and fewer lung abnor-

malities on CT scans [184]. DHA was also shown to protect against particle-exacerbated asthma in children [176]. These studies support the contention that dietary intervention with ω-3 fatty acids might improve lung-related disease outcomes, potentially by reducing the inflammatory response.

Strengths of this study include thorough characterization of a novel AM model over extended time in culture, and detailed investigation of the toxic effects of an inhaled particle in this highly relevant *in vitro* model. Furthermore, our method for investigating $cSiO_2$ phagocytosis has several advantages over measuring side scatter by flow cytometry, which is commonly used to assess particle phagocytosis. Cells can be analyzed without requiring isolation steps which may damage cells or lead to lack of measurement of cells that have already died due to $cSiO_2$ exposure. Additionally, the use of live cell imaging allows individual cells to be tracked over time, while flow cytometric analyses inherently provide an endpoint measurement. Finally, live cell imaging permits tracking cellular events such as lysosomal membrane permeabilization and cell death to better elucidate the timeline of $cSiO_2$-triggered processes.

However, this investigation had limitations that should be addressed in future studies. First, this study only employed concentrations of $cSiO_2$ that were high enough to induce cytotoxicity. It would be useful in future studies to use a lower concentration of $cSiO_2$ and investigate how exposure to sub-cytotoxic of $cSiO_2$ influence functions such as migration and efferocytosis. More detailed mechanisms could be performed to better understand the cellular events occurring following $cSiO_2$ engulfment. For example, while a decrease in LysoTracker staining implies loss of lysosomal membrane integrity, additional assays, such as release of lysosomal cathepsin enzymes, would provide information about how this process contributes to toxicity. More mechanistic details of how DHA and/or its metabolites suppress cell death and cytokine release would be very valuable to field. Finally, the applicability of TMPI cells to study of other airborne toxicants, such as PM2.5, $cSiO_2$ nanoparticles, and multiwalled carbon nanotubes, need to be examined.

In summary, we demonstrate here optimization and applicability of a reproducible *in vitro* cell model for AMs with far-reaching implications for study of the lung, development, immunology, and toxicology. The optimized TMPI cell model may be employed to shed new light on processes

unique to AMs, like phagocytosis and removal of inhaled particles. These cells have great potential to be used to unravel pathways and mechanisms of toxicity in AMs. TMPI cells can be isolated from genetically engineered animals, as previously described [495]. Furthermore, the ability of these cells to self-replicate allows for gene-editing experiments that require large numbers of cells and/or proliferating cells. Taken together, the optimization and application of MPI cells provides an exciting, innovative model to thoroughly investigate AM biology.

6.6 ACKNOWLEDGMENTS

We would like to thank Alexa Richardson, Shamya Harris, and Adrianna Kirby for their excellent technical assistance with AM isolation and *in vitro* assays.

CHAPTER 7

CONCLUSIONS AND FUTURE DIRECTIONS

7.1 CONCLUSION

This research determined how two elements of the exposome – the environmental toxicant crystalline silica ($cSiO_2$) and the dietary ω-3 highly unsaturated fatty acid (HUFA) docosahexaenoic acid (DHA) – influence the development of autoimmune disease in the lupus prone NZBWF1 mouse and the phenotype and activation of macrophages in vitro. This dissertation lays the groundwork for future investigations to understand the molecular and cellular events triggered by both DHA and $cSiO_2$ in greater mechanistic detail.

The results presented herein build upon previous literature describing the protective effects of dietary ω-3 HUFAs by exploring their potential to protect against lupus flaring and macrophage activation triggered by an environmental exposure. The findings of **Chapter 2** confirm the robustness of DHA supplementation as a dietary intervention to protect against lupus flares, as it was found to be effective even in the context of a modified Total Western Diet. **Chapter 3** identifies the ω-3 HUFA Score as a biomarker to of dietary ω-3 intake and reveals a strong negative correlation between this score, which represents the level of ω-3 HUFAs in the red blood cells, with a variety of $cSiO_2$-triggered inflammatory and autoimmune endpoints. In **Chapter 4**, DHA is found to protect against $cSiO_2$-induced inflammasome activation, in part by regulating LPS-induced transcription of IL-1 cytokines and inflammasome proteins. **Chapter 5** uses next-generation sequencing to further profile the influence transcriptional changes mediated by DHA with and without lipopolysaccharide (LPS). Lastly, **Chapter 6** optimizes and employs a novel *in vitro* surrogate for alveolar macrophages (AMs) to investigate cellular events triggered by $cSiO_2$ and ameliorated by DHA in a more translational relevent cell model.

Taken together, these findings support the contention that the environment can shape inflammation and autoimmune disease. The intricately balanced immune system receives nearly constant insult from daily exposures, but is designed to manage these insults and return to a state of homeostasis. However, this balance can be perturbed, resulting in under-activity (more susceptible to infection, less likely to detect and control malignancies) or over-activity (autoimmune disease, chronic inflammation). *In vivo* studies performed by Dr. Pestka's lab, including those presented in

this thesis, show how the interaction of genetic susceptibility (i.e. the lupus-prone genetics of the NZBWF1 mouse) couples with elements of the exposome (i.e. respirable $cSiO_2$ and dietary DHA) to differentially modulate the triggering of autoimmune disease [4, 7, 23]. *In vitro* studies reveal pathways in macrophages that are induced by $cSiO_2$ and by DHA, pointing to the opposing roles of these exposures in the inflammatory response.

While genetic susceptibility is out of the individual's control, it is possible in some circumstances to modify the environment to reestablish balance within the immune system. Published literature and the data presented in this thesis point to the potential benefit of reducing exposure to inhaled particles and increasing consumption of dietary ω-3 HUFAs [24, 513]. Future research will strengthen these findings and provide greater insight into the mechanisms behind $cSiO_2$-induced toxicity and protection by dietary DHA.

7.2 FUTURE RESEARCH

7.2.1 Profile the presence and phenotype of macrophages in the lung following acute $cSiO_2$ exposure *in vivo*.

There have been several recent studies employing single cell technologies to thoroughly profile the changes to myeloid cell populations in the lung following infection or lung injury [514, 97, 515, 98, 497, 99]. In our studies, we observe a transient decrease in macrophages in the bronchoalveolar lavage fluid (BALF) following $cSiO_2$ exposure that increases back to baseline and, given the dose of $cSiO_2$ administered, can remain elevated relative to control animals, concurrent with the increase in inflammatory endpoints [159]. Notably, DHA reduces the number of infiltrating macrophages. Likely, the initial decline in macrophage counts is due to $cSiO_2$-induced cell death, followed by repopulation with monocyte-derived macrophages. Previous studies from our lab used differential cell counts based on morphology to quantify cell populations, prohibiting the ability to distinguish between different sub-types of immune cells [4, 7, 3, 159, 8, 181]. Future studies employing techniques such as flow cytometry or single cell RNA sequencing will reveal key changes induced by DHA and $cSiO_2$ to macrophage sub-populations. I hypothesize that DHA

supplementation will partially protect AMs from $cSiO_2$ induced-cell death *in vivo* and will promote a pro-resolving phenotype (reduced inflammatory cytokine expression, improved capacity for efferocytosis) in infiltrating monocyte-derived macrophages.

Early events following $cSiO_2$ exposure could be elucidated by performing an acute time course study in which DHA-and control diet-fed animals are instilled with a low (sub-pathogenic) and high (pathogenic) dose of $cSiO_2$ samples collected over a period of 1-2 wk. To limit the analysis to cells within the alveolar space, BALF alone could be collected. The number of infiltrating monocytes, monocyte-derived macrophages, and resident alveolar macrophages could be quantified by flow cytometry, and three populations could be sorted by FACS for downstream assays. For example, DHA- and $cSiO_2$-induced transcriptional changes in each cell type could be identified by RNA sequencing. The influence of $cSiO_2$ and DHA on efferocytosis, phagocytosis, and cytokine release could be assessed on cells cultured *ex vivo*.

Further insight into transcriptional differences and treatment-induced changes to individual cell types could be ascertained using single cell RNA sequencing on either the immune cells of the BALF (to focus on the cells localized to the airway) or on the whole lung digest (to investigate all cell types in the lung). Studies using this technique to understand the initiating stages in pulmonary fibrosis have identified a pro-fibrotic macrophage sub-type that exists within the recruited macrophage population [97, 99]. A potential impediment to this study in our lab would be interference by $cSiO_2$ particles, either intra- or extra-cellularly, during the single-cell isolation process. However a recent study from the lab of Dr. Alexander Misharin performed single-cell RNA sequencing on lung digestions from mice exposed to TiO2 particles and asbestos fibers and did not report any concerns of this manner [97].

7.2.2 Relate metabolite profile in the BALF to inflammatory endpoints triggered by $cSiO_2$.

Preliminary studies performed by Dr. Lichchavi Rajasinghe, a post-doctoral research fellow in the lab, show that $cSiO_2$ treatment results in the generation of a wide array of lipid metabolites, and that treatment with DHA shifts the $cSiO_2$-triggered lipidome toward more ω-3 derived pro-resolving

mediators (unpublished). It would be enlightening to profile the plasma lipidome of bronchoalveolar lavage fluid from $cSiO_2$ exposed mice fed DHA or control diets. The BALF lipidome would likely be unique from the lipid metabolite profile observed in the cell culture supernatant, due to the many additional cells *in vivo* that may be producing these metabolites. Previous studies show that inflammation [516], infection [517], particle exposure [518, 519, 520] in both mice and humans influence the metabolite profile in the lungs. These metabolites influence the immune response in the lung [521], including macrophages which express many receptors for these metabolites [201]. I hypothesize that the BALF lipidome of DHA fed animals exposed to $cSiO_2$ would have increased levels of metabolites with anti-inflammatory and pro-resolving properties, contributing to the protective effects of DHA. Metabolites that are the most highly produced in DHA-fed animals following $cSiO_2$ exposure would be good candidates to investigate how individual metabolites influence the macrophage response *in vitro*.

7.2.3 Use genetically modified TMPI cells to elucidate pathways of $cSiO_2$ uptake and toxicity and/or protection by DHA.

TMPI cells could be isolated from genetically engineered mice, as described [450]. Alternatively, the proliferative potential of these cells allow them to be subjected to CRISPR-Cas9 gene editing. TMPI cells lacking genes such as the transmembrane receptors GPR120 and GPR40, or genes encoding enzymes involved in the generation of DHA derived metabolites, such as 12/15-LOX (maresin biosynthesis pathway) and 5-LOX or 15-LOX (resolvin and protectin biosynthetic pathway) could be employed to disentangle anti-inflammatory properties of DHA. Similar techniques could be used to investigate receptors implicated in $cSiO_2$-induced toxicity, such as MARCO, or downstream pathways leading to inflammasome activation, such as knocking out individual lysosomal cathepsins.

A genetic modification that would be particularly relevant to the studies reported herein is the expression of the *C. elegans FAT-1 gene*. This is a fatty acid desaturase absent in mammals that allows the endogenous conversion of ω-6 HUFAs to ω-3 HUFAs. FAT-1 mice have expressed this

gene and have been used since 2004 to study the effects of increased levels of ω-3 HUFAs without the need for dietary supplementation [233]. A recent study from the same group who engineered the FAT-1 mouse recently reported the generation of a FAT-2 mouse, which has increased tissue ω-6 HUFAs due to the expression of the FAT-2 gene which converts monounsaturated fatty acids to ω-6 HUFAs [522]. TMPI cells could be isolated from these mice and compared to wild-type TMPI cells *in vitro*. Experiments performed in this manner would not require a supplementation step, which reduces hands-on experiment time while also removing a potential source of error and variability.

7.2.4 Instill edited TMPI cells into the murine lung to mechanisms of interest in vivo.

In vitro experiments with edited TMPI cells could be followed up by instilling them into the murine lung to determine their roles in vivo. A recent pre-print study cultured murine alveolar macrophages ex vivo in the presence of TGFβ and GM-CSF and successfully engrafted these macrophages back into the lungs of AM-deficient mice [493]. If successful, this technique experiment would allow multiple hypotheses presented in this thesis to be tested. For example, TMPI cells deficient in IL-1α could be instilled to investigate the hypothesis that AM-derived IL-1α is critical for propagating the inflammatory response to $cSiO_2$. It is suggested that migration of viable, $cSiO_2$-filled AMs out of the alveoli is a means by which inhaled $cSiO_2$ is cleared, so TMPI cells lacking the ability to phagocytose silica (e.g. knocking out MARCO or other scavenger receptors) or with impaired migration (e.g. knocking out chemokine receptors) could be employed to text this hypothesis. If a sub-pathogenic dose of $cSiO_2$ in mice instilled with wild type MPI cells is pathogenic to mice instilled with knock out MPI cells, it would support this mechanism of $cSiO_2$ clearance and pathogenesis.

Instillation of FAT-1 MPI cells could test the hypothesis that enriching the AM membrane with ω-3 HUFAs decreases $cSiO_2$-triggered inflammation in the lung. The increased ω-3 HUFAs naturally present in the membrane of cells with this genetic modification would bypass the need to supplement MPI cells with DHA prior to instillation.

7.2.5 Investigate the influence of other HUFAs, including ω-6 HUFA arachidonic acid and ω-3 HUFA eicosapentaenoic acid on the phenotype and function of MPI cells.

While it is generally well accepted that increasing ω-3 HUFA intake has many health benefits and that ω-3 HUFAs counter inflammatory pathways in vitro, preclinically, and clinically, the role of ω-6 HUFAs is less clear. A widely held view is that ω-6 HUFAs are responsible for induction of pro-inflammatory signaling pathways while ω-3 HUFAs inhibit ω-6 HUFA-triggered pathways and promote pro-resolving. The reality appears to be much more nuanced. There are numerous examples of studies with conflicting results relative to the influence of ω-6 and ω-3 HUFAs on inflammation [176, 522, 68, 183, 523, 380]. A recent meta-analysis of cardiovascular disease studies suggested that simply replacing saturated fats with HUFAs (not ω-3 or ω-6 specifically) is protective [524]. However, even the previously widely-held belief that saturated fatty acids contribute to heart disease is subject to debate, as thoroughly explored by Ruiz-Nunez et al. [525].

In a project funded by the Lupus Foundation of America, I performed preliminary studies assessing the effects of free DHA and ARA (provided as an ethanolic suspension of the free fatty acid) on the inflammasome activation and LPS-induced gene expression (**Figure 7.1**). I found that both DHA and ARA were similarly capable of suppressing cell death IL-1β release triggered by LPS and nigericin (**Figure 7.1 A-B**) and *Il1b* and *Il1a* gene expression induced by LPS alone (**Figure 7.1 B-C**). A key difference between this experiment those presented in this thesis was the use of a short-term exposure to the free fatty acids (2 h) rather than the 24 h supplementation with BSA-conjugated fatty acids. Therefore, these findings describe potential anti-inflammatory effects of free ARA, but do not describe how incorporation of this ω-3 HUFA influences the inflammatory response.

Lastly, the effect of EPA should also be assessed. Many studies relate the combination of EPA and DHA (presented as the Omega-3 Index) to disease endpoints [349, 381], but others have shown that there are differences between the two HUFAs [526, 527, 528]. This is likely mediated in part by the different lipid metabolite profiles that are generated [529]. Determining the effects of EPA on the *in vitro* MPI model would be useful in identifying changes induced by ω-3 HUFAs in general

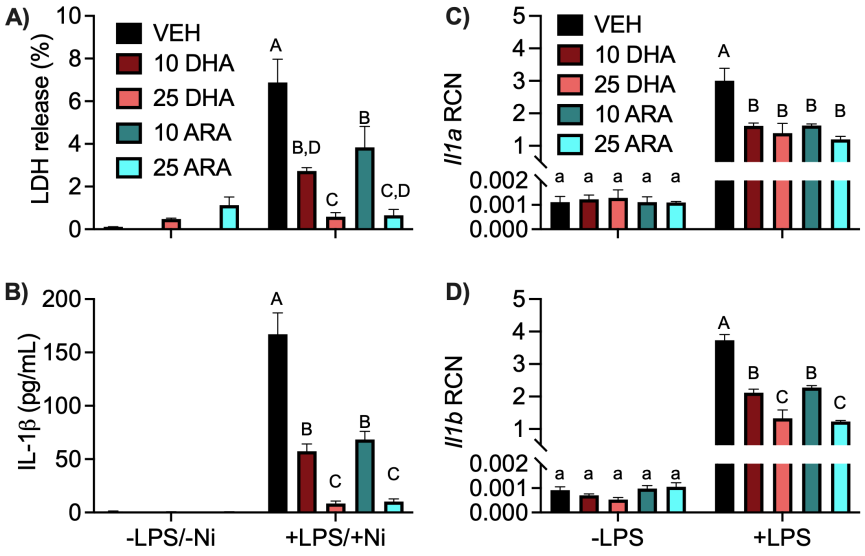


Figure 7.1: Short term exposure to DHA and ARA suppresses cell death, inflammasome activation, and IL-1 gene expression. MPI cells were treated with 10 or 25 μM DHA or arachidonic acid (ARA) as ethanolic suspensions for two hours prior to stimulation with LPS. A 40 ng/mL solution of LPS was added to 1 volume of DHA or ARA-containing media already in the well, reducing the concentrations of the fatty acids to 5 and 12.5 μM and the LPS to a final concentration of 20 ng/mL. To assess **A.** cell death and **B.** IL-1β release, cells incubated in LPS for 3 h followed by 45 min treatment with 5 μM nigericin, added dropwise. In a separate experiment, cells were incubated in LPS for 4 h and RNA extracted, reverse transcribed to cDNA, and expression of **C.** *Il1a* and **D.** *Il1b*.

and by DHA or EPA specifically.

APPENDICES

APPENDIX A

CHAPTER 2 SUPPORTING FIGURES AND TABLES

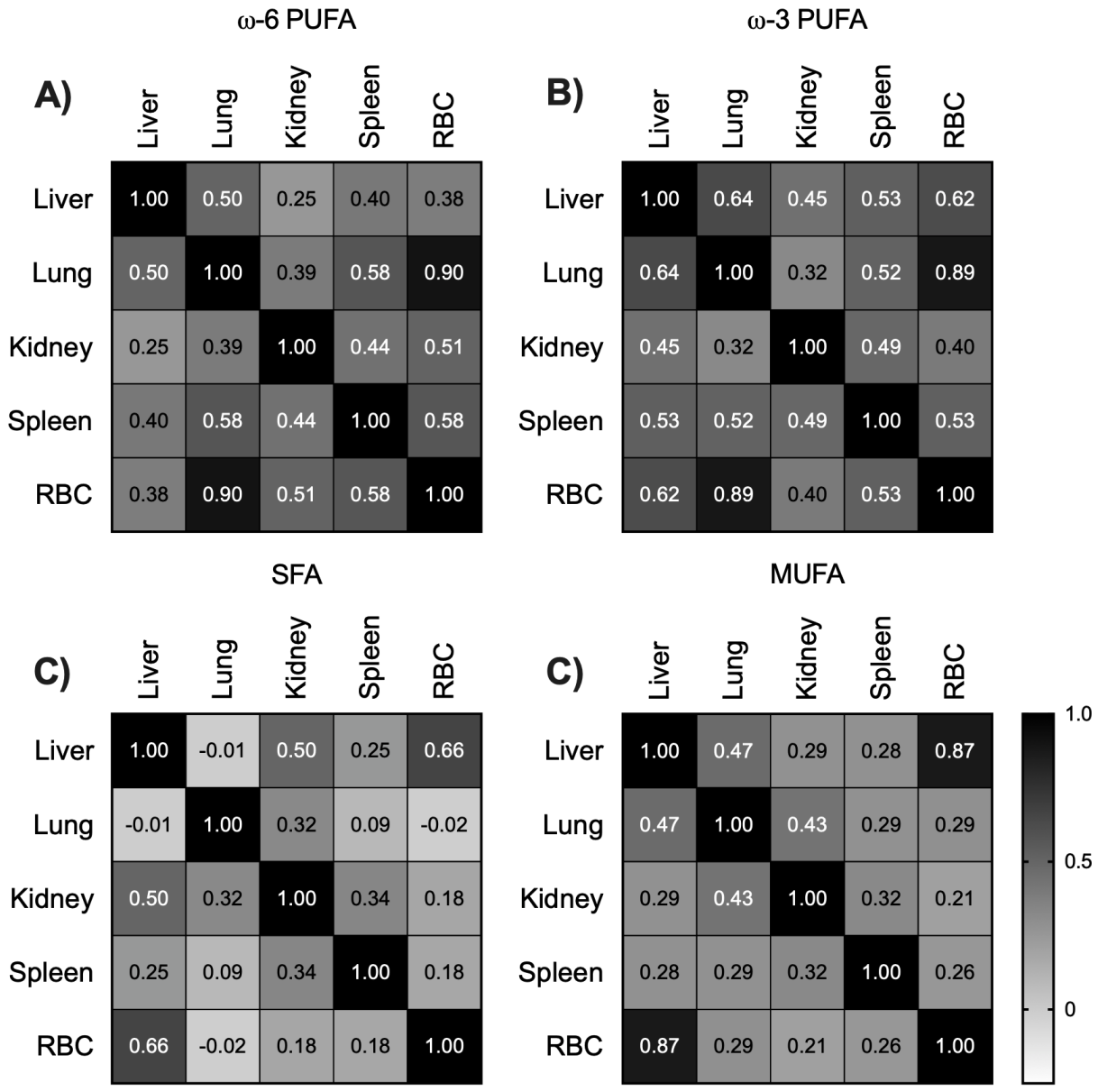


Figure A.1: Correlation between RBC and tissues for SFA, MUFA, ω-6 PUFA, and ω-3 PUFA
Correlation matrix presenting Pearson's correlation coefficients comparing RBC and tissue levels of **A.** saturated fatty acids (SFAs), **B.** monounsaturated fatty acids (MUFAs), **C.** ω-6 polyunsaturated fatty acids (PUFAs), **D.** and ω-3 PUFAs.

Table A.1: Lung fatty acid content as determined by GLC.

		VEH / CON	$cSiO_2$ / CON	$cSiO_2$ /↑DHA	$cSiO_2$ / ↓SF.ω6	$cSiO_2$ / ↓SF.ω6↑DHA
Common Name	**Chemical Formula**	*(% of total fatty acids)*				
Lauric	**C12:0**	0.07 ± 0.02^{A}	0.03 ± 0.01^{B}	0.04 ± 0.01^{AB}	0.02 ± 0.01^{B}	0.03 ± 0.00^{AB}
Myristic	**C14:0**	1.25 ± 0.17^{A}	2.38 ± 0.40^{BC}	2.74 ± 0.36^{B}	2.21 ± 0.45^{C}	2.10 ± 0.22^{C}
Palmitic	**C16:0**	31.76 ± 1.70^{A}	50.09 ± 5.32^{BC}	52.03 ± 3.45^{BC}	54.07 ± 3.86^{B}	48.55 ± 3.01^{C}
Palmitolaidic	**C16:1ω7t**	0.10 ± 0.02^{A}	0.10 ± 0.01^{A}	0.10 ± 0.01^{A}	0.05 ± 0.01^{B}	0.04 ± 0.01^{B}
Palmitoleic	**C16:1ω7c**	3.21 ± 0.63^{A}	4.02 ± 0.24^{B}	3.94 ± 0.32^{B}	3.07 ± 0.31^{A}	2.94 ± 0.38^{A}
Stearic	**C18:0**	10.25 ± 1.26^{A}	5.21 ± 1.02^{B}	4.82 ± 0.87^{BC}	3.85 ± 0.75^{C}	4.39 ± 0.65^{BC}
Elaidic	**C18:1ω9t**	0.00 ± 0.00	0.00 ± 0.00	0.00 ± 0.00	0.00 ± 0.00	0.00 ± 0.00
Oleic	**C18:1ω9c**	21.01 ± 2.91^{A}	13.81 ± 3.37^{B}	10.43 ± 1.40^{C}	15.88 ± 2.10^{BD}	17.10 ± 1.80^{D}
Linoleic	**C18:2ω6**	7.78 ± 0.75^{A}	5.51 ± 1.04^{B}	5.87 ± 0.66^{B}	2.46 ± 0.30^{C}	3.14 ± 0.40^{C}
Arachidic	**C20:0**	0.09 ± 0.04^{A}	0.03 ± 0.01^{B}	0.04 ± 0.02^{AB}	0.03 ± 0.01^{B}	0.04 ± 0.01^{AB}
Gamma-linolenic	**C18:3ω6**	0.18 ± 0.10^{AB}	0.10 ± 0.02^{A}	0.07 ± 0.01^{B}	0.06 ± 0.02^{BC}	0.04 ± 0.01^{C}
Linolenic	**C18:3ω3**	0.44 ± 0.07^{A}	0.17 ± 0.06^{BC}	0.09 ± 0.03^{B}	0.24 ± 0.08^{C}	0.23 ± 0.08^{C}
Eicosanoic	**C20:1ω9**	0.00 ± 0.00	0.00 ± 0.00	0.00 ± 0.00	0.00 ± 0.00	0.00 ± 0.00
Conjugated Linoleic	**CLA 9c,11t**	0.01 ± 0.03^{A}	0.01 ± 0.02^{A}	0.00 ± 0.00^{A}	0.00 ± 0.01^{A}	0.00 ± 0.01^{A}
Eicosadienoic	**C20:2ω6**	0.28 ± 0.03^{A}	0.16 ± 0.04^{B}	0.13 ± 0.03^{B}	0.07 ± 0.01^{C}	0.08 ± 0.02^{C}
Eicosatrienoic	**C20:3ω9**	0.11 ± 0.03^{A}	0.06 ± 0.02^{BC}	0.03 ± 0.02^{B}	0.10 ± 0.02^{A}	0.07 ± 0.02^{C}
Behenic	**C22:0**	0.05 ± 0.01^{A}	0.04 ± 0.02^{AB}	0.04 ± 0.02^{AB}	0.03 ± 0.01^{B}	0.04 ± 0.01^{AB}
Dihomo-g-linolenic	**C20:3ω6**	0.87 ± 0.13^{A}	0.38 ± 0.08^{BC}	0.44 ± 0.09^{B}	0.28 ± 0.05^{C}	0.37 ± 0.07^{BC}
Arachidonic	**C20:4ω6**	7.70 ± 1.18^{A}	5.83 ± 0.30^{B}	1.63 ± 0.20^{CD}	5.47 ± 0.32^{B}	1.02 ± 0.12^{D}
Eicosapentaenoic	**C20:5ω3**	0.08 ± 0.03^{A}	0.09 ± 0.02^{A}	0.76 ± 0.09^{BC}	0.08 ± 0.02^{A}	0.85 ± 0.08^{C}
Lignoceric	**C24:0**	0.09 ± 0.01^{A}	0.07 ± 0.01^{AB}	0.07 ± 0.01^{AB}	0.05 ± 0.01^{BC}	0.04 ± 0.00^{C}
Adrenic	**C22:4ω6**	2.53 ± 0.39^{A}	1.36 ± 0.31^{B}	0.13 ± 0.04^{C}	1.00 ± 0.19^{B}	0.08 ± 0.02^{D}
Docosapentaenoic ω6	**C22:5ω6**	0.61 ± 0.28^{A}	0.70 ± 0.24^{A}	0.91 ± 0.33^{AB}	0.65 ± 0.22^{A}	1.30 ± 0.36^{B}
Docosapentaenoic ω3	**C22:5ω3**	0.89 ± 0.10^{A}	0.50 ± 0.08^{B}	0.70 ± 0.12^{C}	0.26 ± 0.03^{D}	0.68 ± 0.10^{C}
Docosahexaenoic	**C22:6ω3**	3.04 ± 0.47^{A}	2.40 ± 0.09^{B}	8.88 ± 0.77^{C}	2.12 ± 0.12^{D}	8.87 ± 0.53^{C}
Total SF		44.45 ± 3.07^{A}	58.39 ± 4.96^{B}	60.32 ± 2.94^{B}	60.61 ± 3.58^{B}	55.50 ± 2.61^{B}
Total MUFA		28.89 ± 3.46^{A}	22.51 ± 3.62^{B}	18.67 ± 1.32^{C}	25.75 ± 2.67^{AB}	26.90 ± 1.75^{A}
Total ω-3 PUFA		4.45 ± 0.61^{A}	3.12 ± 0.11^{B}	10.44 ± 0.84^{C}	2.69 ± 0.19^{D}	10.64 ± 0.63^{C}
Total ω-6 PUFA		19.93 ± 1.61^{A}	14.31 ± 1.73^{B}	9.17 ± 1.06^{C}	9.98 ± 0.92^{C}	6.02 ± 0.67^{D}
EPA+DHA		3.12 ± 0.47^{A}	2.49 ± 0.09^{B}	9.65 ± 0.75^{C}	2.20 ± 0.12^{D}	9.72 ± 0.49^{C}

Data presented as mean ± SD. Difference between diets compared by ordinary one-way ANOVA followed by Tukey's multiple comparison. non-parametric versions of these tests were used when applicable. Unique letters indicate significant differences between groups (p<0.05). GLC, gas-liquid chromatography; SF, saturated fat; MUFA, monounsaturated fatty acid; PUFA, polyunsaturated fatty acid.

Table A.2: Liver fatty acid content as determined by GLC.

Common Name	Chemical Formula	VEH / CON	cSiO₂ / CON	cSiO₂ /↑DHA	cSiO₂ / ↓SF.ω6	cSiO₂ / ↓SF.ω6↑DHA
		(% of total fatty acids)				
Lauric	**C12:0**	0.03 ± 0.01^{AC}	0.04 ± 0.01^{A}	0.04 ± 0.01^{A}	0.02 ± 0.01^{B}	0.02 ± 0.01^{BC}
Myristic	**C14:0**	0.57 ± 0.12^{AC}	0.54 ± 0.10^{AC}	0.69 ± 0.08^{A}	0.31 ± 0.05^{B}	0.54 ± 0.03^{C}
Palmitic	**C16:0**	20.42 ± 0.55^{A}	20.33 ± 0.62^{A}	24.96 ± 1.01^{B}	14.45 ± 0.61^{C}	20.76 ± 1.15^{A}
Palmitolaidic	**C16:1ω7t**	0.06 ± 0.01^{A}	0.06 ± 0.01^{A}	0.06 ± 0.01^{AB}	0.04 ± 0.01^{B}	0.03 ± 0.01^{C}
Palmitoleic	**C16:1ω7c**	2.98 ± 0.48^{AB}	2.48 ± 0.40^{A}	3.28 ± 0.35^{B}	1.70 ± 0.26^{C}	2.58 ± 0.15^{A}
Stearic	**C18:0**	2.73 ± 0.52^{ACD}	3.55 ± 0.52^{B}	3.41 ± 0.80^{BC}	2.08 ± 0.25^{D}	2.10 ± 0.22^{D}
Elaidic	**C18:1ω9t**	0.07 ± 0.02^{A}	0.07 ± 0.01^{A}	0.06 ± 0.01^{A}	0.05 ± 0.02^{A}	0.04 ± 0.02^{A}
Oleic	**C18:1ω9c**	47.01 ± 1.04^{A}	44.79 ± 1.25^{B}	36.04 ± 4.98^{C}	65.50 ± 1.24^{D}	57.44 ± 0.47^{E}
Linoleic	**C18:2ω6**	15.64 ± 1.37^{A}	16.37 ± 1.64^{A}	17.51 ± 3.12^{A}	5.80 ± 0.46^{B}	6.96 ± 0.99^{B}
Arachidic	**C20:0**	0.00 ± 0.00^{A}	0.00 ± 0.00^{A}	0.00 ± 0.00^{A}	0.01 ± 0.02^{A}	0.00 ± 0.00^{A}
Gamma-linolenic	**C18:3ω6**	0.16 ± 0.05^{A}	0.18 ± 0.03^{A}	0.09 ± 0.02^{C}	0.08 ± 0.02^{C}	0.05 ± 0.02^{C}
Linolenic	**C18:3ω3**	0.50 ± 0.09^{A}	0.46 ± 0.10^{A}	1.17 ± 0.14^{B}	1.03 ± 0.14^{BC}	0.90 ± 0.05^{C}
Eicosanoic	**C20:1ω9**	0.49 ± 0.11^{A}	0.52 ± 0.09^{A}	0.03 ± 0.08^{B}	0.00 ± 0.00^{B}	0.00 ± 0.00^{B}
Conjugated Linoleic	**CLA 9c,11t**	0.14 ± 0.02^{AC}	0.13 ± 0.01^{AC}	0.15 ± 0.00^{A}	0.00 ± 0.00^{B}	0.02 ± 0.03^{C}
Eicosadienoic	**C20:2ω6**	0.12 ± 0.02^{A}	0.15 ± 0.02^{B}	0.14 ± 0.03^{AB}	0.05 ± 0.02^{C}	0.06 ± 0.02^{C}
Eicosatrienoic	**C20:3ω9**	0.05 ± 0.01^{AC}	0.07 ± 0.02^{AB}	0.03 ± 0.01^{AC}	0.13 ± 0.02^{B}	0.03 ± 0.01^{C}
Behenic	**C22:0**	0.00 ± 0.00	0.00 ± 0.00	0.00 ± 0.00	0.00 ± 0.00	0.00 ± 0.00
Dihomo-g-linolenic	**C20:3ω6**	0.23 ± 0.02^{ABC}	0.30 ± 0.05^{AC}	0.32 ± 0.06^{AB}	0.19 ± 0.02^{C}	0.15 ± 0.01^{B}
Arachidonic	**C20:4ω6**	1.39 ± 0.19^{A}	2.44 ± 0.57^{B}	0.73 ± 0.17^{C}	1.30 ± 0.19^{A}	0.27 ± 0.03^{D}
Eicosapentaenoic	**C20:5ω3**	0.06 ± 0.01^{A}	0.06 ± 0.02^{A}	0.88 ± 0.29^{B}	0.03 ± 0.01^{C}	0.59 ± 0.10^{B}
Lignoceric	**C24:0**	0.01 ± 0.01^{A}	0.00 ± 0.00^{B}	0.01 ± 0.01^{AB}	0.00 ± 0.00^{B}	0.00 ± 0.00^{B}
Adrenic	**C22:4ω6**	0.06 ± 0.01^{A}	0.09 ± 0.03^{B}	0.04 ± 0.01^{AC}	0.05 ± 0.02^{A}	0.02 ± 0.01^{C}
Docosapentaenoic ω6	**C22:5ω6**	0.32 ± 0.07^{AB}	0.37 ± 0.04^{A}	0.24 ± 0.03^{B}	0.60 ± 0.07^{C}	0.31 ± 0.06^{AB}
Docosapentaenoic ω3	**C22:5ω3**	0.09 ± 0.02^{A}	0.09 ± 0.02^{A}	0.35 ± 0.13^{B}	0.05 ± 0.02^{C}	0.16 ± 0.03^{D}
Docosahexaenoic	**C22:6ω3**	1.02 ± 0.26^{A}	1.55 ± 0.34^{B}	5.07 ± 2.05^{C}	0.73 ± 0.03^{A}	2.08 ± 0.44^{BD}
Total SF		24.10 ± 0.62^{A}	24.82 ± 0.99^{A}	29.44 ± 0.71^{B}	17.06 ± 0.78^{C}	23.60 ± 0.91^{A}
Total MUFA		55.42 ± 1.82^{A}	52.35 ± 1.75^{B}	43.31 ± 6.03^{C}	72.49 ± 1.31^{D}	64.56 ± 0.87^{E}
Total ω-3 PUFA		1.67 ± 0.31^{A}	2.16 ± 0.38^{A}	7.47 ± 2.54^{B}	1.91 ± 0.19^{A}	3.72 ± 0.60^{C}
Total ω-6 PUFA		18.05 ± 1.64^{A}	19.90 ± 1.65^{A}	19.06 ± 3.35^{A}	8.17 ± 0.63^{B}	7.82 ± 1.05^{B}
EPA+DHA		1.08 ± 0.26^{A}	1.60 ± 0.36^{B}	5.95 ± 2.33^{C}	0.75 ± 0.03^{A}	2.67 ± 0.54^{D}

Data presented as mean ± SD. Difference between diets compared by ordinary one-way ANOVA followed by Tukey's multiple comparison. non-parametric versions of these tests were used when applicable. Unique letters indicate significant differences between groups (p<0.05). GLC, gas-liquid chromatography; SF, saturated fat; MUFA, monounsaturated fatty acid; PUFA, polyunsaturated fatty acid.

Table A.3: Kidney fatty acid content as determined by GLC.

		VEH / CON	$cSiO_2$ / CON	$cSiO_2$ /↑DHA	$cSiO_2$ / ↓SF.ω6	$cSiO_2$ / ↓SF.ω6↑DHA
Common Name	**Chemical Formula**	*(% of total fatty acids)*				
Lauric	**C12:0**	0.12 ± 0.02^{A}	0.11 ± 0.06^{AB}	0.19 ± 0.06^{A}	0.03 ± 0.01^{B}	0.11 ± 0.04^{A}
Myristic	**C14:0**	1.22 ± 0.14^{A}	1.04 ± 0.54^{A}	1.57 ± 0.52^{A}	0.37 ± 0.16^{B}	1.08 ± 0.41^{A}
Palmitic	**C16:0**	19.72 ± 0.51^{A}	18.99 ± 1.30^{A}	22.78 ± 0.95^{B}	15.51 ± 1.18^{C}	18.79 ± 1.52^{A}
Palmitolaidic	**C16:1ω7t**	0.08 ± 0.01^{A}	0.08 ± 0.01^{A}	0.09 ± 0.02^{A}	0.04 ± 0.01^{B}	0.04 ± 0.01^{B}
Palmitoleic	**C16:1ω7c**	5.27 ± 1.49^{A}	3.90 ± 2.05^{AB}	5.21 ± 1.53^{A}	2.09 ± 1.05^{B}	4.29 ± 1.88^{AB}
Stearic	**C18:0**	6.38 ± 1.92^{A}	7.94 ± 5.13^{A}	7.94 ± 2.63^{A}	10.46 ± 4.19^{A}	5.99 ± 3.42^{A}
Elaidic	**C18:1ω9t**	0.09 ± 0.02^{A}	0.08 ± 0.02^{A}	0.07 ± 0.01^{A}	0.04 ± 0.01^{B}	0.04 ± 0.01^{B}
Oleic	**C18:1ω9c**	36.25 ± 4.37^{AB}	33.02 ± 14.35^{AB}	24.46 ± 7.23^{A}	34.15 ± 15.77^{AB}	44.25 ± 12.23^{B}
Linoleic	**C18:2ω6**	14.75 ± 0.60^{A}	14.02 ± 2.13^{A}	15.79 ± 1.49^{A}	7.51 ± 0.05^{B}	8.21 ± 1.20^{B}
Arachidic	**C20:0**	0.06 ± 0.02^{A}	0.09 ± 0.03^{A}	0.06 ± 0.01^{A}	0.08 ± 0.02^{A}	0.06 ± 0.02^{A}
Gamma-linolenic	**C18:3ω6**	0.04 ± 0.01^{A}	0.05 ± 0.02^{A}	0.03 ± 0.01^{AB}	0.04 ± 0.01^{A}	0.02 ± 0.00^{B}
Linolenic	**C18:3ω3**	0.55 ± 0.10^{A}	0.46 ± 0.22^{AC}	0.63 ± 0.15^{A}	0.15 ± 0.07^{B}	0.26 ± 0.09^{BC}
Eicosanoic	**C20:1ω9**	0.26 ± 0.05^{A}	0.28 ± 0.07^{A}	0.16 ± 0.03^{B}	0.35 ± 0.03^{C}	0.23 ± 0.04^{AB}
Conjugated Linoleic	**CLA 9c,11t**	0.15 ± 0.03^{A}	0.14 ± 0.04^{A}	0.14 ± 0.03^{A}	0.05 ± 0.01^{B}	0.05 ± 0.03^{B}
Eicosadienoic	**C20:2ω6**	0.15 ± 0.02^{A}	0.16 ± 0.08^{A}	0.16 ± 0.04^{A}	0.13 ± 0.05^{AB}	0.08 ± 0.03^{B}
Eicosatrienoic	**C20:3ω9**	0.04 ± 0.01^{A}	0.04 ± 0.02^{A}	0.03 ± 0.02^{A}	0.14 ± 0.05^{B}	0.05 ± 0.03^{A}
Behenic	**C22:0**	0.04 ± 0.01^{A}	0.05 ± 0.03^{A}	0.05 ± 0.03^{A}	0.06 ± 0.02^{A}	0.04 ± 0.02^{A}
Dihomo-g-linolenic	**C20:3ω6**	0.31 ± 0.08^{A}	0.40 ± 0.31^{A}	0.50 ± 0.21^{A}	0.64 ± 0.28^{A}	0.37 ± 0.27^{A}
Arachidonic	**C20:4ω6**	6.53 ± 2.56^{AB}	9.11 ± 8.73^{AB}	3.95 ± 2.02^{AB}	15.33 ± 7.30^{A}	2.14 ± 1.72^{A}
Eicosapentaenoic	**C20:5ω3**	0.09 ± 0.02^{A}	0.12 ± 0.11^{A}	2.03 ± 0.98^{B}	0.16 ± 0.07^{A}	2.26 ± 1.73^{B}
Lignoceric	**C24:0**	0.05 ± 0.02^{A}	0.07 ± 0.05^{A}	0.07 ± 0.03^{A}	0.09 ± 0.04^{A}	0.05 ± 0.02^{A}
Adrenic	**C22:4ω6**	0.15 ± 0.05^{AD}	0.24 ± 0.22^{AD}	0.02 ± 0.01^{B}	0.33 ± 0.14^{AC}	0.02 ± 0.01^{BD}
Docosapentaenoic ω6	**C22:5ω6**	0.20 ± 0.04^{A}	0.55 ± 0.55^{AB}	0.55 ± 0.31^{AB}	0.94 ± 0.44^{B}	0.34 ± 0.16^{AB}
Docosapentaenoic ω3	**C22:5ω3**	0.18 ± 0.06^{A}	0.27 ± 0.19^{A}	0.33 ± 0.17^{A}	0.26 ± 0.15^{A}	0.21 ± 0.06^{A}
Docosahexaenoic	**C22:6ω3**	2.84 ± 0.99^{A}	4.12 ± 3.88^{AB}	8.95 ± 4.22^{B}	6.33 ± 2.87^{AB}	7.37 ± 5.17^{AB}
Total SF		27.97 ± 1.67^{A}	28.68 ± 4.35^{AB}	33.07 ± 1.54^{B}	26.87 ± 5.13^{A}	26.33 ± 3.16^{A}
Total MUFA		44.98 ± 4.80^{A}	40.39 ± 16.16^{A}	32.44 ± 8.43^{A}	39.91 ± 16.76^{A}	51.52 ± 13.53^{A}
Total ω-3 PUFA		3.66 ± 1.03^{A}	4.96 ± 3.97^{A}	11.94 ± 5.19^{B}	6.91 ± 3.00^{AB}	10.13 ± 6.93^{AB}
Total ω-6 PUFA		22.12 ± 2.26^{A}	24.53 ± 7.86^{A}	21.00 ± 1.76^{AB}	24.90 ± 8.26^{A}	11.18 ± 3.27^{B}
EPA+DHA		2.93 ± 1.01^{A}	4.24 ± 3.98^{A}	10.98 ± 5.18^{B}	6.94 ± 2.94^{AB}	9.62 ± 6.89^{AB}

Data presented as mean ± SD. Difference between diets compared by ordinary one-way ANOVA followed by Tukey's multiple comparison. non-parametric versions of these tests were used when applicable. Unique letters indicate significant differences between groups (p<0.05). GLC, gas-liquid chromatography; SF, saturated fat; MUFA, monounsaturated fatty acid; PUFA, polyunsaturated fatty acid.

Table A.4: Spleen fatty acid content as determined by GLC.

		VEH / CON	cSiO₂ / CON	cSiO₂ /↑DHA	cSiO₂ / ↓SF.ω6	cSiO₂ / ↓SF.ω6↑DHA
Common Name	**Chemical Formula**	*(% of total fatty acids)*				
Lauric	**C12:0**	0.11 ± 0.03^{A}	0.10 ± 0.03^{A}	0.19 ± 0.07^{B}	0.04 ± 0.01^{C}	0.11 ± 0.04^{AB}
Myristic	**C14:0**	1.18 ± 0.31^{A}	1.17 ± 0.17^{A}	1.85 ± 0.52^{A}	0.61 ± 0.13^{B}	1.22 ± 0.29^{A}
Palmitic	**C16:0**	22.06 ± 2.29^{A}	21.48 ± 1.75^{A}	25.82 ± 1.95^{BC}	19.50 ± 2.89^{A}	23.40 ± 1.98^{C}
Palmitolaidic	**C16:1ω7t**	0.11 ± 0.03^{A}	0.09 ± 0.01^{A}	0.10 ± 0.02^{A}	0.05 ± 0.01^{B}	0.05 ± 0.02^{B}
Palmitoleic	**C16:1ω7c**	5.20 ± 2.10^{A}	4.97 ± 1.14^{A}	5.69 ± 2.08^{A}	3.30 ± 1.46^{A}	4.80 ± 2.18^{A}
Stearic	**C18:0**	7.36 ± 5.00^{A}	6.52 ± 3.01^{A}	7.28 ± 4.02^{A}	8.29 ± 3.95^{A}	7.27 ± 3.27^{A}
Elaidic	**C18:1ω9t**	0.11 ± 0.01^{A}	0.10 ± 0.03^{A}	0.08 ± 0.03^{AB}	0.04 ± 0.02^{B}	0.10 ± 0.06^{A}
Oleic	**C18:1ω9c**	32.81 ± 13.13^{A}	38.21 ± 4.84^{A}	26.20 ± 9.55^{A}	39.67 ± 14.74^{A}	37.40 ± 11.72^{A}
Linoleic	**C18:2ω6**	12.34 ± 2.92^{A}	12.52 ± 1.67^{A}	14.24 ± 2.63^{A}	5.65 ± 0.37^{B}	7.37 ± 0.37^{C}
Arachidic	**C20:0**	0.03 ± 0.03^{A}	0.02 ± 0.04^{A}	0.02 ± 0.03^{A}	0.03 ± 0.03^{A}	0.03 ± 0.04^{A}
Gamma-linolenic	**C18:3ω6**	0.01 ± 0.01^{A}	0.01 ± 0.02^{A}	0.01 ± 0.03^{A}	0.01 ± 0.00^{A}	0.01 ± 0.03^{A}
Linolenic	**C18:3ω3**	0.78 ± 0.13^{A}	0.73 ± 0.11^{A}	0.80 ± 0.14^{A}	0.56 ± 0.12^{AB}	0.33 ± 0.10^{B}
Eicosanoic	**C20:1ω9**	0.00 ± 0.00	0.00 ± 0.00	0.00 ± 0.00	0.00 ± 0.00	0.00 ± 0.00
Conjugated Linoleic	**CLA 9c,11t**	0.08 ± 0.09^{A}	0.11 ± 0.07^{A}	0.09 ± 0.09^{A}	0.02 ± 0.04^{A}	0.01 ± 0.03^{A}
Eicosadienoic	**C20:2ω6**	0.28 ± 0.16^{A}	0.24 ± 0.08^{A}	0.27 ± 0.18^{A}	0.22 ± 0.12^{A}	0.17 ± 0.09^{A}
Eicosatrienoic	**C20:3ω9**	0.04 ± 0.04^{A}	0.06 ± 0.03^{AB}	0.02 ± 0.03^{A}	0.14 ± 0.06^{B}	0.05 ± 0.03^{AB}
Behenic	**C22:0**	0.18 ± 0.17^{A}	0.18 ± 0.09^{A}	0.30 ± 0.31^{A}	0.28 ± 0.24^{A}	0.02 ± 0.02^{A}
Dihomo-g-linolenic	**C20:3ω6**	0.41 ± 0.32^{A}	0.35 ± 0.17^{A}	0.62 ± 0.45^{A}	0.53 ± 0.26^{A}	0.67 ± 0.33^{A}
Arachidonic	**C20:4ω6**	7.21 ± 6.14^{AB}	4.60 ± 3.75^{A}	2.61 ± 2.19^{AB}	9.54 ± 5.28^{A}	1.88 ± 0.98^{B}
Eicosapentaenoic	**C20:5ω3**	0.06 ± 0.05^{A}	0.05 ± 0.02^{A}	0.70 ± 0.51^{AB}	0.06 ± 0.04^{A}	1.19 ± 0.64^{B}
Lignoceric	**C24:0**	0.03 ± 0.05^{A}	0.10 ± 0.08^{AB}	0.09 ± 0.04^{AB}	0.20 ± 0.15^{B}	0.04 ± 0.03^{AB}
Adrenic	**C22:4ω6**	1.11 ± 0.99^{AB}	0.84 ± 0.32^{A}	0.15 ± 0.14^{B}	1.72 ± 0.91^{A}	0.08 ± 0.06^{B}
Docosapentaenoic ω6	**C22:5ω6**	0.70 ± 0.58^{A}	0.56 ± 0.19^{A}	0.98 ± 0.87^{A}	1.08 ± 0.77^{A}	0.34 ± 0.38^{A}
Docosapentaenoic ω3	**C22:5ω3**	0.51 ± 0.42^{A}	0.37 ± 0.16^{A}	0.69 ± 0.54^{A}	0.41 ± 0.19^{A}	0.83 ± 0.46^{A}
Docosahexaenoic	**C22:6ω3**	1.86 ± 1.61^{A}	1.41 ± 0.44^{A}	6.11 ± 4.38^{AB}	2.72 ± 1.42^{AB}	7.66 ± 4.32^{B}
Total SF		31.44 ± 7.13^{A}	30.01 ± 4.74^{A}	36.21 ± 4.50^{A}	29.27 ± 6.99^{A}	32.49 ± 4.85^{A}
Total MUFA		41.77 ± 14.70^{A}	47.29 ± 4.59^{A}	35.17 ± 11.03^{A}	47.14 ± 15.77^{A}	45.83 ± 12.21^{A}
Total ω-3 PUFA		3.21 ± 2.00^{A}	2.54 ± 0.54^{A}	8.29 ± 5.29^{A}	3.74 ± 1.71^{A}	10.01 ± 5.52^{A}
Total ω-6 PUFA		22.05 ± 5.33^{A}	19.85 ± 1.18^{A}	18.89 ± 1.80^{A}	18.75 ± 6.87^{AB}	10.53 ± 1.78^{B}
EPA+DHA		1.92 ± 1.66^{A}	1.45 ± 0.45^{A}	6.81 ± 4.89^{AB}	2.79 ± 1.45^{AB}	8.86 ± 4.96^{B}

Data presented as mean ± SD. Difference between diets compared by ordinary one-way ANOVA followed by Tukey's multiple comparison. non-parametric versions of these tests were used when applicable. Unique letters indicate significant differences between groups (p<0.05). GLC, gas-liquid chromatography; SF, saturated fat; MUFA, monounsaturated fatty acid; PUFA, polyunsaturated fatty acid.

Table A.5: Histopathology severity scores, lungs.

Experimental Group	LYMPHOID AGGREGATES	ECTOPIC LYMPHOID STRUCTURES	ALVEOLITIS
VEH / CON	0 ± 0.1	0 ± 0	0 ± 0.1
$cSiO_2$ / CON	3.4 ± 0.3*	2.8 ± 0.4*	3.5 ± 0.3*
$cSiO_2$ /↑DHA	1.2 ± 0.3#	0.1 ± 0.1#	2.4 ± 0.2#
$cSiO_2$ / ↓SF.ω-6	2.6 ± 0.2	1.5 ± 0.2#	2.4 ± 0.2#
$cSiO_2$ / ↓SF.ω-6↑DHA	1.4 ± 0.3#	0 ± 0#	1.1 ± 0.2#

Mice were graded individually for extent of lymphoid aggregation, ectopic lymphoid structure development, and alveolitis (% of total pulmonary tissue examined) as follows: 0 = no changes; 1, minimal (<10%); 2, slight (10-25%); 3, moderate (26-50%); 4, severe (51-75%); 5, very severe (>75%). Data are mean ± SEM. *Indicates significant difference between VEH/CON and $cSiO_2$/CON groups, as measured by unpaired T test (p<0.05) #Indicates significant difference from $cSiO_2$/Con group, as measured by ordinary one-way ANOVA with Dunnett's multiple comparison test (p<0.05).

Table A.6: Urinary protein at 18, 20, and 22 wk of age.

	Experimental Diets				
	VEH / CON	$cSiO_2$ / CON	$cSiO_2$ /↑DHA	$cSiO_2$ / ↓SF.ω6	$cSiO_2$ / ↓SF.ω6↑DHA
Week	*Protein concentration, mg/dL*				
18	61.73 ± 9.77	62.62 ± 12.05	90.00 ± 8.38	58.45 ± 7.20	69.56 ± 7.66
20	56.88 ± 11.88	64.09 ± 9.21	80.24 ± 5.85	76.65 ± 11.08	106.36 ± 31.53
22	233.84 ± 63.18	183.64 ± 38.50	201. 05 ± 24.86	134.45 ± 21.15	214.09 ± 22.68

Data presented as mean ± SE. No significant difference was observed between $cSiO_2$ and any of the groups in wk 18, 20, or 22. Mice were euthanized at age 22 wk

.

APPENDIX B

CHAPTER 3 SUPPORTING FIGURES AND TABLES

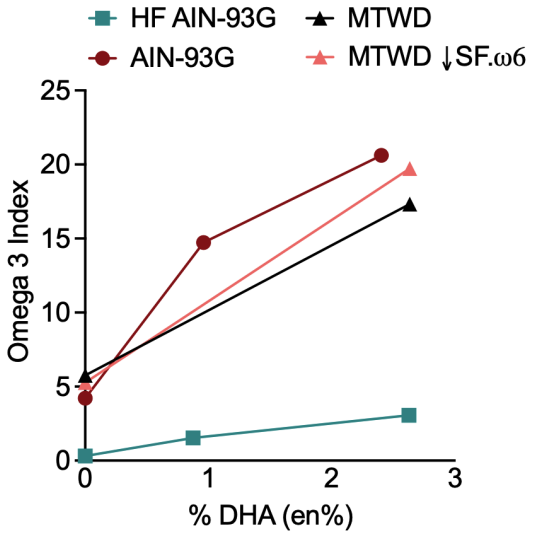


Figure B.1: O3I increases with DHA intake in NZBWF1 mice. Animals were supplemented with DHA on the background of distinct diets, as described in Figure 3.1. RBCs were collected at experiment termination for fatty acid analysis by gas-liquid chromatography (full fatty acid profiles presented in Supplementary Table B.1). The DHA content in the diet is presented as en% and the ω-3 content of the red blood cells (RBCs) is expressed as the Omega 3 Index (O3I). While animals in Studies 2 and 3 (fed the AIN-93G and MTWD diets) had similar O3Is, animals from Study 1 (fed the HF-AIN-93G diet) had significantly lower O3Is. The analysis of the RBC fatty acids for Study 1 were performed in a different lab from those of Studies 2 and 3, which may account for the observed difference.

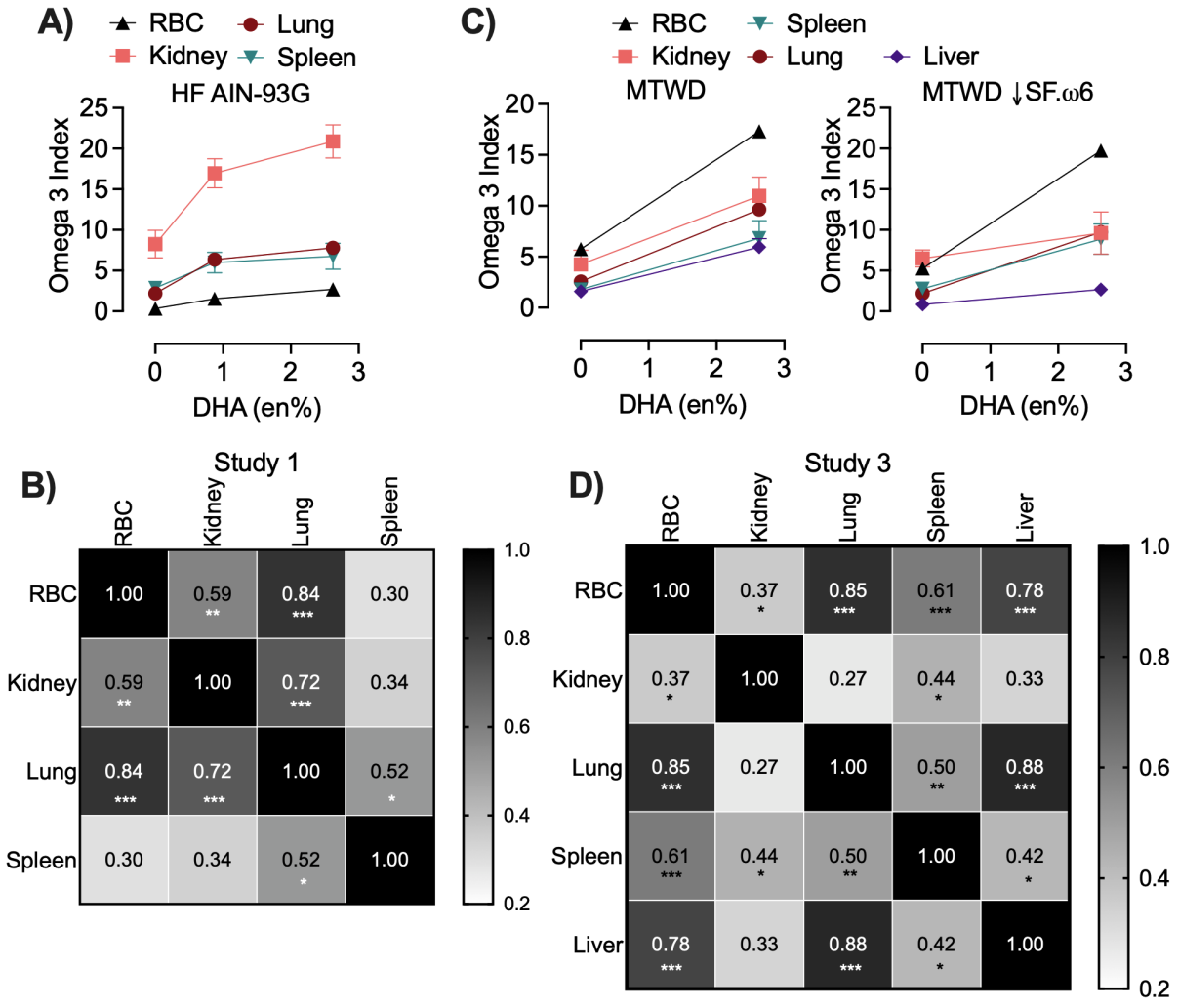


Figure B.2: RBC O3Is do not closely reflect tissue EPA+DHA levels. Animals from **A-B.** Study 1 (HF AIN-93G) and **C-D.** Study 3 (MTWD and MTWD SF.ω6 diet) were analyzed separately to assess the impact of DHA supplementation on red blood cell (RBC) and tissue fatty acid incorporation (**A,C**). The Omega-3 Index (O3I) was clearly distinct among different tissues when animals were supplemented with DHA. (**B,D**) Spearman's correlation was used to identify correlations between the RBC O3I and O3I across multiple tissues (*p<0.05, **p<0.01, ***p<0.001).

Table B.1: Fatty acid content of RBCs for Studies 1,2,and 3a.

		Experimental Diets									
		Study 1			Study 2			Study 3			
	Basal Diet	HF AIN-93G			AIN-93G			MTWD		MTWD ↓SF.w-6	
	DHA (en%)	0.00%	0.96%	2.40%	0.00%	0.87%	2.62%	0.00%	2.63%	0.00%	2.63%
	DHA (%w/w)	0.00%	0.40%	1.20%	0.00%	0.40%	1.00%	0.00%	1.00%	0.00%	1.00%
Common Name	Chemical Formula	*(% of total fatty acids)*									
Myristic	C14:0	0.91 ± 0.30	0.97 ± 0.46	1.66 ± 0.68	0.11 ± 0.01	0.16 ± 0.02	0.17 ± 0.05	0.23 ± 0.03	0.33 ± 0.06	0.13 ± 0.01	0.22 ± 0.02
Palmitic	C16:0	42.20 ± 6.39	40.26 ± 8.67	40.50 ± 8.30	25.06 ± 0.55	27.21 ± 0.80	28.69 ± 0.47	25.47 ± 0.67	27.20 ± 0.49	24.71 ± 0.72	27.05 ± 0.38
Palmitelaidic	C16:1ω7t	0.08 ± 0.03	0.06 ± 0.02	0.06 ± 0.01	0.03 ± 0.00	0.02 ± 0.00	0.02 ± 0.00	0.15 ± 0.01	0.14 ± 0.01	0.07 ± 0.01	0.06 ± 0.01
Palmitoleic	C16:1ω7	1.84 ± 1.13	2.14 ± 1.71	3.84 ± 2.50	0.41 ± 0.07	0.41 ± 0.07	0.52 ± 0.08	0.45 ± 0.06	0.60 ± 0.08	0.32 ± 0.04	0.41 ± 0.03
Stearic	C18:0	20.54 ± 7.08	16.64 ± 7.72	12.60 ± 6.00	15.51 ± 0.89	14.22 ± 0.37	13.81 ± 0.64	16.29 ± 0.84	15.83 ± 0.18	14.84 ± 0.75	13.45 ± 0.41
Elaidic	C18:1t	0.33 ± 0.22	0.18 ± 0.10	0.08 ± 0.04	0.12 ± 0.01	0.11 ± 0.01	0.10 ± 0.01	0.69 ± 0.04	0.62 ± 0.04	0.27 ± 0.02	0.24 ± 0.02
Oleic	C18:1ω9	19.01 ± 10.57	22.52 ± 14.29	22.52 ± 10.58	19.01 ± 0.56	17.70 ± 0.51	17.41 ± 0.70	15.03 ± 0.43	12.99 ± 0.55	21.70 ± 0.19	20.00 ± 0.29
Linoleic	C18:2ω6	4.02 ± 1.85	5.88 ± 2.82	5.59 ± 1.59	7.97 ± 0.76	9.99 ± 0.45	9.90 ± 0.70	10.97 ± 0.39	14.30 ± 0.78	7.80 ± 0.58	9.70 ± 0.47
Arachidic	C20:0	0.33 ± 0.09	0.28 ± 0.11	0.16 ± 0.05	0.12 ± 0.02	0.11 ± 0.01	0.11 ± 0.02	0.13 ± 0.03	0.13 ± 0.03	0.12 ± 0.03	0.11 ± 0.02
gamma-Linolenic	C18:3ω6	0.00 ± 0.00	0.00 ± 0.00	0.00 ± 0.00	0.05 ± 0.01	0.05 ± 0.01	0.04 ± 0.01	0.05 ± 0.01	0.05 ± 0.01	0.05 ± 0.00	0.03 ± 0.01
Eicosenoic	C20:1ω9	0.32 ± 0.14	0.34 ± 0.20	0.24 ± 0.13	0.41 ± 0.04	0.33 ± 0.03	0.27 ± 0.04	0.28 ± 0.02	0.18 ± 0.04	0.49 ± 0.06	0.29 ± 0.03
alpha-Linolenic	C18:3ω3	0.00 ± 0.00	0.00 ± 0.00	0.00 ± 0.00	0.02 ± 0.00	0.02 ± 0.00	0.01 ± 0.00	0.08 ± 0.01	0.08 ± 0.01	0.04 ± 0.01	0.04 ± 0.01
Eicosadienoic	C20:2ω6	0.02 ± 0.04	0.07 ± 0.04	0.11 ± 0.08	0.21 ± 0.03	0.24 ± 0.02	0.20 ± 0.02	0.30 ± 0.03	0.30 ± 0.03	0.21 ± 0.01	0.18 ± 0.01
Behenic	C22:0	0.20 ± 0.13	0.10 ± 0.05	0.06 ± 0.04	0.07 ± 0.02	0.07 ± 0.01	0.05 ± 0.01	0.10 ± 0.04	0.11 ± 0.04	0.07 ± 0.01	0.09 ± 0.02
DGLA	C20:3ω6	0.20 ± 0.08	0.35 ± 0.15	0.25 ± 0.10	1.16 ± 0.12	1.80 ± 0.27	1.47 ± 0.18	1.26 ± 0.09	1.43 ± 0.20	1.41 ± 0.08	1.24 ± 0.14
Arachidonic	C20:4ω6	2.36 ± 0.91	1.68 ± 0.71	0.73 ± 0.25	21.37 ± 0.63	11.05 ± 0.78	5.06 ± 0.54	18.91 ± 0.87	6.84 ± 0.56	19.14 ± 0.45	5.11 ± 0.49
Lignoceric	C24:0	0.29 ± 0.16	0.17 ± 0.09	0.13 ± 0.07	0.10 ± 0.03	0.12 ± 0.03	0.10 ± 0.02	0.18 ± 0.07	0.19 ± 0.06	0.14 ± 0.03	0.19 ± 0.01
Eicosapentaenoic	C20:5ω3	0.01 ± 0.02	0.18 ± 0.13	0.72 ± 0.31	0.07 ± 0.01	1.98 ± 0.29	4.95 ± 0.51	0.25 ± 0.02	2.98 ± 0.16	0.20 ± 0.02	4.73 ± 0.18
Nervonic	C24:1ω9	0.25 ± 0.31	0.05 ± 0.02	0.03 ± 0.01	0.19 ± 0.05	0.22 ± 0.05	0.20 ± 0.01	0.14 ± 0.06	0.13 ± 0.04	0.21 ± 0.04	0.26 ± 0.02
Docosatetraenoic	C22:4ω6	0.31 ± 0.13	0.07 ± 0.04	0.03 ± 0.01	2.40 ± 0.32	0.54 ± 0.08	0.14 ± 0.02	2.22 ± 0.13	0.22 ± 0.03	1.98 ± 0.15	0.14 ± 0.01
Docosapentaenoic - ω6	C22:5ω6	0.13 ± 0.04	0.00 ± 0.01	0.00 ± 0.00	1.18 ± 0.12	0.08 ± 0.01	0.03 ± 0.00	0.47 ± 0.03	0.04 ± 0.01	0.51 ± 0.04	0.03 ± 0.01
Docosapentaenoic - ω3	C22:5ω3	0.02 ± 0.02	0.11 ± 0.06	0.19 ± 0.06	0.25 ± 0.03	0.78 ± 0.04	1.01 ± 0.07	0.75 ± 0.08	0.86 ± 0.04	0.45 ± 0.05	0.90 ± 0.04
Docosahexaenoic	C22:6ω3	0.31 ± 0.14	1.36 ± 0.77	2.35 ± 0.92	4.14 ± 0.22	12.75 ± 0.23	15.67 ± 0.70	5.50 ± 0.19	14.35 ± 0.49	5.06 ± 0.17	15.01 ± 0.28
SFA		64.46 ± 13.20	58.42 ± 16.04	55.11 ± 13.75	40.97 ± 0.78	41.89 ± 0.92	42.94 ± 0.42	42.39 ± 0.72	43.79 ± 0.45	40.01 ± 1.13	41.12 ± 0.63
MUFA		21.84 ± 11.38	25.29 ± 15.98	26.77 ± 13.09	20.17 ± 0.60	18.80 ± 0.54	18.53 ± 0.75	16.73 ± 0.46	14.65 ± 0.57	23.06 ± 0.19	21.26 ± 0.30
Total ω-3 PUFA		0.33 ± 0.16	1.65 ± 0.95	3.26 ± 1.27	4.48 ± 0.22	15.52 ± 0.43	21.64 ± 0.72	6.58 ± 0.17	18.27 ± 0.56	5.76 ± 0.21	20.67 ± 0.27
Total ω-6 PUFA		7.04 ± 2.92	8.06 ± 3.33	6.72 ± 1.67	34.38 ± 0.89	23.79 ± 0.63	16.89 ± 1.05	34.30 ± 0.89	23.29 ± 0.33	31.17 ± 0.90	16.49 ± 0.37
Omega-3 Index		0.32 ± 0.14	1.47 ± 0.83	2.54 ± 0.96	4.21 ± 0.22	14.73 ± 0.40	20.62 ± 0.68	5.75 ± 0.18	17.32 ± 0.56	5.26 ± 0.17	19.74 ± 0.28
ω-3 HUFA Score		11.24 7.90	41.13 9.24	75.83 3.81	14.61 ± 0.81	53.57 ± 2.25	76.34 ± 2.35	22.16 ± 0.66	68.08 ± 2.42	19.88 ± 0.48	76.04 ± 1.94

Study 1 analyzed in house. Study 2 and 3 analyzed at OmegaQuant Analytics, LLC. SFA, saturated fatty acid; MUFA, monounsaturated fatty acid; PUFA, polyunsaturated fatty acid; HUFA, highly unsaturated fatty acid.

APPENDIX C

CHAPTER 4 SUPPORTING FIGURES

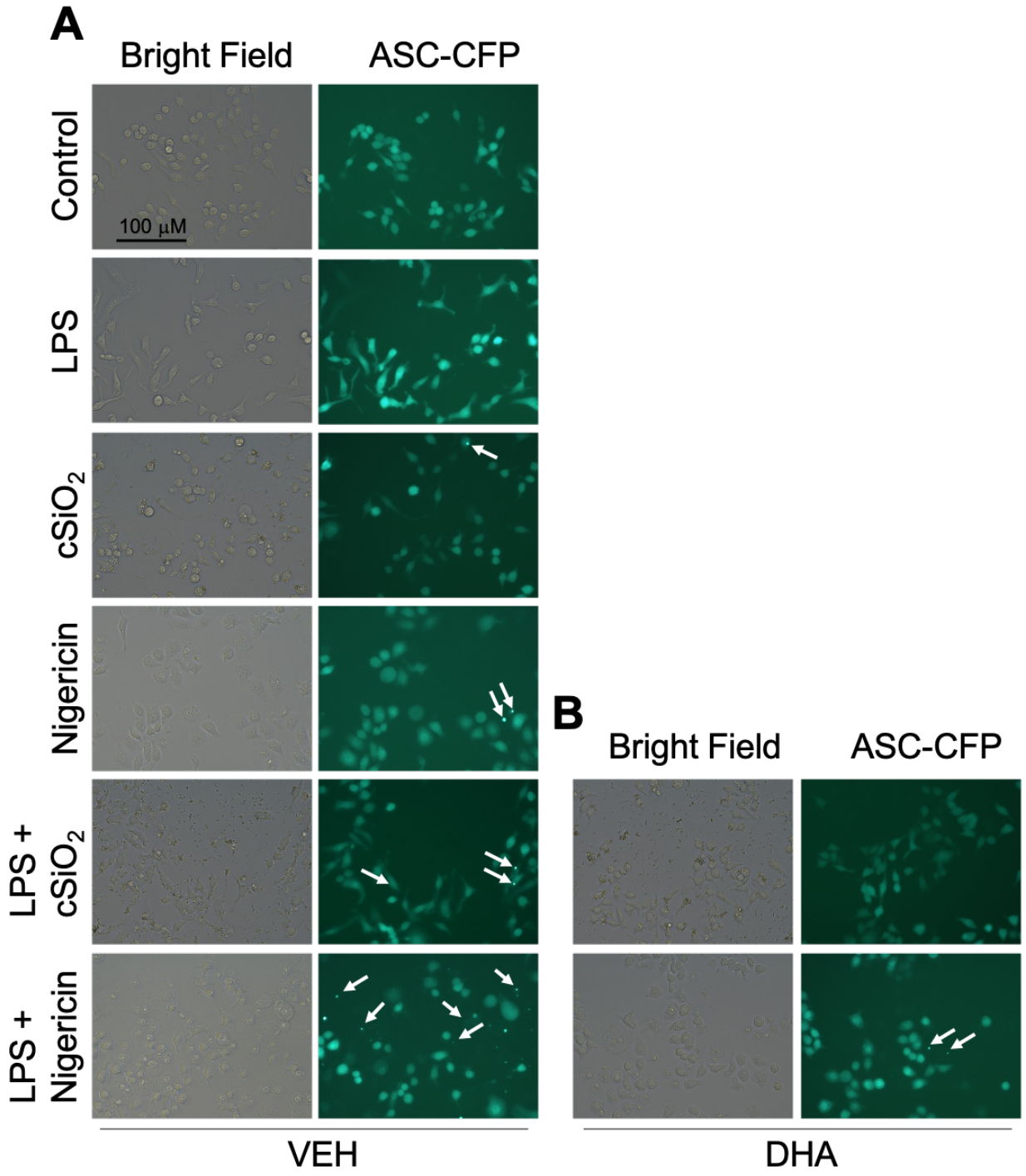


Figure C.1: Visualization of ASC-CFP specks in RAW-ASC cells stimulated with LPS, nigericin and/or $cSiO_2$. Cells were incubated in **A.** serum-deprived media containing vehicle (BSA) or **B.** 25 μM DHA for 24 h. Cells were then primed for 2 h with 500 ng/mL LPS and treated with 5 μM nigericin (45 min) or 25 μg/mL $cSiO_2$ (4 h). ASC specks (white arrows) were visualized using an EVOS FL Auto Cell Imaging System equipped with a CFP light cube. Photomicrographs representative of two independent experiments.

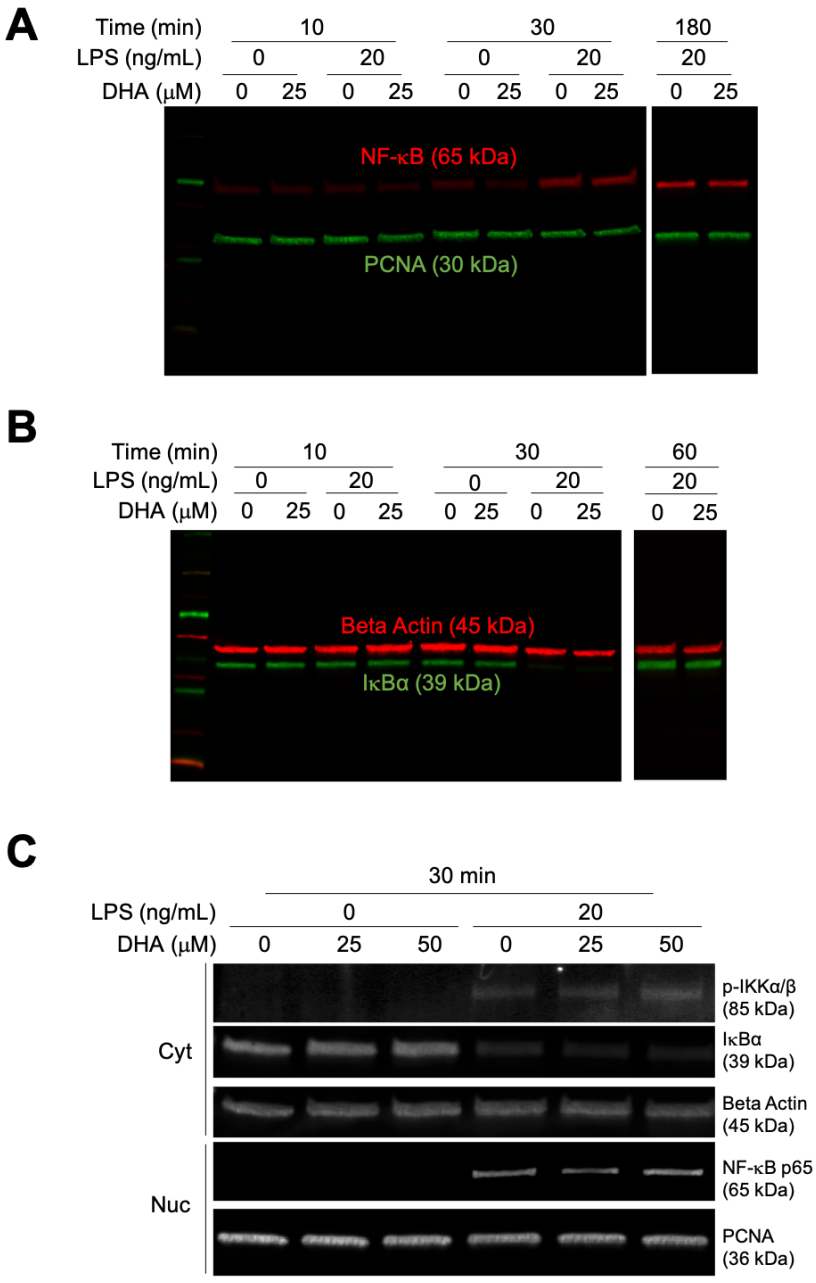


Figure C.2: Assessment of NF-κB activation. RAW-ASC cells were incubated in serum-deprived media containing the indicated concentration DHA or vehicle (BSA) for 24 h. Cells were then treated with 20 ng/mL LPS and collected at the indicated times. Cell lysates were fractionated to obtain separate cytoplasmic and nuclear extracts. **A.** NF-κB translocation was assessed by the presence of NF-κB in nuclear extracts. PCNA was used as a loading control. **B.** Canonical NF-κB signaling was assessed by IκBα degradation in cytoplasmic extracts. Beta actin was used as a loading control. **C.** Cells were treated with 20 ng/mL LPS for 30 min. In the cytoplasm, phosphorylation of IKKα/β and degradation of IκBα were measured to assess activation of the NF-κB signaling pathway. In the nucleus, the NF-κB p65 subunit was measured to evaluate nuclear translocation. Actin and PCNA were used as cytoplasmic and nuclear loading controls, respectively.

APPENDIX D

CHAPTER 5 SUPPORTING FIGURES AND TABLES

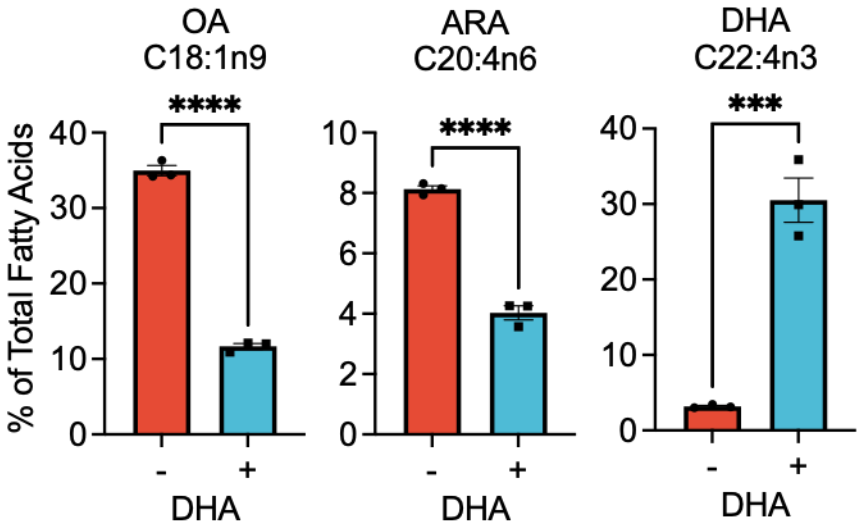


Figure D.1: DHA supplementation results in increased DHA levels in the phospholipid membrane at the expense of oleic acid and arachidonic acid. Cells were treated with 25 μM DHA or Veh (8.3 μM BSA) for 24 h. Cell pellets were collected in methanol and analyzed by gas-liquid chromatography at OmegaQuant Analytics LLC. Fatty acid levels of oleic acid (OA), arachidonic acid (ARA), and DHA expressed as a percent of all fatty acids measured. Asterisks indicate significant differences (****p<0.0001, ***p<0.001) between Veh (-) and DHA (+) treatment groups, as assessed by Student's T-tests.

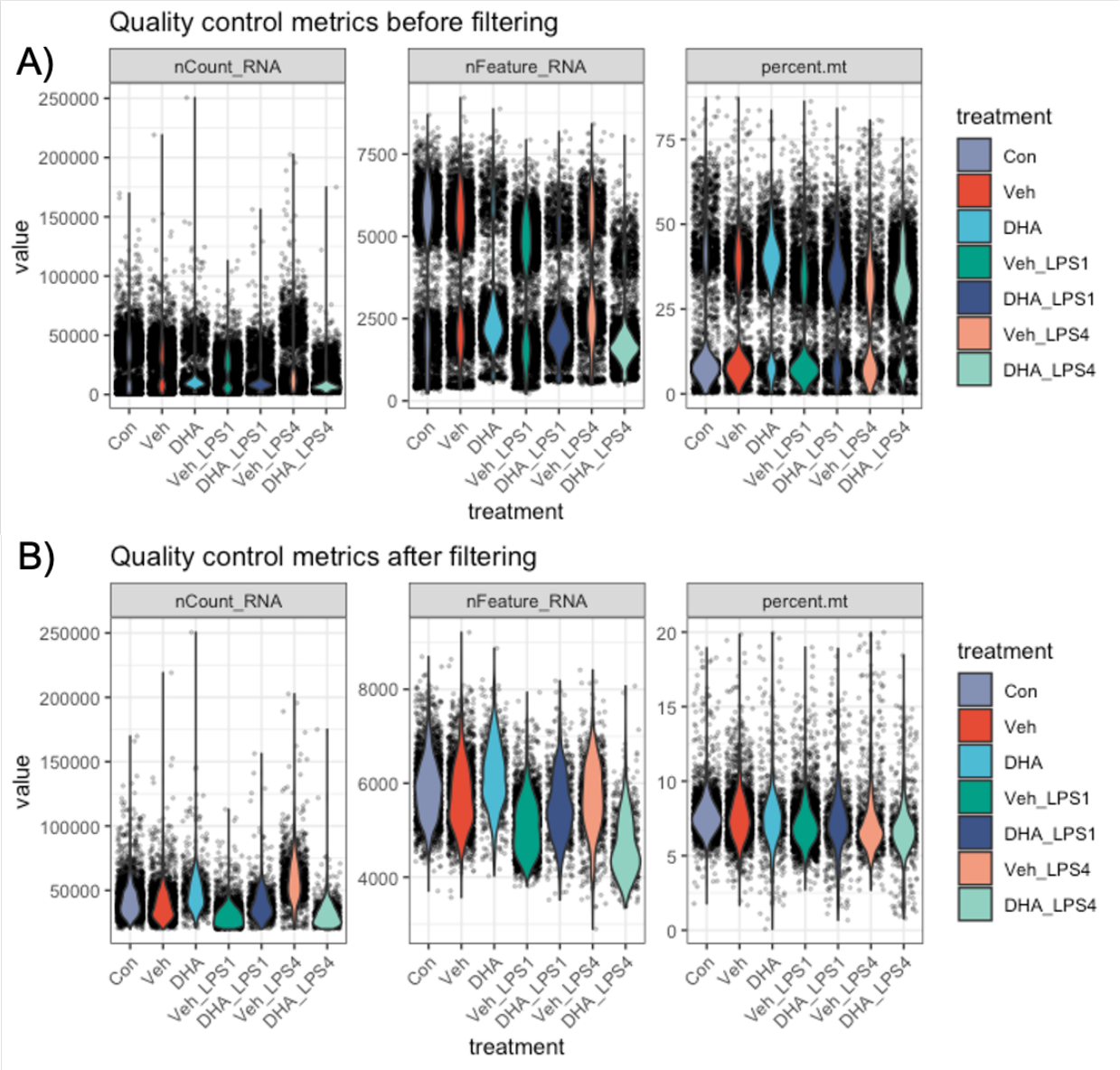


Figure D.2: Quality control metrics before and after filtering. Only high quality cells were used for downstream analysis. Low quality cells were filtered out based on the presence of excess mitochondrial RNA (>20%) and low gene counts (nCount_RNA<20,000, nFeature_RNA <3000) **(A)**. After filtering, each treatment group showed similar levels of the indicated quality control metrics **(B)**.

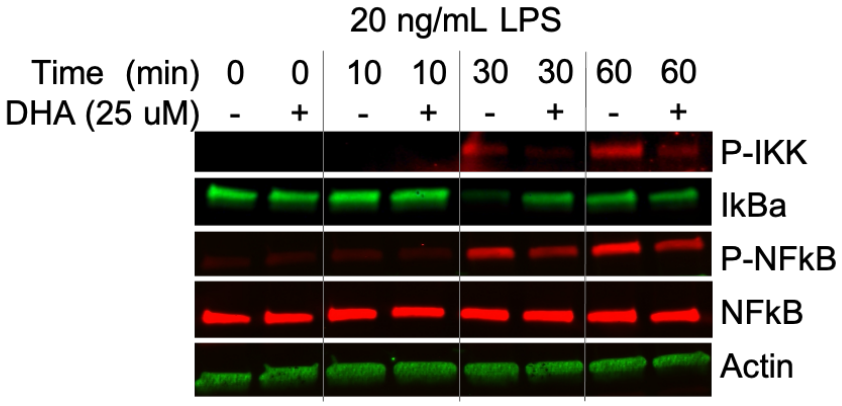


Figure D.3: DHA inhibits NFkB signaling pathway. MPI cells were treated with 20 ng/mL LPS and 25 μM DHA for the indicated times and cell lysates collected and processed for Western blots. Equal amounts of protein were loaded in each well of precast SDS-PAGE gels and proteins transferred to low-fluorescence nitrocellulose membranes. Membranes were probed for the indicated proteins and phospho-proteins and scanned using a Licor Odyssey Imaging System. Actin and non-phosphorylated proteins were used as loading controls. Representative of 3 independent experiments.

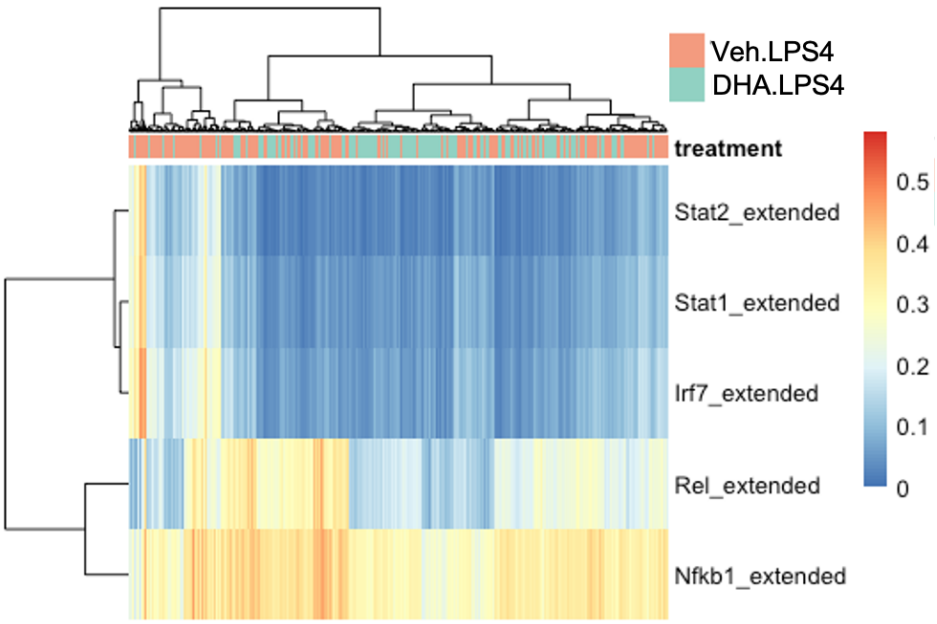


Figure D.4: Heatmap of Regulon scores reveals cluster of cells with high expression of *Stat1*, *Stat2*, and *Irf7* regulons. Regulon scores were applied to each cell. Cells in the Veh.LPS4 and Veh.DHA4 treatment groups (as indicated by the horizontal bar above the heatmap) were analyzed for *Stat2, Stat1, Irf7, Rel*, and *Nfkb1* regulons. Clustering was performed using Ward's method in the pheatmap tool in R Studio.

Table D.1: Fatty acid profile of Veh- and DHA-supplemented MPI cells.

		Veh	DHA
Fatty Acid	**Chemical formula**	*% of total fatty acids, mean±SD*	
Myristic	C14:0	2.18 ± 0.19	3.23 ± 0.43*
Palmitic	C16:0	10.76 ± 0.7	19.54 ± 5.32*
Palmitelaidic	C16:1ω7t	0.73 ± 0.34	0.57 ± 0.29
Palmitoleic	C16:1ω7	4.39 ± 0.64	0.77 ± 0.31***
Stearic	C18:0	12.85 ± 0.47	13.54 ± 3.75
Elaidic	C18:1t	1.64 ± 0.07	0.66 ± 0.64
Oleic	C18:1ω9	34.97 ± 1.17	11.68 ± 0.66***
Linolaidic	C18:2ω6t	1.68 ± 0.81	1.78 ± 0.48
LInoleic	C18:2ω6	3.10 ± 0.56	1.95 ± 0.32*
Arachidic	C20:0	0.47 ± 0.16	0.63 ± 0.20
Gamma-Linolenic	C18:3ω6	0.48 ± 0.15	0.30 ± 0.04
Eicosenoic	C20:1ω9	2.32 ± 0.21	1.25 ± 0.34**
Alpha-Linolenic	C18:3ω3	0.35 ± 0.04	0.29 ± 0.09
Eicosadienoic	C20:2ω6	0.28 ± 0.19	0.38 ± 0.18
Behenic	C22:0	1.23 ± 0.41	1.01 ± 0.22
DGLA	C20:3ω6	0.72 ± 0.21	1.14 ± 0.39
Arachidonic	C20:4ω6	8.13 ± 0.19	4.03 ± 0.40***
Lignoceric	C24:0	1.04 ± 0.34	0.71 ± 0.22
Eicosapentaenoic	C20:5ω3	0.73 ± 0.18	1.17 ± 0.35
Nervonic	C24:1ω9	0.58 ± 0.21	0.52 ± 0.32
Docosatetraenoic	C22:4ω6	3.36 ± 0.36	1.48 ± 0.22**
Docosapentaenoic-ω6	C22:5ω6	1.59 ± 0.16	0.56 ± 0.40*
Docosapentaenoic-ω6	C22:5ω3	3.19 ± 0.09	2.30 ± 0.41*
Docosahexaenoic	C22:6ω3	3.20 ± 0.21	30.53 ± 5.09***
	Total SFA	28.54 ± 1.22	38.66 ± 9.08
	Total MUFA	44.64 ± 1.70	15.45 ± 2.10***
	Total n6	19.35 ± 0.66	11.60 ± 1.68**
	Total n3	6.74 ± 0.20	33.11 ± 5.45**
	Omega-3 Index	3.93 ± 0.37	31.70 ± 5.15***
	ω-3 HUFA Score	35.26 ± 1.30	84.94 ± 0.22***

Cells were supplemented with Veh (8.3 μM BSA) or 25 μM DHA as a 3:1 complex with BSA for 24 h and cell pellets collected for fatty acid analysis by gas-liquid chromatography. Data presented as mean percent of totally fatty acids, ± SEM. ***p<0.001, **p<0.01, *p<0.05. SFA, saturated fatty acid; MUFA, monounsaturated fatty acid; PUFA, polyunsaturated fatty acid; HUFA, highly unsaturated fatty acid.

APPENDIX E

CHAPTER 6 SUPPORTING FIGURES

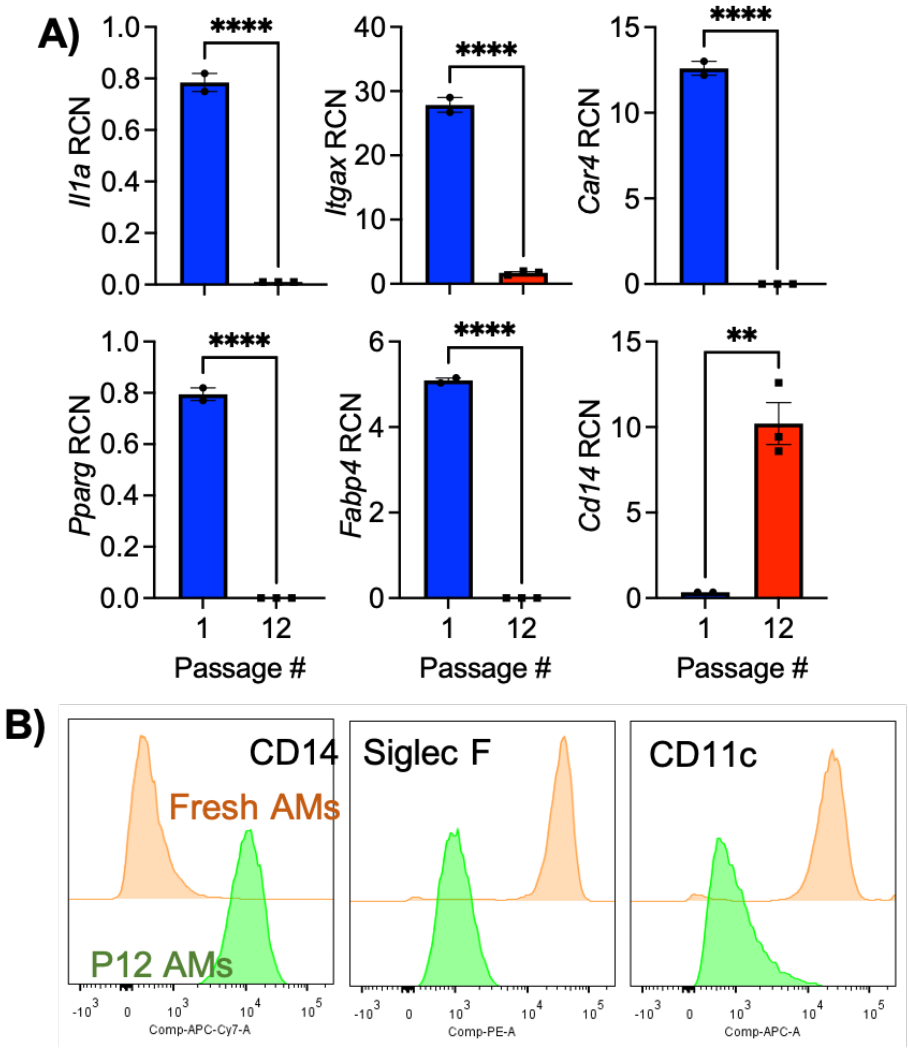


Figure E.1: AMs cultured over time lose AM-specific gene and surface marker expression. Freshly isolated alveolar macrophages (AMs) were cultured overnight (P1) or maintained in culture >2 months (P7, P12). **A.** Recently isolated AMs expressed many AM-specific genes and low levels of *Cd14*, but lose expression of AM-specific genes and gain Cd14 expression by P12. **B.** AMs lose surface expression of Siglec F and CD11c over time.

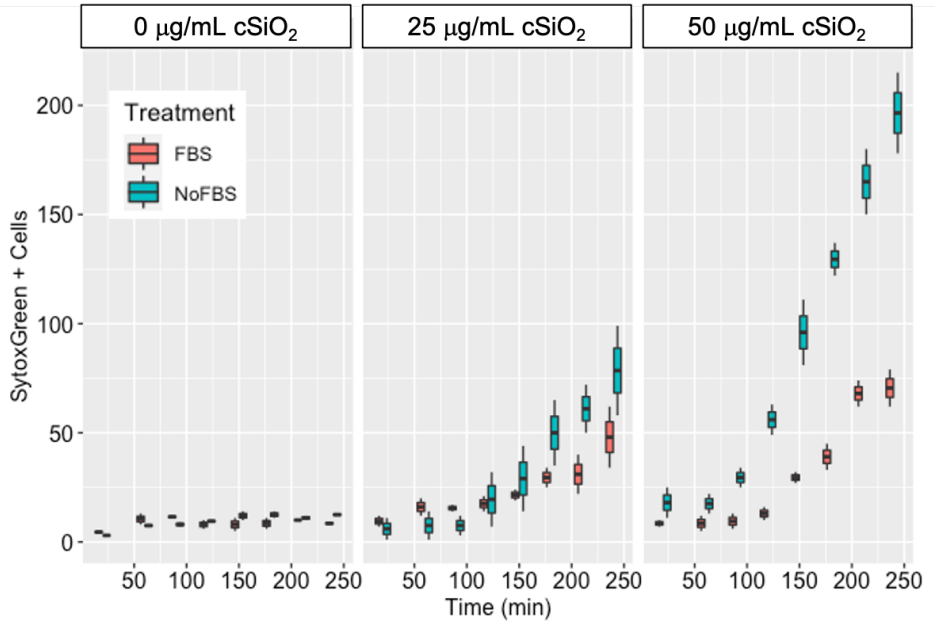


Figure E.2: FBS supplemented media slows cell death in response to $cSiO_2$. Cells were stained with 200 nM SYTOX Green in FluoroBrite DMEM containing 0 or 10% fetal bovine serum (FBS). $cSiO_2$ as a suspension in PBS was added dropwise to achieve the indicated concentrations. Images were taken at the indicated timepoints using an EVOS FL2 fluorescent microscope with an onstage temperature- and CO_2-controlled incubator. $SYTOX^+$ cells were quantified using the CellProfiler software and data.

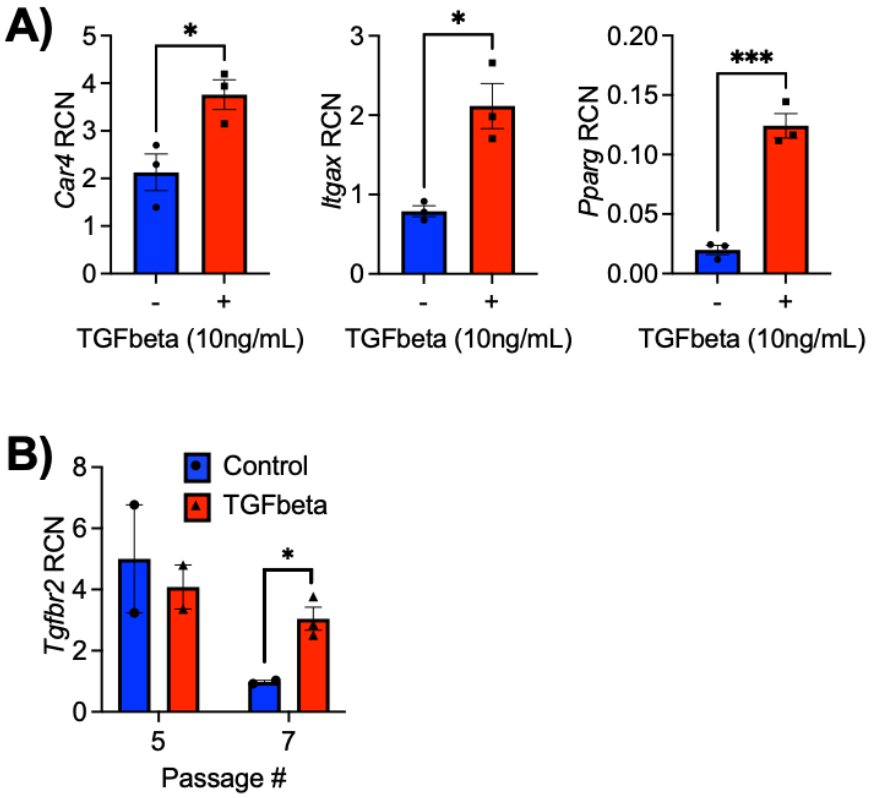


Figure E.3: Short term incubation with TGFβ increases expression of AM-specific genes. A. Early MPI cells were incubated with 10 ng/mL TGFβ for 24 h prior collecting RNA for qPCR analysis of *Car4, Itgax,* and *PPAR*γ gene expression. Asterisks indicate significant differences (***p<0.001, *p<0.05) between control and TGFβ-treated cells, as determined by Student's t-test. **B.** Expression of *Tgfbr2* in MPI and TMPI was assessed at P5 and P7. At P5, MPI still retained alveolar macrophage (AM)-likeness, at P7, they lost expression of AM-specific surface markers and gene expression, as shown in Figure 6.3B.

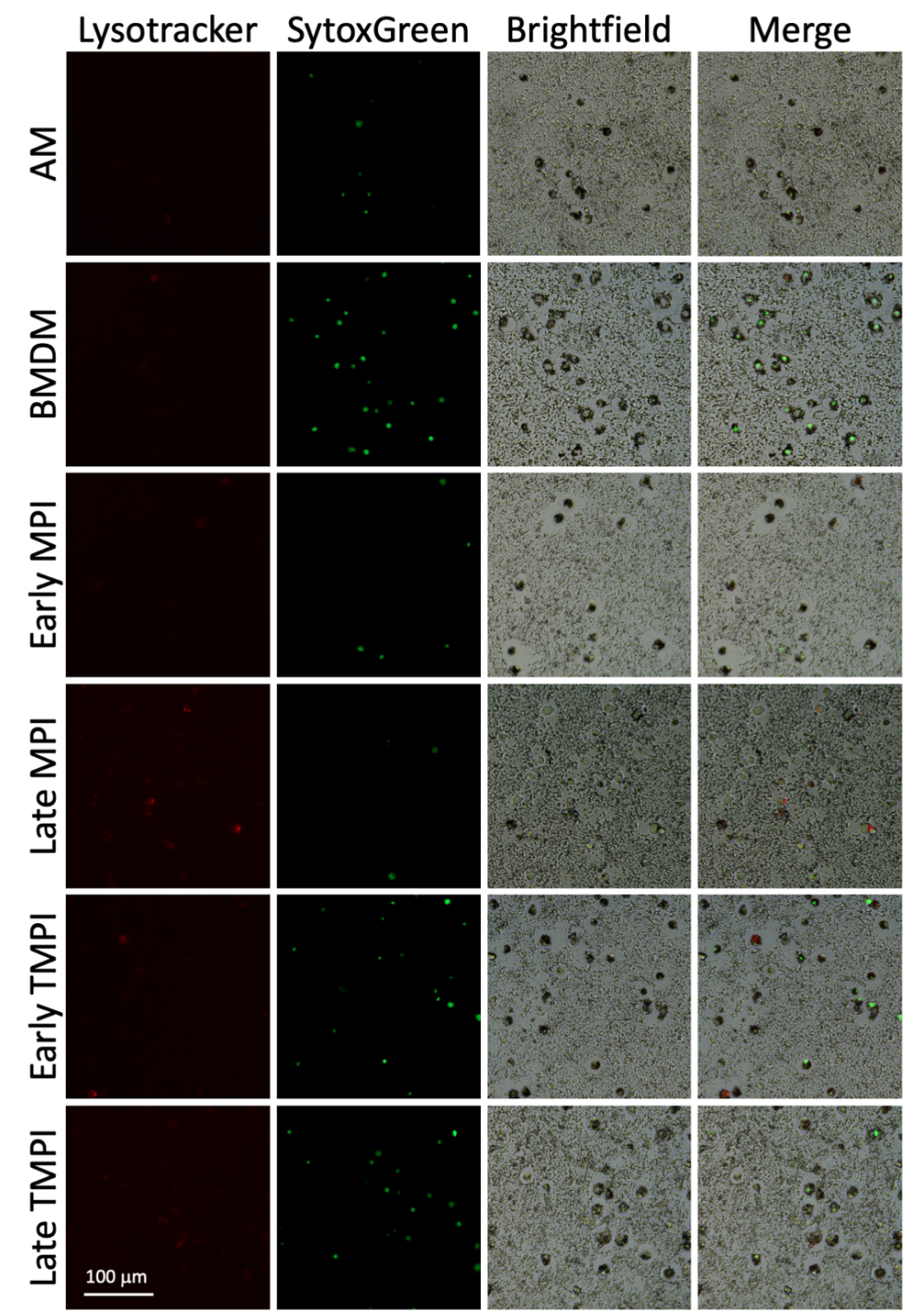


Figure E.4: Cells with high rates of $cSiO_2$ engulfment show loss of lysosomal membrane integrity following $cSiO_2$ exposure. Representative images from samples analyzed in Figure 6.4. Cells were treated with 50 μg/cm^2 $cSiO_2$ for 8 h. Late MPI cells have the highest degree of LysoTracker staining, suggesting that their reduced rate of $cSiO_2$ uptake prevented loss of lysosomal membrane integrity.

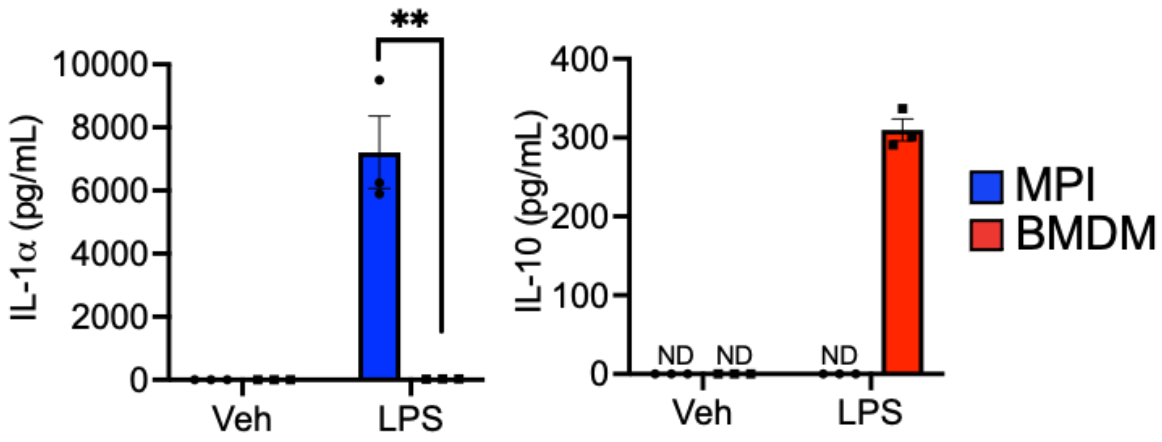


Figure E.5: MPI cells and BMDM have different patterns of cytokine release following LPS stimulation. Early MPI cells and bone marrow-derived macrophages (BMDMs) were treated with 100 ng/mL LPS for 24 h and cell-free supernatant was analyzed for release of IL-1α and IL-10 by ELISA. Asterisks indicate significant differences (**p<0.01) between MPI cells and BMDMs. ND=not detected.

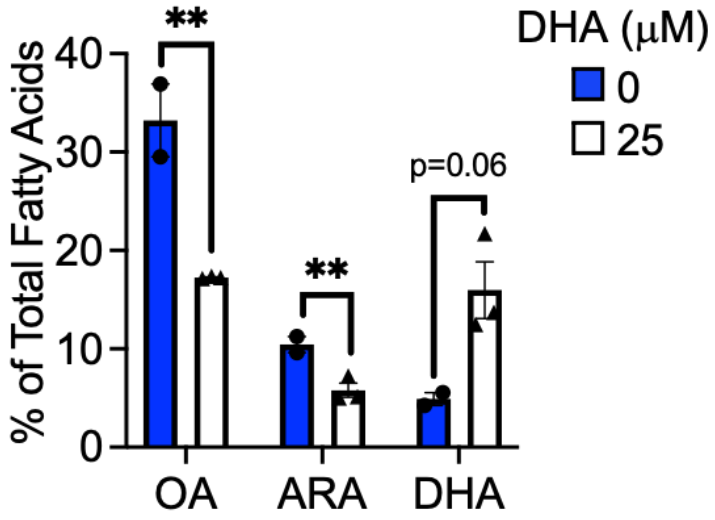


Figure E.6: DHA supplementation enhances DHA in the TMPI cell membrane at the expense of oleic acid and arachidonic acid. TMPI cells were supplemented for 24 h with Veh (8.3 μM BSA) or 25 μM DHA as a 3:1 complex with BSA and cells collected for analysis of phospholipid fatty acid content. Values presented as percent of total fatty acids, mean $\pm$ SEM. **p<0.01.

APPENDIX F

REAGENTS AND MATERIALS

F.1 Frequently Used Reagents and Materials

Item; Product Number; Manufacturer; Location

Rabbit anti-CD3 polyclonal antibody; ab5690; Abcam; Cambridge, MA

Nuclear Extract Kit; 40010; Active Motif; Carlsbad, CA

TransAM® PPARγ Transcription Factor ELISA kit; 40196; Active Motif; Carlsbad, CA

Mouse anti-mouse IL-1α antibody; AG-20B-0064-C100; AdipoGen; San Diego, CA

Gas Chromatography Capillary Column; DB-23; Agilent J&W; Santa Clara, CA

Mouse RBC lysis buffer; J62150; Alfa Aesar; Ward Hill, MA

RBC lysis buffer for mouse; J62150; Alfa Aesar; Waltham, MA

Anti-dsDNA IgG ELISA; 5120; Alpha Diagnostics; San Antonio, TX

High Capacity RNA to cDNA RT Kit; 4387406; Applied Biosystems; Waltham, MA

Accutase; 561527; BD Biosciences; Franklin Lakes, NJ

Rat anti-mouse CD45R monoclonal antibody; 550286; Becton Dickenson; Franklin Lakes, NJ

APC anti-mouse CD11c; 11730; Biolegend; San Diego, CA

APC/Cy7 anti-mouse CD14; 123317; Biolegend; San Diego, CA

Mouse FC Block; 101319; Biolegend; San Diego, CA

PE anti-mouse CD170; 155505; Biolegend; San Diego, CA

4-20% TGX precast protein gel; 4561094; BioRad; Hercules, CA

10x TGS Running buffer; 1610732; BioRad; Hercules, CA

Gel transfer stacks (RTA Mini PVDF Transfer Kit); 1704272; BioRad; Hercules, CA

TransBlot Turbo; 1704510; BioRad; Hercules, CA

Trans-Blot® Turbo™ RTA Mini PVDF transfer kit; 1704274; BioRad; Hercules, CA

Mouse anti-mouse IκBα Antibody; 4814; Cell Signaling Technology; Danvers, MA

Mouse anti-mouse PCNA antibody; 2586; Cell Signaling Technology; Danvers, MA

Rabbit anti-mouse beta-actin antibody; 4970; Cell Signaling Technology; Danvers, MA

Rabbit anti-mouse GAPDH Antibody; 3907; Cell Signaling Technology; Danvers, MA

Rabbit anti-mouse IL-1α Antibody; 50794; Cell Signaling Technology; Danvers, MA

Rabbit anti-mouse NF-κB p65 Antibody; 8242; Cell Signaling Technology; Danvers, MA

Rabbit anti-mouse phosphoIKKα/β Cell Antibody; 2697; Cell Signaling Technology; Danvers, MA

Urine reagent strip; URS-1P; Cortez diagnostics; Calabasas, CA

Circular coverslips ; 72196-12; Electron Microscopy Sciences; Hatfield, PA

DMEM; 11965092; Gibco; Waltham, MA

RPMI; 21875034; Gibco; Grand Island, NY

Fetal Bovine Serum; 100099141; Gibco; Waltham, MA

Phenol red-free RPMI 1640; 11835030; Gibco; Waltham, MA

Low Fluorescence PVDF membrane; IPFL00010; Immobilon-FL; Billerica, MA

FAM-FLICA Caspase 1 Assay Kit; 97; Immuno-Chemistry Technologies; Bloomington, MN

Blasticidin; ant-bl-05; Inivogen; San Diego, CA

0.5 M EDTA; 15575-038; Invitrogen; Grand Island, NY

Lipofectamine 2000; 11668030; Invitrogen; Carlsbad, CA

Penicillin-Streptomycin; 15140122; Invitrogen; Carlsbad, CA

Alum Crystals; tlrl-alk; Invivogen; San Diego, CA

Monosodium Urate Crystals; tlrl-msu; Invivogen; San Diego, CA

Bovine Serum Albumin; A3912-100G; Millipore Sigma; Burlington, MA

Dulbecco's Phosphate Buffered Saline; D8537; Millipore Sigma; Burlington, MA

Fatty acid-free Bovine Serum Albumin (BSA); A8806 5G; Millipore Sigma; Burlington, MA

Lipopolysaccharide from Salmonella Enterica; L6143; Millipore Sigma; Burlington, MA

Methanolic BF3; 61626; Millipore Sigma; Burlington, MA

Nigericin; N7143; Millipore Sigma; Burlington, MA

Triton X-100; T8787; Millipore Sigma; Burlington, MA

Docosahexaenoic Acid; U-84-A; NuChek Prep; Elysian, MN

Fatty acid Standard Mix; GLC682; NuChek Prep; Elysian, MN

Heptadecanoic Acid Standard; N-17-A; NuChek Prep; Elysian, MN

hTGFbeta; 100-21; Peprotech; Cranbury, NJ

mGM-CSF; 315-03; Peprotech; Cranbury, NJ

RNeasy Isolation Kit; 74106; Qiagen; Germantown, MD

RNEasy Mini Kit; 74104; Qiagen; Germantown, MD

Fetal Bovine Serum; S11150H; R&D Systems; Minneapolis, MN

Goat anti-mouse IL-1β Antibody; AF-401-NA; R&D Systems; Minneapolis, MN

IL-1α DuoSet ELISA; DY400; R&D Systems; Minneapolis, MN

IL-1β DuoSet ELISA; DY401; R&D Systems; Minneapolis, MN

Mouse GM-CSF DuoSet ELISA; DY415; R&D Systems; Minneapolis, MN

Mouse IL-1 alpha/IL-1F1 DuoSet ELISA; DY400; R&D Systems; Minneapolis, MN

Mouse IL-1 beta/IL-1F2 Duoset ELISA; DY401; R&D Systems; Minneapolis, MN

Mouse IL-10 DuoSet ELISA; DY417; R&D Systems; Minneapolis, MN

Tri Reagent; 93289; Sigma Aldrich; St. Louis, MO

Sytems Three Quick Cure 5 epoxy glue; 1000A000, 1000B00; Systems 3 Resins; Auburn WA

Halt Protease and Phosphatase inhibitor; 78440; Thermo Fisher; Rockford, IL

High Capacity Reverse Transcriptase kit; 4368814; Thermo Fisher; Carlsbad, CA

LysoTracker Red; L7528; Thermo Fisher; Carlsbad, CA

Penn-Strep; 15140122; Thermo Fisher; Carlsbad, CA

Pierce BCA Protein Assay; 23225; Thermo Fisher; Rockford, IL

RIPA buffer; 89900; Thermo Fisher; Rockford, IL

SYTOX Green; S7020; Thermo Fisher; Carlsbad, CA

TaqMan Gene Expression Master Mix; 4304437; Thermo Fisher; Carlsbad, CA

Halt Protease Inhibitor; 87785; Thermo Fisher Scientific; Waltham, MA

High-capacity cDNA Reverse Transcription Kit; 4368814; Thermo Fisher Scientific; Waltham,

MA

iBind Flex Western Blot System; SLF2000; Thermo Fisher Scientific; Waltham, MA

Mouse FAM-MGB Taqman probes; 4331182; Thermo Fisher Scientific; Waltham, MA

Immune Monitoring 48-plex ProcarataPlex Mouse Luminex Bead-based Immunoassay; EPX480-20834-901; Thermo Fisher Scientific; Waltham, MA

NE-PER Nuclear and Cytoplasmic Extraction Reagents; 78833; Thermo Fisher Scientific; MA

Pierce BCA Protein Assay Kit; 23225; Thermo Fisher Scientific; Waltham, MA

Pierce™ TMB Substrate Kit; 34021; Thermo Fisher Scientific; Waltham, MA

RNAlater; AM7020; Thermo Fisher Scientific; Waltham, MA

TaqMan Fast Advanced Master Mix; 4444963; Thermo Fisher Scientific; Waltham, MA

FluoroBrite DMEM; A1896701; Thermo Fisher Scientific; Carlsbad, CA

Silica; Min-U-Sil-5; U.S. Silica; Pittsburgh, PA

RNA Clean and Concentrator Kit; R1017; Zymo Research; Irvine, CA

F.2 Frequently used Taqman Probes (all Mouse, FAM-MGB)

Gene; Probe Code

Ifi27; Mm00835449_g1

Ifi44; Mm00505670_m1

Ifih1; Mm00459183_m1

Ifit1; Mm00515153_m1

Ifit3; Mm01704846_s1

Ifitm3; Mm00847057_s1

Stat1; Mm01257286_m1

Stat2; Mm00490880_m1

Irf7; Mm00516793_g1

Irf9; Mm00492679_m1

Isg15; Mm01705338_s1

Isg20; Mm00469585_m1

Mx1; Mm00487796_m1

Oas2; Mm00460961_m1

Oasl1; Mm00455081_m1

Rsad2; Mm00491265_m1

Sqstm1; Mm00448091_m1

Hmox1; Mm00516004_m1

Oas1a; Mm00836412_m1

Cxcl5; Mm00436451_g1

Cxcl13; Mm0421485_s1

Tgfb1; Mm01178820_m1

Tgfbr1; Mm00436964_m1

Tgfbr2; Mm03024091_m1

Cd14; Mm00438094_g1

Siglecf; Mm00523987_m1

Marco; Mm00440265_m1

Pparg; Mm00440945_m1

Car4; Mm00483021_m1

Fabp4; Mm00445880_m1

Itgax; Mm0498708_g1

Itgam; Mm00434455_m1

Cd36; Mm00432403_m1

Epcam; Mm00493214_m1

Itga3; Mm00442910_m1

Mrc1; Mm01329359_m1

Il1a; Mm00439621_m1

Il1b; Mm00434228_m1

Gapdh; Mm99999915_g1

Caspase-1; Mm00438023_m1

Gapdh; Mm99999915_g1

APPENDIX G

FULL LIST OF PUBLISHED MANUSCRIPTS

Pestka JJ, Akbari P, Wierenga KA, Bates MA, Gilley KN, Wagner JG, Lewandowski RP, Rajasinghe LD, Chauhan PS, Lock AL, Li Q, Harkema JR. "Docosahexaenoic Acid Supplementation as an Intervention Against Established Autoimmunity in a Murine Model of Toxicant-Triggered Lupus Flaring". Front Immunol. (2021). **Contribution:** Necropsy, figure preparation, manuscript writing

Chauhan PS, Wagner JG, Benninghoff AD, Lewandowski RK, Favor OK, Wierenga KA, Gilley KN, Ross EA, Harkema JR, Pestka JJ. "Rapid Induction of Pulmonary Inflammation, Autoimmune Gene Expression, and Ectopic Lymphoid Neogenesis Following Acute Silica Exposure in Lupus-Prone Mice". Front Immunol. (2021). **Contribution:** *In vivo* $cSiO_2$ exposures, necropsy, manuscript preparation

Rajasinghe LD, Chauhan PS, Wierenga KA, Evered AO, Harris S, Gavrilin MA, Pestka JJ. "Omega-3 docosahexaenoic acid (DHA) impedes silica-induced macrophage corpse accumulation by attenuating cell death and potentiating efferocytosis". Front Immunol. (2020). **Contribution:** Development of *in vitro* cell model, manuscript preparation

Wierenga KA, Bates MA, Lock AL, Strakovsky RS, Rajasinghe LD, Harkema JR, Holian A, Pestka JJ. "Requisite Omega-3 HUFA Biomarker Thresholds for Preventing Murine Lupus Flaring". Front Immunol. (2020). **(Thesis Chapter 3)**

Rajasinghe LD, Li Q, Zhu C, Yan M, Chauhan PS, Wierenga KA, Bates MA, Holian A, Harkema JR, Benninghoff AD, and Pestka JJ. "Increasing Omega-3 Index Suppresses Broad Autoantibody Repertoire Induced by Silica in Lupus-Prone Mice". Autoimmunity. (2020). **Contribution:** Data

analysis, figure preparation, manuscript preparation

Gilley KN*, Wierenga KA*, Chauhuan PS, Wagner JG, Lewandowski RP, Ross EA, Lock AL, Harkema JR, Benninghoff AD, Pestka JJ. "Docosahexaenoic acid supplementation prevents silica-triggered lupus flaring in NZBWF1 mice fed the Total Western Diet". PLos One. (2020). *Co-first authors **(Thesis Chapter 2)**

Wierenga KA, Harkema JR, Pestka JJ. "Lupus, Silica, and Dietary Omega-3 Fatty Acid Interventions". Toxicol Pathol. (2019). Review Article. **(Thesis Chapter 1)**

Wierenga KA, Wee J, Gilley KN, Rajasinghe LD, Bates MA, Gavrilin MA, Holian A, Pestka JJ. "Docosahexaenoic Acid Suppresses Silica-induced NRLP3 Inflammasome Activation and Release of IL-1 Cytokines but not Cell Death in the Macrophage". Front Immunol. (2019). **(Thesis Chapter 4)**

Benninghoff AD, Bates MA, Wierenga KA, Gilley KN, Holian A, Harkema JR, Pestka JJ. "Docosahexaenoic Acid Consumption Impedes Early Interferon- and Chemokine- related Gene Expression While Suppressing Silica-Triggered Flaring of Murine Lupus". Front Immunol. (2019). **Contribution:** Analysis and presentation of fatty acid data, manuscript preparation

Bates MA, Akbari P, Gilley KN, Jackson-Humbles DN, Wagner JG, Li N, Kopec AK, Wierenga KA, Brandenberger C, Holian A, Benninghoff AD, Harkema JR, Pestka JJ. "Dietary docosahexaenoic acid prevents silica-induced development of pulmonary ectopic germinal centers and glomerulonephritis in the lupus-prone NZBWF1 mouse". Front Immunol. (2018). **Contribution:** Analysis and presentation of fatty acid data, manuscript preparation

BIBLIOGRAPHY

BIBLIOGRAPHY

[1] M. Pristner and B. Warth. “Drug-Exposome Interactions: The Next Frontier in Precision Medicine”. In: *Trends Pharmacol Sci* 41.12 (2020), pp. 994–1005. ISSN: 1873-3735 (Electronic) 0165-6147 (Linking). DOI: 10.1016/j.tips.2020.09.012. URL: https://www.ncbi.nlm.nih.gov/pubmed/33186555.

[2] C. G. Parks and G. S. Cooper. “Occupational exposures and risk of systemic lupus erythematosus”. In: *Autoimmunity* 38.7 (2005), pp. 497–506. ISSN: 0891-6934. DOI: 10.1080/08916930500285493. URL: %3CGo%20to%20ISI%3E://000233776800005%20http://informahealthcare.com/doi/abs/10.1080/08916930500285493.

[3] Melissa A. Bates et al. “Silica triggers inflammation and ectopic lymphoid neogenesis in the lungs in parallel with accelerated onset of systemic autoimmunity and glomerulonephritis in the lupus-prone NZBWF1 mouse”. In: *PLoS ONE* 10.5 (2015), e0125481. DOI: 10.1371/journal.pone.0125481. URL: http://dx.doi.org/10.1371%2Fjournal.pone.0125481%20https://www.ncbi.nlm.nih.gov/pmc/articles/PMC4433215/pdf/pone.0125481.pdf.

[4] M. A. Bates et al. “Dietary Docosahexaenoic Acid Prevents Silica-Induced Development of Pulmonary Ectopic Germinal Centers and Glomerulonephritis in the Lupus-Prone NZBWF1 Mouse”. In: *Front Immunol* 9 (2018), p. 2002. ISSN: 1664-3224 (Electronic) 1664-3224 (Linking). DOI: 10.3389/fimmu.2018.02002. URL: https://www.ncbi.nlm.nih.gov/pubmed/30258439.

[5] G. Ruiz-Irastorza, A. Danza, and M. Khamashta. “Glucocorticoid use and abuse in SLE”. In: *Rheumatology (Oxford)* 51.7 (2012), pp. 1145–53. ISSN: 1462-0332 (Electronic) 1462-0324 (Linking). DOI: 10.1093/rheumatology/ker410. URL: https://www.ncbi.nlm.nih.gov/pubmed/22271756.

[6] H. J. Anders et al. “Lupus nephritis”. In: *Nat Rev Dis Primers* 6.1 (2020), p. 7. ISSN: 2056-676X (Electronic) 2056-676X (Linking). DOI: 10.1038/s41572-019-0141-9. URL: https://www.ncbi.nlm.nih.gov/pubmed/31974366.

[7] M. A. Bates et al. “Silica-triggered autoimmunity in lupus-prone mice blocked by docosahexaenoic acid consumption”. In: *PLoS One* 11.8 (2016), e0160622. ISSN: 1932-6203 (Electronic) 1932-6203 (Linking). DOI: 10.1371/journal.pone.0160622. URL: https://www.ncbi.nlm.nih.gov/pubmed/27513935.

[8] K.N. Gilley et al. “Influence of total western diet on docosahexaenoic acid suppression of silica-triggered lupus flaring in NZBWF1 mice”. In: *PLoS One* (In Press) (2020).

[9] G. J. Pons-Estel, M. F. Ugarte-Gil, and G. S. Alarcon. “Epidemiology of systemic lupus erythematosus”. In: *Expert Rev Clin Immunol* 13.8 (2017), pp. 799–814. ISSN: 1744-8409 (Electronic) 1744-666X (Linking). DOI: 10.1080/1744666x.2017.1327352.

[10] L. Durcan, T. O'Dwyer, and M. Petri. "Management strategies and future directions for systemic lupus erythematosus in adults". In: *Lancet* 393.10188 (2019), pp. 2332–2343. ISSN: 1474-547X (Electronic) 0140-6736 (Linking). DOI: 10.1016/S0140-6736(19)30237-5. URL: https://www.ncbi.nlm.nih.gov/pubmed/31180030.

[11] C. G. Parks et al. "Expert panel workshop consensus statement on the role of the environment in the development of autoimmune disease". In: *Int J Mol Sci* 15.8 (2014), pp. 14269–97. ISSN: 1422-0067 (Electronic) 1422-0067 (Linking). DOI: 10.3390/ijms150814269. URL: https://www.ncbi.nlm.nih.gov/pubmed/25196523.

[12] P. Charoenwoodhipong et al. "Dietary omega polyunsaturated fatty acid intake and patient-reported outcomes in systemic lupus erythematosus: The Michigan Lupus Epidemiology Surveillance (MILES) Program". In: *Arthritis Care Res (Hoboken)* (2019). ISSN: 2151-4658 (Electronic) 2151-464X (Linking). DOI: 10.1002/acr.23925. URL: https://www.ncbi.nlm.nih.gov/pubmed/31074595.

[13] B. C. Doney et al. "Estimation of the number of workers exposed to respirable crystalline silica by industry: Analysis of OSHA compliance data (1979-2015)". In: *Am J Ind Med* 63.6 (2020), pp. 465–477. ISSN: 1097-0274 (Electronic) 0271-3586 (Linking). DOI: 10.1002/ajim.23109. URL: https://www.ncbi.nlm.nih.gov/pubmed/32270550.

[14] C. C. Leung, I. T. Yu, and W. Chen. "Silicosis". In: *Lancet* 379.9830 (2012), pp. 2008–18. ISSN: 1474-547X (Electronic) 0140-6736 (Linking). DOI: 10.1016/S0140-6736(12)60235-9. URL: https://www.ncbi.nlm.nih.gov/pubmed/22534002.

[15] R. A. Cohen et al. "Lung Pathology in U.S. Coal Workers with Rapidly Progressive Pneumoconiosis Implicates Silica and Silicates". In: *Am J Respir Crit Care Med* 193.6 (2016), pp. 673–80. ISSN: 1535-4970 (Electronic) 1073-449X (Linking). DOI: 10.1164/rccm.201505-1014OC. URL: https://www.ncbi.nlm.nih.gov/pubmed/26513613.

[16] H. Kawasaki. "A review of the fate of inhaled alpha-quartz in the lungs of rats". In: *Inhal Toxicol* 31.1 (2019), pp. 25–34. ISSN: 1091-7691 (Electronic) 0895-8378 (Linking). DOI: 10.1080/08958378.2019.1597218. URL: https://www.ncbi.nlm.nih.gov/pubmed/30997849.

[17] H. Kawasaki. "A mechanistic review of silica-induced inhalation toxicity". In: *Inhal Toxicol* 27.8 (2015), pp. 363–77. ISSN: 1091-7691 (Electronic) 0895-8378 (Linking). DOI: 10.3109/08958378.2015.1066905. URL: https://www.ncbi.nlm.nih.gov/pubmed/26194035.

[18] J. M. Brown, J. C. Pfau, and A. Holian. "Immunoglobulin and lymphocyte responses following silica exposure in New Zealand mixed mice". In: *Inhal Toxicol* 16.3 (2004), pp. 133–9. ISSN: 0895-8378 (Print) 0895-8378 (Linking). DOI: 10.1080/08958370490270936. URL: https://www.ncbi.nlm.nih.gov/pubmed/15204774.

[19] C. G. Parks and G. S. Cooper. “Occupational exposures and risk of systemic lupus erythematosus: a review of the evidence and exposure assessment methods in population- and clinic-based studies”. In: *Lupus* 15.11 (2006), pp. 728–36. ISSN: 0961-2033 (Print) 0961-2033 (Linking). DOI: 10.1177/0961203306069346. URL: https://www.ncbi.nlm.nih.gov/pubmed/17153843.

[20] A. B. Hill. “The Environment and Disease: Association or Causation?” In: *Proc R Soc Med* 58 (1965), pp. 295–300. ISSN: 0035-9157 (Print) 0035-9157 (Linking). URL: https://www.ncbi.nlm.nih.gov/pubmed/14283879.

[21] A. Gioxari et al. “Intake of omega-3 polyunsaturated fatty acids in patients with rheumatoid arthritis: A systematic review and meta-analysis”. In: *Nutrition* 45 (2018), 114–124 e4. ISSN: 1873-1244 (Electronic) 0899-9007 (Linking). DOI: 10.1016/j.nut.2017.06.023. URL: https://www.ncbi.nlm.nih.gov/pubmed/28965775.

[22] P. C. Calder. “Marine omega-3 fatty acids and inflammatory processes: Effects, mechanisms and clinical relevance”. In: *Biochim Biophys Acta* 1851.4 (2015), pp. 469–484. ISSN: 0006-3002 (Print) 0006-3002. DOI: 10.1016/j.bbalip.2014.08.010. URL: http://ac.els-cdn.com/S1388198114001656/1-s2.0-S1388198114001656-main.pdf?_tid=621ecfd0-4628-11e7-96c9-00000aacb362&acdnat=1496252671_a7ee29c5742104f4c777d18547e81184.

[23] J. J. Pestka. “n-3 polyunsaturated fatty acids and autoimmune-mediated glomerulonephritis”. In: *Prostaglandins Leukot Essent Fatty Acids* 82.4-6 (2010), pp. 251–8. ISSN: 1532-2823 (Electronic) 0952-3278 (Linking). DOI: 10.1016/j.plefa.2010.02.013. URL: http://www.ncbi.nlm.nih.gov/pubmed/20189790%20https://www.ncbi.nlm.nih.gov/pmc/articles/PMC2885141/pdf/nihms181390.pdf.

[24] W. S. Harris et al. “Blood n-3 fatty acid levels and total and cause-specific mortality from 17 prospective studies”. In: *Nat Commun* 12.1 (2021), p. 2329. ISSN: 2041-1723 (Electronic) 2041-1723 (Linking). DOI: 10.1038/s41467-021-22370-2. URL: https://www.ncbi.nlm.nih.gov/pubmed/33888689.

[25] J. T. Brenna. “Efficiency of conversion of alpha-linolenic acid to long chain n-3 fatty acids in man”. In: *Curr Opin Clin Nutr Metab Care* 5.2 (2002), pp. 127–32. ISSN: 1363-1950 (Print) 1363-1950 (Linking). DOI: 10.1097/00075197-200203000-00002. URL: https://www.ncbi.nlm.nih.gov/pubmed/11844977.

[26] S. V. Thuppal et al. “Discrepancy between Knowledge and Perceptions of Dietary Omega-3 Fatty Acid Intake Compared with the Omega-3 Index”. In: *Nutrients* 9.9 (2017). ISSN: 2072-6643 (Electronic) 2072-6643 (Linking). DOI: 10.3390/nu9090930. URL: https://www.ncbi.nlm.nih.gov/pubmed/28837086.

[27] Y. Papanikolaou et al. “U.S. adults are not meeting recommended levels for fish and omega-3 fatty acid intake: results of an analysis using observational data from NHANES 2003-

2008". In: *Nutr J* 13 (2014), p. 31. ISSN: 1475-2891 (Electronic) 1475-2891 (Linking). DOI: 10.1186/1475-2891-13-31. URL: https://www.ncbi.nlm.nih.gov/pubmed/24694001.

[28] L. M. Browning et al. "Incorporation of eicosapentaenoic and docosahexaenoic acids into lipid pools when given as supplements providing doses equivalent to typical intakes of oily fish". In: *Am J Clin Nutr* 96.4 (2012), pp. 748–58. ISSN: 1938-3207 (Electronic) 0002-9165 (Linking). DOI: 10.3945/ajcn.112.041343. URL: https://www.ncbi.nlm.nih.gov/pubmed/22932281.

[29] R. Micha et al. "Global, regional, and national consumption levels of dietary fats and oils in 1990 and 2010: a systematic analysis including 266 country-specific nutrition surveys". In: *BMJ* 348 (2014), g2272. ISSN: 1756-1833 (Electronic) 0959-8138 (Linking). DOI: 10.1136/bmj.g2272. URL: https://www.ncbi.nlm.nih.gov/pubmed/24736206.

[30] T. C. Clarke et al. "Trends in the use of complementary health approaches among adults: United States, 2002-2012". In: *Natl Health Stat Report* 79 (2015), pp. 1–16. ISSN: 2164-8344 (Print) 2164-8344 (Linking). URL: https://www.ncbi.nlm.nih.gov/pubmed/25671660.

[31] P. C. Calder. "Omega-3 fatty acids and inflammatory processes: from molecules to man". In: *Biochem Soc Trans* 45.5 (2017), pp. 1105–1115. ISSN: 1470-8752 (Electronic) 0300-5127 (Linking). DOI: 10.1042/bst20160474.

[32] U. Akbar et al. "Omega-3 fatty acids in rheumatic diseases: a critical review". In: *J Clin Rheumatol* 23.6 (2017), pp. 330–339. ISSN: 1536-7355 (Electronic) 1076-1608 (Linking). DOI: 10.1097/rhu.0000000000000563. URL: http://ovidsp.tx.ovid.com/ovftpdfs/FPDDNCIBCDDMPB00/fs047/ovft/live/gv024/00124743/00124743-201709000-00006.pdf.

[33] S. P. Crampton, P. A. Morawski, and S. Bolland. "Linking susceptibility genes and pathogenesis mechanisms using mouse models of systemic lupus erythematosus". In: *Dis Model Mech* 7.9 (2014), pp. 1033–46. ISSN: 1754-8411 (Electronic) 1754-8403 (Linking). DOI: 10.1242/dmm.016451. URL: https://www.ncbi.nlm.nih.gov/pubmed/25147296.

[34] E. L. Dubois et al. "NZB/NZW mice as a model of systemic lupus erythematosus". In: *JAMA* 195.4 (1966), pp. 285–9. ISSN: 0098-7484 (Print) 0098-7484 (Linking). URL: https://www.ncbi.nlm.nih.gov/pubmed/4159181.

[35] J. J. Pestka et al. "Comparative effects of n-3, n-6 and n-9 unsaturated fatty acid-rich diet consumption on lupus nephritis, autoantibody production and CD4+ T cell-related gene responses in the autoimmune NZBWF1 mouse". In: *PloS one* 9.6 (2014), e100255. ISSN: 1932-6203 (Electronic) 1932-6203 (Linking). DOI: 10.1371/journal.pone.0100255. URL: http://www.ncbi.nlm.nih.gov/pubmed/24945254%20https://www.ncbi.nlm.nih.gov/pmc/articles/PMC4063768/pdf/pone.0100255.pdf.

[36] E. Corsiero et al. “Ectopic Lymphoid Structures: Powerhouse of Autoimmunity”. In: *Front Immunol* 7 (2016), p. 430. ISSN: 1664-3224 (Print) 1664-3224 (Linking). DOI: 10.3389/fimmu.2016.00430. URL: https://www.ncbi.nlm.nih.gov/pubmed/27799933.

[37] D. C. Nacionales et al. “B cell proliferation, somatic hypermutation, class switch recombination, and autoantibody production in ectopic lymphoid tissue in murine lupus”. In: *J Immunol* 182.7 (2009), pp. 4226–36. ISSN: 1550-6606 (Electronic) 0022-1767 (Linking). DOI: 10.4049/jimmunol.0800771. URL: https://www.ncbi.nlm.nih.gov/pubmed/19299721.

[38] G. W. Jones and S. A. Jones. “Ectopic lymphoid follicles: inducible centres for generating antigen-specific immune responses within tissues”. In: *Immunology* 147.2 (2016), pp. 141–51. ISSN: 1365-2567 (Electronic) 0019-2805 (Linking). DOI: 10.1111/imm.12554. URL: https://www.ncbi.nlm.nih.gov/pubmed/26551738.

[39] L. Rajasinghe et al. “Docosahexaenoic acid (DHA) suppresses broad spectrum of pathogenic autoantibodies elicited in murine model of lupus flaring”. Unpublished Work. Current Developments in Nutrition, 2019. URL: %3CGo%20to%20ISI%3E://FSTA:2019-11-Ge5643.

[40] Q. Z. Li et al. “Protein array autoantibody profiles for insights into systemic lupus erythematosus and incomplete lupus syndromes”. In: *Clin Exp Immunol* 147.1 (2007), pp. 60–70. ISSN: 0009-9104 (Print) 0009-9104 (Linking). DOI: 10.1111/j.1365-2249.2006.03251.x. URL: https://www.ncbi.nlm.nih.gov/pubmed/17177964.

[41] A. D. Benninghoff et al. “Docosahexaenoic Acid Consumption Impedes Early Interferon- and Chemokine-Related Gene Expression While Suppressing Silica-Triggered Flaring of Murine Lupus”. In: *Front Immunol* 10 (2019), p. 2851. ISSN: 1664-3224 (Electronic) 1664-3224 (Linking). DOI: 10.3389/fimmu.2019.02851. URL: https://www.ncbi.nlm.nih.gov/pubmed/31921124.

[42] M. K. Crow, M. Olferiev, and K. A. Kirou. “Type I Interferons in Autoimmune Disease”. In: *Annu Rev Pathol* 14 (2019), pp. 369–393. ISSN: 1553-4014 (Electronic) 1553-4006 (Linking). DOI: 10.1146/annurev-pathol-020117-043952.

[43] A. D. Steinberg, S. Baron, and N. Talal. “The pathogenesis of autoimmunity in New Zealand mice, I. Induction of antinucleic acid antibodies by polyinosinic-polycytidylic acid”. In: *Proc Natl Acad Sci U S A* 63.4 (1969), pp. 1102–7. ISSN: 0027-8424 (Print) 0027-8424 (Linking). DOI: 10.1073/pnas.63.4.1102. URL: https://www.ncbi.nlm.nih.gov/pubmed/5307809.

[44] J. J. Hooks et al. “Immune interferon in the circulation of patients with autoimmune disease”. In: *N Engl J Med* 301.1 (1979), pp. 5–8. ISSN: 0028-4793 (Print) 0028-4793 (Linking). DOI: 10.1056/NEJM197907053010102. URL: https://www.ncbi.nlm.nih.gov/pubmed/449915.

[45] C. Gota and L. Calabrese. “Induction of clinical autoimmune disease by therapeutic interferon-alpha”. In: *Autoimmunity* 36.8 (2003), pp. 511–8. ISSN: 0891-6934 (Print) 0891-6934 (Linking). DOI: 10.1080/08916930310001605873. URL: https://www.ncbi.nlm.nih.gov/pubmed/14984028.

[46] R. Rizvi and M. Hojjati. “Interferon-alpha induced lupus in a patient with chronic hepatitis C virus”. In: *J Clin Rheumatol* 17.3 (2011), pp. 152–3. ISSN: 1536-7355 (Electronic) 1076-1608 (Linking). DOI: 10.1097/RHU.0b013e31821557e7. URL: https://www.ncbi.nlm.nih.gov/pubmed/21441813.

[47] L. E. Ronnblom, G. V. Alm, and K. E. Oberg. “Autoimmunity after alpha-interferon therapy for malignant carcinoid tumors”. In: *Ann Intern Med* 115.3 (1991), pp. 178–83. ISSN: 0003-4819 (Print) 0003-4819 (Linking). DOI: 10.7326/0003-4819-115-3-178. URL: https://www.ncbi.nlm.nih.gov/pubmed/2058872.

[48] E. C. Baechler et al. “Interferon-inducible gene expression signature in peripheral blood cells of patients with severe lupus”. In: *Proc Natl Acad Sci U S A* 100.5 (2003), pp. 2610–5. ISSN: 0027-8424 (Print) 0027-8424 (Linking). DOI: 10.1073/pnas.0337679100. URL: https://www.ncbi.nlm.nih.gov/pubmed/12604793.

[49] S. Benmerzoug et al. “STING-dependent sensing of self-DNA drives silica-induced lung inflammation”. In: *Nat Commun* 9.1 (2018), p. 5226. ISSN: 2041-1723 (Electronic) 2041-1723 (Linking). DOI: 10.1038/s41467-018-07425-1. URL: https://www.ncbi.nlm.nih.gov/pubmed/30523277.

[50] S. R. Paludan and A. G. Bowie. “Immune sensing of DNA”. In: *Immunity* 38.5 (2013), pp. 870–80. ISSN: 1097-4180 (Electronic) 1074-7613 (Linking). DOI: 10.1016/j.immuni.2013.05.004. URL: https://www.ncbi.nlm.nih.gov/pubmed/23706668.

[51] F. Abdolmaleki et al. “The Role of Efferocytosis in Autoimmune Diseases”. In: *Front Immunol* 9 (2018), p. 1645. ISSN: 1664-3224 (Print) 1664-3224 (Linking). DOI: 10.3389/fimmu.2018.01645. URL: https://www.ncbi.nlm.nih.gov/pubmed/30083153.

[52] M. Rizzi et al. “Charged molecular silica trigger in vitro NETosis in human granulocytes via both oxidative and autophagic pathways”. In: *Eur Rev Med Pharmacol Sci* 22.20 (2018), pp. 7058–7068. ISSN: 2284-0729 (Electronic) 1128-3602 (Linking). DOI: 10.26355/eurrev_201810_16178. URL: https://www.ncbi.nlm.nih.gov/pubmed/30402874.

[53] F. McNab et al. “Type I interferons in infectious disease”. In: *Nat Rev Immunol* 15.2 (2015), pp. 87–103. ISSN: 1474-1741 (Electronic) 1474-1733 (Linking). DOI: 10.1038/nri3787. URL: https://www.ncbi.nlm.nih.gov/pubmed/25614319.

[54] F. Chasset and L. Arnaud. “Targeting interferons and their pathways in systemic lupus erythematosus”. In: *Autoimmun Rev* 17.1 (2018), pp. 44–52. ISSN: 1873-0183 (Electronic) 1568-9972 (Linking). DOI: 10.1016/j.autrev.2017.11.009.

[55] G. S. Garcia-Romo et al. “Netting neutrophils are major inducers of type I IFN production in pediatric systemic lupus erythematosus”. In: *Sci Transl Med* 3.73 (2011), 73ra20. ISSN: 1946-6242 (Electronic) 1946-6234 (Linking). DOI: 10.1126/scitranslmed.3001201. URL: https://www.ncbi.nlm.nih.gov/pubmed/21389264.

[56] N. Jacob et al. “B Cell and BAFF dependence of IFN-alpha-exaggerated disease in systemic lupus erythematosus-prone NZM 2328 mice”. In: *J Immunol* 186.8 (2011), pp. 4984–93. ISSN: 1550-6606 (Electronic) 0022-1767 (Linking). DOI: 10.4049/jimmunol.1000466.

[57] P. Lopez et al. “Interferon-alpha-induced B-lymphocyte stimulator expression and mobilization in healthy and systemic lupus erthymatosus monocytes”. In: *Rheumatology (Oxford)* 53.12 (2014), pp. 2249–58. ISSN: 1462-0332 (Electronic) 1462-0324 (Linking). DOI: 10.1093/rheumatology/keu249. URL: https://www.ncbi.nlm.nih.gov/pubmed/24942493.

[58] 3rd Lamore R. et al. “Belimumab (benlysta): a breakthrough therapy for systemic lupus erythematosus”. In: *P T* 37.4 (2012), pp. 212–26. ISSN: 1052-1372 (Print) 1052-1372 (Linking). URL: https://www.ncbi.nlm.nih.gov/pubmed/22593633.

[59] M. Guzman and J. S. Hui-Yuen. “Management of Pediatric Systemic Lupus Erythematosus: Focus on Belimumab”. In: *Drug Des Devel Ther* 14 (2020), pp. 2503–2513. ISSN: 1177-8881 (Electronic) 1177-8881 (Linking). DOI: 10.2147/DDDT.S216193. URL: https://www.ncbi.nlm.nih.gov/pubmed/32612353.

[60] H. A. Blair and E. D. Deeks. “Infliximab Biosimilar (CT-P13; Infliximab-dyyb): A Review in Autoimmune Inflammatory Diseases”. In: *BioDrugs* 30.5 (2016), pp. 469–480. ISSN: 1179-190X (Electronic) 1173-8804 (Linking). DOI: 10.1007/s40259-016-0193-2. URL: https://www.ncbi.nlm.nih.gov/pubmed/27650650.

[61] J. Menne et al. “C-C motif-ligand 2 inhibition with emapticap pegol (NOX-E36) in type 2 diabetic patients with albuminuria”. In: *Nephrol Dial Transplant* 32.2 (2017), pp. 307–315. ISSN: 1460-2385 (Electronic) 0931-0509 (Linking). DOI: 10.1093/ndt/gfv459. URL: https://www.ncbi.nlm.nih.gov/pubmed/28186566.

[62] L. Chatenoud. “CD3-specific antibody-induced active tolerance: from bench to bedside”. In: *Nat Rev Immunol* 3.2 (2003), pp. 123–32. ISSN: 1474-1733 (Print) 1474-1733 (Linking). DOI: 10.1038/nri1000. URL: https://www.ncbi.nlm.nih.gov/pubmed/12563296.

[63] E. Pelechas, P. V. Voulgari, and A. A. Drosos. “Sirukumab: a promising therapy for rheumatoid arthritis”. In: *Expert Opin Biol Ther* 17.6 (2017), pp. 755–763. ISSN: 1744-7682 (Electronic) 1471-2598 (Linking). DOI: 10.1080/14712598.2017.1315099. URL: https://www.ncbi.nlm.nih.gov/pubmed/28374627.

[64] M. Sheppard et al. “Tocilizumab (Actemra)”. In: *Hum Vaccin Immunother* 13.9 (2017), pp. 1972–1988. ISSN: 2164-554X (Electronic) 2164-5515 (Linking). DOI: 10.1080/21645515.2017.1316909. URL: https://www.ncbi.nlm.nih.gov/pubmed/28841363.

[65] R. Furie et al. “Anifrolumab reduces flare rates in patients with moderate to severe systemic lupus erythematosus”. In: *Lupus* (2021), p. 9612033211014267. ISSN: 1477-0962 (Electronic) 0961-2033 (Linking). DOI: 10.1177/09612033211014267. URL: https://www.ncbi.nlm.nih.gov/pubmed/33977796.

[66] A. F. Shaughnessy. “Monoclonal antibodies: magic bullets with a hefty price tag”. In: *BMJ* 345 (2012), e8346. ISSN: 1756-1833 (Electronic) 0959-8138 (Linking). DOI: 10.1136/bmj.e8346. URL: https://www.ncbi.nlm.nih.gov/pubmed/23236036.

[67] P. Panopalis et al. “Health care costs and costs associated with changes in work productivity among persons with systemic lupus erythematosus”. In: *Arthritis Rheum* 59.12 (2008), pp. 1788–95. ISSN: 0004-3591 (Print) 0004-3591 (Linking). DOI: 10.1002/art.24063. URL: https://www.ncbi.nlm.nih.gov/pubmed/19035422.

[68] B. Lands, D. Bibus, and K. D. Stark. “Dynamic interactions of n-3 and n-6 fatty acid nutrients”. In: *Prostaglandins Leukot Essent Fatty Acids* 136 (2018), pp. 15–21. ISSN: 1532-2823 (Electronic) 0952-3278 (Linking). DOI: 10.1016/j.plefa.2017.01.012.

[69] S. W. Wong et al. “Fatty acids modulate Toll-like receptor 4 activation through regulation of receptor dimerization and recruitment into lipid rafts in a reactive oxygen species-dependent manner”. In: *J Biol Chem* 284.40 (2009), pp. 27384–92. ISSN: 1083-351X (Electronic) 0021-9258 (Linking). DOI: 10.1074/jbc.M109.044065. URL: https://www.ncbi.nlm.nih.gov/pubmed/19648648.

[70] P. C. Norris and E. A. Dennis. “Omega-3 fatty acids cause dramatic changes in TLR4 and purinergic eicosanoid signaling”. In: *Proc Natl Acad Sci U S A* 109.22 (2012), pp. 8517–22. ISSN: 1091-6490 (Electronic) 0027-8424 (Linking). DOI: 10.1073/pnas.1200189109. URL: https://www.ncbi.nlm.nih.gov/pmc/articles/PMC3365225/pdf/pnas.201200189.pdf.

[71] P. C. Norris et al. “Phospholipase A2 regulates eicosanoid class switching during inflammasome activation”. In: *Proc Natl Acad Sci U S A* 111.35 (2014), pp. 12746–51. ISSN: 1091-6490 (Electronic) 0027-8424 (Linking). DOI: 10.1073/pnas.1404372111. URL: https://www.ncbi.nlm.nih.gov/pubmed/25139986.

[72] X. Li, Y. Yu, and C. D. Funk. “Cyclooxygenase-2 induction in macrophages is modulated by docosahexaenoic acid via interactions with free fatty acid receptor 4 (FFA4)”. In: *FASEB J* 27.12 (2013), pp. 4987–97. ISSN: 1530-6860 (Electronic) 0892-6638 (Linking). DOI: 10.1096/fj.13-235333. URL: http://www.fasebj.org/content/27/12/4987.full.pdf.

[73] Y. Yan et al. “Omega-3 fatty acids prevent inflammation and metabolic disorder through inhibition of NLRP3 inflammasome activation”. In: *Immunity* 38.6 (2013), pp. 1154–63. ISSN: 1097-4180 (Electronic) 1074-7613 (Linking). DOI: 10.1016/j.immuni.2013.05.015. URL: https://www.ncbi.nlm.nih.gov/pubmed/23809162.

[74] Mercedes Ricote and Christopher K. Glass. “PPARs and molecular mechanisms of transrepression”. In: *Biochim Biophys Acta* 1771.8 (2007), pp. 926–935. ISSN: 1388-1981. DOI: 10.1016/j.bbalip.2007.02.013. URL: %3CGo%20to%20ISI%3E://WOS:000249149100003.

[75] Hae Yeun Chang et al. “Docosahexaenoic acid induces M2 macrophage polarization through peroxisome proliferator-activated receptor gamma activation”. In: *Life Sciences* 120 (2015), pp. 39–47. ISSN: 0024-3205. DOI: 10.1016/j.lfs.2014.10.014. URL: %3CGo%20to%20ISI%3E://WOS:000348693700006.

[76] A. I. Ostermann et al. “Determining the fatty acid composition in plasma and tissues as fatty acid methyl esters using gas chromatography - a comparison of different derivatization and extraction procedures”. In: *Prostaglandins Leukot Essent Fatty Acids* 91.6 (2014), pp. 235–41. ISSN: 1532-2823 (Electronic) 0952-3278 (Linking). DOI: 10.1016/j.plefa.2014.10.002. URL: https://www.ncbi.nlm.nih.gov/pubmed/25458899.

[77] G. Fredman et al. “An imbalance between specialized pro-resolving lipid mediators and pro-inflammatory leukotrienes promotes instability of atherosclerotic plaques”. In: *Nat Commun* 7 (2016), p. 12859. ISSN: 2041-1723 (Electronic) 2041-1723 (Linking). DOI: 10.1038/ncomms12859. URL: https://www.ncbi.nlm.nih.gov/pubmed/27659679.

[78] D. T. Johnston et al. “Red blood cell omega-3 fatty acid levels and neurocognitive performance in deployed U.S. Servicemembers”. In: *Nutr Neurosci* 16.1 (2013), pp. 30–8. ISSN: 1476-8305 (Electronic) 1028-415X (Linking). DOI: 10.1179/1476830512Y.0000000025. URL: https://www.ncbi.nlm.nih.gov/pubmed/22748167.

[79] K. D. Stark. “The percentage of n-3 highly unsaturated fatty acids in total HUFA as a biomarker for omega-3 fatty acid status in tissues”. In: *Lipids* 43.1 (2008), pp. 45–53. ISSN: 0024-4201 (Print) 0024-4201. DOI: 10.1007/s11745-007-3128-3.

[80] S. E. Strandjord, B. Lands, and J. R. Hibbeln. “Validation of an equation predicting highly unsaturated fatty acid (HUFA) compositions of human blood fractions from dietary intakes of both HUFAs and their precursors”. In: *Prostaglandins Leukotrienes and Essential Fatty Acids* 136 (2018), pp. 171–176. ISSN: 0952-3278. DOI: 10.1016/j.plefa.2017.03.005. URL: %3CGo%20to%20ISI%3E://WOS:000449447000021.

[81] S. Gordon. “Phagocytosis: The Legacy of Metchnikoff”. In: *Cell* 166.5 (2016), pp. 1065–1068. ISSN: 1097-4172 (Electronic) 0092-8674 (Linking). DOI: 10.1016/j.cell.2016.08.017. URL: https://www.ncbi.nlm.nih.gov/pubmed/27565334.

[82] S. Watanabe et al. “The role of macrophages in the resolution of inflammation”. In: *J Clin Invest* 129.7 (2019), pp. 2619–2628. ISSN: 1558-8238 (Electronic) 0021-9738 (Linking). DOI: 10.1172/JCI124615. URL: https://www.ncbi.nlm.nih.gov/pubmed/31107246.

[83] E. A. Dennis et al. “A mouse macrophage lipidome”. In: *J Biol Chem* 285.51 (2010), pp. 39976–85. ISSN: 1083-351X (Electronic) 0021-9258 (Linking). DOI: 10.1074/jbc.M110.182915. URL: https://www.ncbi.nlm.nih.gov/pubmed/20923771.

[84] C. N. Serhan. “Pro-resolving lipid mediators are leads for resolution physiology”. In: *Nature* 510.7503 (2014), pp. 92–101. ISSN: 1476-4687 (Electronic) 0028-0836 (Linking). DOI: 10.1038/nature13479. URL: https://www.ncbi.nlm.nih.gov/pubmed/24899309.

[85] I. A. Udalova, A. Mantovani, and M. Feldmann. “Macrophage heterogeneity in the context of rheumatoid arthritis”. In: *Nat Rev Rheumatol* 12.8 (2016), pp. 472–85. ISSN: 1759-4804 (Electronic) 1759-4790 (Linking). DOI: 10.1038/nrrheum.2016.91. URL: https://www.ncbi.nlm.nih.gov/pubmed/27383913.

[86] L. C. Davies et al. “Tissue-resident macrophages”. In: *Nat Immunol* 14.10 (2013), pp. 986–95. ISSN: 1529-2916 (Electronic) 1529-2908 (Linking). DOI: 10.1038/ni.2705. URL: https://www.ncbi.nlm.nih.gov/pubmed/24048120.

[87] F. Ginhoux and M. Guilliams. “Tissue-Resident Macrophage Ontogeny and Homeostasis”. In: *Immunity* 44.3 (2016), pp. 439–449. ISSN: 1097-4180 (Electronic) 1074-7613 (Linking). DOI: 10.1016/j.immuni.2016.02.024. URL: https://www.ncbi.nlm.nih.gov/pubmed/26982352.

[88] Y. Lavin et al. “Tissue-resident macrophage enhancer landscapes are shaped by the local microenvironment”. In: *Cell* 159.6 (2014), pp. 1312–26. ISSN: 1097-4172 (Electronic) 0092-8674 (Linking). DOI: 10.1016/j.cell.2014.11.018. URL: https://www.ncbi.nlm.nih.gov/pubmed/25480296.

[89] E. Mass et al. “Specification of tissue-resident macrophages during organogenesis”. In: *Science* 353.6304 (2016). ISSN: 1095-9203 (Electronic) 0036-8075 (Linking). DOI: 10.1126/science.aaf4238. URL: https://www.ncbi.nlm.nih.gov/pubmed/27492475.

[90] C. Schneider et al. “Induction of the nuclear receptor PPAR-gamma by the cytokine GM-CSF is critical for the differentiation of fetal monocytes into alveolar macrophages”. In: *Nat Immunol* 15.11 (2014), pp. 1026–37. ISSN: 1529-2916 (Electronic) 1529-2908 (Linking). DOI: 10.1038/ni.3005. URL: https://www.ncbi.nlm.nih.gov/pubmed/25263125.

[91] X. Yu et al. “The Cytokine TGF-beta Promotes the Development and Homeostasis of Alveolar Macrophages”. In: *Immunity* 47.5 (2017), 903–912 e4. ISSN: 1097-4180 (Electronic) 1074-7613 (Linking). DOI: 10.1016/j.immuni.2017.10.007. URL: https://www.ncbi.nlm.nih.gov/pubmed/29126797.

[92] E. Y. Bissonnette et al. “Cross-Talk Between Alveolar Macrophages and Lung Epithelial Cells is Essential to Maintain Lung Homeostasis”. In: *Front Immunol* 11 (2020), p. 583042. ISSN: 1664-3224 (Electronic) 1664-3224 (Linking). DOI: 10.3389/fimmu.2020.583042. URL: https://www.ncbi.nlm.nih.gov/pubmed/33178214.

[93] M. Hetzel, M. Ackermann, and N. Lachmann. “Beyond ”Big Eaters”: The Versatile Role of Alveolar Macrophages in Health and Disease”. In: *Int J Mol Sci* 22.7 (2021). ISSN: 1422-0067 (Electronic) 1422-0067 (Linking). DOI: 10.3390/ijms22073308. URL: https://www.ncbi.nlm.nih.gov/pubmed/33804918.

[94] P. P. Lamichhane and A. E. Samarasinghe. “The Role of Innate Leukocytes during Influenza Virus Infection”. In: *J Immunol Res* 2019 (2019), p. 8028725. ISSN: 2314-7156 (Electronic) 2314-7156 (Linking). DOI: 10.1155/2019/8028725. URL: https://www.ncbi.nlm.nih.gov/pubmed/31612153.

[95] H. Aegerter et al. “Influenza-induced monocyte-derived alveolar macrophages confer prolonged antibacterial protection”. In: *Nat Immunol* 21.2 (2020), pp. 145–157. ISSN: 1529-2916 (Electronic) 1529-2908 (Linking). DOI: 10.1038/s41590-019-0568-x. URL: https://www.ncbi.nlm.nih.gov/pubmed/31932810.

[96] D. Aran et al. “Reference-based analysis of lung single-cell sequencing reveals a transitional profibrotic macrophage”. In: *Nat Immunol* 20.2 (2019), pp. 163–172. ISSN: 1529-2916 (Electronic) 1529-2908 (Linking). DOI: 10.1038/s41590-018-0276-y. URL: https://www.ncbi.nlm.nih.gov/pubmed/30643263.

[97] N. Joshi et al. “A spatially restricted fibrotic niche in pulmonary fibrosis is sustained by M-CSF/M-CSFR signalling in monocyte-derived alveolar macrophages”. In: *Eur Respir J* 55.1 (2020). ISSN: 1399-3003 (Electronic) 0903-1936 (Linking). DOI: 10.1183/13993003.00646-2019. URL: https://www.ncbi.nlm.nih.gov/pubmed/31601718.

[98] A. V. Misharin et al. “Monocyte-derived alveolar macrophages drive lung fibrosis and persist in the lung over the life span”. In: *J Exp Med* 214.8 (2017), pp. 2387–2404. ISSN: 1540-9538 (Electronic) 0022-1007 (Linking). DOI: 10.1084/jem.20162152. URL: https://www.ncbi.nlm.nih.gov/pubmed/28694385.

[99] P. A. Reyfman et al. “Single-Cell Transcriptomic Analysis of Human Lung Provides Insights into the Pathobiology of Pulmonary Fibrosis”. In: *Am J Respir Crit Care Med* 199.12 (2019), pp. 1517–1536. ISSN: 1535-4970 (Electronic) 1073-449X (Linking). DOI: 10.1164/rccm.201712-2410OC. URL: https://www.ncbi.nlm.nih.gov/pubmed/30554520.

[100] S. Shichino et al. “Reduced supply of monocyte-derived macrophages leads to a transition from nodular to diffuse lesions and tissue cell activation in silica-induced pulmonary fibrosis in mice”. In: *Am J Pathol* 185.11 (2015), pp. 2923–38. ISSN: 1525-2191 (Electronic) 0002-9440 (Linking). DOI: 10.1016/j.ajpath.2015.07.013. URL: https://www.ncbi.nlm.nih.gov/pubmed/26456580.

[101] J. Heyder. “Deposition of inhaled particles in the human respiratory tract and consequences for regional targeting in respiratory drug delivery”. In: *Proc Am Thorac Soc* 1.4 (2004), pp. 315–20. ISSN: 1546-3222 (Print) 1546-3222 (Linking). DOI: 10.1513/pats.200409-046TA. URL: https://www.ncbi.nlm.nih.gov/pubmed/16113452.

[102] A. A. Rostami. “Computational modeling of aerosol deposition in respiratory tract: a review”. In: *Inhal Toxicol* 21.4 (2009), pp. 262–90. ISSN: 1091-7691 (Electronic) 0895-8378 (Linking). DOI: 10.1080/08958370802448987. URL: https://www.ncbi.nlm.nih.gov/pubmed/19235608.

[103] G. Oberdorster, E. Oberdorster, and J. Oberdorster. “Nanotoxicology: an emerging discipline evolving from studies of ultrafine particles”. In: *Environ Health Perspect* 113.7 (2005), pp. 823–39. ISSN: 0091-6765 (Print) 0091-6765 (Linking). DOI: 10.1289/ehp.7339. URL: https://www.ncbi.nlm.nih.gov/pubmed/16002369.

[104] J. C. Prata. “Airborne microplastics: Consequences to human health?” In: *Environ Pollut* 234 (2018), pp. 115–126. ISSN: 1873-6424 (Electronic) 0269-7491 (Linking). DOI: 10.1016/j.envpol.2017.11.043. URL: https://www.ncbi.nlm.nih.gov/pubmed/29172041.

[105] G. Oberdorster. “Lung dosimetry: Pulmonary clearance of inhaled particles”. In: *Aerosol Sci Tech* 18.3 (1993), pp. 279–289. ISSN: 0278-8826. DOI: 10.1080/02786829308959605. URL: https://www.tandfonline.com/doi/pdf/10.1080/02786829308959605.

[106] X. M. Bustamante-Marin and L. E. Ostrowski. “Cilia and Mucociliary Clearance”. In: *Cold Spring Harb Perspect Biol* 9.4 (2017). ISSN: 1943-0264 (Electronic) 1943-0264 (Linking). DOI: 10.1101/cshperspect.a028241. URL: https://www.ncbi.nlm.nih.gov/pubmed/27864314.

[107] M. B. Snipes. “Long-term retention and clearance of particles inhaled by mammalian species”. In: *Crit Rev Toxicol* 20.3 (1989), pp. 175–211. ISSN: 1040-8444 (Print) 1040-8444 (Linking). DOI: 10.3109/10408448909017909. URL: https://www.ncbi.nlm.nih.gov/pubmed/2692607.

[108] K. J. Nikula et al. “Sites of particle retention and lung tissue responses to chronically inhaled diesel exhaust and coal dust in rats and cynomolgus monkeys”. In: *Environ Health Perspect* 105 Suppl 5 (1997), pp. 1231–4. ISSN: 0091-6765 (Print) 0091-6765 (Linking). DOI: 10.1289/ehp.97105s51231. URL: https://www.ncbi.nlm.nih.gov/pubmed/9400729.

[109] S. Honnons and J. M. Porcher. “In vivo experimental model for silicosis”. In: *J Environ Pathol Toxicol Oncol* 19.4 (2000), pp. 391–400. ISSN: 0731-8898 (Print) 0731-8898 (Linking). URL: https://www.ncbi.nlm.nih.gov/pubmed/11213022.

[110] B. Moore et al. “Animal models of fibrotic lung disease”. In: *Am J Respir Cell Mol Biol* 49.2 (2013), pp. 167–79. ISSN: 1535-4989 (Electronic) 1044-1549 (Linking). DOI: 10.1165/rcmb.2013-0094TR. URL: https://www.ncbi.nlm.nih.gov/pubmed/23526222.

[111] A. Elder et al. “Effects of subchronically inhaled carbon black in three species. I. Retention kinetics, lung inflammation, and histopathology”. In: *Toxicol Sci* 88.2 (2005), pp. 614–29. ISSN: 1096-6080 (Print) 1096-0929 (Linking). DOI: 10.1093/toxsci/kfi327. URL: https://www.ncbi.nlm.nih.gov/pubmed/16177241.

[112] "IARC working group on the evaluation of carcinogenic risks to Humans: Silica, Some Silicates, Coal Dust and Para-Aramid Fibrils. Lyon, 15-22 October 1996". In: *IARC Monogr Eval Carcinog Risks Hum* 68 (1997), pp. 1–475. ISSN: 1017-1606 (Print) 1017-1606 (Linking). URL: https://www.ncbi.nlm.nih.gov/pubmed/9303953.

[113] G. Oberdorster, J. Ferin, and P. E. Morrow. "Volumetric loading of alveolar macrophages (AM): a possible basis for diminished AM-mediated particle clearance". In: *Exp Lung Res* 18.1 (1992), pp. 87–104. ISSN: 0190-2148 (Print) 0190-2148 (Linking). DOI: 10.3109/01902149209020653. URL: https://www.ncbi.nlm.nih.gov/pubmed/1572327.

[114] A. R. Brody et al. "Deposition and translocation of inhaled silica in rats. Quantification of particle distribution, macrophage participation, and function". In: *Lab Invest* 47.6 (1982), pp. 533–42. ISSN: 0023-6837 (Print) 0023-6837 (Linking). URL: https://www.ncbi.nlm.nih.gov/pubmed/6292578.

[115] D. W. Porter et al. "Nitric oxide and reactive oxygen species production causes progressive damage in rats after cessation of silica inhalation". In: *Toxicol Sci* 90.1 (2006), pp. 188–97. ISSN: 1096-6080 (Print) 1096-0929 (Linking). DOI: 10.1093/toxsci/kfj075. URL: https://www.ncbi.nlm.nih.gov/pubmed/16339787.

[116] M. Sjostrand and R. Rylander. "Enzymes in lung lavage fluid after inhalation exposure to silica dust". In: *Environ Res* 33.2 (1984), pp. 307–11. ISSN: 0013-9351 (Print) 0013-9351 (Linking). DOI: 10.1016/0013-9351(84)90028-8. URL: https://www.ncbi.nlm.nih.gov/pubmed/6325142.

[117] I. Y. Adamson. "Radiation enhances silica translocation to the pulmonary interstitium and increases fibrosis in mice". In: *Environ Health Perspect* 97 (1992), pp. 233–8. ISSN: 0091-6765 (Print) 0091-6765 (Linking). DOI: 10.1289/ehp.9297233. URL: https://www.ncbi.nlm.nih.gov/pubmed/1327737.

[118] Y. Nakano-Narusawa et al. "Single Intratracheal Quartz Instillation Induced Chronic Inflammation and Tumourigenesis in Rat Lungs". In: *Sci Rep* 10.1 (2020), p. 6647. ISSN: 2045-2322 (Electronic) 2045-2322 (Linking). DOI: 10.1038/s41598-020-63667-4. URL: https://www.ncbi.nlm.nih.gov/pubmed/32313071.

[119] I. Y. Adamson, H. Prieditis, and D. H. Bowden. "Instillation of chemotactic factor to silica-injected lungs lowers interstitial particle content and reduces pulmonary fibrosis". In: *Am J Pathol* 141.2 (1992), pp. 319–26. ISSN: 0002-9440 (Print) 0002-9440 (Linking). URL: https://www.ncbi.nlm.nih.gov/pubmed/1323217.

[120] I. Y. Adamson, H. Prieditis, and D. H. Bowden. "Enhanced clearance of silica from mouse lung after instillation of a leukocyte chemotactic factor". In: *Exp Lung Res* 20.3 (1994), pp. 223–33. ISSN: 0190-2148 (Print) 0190-2148 (Linking). DOI: 10.3109/01902149409064384. URL: https://www.ncbi.nlm.nih.gov/pubmed/7925140.

[121] J. H. Vincent et al. “Accumulation of inhaled mineral dust in the lung and associated lymph nodes: implications for exposure and dose in occupational lung disease”. In: *Ann Occup Hyg* 31.3 (1987), pp. 375–93. ISSN: 0003-4878 (Print) 0003-4878 (Linking). DOI: 10.1093/annhyg/31.3.375. URL: https://www.ncbi.nlm.nih.gov/pubmed/3426036.

[122] R. Iyer et al. “Silica-induced apoptosis mediated via scavenger receptor in human alveolar macrophages”. In: *Toxicol Appl Pharmacol* 141.1 (1996), pp. 84–92. ISSN: 0041-008X (Print) 0041-008X (Linking). DOI: 10.1006/taap.1996.0263. URL: https://www.ncbi.nlm.nih.gov/pubmed/8917679.

[123] K. Donaldson et al. “Impaired chemotactic responses of bronchoalveolar leukocytes in experimental pneumoconiosis”. In: *J Pathol* 160.1 (1990), pp. 63–9. ISSN: 0022-3417 (Print) 0022-3417 (Linking). DOI: 10.1002/path.1711600113. URL: https://www.ncbi.nlm.nih.gov/pubmed/2156037.

[124] G. N. Joshi and D. A. Knecht. “Silica phagocytosis causes apoptosis and necrosis by different temporal and molecular pathways in alveolar macrophages”. In: *Apoptosis* 18.3 (2013), pp. 271–85. ISSN: 1360-8185. DOI: 10.1007/s10495-012-0798-y. URL: http://download.springer.com/static/pdf/716/art%253A10.1007%252Fs10495-012-0798-y.pdf?originUrl=http%3A%2F%2Flink.springer.com%2Farticle%2F10.1007%2Fs10495-012-0798-y&token2=exp=1496253678~acl=%2Fstatic%2Fpdf%2F716%2Fart%25253A10.1007%25252Fs10495-012-0798-y.pdf%3ForiginUrl%3Dhttp%253A%252F%252Flink.springer.com%252Farticle%252F10.1007%252Fs10495-012-0798-y*~hmac=edf2ae95ae1cc9fd8a9a7c572a2d6145af5633d2b1e76eab91b35bf823e31aae.

[125] V. Hornung et al. “Silica crystals and aluminum salts activate the NALP3 inflammasome through phagosomal destabilization”. In: *Nat Immunol* 9.8 (2008), pp. 847–56. ISSN: 1529-2916 (Electronic) 1529-2908 (Linking). DOI: 10.1038/ni.1631. URL: https://www.ncbi.nlm.nih.gov/pubmed/18604214.

[126] F. Jessop et al. “Phagolysosome acidification is required for silica and engineered nanoparticle-induced lysosome membrane permeabilization and resultant NLRP3 inflammasome activity”. In: *Toxicol Appl Pharmacol* 318 (2017), pp. 58–68. ISSN: 1096-0333 (Electronic) 0041-008X (Linking). DOI: 10.1016/j.taap.2017.01.012. URL: https://www.ncbi.nlm.nih.gov/pubmed/28126413.

[127] M. S. Thibodeau et al. “Silica-induced apoptosis in mouse alveolar macrophages is initiated by lysosomal enzyme activity”. In: *Toxicol Sci* 80.1 (2004), pp. 34–48. ISSN: 1096-6080 (Print) 1096-0929 (Linking). DOI: 10.1093/toxsci/kfh121. URL: https://www.ncbi.nlm.nih.gov/pubmed/15056807.

[128] P. Boya and G. Kroemer. “Lysosomal membrane permeabilization in cell death”. In: *Oncogene* 27.50 (2008), pp. 6434–51. ISSN: 1476-5594 (Electronic) 0950-9232 (Linking). DOI: 10.1038/onc.2008.310. URL: https://www.ncbi.nlm.nih.gov/pubmed/18955971.

[129] A. Lescoat et al. “Crystalline Silica Impairs Efferocytosis Abilities of Human and Mouse Macrophages: Implication for Silica-Associated Systemic Sclerosis”. In: *Front Immunol* 11 (2020), p. 219. ISSN: 1664-3224 (Electronic) 1664-3224 (Linking). DOI: 10.3389/fimmu.2020.00219. URL: https://www.ncbi.nlm.nih.gov/pubmed/32133004.

[130] U. S. Gaipl et al. “Clearance of apoptotic cells in human SLE”. In: *Curr Dir Autoimmun* 9 (2006), pp. 173–87. ISSN: 1422-2132 (Print) 1422-2132 (Linking). DOI: 10.1159/000090781. URL: https://www.ncbi.nlm.nih.gov/pubmed/16394661.

[131] L. Franchi, T. Eigenbrod, and G. Nunez. “Cutting edge: TNF-alpha mediates sensitization to ATP and silica via the NLRP3 inflammasome in the absence of microbial stimulation”. In: *J Immunol* 183.2 (2009), pp. 792–6. ISSN: 1550-6606 (Electronic) 0022-1767 (Linking). DOI: 10.4049/jimmunol.0900173. URL: https://www.ncbi.nlm.nih.gov/pubmed/19542372.

[132] V. Rabolli et al. “The alarmin IL-1alpha is a master cytokine in acute lung inflammation induced by silica micro- and nanoparticles”. In: *Part Fibre Toxicol* 11 (2014), p. 69. ISSN: 1743-8977 (Electronic) 1743-8977 (Linking). DOI: 10.1186/s12989-014-0069-x. URL: https://www.ncbi.nlm.nih.gov/pubmed/25497724.

[133] V. Rabolli, D. Lison, and F. Huaux. “The complex cascade of cellular events governing inflammasome activation and IL-1beta processing in response to inhaled particles”. In: *Part Fibre Toxicol* 13.1 (2016), p. 40. ISSN: 1743-8977 (Electronic) 1743-8977 (Linking). DOI: 10.1186/s12989-016-0150-8. URL: https://www.ncbi.nlm.nih.gov/pubmed/27519871.

[134] R. Mezzapelle, E. Venereau, and M. E. Bianchi. “Stress and Alarmins. Report from the 9th iDEAs meeting”. In: *Cell Death Dis* 10.12 (2019), p. 937. ISSN: 2041-4889 (Electronic). DOI: 10.1038/s41419-019-2165-1. URL: https://www.ncbi.nlm.nih.gov/pubmed/31819042.

[135] F. Huaux et al. “IL-1alpha induces CD11b(low) alveolar macrophage proliferation and maturation during granuloma formation”. In: *J Pathol* 235.5 (2015), pp. 698–709. ISSN: 1096-9896 (Electronic) 0022-3417 (Linking). DOI: 10.1002/path.4487. URL: https://www.ncbi.nlm.nih.gov/pubmed/25421226.

[136] J. Ma et al. “High-mobility group box 1 promotes epithelial-to-mesenchymal transition in crystalline silica induced pulmonary inflammation and fibrosis”. In: *Toxicol Lett* 330 (2020), pp. 134–143. ISSN: 1879-3169 (Electronic) 0378-4274 (Linking). DOI: 10.1016/j.toxlet.2020.05.016. URL: https://www.ncbi.nlm.nih.gov/pubmed/32428545.

[137] G. Fejer, S. Sharma, and I. Gyory. “Self-renewing macrophages–a new line of enquiries in mononuclear phagocytes”. In: *Immunobiology* 220.2 (2015), pp. 169–74. ISSN: 1878-3279 (Electronic) 0171-2985 (Linking). DOI: 10.1016/j.imbio.2014.11.005. URL: https://www.ncbi.nlm.nih.gov/pubmed/25468723.

[138] E. Kuroda et al. “Inhaled Fine Particles Induce Alveolar Macrophage Death and Interleukin-1alpha Release to Promote Inducible Bronchus-Associated Lymphoid Tissue Formation”. In: *Immunity* 45.6 (2016), pp. 1299–1310. ISSN: 1097-4180 (Electronic) 1074-7613 (Linking). DOI: 10.1016/j.immuni.2016.11.010. URL: https://www.ncbi.nlm.nih.gov/pubmed/28002730.

[139] T. Skuland et al. “Pro-inflammatory effects of crystalline- and nano-sized non-crystalline silica particles in a 3D alveolar model”. In: *Part Fibre Toxicol* 17.1 (2020), p. 13. ISSN: 1743-8977 (Electronic) 1743-8977 (Linking). DOI: 10.1186/s12989-020-00345-3. URL: https://www.ncbi.nlm.nih.gov/pubmed/32316988.

[140] S. L. Cassel et al. “The Nalp3 inflammasome is essential for the development of silicosis”. In: *Proc Natl Acad Sci U S A* 105.26 (2008), pp. 9035–40. ISSN: 1091-6490 (Electronic) 0027-8424 (Linking). DOI: 10.1073/pnas.0803933105. URL: https://www.ncbi.nlm.nih.gov/pubmed/18577586.

[141] O. Gross et al. “Inflammasome activators induce interleukin-1alpha secretion via distinct pathways with differential requirement for the protease function of caspase-1”. In: *Immunity* 36.3 (2012), pp. 388–400. ISSN: 1097-4180 (Electronic) 1074-7613 (Linking). DOI: 10.1016/j.immuni.2012.01.018. URL: https://www.ncbi.nlm.nih.gov/pubmed/22444631.

[142] N. C. Di Paolo and D. M. Shayakhmetov. “Interleukin 1alpha and the inflammatory process”. In: *Nat Immunol* 17.8 (2016), pp. 906–13. ISSN: 1529-2916 (Electronic) 1529-2908 (Linking). DOI: 10.1038/ni.3503.

[143] D. E. Damby et al. “Volcanic Ash Activates the NLRP3 Inflammasome in Murine and Human Macrophages”. In: *Front Immunol* 8 (2017), p. 2000. ISSN: 1664-3224 (Print) 1664-3224 (Linking). DOI: 10.3389/fimmu.2017.02000. URL: https://www.ncbi.nlm.nih.gov/pubmed/29403480.

[144] S. Deville et al. “Time-resolved characterization of the mechanisms of toxicity induced by silica and amino-modified polystyrene on alveolar-like macrophages”. In: *Arch Toxicol* 94.1 (2020), pp. 173–186. ISSN: 1432-0738 (Electronic) 0340-5761 (Linking). DOI: 10.1007/s00204-019-02604-5. URL: https://www.ncbi.nlm.nih.gov/pubmed/31677074.

[145] P. Duewell et al. “NLRP3 inflammasomes are required for atherogenesis and activated by cholesterol crystals”. In: *Nature* 464.7293 (2010), pp. 1357–61. ISSN: 1476-4687 (Electronic) 0028-0836 (Linking). DOI: 10.1038/nature08938. URL: https://www.ncbi.nlm.nih.gov/pubmed/20428172.

[146] R. E. Tweedell and T. D. Kanneganti. “Advances in Inflammasome Research: Recent Breakthroughs and Future Hurdles”. In: *Trends Mol Med* 26.11 (2020), pp. 969–971. ISSN: 1471-499X (Electronic) 1471-4914 (Linking). DOI: 10.1016/j.molmed.2020.07.010. URL: https://www.ncbi.nlm.nih.gov/pubmed/32948447.

[147] Y. Yang et al. “Recent advances in the mechanisms of NLRP3 inflammasome activation and its inhibitors”. In: *Cell Death Dis* 10.2 (2019), p. 128. ISSN: 2041-4889 (Electronic). DOI: 10.1038/s41419-019-1413-8. URL: https://www.ncbi.nlm.nih.gov/pubmed/30755589.

[148] C. Dostert et al. “Innate immune activation through Nalp3 inflammasome sensing of asbestos and silica”. In: *Science* 320.5876 (2008), pp. 674–7. ISSN: 1095-9203 (Electronic) 0036-8075 (Linking). DOI: 10.1126/science.1156995. URL: https://www.ncbi.nlm.nih.gov/pubmed/18403674.

[149] E. Kuroda et al. “Silica crystals and aluminum salts regulate the production of prostaglandin in macrophages via NALP3 inflammasome-independent mechanisms”. In: *Immunity* 34.4 (2011), pp. 514–26. ISSN: 1097-4180 (Electronic) 1074-7613 (Linking). DOI: 10.1016/j.immuni.2011.03.019. URL: https://www.ncbi.nlm.nih.gov/pubmed/21497116.

[150] T. Ziglari, Z. Wang, and A. Holian. “Contribution of Particle-Induced Lysosomal Membrane Hyperpolarization to Lysosomal Membrane Permeabilization”. In: *Int J Mol Sci* 22.5 (2021). ISSN: 1422-0067 (Electronic) 1422-0067 (Linking). DOI: 10.3390/ijms22052277. URL: https://www.ncbi.nlm.nih.gov/pubmed/33668885.

[151] G. N. Joshi, A. M. Goetjen, and D. A. Knecht. “Silica particles cause NADPH oxidase-independent ROS generation and transient phagolysosomal leakage”. In: *Mol Biol Cell* 26.18 (2015), pp. 3150–64. ISSN: 1939-4586 (Electronic) 1059-1524 (Linking). DOI: 10.1091/mbc.E15-03-0126. URL: https://www.ncbi.nlm.nih.gov/pubmed/26202463.

[152] T. Murakami et al. “Critical role for calcium mobilization in activation of the NLRP3 inflammasome”. In: *Proc Natl Acad Sci U S A* 109.28 (2012), pp. 11282–7. ISSN: 1091-6490 (Electronic) 0027-8424 (Linking). DOI: 10.1073/pnas.1117765109. URL: https://www.ncbi.nlm.nih.gov/pubmed/22733741.

[153] A. Hari et al. “Activation of NLRP3 inflammasome by crystalline structures via cell surface contact”. In: *Sci Rep* 4 (2014), p. 7281. ISSN: 2045-2322 (Electronic) 2045-2322 (Linking). DOI: 10.1038/srep07281. URL: https://www.ncbi.nlm.nih.gov/pubmed/25445147.

[154] P. M. Peeters et al. “Silica-induced NLRP3 inflammasome activation in vitro and in rat lungs”. In: *Part Fibre Toxicol* 11 (2014), p. 58. ISSN: 1743-8977 (Electronic) 1743-8977 (Linking). DOI: 10.1186/s12989-014-0058-0. URL: https://www.ncbi.nlm.nih.gov/pubmed/25406505.

[155] H. M. Shen et al. “Reactive oxygen species and caspase activation mediate silica-induced apoptosis in alveolar macrophages”. In: *Am J Physiol Lung Cell Mol Physiol* 280.1 (2001), pp. L10–7. ISSN: 1040-0605 (Print) 1040-0605 (Linking). DOI: 10.1152/ajplung.2001.280.1.L10. URL: https://www.ncbi.nlm.nih.gov/pubmed/11133490.

[156] Z. Zhong et al. “TRPM2 links oxidative stress to NLRP3 inflammasome activation”. In: *Nat Commun* 4 (2013), p. 1611. ISSN: 2041-1723 (Electronic) 2041-1723 (Linking). DOI: 10.1038/ncomms2608. URL: https://www.ncbi.nlm.nih.gov/pubmed/23511475.

[157] Z. Zhong et al. “New mitochondrial DNA synthesis enables NLRP3 inflammasome activation”. In: *Nature* 560.7717 (2018), pp. 198–203. ISSN: 1476-4687 (Electronic) 0028-0836 (Linking). DOI: 10.1038/s41586-018-0372-z. URL: https://www.ncbi.nlm.nih.gov/pubmed/30046112.

[158] C. Dai et al. “Interferon alpha on NZM2328.Lc1R27: enhancing autoimmunity and immune complex-mediated glomerulonephritis without end stage renal failure”. In: *Clin Immunol* 154.1 (2014), pp. 66–71. ISSN: 1521-7035 (Electronic) 1521-6616 (Linking). DOI: 10.1016/j.clim.2014.06.008.

[159] P. S. Chauhan et al. “Rapid Induction of Pulmonary Inflammation, Autoimmune Gene Expression, and Ectopic Lymphoid Neogenesis Following Acute Silica Exposure in Lupus-Prone Mice”. In: *Front Immunol* 12 (2021), p. 635138. ISSN: 1664-3224 (Electronic) 1664-3224 (Linking). DOI: 10.3389/fimmu.2021.635138. URL: https://www.ncbi.nlm.nih.gov/pubmed/33732257.

[160] M. H. Foster et al. “Silica Exposure Differentially Modulates Autoimmunity in Lupus Strains and Autoantibody Transgenic Mice”. In: *Front Immunol* 10 (2019), p. 2336. ISSN: 1664-3224 (Electronic) 1664-3224 (Linking). DOI: 10.3389/fimmu.2019.02336. URL: https://www.ncbi.nlm.nih.gov/pubmed/31632407.

[161] C. Gago da Graca, L. G. M. van Baarsen, and R. E. Mebius. “Tertiary Lymphoid Structures: Diversity in Their Development, Composition, and Role”. In: *J Immunol* 206.2 (2021), pp. 273–281. ISSN: 1550-6606 (Electronic) 0022-1767 (Linking). DOI: 10.4049/jimmunol.2000873. URL: https://www.ncbi.nlm.nih.gov/pubmed/33397741.

[162] A. Ager. “High Endothelial Venules and Other Blood Vessels: Critical Regulators of Lymphoid Organ Development and Function”. In: *Front Immunol* 8 (2017), p. 45. ISSN: 1664-3224 (Print) 1664-3224 (Linking). DOI: 10.3389/fimmu.2017.00045. URL: https://www.ncbi.nlm.nih.gov/pubmed/28217126.

[163] N. H. Ruddle. “High Endothelial Venules and Lymphatic Vessels in Tertiary Lymphoid Organs: Characteristics, Functions, and Regulation”. In: *Front Immunol* 7 (2016), p. 491. ISSN: 1664-3224 (Print) 1664-3224 (Linking). DOI: 10.3389/fimmu.2016.00491. URL: https://www.ncbi.nlm.nih.gov/pubmed/27881983.

[164] A. L. Tatler and G. Jenkins. “TGF-beta activation and lung fibrosis”. In: *Proc Am Thorac Soc* 9.3 (2012), pp. 130–6. ISSN: 1943-5665 (Electronic) 1546-3222 (Linking). DOI: 10.1513/pats.201201-003AW. URL: https://www.ncbi.nlm.nih.gov/pubmed/22802287.

[165] Y. Chen et al. “Antifibrotic effect of interferon gamma in silicosis model of rat”. In: *Toxicol Lett* 155.3 (2005), pp. 353–60. ISSN: 0378-4274 (Print) 0378-4274 (Linking). DOI: 10.1016/j.toxlet.2004.10.011. URL: https://www.ncbi.nlm.nih.gov/pubmed/15649618.

[166] M. Kolb et al. “Transient expression of IL-1beta induces acute lung injury and chronic repair leading to pulmonary fibrosis”. In: *J Clin Invest* 107.12 (2001), pp. 1529–36. ISSN: 0021-9738 (Print) 0021-9738 (Linking). DOI: 10.1172/JCI12568. URL: https://www.ncbi.nlm.nih.gov/pubmed/11413160.

[167] J. A. Markovics et al. “Interleukin-1beta induces increased transcriptional activation of the transforming growth factor-beta-activating integrin subunit beta8 through altering chromatin architecture”. In: *J Biol Chem* 286.42 (2011), pp. 36864–74. ISSN: 1083-351X (Electronic) 0021-9258 (Linking). DOI: 10.1074/jbc.M111.276790. URL: https://www.ncbi.nlm.nih.gov/pubmed/21878622.

[168] G. F. Hoyne et al. “Idiopathic pulmonary fibrosis and a role for autoimmunity”. In: *Immunol Cell Biol* 95.7 (2017), pp. 577–583. ISSN: 1440-1711 (Electronic) 0818-9641 (Linking). DOI: 10.1038/icb.2017.22. URL: https://www.ncbi.nlm.nih.gov/pubmed/28356570.

[169] P. G. Holt et al. “Downregulation of the antigen presenting cell function(s) of pulmonary dendritic cells in vivo by resident alveolar macrophages”. In: *J Exp Med* 177.2 (1993), pp. 397–407. ISSN: 0022-1007 (Print) 0022-1007 (Linking). DOI: 10.1084/jem.177.2.397. URL: https://www.ncbi.nlm.nih.gov/pubmed/8426110.

[170] C. Jakubzick et al. “Modulation of dendritic cell trafficking to and from the airways”. In: *J Immunol* 176.6 (2006), pp. 3578–84. ISSN: 0022-1767 (Print) 0022-1767 (Linking). DOI: 10.4049/jimmunol.176.6.3578. URL: https://www.ncbi.nlm.nih.gov/pubmed/16517726.

[171] T. Thepen, N. Van Rooijen, and G. Kraal. “Alveolar macrophage elimination in vivo is associated with an increase in pulmonary immune response in mice”. In: *J Exp Med* 170.2 (1989), pp. 499–509. ISSN: 0022-1007 (Print) 0022-1007 (Linking). DOI: 10.1084/jem.170.2.499. URL: https://www.ncbi.nlm.nih.gov/pubmed/2526847.

[172] J. F. Lauzon-Joset et al. “Dysregulation of alveolar macrophages unleashes dendritic cell-mediated mechanisms of allergic airway inflammation”. In: *Mucosal Immunol* 7.1 (2014), pp. 155–64. ISSN: 1935-3456 (Electronic) 1933-0219 (Linking). DOI: 10.1038/mi.2013.34. URL: https://www.ncbi.nlm.nih.gov/pubmed/23715174.

[173] W. Duan and M. Croft. “Control of regulatory T cells and airway tolerance by lung macrophages and dendritic cells”. In: *Ann Am Thorac Soc* 11 Suppl 5 (2014), S306–13. ISSN: 2325-6621 (Electronic) 2325-6621 (Linking). DOI: 10.1513/AnnalsATS.201401-028AW. URL: https://www.ncbi.nlm.nih.gov/pubmed/25525738.

[174] K. Neyt et al. “Early IL-1 Signaling Promotes iBALT Induction after Influenza Virus Infection”. In: *Front Immunol* 7 (2016), p. 312. ISSN: 1664-3224 (Print) 1664-3224 (Linking).

DOI: 10.3389/fimmu.2016.00312. URL: https://www.ncbi.nlm.nih.gov/pubmed/27579026.

[175] M. A. Bates et al. "Mapping of dynamic transcriptome changes associated with silica-triggered autoimmune pathogenesis in the lupus-prone NZBWF1 mouse". In: *Front Immunol* 10 (2019), p. 632. ISSN: 1664-3224 (Electronic) 1664-3224 (Linking). DOI: 10.3389/fimmu.2019.00632. URL: http://www.ncbi.nlm.nih.gov/pubmed/30984195%20https://fjfsdata01prod.blob.core.windows.net/articles/files/439767/pubmed-zip/.versions/2/.package-entries/fimmu-10-00632-r1/fimmu-10-00632.pdf?sv=2015-12-11&sr=b&sig=o%2B0boKVJKtMGl5by5T7YVowCGfGHRbWqajzHnUd%2BtUs%3D&se=2020-01-06T20%3A03%3A34Z&sp=r&rscd=attachment%3B%20filename%2A%3DUTF-8%27%27fimmu-10-00632.pdf.

[176] E. P. Brigham et al. "Omega-3 and Omega-6 Intake Modifies Asthma Severity and Response to Indoor Air Pollution in Children". In: *Am J Respir Crit Care Med* 199.12 (2019), pp. 1478–1486. ISSN: 1535-4970 (Electronic) 1073-449X (Linking). DOI: 10.1164/rccm.201808-1474OC. URL: https://www.ncbi.nlm.nih.gov/pubmed/30922077.

[177] X. Du et al. "Combined effects of vitamin E and omega-3 fatty acids on protecting ambient PM2.5-induced cardiovascular injury in rats". In: *Chemosphere* 173 (2017), pp. 14–21. ISSN: 1879-1298 (Electronic) 0045-6535 (Linking). DOI: 10.1016/j.chemosphere.2017.01.042. URL: https://www.ncbi.nlm.nih.gov/pubmed/28104476.

[178] X. Y. Li et al. "Protection against fine particle-induced pulmonary and systemic inflammation by omega-3 polyunsaturated fatty acids". In: *Biochim Biophys Acta Gen Subj* 1861.3 (2017), pp. 577–584. ISSN: 0304-4165 (Print) 0304-4165 (Linking). DOI: 10.1016/j.bbagen.2016.12.018. URL: https://www.ncbi.nlm.nih.gov/pubmed/28011301.

[179] I. Romieu et al. "The effect of supplementation with omega-3 polyunsaturated fatty acids on markers of oxidative stress in elderly exposed to PM(2.5)". In: *Environ Health Perspect* 116.9 (2008), pp. 1237–42. ISSN: 0091-6765 (Print) 0091-6765 (Linking). DOI: 10.1289/ehp.10578. URL: https://www.ncbi.nlm.nih.gov/pubmed/18795169.

[180] E. F. Wiest, M. T. Walsh-Wilcox, and M. K. Walker. "Omega-3 Polyunsaturated Fatty Acids Protect Against Cigarette Smoke-Induced Oxidative Stress and Vascular Dysfunction". In: *Toxicol Sci* 156.1 (2017), pp. 300–310. ISSN: 1096-0929 (Electronic) 1096-0929 (Linking). DOI: 10.1093/toxsci/kfw255. URL: https://www.ncbi.nlm.nih.gov/pubmed/28115642.

[181] J. J. Pestka et al. "Omega-3 Polyunsaturated Fatty Acid Intervention Against Established Autoimmunity in a Murine Model of Toxicant-Triggered Lupus". In: *Front Immunol* 12 (2021), p. 653464. ISSN: 1664-3224 (Electronic) 1664-3224 (Linking). DOI: 10.3389/fimmu.2021.653464. URL: https://www.ncbi.nlm.nih.gov/pubmed/33897700.

[182] I. Stoodley et al. "Higher Omega-3 Index Is Associated with Better Asthma Control and Lower Medication Dose: A Cross-Sectional Study". In: *Nutrients* 12.1 (2019). ISSN: 2072-

6643 (Electronic) 2072-6643 (Linking). DOI: 10.3390/nu12010074. URL: https://www.ncbi.nlm.nih.gov/pubmed/31892115.

[183] C. Lemoine et al. “Relationship between Omega-3 and Omega-6 Fatty Acid Intake and Chronic Obstructive Pulmonary Disease Morbidity”. In: *Ann Am Thorac Soc* 17.3 (2020), pp. 378–381. ISSN: 2325-6621 (Electronic) 2325-6621 (Linking). DOI: 10.1513/AnnalsATS.201910-740RL. URL: https://www.ncbi.nlm.nih.gov/pubmed/31751155.

[184] J. S. Kim et al. “Associations of omega-3 Fatty Acids With Interstitial Lung Disease and Lung Imaging Abnormalities Among Adults”. In: *Am J Epidemiol* 190.1 (2021), pp. 95–108. ISSN: 1476-6256 (Electronic) 0002-9262 (Linking). DOI: 10.1093/aje/kwaa168. URL: https://www.ncbi.nlm.nih.gov/pubmed/32803215.

[185] S. Gutierrez, S. L. Svahn, and M. E. Johansson. “Effects of omega-3 fatty acids on immune cells”. In: *Int J Mol Sci* 20.20 (2019). ISSN: 1422-0067 (Electronic) 1422-0067 (Linking). DOI: 10.3390/ijms20205028. URL: https://www.ncbi.nlm.nih.gov/pubmed/31614433.

[186] I. Kimura et al. “Free Fatty Acid Receptors in Health and Disease”. In: *Physiol Rev* 100.1 (2020), pp. 171–210. ISSN: 1522-1210 (Electronic) 0031-9333 (Linking). DOI: 10.1152/physrev.00041.2018. URL: https://www.ncbi.nlm.nih.gov/pubmed/31487233.

[187] W. E. Lands. “Metabolism of glycerolipides; a comparison of lecithin and triglyceride synthesis”. In: *J Biol Chem* 231.2 (1958), pp. 883–8. ISSN: 0021-9258 (Print) 0021-9258 (Linking). URL: https://www.ncbi.nlm.nih.gov/pubmed/13539023.

[188] W. E. Lands et al. “Selective incorporation of polyunsaturated fatty acids into phosphatidylcholine by rat liver microsomes”. In: *J Biol Chem* 257.24 (1982), pp. 14968–72. ISSN: 0021-9258 (Print) 0021-9258 (Linking). URL: https://www.ncbi.nlm.nih.gov/pubmed/7174678.

[189] S. K. Abbott et al. “Fatty acid composition of membrane bilayers: importance of diet polyunsaturated fat balance”. In: *Biochim Biophys Acta* 1818.5 (2012), pp. 1309–17. ISSN: 0006-3002 (Print) 0006-3002 (Linking). DOI: 10.1016/j.bbamem.2012.01.011. URL: https://www.ncbi.nlm.nih.gov/pubmed/22285120.

[190] J. Faber et al. “Supplementation with a fish oil-enriched, high-protein medical food leads to rapid incorporation of EPA into white blood cells and modulates immune responses within one week in healthy men and women”. In: *J Nutr* 141.5 (2011), pp. 964–70. ISSN: 1541-6100 (Electronic) 0022-3166 (Linking). DOI: 10.3945/jn.110.132985. URL: https://www.ncbi.nlm.nih.gov/pubmed/21430245.

[191] D. Rees et al. “Dose-related effects of eicosapentaenoic acid on innate immune function in healthy humans: a comparison of young and older men”. In: *Am J Clin Nutr* 83.2 (2006), pp. 331–42. ISSN: 0002-9165 (Print) 0002-9165 (Linking). DOI: 10.1093/ajcn/83.2.331. URL: https://www.ncbi.nlm.nih.gov/pubmed/16469992.

[192] B. S. Solvik et al. “Biomarkers and Fatty Fish Intake: A Randomized Controlled Trial in Norwegian Preschool Children”. In: *J Nutr* (2021). ISSN: 1541-6100 (Electronic) 0022-3166 (Linking). DOI: 10.1093/jn/nxab112. URL: https://www.ncbi.nlm.nih.gov/pubmed/33978160.

[193] P. Yaqoob et al. “Encapsulated fish oil enriched in alpha-tocopherol alters plasma phospholipid and mononuclear cell fatty acid compositions but not mononuclear cell functions”. In: *Eur J Clin Invest* 30.3 (2000), pp. 260–74. ISSN: 0014-2972 (Print) 0014-2972 (Linking). DOI: 10.1046/j.1365-2362.2000.00623.x. URL: https://www.ncbi.nlm.nih.gov/pubmed/10692004.

[194] Y. Y. Fan et al. “Remodelling of primary human CD4+ T cell plasma membrane order by n-3 PUFA”. In: *Br J Nutr* 119.2 (2018), pp. 163–175. ISSN: 1475-2662 (Electronic) 0007-1145 (Linking). DOI: 10.1017/S0007114517003385. URL: https://www.ncbi.nlm.nih.gov/pubmed/29249211.

[195] M. J. Gibney and B. Hunter. “The effects of short- and long-term supplementation with fish oil on the incorporation of n-3 polyunsaturated fatty acids into cells of the immune system in healthy volunteers”. In: *Eur J Clin Nutr* 47.4 (1993), pp. 255–9. ISSN: 0954-3007 (Print) 0954-3007 (Linking). URL: https://www.ncbi.nlm.nih.gov/pubmed/8491162.

[196] D. A. Healy et al. “Effect of low-to-moderate amounts of dietary fish oil on neutrophil lipid composition and function”. In: *Lipids* 35.7 (2000), pp. 763–8. ISSN: 0024-4201 (Print) 0024-4201 (Linking). DOI: 10.1007/s11745-000-0583-1. URL: https://www.ncbi.nlm.nih.gov/pubmed/10941877.

[197] N. Bie et al. “The immunomodulatory effect of docosahexaenoic acid (DHA) on the RAW264.7 cells by modification of the membrane structure and function”. In: *Food Funct* 11.3 (2020), pp. 2603–2616. ISSN: 2042-650X (Electronic) 2042-6496 (Linking). DOI: 10.1039/c9fo02618e. URL: https://www.ncbi.nlm.nih.gov/pubmed/32154543.

[198] N. R. Fuentes et al. “Omega-3 fatty acids, membrane remodeling and cancer prevention”. In: *Mol Aspects Med* 64 (2018), pp. 79–91. ISSN: 1872-9452 (Electronic) 0098-2997 (Linking). DOI: 10.1016/j.mam.2018.04.001. URL: https://www.ncbi.nlm.nih.gov/pubmed/29627343.

[199] M. L. Jacobs et al. “EPA and DHA differentially modulate membrane elasticity in the presence of cholesterol”. In: *Biophys J* (2021). ISSN: 1542-0086 (Electronic) 0006-3495 (Linking). DOI: 10.1016/j.bpj.2021.04.009. URL: https://www.ncbi.nlm.nih.gov/pubmed/33887229.

[200] B. Katrencikova et al. “Lipid Profile, Lipoprotein Subfractions, and Fluidity of Membranes in Children and Adolescents with Depressive Disorder: Effect of Omega-3 Fatty Acids in a Double-Blind Randomized Controlled Study”. In: *Biomolecules* 10.10 (2020). ISSN:

2218-273X (Electronic) 2218-273X (Linking). DOI: 10.3390/biom10101427. URL: https://www.ncbi.nlm.nih.gov/pubmed/33050072.

[201] M. G. Balta, E. Papathanasiou, and P. F. Christopoulos. “Specialized Pro-Resolving Mediators as Potential Regulators of Inflammatory Macrophage Responses in COVID-19”. In: *Front Immunol* 12 (2021), p. 632238. ISSN: 1664-3224 (Electronic) 1664-3224 (Linking). DOI: 10.3389/fimmu.2021.632238. URL: https://www.ncbi.nlm.nih.gov/pubmed/33717168.

[202] N. Chiang and C. N. Serhan. “Structural elucidation and physiologic functions of specialized pro-resolving mediators and their receptors”. In: *Mol Aspects Med* 58 (2017), pp. 114–129. ISSN: 1872-9452 (Electronic) 0098-2997 (Linking). DOI: 10.1016/j.mam.2017.03.005. URL: https://www.ncbi.nlm.nih.gov/pubmed/28336292.

[203] C. N. Serhan, N. Chiang, and J. Dalli. “New pro-resolving n-3 mediators bridge resolution of infectious inflammation to tissue regeneration”. In: *Mol Aspects Med* 64 (2018), pp. 1–17. ISSN: 1872-9452 (Electronic) 0098-2997 (Linking). DOI: 10.1016/j.mam.2017.08.002. URL: https://www.ncbi.nlm.nih.gov/pubmed/28802833.

[204] P. C. Calder et al. “Uptake and incorporation of saturated and unsaturated fatty acids into macrophage lipids and their effect upon macrophage adhesion and phagocytosis”. In: *Biochem J* 269.3 (1990), pp. 807–14. ISSN: 0264-6021 (Print) 0264-6021 (Linking). DOI: 10.1042/bj2690807. URL: https://www.ncbi.nlm.nih.gov/pubmed/2117922.

[205] S. Kew et al. “Relation between the fatty acid composition of peripheral blood mononuclear cells and measures of immune cell function in healthy, free-living subjects aged 25-72 y”. In: *Am J Clin Nutr* 77.5 (2003), pp. 1278–86. ISSN: 0002-9165 (Print) 0002-9165 (Linking). DOI: 10.1093/ajcn/77.5.1278. URL: https://www.ncbi.nlm.nih.gov/pubmed/12716683.

[206] A. Sobrino et al. “Protective activities of distinct omega-3 enriched oils are linked to their ability to upregulate specialized pro-resolving mediators”. In: *PLoS One* 15.12 (2020), e0242543. ISSN: 1932-6203 (Electronic) 1932-6203 (Linking). DOI: 10.1371/journal.pone.0242543. URL: https://www.ncbi.nlm.nih.gov/pubmed/33326419.

[207] L. H. Chen et al. “Modulation of the G-Protein-Coupled Receptor 84 (GPR84) by Agonists and Antagonists”. In: *J Med Chem* 63.24 (2020), pp. 15399–15409. ISSN: 1520-4804 (Electronic) 0022-2623 (Linking). DOI: 10.1021/acs.jmedchem.0c01378. URL: https://www.ncbi.nlm.nih.gov/pubmed/33267584.

[208] E. Isopi et al. “Resolvin D1 Reduces Lung Infection and Inflammation Activating Resolution in Cystic Fibrosis”. In: *Front Immunol* 11 (2020), p. 581. ISSN: 1664-3224 (Electronic) 1664-3224 (Linking). DOI: 10.3389/fimmu.2020.00581. URL: https://www.ncbi.nlm.nih.gov/pubmed/32528461.

[209] M. Codagnone et al. “Resolvin D1 enhances the resolution of lung inflammation caused by long-term Pseudomonas aeruginosa infection”. In: *Mucosal Immunol* 11.1 (2018), pp. 35–49. ISSN: 1935-3456 (Electronic) 1933-0219 (Linking). DOI: 10.1038/mi.2017.36. URL: https://www.ncbi.nlm.nih.gov/pubmed/28422188.

[210] Z. Hosseini et al. “Resolvin D1 Enhances Necroptotic Cell Clearance Through Promoting Macrophage Fatty Acid Oxidation and Oxidative Phosphorylation”. In: *Arterioscler Thromb Vasc Biol* 41.3 (2021), pp. 1062–1075. ISSN: 1524-4636 (Electronic) 1079-5642 (Linking). DOI: 10.1161/ATVBAHA.120.315758. URL: https://www.ncbi.nlm.nih.gov/pubmed/33472399.

[211] B. D. Gerlach et al. “Resolvin D1 promotes the targeting and clearance of necroptotic cells”. In: *Cell Death Differ* 27.2 (2020), pp. 525–539. ISSN: 1476-5403 (Electronic) 1350-9047 (Linking). DOI: 10.1038/s41418-019-0370-1. URL: https://www.ncbi.nlm.nih.gov/pubmed/31222041.

[212] N. Rymut et al. “Resolvin D1 promotes efferocytosis in aging by limiting senescent cell-induced MerTK cleavage”. In: *FASEB J* 34.1 (2020), pp. 597–609. ISSN: 1530-6860 (Electronic) 0892-6638 (Linking). DOI: 10.1096/fj.201902126R. URL: https://www.ncbi.nlm.nih.gov/pubmed/31914705.

[213] R. Ganesan et al. “D-series Resolvins activate Phospholipase D in phagocytes during inflammation and resolution”. In: *FASEB J* 34.12 (2020), pp. 15888–15906. ISSN: 1530-6860 (Electronic) 0892-6638 (Linking). DOI: 10.1096/fj.201903025RR. URL: https://www.ncbi.nlm.nih.gov/pubmed/33047359.

[214] M. Bolomini-Vittori et al. “PLD-dependent phosphatidic acid microdomains are signaling platforms for podosome formation”. In: *Sci Rep* 9.1 (2019), p. 3556. ISSN: 2045-2322 (Electronic) 2045-2322 (Linking). DOI: 10.1038/s41598-019-39358-0. URL: https://www.ncbi.nlm.nih.gov/pubmed/30837487.

[215] S. S. Iyer et al. “Phospholipases D1 and D2 coordinately regulate macrophage phagocytosis”. In: *J Immunol* 173.4 (2004), pp. 2615–23. ISSN: 0022-1767 (Print) 0022-1767 (Linking). DOI: 10.4049/jimmunol.173.4.2615. URL: https://www.ncbi.nlm.nih.gov/pubmed/15294978.

[216] L. D. Rajasinghe et al. “Omega-3 Docosahexaenoic Acid (DHA) Impedes Silica-Induced Macrophage Corpse Accumulation by Attenuating Cell Death and Potentiating Efferocytosis”. In: *Front Immunol* 11 (2020), p. 2179. ISSN: 1664-3224 (Electronic) 1664-3224 (Linking). DOI: 10.3389/fimmu.2020.02179. URL: https://www.ncbi.nlm.nih.gov/pubmed/33123123.

[217] M. K. Chang et al. “Monoclonal antibodies against oxidized low-density lipoprotein bind to apoptotic cells and inhibit their phagocytosis by elicited macrophages: evidence that oxidation-specific epitopes mediate macrophage recognition”. In: *Proc Natl Acad Sci U S*

A 96.11 (1999), pp. 6353–8. ISSN: 0027-8424 (Print) 0027-8424 (Linking). DOI: 10.1073/pnas.96.11.6353. URL: https://www.ncbi.nlm.nih.gov/pubmed/10339591.

[218] M. E. Greenberg et al. "Oxidized phosphatidylserine-CD36 interactions play an essential role in macrophage-dependent phagocytosis of apoptotic cells". In: *J Exp Med* 203.12 (2006), pp. 2613–25. ISSN: 0022-1007 (Print) 0022-1007 (Linking). DOI: 10.1084/jem.20060370. URL: https://www.ncbi.nlm.nih.gov/pubmed/17101731.

[219] V. E. Kagan et al. "A role for oxidative stress in apoptosis: oxidation and externalization of phosphatidylserine is required for macrophage clearance of cells undergoing Fas-mediated apoptosis". In: *J Immunol* 169.1 (2002), pp. 487–99. ISSN: 0022-1767 (Print) 0022-1767 (Linking). DOI: 10.4049/jimmunol.169.1.487. URL: https://www.ncbi.nlm.nih.gov/pubmed/12077280.

[220] V. A. Tyurin et al. "Oxidatively modified phosphatidylserines on the surface of apoptotic cells are essential phagocytic 'eat-me' signals: cleavage and inhibition of phagocytosis by Lp-PLA2". In: *Cell Death Differ* 21.5 (2014), pp. 825–35. ISSN: 1476-5403 (Electronic) 1350-9047 (Linking). DOI: 10.1038/cdd.2014.1. URL: https://www.ncbi.nlm.nih.gov/pubmed/24464221.

[221] R. S. Chapkin et al. "Docosahexaenoic acid alters the size and distribution of cell surface microdomains". In: *Biochim Biophys Acta* 1778.2 (2008), pp. 466–71. ISSN: 0006-3002 (Print) 0006-3002 (Linking). DOI: 10.1016/j.bbamem.2007.11.003. URL: https://www.ncbi.nlm.nih.gov/pubmed/18068112.

[222] S. K. Pierce. "Lipid rafts and B-cell activation". In: *Nat Rev Immunol* 2.2 (2002), pp. 96–105. ISSN: 1474-1733 (Print) 1474-1733 (Linking). DOI: 10.1038/nri726. URL: https://www.ncbi.nlm.nih.gov/pubmed/11910900.

[223] K. Simons and D. Toomre. "Lipid rafts and signal transduction". In: *Nat Rev Mol Cell Biol* 1.1 (2000), pp. 31–9. ISSN: 1471-0072 (Print) 1471-0072 (Linking). DOI: 10.1038/35036052. URL: https://www.ncbi.nlm.nih.gov/pubmed/11413487.

[224] N. R. Fuentes et al. "Long-Chain n-3 Fatty Acids Attenuate Oncogenic KRas-Driven Proliferation by Altering Plasma Membrane Nanoscale Proteolipid Composition". In: *Cancer Res* 78.14 (2018), pp. 3899–3912. ISSN: 1538-7445 (Electronic) 0008-5472 (Linking). DOI: 10.1158/0008-5472.CAN-18-0324. URL: https://www.ncbi.nlm.nih.gov/pubmed/29769200.

[225] N. R. Fuentes et al. "Emerging role of chemoprotective agents in the dynamic shaping of plasma membrane organization". In: *Biochim Biophys Acta Biomembr* 1859.9 Pt B (2017), pp. 1668–1678. ISSN: 0005-2736 (Print) 0005-2736 (Linking). DOI: 10.1016/j.bbamem.2017.03.014. URL: https://www.ncbi.nlm.nih.gov/pubmed/28342710.

[226] K. L. Honda et al. “EPA and DHA exposure alters the inflammatory response but not the surface expression of Toll-like receptor 4 in macrophages”. In: *Lipids* 50.2 (2015), pp. 121–9. ISSN: 1558-9307 (Electronic) 0024-4201 (Linking). DOI: 10.1007/s11745-014-3971-y. URL: https://www.ncbi.nlm.nih.gov/pubmed/25408476.

[227] A. Schoeniger, H. Fuhrmann, and J. Schumann. “LPS- or Pseudomonas aeruginosa-mediated activation of the macrophage TLR4 signaling cascade depends on membrane lipid composition”. In: *PeerJ* 4 (2016), e1663. ISSN: 2167-8359 (Print) 2167-8359 (Linking). DOI: 10.7717/peerj.1663. URL: https://www.ncbi.nlm.nih.gov/pubmed/26870615.

[228] C. K. Wong et al. “Activation profile of Toll-like receptors of peripheral blood lymphocytes in patients with systemic lupus erythematosus”. In: *Clin Exp Immunol* 159.1 (2010), pp. 11–22. ISSN: 1365-2249 (Electronic) 0009-9104 (Linking). DOI: 10.1111/j.1365-2249.2009.04036.x.

[229] D. L. Bonilla et al. “Incorporation of a dietary omega 3 fatty acid impairs murine macrophage responses to Mycobacterium tuberculosis”. In: *PLoS One* 5.5 (2010), e10878. ISSN: 1932-6203 (Electronic) 1932-6203 (Linking). DOI: 10.1371/journal.pone.0010878. URL: https://www.ncbi.nlm.nih.gov/pubmed/20526363.

[230] R. Irons and K. L. Fritsche. “Omega-3 polyunsaturated fatty acids impair in vivo interferon-gamma responsiveness via diminished receptor signaling”. In: *J Infect Dis* 191.3 (2005), pp. 481–6. ISSN: 0022-1899 (Print) 0022-1899 (Linking). DOI: 10.1086/427264. URL: https://www.ncbi.nlm.nih.gov/pubmed/15633108.

[231] T. Koppelmann et al. “The Mechanisms of the Anti-Inflammatory and Anti-Apoptotic Effects of Omega-3 Polyunsaturated Fatty Acids during Methotrexate-Induced Intestinal Damage in Cell Line and in a Rat Model”. In: *Nutrients* 13.3 (2021). ISSN: 2072-6643 (Electronic) 2072-6643 (Linking). DOI: 10.3390/nu13030888. URL: https://www.ncbi.nlm.nih.gov/pubmed/33801889.

[232] Z. Li et al. “DHA attenuates hepatic ischemia reperfusion injury by inhibiting pyroptosis and activating PI3K/Akt pathway”. In: *Eur J Pharmacol* 835 (2018), pp. 1–10. ISSN: 1879-0712 (Electronic) 0014-2999 (Linking). DOI: 10.1016/j.ejphar.2018.07.054. URL: https://www.ncbi.nlm.nih.gov/pubmed/30075219.

[233] J. X. Kang et al. “Transgenic mice: fat-1 mice convert n-6 to n-3 fatty acids”. In: *Nature* 427.6974 (2004), p. 504. ISSN: 1476-4687 (Electronic) 0028-0836 (Linking). DOI: 10.1038/427504a. URL: https://www.ncbi.nlm.nih.gov/pubmed/14765186.

[234] J. P. McGeown et al. “Nutritional interventions to improve neurophysiological impairments following traumatic brain injury: A systematic review”. In: *J Neurosci Res* 99.2 (2021), pp. 573–603. ISSN: 1097-4547 (Electronic) 0360-4012 (Linking). DOI: 10.1002/jnr.24746. URL: https://www.ncbi.nlm.nih.gov/pubmed/33107071.

[235] H. Ren et al. “Enriched Endogenous Omega-3 Fatty Acids in Mice Ameliorate Parenchymal Cell Death After Traumatic Brain Injury”. In: *Mol Neurobiol* 54.5 (2017), pp. 3317–3326. ISSN: 1559-1182 (Electronic) 0893-7648 (Linking). DOI: 10.1007/s12035-016-9931-1. URL: https://www.ncbi.nlm.nih.gov/pubmed/27167127.

[236] G. Lin et al. “Omega-3 free fatty acids and all-trans retinoic acid synergistically induce growth inhibition of three subtypes of breast cancer cell lines”. In: *Sci Rep* 7.1 (2017), p. 2929. ISSN: 2045-2322 (Electronic) 2045-2322 (Linking). DOI: 10.1038/s41598-017-03231-9. URL: https://www.ncbi.nlm.nih.gov/pubmed/28592877.

[237] F. Picou et al. “n-3 Polyunsaturated fatty acids induce acute myeloid leukemia cell death associated with mitochondrial glycolytic switch and Nrf2 pathway activation”. In: *Pharmacol Res* 136 (2018), pp. 45–55. ISSN: 1096-1186 (Electronic) 1043-6618 (Linking). DOI: 10.1016/j.phrs.2018.08.015. URL: https://www.ncbi.nlm.nih.gov/pubmed/30142422.

[238] N. Pizato et al. “Omega-3 docosahexaenoic acid induces pyroptosis cell death in triple-negative breast cancer cells”. In: *Sci Rep* 8.1 (2018), p. 1952. ISSN: 2045-2322 (Electronic) 2045-2322 (Linking). DOI: 10.1038/s41598-018-20422-0. URL: https://www.ncbi.nlm.nih.gov/pubmed/29386662.

[239] G. Fan et al. “DHA/AA alleviates LPS-induced Kupffer cells pyroptosis via GPR120 interaction with NLRP3 to inhibit inflammasome complexes assembly”. In: *Cell Death Dis* 12.1 (2021), p. 73. ISSN: 2041-4889 (Electronic). DOI: 10.1038/s41419-020-03347-3. URL: https://www.ncbi.nlm.nih.gov/pubmed/33436541.

[240] M. Srikanth et al. “Metabolism of Docosahexaenoic Acid (DHA) Induces Pyroptosis in BV-2 Microglial Cells”. In: *Neuromolecular Med* 20.4 (2018), pp. 504–514. ISSN: 1559-1174 (Electronic) 1535-1084 (Linking). DOI: 10.1007/s12017-018-8511-0. URL: https://www.ncbi.nlm.nih.gov/pubmed/30232677.

[241] A. Perl. “Oxidative stress in the pathology and treatment of systemic lupus erythematosus”. In: *Nat Rev Rheumatol* 9.11 (2013), pp. 674–86. ISSN: 1759-4804 (Electronic) 1759-4790 (Linking). DOI: 10.1038/nrrheum.2013.147. URL: https://www.ncbi.nlm.nih.gov/pubmed/24100461.

[242] E. A. Song, J. W. Lim, and H. Kim. “Docosahexaenoic acid inhibits IL-6 expression via PPARgamma-mediated expression of catalase in cerulein-stimulated pancreatic acinar cells”. In: *Int J Biochem Cell Biol* 88 (2017), pp. 60–68. ISSN: 1878-5875 (Electronic) 1357-2725 (Linking). DOI: 10.1016/j.biocel.2017.05.011. URL: https://www.ncbi.nlm.nih.gov/pubmed/28483666.

[243] W. Komatsu et al. “Docosahexaenoic acid suppresses nitric oxide production and inducible nitric oxide synthase expression in interferon-gamma plus lipopolysaccharide-stimulated murine macrophages by inhibiting the oxidative stress”. In: *Free Radic Biol Med* 34.8

(2003), pp. 1006–16. ISSN: 0891-5849 (Print) 0891-5849 (Linking). DOI: 10.1016/s0891-5849(03)00027-3. URL: https://www.ncbi.nlm.nih.gov/pubmed/12684085.

[244] H. Wang et al. "Role of Nrf2 in suppressing LPS-induced inflammation in mouse peritoneal macrophages by polyunsaturated fatty acids docosahexaenoic acid and eicosapentaenoic acid". In: *Mol Pharm* 7.6 (2010), pp. 2185–93. ISSN: 1543-8392 (Electronic) 1543-8384 (Linking). DOI: 10.1021/mp100199m. URL: https://www.ncbi.nlm.nih.gov/pubmed/20831192.

[245] M. L. Kielar et al. "Docosahexaenoic acid decreases IRF-1 mRNA and thus inhibits activation of both the IRF-E and NFkappa d response elements of the iNOS promoter". In: *Transplantation* 69.10 (2000), pp. 2131–7. ISSN: 0041-1337 (Print) 0041-1337 (Linking). DOI: 10.1097/00007890-200005270-00030. URL: https://www.ncbi.nlm.nih.gov/pubmed/10852612.

[246] B. Xue et al. "Omega-3 polyunsaturated fatty acids antagonize macrophage inflammation via activation of AMPK/SIRT1 pathway". In: *PLoS One* 7.10 (2012), e45990. ISSN: 1932-6203 (Electronic) 1932-6203 (Linking). DOI: 10.1371/journal.pone.0045990. URL: https://www.ncbi.nlm.nih.gov/pubmed/23071533.

[247] C. Hunsche et al. "Immune dysfunction and increased oxidative stress state in diet-induced obese mice are reverted by nutritional supplementation with monounsaturated and n-3 polyunsaturated fatty acids". In: *Eur J Nutr* 57.3 (2018), pp. 1123–1135. ISSN: 1436-6215 (Electronic) 1436-6207 (Linking). DOI: 10.1007/s00394-017-1395-1. URL: https://www.ncbi.nlm.nih.gov/pubmed/28229279.

[248] L. T. Meital et al. "Omega-3 fatty acids decrease oxidative stress and inflammation in macrophages from patients with small abdominal aortic aneurysm". In: *Sci Rep* 9.1 (2019), p. 12978. ISSN: 2045-2322 (Electronic) 2045-2322 (Linking). DOI: 10.1038/s41598-019-49362-z. URL: https://www.ncbi.nlm.nih.gov/pubmed/31506475.

[249] H. Y. Bang et al. "Docosahexaenoic Acid Induces Expression of Heme Oxygenase-1 and NAD(P)H:quinone Oxidoreductase through Activation of Nrf2 in Human Mammary Epithelial Cells". In: *Molecules* 22.6 (2017). ISSN: 1420-3049 (Electronic) 1420-3049 (Linking). DOI: 10.3390/molecules22060969. URL: https://www.ncbi.nlm.nih.gov/pubmed/28604588.

[250] J. Mildenberger et al. "N-3 PUFAs induce inflammatory tolerance by formation of KEAP1-containing SQSTM1/p62-bodies and activation of NFE2L2". In: *Autophagy* 13.10 (2017), pp. 1664–1678. ISSN: 1554-8635 (Electronic) 1554-8627 (Linking). DOI: 10.1080/15548627.2017.1345411. URL: https://www.ncbi.nlm.nih.gov/pubmed/28820283.

[251] E. Wheeler et al. "Interactive Effects of Omega-3 Polyunsaturated Fatty Acids and Secondhand Smoke in Mice and Human Subjects". In: *Cardiovasc Toxicol* 21.2 (2021), pp. 115–

126. ISSN: 1559-0259 (Electronic) 1530-7905 (Linking). DOI: 10.1007/s12012-020-09601-6. URL: https://www.ncbi.nlm.nih.gov/pubmed/32844369.

[252] G. P. Zaloga. "Narrative Review of n-3 Polyunsaturated Fatty Acid Supplementation upon Immune Functions, Resolution Molecules and Lipid Peroxidation". In: *Nutrients* 13.2 (2021). ISSN: 2072-6643 (Electronic) 2072-6643 (Linking). DOI: 10.3390/nu13020662. URL: https://www.ncbi.nlm.nih.gov/pubmed/33670710.

[253] M. Oarada et al. "Effects of dietary fish oil on lipid peroxidation and serum triacylglycerol levels in psychologically stressed mice". In: *Nutrition* 24.1 (2008), pp. 67–75. ISSN: 0899-9007 (Print) 0899-9007 (Linking). DOI: 10.1016/j.nut.2007.10.006. URL: https://www.ncbi.nlm.nih.gov/pubmed/18070659.

[254] J. Heshmati et al. "Omega-3 fatty acids supplementation and oxidative stress parameters: A systematic review and meta-analysis of clinical trials". In: *Pharmacol Res* 149 (2019), p. 104462. ISSN: 1096-1186 (Electronic) 1043-6618 (Linking). DOI: 10.1016/j.phrs.2019.104462. URL: https://www.ncbi.nlm.nih.gov/pubmed/31563611.

[255] K. Miloudi et al. "The mode of administration of total parenteral nutrition and nature of lipid content influence the generation of peroxides and aldehydes". In: *Clin Nutr* 31.4 (2012), pp. 526–34. ISSN: 1532-1983 (Electronic) 0261-5614 (Linking). DOI: 10.1016/j.clnu.2011.12.012. URL: https://www.ncbi.nlm.nih.gov/pubmed/22230256.

[256] D. Y. Oh and E. Walenta. "Omega-3 Fatty Acids and FFAR4". In: *Front Endocrinol (Lausanne)* 5 (2014), p. 115. ISSN: 1664-2392 (Print) 1664-2392 (Linking). DOI: 10.3389/fendo.2014.00115. URL: https://www.ncbi.nlm.nih.gov/pubmed/25076939.

[257] R. Prihandoko et al. "Pathophysiological regulation of lung function by the free fatty acid receptor FFA4". In: *Sci Transl Med* 12.557 (2020). ISSN: 1946-6242 (Electronic) 1946-6234 (Linking). DOI: 10.1126/scitranslmed.aaw9009. URL: https://www.ncbi.nlm.nih.gov/pubmed/32817367.

[258] P. J. Thul et al. "A subcellular map of the human proteome". In: *Science* 356.6340 (2017). ISSN: 1095-9203 (Electronic) 0036-8075 (Linking). DOI: 10.1126/science.aal3321. URL: https://www.ncbi.nlm.nih.gov/pubmed/28495876.

[259] D. Y. Oh et al. "GPR120 is an omega-3 fatty acid receptor mediating potent anti-inflammatory and insulin-sensitizing effects". In: *Cell* 142.5 (2010), pp. 687–98. ISSN: 1097-4172 (Electronic) 0092-8674 (Linking). DOI: 10.1016/j.cell.2010.07.041. URL: https://www.ncbi.nlm.nih.gov/pubmed/20813258.

[260] Z. Mo et al. "Eicosapentaenoic acid prevents inflammation induced by acute cerebral infarction through inhibition of NLRP3 inflammasome activation". In: *Life Sci* 242 (2020), p. 117133. ISSN: 1879-0631 (Electronic) 0024-3205 (Linking). DOI: 10.1016/j.lfs.2019.117133. URL: https://www.ncbi.nlm.nih.gov/pubmed/31830477.

[261] D. A. Raptis et al. “GPR120 on Kupffer cells mediates hepatoprotective effects of omega3-fatty acids”. In: *J Hepatol* 60.3 (2014), pp. 625–32. ISSN: 1600-0641 (Electronic) 0168-8278 (Linking). DOI: 10.1016/j.jhep.2013.11.006. URL: https://www.ncbi.nlm.nih.gov/pubmed/24262133.

[262] Z. Ren et al. “Activation of the Omega-3 Fatty Acid Receptor GPR120 Protects against Focal Cerebral Ischemic Injury by Preventing Inflammation and Apoptosis in Mice”. In: *J Immunol* 202.3 (2019), pp. 747–759. ISSN: 1550-6606 (Electronic) 0022-1767 (Linking). DOI: 10.4049/jimmunol.1800637. URL: https://www.ncbi.nlm.nih.gov/pubmed/30598514.

[263] C. Feng et al. “Docosahexaenoic acid ameliorates autoimmune inflammation by activating GPR120 signaling pathway in dendritic cells”. In: *Int Immunopharmacol* 97 (2021), p. 107698. ISSN: 1878-1705 (Electronic) 1567-5769 (Linking). DOI: 10.1016/j.intimp.2021.107698. URL: https://www.ncbi.nlm.nih.gov/pubmed/33932699.

[264] P. R. Souza et al. “The GPR40 Agonist GW9508 Enhances Neutrophil Function to Aid Bacterial Clearance During E. coli Infections”. In: *Front Immunol* 11 (2020), p. 573019. ISSN: 1664-3224 (Electronic) 1664-3224 (Linking). DOI: 10.3389/fimmu.2020.573019. URL: https://www.ncbi.nlm.nih.gov/pubmed/33133087.

[265] R. C. Reddy. “Immunomodulatory role of PPAR-gamma in alveolar macrophages”. In: *J Investig Med* 56.2 (2008), pp. 522–7. ISSN: 1081-5589 (Print) 1081-5589 (Linking). DOI: 10.2310/JIM.0b013e3181659972. URL: https://www.ncbi.nlm.nih.gov/pubmed/18317435.

[266] S. Huang et al. “Macrophage PPAR-gamma suppresses long-term lung fibrotic sequelae following acute influenza infection”. In: *PLoS One* 14.10 (2019), e0223430. ISSN: 1932-6203 (Electronic) 1932-6203 (Linking). DOI: 10.1371/journal.pone.0223430. URL: https://www.ncbi.nlm.nih.gov/pubmed/31584978.

[267] S. Huang et al. “Targeting Peroxisome Proliferator-Activated Receptor-Gamma Decreases Host Mortality After Influenza Infection in Obese Mice”. In: *Viral Immunol* 32.4 (2019), pp. 161–169. ISSN: 1557-8976 (Electronic) 0882-8245 (Linking). DOI: 10.1089/vim.2019.0016. URL: https://www.ncbi.nlm.nih.gov/pubmed/31009317.

[268] S. Huang et al. “PPAR-gamma in Macrophages Limits Pulmonary Inflammation and Promotes Host Recovery following Respiratory Viral Infection”. In: *J Virol* 93.9 (2019). ISSN: 1098-5514 (Electronic) 0022-538X (Linking). DOI: 10.1128/JVI.00030-19. URL: https://www.ncbi.nlm.nih.gov/pubmed/30787149.

[269] A. Malur et al. “Restoration of PPARgamma reverses lipid accumulation in alveolar macrophages of GM-CSF knockout mice”. In: *Am J Physiol Lung Cell Mol Physiol* 300.1 (2011), pp. L73–80. ISSN: 1522-1504 (Electronic) 1040-0605 (Linking). DOI: 10.1152/ajplung.00128.2010. URL: https://www.ncbi.nlm.nih.gov/pubmed/21036914.

[270] A. T. Reddy et al. “Endothelial cell peroxisome proliferator-activated receptor gamma reduces endotoxemic pulmonary inflammation and injury”. In: *J Immunol* 189.11 (2012), pp. 5411–20. ISSN: 1550-6606 (Electronic) 0022-1767 (Linking). DOI: 10 . 4049 / jimmunol.1201487. URL: https://www.ncbi.nlm.nih.gov/pubmed/23105142.

[271] J. Kaplan et al. “Pioglitazone reduces inflammation through inhibition of NF-kappaB in polymicrobial sepsis”. In: *Innate Immun* 20.5 (2014), pp. 519–28. ISSN: 1753-4267 (Electronic) 1753-4259 (Linking). DOI: 10.1177/1753425913501565. URL: https://www.ncbi.nlm.nih.gov/pubmed/24029145.

[272] H. Y. Chang et al. “Docosahexaenoic acid induces M2 macrophage polarization through peroxisome proliferator-activated receptor gamma activation”. In: *Life Sci* 120 (2015), pp. 39–47. ISSN: 1879-0631 (Electronic) 0024-3205 (Linking). DOI: 10.1016/j.lfs.2014.10.014. URL: https://www.ncbi.nlm.nih.gov/pubmed/25445227.

[273] Y. Hou, F. Moreau, and K. Chadee. “PPARgamma is an E3 ligase that induces the degradation of NFkappaB/p65”. In: *Nat Commun* 3 (2012), p. 1300. ISSN: 2041-1723 (Electronic) 2041-1723 (Linking). DOI: 10.1038/ncomms2270. URL: https://www.ncbi.nlm.nih.gov/pubmed/23250430.

[274] G. Zhao et al. “Anti-inflammatory effects of polyunsaturated fatty acids in THP-1 cells”. In: *Biochem Biophys Res Commun* 336.3 (2005), pp. 909–17. ISSN: 0006-291X (Print) 0006-291X (Linking). DOI: 10.1016/j.bbrc.2005.08.204. URL: https://www.ncbi.nlm.nih.gov/pubmed/16169525.

[275] S. Sauer. “Ligands for the Nuclear Peroxisome Proliferator-Activated Receptor Gamma”. In: *Trends Pharmacol Sci* 36.10 (2015), pp. 688–704. ISSN: 1873-3735 (Electronic) 0165-6147 (Linking). DOI: 10.1016/j.tips.2015.06.010. URL: https://www.ncbi.nlm.nih.gov/pubmed/26435213.

[276] Z. Czimmerer, L. Halasz, and L. Nagy. “Unorthodox Transcriptional Mechanisms of Lipid-Sensing Nuclear Receptors in Macrophages: Are We Opening a New Chapter?” In: *Front Endocrinol (Lausanne)* 11 (2020), p. 609099. ISSN: 1664-2392 (Print) 1664-2392 (Linking). DOI: 10.3389/fendo.2020.609099. URL: https://www.ncbi.nlm.nih.gov/pubmed/33362723.

[277] F. Zapata-Gonzalez et al. “Human dendritic cell activities are modulated by the omega-3 fatty acid, docosahexaenoic acid, mainly through PPAR(gamma):RXR heterodimers: comparison with other polyunsaturated fatty acids”. In: *J Leukoc Biol* 84.4 (2008), pp. 1172–82. ISSN: 0741-5400 (Print) 0741-5400 (Linking). DOI: 10.1189/jlb.1007688. URL: https://www.ncbi.nlm.nih.gov/pubmed/18632990.

[278] J. Lengqvist et al. “Polyunsaturated fatty acids including docosahexaenoic and arachidonic acid bind to the retinoid X receptor alpha ligand-binding domain”. In: *Mol Cell Proteomics*

3.7 (2004), pp. 692–703. ISSN: 1535-9476 (Print) 1535-9476 (Linking). DOI: 10.1074/mcp.M400003-MCP200. URL: https://www.ncbi.nlm.nih.gov/pubmed/15073272.

[279] E. Glaria, N. A. Letelier, and A. F. Valledor. "Integrating the roles of liver X receptors in inflammation and infection: mechanisms and outcomes". In: *Curr Opin Pharmacol* 53 (2020), pp. 55–65. ISSN: 1471-4973 (Electronic) 1471-4892 (Linking). DOI: 10.1016/j.coph.2020.05.001. URL: https://www.ncbi.nlm.nih.gov/pubmed/32599447.

[280] Web Page. 2005 2005. URL: https://www.niaid.nih.gov/topics/autoimmune/Documents/adccfinal.pdf.

[281] N Ruperto et al. "International consensus for a definition of disease flare in lupus". In: *Lupus* 20.5 (2011), pp. 453–462. DOI: 10.1177/0961203310388445. URL: https://journals.sagepub.com/doi/abs/10.1177/0961203310388445.

[282] A. Sang et al. "Animal models of molecular pathology systemic lupus erythematosus". In: *Prog Mol Biol Transl Sci* 105 (2012), pp. 321–70. ISSN: 1878-0814 (Electronic) 1877-1173 (Linking). DOI: 10.1016/b978-0-12-394596-9.00010-x.

[283] C. M. Syrett et al. "Loss of epigenetic modifications on the inactive X chromosome and sex-biased gene expression profiles in B cells from NZB/W F1 mice with lupus-like disease". In: *J Autoimmun* 107 (2020), p. 102357. ISSN: 1095-9157 (Electronic) 0896-8411 (Linking). DOI: 10.1016/j.jaut.2019.102357. URL: https://www.ncbi.nlm.nih.gov/pubmed/31780316.

[284] J. C. Ansel et al. "Effects of UV radiation on autoimmune strains of mice: increased mortality and accelerated autoimmunity in BXSB male mice". In: *J Invest Dermatol* 85.3 (1985), pp. 181–6. ISSN: 0022-202X (Print) 0022-202X (Linking). DOI: 10.1111/1523-1747.ep12276652.

[285] S. J. Wolf et al. "Ultraviolet light induces increased T cell activation in lupus-prone mice via type I IFN-dependent inhibition of T regulatory cells". In: *J Autoimmun* 103 (2019), p. 102291. ISSN: 1095-9157 (Electronic) 0896-8411 (Linking). DOI: 10.1016/j.jaut.2019.06.002.

[286] K. L. Clark et al. "Epidermal injury promotes nephritis flare in lupus-prone mice". In: *J Autoimmun* 65 (2015), pp. 38–48. ISSN: 1095-9157 (Electronic) 0896-8411 (Linking). DOI: 10.1016/j.jaut.2015.08.005.

[287] Zheng Liu et al. "Interferon-α accelerates murine systemic lupus erythematosus in a T cell–dependent manner". In: *Arthr Rheumatol* 63.1 (2011), pp. 219–229. ISSN: 1529-0131. DOI: 10.1002/art.30087. URL: http://dx.doi.org/10.1002/art.30087.

[288] C. G. Parks et al. "Occupational exposure to crystalline silica and risk of systemic lupus erythematosus - A population-based, case-control study in the southeastern United States".

In: *Arthritus Rheum* 46.7 (2002), pp. 1840–1850. ISSN: 0004-3591. DOI: 10.1002/art.10368. URL: %3CGo%20to%20ISI%3E://000176773200018.

[289] C. G. Parks and A. J. De Roos. "Pesticides, chemical and industrial exposures in relation to systemic lupus erythematosus". In: *Lupus* 23.6 (2014), pp. 527–536. ISSN: 0961-2033. DOI: 10.1177/0961203313511680. URL: %3CGo%20to%20ISI%3E://WOS:000334824800004%20https://www.ncbi.nlm.nih.gov/pmc/articles/PMC4020505/pdf/nihms532384.pdf.

[290] S. Vupputuri et al. "Occupational silica exposure and chronic kidney disease". In: *Ren Fail* 34.1 (2012), pp. 40–6. ISSN: 1525-6049 (Electronic) 0886-022X (Linking). DOI: 10.3109/0886022X.2011.623496. URL: https://www.ncbi.nlm.nih.gov/pubmed/22032652.

[291] K. A. Wierenga, J. R. Harkema, and J. J. Pestka. "Lupus, Silica, and Dietary Omega-3 Fatty Acid Interventions". In: *Toxicol Pathol* 47.8 (2019), pp. 1004–1011. ISSN: 1533-1601 (Electronic) 0192-6233 (Linking). DOI: 10.1177/0192623319878398. URL: https://www.ncbi.nlm.nih.gov/pubmed/31725357.

[292] G. N. Joshi, R. M. Gilberti, and D. A. Knecht. "Single cell snalysis of phagocytosis, phagosome maturation, phagolysosomal leakage, and cell death following exposure of macrophages to silica particles". In: *Meth Mol Biol* 1519 (2017), pp. 55–77. ISSN: 1940-6029 (Electronic) 1064-3745 (Linking). DOI: 10.1007/978-1-4939-6581-6_5.

[293] M. Gatto et al. "New therapeutic strategies in systemic lupus erythematosus management". In: *Nature reviews. Rheumatology* 15.1 (2019), pp. 30–48. ISSN: 1759-4804 (Electronic) 1759-4790 (Linking). DOI: 10.1038/s41584-018-0133-2. URL: http://www.ncbi.nlm.nih.gov/pubmed/30538302%20https://www.nature.com/articles/s41584-018-0133-2%20https://www.nature.com/articles/s41584-018-0133-2.pdf.

[294] E. M. Duffy et al. "The clinical effect of dietary supplementation with omega-3 fish oils and/or copper in systemic lupus erythematosus". In: *J Rheumatol.* 31.8 (2004), pp. 1551–1556. URL: PM:15290734.

[295] M. A. Lozovoy et al. "Fish oil N-3 fatty acids increase adiponectin and decrease leptin levels in patients with systemic lupus erythematosus". In: *Marine drugs* 13.2 (2015), pp. 1071–83. ISSN: 1660-3397 (Electronic) 1660-3397 (Linking). DOI: 10.3390/md13021071. URL: http://www.ncbi.nlm.nih.gov/pubmed/25690094.

[296] S. A. Wright et al. "A randomised interventional trial of omega-3-polyunsaturated fatty acids on endothelial function and disease activity in systemic lupus erythematosus". In: *Ann Rheum Dis* 67.6 (2008), pp. 841–8. ISSN: 1468-2060 (Electronic) 0003-4967 (Linking). DOI: ard.2007.077156[pii]10.1136/ard.2007.077156. URL: http://www.ncbi.nlm.nih.gov/pubmed/17875549.

[297] K. J. Hintze, A. D. Benninghoff, and R. E. Ward. “Formulation of the Total Western Diet (TWD) as a basal diet for rodent cancer studies”. In: *J Agric Food Chem* 60.27 (2012), pp. 6736–42. ISSN: 1520-5118 (Electronic) 0021-8561 (Linking). DOI: 10.1021/jf204509a. URL: https://www.ncbi.nlm.nih.gov/pubmed/22224871.

[298] K. J. Hintze, J. Tawzer, and R. E. Ward. “Concentration and ratio of essential fatty acids influences the inflammatory response in lipopolysaccharide challenged mice”. In: *Prostaglandins Leukot Essent Fatty Acids* 111 (2016), pp. 37–44. ISSN: 1532-2823 (Electronic) 0952-3278 (Linking). DOI: 10.1016/j.plefa.2016.03.003.

[299] K. J. Hintze et al. “Modeling the western diet for preclinical investigations”. In: *Adv Nutr* 9.3 (2018), pp. 263–271. ISSN: 2156-5376 (Electronic) 2161-8313 (Linking). DOI: 10.1093/advances/nmy002. URL: http://www.ncbi.nlm.nih.gov/pubmed/29635305.

[300] C. Brandenberger et al. “Engineered silica nanoparticles act as adjuvants to enhance allergic airway disease in mice”. In: *Part Fibre Toxicol* 10 (2013), p. 26. ISSN: 1743-8977 (Electronic) 1743-8977 (Linking). DOI: 10.1186/1743-8977-10-26.

[301] R. J. Fahy et al. “Inflammasome mRNA expression in human monocytes during early septic shock”. In: *Am J Respir Crit Care Med* 177.9 (2008), pp. 983–8. ISSN: 1535-4970 (Electronic) 1073-449X (Linking). DOI: 10.1164/rccm.200703-418OC. URL: https://www.ncbi.nlm.nih.gov/pubmed/18263805.

[302] M. A. Gavrilin et al. “Pyrin critical to macrophage IL-1beta response to Francisella challenge”. In: *J Immunol* 182.12 (2009), pp. 7982–9. ISSN: 1550-6606 (Electronic) 0022-1767 (Linking). DOI: 10.4049/jimmunol.0803073. URL: https://www.ncbi.nlm.nih.gov/pubmed/19494323.

[303] F. Yu et al. “Redefining lupus nephritis: clinical implications of pathophysiologic subtypes”. In: *Nat Rev Nephrol* 13.8 (2017), pp. 483–495. ISSN: 1759-507X (Electronic) 1759-5061 (Linking). DOI: 10.1038/nrneph.2017.85.

[304] J. I. Fenton et al. “Red blood cell PUFAs reflect the phospholipid PUFA composition of major organs”. In: *Prostaglandins Leukot Essent Fatty Acids* 112 (2016), pp. 12–23. ISSN: 1532-2823 (Electronic) 0952-3278 (Linking). DOI: 10.1016/j.plefa.2016.06.004. URL: https://www.ncbi.nlm.nih.gov/pubmed/27637336.

[305] E. A. Gurzell et al. “Marine fish oils are not equivalent with respect to B-cell membrane organization and activation”. In: *J Nutr Biochem* 26.4 (2015), pp. 369–77. ISSN: 1873-4847 (Electronic) 0955-2863 (Linking). DOI: 10.1016/j.jnutbio.2014.11.005. URL: https://www.ncbi.nlm.nih.gov/pubmed/25616447.

[306] R. G. Metcalf et al. “Relation between blood and atrial fatty acids in patients undergoing cardiac bypass surgery”. In: *Am J Clin Nutr* 91.3 (2010), pp. 528–34. ISSN: 1938-3207

(Electronic) 0002-9165 (Linking). DOI: 10.3945/ajcn.2009.28302. URL: https://www.ncbi.nlm.nih.gov/pubmed/20089730.

[307] A. C. Beynen, R. J. Hermus, and J. G. Hautvast. "A mathematical relationship between the fatty acid composition of the diet and that of the adipose tissue in man". In: *Am J Clin Nutr* 33.1 (1980), pp. 81–5. ISSN: 0002-9165 (Print) 0002-9165 (Linking). DOI: 10.1093/ajcn/33.1.81. URL: https://www.ncbi.nlm.nih.gov/pubmed/7355785.

[308] L. Hodson, C. M. Skeaff, and B. A. Fielding. "Fatty acid composition of adipose tissue and blood in humans and its use as a biomarker of dietary intake". In: *Prog Lipid Res* 47.5 (2008), pp. 348–80. ISSN: 0163-7827 (Print) 0163-7827 (Linking). DOI: 10.1016/j.plipres.2008.03.003. URL: https://www.ncbi.nlm.nih.gov/pubmed/18435934.

[309] S. D. Poppitt et al. "Assessment of erythrocyte phospholipid fatty acid composition as a biomarker for dietary MUFA, PUFA or saturated fatty acid intake in a controlled cross-over intervention trial". In: *Lipids Health Dis* 4 (2005), p. 30. ISSN: 1476-511X (Electronic) 1476-511X (Linking). DOI: 10.1186/1476-511X-4-30. URL: https://www.ncbi.nlm.nih.gov/pubmed/16329761.

[310] P. L. Zock et al. "Fatty acids in serum cholesteryl esters as quantitative biomarkers of dietary intake in humans". In: *Am J Epidemiol* 145.12 (1997), pp. 1114–22. ISSN: 0002-9262 (Print) 0002-9262 (Linking). DOI: 10.1093/oxfordjournals.aje.a009074. URL: https://www.ncbi.nlm.nih.gov/pubmed/9199541.

[311] A. H. Metherel et al. "Compound-specific isotope analysis reveals no retroconversion of DHA to EPA but substantial conversion of EPA to DHA following supplementation: a randomized control trial". In: *Am J Clin Nutr* 110.4 (2019), pp. 823–831. ISSN: 1938-3207 (Electronic) 0002-9165 (Linking). DOI: 10.1093/ajcn/nqz097. URL: https://www.ncbi.nlm.nih.gov/pubmed/31204771.

[312] J. P. Schuchardt and A. Hahn. "Bioavailability of long-chain omega-3 fatty acids". In: *Prostaglandins Leukot Essent Fatty Acids* 89.1 (2013), pp. 1–8. ISSN: 1532-2823 (Electronic) 0952-3278 (Linking). DOI: 10.1016/j.plefa.2013.03.010. URL: https://www.ncbi.nlm.nih.gov/pubmed/23676322.

[313] M. L. Bonet, J. Ribot, and A. Palou. "Lipid metabolism in mammalian tissues and its control by retinoic acid". In: *Biochim Biophys Acta* 1821.1 (2012), pp. 177–89. ISSN: 0006-3002 (Print) 0006-3002 (Linking). DOI: 10.1016/j.bbalip.2011.06.001. URL: https://www.ncbi.nlm.nih.gov/pubmed/21669299.

[314] K. L. Donnelly et al. "Sources of fatty acids stored in liver and secreted via lipoproteins in patients with nonalcoholic fatty liver disease". In: *J Clin Invest* 115.5 (2005), pp. 1343–51. ISSN: 0021-9738 (Print) 0021-9738 (Linking). DOI: 10.1172/JCI23621. URL: https://www.ncbi.nlm.nih.gov/pubmed/15864352.

[315] E. J. Parks et al. “Effects of a low-fat, high-carbohydrate diet on VLDL-triglyceride assembly, production, and clearance”. In: *J Clin Invest* 104.8 (1999), pp. 1087–96. ISSN: 0021-9738 (Print) 0021-9738 (Linking). DOI: 10.1172/JCI6572. URL: https://www.ncbi.nlm.nih.gov/pubmed/10525047.

[316] B. S. Andrews et al. “Spontaneous murine lupus-like syndromes. Clinical and immunopathological manifestations in several strains”. In: *J Exp Med* 148.5 (1978), pp. 1198–215. ISSN: 0022-1007 (Print) 0022-1007 (Linking). DOI: 10.1084/jem.148.5.1198.

[317] A. Mathian et al. “IFN-alpha induces early lethal lupus in preautoimmune (New Zealand black x New Zealand White)F-1 but not in BALB/c mice”. In: *J Immunol* 174.5 (2005), pp. 2499–2506. ISSN: 0022-1767. URL: %3CGo % 20to % 20ISI % 3E : / / WOS : 000227172100011.

[318] R. Gonzalez-Quintial et al. “Silica exposure and chronic virus infection synergistically promote lupus-like systemic autoimmunity in mice with low genetic predisposition”. In: *Clin Immunol* 205 (2019), pp. 75–82. ISSN: 1521-7035 (Electronic) 1521-6616 (Linking). DOI: 10.1016/j.clim.2019.06.003.

[319] J. W. Bauer et al. “Interferon-regulated chemokines as biomarkers of systemic lupus erythematosus disease activity: a validation study”. In: *Arthritis Rheum* 60.10 (2009), pp. 3098–107. ISSN: 0004-3591 (Print) 0004-3591 (Linking). DOI: 10.1002/art.24803.

[320] C. J. Ulff-Moller et al. “Twin DNA methylation profiling reveals flare-dependent interferon signature and B cell promoter hypermethylation in systemic lupus erythematosus”. In: *Arthritis Rheumatol* 70.6 (2018), pp. 878–890. ISSN: 2326-5205 (Electronic) 2326-5191 (Linking). DOI: 10.1002/art.40422. URL: https://onlinelibrary.wiley.com/doi/full/10.1002/art.40422.

[321] M. Khamashta et al. “Sifalimumab, an anti-interferon-alpha monoclonal antibody, in moderate to severe systemic lupus erythematosus: a randomised, double-blind, placebo-controlled study”. In: *Ann Rheum Dis* 75.11 (2016), pp. 1909–1916. ISSN: 1468-2060 (Electronic) 0003-4967 (Linking). DOI: 10.1136/annrheumdis-2015-208562. URL: http://www.ncbi.nlm.nih.gov/pubmed/27009916%20https://ard.bmj.com/content/annrheumdis/75/11/1909.full.pdf.

[322] R. Furie et al. “Anifrolumab, an anti-interferon-alpha receptor monoclonal antibody, in moderate-to-severe systemic lupus erythematosus”. In: *Arthritis Rheumatol* 69.2 (2017), pp. 376–386. ISSN: 2326-5205 (Electronic) 2326-5191 (Linking). DOI: 10.1002/art.39962. URL: http://www.ncbi.nlm.nih.gov/pubmed/28130918%20https://onlinelibrary.wiley.com/doi/full/10.1002/art.39962.

[323] R. E. Walker et al. “Predicting the effects of supplemental EPA and DHA on the omega-3 index”. In: *Am J Clin Nutr* 110.4 (2019), pp. 1034–1040. ISSN: 1938-3207 (Electronic) 0002-9165 (Linking). DOI: 10.1093/ajcn/nqz161.

[324] J. K. Innes and P. C. Calder. “Omega-6 fatty acids and inflammation”. In: *Prostaglandins Leukot Essent Fatty Acids* 132 (2018), pp. 41–48. ISSN: 1532-2823 (Electronic) 0952-3278 (Linking). DOI: 10.1016/j.plefa.2018.03.004. URL: https://www.ncbi.nlm.nih.gov/pubmed/29610056.

[325] A. I. Ostermann and N. H. Schebb. “Effects of omega-3 fatty acid supplementation on the pattern of oxylipins: a short review about the modulation of hydroxy-, dihydroxy-, and epoxy-fatty acids”. In: *Food Funct* (2017). ISSN: 2042-650X (Electronic) 2042-6496 (Linking). DOI: 10.1039/c7fo00403f. URL: http://pubs.rsc.org/en/Content/ArticleLanding/2017/FO/C7FO00403F.

[326] S. Vordenbaumen et al. “Erythrocyte membrane polyunsaturated fatty acid profiles are associated with systemic inflammation and fish consumption in systemic lupus erythematosus: a cross-sectional study”. In: *Lupus* (2020), p. 961203320912326. ISSN: 1477-0962 (Electronic) 0961-2033 (Linking). DOI: 10.1177/0961203320912326. URL: https://www.ncbi.nlm.nih.gov/pubmed/32188303.

[327] E. Aghdassi et al. “Alterations in circulating fatty acid composition in patients with systemic lupus erythematosus: a pilot study”. In: *JPEN J Parenter Enteral Nutr* 35.2 (2011), pp. 198–208. ISSN: 1941-2444 (Electronic) 0148-6071 (Linking). DOI: 10.1177/0148607110386378. URL: https://www.ncbi.nlm.nih.gov/pubmed/21378249.

[328] L. Navarini et al. “Role of the specialized proresolving mediator resolvin D1 in systemic lupus erythematosus: preliminary results”. In: *J Immunol Res* 2018 (2018), p. 5264195. ISSN: 2314-7156 (Electronic) 2314-7156 (Linking). DOI: 10.1155/2018/5264195. URL: https://www.ncbi.nlm.nih.gov/pubmed/30420970.

[329] J. E. Davidson et al. “Quantifying the burden of steroid-related damage in SLE in the Hopkins Lupus Cohort”. In: *Lupus Sci Med* 5.1 (2018), e000237. ISSN: 2053-8790 (Print) 2053-8790 (Linking). DOI: 10.1136/lupus-2017-000237. URL: https://www.ncbi.nlm.nih.gov/pubmed/29765616.

[330] X. Li et al. “Therapeutic Potential of omega-3 Polyunsaturated Fatty Acids in Human Autoimmune Diseases”. In: *Front Immunol* 10 (2019), p. 2241. ISSN: 1664-3224 (Electronic) 1664-3224 (Linking). DOI: 10.3389/fimmu.2019.02241. URL: https://www.ncbi.nlm.nih.gov/pubmed/31611873.

[331] A. C. Elkan et al. “Diet and fatty acid pattern among patients with SLE: associations with disease activity, blood lipids and atherosclerosis”. In: *Lupus* 21.13 (2012), pp. 1405–11. ISSN: 1477-0962 (Electronic) 0961-2033 (Linking). DOI: 10.1177/0961203312458471. URL: https://www.ncbi.nlm.nih.gov/pubmed/22930204.

[332] C. Arriens et al. “Placebo-controlled randomized clinical trial of fish oil’s impact on fatigue, quality of life, and disease activity in Systemic Lupus Erythematosus”. In: *Nutr J* 14 (2015),

p. 82. ISSN: 1475-2891 (Electronic) 1475-2891 (Linking). DOI: 10.1186/s12937-015-0068-2. URL: https://www.ncbi.nlm.nih.gov/pubmed/26283629.

[333] K. J. Bello et al. “Omega-3 in SLE: a double-blind, placebo-controlled randomized clinical trial of endothelial dysfunction and disease activity in systemic lupus erythematosus”. In: *Rheumatol Int* 33.11 (2013), pp. 2789–96. ISSN: 1437-160X (Electronic) 0172-8172 (Linking). DOI: 10.1007/s00296-013-2811-3. URL: https://www.ncbi.nlm.nih.gov/pubmed/23817872.

[334] M. C. Borges et al. “Omega-3 fatty acids, inflammatory status and biochemical markers of patients with systemic lupus erythematosus: a pilot study”. In: *Rev Bras Reumatol* (2016). ISSN: 1809-4570 (Electronic) 0482-5004 (Linking). DOI: 10.1016/j.rbr.2016.08.002. URL: http://ac.els-cdn.com/S048250041630078X/1-s2.0-S048250041630078X-main.pdf?_tid=efe5f4c2-4620-11e7-9730-00000aab0f26&acdnat=1496249473_55aecda4ed64f1d5148212f5cba9f855.

[335] W. F. Clark et al. “Omega-3 fatty acid dietary supplementation in systemic lupus erythematosus”. In: *Kidney Int* 36.4 (1989), pp. 653–60. ISSN: 0085-2538 (Print) 0085-2538 (Linking). DOI: 10.1038/ki.1989.242. URL: https://www.ncbi.nlm.nih.gov/pubmed/2811063.

[336] W. F. Clark et al. “Fish oil in lupus nephritis: clinical findings and methodological implications”. In: *Kidney Int* 44.1 (1993), pp. 75–86. ISSN: 0085-2538 (Print) 0085-2538 (Linking). DOI: 10.1038/ki.1993.215. URL: https://www.ncbi.nlm.nih.gov/pubmed/8355469.

[337] N. Nakamura et al. “Effects of eicosapentaenoic acids on oxidative stress and plasma fatty acid composition in patients with lupus nephritis”. In: *In Vivo* 19.5 (2005), pp. 879–82. ISSN: 0258-851X (Print) 0258-851X (Linking). URL: https://www.ncbi.nlm.nih.gov/pubmed/16097442.

[338] A. J. Walton et al. “Dietary fish oil and the severity of symptoms in patients with systemic lupus erythematosus”. In: *Ann Rheum Dis* 50.7 (1991), pp. 463–6. ISSN: 0003-4967 (Print) 0003-4967 (Linking). DOI: 10.1136/ard.50.7.463. URL: https://www.ncbi.nlm.nih.gov/pubmed/1877851.

[339] R. H. M. de Groot and B. J. Meyer. “ISSFAL Official Statement Number 6: The importance of measuring blood omega-3 long chain polyunsaturated fatty acid levels in research”. In: *Prostaglandins Leukot Essent Fatty Acids* (2019), p. 102029. ISSN: 1532-2823 (Electronic) 0952-3278 (Linking). DOI: 10.1016/j.plefa.2019.102029.

[340] M. C. Gelfand and A. D. Steinberg. “Therapeutic studies in NZB-W mice. II. Relative efficacy of azathioprine, cyclophosphamide and methylprednisolone”. In: *Arthritis Rheum* 15.3 (1972), pp. 247–52. ISSN: 0004-3591 (Print) 0004-3591 (Linking).

[341] M. C. Gelfand et al. “Therapeutic studies in NZB-W mice. I. Synergy of azathioprine, cyclophosphamide and methylprednisolone in combination”. In: *Arthritis Rheum* 15.3 (1972), pp. 239–46. ISSN: 0004-3591 (Print) 0004-3591 (Linking).

[342] B. Chandrasekar et al. “Dietary omega-3 lipids delay the onset and progression of autoimmune lupus nephritis by inhibiting transforming growth factor beta mRNA and protein expression”. In: *J Autoimmun* 8.3 (1995), pp. 381–93. ISSN: 0896-8411 (Print) 0896-8411 (Linking). DOI: 10.1006/jaut.1995.0030. URL: https://www.ncbi.nlm.nih.gov/pubmed/7575999.

[343] G. V. Halade et al. “Docosahexaenoic acid-enriched fish oil attenuates kidney disease and prolongs median and maximal life span of autoimmune lupus-prone mice”. In: *J Immunol* 184.9 (2010), pp. 5280–6. ISSN: 1550-6606 (Electronic) 0022-1767 (Linking). DOI: 10.4049/jimmunol.0903282. URL: http://www.jimmunol.org/content/184/9/5280.full.pdf.

[344] G. V. Halade et al. “Concentrated fish oil (Lovaza (R)) extends lifespan and attenuates kidney disease in lupus-prone short-lived (NZBxNZW)F1 mice”. In: *Exp Bio Med* 238.6 (2013), pp. 610–622. ISSN: 1535-3702. DOI: 10.1177/1535370213489485. URL: %3CGo%20to%20ISI%3E://WOS:000322771400003.

[345] K. C. Jeng and G. Fernandes. “Effect of fish oil diet on immune response and proteinuria in mice”. In: *Proc Natl Sci Counc Repub China B* 15.2 (1991), pp. 105–10. ISSN: 0255-6596 (Print) 0255-6596 (Linking). URL: https://www.ncbi.nlm.nih.gov/pubmed/1946815.

[346] C. A. Jolly et al. “Life span is prolonged in food-restricted autoimmune-prone (NZB x NZW)F(1) mice fed a diet enriched with (n-3) fatty acids”. In: *J Nutr* 131.10 (2001), pp. 2753–60. ISSN: 0022-3166 (Print) 0022-3166 (Linking). DOI: 10.1093/jn/131.10.2753. URL: https://www.ncbi.nlm.nih.gov/pubmed/11584100.

[347] J. A. Gomez-Puerta, L. Gedmintas, and K. H. Costenbader. “The association between silica exposure and development of ANCA-associated vasculitis: Systematic review and meta-analysis”. In: *Autoimmunity Reviews* 12.12 (2013), pp. 1129–1135. ISSN: 1568-9972. DOI: 10.1016/j.autrev.2013.06.016. URL: %3CGo%20to%20ISI%3E://WOS:000326010000004%20http://ac.els-cdn.com/S1568997213001201/1-s2.0-S1568997213001201-main.pdf?_tid=676f4582-4628-11e7-b83f-00000aacb35e&acdnat=1496252680_96529b3d65df9c49fd6d65a24d4741f6.

[348] Ashima Makol, Mary Jo Reilly, and Kenneth D. Rosenman. “Prevalence of connective tissue disease in silicosis (1985–2006)—a report from the state of Michigan surveillance system for silicosis”. In: *Amer J Ind Med* 54.4 (2011), pp. 255–262. ISSN: 1097-0274. DOI: 10.1002/ajim.20917. URL: http://dx.doi.org/10.1002/ajim.20917.

[349] W. S. Harris. “The omega-3 index: clinical utility for therapeutic intervention”. In: *Curr Cardiol Rep* 12.6 (2010), pp. 503–8. ISSN: 1523-3782. DOI: 10.1007/s11886-010-0141-6.

[350] M. Petri et al. “Derivation and validation of the Systemic Lupus International Collaborating Clinics classification criteria for systemic lupus erythematosus”. In: *Arthritis Rheum* 64.8 (2012), pp. 2677–86. ISSN: 1529-0131 (Electronic) 0004-3591 (Linking). DOI: 10.1002/art.34473. URL: https://www.ncbi.nlm.nih.gov/pubmed/22553077.

[351] J. M. Brown et al. “Silica accelerated systemic autoimmune disease in lupus-prone New Zealand mixed mice”. In: *Clin Exp Immunol.* 131.3 (2003), pp. 415–21. ISSN: 0009-9104 (Print) 0009-9104 (Linking). URL: http://www.ncbi.nlm.nih.gov/pubmed/12605693%20https://www.ncbi.nlm.nih.gov/pmc/articles/PMC1808650/pdf/cei0131-0415.pdf.

[352] J. C. Pfau, J. M. Brown, and A. Holian. “Silica-exposed mice generate autoantibodies to apoptotic cells”. In: *Toxicology* 195.2-3 (2004), pp. 167–76. ISSN: 0300-483X (Print) 0300-483X (Linking). DOI: S0300483X03004530[pii]. URL: http://www.ncbi.nlm.nih.gov/pubmed/14751672.

[353] R. M. Gilberti, G. N. Joshi, and D. A. Knecht. “The phagocytosis of crystalline silica particles by macrophages”. In: *Am J Respir Cell Mol Biol* 39.5 (2008), pp. 619–27. ISSN: 1535-4989 (Electronic) 1044-1549 (Linking). DOI: 10.1165/rcmb.2008-0046OC. URL: https://www.ncbi.nlm.nih.gov/pubmed/18556590.

[354] K. A. Wierenga et al. “Docosahexaenoic acid suppresses silica-induced inflammasome activation and IL-1 cytokine release by interfering with priming signal”. In: *Front Immunol* 10 (2019), p. 2130. ISSN: 1664-3224 (Electronic) 1664-3224 (Linking). DOI: 10.3389/fimmu.2019.02130. URL: https://www.ncbi.nlm.nih.gov/pubmed/31616405.

[355] R. P. Mason, P. Libby, and D. L. Bhatt. “Emerging mechanisms of cardiovascular protection for the omega-3 fatty acid eicosapentaenoic acid”. In: *Arterioscler Thromb Vasc Biol* (2020), ATVBAHA119313286. ISSN: 1524-4636 (Electronic) 1079-5642 (Linking). DOI: 10.1161/ATVBAHA.119.313286. URL: https://www.ncbi.nlm.nih.gov/pubmed/32212849.

[356] N. Martinelli et al. “FADS genotypes and desaturase activity estimated by the ratio of arachidonic acid to linoleic acid are associated with inflammation and coronary artery disease”. In: *Am J Clin Nutr* 88.4 (2008), pp. 941–9. ISSN: 1938-3207 (Electronic) 0002-9165 (Linking). DOI: 10.1093/ajcn/88.4.941. URL: https://www.ncbi.nlm.nih.gov/pubmed/18842780.

[357] L. Schaeffer et al. “Common genetic variants of the FADS1 FADS2 gene cluster and their reconstructed haplotypes are associated with the fatty acid composition in phospholipids”. In: *Hum Mol Genet* 15.11 (2006), pp. 1745–56. ISSN: 0964-6906 (Print) 0964-6906 (Linking). DOI: 10.1093/hmg/ddl117. URL: https://www.ncbi.nlm.nih.gov/pubmed/16670158.

[358] J. Madden et al. “The impact of common gene variants on the response of biomarkers of cardiovascular disease (CVD) risk to increased fish oil fatty acids intakes”. In: *Annu Rev Nutr* 31 (2011), pp. 203–34. ISSN: 1545-4312 (Electronic) 0199-9885 (Linking). DOI:

10.1146/annurev-nutr-010411-095239. URL: https://www.ncbi.nlm.nih.gov/pubmed/21568708.

[359] K. Fritsche. “Important differences exist in the dose-response relationship between diet and immune cell fatty acids in humans and rodents”. In: *Lipids* 42.11 (2007), pp. 961–79. ISSN: 0024-4201 (Print) 0024-4201 (Linking). DOI: 10.1007/s11745-007-3106-9. URL: https://www.ncbi.nlm.nih.gov/pubmed/17713802.

[360] J. G. Bell et al. “Using a fingertip whole blood sample for rapid fatty acid measurement: method validation and correlation with erythrocyte polar lipid compositions in UK subjects”. In: *Br J Nutr* 106.9 (2011), pp. 1408–15. ISSN: 1475-2662 (Electronic) 0007-1145 (Linking). DOI: 10.1017/S0007114511001978. URL: https://www.ncbi.nlm.nih.gov/pubmed/21736805.

[361] P. C. Calder. “Omega-3 polyunsaturated fatty acids and inflammatory processes: nutrition or pharmacology?” In: *Br J Clin Pharmacol* 75.3 (2013), pp. 645–62. ISSN: 1365-2125 (Electronic) 0306-5251 (Linking). DOI: 10.1111/j.1365-2125.2012.04374.x. URL: https://www.ncbi.nlm.nih.gov/pubmed/22765297.

[362] P. C. Norris and E. A. Dennis. “A lipidomic perspective on inflammatory macrophage eicosanoid signaling”. In: *Adv Biol Regul* 54 (2014), pp. 99–110. ISSN: 2212-4934 (Electronic) 2212-4926 (Linking). DOI: 10.1016/j.jbior.2013.09.009.

[363] D. H. Hwang, J. A. Kim, and J. Y. Lee. “Mechanisms for the activation of Toll-like receptor 2/4 by saturated fatty acids and inhibition by docosahexaenoic acid”. In: *Eur J Pharmacol* 785 (2016), pp. 24–35. ISSN: 1879-0712 (Electronic) 0014-2999 (Linking). DOI: 10.1016/j.ejphar.2016.04.024. URL: https://www.ncbi.nlm.nih.gov/pubmed/27085899.

[364] A. R. Weatherill et al. “Saturated and polyunsaturated fatty acids reciprocally modulate dendritic cell functions mediated through TLR4”. In: *J Immunol* 174.9 (2005), pp. 5390–7. ISSN: 0022-1767 (Print) 0022-1767 (Linking). DOI: 10.4049/jimmunol.174.9.5390. URL: https://www.ncbi.nlm.nih.gov/pubmed/15843537.

[365] C. N. Serhan et al. “Maresins: novel macrophage mediators with potent antiinflammatory and proresolving actions”. In: *J Exp Med* 206.1 (2009), pp. 15–23. ISSN: 1540-9538 (Electronic) 0022-1007 (Linking). DOI: jem.20081880[pii]10.1084/jem.20081880. URL: http://www.ncbi.nlm.nih.gov/pubmed/19103881.

[366] Ho Pan Sham et al. “15-epi-lipoxin A(4), resolvin D2, and resolvin D3 induce NF-kappa B regulators in bacterial pneumonia”. In: *Immunol* 200.8 (2018), pp. 2757–2766. ISSN: 0022-1767. DOI: 10.4049/jimmunol.1602090. URL: %3CGo%20to%20ISI%3E://WOS:000429500400025.

[367] Esther Titos et al. “Signaling and immunoresolving actions of resolvin D1 in inflamed human visceral adipose tissue”. In: *Journal of Immunology* 197.8 (2016), pp. 3360–3370.

ISSN: 0022-1767. DOI: 10.4049/jimmunol.1502522. URL: %3CGo%20to%20ISI%3E://WOS:000387965100037.

[368] Nan Chiang et al. “Infection regulates pro-resolving mediators that lower antibiotic requirements”. In: *Nature* 484.7395 (2012), 524–U152. ISSN: 0028-0836. DOI: 10.1038/nature11042. URL: %3CGo%20to%20ISI%3E://WOS:000303200400053.

[369] H. B. Rice et al. “Conducting omega-3 clinical trials with cardiovascular outcomes: Proceedings of a workshop held at ISSFAL 2014”. In: *Prostaglandins Leukot Essent Fatty Acids* 107 (2016), pp. 30–42. ISSN: 1532-2823 (Electronic) 0952-3278 (Linking). DOI: 10.1016/j.plefa.2016.01.003. URL: https://www.ncbi.nlm.nih.gov/pubmed/26858145.

[370] A. L. Farquharson et al. “Effect of dietary fish oil on atrial fibrillation after cardiac surgery”. In: *Am J Cardiol* 108.6 (2011), pp. 851–6. ISSN: 1879-1913 (Electronic) 0002-9149 (Linking). DOI: 10.1016/j.amjcard.2011.04.036. URL: https://www.ncbi.nlm.nih.gov/pubmed/21762871.

[371] M. J. James et al. “Pitfalls in the use of randomised controlled trials for fish oil studies with cardiac patients”. In: *Br J Nutr* 112.5 (2014), pp. 812–20. ISSN: 1475-2662 (Electronic) 0007-1145 (Linking). DOI: 10.1017/S0007114514001408. URL: https://www.ncbi.nlm.nih.gov/pubmed/24933212.

[372] D. L. Bhatt et al. “Cardiovascular Risk Reduction with Icosapent Ethyl for Hypertriglyceridemia”. In: *N Engl J Med* 380.1 (2019), pp. 11–22. ISSN: 1533-4406 (Electronic) 0028-4793 (Linking). DOI: 10.1056/NEJMoa1812792. URL: https://www.ncbi.nlm.nih.gov/pubmed/30415628.

[373] E. L. O’Keefe et al. “Sea change for marine omega-3s: Randomized trials show fish oil reduces cardiovascular events”. In: *Mayo Clin Proc* 94.12 (2019), pp. 2524–2533. ISSN: 1942-5546 (Electronic) 0025-6196 (Linking). DOI: 10.1016/j.mayocp.2019.04.027. URL: https://www.ncbi.nlm.nih.gov/pubmed/31627938.

[374] U. N. Das. “Beneficial effect of eicosapentaenoic and docosahexaenoic acids in the management of systemic lupus erythematosus and its relationship to the cytokine network”. In: *Prostaglandins Leukot Essent Fatty Acids* 51.3 (1994), pp. 207–13. ISSN: 0952-3278 (Print) 0952-3278 (Linking). DOI: 10.1016/0952-3278(94)90136-8. URL: https://www.ncbi.nlm.nih.gov/pubmed/7824535.

[375] P. Piranavan and A. Perl. “Management of cardiovascular disease in patients with systemic lupus erythematosus”. In: *Expert Opin Pharmacother* (2020), pp. 1–11. ISSN: 1744-7666 (Electronic) 1465-6566 (Linking). DOI: 10.1080/14656566.2020.1770227. URL: https://www.ncbi.nlm.nih.gov/pubmed/32511034.

[376] Y. Liu and M. J. Kaplan. “Cardiovascular disease in systemic lupus erythematosus: an update”. In: *Curr Opin Rheumatol* 30.5 (2018), pp. 441–448. ISSN: 1531-6963 (Electronic)

1040-8711 (Linking). DOI: 10.1097/BOR.0000000000000528. URL: https://www.ncbi.nlm.nih.gov/pubmed/29870498.

[377] H. E. Bays et al. “Icosapent ethyl, a pure ethyl ester of eicosapentaenoic acid: effects on circulating markers of inflammation from the MARINE and ANCHOR studies”. In: *Am J Cardiovasc Drugs* 13.1 (2013), pp. 37–46. ISSN: 1179-187X (Electronic) 1175-3277 (Linking). DOI: 10.1007/s40256-012-0002-3. URL: https://www.ncbi.nlm.nih.gov/pubmed/23325450.

[378] T. A. Mori et al. “Effect of omega 3 fatty acids on oxidative stress in humans: GC-MS measurement of urinary F2-isoprostane excretion”. In: *Redox Rep* 5.1 (2000), pp. 45–6. ISSN: 1351-0002 (Print) 1351-0002 (Linking). DOI: 10.1179/rer.2000.5.1.45. URL: https://www.ncbi.nlm.nih.gov/pubmed/10905544.

[379] W. E. Lands. “Diets could prevent many diseases”. In: *Lipids* 38.4 (2003), pp. 317–21. ISSN: 0024-4201 (Print) 0024-4201 (Linking). DOI: 10.1007/s11745-003-1066-0. URL: https://www.ncbi.nlm.nih.gov/pubmed/12848276.

[380] C. E. Ramsden et al. “Targeted alteration of dietary n-3 and n-6 fatty acids for the treatment of chronic headaches: a randomized trial”. In: *Pain* 154.11 (2013), pp. 2441–51. ISSN: 1872-6623 (Electronic) 0304-3959 (Linking). DOI: 10.1016/j.pain.2013.07.028. URL: https://www.ncbi.nlm.nih.gov/pubmed/23886520.

[381] W. S. Harris and C. Von Schacky. “The Omega-3 Index: a new risk factor for death from coronary heart disease?” In: *Prev Med* 39.1 (2004), pp. 212–20. ISSN: 0091-7435 (Print) 0091-7435 (Linking). DOI: 10.1016/j.ypmed.2004.02.030. URL: https://www.ncbi.nlm.nih.gov/pubmed/15208005.

[382] L. C. Del Gobbo et al. “Omega-3 polyunsaturated fatty Acid biomarkers and coronary heart disease: Pooling project of 19 cohort studies”. In: *JAMA Intern Med* 176.8 (2016), pp. 1155–66. ISSN: 2168-6114 (Electronic) 2168-6106 (Linking). DOI: 10.1001/jamainternmed.2016.2925. URL: https://www.ncbi.nlm.nih.gov/pubmed/27357102.

[383] Nutrition EFSA Panel on Dietetic Products and Allergies (NDA). “Scientific opinion related to the tolerable upper intake level of eicosapentaenoic acid (EPA), docosahexaenoic acid (DHA) and docosapentaenoic acid (DPA).” In: *EFSA Journal* 10.7 (2012), pp. 1–48. DOI: 10.2903/j.efsa.2012.2815.. URL: https://www.efsa.europa.eu/en/efsajournal/pub/2815.

[384] J. M. Brown et al. “Silica, apoptosis, and autoimmunity”. In: *J Immunotoxicol* 1.3 (2005), pp. 177–87. ISSN: 1547-6901 (Electronic) 1547-691X (Linking). DOI: 10.1080/15476910490911922. URL: https://www.ncbi.nlm.nih.gov/pubmed/18958651.

[385] R. F. Hamilton, S. A. Thakur, and A. Holian. “Silica binding and toxicity in alveolar macrophages”. In: *Free Radic Biol Med* 44.7 (2008), pp. 1246–58. ISSN: 0891-5849. DOI:

10.1016/j.freeradbiomed.2007.12.027. URL: https://www.ncbi.nlm.nih.gov/pubmed/18226603.

[386] D. Frank and J. E. Vince. “Pyroptosis versus necroptosis: similarities, differences, and crosstalk”. In: *Cell Death Differ* (2018). ISSN: 1350-9047. DOI: 10.1038/s41418-018-0212-6.

[387] A. C. Reisetter et al. “Induction of inflammasome-dependent pyroptosis by carbon black nanoparticles”. In: *J Biol Chem* 286.24 (2011), pp. 21844–52. ISSN: 1083-351X (Electronic) 0021-9258 (Linking). DOI: 10.1074/jbc.M111.238519. URL: https://www.ncbi.nlm.nih.gov/pubmed/21525001.

[388] F. Martinon et al. “Gout-associated uric acid crystals activate the NALP3 inflammasome”. In: *Nature* 440.7081 (2006), pp. 237–41. ISSN: 1476-4687 (Electronic) 0028-0836 (Linking). DOI: 10.1038/nature04516. URL: https://www.ncbi.nlm.nih.gov/pubmed/16407889.

[389] F. G. Bauernfeind et al. “Cutting edge: NF-kappaB activating pattern recognition and cytokine receptors license NLRP3 inflammasome activation by regulating NLRP3 expression”. In: *J Immunol* 183.2 (2009), pp. 787–91. ISSN: 1550-6606 (Electronic) 0022-1767 (Linking). DOI: 10.4049/jimmunol.0901363. URL: https://www.ncbi.nlm.nih.gov/pubmed/19570822.

[390] M. P. Absher et al. “Intrathoracic distribution and transport of aerosolized silica in the rat”. In: *Exp Lung Res* 18.5 (1992), pp. 743–57. ISSN: 0190-2148 (Print) 0190-2148 (Linking). DOI: 10.3109/01902149209031705. URL: https://www.ncbi.nlm.nih.gov/pubmed/1327732.

[391] M. G. Duvall and B. D. Levy. “DHA- and EPA-derived resolvins, protectins, and maresins in airway inflammation”. In: *Eur J Pharmacol* 785 (2016), pp. 144–155. ISSN: 1879-0712 (Electronic) 0014-2999 (Linking). DOI: 10.1016/j.ejphar.2015.11.001. URL: https://www.ncbi.nlm.nih.gov/pubmed/26546247.

[392] A. Lopategi et al. “Frontline Science: Specialized proresolving lipid mediators inhibit the priming and activation of the macrophage NLRP3 inflammasome”. In: *J Leukoc Biol* (2018). ISSN: 0741-5400. DOI: 10.1002/jlb.3hi0517-206rr.

[393] N. Martinez-Micaelo et al. “Dietary fatty acid composition is sensed by the NLRP3 inflammasome: omega-3 fatty acid (DHA) prevents NLRP3 activation in human macrophages”. In: *Food Funct* 7.8 (2016), pp. 3480–7. ISSN: 2042-6496. DOI: 10.1039/c6fo00477f.

[394] L. Shen et al. “Dietary PUFAs attenuate NLRP3 inflammasome activation via enhancing macrophage autophagy”. In: *J Lipid Res* 58.9 (2017), pp. 1808–1821. ISSN: 0022-2275. DOI: 10.1194/jlr.M075879.

[395] W. C. Raschke et al. “Functional macrophage cell lines transformed by Abelson leukemia virus”. In: *Cell* 15.1 (1978), pp. 261–7. ISSN: 0092-8674 (Print) 0092-8674 (Linking). URL: https://www.ncbi.nlm.nih.gov/pubmed/212198.

[396] P. Pelegrin, C. Barroso-Gutierrez, and A. Surprenant. “P2X7 receptor differentially couples to distinct release pathways for IL-1beta in mouse macrophage”. In: *J Immunol* 180.11 (2008), pp. 7147–57. ISSN: 0022-1767 (Print) 0022-1767 (Linking). URL: https://www.ncbi.nlm.nih.gov/pubmed/18490713.

[397] W. T. He et al. “Gasdermin D is an executor of pyroptosis and required for interleukin-1beta secretion”. In: *Cell Res* 25.12 (2015), pp. 1285–98. ISSN: 1748-7838 (Electronic) 1001-0602 (Linking). DOI: 10.1038/cr.2015.139. URL: https://www.ncbi.nlm.nih.gov/pubmed/26611636.

[398] H. Hara et al. “Phosphorylation of the adaptor ASC acts as a molecular switch that controls the formation of speck-like aggregates and inflammasome activity”. In: *Nat Immunol* 14.12 (2013), pp. 1247–55. ISSN: 1529-2916 (Electronic) 1529-2908 (Linking). DOI: 10.1038/ni.2749. URL: https://www.ncbi.nlm.nih.gov/pubmed/24185614.

[399] J. Weischenfeldt and B. Porse. “Bone Marrow-Derived Macrophages (BMM): Isolation and Applications”. In: *CSH Protoc* 2008 (2008), pdb prot5080. ISSN: 1559-6095 (Linking). DOI: 10.1101/pdb.prot5080. URL: https://www.ncbi.nlm.nih.gov/pubmed/21356739.

[400] R. Biswas et al. “Imipramine blocks acute silicosis in a mouse model”. In: *Part Fibre Toxicol* 14.1 (2017), p. 36. ISSN: 1743-8977 (Electronic) 1743-8977 (Linking). DOI: 10.1186/s12989-017-0217-1. URL: https://www.ncbi.nlm.nih.gov/pubmed/28893276.

[401] R. D. Lynch. “Utilization of polyunsaturated fatty acids by human diploid cells aging in vitro”. In: *Lipids* 15.6 (1980), pp. 412–20. ISSN: 0024-4201 (Print) 0024-4201 (Linking). URL: https://www.ncbi.nlm.nih.gov/pubmed/7401939.

[402] P. W. Wiesenfeld, U. S. Babu, and M. W. O’Donnell. “Effect of long-chain fatty acids in the culture medium on fatty acid composition of WEHI-3 and J774A.1 cells”. In: *Comp Biochem Physiol B Biochem Mol Biol* 128.1 (2001), pp. 123–134. ISSN: 1096-4959. DOI: 10 . 1016 / s1096 - 4959(00) 00305 - 5. URL: %3CGo % 20to % 20ISI % 3E : / / WOS : 000166624300013.

[403] F. K. Chan, K. Moriwaki, and M. J. De Rosa. “Detection of necrosis by release of lactate dehydrogenase activity”. In: *Methods Mol Biol* 979 (2013), pp. 65–70. ISSN: 1940-6029 (Electronic) 1064-3745 (Linking). DOI: 10.1007/978-1-62703-290-2_7. URL: https://www.ncbi.nlm.nih.gov/pubmed/23397389.

[404] D. Wessel and U. I. Flugge. “A method for the quantitative recovery of protein in dilute solution in the presence of detergents and lipids”. In: *Anal Biochem* 138.1 (1984), pp. 141–

3. ISSN: 0003-2697 (Print) 0003-2697 (Linking). URL: https://www.ncbi.nlm.nih.gov/pubmed/6731838.

[405] H. Y. Choi, J. E. Lim, and J. H. Hong. "Curcumin interrupts the interaction between the androgen receptor and Wnt/beta-catenin signaling pathway in LNCaP prostate cancer cells". In: *Prostate Cancer Prostatic Dis* 13.4 (2010), pp. 343–9. ISSN: 1476-5608 (Electronic) 1365-7852 (Linking). DOI: 10.1038/pcan.2010.26. URL: https://www.ncbi.nlm.nih.gov/pubmed/20680030.

[406] E. G. Bligh and W. J. Dyer. "A rapid method of total lipid extraction and purification". In: *Can J Biochem Physiol* 37.8 (1959), pp. 911–7. DOI: 10.1139/o59-099. URL: https://www.ncbi.nlm.nih.gov/pubmed/13671378.

[407] L. L. Stoll and A. A. Spector. "Changes in serum influence the fatty acid composition of established cell lines". In: *In vitro* 20.9 (1984), pp. 732–8. ISSN: 0073-5655 (Print) 0073-5655 (Linking). URL: http://www.ncbi.nlm.nih.gov/pubmed/6500611.

[408] J. M. Kahlenberg and M. J. Kaplan. "The inflammasome and lupus: another innate immune mechanism contributing to disease pathogenesis?" In: *Curr Opin Rheumatol* 26.5 (2014), pp. 475–81. ISSN: 1040-8711. DOI: 10.1097/bor.0000000000000088.

[409] I. S. Afonina et al. "Proteolytic Processing of Interleukin-1 Family Cytokines: Variations on a Common Theme". In: *Immunity* 42.6 (2015), pp. 991–1004. ISSN: 1097-4180 (Electronic) 1074-7613 (Linking). DOI: 10.1016/j.immuni.2015.06.003. URL: https://www.ncbi.nlm.nih.gov/pubmed/26084020.

[410] Yifei Zhang et al. "A Membrane Potential- and Calpain-Dependent Reversal of Caspase-1 Inhibition Regulates Canonical NLRP3 Inflammasome". In: *Cell Reports* 24.9 (2018), 2356–2369.e5. ISSN: 2211-1247. DOI: https://doi.org/10.1016/j.celrep.2018.07.098. URL: http://www.sciencedirect.com/science/article/pii/S2211124718312312.

[411] C. A. Dinarello. "Overview of the IL-1 family in innate inflammation and acquired immunity". In: *Immunol Rev* 281.1 (2018), pp. 8–27. ISSN: 1600-065X (Electronic) 0105-2896 (Linking). DOI: 10.1111/imr.12621. URL: https://www.ncbi.nlm.nih.gov/pubmed/29247995.

[412] J. Ding et al. "Pore-forming activity and structural autoinhibition of the gasdermin family". In: *Nature* 535.7610 (2016), pp. 111–6. ISSN: 1476-4687 (Electronic) 0028-0836 (Linking). DOI: 10.1038/nature18590. URL: https://www.ncbi.nlm.nih.gov/pubmed/27281216.

[413] C. L. Evavold et al. "The Pore-Forming Protein Gasdermin D Regulates Interleukin-1 Secretion from Living Macrophages". In: *Immunity* 48.1 (2018), 35–44 e6. ISSN: 1097-4180 (Electronic) 1074-7613 (Linking). DOI: 10.1016/j.immuni.2017.11.013. URL: https://www.ncbi.nlm.nih.gov/pubmed/29195811.

[414] X. Liu et al. “Inflammasome-activated gasdermin D causes pyroptosis by forming membrane pores”. In: *Nature* 535.7610 (2016), pp. 153–8. ISSN: 1476-4687 (Electronic) 0028-0836 (Linking). DOI: 10.1038/nature18629. URL: https://www.ncbi.nlm.nih.gov/pubmed/27383986.

[415] C. Schorn et al. “Sodium overload and water influx activate the NALP3 inflammasome”. In: *J Biol Chem* 286.1 (2011), pp. 35–41. ISSN: 1083-351X (Electronic) 0021-9258 (Linking). DOI: 10.1074/jbc.M110.139048. URL: https://www.ncbi.nlm.nih.gov/pubmed/21051542.

[416] T. Shirahama and A. S. Cohen. “Ultrastructural evidence for leakage of lysosomal contents after phagocytosis of monosodium urate crystals. A mechanism of gouty inflammation”. In: *Am J Pathol* 76.3 (1974), pp. 501–20. ISSN: 0002-9440 (Print) 0002-9440 (Linking). URL: https://www.ncbi.nlm.nih.gov/pubmed/4370533.

[417] S. B. Kovacs and E. A. Miao. “Gasdermins: Effectors of Pyroptosis”. In: *Trends Cell Biol* 27.9 (2017), pp. 673–684. ISSN: 1879-3088 (Electronic) 0962-8924 (Linking). DOI: 10.1016/j.tcb.2017.05.005.

[418] M. Honarpisheh et al. “Phagocytosis of environmental or metabolic crystalline particles induces cytotoxicity by triggering necroptosis across a broad range of particle size and shape”. In: *Sci Rep* 7.1 (2017), p. 15523. ISSN: 2045-2322 (Electronic) 2045-2322 (Linking). DOI: 10.1038/s41598-017-15804-9. URL: http://www.ncbi.nlm.nih.gov/pubmed/29138474.

[419] J. Desai et al. “Particles of different sizes and shapes induce neutrophil necroptosis followed by the release of neutrophil extracellular trap-like chromatin”. In: *Sci Rep* 7.1 (2017), p. 15003. ISSN: 2045-2322 (Electronic) 2045-2322 (Linking). DOI: 10.1038/s41598-017-15106-0. URL: https://www.ncbi.nlm.nih.gov/pubmed/29101355.

[420] Hazel England et al. “Release of interleukin-1α or interleukin-1β depends on mechanism of cell death”. In: *J Biol Chem* 289.23 (2014), pp. 15942–15950. ISSN: 1083-351X 0021-9258. DOI: 10.1074/jbc.M114.557561. URL: https://www.ncbi.nlm.nih.gov/pubmed/24790078%20https://www.ncbi.nlm.nih.gov/pmc/PMC4047367/.

[421] B. Lands, D. Bibus, and K. D. Stark. “Dynamic interactions of n-3 and n-6 fatty acid nutrients”. In: *Prostaglandins Leukot Essent Fatty Acids* (2017). ISSN: 1532-2823 (Electronic) 0952-3278 (Linking). DOI: 10.1016/j.plefa.2017.01.012. URL: http://ac.els-cdn.com/S0952327816301521/1-s2.0-S0952327816301521-main.pdf?_tid=77e29a64-4622-11e7-9aae-00000aab0f01&acdnat=1496250131_e58fdec00fd3140d18689db082bff76c.

[422] T. C. Adarme-Vega, S. R. Thomas-Hall, and P. M. Schenk. “Towards sustainable sources for omega-3 fatty acids production”. In: *Curr Opin Biotechnol* 26 (2014), pp. 14–8. ISSN: 1879-0429 (Electronic) 0958-1669 (Linking). DOI: 10.1016/j.copbio.2013.08.003.

[423] Y. Williams-Bey et al. “Omega-3 free fatty acids suppress macrophage inflammasome activation by inhibiting NF-kappaB activation and enhancing autophagy”. In: *PLoS One*

9.6 (2014), e97957. ISSN: 1932-6203 (Electronic) 1932-6203 (Linking). DOI: 10.1371/journal.pone.0097957. URL: https://www.ncbi.nlm.nih.gov/pubmed/24911523.

[424] J. S. Hwang et al. "Activation of peroxisome proliferator-activated receptor gamma by rosiglitazone inhibits lipopolysaccharide-induced release of high mobility group box 1". In: *Mediators Inflamm* 2012 (2012), p. 352807. ISSN: 1466-1861 (Electronic) 0962-9351 (Linking). DOI: 10.1155/2012/352807. URL: https://www.ncbi.nlm.nih.gov/pubmed/23316104.

[425] C. F. Lin et al. "Rosiglitazone regulates anti-inflammation and growth inhibition via PTEN". In: *Biomed Res Int* 2014 (2014), p. 787924. ISSN: 2314-6141 (Electronic). DOI: 10.1155/2014/787924. URL: https://www.ncbi.nlm.nih.gov/pubmed/24757676.

[426] A. Croasdell et al. "PPARgamma and the Innate Immune System Mediate the Resolution of Inflammation". In: *PPAR Res* 2015 (2015), p. 549691. ISSN: 1687-4757 (Print). DOI: 10.1155/2015/549691. URL: https://www.ncbi.nlm.nih.gov/pubmed/26713087.

[427] G. Pascual et al. "A SUMOylation-dependent pathway mediates transrepression of inflammatory response genes by PPAR-gamma". In: *Nature* 437.7059 (2005), pp. 759–63. ISSN: 1476-4687 (Electronic) 0028-0836 (Linking). DOI: 10.1038/nature03988. URL: https://www.ncbi.nlm.nih.gov/pubmed/16127449.

[428] S. W. Chung et al. "Oxidized low density lipoprotein inhibits interleukin-12 production in lipopolysaccharide-activated mouse macrophages via direct interactions between peroxisome proliferator-activated receptor-gamma and nuclear factor-kappa B". In: *J Biol Chem* 275.42 (2000), pp. 32681–7. ISSN: 0021-9258 (Print) 0021-9258 (Linking). DOI: 10.1074/jbc.M002577200. URL: https://www.ncbi.nlm.nih.gov/pubmed/10934192.

[429] D. Kelly et al. "Commensal anaerobic gut bacteria attenuate inflammation by regulating nuclear-cytoplasmic shuttling of PPAR-gamma and RelA". In: *Nat Immunol* 5.1 (2004), pp. 104–12. ISSN: 1529-2908 (Print) 1529-2908 (Linking). DOI: 10.1038/ni1018. URL: https://www.ncbi.nlm.nih.gov/pubmed/14691478.

[430] A. Castrillo et al. "Peroxisome proliferator-activated receptor-gamma-independent inhibition of macrophage activation by the non-thiazolidinedione agonist L-796,449. Comparison with the effects of 15-deoxy-delta(12,14)-prostaglandin J(2)". In: *J Biol Chem* 276.36 (2001), pp. 34082–8. ISSN: 0021-9258 (Print) 0021-9258 (Linking). DOI: 10.1074/jbc.M102472200. URL: https://www.ncbi.nlm.nih.gov/pubmed/11438523.

[431] M. Ricote et al. "The peroxisome proliferator-activated receptor-gamma is a negative regulator of macrophage activation". In: *Nature* 391.6662 (1998), pp. 79–82. ISSN: 0028-0836 (Print) 0028-0836 (Linking). DOI: 10.1038/34178. URL: https://www.ncbi.nlm.nih.gov/pubmed/9422508.

[432] J. Y. Lee et al. “Saturated fatty acids, but not unsaturated fatty acids, induce the expression of cyclooxygenase-2 mediated through Toll-like receptor 4”. In: *J Biol Chem* 276.20 (2001), pp. 16683–9. ISSN: 0021-9258 (Print) 0021-9258 (Linking). DOI: 10.1074/jbc.M011695200. URL: https://www.ncbi.nlm.nih.gov/pubmed/11278967.

[433] S. Bang et al. “GPR37 regulates macrophage phagocytosis and resolution of inflammatory pain”. In: *J Clin Invest* 128.8 (2018), pp. 3568–3582. ISSN: 1558-8238 (Electronic) 0021-9738 (Linking). DOI: 10.1172/JCI99888. URL: https://www.ncbi.nlm.nih.gov/pubmed/30010619.

[434] H. Hao et al. “Lipoxin A4 suppresses lipopolysaccharide-induced hela cell proliferation and migration via NF-kappaB pathway”. In: *Inflammation* 38.1 (2015), pp. 400–8. ISSN: 1573-2576 (Electronic) 0360-3997 (Linking). DOI: 10.1007/s10753-014-0044-6. URL: https://www.ncbi.nlm.nih.gov/pubmed/25348861.

[435] H. M. Hsiao et al. “Resolvin D1 attenuates polyinosinic-polycytidylic acid-induced inflammatory signaling in human airway epithelial cells via TAK1”. In: *J Immunol* 193.10 (2014), pp. 4980–7. ISSN: 1550-6606 (Electronic) 0022-1767 (Linking). DOI: 10.4049/jimmunol.1400313. URL: https://www.ncbi.nlm.nih.gov/pubmed/25320283.

[436] S. Krishnamoorthy et al. “Resolvin D1 binds human phagocytes with evidence for proresolving receptors”. In: *Proc Natl Acad Sci U S A* 107.4 (2010), pp. 1660–5. ISSN: 1091-6490 (Electronic) 0027-8424 (Linking). DOI: 10.1073/pnas.0907342107. URL: https://www.ncbi.nlm.nih.gov/pubmed/20080636.

[437] P. J. White et al. “Protectin DX alleviates insulin resistance by activating a myokine-liver glucoregulatory axis”. In: *Nat Med* 20.6 (2014), pp. 664–9. ISSN: 1546-170X (Electronic) 1078-8956 (Linking). DOI: 10.1038/nm.3549. URL: https://www.ncbi.nlm.nih.gov/pubmed/24813250.

[438] L. V. Norling et al. “Proresolving and cartilage-protective actions of resolvin D1 in inflammatory arthritis”. In: *JCI Insight* 1.5 (2016), e85922. ISSN: 2379-3708 (Print) 2379-3708 (Linking). DOI: 10.1172/jci.insight.85922. URL: https://www.ncbi.nlm.nih.gov/pubmed/27158677.

[439] S. G. Wendell et al. “15-Hydroxyprostaglandin dehydrogenase generation of electrophilic lipid signaling mediators from hydroxy omega-3 fatty acids”. In: *J Biol Chem* 290.9 (2015), pp. 5868–80. ISSN: 1083-351X (Electronic) 0021-9258 (Linking). DOI: 10.1074/jbc.M114.635151. URL: https://www.ncbi.nlm.nih.gov/pubmed/25586183.

[440] S. Yang et al. “Macrophage polarization in atherosclerosis”. In: *Clin Chim Acta* 501 (2020), pp. 142–146. ISSN: 1873-3492 (Electronic) 0009-8981 (Linking). DOI: 10.1016/j.cca.2019.10.034. URL: https://www.ncbi.nlm.nih.gov/pubmed/31730809.

[441] C. N. Lumeng, J. L. Bodzin, and A. R. Saltiel. “Obesity induces a phenotypic switch in adipose tissue macrophage polarization”. In: *J Clin Invest* 117.1 (2007), pp. 175–84. ISSN: 0021-9738 (Print) 0021-9738 (Linking). DOI: 10.1172/JCI29881. URL: https://www.ncbi.nlm.nih.gov/pubmed/17200717.

[442] A. A. Herrada et al. “Innate Immune Cells’ Contribution to Systemic Lupus Erythematosus”. In: *Front Immunol* 10 (2019), p. 772. ISSN: 1664-3224 (Electronic) 1664-3224 (Linking). DOI: 10.3389/fimmu.2019.00772. URL: https://www.ncbi.nlm.nih.gov/pubmed/31037070.

[443] E. M. Palsson-McDermott and L. A. O’Neill. “Signal transduction by the lipopolysaccharide receptor, Toll-like receptor-4”. In: *Immunology* 113.2 (2004), pp. 153–62. ISSN: 0019-2805 (Print) 0019-2805 (Linking). DOI: 10.1111/j.1365-2567.2004.01976.x. URL: https://www.ncbi.nlm.nih.gov/pubmed/15379975.

[444] J. K. Baillie et al. “Analysis of the human monocyte-derived macrophage transcriptome and response to lipopolysaccharide provides new insights into genetic aetiology of inflammatory bowel disease”. In: *PLoS Genet* 13.3 (2017), e1006641. ISSN: 1553-7404 (Electronic) 1553-7390 (Linking). DOI: 10.1371/journal.pgen.1006641. URL: https://www.ncbi.nlm.nih.gov/pubmed/28263993.

[445] R. Nilsson et al. “Transcriptional network dynamics in macrophage activation”. In: *Genomics* 88.2 (2006), pp. 133–42. ISSN: 0888-7543 (Print) 0888-7543 (Linking). DOI: 10.1016/j.ygeno.2006.03.022. URL: https://www.ncbi.nlm.nih.gov/pubmed/16698233.

[446] C. Barnig et al. “Activation of Resolution Pathways to Prevent and Fight Chronic Inflammation: Lessons From Asthma and Inflammatory Bowel Disease”. In: *Front Immunol* 10 (2019), p. 1699. ISSN: 1664-3224 (Electronic) 1664-3224 (Linking). DOI: 10.3389/fimmu.2019.01699. URL: https://www.ncbi.nlm.nih.gov/pubmed/31396220.

[447] T. Lawrence and D. W. Gilroy. “Chronic inflammation: a failure of resolution?” In: *Int J Exp Pathol* 88.2 (2007), pp. 85–94. ISSN: 0959-9673 (Print) 0959-9673 (Linking). DOI: 10.1111/j.1365-2613.2006.00507.x. URL: https://www.ncbi.nlm.nih.gov/pubmed/17408451.

[448] O. Adam et al. “Anti-inflammatory effects of a low arachidonic acid diet and fish oil in patients with rheumatoid arthritis”. In: *Rheumatol Int* 23.1 (2003), pp. 27–36. ISSN: 0172-8172 (Print) 0172-8172 (Linking). DOI: 10.1007/s00296-002-0234-7. URL: https://www.ncbi.nlm.nih.gov/pubmed/12548439.

[449] K. A. Wierenga et al. “Requisite Omega-3 HUFA Biomarker Thresholds for Preventing Murine Lupus Flaring”. In: *Front Immunol* 11 (2020), p. 1796. ISSN: 1664-3224 (Electronic) 1664-3224 (Linking). DOI: 10.3389/fimmu.2020.01796. URL: https://www.ncbi.nlm.nih.gov/pubmed/32973753.

[450] G. Fejer et al. “Nontransformed, GM-CSF-dependent macrophage lines are a unique model to study tissue macrophage functions”. In: *Proc Natl Acad Sci U S A* 110.24 (2013), E2191–8. ISSN: 1091-6490 (Electronic) 0027-8424 (Linking). DOI: 10.1073/pnas.1302877110. URL: https://www.ncbi.nlm.nih.gov/pubmed/23708119.

[451] G. X. Zheng et al. “Massively parallel digital transcriptional profiling of single cells”. In: *Nat Commun* 8 (2017), p. 14049. ISSN: 2041-1723 (Electronic) 2041-1723 (Linking). DOI: 10.1038/ncomms14049. URL: https://www.ncbi.nlm.nih.gov/pubmed/28091601.

[452] T. Stuart et al. “Comprehensive Integration of Single-Cell Data”. In: *Cell* 177.7 (2019), 1888–1902 e21. ISSN: 1097-4172 (Electronic) 0092-8674 (Linking). DOI: 10.1016/j.cell.2019.05.031. URL: https://www.ncbi.nlm.nih.gov/pubmed/31178118.

[453] S. Aibar et al. “SCENIC: single-cell regulatory network inference and clustering”. In: *Nat Methods* 14.11 (2017), pp. 1083–1086. ISSN: 1548-7105 (Electronic) 1548-7091 (Linking). DOI: 10.1038/nmeth.4463. URL: https://www.ncbi.nlm.nih.gov/pubmed/28991892.

[454] Hadley Wickham. *ggplot2: Elegant Graphics for Data Analysis*. Springer-Verlag New York, 2016. ISBN: 978-3-319-24277-4. URL: https://ggplot2.tidyverse.org.

[455] W. Stillwell and S. R. Wassall. “Docosahexaenoic acid: membrane properties of a unique fatty acid”. In: *Chem Phys Lipids* 126.1 (2003), pp. 1–27. ISSN: 0009-3084 (Print) 0009-3084 (Linking). DOI: 10.1016/s0009-3084(03)00101-4. URL: https://www.ncbi.nlm.nih.gov/pubmed/14580707.

[456] H. Rajagopalan and C. Lengauer. “hCDC4 and genetic instability in cancer”. In: *Cell Cycle* 3.6 (2004), pp. 693–4. ISSN: 1551-4005 (Electronic) 1551-4005 (Linking). DOI: 10.4161/cc.3.6.940. URL: https://www.ncbi.nlm.nih.gov/pubmed/15118416.

[457] B. Chenais et al. “Transcriptomic Response of Breast Cancer Cells MDA-MB-231 to Docosahexaenoic Acid: Downregulation of Lipid and Cholesterol Metabolism Genes and Upregulation of Genes of the Pro-Apoptotic ER-Stress Pathway”. In: *Int J Environ Res Public Health* 17.10 (2020). ISSN: 1660-4601 (Electronic) 1660-4601 (Linking). DOI: 10.3390/ijerph17103746. URL: https://www.ncbi.nlm.nih.gov/pubmed/32466294.

[458] E. Grajchen et al. “CD36-mediated uptake of myelin debris by macrophages and microglia reduces neuroinflammation”. In: *J Neuroinflammation* 17.1 (2020), p. 224. ISSN: 1742-2094 (Electronic) 1742-2094 (Linking). DOI: 10.1186/s12974-020-01899-x. URL: https://www.ncbi.nlm.nih.gov/pubmed/32718316.

[459] C. Tonelli, I. I. C. Chio, and D. A. Tuveson. “Transcriptional Regulation by Nrf2”. In: *Antioxid Redox Signal* 29.17 (2018), pp. 1727–1745. ISSN: 1557-7716 (Electronic) 1523-0864 (Linking). DOI: 10.1089/ars.2017.7342. URL: https://www.ncbi.nlm.nih.gov/pubmed/28899199.

[460] R. Gozzelino, V. Jeney, and M. P. Soares. “Mechanisms of cell protection by heme oxygenase-1”. In: *Annu Rev Pharmacol Toxicol* 50 (2010), pp. 323–54. ISSN: 1545-4304 (Electronic) 0362-1642 (Linking). DOI: 10.1146/annurev.pharmtox.010909.105600. URL: https://www.ncbi.nlm.nih.gov/pubmed/20055707.

[461] A. Jain et al. “p62/SQSTM1 is a target gene for transcription factor NRF2 and creates a positive feedback loop by inducing antioxidant response element-driven gene transcription”. In: *J Biol Chem* 285.29 (2010), pp. 22576–91. ISSN: 1083-351X (Electronic) 0021-9258 (Linking). DOI: 10.1074/jbc.M110.118976. URL: https://www.ncbi.nlm.nih.gov/pubmed/20452972.

[462] E. C. Genin et al. “CHCHD10 mutations promote loss of mitochondrial cristae junctions with impaired mitochondrial genome maintenance and inhibition of apoptosis”. In: *EMBO Mol Med* 8.1 (2016), pp. 58–72. ISSN: 1757-4684 (Electronic) 1757-4676 (Linking). DOI: 10.15252/emmm.201505496. URL: https://www.ncbi.nlm.nih.gov/pubmed/26666268.

[463] T. L. Roberts et al. “HIN-200 proteins regulate caspase activation in response to foreign cytoplasmic DNA”. In: *Science* 323.5917 (2009), pp. 1057–60. ISSN: 1095-9203 (Electronic) 0036-8075 (Linking). DOI: 10.1126/science.1169841. URL: https://www.ncbi.nlm.nih.gov/pubmed/19131592.

[464] O. Zenarruzabeitia et al. “The Biology and Disease Relevance of CD300a, an Inhibitory Receptor for Phosphatidylserine and Phosphatidylethanolamine”. In: *J Immunol* 194.11 (2015), pp. 5053–60. ISSN: 1550-6606 (Electronic) 0022-1767 (Linking). DOI: 10.4049/jimmunol.1500304. URL: https://www.ncbi.nlm.nih.gov/pubmed/25980030.

[465] M. Lee et al. “Tissue-specific Role of CX3CR1 Expressing Immune Cells and Their Relationships with Human Disease”. In: *Immune Netw* 18.1 (2018), e5. ISSN: 1598-2629 (Print) 1598-2629 (Linking). DOI: 10.4110/in.2018.18.e5. URL: https://www.ncbi.nlm.nih.gov/pubmed/29503738.

[466] K. Watari et al. “Impaired differentiation of macrophage lineage cells attenuates bone remodeling and inflammatory angiogenesis in Ndrg1 deficient mice”. In: *Sci Rep* 6 (2016), p. 19470. ISSN: 2045-2322 (Electronic) 2045-2322 (Linking). DOI: 10.1038/srep19470. URL: https://www.ncbi.nlm.nih.gov/pubmed/26778110.

[467] F. O. Martinez et al. “Genetic programs expressed in resting and IL-4 alternatively activated mouse and human macrophages: similarities and differences”. In: *Blood* 121.9 (2013), e57–69. ISSN: 1528-0020 (Electronic) 0006-4971 (Linking). DOI: 10.1182/blood-2012-06-436212. URL: https://www.ncbi.nlm.nih.gov/pubmed/23293084.

[468] E. Y. Chen et al. “Enrichr: interactive and collaborative HTML5 gene list enrichment analysis tool”. In: *BMC Bioinformatics* 14 (2013), p. 128. ISSN: 1471-2105 (Electronic) 1471-2105 (Linking). DOI: 10.1186/1471-2105-14-128. URL: https://www.ncbi.nlm.nih.gov/pubmed/23586463.

[469] R. G. Carroll et al. “An unexpected link between fatty acid synthase and cholesterol synthesis in proinflammatory macrophage activation”. In: *J Biol Chem* 293.15 (2018), pp. 5509–5521. ISSN: 1083-351X (Electronic) 0021-9258 (Linking). DOI: 10.1074/jbc.RA118.001921. URL: https://www.ncbi.nlm.nih.gov/pubmed/29463677.

[470] C. Recio et al. “Activation of the Immune-Metabolic Receptor GPR84 Enhances Inflammation and Phagocytosis in Macrophages”. In: *Front Immunol* 9 (2018), p. 1419. ISSN: 1664-3224 (Print) 1664-3224 (Linking). DOI: 10.3389/fimmu.2018.01419. URL: https://www.ncbi.nlm.nih.gov/pubmed/29973940.

[471] C. Cochain et al. “Single-Cell RNA-Seq Reveals the Transcriptional Landscape and Heterogeneity of Aortic Macrophages in Murine Atherosclerosis”. In: *Circ Res* 122.12 (2018), pp. 1661–1674. ISSN: 1524-4571 (Electronic) 0009-7330 (Linking). DOI: 10.1161/CIRCRESAHA.117.312509. URL: https://www.ncbi.nlm.nih.gov/pubmed/29545365.

[472] H. Yu et al. “Targeting NF-kappaB pathway for the therapy of diseases: mechanism and clinical study”. In: *Signal Transduct Target Ther* 5.1 (2020), p. 209. ISSN: 2059-3635 (Electronic) 2059-3635 (Linking). DOI: 10.1038/s41392-020-00312-6. URL: https://www.ncbi.nlm.nih.gov/pubmed/32958760.

[473] Q. Zhang, M. J. Lenardo, and D. Baltimore. “30 Years of NF-kappaB: A Blossoming of Relevance to Human Pathobiology”. In: *Cell* 168.1-2 (2017), pp. 37–57. ISSN: 1097-4172 (Electronic) 0092-8674 (Linking). DOI: 10.1016/j.cell.2016.12.012. URL: https://www.ncbi.nlm.nih.gov/pubmed/28086098.

[474] T. Kawasaki and T. Kawai. “Toll-like receptor signaling pathways”. In: *Front Immunol* 5 (2014), p. 461. ISSN: 1664-3224 (Print) 1664-3224 (Linking). DOI: 10.3389/fimmu.2014.00461. URL: https://www.ncbi.nlm.nih.gov/pubmed/25309543.

[475] W. X. Sin et al. “IRF-7 Mediates Type I IFN Responses in Endotoxin-Challenged Mice”. In: *Front Immunol* 11 (2020), p. 640. ISSN: 1664-3224 (Electronic) 1664-3224 (Linking). DOI: 10.3389/fimmu.2020.00640. URL: https://www.ncbi.nlm.nih.gov/pubmed/32373120.

[476] A. I. Ostermann et al. “Plasma oxylipins respond in a linear dose-response manner with increased intake of EPA and DHA: results from a randomized controlled trial in healthy humans”. In: *Am J Clin Nutr* 109.5 (2019), pp. 1251–1263. ISSN: 1938-3207 (Electronic) 0002-9165 (Linking). DOI: 10.1093/ajcn/nqz016. URL: https://www.ncbi.nlm.nih.gov/pubmed/31006007.

[477] Y. Gong et al. “Sterol-regulated ubiquitination and degradation of Insig-1 creates a convergent mechanism for feedback control of cholesterol synthesis and uptake”. In: *Cell Metab* 3.1 (2006), pp. 15–24. ISSN: 1550-4131 (Print) 1550-4131 (Linking). DOI: 10.1016/j.cmet.2005.11.014. URL: https://www.ncbi.nlm.nih.gov/pubmed/16399501.

[478] B. D. Reed et al. “Genome-wide occupancy of SREBP1 and its partners NFY and SP1 reveals novel functional roles and combinatorial regulation of distinct classes of genes”. In: *PLoS Genet* 4.7 (2008), e1000133. ISSN: 1553-7404 (Electronic) 1553-7390 (Linking). DOI: 10.1371/journal.pgen.1000133. URL: https://www.ncbi.nlm.nih.gov/pubmed/18654640.

[479] R. Streicher et al. “SREBP-1 mediates activation of the low density lipoprotein receptor promoter by insulin and insulin-like growth factor-I”. In: *J Biol Chem* 271.12 (1996), pp. 7128–33. ISSN: 0021-9258 (Print) 0021-9258 (Linking). DOI: 10.1074/jbc.271.12.7128. URL: https://www.ncbi.nlm.nih.gov/pubmed/8636148.

[480] D. Hishikawa et al. “Hepatic Levels of DHA-Containing Phospholipids Instruct SREBP1-Mediated Synthesis and Systemic Delivery of Polyunsaturated Fatty Acids”. In: *iScience* 23.9 (2020), p. 101495. ISSN: 2589-0042 (Electronic) 2589-0042 (Linking). DOI: 10.1016/j.isci.2020.101495. URL: https://www.ncbi.nlm.nih.gov/pubmed/32891885.

[481] L. H. Huang, H. Y. Chung, and H. M. Su. “Docosahexaenoic acid reduces sterol regulatory element binding protein-1 and fatty acid synthase expression and inhibits cell proliferation by inhibiting pAkt signaling in a human breast cancer MCF-7 cell line”. In: *BMC Cancer* 17.1 (2017), p. 890. ISSN: 1471-2407 (Electronic) 1471-2407 (Linking). DOI: 10.1186/s12885-017-3936-7. URL: https://www.ncbi.nlm.nih.gov/pubmed/29282029.

[482] X. Zhu et al. “Macrophage ABCA1 reduces MyD88-dependent Toll-like receptor trafficking to lipid rafts by reduction of lipid raft cholesterol”. In: *J Lipid Res* 51.11 (2010), pp. 3196–206. ISSN: 1539-7262 (Electronic) 0022-2275 (Linking). DOI: 10.1194/jlr.M006486. URL: https://www.ncbi.nlm.nih.gov/pubmed/20650929.

[483] J. S. Riley and S. W. Tait. “Mitochondrial DNA in inflammation and immunity”. In: *EMBO Rep* 21.4 (2020), e49799. ISSN: 1469-3178 (Electronic) 1469-221X (Linking). DOI: 10.15252/embr.201949799. URL: https://www.ncbi.nlm.nih.gov/pubmed/32202065.

[484] E. V. Dang et al. “Oxysterol Restraint of Cholesterol Synthesis Prevents AIM2 Inflammasome Activation”. In: *Cell* 171.5 (2017), 1057–1071 e11. ISSN: 1097-4172 (Electronic) 0092-8674 (Linking). DOI: 10.1016/j.cell.2017.09.029. URL: https://www.ncbi.nlm.nih.gov/pubmed/29033131.

[485] S. J. Bush et al. “Species-Specificity of Transcriptional Regulation and the Response to Lipopolysaccharide in Mammalian Macrophages”. In: *Front Cell Dev Biol* 8 (2020), p. 661. ISSN: 2296-634X (Print) 2296-634X (Linking). DOI: 10.3389/fcell.2020.00661. URL: https://www.ncbi.nlm.nih.gov/pubmed/32793601.

[486] C. Pridans et al. “Transcriptomic Analysis of Rat Macrophages”. In: *Front Immunol* 11 (2020), p. 594594. ISSN: 1664-3224 (Electronic) 1664-3224 (Linking). DOI: 10.3389/fimmu.2020.594594. URL: https://www.ncbi.nlm.nih.gov/pubmed/33633725.

[487] S. H. Boudigaard et al. “Occupational exposure to respirable crystalline silica and risk of autoimmune rheumatic diseases: a nationwide cohort study”. In: *Int J Epidemiol* (2021). ISSN: 1464-3685 (Electronic) 0300-5771 (Linking). DOI: 10.1093/ije/dyaa287. URL: https://www.ncbi.nlm.nih.gov/pubmed/33462590.

[488] C. G. Parks et al. “Understanding the role of environmental factors in the development of systemic lupus erythematosus”. In: *Best Pract Res Clin Rheumatol* 31.3 (2017), pp. 306–320. ISSN: 1532-1770 (Electronic) 1521-6942 (Linking). DOI: 10.1016/j.berh.2017.09.005. URL: https://www.ncbi.nlm.nih.gov/pubmed/29224673.

[489] C. J. Busch et al. “Isolation and Long-term Cultivation of Mouse Alveolar Macrophages”. In: *Bio Protoc* 9.14 (2019). ISSN: 2331-8325 (Print) 2331-8325 (Linking). DOI: 10.21769/BioProtoc.3302. URL: https://www.ncbi.nlm.nih.gov/pubmed/31909091.

[490] Y. W. Chen et al. “PM2.5 impairs macrophage functions to exacerbate pneumococcus-induced pulmonary pathogenesis”. In: *Part Fibre Toxicol* 17.1 (2020), p. 37. ISSN: 1743-8977 (Electronic) 1743-8977 (Linking). DOI: 10.1186/s12989-020-00362-2. URL: https://www.ncbi.nlm.nih.gov/pubmed/32753046.

[491] T. A. Brenner et al. “Immortalized MH-S cells lack defining features of primary alveolar macrophages and do not support mouse pneumovirus replication”. In: *Immunol Lett* 172 (2016), pp. 106–12. ISSN: 1879-0542 (Electronic) 0165-2478 (Linking). DOI: 10.1016/j.imlet.2016.02.012. URL: https://www.ncbi.nlm.nih.gov/pubmed/26916143.

[492] M. Guilliams et al. “Alveolar macrophages develop from fetal monocytes that differentiate into long-lived cells in the first week of life via GM-CSF”. In: *J Exp Med* 210.10 (2013), pp. 1977–92. ISSN: 1540-9538 (Electronic) 0022-1007 (Linking). DOI: 10.1084/jem.20131199. URL: https://www.ncbi.nlm.nih.gov/pubmed/24043763.

[493] A.D. Gorki et al. “Murine ex vivo cultured alveolar macrophages provide a novel tool to study tissue-resident macrophage behavior and function”. In: *bioRxiv* (2021). DOI: 10.1101/2021.02.11.430791. URL: https://www.biorxiv.org/content/10.1101/2021.02.11.430791v1.

[494] A. E. Carpenter et al. “CellProfiler: image analysis software for identifying and quantifying cell phenotypes”. In: *Genome Biol* 7.10 (2006), R100. ISSN: 1474-760X (Electronic) 1474-7596 (Linking). DOI: 10.1186/gb-2006-7-10-r100. URL: https://www.ncbi.nlm.nih.gov/pubmed/17076895.

[495] M. D. Maler et al. “Key Role of the Scavenger Receptor MARCO in Mediating Adenovirus Infection and Subsequent Innate Responses of Macrophages”. In: *mBio* 8.4 (2017). ISSN: 2150-7511 (Electronic). DOI: 10.1128/mBio.00670-17. URL: https://www.ncbi.nlm.nih.gov/pubmed/28765216.

[496] M. Woo et al. “Mycobacterium tuberculosis Infection and Innate Responses in a New Model of Lung Alveolar Macrophages”. In: *Front Immunol* 9 (2018), p. 438. ISSN: 1664-3224 (Print) 1664-3224 (Linking). DOI: 10.3389/fimmu.2018.00438. URL: https://www.ncbi.nlm.nih.gov/pubmed/29593716.

[497] K. J. Mould et al. “Single cell RNA sequencing identifies unique inflammatory airspace macrophage subsets”. In: *JCI Insight* 4.5 (2019). ISSN: 2379-3708 (Electronic) 2379-3708 (Linking). DOI: 10.1172/jci.insight.126556. URL: https://www.ncbi.nlm.nih.gov/pubmed/30721157.

[498] P. Fletcher et al. “Docosahexaenoic acid impacts macrophage phenotype subsets and phagolysosomal membrane permeability with particle exposure”. In: *J Toxicol Environ Health A* 84.4 (2021), pp. 152–172. ISSN: 1528-7394 (Print) 0098-4108 (Linking). DOI: 10.1080/15287394.2020.1842826. URL: https://www.ncbi.nlm.nih.gov/pubmed/33148135.

[499] E. H. Budi, D. Duan, and R. Derynck. “Transforming Growth Factor-beta Receptors and Smads: Regulatory Complexity and Functional Versatility”. In: *Trends Cell Biol* 27.9 (2017), pp. 658–672. ISSN: 1879-3088 (Electronic) 0962-8924 (Linking). DOI: 10.1016/j.tcb.2017.04.005. URL: https://www.ncbi.nlm.nih.gov/pubmed/28552280.

[500] K. Tzavlaki and A. Moustakas. “TGF-beta Signaling”. In: *Biomolecules* 10.3 (2020). ISSN: 2218-273X (Electronic) 2218-273X (Linking). DOI: 10.3390/biom10030487. URL: https://www.ncbi.nlm.nih.gov/pubmed/32210029.

[501] D. Duan and R. Derynck. “Transforming growth factor-beta (TGF-beta)-induced up-regulation of TGF-beta receptors at the cell surface amplifies the TGF-beta response”. In: *J Biol Chem* 294.21 (2019), pp. 8490–8504. ISSN: 1083-351X (Electronic) 0021-9258 (Linking). DOI: 10.1074/jbc.RA118.005763. URL: https://www.ncbi.nlm.nih.gov/pubmed/30948511.

[502] Y. Yao et al. “Histone deacetylase 3 controls lung alveolar macrophage development and homeostasis”. In: *Nat Commun* 11.1 (2020), p. 3822. ISSN: 2041-1723 (Electronic) 2041-1723 (Linking). DOI: 10.1038/s41467-020-17630-6. URL: https://www.ncbi.nlm.nih.gov/pubmed/32732898.

[503] A. D. Baker et al. “Targeted PPARgamma deficiency in alveolar macrophages disrupts surfactant catabolism”. In: *J Lipid Res* 51.6 (2010), pp. 1325–31. ISSN: 1539-7262 (Electronic) 0022-2275 (Linking). DOI: 10.1194/jlr.M001651. URL: https://www.ncbi.nlm.nih.gov/pubmed/20064973.

[504] P. Hallenborg et al. “The elusive endogenous adipogenic PPARgamma agonists: Lining up the suspects”. In: *Prog Lipid Res* 61 (2016), pp. 149–62. ISSN: 1873-2194 (Electronic) 0163-7827 (Linking). DOI: 10.1016/j.plipres.2015.11.002. URL: https://www.ncbi.nlm.nih.gov/pubmed/26703188.

[505] T. L. Bonfield et al. “Peroxisome proliferator-activated receptor-gamma is deficient in alveolar macrophages from patients with alveolar proteinosis”. In: *Am J Respir Cell Mol Biol* 29.6 (2003), pp. 677–82. ISSN: 1044-1549 (Print) 1044-1549 (Linking). DOI: 10.1165/rcmb.2003-0148OC. URL: https://www.ncbi.nlm.nih.gov/pubmed/12805087.

[506] S. L. Gibbings et al. “Transcriptome analysis highlights the conserved difference between embryonic and postnatal-derived alveolar macrophages”. In: *Blood* 126.11 (2015), pp. 1357–66. ISSN: 1528-0020 (Electronic) 0006-4971 (Linking). DOI: 10.1182/blood-2015-01-624809. URL: https://www.ncbi.nlm.nih.gov/pubmed/26232173.

[507] M. S. Arredouani et al. “MARCO is the major binding receptor for unopsonized particles and bacteria on human alveolar macrophages”. In: *J Immunol* 175.9 (2005), pp. 6058–64. ISSN: 0022-1767 (Print) 0022-1767 (Linking). DOI: 10.4049/jimmunol.175.9.6058. URL: https://www.ncbi.nlm.nih.gov/pubmed/16237101.

[508] Jr. Hamilton R. F. et al. “MARCO mediates silica uptake and toxicity in alveolar macrophages from C57BL/6 mice”. In: *J Biol Chem* 281.45 (2006), pp. 34218–26. ISSN: 0021-9258 (Print) 0021-9258 (Linking). DOI: 10.1074/jbc.M605229200. URL: https://www.ncbi.nlm.nih.gov/pubmed/16984918.

[509] P. C. Calder and R. J. Deckelbaum. “Editorial: Omega-3 fatty acids: new studies, new data, new questions”. In: *Curr Opin Clin Nutr Metab Care* 24.2 (2021), pp. 109–113. ISSN: 1473-6519 (Electronic) 1363-1950 (Linking). DOI: 10.1097/MCO.0000000000000726. URL: https://www.ncbi.nlm.nih.gov/pubmed/33394717.

[510] B. Troesch et al. “Expert Opinion on Benefits of Long-Chain Omega-3 Fatty Acids (DHA and EPA) in Aging and Clinical Nutrition”. In: *Nutrients* 12.9 (2020). ISSN: 2072-6643 (Electronic) 2072-6643 (Linking). DOI: 10.3390/nu12092555. URL: https://www.ncbi.nlm.nih.gov/pubmed/32846900.

[511] A. Pizzini et al. “The Role of Omega-3 Fatty Acids in the Setting of Coronary Artery Disease and COPD: A Review”. In: *Nutrients* 10.12 (2018). ISSN: 2072-6643 (Electronic) 2072-6643 (Linking). DOI: 10.3390/nu10121864. URL: https://www.ncbi.nlm.nih.gov/pubmed/30513804.

[512] A. Pontes-Arruda et al. “The use of an inflammation-modulating diet in patients with acute lung injury or acute respiratory distress syndrome: a meta-analysis of outcome data”. In: *JPEN J Parenter Enteral Nutr* 32.6 (2008), pp. 596–605. ISSN: 0148-6071 (Print) 0148-6071 (Linking). DOI: 10.1177/0148607108324203. URL: https://www.ncbi.nlm.nih.gov/pubmed/18974237.

[513] D. E. Schraufnagel et al. “Health Benefits of Air Pollution Reduction”. In: *Ann Am Thorac Soc* 16.12 (2019), pp. 1478–1487. ISSN: 2325-6621 (Electronic) 2325-6621 (Linking). DOI: 10.1513/AnnalsATS.201907-538CME. URL: https://www.ncbi.nlm.nih.gov/pubmed/31774324.

[514] R. S. Gangwar et al. “Differential contribution of bone marrow-derived infiltrating monocytes and resident macrophages to persistent lung inflammation in chronic air pollution exposure”. In: *Sci Rep* 10.1 (2020), p. 14348. ISSN: 2045-2322 (Electronic) 2045-2322 (Linking). DOI: 10.1038/s41598-020-71144-1. URL: https://www.ncbi.nlm.nih.gov/pubmed/32873817.

[515] A. C. McQuattie-Pimentel et al. “The lung microenvironment shapes a dysfunctional response of alveolar macrophages in aging”. In: *J Clin Invest* 131.4 (2021). ISSN: 1558-8238 (Electronic) 0021-9738 (Linking). DOI: 10.1172/JCI140299. URL: https://www.ncbi.nlm.nih.gov/pubmed/33586677.

[516] N. Krishnamoorthy et al. “Cutting edge: maresin-1 engages regulatory T cells to limit type 2 innate lymphoid cell activation and promote resolution of lung inflammation”. In: *J Immunol* 194.3 (2015), pp. 863–7. ISSN: 1550-6606 (Electronic) 0022-1767 (Linking). DOI: 10.4049/jimmunol.1402534. URL: https://www.ncbi.nlm.nih.gov/pubmed/25539814.

[517] R. E. Abdulnour et al. “Aspirin-triggered resolvin D1 is produced during self-resolving gram-negative bacterial pneumonia and regulates host immune responses for the resolution of lung inflammation”. In: *Mucosal Immunol* 9.5 (2016), pp. 1278–87. ISSN: 1935-3456 (Electronic) 1933-0219 (Linking). DOI: 10.1038/mi.2015.129. URL: https://www.ncbi.nlm.nih.gov/pubmed/26647716.

[518] S. Gouveia-Figueira et al. “Mass spectrometry profiling of oxylipins, endocannabinoids, and N-acylethanolamines in human lung lavage fluids reveals responsiveness of prostaglandin E2 and associated lipid metabolites to biodiesel exhaust exposure”. In: *Anal Bioanal Chem* 409.11 (2017), pp. 2967–2980. ISSN: 1618-2650 (Electronic) 1618-2642 (Linking). DOI: 10.1007/s00216-017-0243-8. URL: https://www.ncbi.nlm.nih.gov/pubmed/28235994.

[519] B. Kilburg-Basnyat et al. “Specialized Pro-Resolving Lipid Mediators Regulate Ozone-Induced Pulmonary and Systemic Inflammation”. In: *Toxicol Sci* 163.2 (2018), pp. 466–477. ISSN: 1096-0929 (Electronic) 1096-0929 (Linking). DOI: 10.1093/toxsci/kfy040. URL: https://www.ncbi.nlm.nih.gov/pubmed/29471542.

[520] O. Koltsida et al. “Toll-like receptor 7 stimulates production of specialized pro-resolving lipid mediators and promotes resolution of airway inflammation”. In: *EMBO Mol Med* 5.5 (2013), pp. 762–75. ISSN: 1757-4684 (Electronic) 1757-4676 (Linking). DOI: 10.1002/emmm.201201891. URL: https://www.ncbi.nlm.nih.gov/pubmed/23584892.

[521] N. Krishnamoorthy et al. “Specialized Proresolving Mediators in Innate and Adaptive Immune Responses in Airway Diseases”. In: *Physiol Rev* 98.3 (2018), pp. 1335–1370. ISSN: 1522-1210 (Electronic) 0031-9333 (Linking). DOI: 10.1152/physrev.00026.2017. URL: https://www.ncbi.nlm.nih.gov/pubmed/29717929.

[522] K. Kaliannan et al. “Multi-omic analysis in transgenic mice implicates omega-6/omega-3 fatty acid imbalance as a risk factor for chronic disease”. In: *Commun Biol* 2 (2019), p. 276. ISSN: 2399-3642 (Electronic) 2399-3642 (Linking). DOI: 10.1038/s42003-019-0521-4. URL: https://www.ncbi.nlm.nih.gov/pubmed/31372515.

[523] M. Marklund et al. “Biomarkers of Dietary Omega-6 Fatty Acids and Incident Cardiovascular Disease and Mortality”. In: *Circulation* 139.21 (2019), pp. 2422–2436. ISSN: 1524-4539 (Electronic) 0009-7322 (Linking). DOI: 10.1161/CIRCULATIONAHA.118.038908. URL: https://www.ncbi.nlm.nih.gov/pubmed/30971107.

[524] P. M. Clifton and J. B. Keogh. “A systematic review of the effect of dietary saturated and polyunsaturated fat on heart disease”. In: *Nutr Metab Cardiovasc Dis* 27.12 (2017), pp. 1060–1080. ISSN: 1590-3729 (Electronic) 0939-4753 (Linking). DOI: 10.1016/j.numecd.2017.10.010. URL: https://www.ncbi.nlm.nih.gov/pubmed/29174025.

[525] B. Ruiz-Nunez, D. A. Dijck-Brouwer, and F. A. Muskiet. “The relation of saturated fatty acids with low-grade inflammation and cardiovascular disease”. In: *J Nutr Biochem* 36 (2016), pp. 1–20. ISSN: 1873-4847 (Electronic) 0955-2863 (Linking). DOI: 10.1016/j.jnutbio.2015.12.007. URL: https://www.ncbi.nlm.nih.gov/pubmed/27692243.

[526] J. Allaire et al. “A randomized, crossover, head-to-head comparison of eicosapentaenoic acid and docosahexaenoic acid supplementation to reduce inflammation markers in men and women: the Comparing EPA to DHA (ComparED) Study”. In: *Am J Clin Nutr* 104.2 (2016), pp. 280–7. ISSN: 1938-3207 (Electronic) 0002-9165 (Linking). DOI: 10.3945/ajcn.116.131896. URL: https://www.ncbi.nlm.nih.gov/pubmed/27281302.

[527] S. C. Dyall. “Long-chain omega-3 fatty acids and the brain: a review of the independent and shared effects of EPA, DPA and DHA”. In: *Front Aging Neurosci* 7 (2015), p. 52. ISSN: 1663-4365 (Print) 1663-4365 (Linking). DOI: 10.3389/fnagi.2015.00052. URL: https://www.ncbi.nlm.nih.gov/pubmed/25954194.

[528] D. S. Kelley and Y. Adkins. “Similarities and differences between the effects of EPA and DHA on markers of atherosclerosis in human subjects”. In: *Proc Nutr Soc* 71.2 (2012), pp. 322–31. ISSN: 1475-2719 (Electronic) 0029-6651 (Linking). DOI: 10.1017/S0029665112000080. URL: https://www.ncbi.nlm.nih.gov/pubmed/22369859.

[529] J. So et al. “EPA and DHA differentially modulate monocyte inflammatory response in subjects with chronic inflammation in part via plasma specialized pro-resolving lipid mediators: A randomized, double-blind, crossover study”. In: *Atherosclerosis* 316 (2021), pp. 90–98. ISSN: 1879-1484 (Electronic) 0021-9150 (Linking). DOI: 10.1016/j.atherosclerosis.2020.11.018. URL: https://www.ncbi.nlm.nih.gov/pubmed/33303222.